



**Visualization of the Subcellular Localization of Inhaled
PI3K δ Inhibitors Using Bioorthogonal Approaches**

Thesis presented by

Maxime Rouah

In fulfilment of the requirements for a degree of
Doctor of Philosophy

2020

Declaration of Copyright

This thesis is the result of the author's original research. It has been composed by the author and has not been previously submitted for examination which has led to the award of a degree.

The copyright of this thesis belongs to the author under the terms of the United Kingdom Copyright Acts as qualified by University of Strathclyde Regulation 3.50. Due acknowledgement must always be made of the use of any material contained in, or derived from, this thesis.

Maxime Rouah

Signed:

Date:

Acknowledgements

Firstly, I would like to thank my GSK supervisor Dr Zoë Henley for her continual guidance, dedication and enthusiasm. It has been a pleasure to work with you and I have gained so much from your experience and scientific rigour. Thank you for ensuring that your supervision would always contribute to both my scientific and personal development. I would also like to thank my second GSK supervisor Dr Jonathan Taylor for stepping in and providing me with supervision in the last months of my PhD. I am really grateful for your guidance, your contribution proof-reading this thesis and your support as I was going through the end of my PhD. I would also like to thank my academic supervisor Dr Craig Jamieson for his complementary support and his enduring positive attitude throughout my PhD. I would also like to thank my line manager at GSK, Dr Diane Coe, for her guidance, availability and her help proof-reading this thesis.

I would like to thank Professor Harry Kelly and Professor Billy Kerr for offering me the opportunity to join the collaborative GSK/University of Strathclyde PhD Programme. I would also like to thank Harry for supporting my participation to attend and present my research at numerous scientific conferences throughout my PhD, therefore giving me the opportunity to benefit from significant peer-to-peer interactions and strongly bolstering my profile as a researcher. In addition, I would like to thank Andrea Malley, Abby Mullord and Laura Paterson for their administrative support.

This thesis is also the result of successful multidisciplinary collaborations. Therefore, I would like to thank all the talented scientists with whom I have had pleasure to work with throughout my PhD. Firstly, Anna Rutkowska at Cellzome for her precious guidance and her help supervising and also conducting some of the imaging experiments described in this thesis. You have been an incommensurable support and I am really grateful for your time answering the many questions I had as a chemist attempting biology. I would also like to thank Cécile Echaliier with whom I have been able to collaborate on this project. I am incredibly thankful for your

contribution to some of the imaging work, your help arranging my secondment at Cellzome as well as your trainings on some of the biological assays. I would like to address a special thank you to Douglas Thomson, Jana Krause, Marcel Mulbaier and Giovanna Bergamini for their input and contribution to the project. More generally, I would like to thank all the scientists at Cellzome for their warm welcome and making my secondment such a rewarding experience.

I would also like to thank Carla Newman from the Bio-imaging group at GSK for her supervision of the NanoSIMS experiments, her help setting out this collaboration with the National Physical Laboratory (NPL), and her time answering my several questions on mass-spectrometry imaging techniques. I would also like to thank Greg McMahon at the NPL for his precious help with the NanoSIMS work.

I would also like to thank current and past scientists from the former Refractory Respiratory Inflammation (RRI) DPU at GSK for their support and their time engaging in scientific conversations on PI3K: Sophie Bertrand, Ken Down, Charlotte Hardy, Nicole Hamblin, Gus Amour and Edith Hessel.

I would also like to address a special thank you to Richard Briers for his help and advice on the purification of some of the compounds described in this thesis. James Rowedder and Jonathan Lea for their contribution to the PI3K δ assays.

There are also many individuals that have made the last few years such an enjoyable experience and helped me keeping my spirits up during stressful times: Lucia Fusani, Sam Holman, the former members of the RRI Social Committee: Caitlin Lapworth, Hannah Wajdner, Natalie Zimmerman, Nate Lam, the members of the Jamieson Research Group at Strathclyde and the fantastic lab coordinators in the GSK Smartlab: Kerry Mullen and Hannah Paine. I hope our paths cross again.

Finally, I would like to thank my family for their endless support, despite still not fully understanding what I really do. None of this would have been possible without your love and encouragements.

Abstract

In contrast to oral delivery, administering small molecules by the inhaled route is inherently complex and relatively limited information is available on the regional localisation of drug retention following inhalation. Therefore, new tools and methodologies that can help to correlate molecular properties of inhaled drug molecules to their cellular distribution are of considerable interest. The programme of research described in this thesis uses bioorthogonal chemistry approaches to provide molecular tools that can contribute to the understanding of the cellular localisation of inhaled drug molecules *via* cellular imaging. More specifically, a tagging methodology based on bioorthogonal chemistry and the inverse electron demand Diels-Alder (IEDDA) reaction between *trans*-cyclooctene-(TCO)-tagged chemical probes and fluorescent tetrazine reporters was utilised to enable the visualization of drug subcellular localisation at high resolution. This strategy has been applied for the cellular imaging of chemical probe molecules derived from nemiralisib and GSK2292767, two inhaled clinical candidates inhibiting the lipid kinase PI3K δ , currently being investigated for the treatment of respiratory diseases such as asthma and COPD. In rat lung tissue studies by MALDI imaging mass spectrometry, these two molecules exhibited distinct deposition and distribution profiles, and were therefore an ideal case for such studies.

The syntheses of these bioorthogonal chemical probes required the development of robust synthetic routes for which a novel common intermediate was designed, thereby enabling the access of probes derived from both nemiralisib and GSK2292767 in a more convergent approach. Novel monomers were also derivatised to allow the late-stage installation of the *trans*-cyclooctene (TCO) tag at tolerated sites. This strategy relied on design of optimal linkers to ensure that the TCO tag would not disrupt the binding of the chemical probe to the target, whilst ensuring that it would remain available for IEDDA reaction with the tetrazine partner. Based on their properties, several chemical probes were selected for subsequent profiling in the cellular imaging assay. These experiments highlighted different subcellular localisation for the chemical probes derived from the inhaled PI3K δ inhibitors, along

with varying degrees of non-specific accumulation in acidic and membrane-rich subcellular organelles such as the endoplasmic reticulum and the Golgi apparatus. Interestingly, this aggregation was much more prominent for probes derived from nemiralisib and could not be observed for the probe derived from an oral PI3K δ inhibitor. In addition, this cellular behaviour was shown to be independent from PI3K δ as a similar accumulation outcome was observed in cells which do not express the target. Therefore, these findings suggest that the observed accumulation is independent from the target binding and could be caused by compound properties.

To confirm that the subcellular localisation of the TCO probes derived from inhaled PI3K δ inhibitors is a true reflection of the cellular behaviour of the parent molecules due to their intrinsic properties, rather than driven by the TCO tag and its influence on the physico-chemical properties of the functionalised chemical probes, a complementary strategy based on a relatively new mass spectrometry imaging technique called NanoSIMS was conducted. This approach relied on the design and synthesis of analogues of the inhaled compounds labelled with stable isotopes (^{15}N). These complementary investigations corroborated the observations of the TCO bioorthogonal chemical probes and helped to explore the potential and limitation of these two orthogonal cellular imaging methods. Overall, these observations were key to correlate the molecular properties of inhaled PI3K δ inhibitors to their lung distribution and aid in the understanding of their lung retention mechanisms. Thus, the PI3K δ chemical probes developed here have proven to be very useful tools supporting the design of efficacious inhaled therapies. This is particularly important since several PI3K δ inhibitors for delivery by both the inhaled and oral route are currently undergoing clinical development for various therapeutic indications. In addition, selective TCO-probes provide new ways to further study the biology of PI3K δ by enabling specific visualization of the target localization and thereby overcoming the low selectivity problem of available antibodies. Overall, the demonstrated high impact of this strategy makes it an important tool for the development of inhaled therapies that could be applied to other targets.

Finally, even though the IEDDA reaction between *trans*-cyclooctenes and tetrazines has become one of the most widely employed bioorthogonal reactions for

the cellular imaging of biomolecules, and has proven to be impactful in this study, there is still a need for optimized transformations that would overcome some of the limitations associated with the TCO tag. In this context, additional strained alkenes such as cyclopropenes are of significant interest and have recently been investigated as alternative bioorthogonal “mini-tags”. To enable direct comparison of both tags, the synthesis of a cyclopropene chemical probe was successfully carried out and the suitability of cyclopropenes to act as a bioorthogonal reagent in the IEDDA cycloaddition was investigated. The kinetics of the IEDDA reaction with cyclopropene was evaluated by comparison of the second-order rate constants for different types of tetrazines synthesized in the course of this work. However, this alternative “mini-tag” for IEDDA reaction has not proven to be successful, therefore confirming the significant advantage of the chosen TCO strategy, whilst emphasizing a need to further develop small and reactive bioorthogonal reagents.

Abbreviations

° C	Degree Celsius
2-MeTHF	2-Methyltetrahydrofuran
AcOH	Acetic acid
ADP	Adenosine diphosphate
AGP	α -acid–glycoprotein
Akt	V-akt murine thymoma viral oncogene homolog 1
AMP	Artificial membrane permeability
ATP	Adenosine triphosphate
Asp	Aspartic acid
B ₂ Pin ₂	Bis(pinacolato)diboron
BARAC	Biarylazacyclooctynone
Boc	<i>tert</i> -Butyloxycarbonyl
br	Broad
Calc.	Calculated
CBz	Carboxybenzyl
CbzCl	Benzyl chloroformate
ChromLogD _{pH7.4}	log(distribution coefficient) at pH 7.4, either measured chromatographically or calculated using a Chromatographic LogD model
CLL	Chronic lymphocytic leukemia
CLND	Chemiluminescent nitrogen detection
cLogP	Calculated log(partition coefficient)
cm ⁻¹	Wavenumber
CMD	Concerted metalation-deprotonation
CPME	Cyclopentyl methyl ether
COPD	Chronic obstructive pulmonary disease
d	Doublet
DCM	Dichloromethane
DEAD	Diethyl azodicarboxylate
DFT	Density functional theory

DIBAL-H	Diisobutylaluminium hydride
DIBO	Dibenzocyclooctyne
DIFO	Difluorinated cyclooctyne
DIMAC	Dimethoxyazacyclooctyne
DIPEA	Diisopropylethylamine
DMF	<i>N,N</i> -Dimethylformamide
DMP	Dess-Martin periodinane
DMPK	Drug metabolism and pharmacokinetics
DMSO	Dimethyl sulfoxide
DNA	Deoxyribonucleic acid
DoA	Duration of action
DPPA	Diphenyl phosphorazidate
DSC	<i>N,N'</i> -Disuccinimidyl carbonate
EDG	Electron-donating group
equiv.	Equivalents
<i>et al.</i>	et alii
ER	Endoplasmic reticulum
Et ₂ O	Diethylether
EtOAc	Ethyl acetate
Et ₃ N	Triethylamine
(EtO) ₃ SiH	Triethoxysilane
EtOAc	Ethyl acetate
EWG	Electron-withdrawing group
FA	Formic acid
FACS	Fluorescence-activated cell sorting
FDA	US Food and Drug Administration
FTIH	First Time in Human
f_u	Unbound fraction
g	Gram
GFP	Green fluorescent protein
Glu	Glutamic acid

GPCR	G-protein coupled receptor
GSK	GlaxoSmithKline
h	Hour
HATU	2-(7-Aza-1 <i>H</i> -benzotriazol-1-yl)-1,1,3,3-tetramethyluronium hexafluorophosphate
HBPIn	Pinacolborane
HATU	2-(7-Aza-1 <i>H</i> -benzotriazol-1-yl)-1,1,3,3-tetramethyluronium hexafluorophosphate
HBTU	2-(1 <i>H</i> -benzotriazol-1-yl)-1,1,3,3-tetramethyluronium hexafluorophosphate
HOMO	Highest Occupied Molecular Orbital
HPLC	High Performance Liquid Chromatography
HRMS	High Resolution Mass Spectrometry
HSA	Human Serum Albumin
HTRF	Homogeneous Time Resolved Fluorescence
hWB	Human whole blood
Hz	Hertz
IC ₅₀	Half maximal inhibitory concentration
IEDDA	Inverse electron demand Diels-Alder
IFN γ	Interferon gamma
IPA	Isopropanol
<i>i</i> Pr	Isopropyl
Ir	Iridium
IR	Infrared
<i>J</i>	Coupling constant Hertz
k ₂	Second-order rate constant
K ₂ CO ₃	Potassium carbonate
kcal mol ⁻¹	Kilocalories per mol
K _i	Inhibition constant
K _M	Enzyme Michaelis constant
KOAc	Potassium acetate

LCMS	Liquid Chromatography Mass Spectroscopy
LDA	Lithium diisopropylamide
LiHMDS	Lithium bis(trimethylsilyl)amide
logP	log(partition coefficient)
LUMO	Lowest Unoccupied Molecular Orbital
Lys	Lysine
m	Multiplet
M	Molarity
$[M-H]^+$	Positive molecular ion
MALDI	Matrix-assisted laser desorption/ionization
MDAP	Mass directed auto purification system
MDCK	Madin-Darby canine kidney
Me	Methyl
Me4phen	3,4,7,8-Tetramethyl-1,10-phenanthroline
MeCN	Acetonitrile
MeOH	Methanol
mg	Milligram
Min	Minutes
mL	Millilitre
mM	Millimolar
MW	Molecular weight
MOE	Molecular Operating Environment
MOFO	Monofluorinated cyclooctene
mol	Mole
MOPS	3-(<i>N</i> -morpholino)propanesulfonic acid
n	Number of test occasions
NanoSIMS	Nanoscale secondary ion mass spectrometry
NHS	<i>N</i> -Hydroxysuccinimide
Ni(OTf) ₂	Nickel(II) trifluoromethanesulfonate
nM	Nanomolar
NMR	Nuclear Magnetic Resonance

nm.sec ⁻¹	Nanometre per second
PARP	Poly(ADP-ribose) polymerase 1
PBMC	Peripheral Blood Mononuclear Cell
PBS	Phosphate buffered saline
PDB	Protein data bank
PG	Protecting group
Phth	Phthalimide
PI3K	Phosphoinositide 3-kinase
pIC ₅₀	-log(IC ₅₀)
pin	Pinacolato
PIP2	Phosphatidylinositol-(4,5)-diphosphate
PIP3	Phosphatidylinositol (3,4,5)-triphosphate
PK	Pharmacokinetics
pK _a	Acid dissociation constant at logarithmic scale
pK _i	-log(K _i)
PPh ₃	Triphenylphosphine
ppm	Parts per million
PtdIns	Phosphatidylinositol
PtdIns(3)P	Phosphatidylinositol-3-phosphate
PtdIns(3,4)P ₂	Phosphatidylinositol-3,4-bisphosphate
PtdIns(3,4,5)P ₃	Phosphatidylinositol-3,4,5-trisphosphate
PtdIns(4,5)P ₂	Phosphatidylinositol-4,5-bisphosphate
PTEN	Phosphatase and Tensin Homolog Protein
QC	Quality control
quant	Quantitative
RED	Rapid equilibrium dialysis
rt	Room temperature
s	Singlet
SHIP	SH2-containing inositol phosphatase
SIMS	Secondary ion mass spectrometry
SLF	Simulated lung fluid

STAB	Sodium triacethoxyborohydride
STDEV	Standard deviation
t	Triplet
T3P	Propylphosphonic anhydride
TBAF	Tetrabutylammonium fluoride
TCO	<i>trans</i> -Cyclooctene
TCO-PNB ester	(<i>E</i>)-Cyclooct-4-en-1-yl (<i>p</i> -nitrophenyl) carbonate
TFA	Trifluoroacetic acid
THF	Tetrahydrofuran
TMS	Trimethylsilyl
t _R	Retention time
Trp	Tryptophan
Val	Valine
XPhos Pd G1	(2-Dicyclohexylphosphino-2',4',6'-triisopropyl-1,1'-biphenyl)[2-(2-aminoethyl)phenyl]palladium(II) chloride
XPhos Pd G2	Chloro(2-dicyclohexylphosphino-2',4',6'-triisopropyl-1,1'-biphenyl)[2-(2'-amino-1,1'-biphenyl)]palladium(II)
δ	NMR chemical shift in ppm downfield from a standard (tetramethylsilane)
μL	Microlitre
μM	Micromolar
μg.mL ⁻¹	Microgram per millilitre
μwave	Microwave

Table of Contents

Declaration of Copyright.....	ii
Acknowledgements	iii
Abstract	v
Abbreviations	viii
Table of Contents	xiv
1. Introduction.....	1
1.1. Bioorthogonal Chemistry	2
1.1.1. The Staudinger Ligation of Azides	4
1.1.2. The Copper-Catalysed Azide-Alkyne Cycloaddition (CuAAC).....	5
1.1.3. The Strain-Promoted Azide-Alkyne Cycloaddition (SPAAC)	7
1.1.4. The Inverse Electron Demand Diels-Alder Cycloaddition (IEDDA)	9
1.2. A Bioorthogonal Strategy for Drug Localisation, Target Identification and Target Occupancy Measurement.....	23
1.3. Inhaled PI3K δ Inhibitors for the Treatment of Respiratory Diseases	25
1.3.1. The PI3K Pathway.....	25
1.3.2. Class I PI3Ks in Disease	28
1.3.3. PI3K δ Inhibition.....	28
2. Aims.....	41
2.1. Design of Chemical Probes Derived from Nemiralisib	43
2.2. Design of Chemical Probes Derived from GSK2292767	47
3. Results and discussion	48
3.1. Synthesis of Chemical Probes Derived from Nemiralisib	50
3.2. Synthesis of Chemical Probes derived from GSK2292767	65
3.3. Profiling of TCO Chemical Probes	74

3.3.1.	Enzyme Potency in TR-FRET Assay	75
3.3.2.	Kinobead Potency in Cell Lysates.....	77
3.3.3.	Human Whole Blood Assay	79
3.3.4.	Properties of Chemical Probes Derived from Nemiralisib.....	80
3.3.5.	Properties of Chemical Probes Derived from GSK2292767.....	85
3.3.6.	Blood Binding of TCO Chemical Probes	86
3.4.	Cellular Imaging of PI3K δ Chemical probes	89
3.4.1.	Synthesis and Selection of Unlabelled PI3K δ Competitors	93
3.4.2.	Imaging Design	98
3.4.3.	Imaging of Chemical Probes Derived from Inhaled PI3K δ Inhibitors.....	103
3.4.4.	Imaging Conclusions of TCO Probes in Hut78 Cells	123
3.4.5.	Imaging of TCO Chemical Probes in HeLa Cells to Investigate Compound Accumulation	126
4.	NanoSIMS Imaging	142
5.	Cyclopropenes as “Mini-Tags”.....	161
6.	Conclusion	186
7.	Future Work.....	190
8.	Experimental.....	191
8.1.	General Chemistry Experimental Data Methods	191
8.2.	General Experimental Procedures.....	201
8.3.	2 nd order rate constant (k_2) determination	328
8.4.	Cellular Imaging of PI3K δ TCO Chemical Probes.....	329
8.4.1.	Imaging of PI3K δ TCO chemical probes in Hut78 cells.....	329
8.4.2.	Imaging of PI3K δ TCO chemical probes in HeLa cells.....	332
8.5.	NanoSIMS Imaging	333
9.	References.....	336

1. Introduction

Living systems are composed of various components interacting as a machine to drive a large array of physiological processes. However, many of these processes can only be observed in the context of living systems.^[1] Therefore, in order to be able to study these biological mechanisms and gain a better understanding of cell biology, chemists and biologists have started working together to develop new strategies to tag and track molecules within their native environment.^[2]

Today, one of the most widespread tagging strategies involves the use of the green fluorescent protein (GFP) isolated from the jellyfish *Aequorea Victoria*.^[3] The fusion of the GFP protein to a target protein acts as a biological marker that enables the study of both protein expression and localisation in living cells.^[4,5] Although fluorescent proteins have significantly revolutionized cell biology and represent a powerful tool for imaging biopolymers within living systems, they are not without their limitations.^[6,7] First, fluorescent protein fusions can only be visualized by optical methods. Second, these proteins are relatively large, which can lead to significant structural perturbations and therefore influence the expression, localisation or function of the target protein to which they are attached. Finally, fluorescent proteins cannot be used to visualize several other interesting classes of biomolecules such as lipids, glycans, nucleic acids or the various organic metabolites which, taken together, represent a large fraction of a cell's components.^[8] Therefore, methods that would enable the visualisation of both proteins and non-proteinaceous biomolecules would significantly enhance the understanding of complex cellular mechanisms occurring in living systems.

Over the last decade, an alternative strategy has emerged that uses reactive probes to tag biomolecules in complex biological systems or, in some cases, living organisms.^[1] This strategy is based on 'bioorthogonal chemistry', a term initially coined by Bertozzi referring to any chemical reaction that can occur inside living systems without interfering with their inherent biochemical processes.^[1,9]

1.1. Bioorthogonal Chemistry

Bioorthogonal chemistry usually proceeds in a two-step sequence, commonly referred to as the ‘bioorthogonal chemical reporter strategy’ (Figure 1).^[1,10]

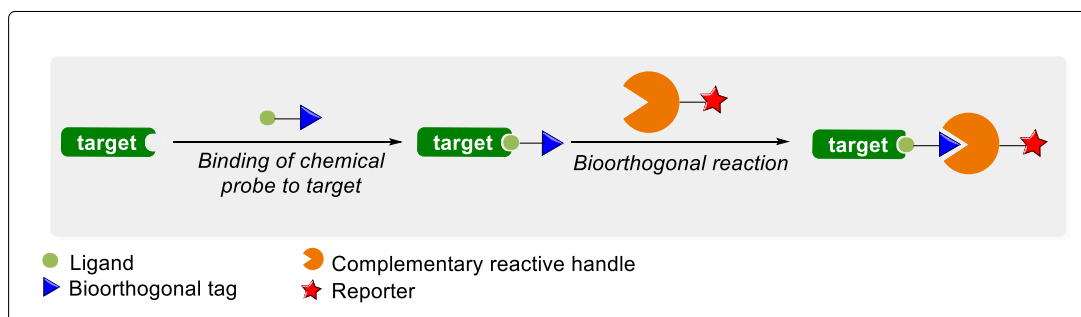


Figure 1. The two-step bioorthogonal chemical reporter strategy as described by Bertozzi.^[1]

First, a unique chemical functionality known as a bioorthogonal chemical tag (blue triangle, Figure 1) is attached to a cellular substrate to generate a chemical probe (light green circle, Figure 1). Some examples of substrates suitable for bioorthogonal chemical reactions include metabolites, enzyme inhibitors or small molecule ligands. The labelled substrate is then introduced into a target biomolecule of interest (dark green box, Figure 1). The second step involves the introduction of an exogenous reporter (red star, Figure 1) bearing a complementary chemical moiety that must react with the bioorthogonal tag. The selective and covalent tagging of biomolecules is a challenging task since bioorthogonal reactions must meet various criteria to be likely to be feasible in living cells.^[11,12]

First, the bioorthogonal chemical tag should be as small as possible since a large functional group will result in structural modifications to the substrate, which could affect its physico-chemical properties and bioactivity.^[1] The two bioorthogonal partners should also be metabolically stable and sufficiently permeable in order to be used in living systems, and react selectively with each other under physiological conditions while remaining inert to the surrounding biological environment.^[9,12]

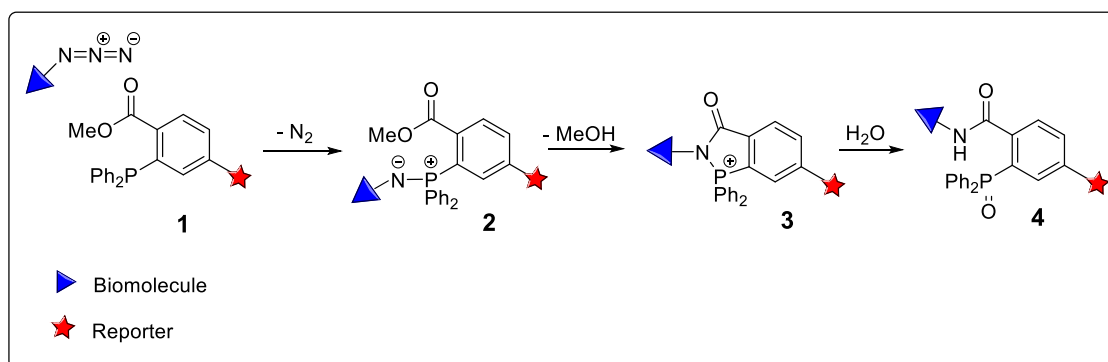
Any side reaction between the bioorthogonal reagents and the array of functionality found in the endogenous biological compounds present in the cells (grey shapes, Figure 1) could disrupt the native processes occurring in the system under study. Finally, the reaction between the bioorthogonal tag and the complementary chemical reporter must be rapid in order to form a strong covalent ligation adduct with no or innocuous by-products. Most of the bioorthogonal reactions developed to date follow second-order kinetics and display rate constants (k_2) ranging from 10^{-4} to 10^4 $\text{M}^{-1}\text{s}^{-1}$.^[13] The rate constant of a bioorthogonal reaction is a valuable piece of information that allows individual processes to be compared, so as to choose the most efficient transformation to track molecules in living systems. Finally, the two-step bioorthogonal chemical reporter strategy offers the opportunity to label the biomolecule of interest with a small bioorthogonal tag, when direct covalent attachment of a reporter to the biomolecule would generate a probe with high molecular weight, which might not be cell permeable.

To date, about 20 bioorthogonal reactions have been reported and most can be classified as either polar reactions or cycloadditions.^[11,14] These bioorthogonal reactions rely on the use of non-natural functional groups to avoid cross-reactivity with biomolecules.

Azides are one of the most commonly used chemical reporters in the context of bioorthogonal reactions as this functional group is absent from naturally occurring biological systems.^[15] The azide group is also small and, therefore, less likely to cause any structural perturbation to the substrate to which it is attached.^[16] However, whilst being inert to most biochemical functionalities under physiological conditions,^[17] azides are weak electrophiles and therefore appear to be reactive with ‘soft’ nucleophiles such as thiols which are found endogenously (e.g. glutathione).^[1] Despite this, and given their unique features, azides have been exploited in several bioorthogonal reactions.^[17]

1.1.1. The Staudinger Ligation of Azides

The first reaction that launched the field of bioorthogonal chemistry was the Staudinger ligation of azides. This reaction was developed by Bertozzi^[18] in 2000 and is largely inspired from the classical Staudinger reduction of azides with triphenylphosphine.^[19] In the Staudinger ligation of azides (Scheme 1),^[9] a substrate of interest is first appended to an azide reporter that undergoes nucleophilic attack by an exogenous probe containing phosphine (**1**), releasing N₂ in the process. The resulting aza-ylide intermediate (**2**) is then trapped intramolecularly by an ortho substituted methyl ester. This forms a cyclic adduct (**3**) that gives a stable amide-ligated phosphine oxide product (**4**) upon hydrolysis, with methanol as a side-product. This intramolecular cyclization step is key to the bioorthogonal aspect of this reaction, otherwise the aza-ylide intermediate would simply hydrolyse to afford the corresponding amine and phosphine oxide.^[20] The reaction is therefore termed a ligation as it ligates two biomolecules together whereas the two reactive partners would not be covalently linked after hydrolysis in the classical Staudinger reaction.



Scheme 1. The Staudinger ligation of azides as described by Bertozzi.^[9]

Due to its high selectivity, the Staudinger ligation remains widely used to track biomolecules in cellular environments and *in vivo*.^[21,22] Some limitations of the reaction include potential oxidation of the phosphine reagent by air or metabolic enzymes and slow kinetics ($k_2 \sim 10^{-3} \text{ M}^{-1}\text{s}^{-1}$).^[23] Efforts to improve the reaction rate, for example by increasing the nucleophilicity of the phosphine *via* the addition of electron-donating groups to its aryl substituents, tend to increase the likelihood of the

phosphine to undergo oxidation, therefore reducing the amount of probe available in the biological system.^[9] Shortly after the description of the Staudinger ligation, Bertozzi and Raines simultaneously reported modified strategies utilizing modified phosphine reagents, whereby the resulting phosphine oxide moiety is cleaved by hydrolysis and therefore not appended to the final adduct, leaving a native amide bond. Even though the phosphine oxide constitutes a stable linkage that may have negligible impact for typical biomolecules labelling, the so-called traceless Staudinger ligation has found widespread application in peptide assembly, overcoming limitations from alternative chemical synthesis approaches.^[24,25]

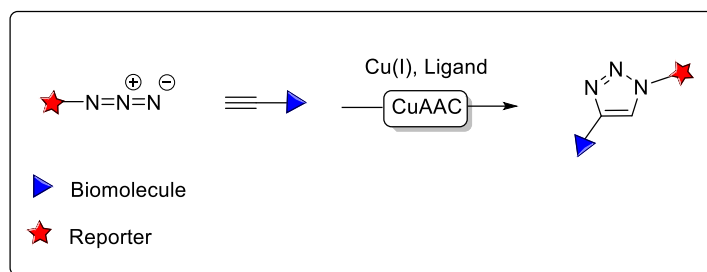
The Staudinger ligation is not the only bioorthogonal reaction where azides feature a prominent role as bioorthogonal participants. Other transformations based on their 1,3-dipole reactivity have been developed and are commonly known as ‘Click Chemistries’.^[26]

1.1.2. The Copper-Catalysed Azide-Alkyne Cycloaddition (CuAAC)

“Click” reactions are a class of biocompatible reactions that have been broadly applied to imaging of biomolecules in living systems.^[27] The term “click chemistry” was initially coined by Sharpless in 1998 and subsequently described in more details by Kolb, Finn and Sharpless in 2001.^[28]

The authors described “click chemistry” as a strategy to generate substances quickly and efficiently by joining small units, or “blocks”, together. Therefore, the term does not refer to a specific chemical reaction but rather encompasses a class of transformations that meet a list of stringent criteria. According to the authors, a suitable “click” reaction should be modular, wide in scope, involve readily available starting materials, be chemically high yielding, have high atom economy, and provide simple product isolation. Based on this description that shares intrinsic similarities with bioorthogonal chemistry, it is not surprising that several “click” reactions have found widespread applications for the labelling of biomolecules.

One reaction that fits the concept of “click chemistry” is the Copper-Catalysed Azide-Alkyne Cycloaddition (CuAAC), which involves the 1,3-dipolar cycloaddition of azides with alkynes to form substituted 1,2,3-triazoles (Scheme 2).^[29]



Scheme 2. The copper-catalysed azide-alkyne cycloaddition (CuAAC) applied to bioorthogonal chemistry.^[27]

Alongside azides, alkynes are another important functionality in bioorthogonal chemistry due again to their small size and absence from most biological systems.^[30] The 1,3-dipolar cycloaddition reaction between azides and alkynes to give 1,4-disubstituted 1,2,3-triazoles was initially reported by Huisgen in 1963.^[31,32]

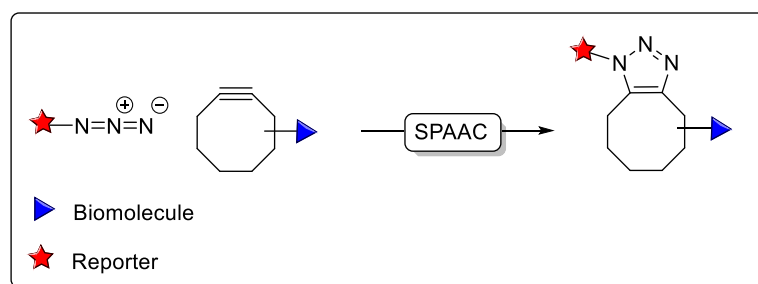
In 2002, Sharpless discovered that the addition of a Cu(I) salt significantly increased the rate of the reaction.^[33] The CuAAC reaction occurs readily in aqueous environments and is significantly faster than the Staudinger ligation, with second-order rate constants $k_2 \sim 10\text{--}200 \text{ M}^{-1}\text{s}^{-1}$ in the presence of 20–500 μM of Cu(I).^[34] However, the requirement of copper to act as a catalyst in cycloaddition reactions between azides and alkynes raises toxicity issues for its direct application in living cells. Indeed, copper is a cytotoxic metal that promotes the formation of reactive oxygen species (ROS) from O_2 , thereby limiting the utilization of the CuAAC *in vivo*.^[35] Therefore, the CuAAC reaction has been mostly used to label biomolecules in an extracellular context.^[29]

A potential solution for the application of the CuAAC reaction in living cells would be to decrease the concentration of Cu(I) catalyst since mammalian cells have been shown to be able to survive low concentrations ($<500 \mu\text{M}$) of Cu(I). However, the CuAAC reaction often proceeds in significantly reduced reaction rates at such concentrations, which might not be compatible with biological time scales.^[36] To overcome this issue, the CuAAC has been further optimized to improve its

biocompatibility. Rather than using a cytotoxic copper catalyst, copper-free ‘click chemistry’ has been developed, which relies on the activation of alkynes by ring strain in order to increase the rate of the reaction. Therefore, this strategy is usually referred to as ‘the strain-promoted alkyne-azide cycloaddition’ (SPAAC).^[17,37]

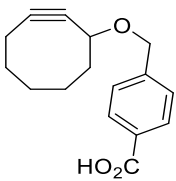
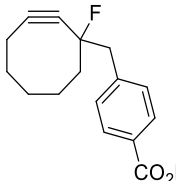
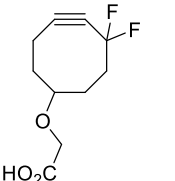
1.1.3. The Strain-Promoted Azide-Alkyne Cycloaddition (SPAAC)

Based on initial work from Wittig and Krebs who investigated the reactivity of cyclooctyne with neat phenyl azide in 1,3-dipolar cycloadditions,^[38] Bertozzi and co-workers investigated the use of strained cyclooctynes as reagents in the SPAAC bioorthogonal reaction.^[37] Constraining the alkyne within an eight-membered ring creates 18 kcal mol⁻¹ of strain that can be favourably released upon [3+2] cycloaddition with azides (Scheme 3).^[39]



Scheme 3. The strain-promoted azide-alkyne cycloaddition (SPAAC).^[27]

Although, the first cyclooctyne that was evaluated named OCT underwent cycloaddition with azides at room temperature without the need for a metal catalyst (Table 1), the reaction kinetics were no faster than the Staudinger ligation ($k_2 \sim 10^{-3} \text{ M}^{-1} \text{ s}^{-1}$) and much slower than CuAAC ($k_2 \sim 10\text{-}200 \text{ M}^{-1} \text{ s}^{-1}$).^[37] Accordingly, additional cyclooctynes have since been developed in order to improve reaction rate (Table 1).^[40]

Structure			
Name	OCT	MOFO	DIFO
k₂ (M⁻¹s⁻¹)	0.0024	0.0043	0.076

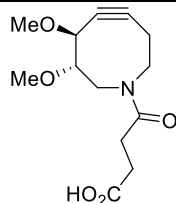
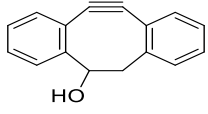
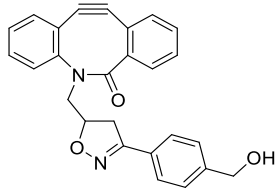
Structure			
Name	DIMAC	DIBO	BARAC
k₂ (M⁻¹s⁻¹)	0.0030	0.057	0.96

Table 1. Cyclooctynes for SPAAC reactions.^[40]

Bertozzi reasoned that the reactivity of strained alkynes with azides could be governed by the Frontier Molecular Orbital Theory,^[41] and therefore suggested that the introduction of electron-withdrawing substituents at the propargylic position should lower the energy of the LUMO of the cyclooctyne and therefore increase its reactivity in the SPAAC reaction. The addition of a fluorine atom in the monofluorinated cyclooctyne (MOFO) gave a modest increase in the reaction rate^[17] whilst the *gem*-difluoro substituent in the difluorinated cyclooctyne (DIFO) considerably increased the kinetics, with a second-order rate constant of $k_2 = 0.076 \text{ M}^{-1} \text{ s}^{-1}$.^[10,42] However, DIFO proved to be poorly soluble in water, which hinders its reactivity under physiological conditions. This issue was later addressed by the synthesis of new strained cyclooctynes bearing heteroatoms, such as dimethoxyazacyclooctyne (DIMAC).^[43] 4-Dibenzocyclooctynol (DIBO) and biarylazacyclooctynone (BARAC) cyclooctynes containing fused benzyl rings possess enhanced ring strain, which significantly improves the rate of the [3+2] cycloaddition reaction with azides ($k_2 = 0.057 \text{ M}^{-1} \text{ s}^{-1}$ and $k_2 = 0.096 \text{ M}^{-1} \text{ s}^{-1}$, respectively).^[44]

Cyclooctynes containing both a fused benzyl ring and a *gem*-difluoro substituent were envisioned to further enhance the reactivity of cyclooctynes in the SPAAC but the resulting compounds suffered from a lack of stability.^[45]

Since SPAAC does not rely on the use of a toxic metal, the reaction has found a wide variety of biomolecule labelling applications, both *in vitro* and *in vivo*.^[46] However, the main restriction to the use of cyclooctynes in the SPAAC bioorthogonal reaction is their relatively large size and hydrophobic nature, which can compromise their exposure to the cell and significantly alter the properties of the substrate to which they are attached.^[27]

Alongside alkynes, strained alkenes have also been considered for “click chemistry”.^[47] One of the most studied transformations is the reaction of strained alkenes with 1,2,4,5-tetrazines in an inverse-electron demand Diels-Alder cycloaddition (IEDDA).^[48]

1.1.4. The Inverse Electron Demand Diels-Alder Cycloaddition (IEDDA)

The Diels–Alder reaction can be defined as a [4+2] cycloaddition between a conjugated diene and a substituted dienophile to form a substituted 6-membered ring.^[49] Depending on the electronic nature of the diene and dienophile, Diels–Alder reactions can be classified as either normal or inverse electron demand (IEDDA). In contrast to the normal electron demand Diels–Alder reaction, where an electron-rich diene reacts with an electron-deficient dienophile, the IEDDA reaction involves an electron-deficient diene (*e.g.* 1,2,4,5-tetrazines) and an electron-rich dienophile (alkene or alkyne). The reactivity of the Diels-Alder reaction can therefore be described using the frontier molecular orbitals by considering the energy difference between the HOMO and LUMO of the cycloaddends. This can be visualised in a molecular orbital diagram as depicted in Figure 2.^[14]

In the normal IEDDA cycloaddition, the energy difference between the HOMO_{diene} and the LUMO_{dienophile} is smaller than the one between the HOMO_{dienophile} and LUMO_{diene}. Accordingly, there is a stronger orbital overlap between the

$\text{HOMO}_{\text{diene}}$ and $\text{LUMO}_{\text{diene}}$ which results in the most energetically favorable bond formation.

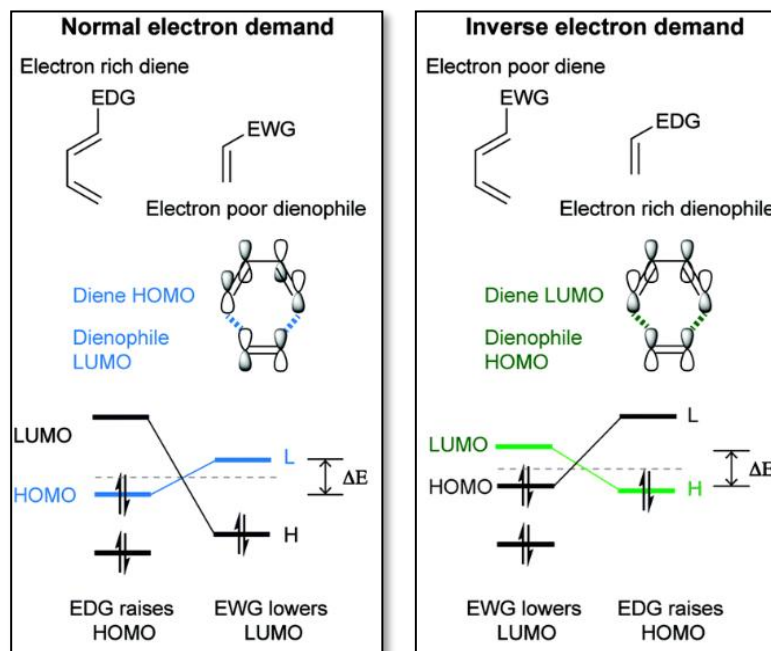
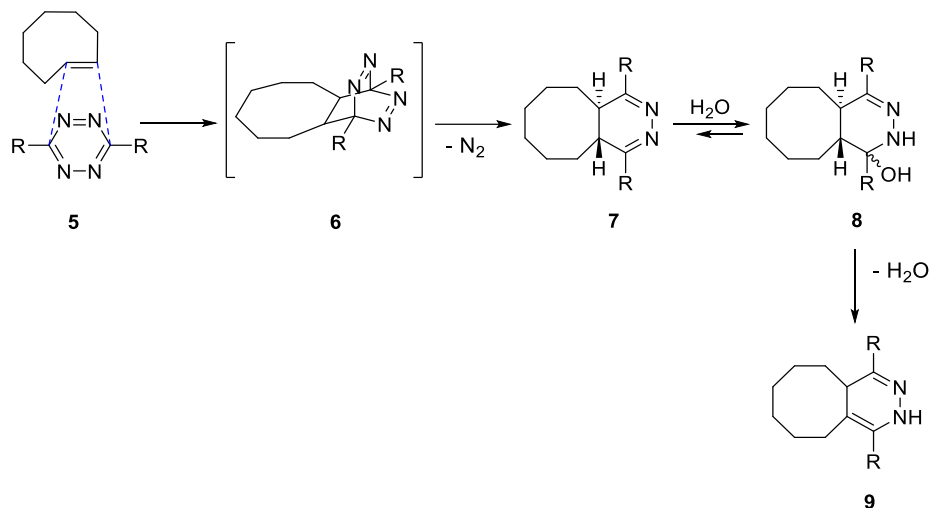


Figure 2. Frontier molecular orbitals of the normal and inverse electron demand Diels-Alder reaction (EDG = electron-donating group, EWG = electron-withdrawing group). Reprinted with permission from Bernardes *et al.*^[14] (Copyright 2017 Royal Society of Chemistry).

Alternatively, in the IEDDA cycloaddition, the presence of electron-withdrawing groups on the diene and electron-donating groups on the dienophile results in a smaller energy difference between the $\text{HOMO}_{\text{dienophile}}$ and $\text{LUMO}_{\text{diene}}$.

Due to a unique ring system that consists of an electron-deficient heterocycle containing four nitrogen atoms, 1,2,4,5-tetrazines have received considerable attention as dienes in IEDDA cycloaddition.^[50] The ability of 1,2,4,5-tetrazine derivatives to undergo cycloaddition with alkenes was initially reported by Carboni and Lindsey in 1959 who observed the disappearance of the characteristic red-purple colour of 3,6-substituted tetrazines upon heating with styrene derivatives and simultaneous formation of nitrogen gas evolution to yield functionalised pyridazines.^[51]

Based on this seminal study, Fox and co-workers reported in 2008 one of the first examples of a bioorthogonal reaction involving the IEDDA cycloaddition between 1,2,4,5-tetrazines and *trans*-cyclooctene (TCO), a transformation which is commonly referred to as the tetrazine ligation (Scheme 4).^[52]



Scheme 4. IEDDA mechanism of the tetrazine ligation with TCO.

The reaction proceeds through an initial rate-determining inverse-electron demand Diels-Alder step (5) to give the highly strained bicyclic adduct 6, which then undergoes a *retro*-Diels-Alder reaction, releasing nitrogen gas in an irreversible step. This generates a 4,5-dihydropyridazine (7), which rearranges to the corresponding 1,4-dihydro-isomer 9.^[12] Several investigations have been conducted to explain the mechanism leading to the formation of the 1,4-dihydropyridazine. NMR studies have revealed that water can add to the 4,5-dihydropyridazine (7) to generate an aminated intermediate (8) which subsequently eliminates to give the 1,4-dihydropyridazine 9.^[48,53,54]

Additional studies by Robillard *et al.* focusing on the reactivity of axial versus equatorial linked TCO derivatives demonstrated that the axial isomer tends to be more reactive than the corresponding equatorial isomer in IEDDA reaction with tetrazines.^[55] The axial diastereomer of 5-hydroxy-*trans*-cyclooctene (10, Figure 3) was found to be approximately 4 times more reactive than the equatorial diastereomer (11, Figure 3) when reacting with 3,6-substituted-1,2,4,5-tetrazines. Robillard *et al.*

reasoned that the axial diastereomer was more reactive due to instability of the ring system caused by transannular interactions.

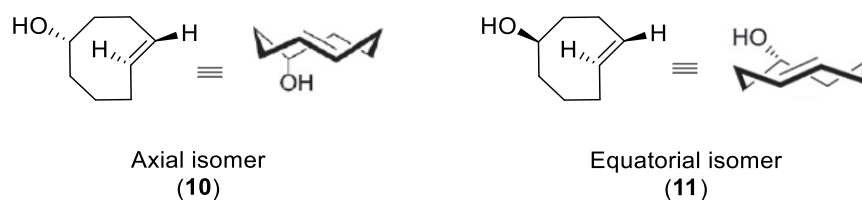
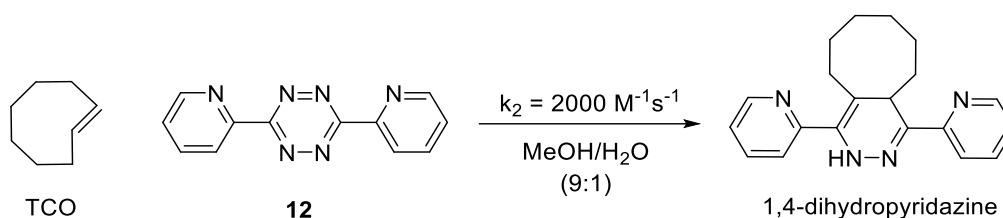


Figure 3. Axial and equatorial isomers of 5-hydroxy *trans*-cyclooctene.

When initially reported by Fox in 2008, the tetrazine ligation appeared as one of the fastest bioorthogonal transformations developed, with rate constants $k_2 = 2000 \text{ M}^{-1}\text{s}^{-1}$ in 9:1 methanol/water with 3,6-dipyridyl-1,2,4,5-tetrazine (**12**) (Scheme 5).^[48]



Scheme 5. Bioorthogonal tetrazine ligation.

The enhanced reactivity of *trans*-cyclooctene in this transformation compared to other strained cyclic alkene was shown to arise from the highly strained twisted carbon-carbon double bond and the fact that the TCO can adopt a highly reactive “half chair” conformation, which was computationally estimated to be $5.6 \text{ kcal mol}^{-1}$ higher in energy than the lowest energy ‘crown’ conformation (Figure 4)^[56].

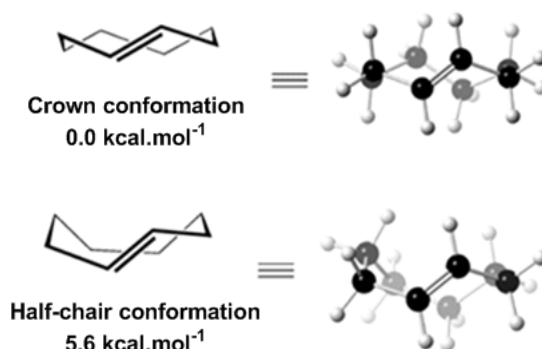


Figure 4. Calculated relative energies for two conformations of *trans*-cyclooctene. Reprinted with permission from Fox *et al.*^[57] (Copyright 2014 Royal Society of Chemistry).

More recently, considerable attention has been given to the design of novel *trans*-cyclooctene derivatives with enhanced reactivity in the tetrazine ligation, whilst also featuring optimized properties. In 2011, Fox *et al.* reported the synthesis of the new *trans*-cyclooctene moiety s-TCO (**13**) which consists of a *trans*-cyclooctene fused to a cyclopropane moiety with a *cis* ring fusion, forcing the *trans*-cyclooctene to adopt the highly reactive half-chair type conformation (Figure 5).^[53] This s-TCO derivative was shown to be 19 times more reactive than the parent monocyclic *trans*-cyclooctene when reacting with 3,6-dipyridyl-1,2,4-5-tetrazine derivative with second order rate constants (k_2) up to 22 000 M⁻¹s⁻¹ in methanol at 25 °C. The reactivity of a water-soluble analogue of s-TCO with a 3,6-dipyridyl tetrazine derivative was later investigated in water at 25 °C and revealed an extremely fast rate constant; $k_2 = 3\,300\,000\text{ M}^{-1}\text{s}^{-1}$.^[57]

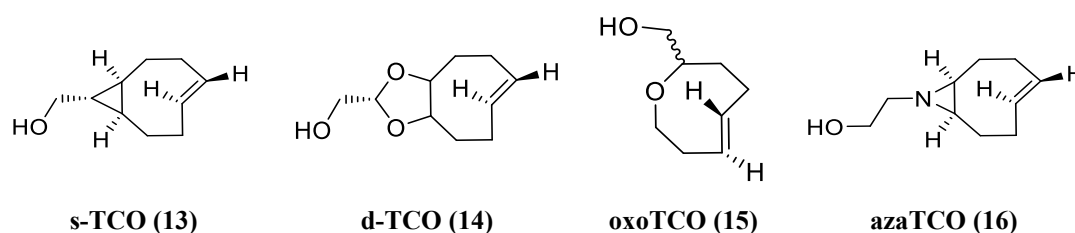


Figure 5. Novel TCO derivatives.

Similarly, Fox reported in 2014 the design of a novel conformationally strained *cis*-dioxolane-fused *trans*-cyclooctene d-TCO (**14**) (Figure 5), which aimed to improve the stability and aqueous solubility of s-TCO while maintaining high reactivity towards tetrazines.^[57] However, it was reasoned that the presence of inductively electron-withdrawing oxygens in the dioxolane moiety of d-TCO could render the cycloalkene less reactive than s-TCO, but this could be compensated by its enhanced stability. Similar to s-TCO, the fused 8-membered ring system of d-TCO also adopts the energetic “half-chair” conformation, and reaction of d-TCO with diphenyltetrazine in methanol at 25 °C was measured to be 27 times faster than with unfunctionalized TCO.^[57] Reaction of d-TCO with a 3,6-dipyridyl-1,2,4,5-tetrazine derivative also displayed extremely high kinetics with a second order rate constant (k_2) of 366 000 M⁻¹s⁻¹ in water at 25 °C.^[57]

An important aspect to consider towards the development of optimized bioorthogonal partners for cellular imaging purposes is the lipophilicity of the reactants. Increased lipophilicity can be associated with higher fluorescent background if the bioorthogonal moieties tend to interact and bind non-specifically to undesired biological targets within the cells.^[58] In addition to this, the removal of excess reagents from the cells often requires extensive washing steps, which can significantly reduce the selective fluorescent signal.^[59] Although TCO derivatives are achieving extremely fast kinetics in the IEDDA reaction with tetrazines, their large structural sizes along with high lipophilicity can limit their application as effective bioorthogonal moieties for the cellular imaging of certain biomolecules. Although d-TCO displays reduced lipophilicity compared to 5-hydroxy-*trans*-cyclooctene TCO and s-TCO (

Table 2),^[60] there is a need for less bulky bioorthogonal reagents with improved lipophilicity. Towards that aim, Fox and co-workers reported in 2017 the computationally-guided discovery of oxoTCO (**15**) (Figure 5), where the insertion of an oxygen atom within the *trans*-cyclooctene ring system results in decreased lipophilicity (Table 2) and improved aqueous solubility, whilst maintaining very fast kinetics.^[60] The rationale behind the design of this compound came from the reasoning that a shorter C-O bond within the *trans*-5-oxocene ring system would increase the angle therefore promoting reactivity of the *trans*-5-oxocene derivative with tetrazines.

Indeed, the reaction of oxoTCO with a 3,6-dipyridyl-1,2,4,5-tetrazine derivative occurred with a second order rate constant (k_2) of $94\,600\text{ M}^{-1}\text{s}^{-1}$ in PBS at $25\text{ }^{\circ}\text{C}$,^[60] much faster than the unfunctionalized TCO.

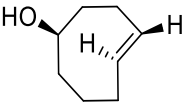
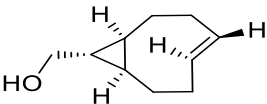
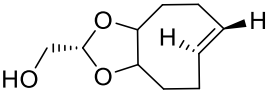
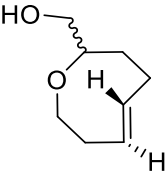
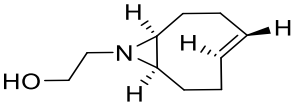
TCO derivative	Structure	cLogP
Eq-TCO-ol (11)		1.9 (measured LogP = 1.1) ^[53]
s-TCO (13)		2.3
d-TCO (14)		1.3 (measured LogP = 0.9) ^[53]
oxoTCO (15)		0.9 (measured LogP = 0.5) ^[60]
aza-TCO (16)		1.2

Table 2. Comparison of calculated lipophilicity (cLogP) of several trans-cyclooctenes derivatives.^[61,62]

Similarly, Vrabel *et al.* reported in 2018 the design of azaTCO (**16**), a novel *trans*-cyclooctene derivative fused to an aziridine.^[63] As intended, the azaTCO also adopts the highly strained “half-chair” conformation, which was confirmed by X-ray crystallography. Reaction with 3,3-diphenyl-1,2,4,5-tetrazine in methanol at $21\text{ }^{\circ}\text{C}$ showed that azaTCO underwent tetrazine ligation 20 times faster than axial isomer of 5-hydroxy-TCO (**10**) and 1.5 times faster than d-TCO (**14**). Even though the LogP was not reported by the authors, comparison of cLogP values with other TCO derivatives (Table 2) showed that azaTCO is less lipophilic than 5-hydroxy-TCO, displaying similar lipophilicity to d-TCO.

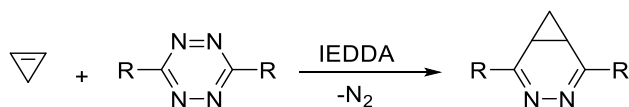
The high reaction rates of TCO derivatives and 1,2,4,5-tetrazines in IEDDA cycloadditions, and the fact that the reaction proceeds at low concentrations in aqueous environments, have allowed the TCO-tetrazine ligation to become one of the most widely employed bioorthogonal reactions for a variety of biological applications, enabling the *in vitro* and *in vivo* labelling of various biomolecules, including nucleic acids, glycans, peptides and proteins.^[64] An important feature is that *trans*-cyclooctene-labelled substrates can be visualized inside living cells *via* the use of tetrazines reporters conjugated to a fluorophore.^[65] Indeed, a standard technique for fluorescent labelling involves a classical IEDDA bioorthogonal reaction where a bioorthogonal tag (*e.g.* TCO derivative) is appended to a biomolecule of interest, with subsequent introduction of a tetrazine-fluorophore reporter (*e.g.* fluorescent dye) followed by washing steps to remove excess dye contributing to the background.^[23,66]

Despite the cornerstone reputation of the TCO tetrazine ligation in the chemical biology field for the labelling and imaging of biomolecules, the reaction still suffers from limitations that can prevent its more widespread use. The main limitation is isomerization of the *trans*-cyclooctene moiety to its *cis* isomer, which has been observed in the presence of certain biological functional groups that are abundant in the cellular environment, such as thiols.^[55] This deactivation is a major issue since *cis*-cyclooctenes are much less reactive species in the tetrazine ligation than their *trans* counterparts.^[67,68] Indeed, unlike *cis*-cyclooctenes, the double bond of *trans*-cyclooctenes is severely twisted, which results in a pre-distorted conformation that requires less distortion energy to achieve the transition state, explaining why *trans*-cyclooctenes are more reactive in IEDDA reactions.^[68]

Another limitation of *trans*-cyclooctenes moieties is their large structural size, which can cause structural and physico-chemical perturbations to the biomolecules to which they are attached and hence disrupt their native behaviour. Finally, despite the recent investigations to improve their physico-chemical properties, most *trans*-cyclooctene bioorthogonal tags are lipophilic, which can influence the cellular effects of the appended biomolecules.^[53] Overall, these limitations impair the use of the TCO tetrazine ligation in applications that require minimally-impacting bioorthogonal tags,

hence there remains a need for smaller, stable and reactive dienophiles for rapid tetrazine cycloadditions.

In this regard, additional classes of strained alkenes have been evaluated for their suitability as dienophile partners in the tetrazine ligation. Recently, there has been a significantly growing interest for cyclopropenes as “mini-tags” for bioorthogonal reactions.^[69-73] Indeed, whilst being slightly larger than the azide and alkyne functionalities, cyclopropenes remain small in size and are the simplest of isolable strained alkenes. In addition, cyclopropenes are absent from endogenous biomolecules and have been found in natural products, suggesting that they can be metabolically stable.^[74,75] The small size of cyclopropenes combined with their reactivity in IEDDA cycloaddition reactions with tetrazines to generate diazanorcaradiene species (Scheme 6) make them very promising dienophiles for reaction in the tetrazine ligation. In addition to this, unlike *trans*-cyclooctenes, cyclopropenes are less likely to cause structural perturbations to the biomolecules to which they are attached and can therefore display improved physico-chemical properties.



Scheme 6. Reaction of unsubstituted cyclopropene with a generic 1,2,4,5-tetrazine.

The first description of cyclopropenes as dienophiles in IEDDA cycloadditions with tetrazines came from Sauer and co-workers who reported the rate constants for the reaction of several acyclic and cyclic alkenes with dimethyl 1,2,4,5-tetrazine-3,6-dicarboxylate in organic solvents.^[68] The reactivity of the cyclic alkenes (from cyclopropene to cyclohexene,) was shown to decrease as the ring size increased, therefore potentially suggesting that the reactivity was governed by the ring strain of the dienophile (Table 3). The main exception to this observed trend was *trans*-cyclooctene which displayed extremely fast kinetics in IEDDA cycloadditions ($k_2 = 1.27 \times 10^4 \text{ M}^{-1}\text{-s}^{-1}$, Table 3). The main exception to this observed trend was *trans*-cyclooctene which displayed extremely fast kinetics in IEDDA cycloadditions ($k_2 = 1.27 \times 10^4 \text{ M}^{-1}\text{-s}^{-1}$, Table 3), as previously discussed in this section.




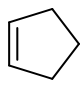
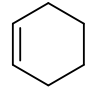
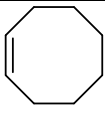

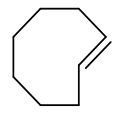
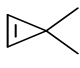
$\text{MeO}_2\text{C}-\text{C}_2\text{N}_2-\text{CO}_2\text{Me} + \text{alkene} \xrightarrow[1,4\text{-dioxane, } 20^\circ\text{C}]{k_2 \text{ M}^{-1}\text{s}^{-1}} \text{product}$					
					
3.63×10^{-1}	4.48×10^2	3.29	2.35×10^{-1}	8.66×10^{-4}	3.38×10^{-2}
					
	5.49×10^2				1.27×10^4
					
	7.77×10^{-2}				

Table 3. Second-order rate constants of different alkenes with dimethyl 1,2,4,5-tetrazine-3,6-dicarboxylate.^[68]

In this experiment, unsubstituted cyclopropene reacted rapidly with a measured rate constant of $k_2 = 448 \text{ M}^{-1}\text{s}^{-1}$. However, unsubstituted cyclopropenes are known to suffer from poor stability at room temperature and are susceptible to polymerisation.^[76-78] To overcome these limitations, Sauer and co-workers investigated synthetic modifications to the cyclopropene scaffold, and observed that varying the substituents on the cyclopropene ring could have a dramatic impact on their reactivity towards tetrazines in the IEDDA reaction. For instance, 3-methylcycloprop-1-ene underwent cycloaddition with tetrazines at a slightly faster rate than unsubstituted cyclopropene ($k_2 = 549 \text{ M}^{-1}\text{s}^{-1}$). However, the reaction of 3,3-dimethylcycloprop-1-ene was found to be significantly lower ($k_2 = 7.77 \times 10^{-2} \text{ M}^{-1}\text{s}^{-1}$, Table 3), whereby the addition of a second methyl substituent at the cyclopropene C3 position was hypothesised to cause a steric clash that impedes the approach of the tetrazine to undergo the IEDDA cycloaddition.^[69]

Based on the observations from Sauer who demonstrated that 3-methyl substituted cyclopropene was the second most reactive dienophile after *trans*-cyclooctene in the IEDDA cycloaddition with tetrazines, Devaraj *et al.* also showed an interest in the development of novel substituted cyclopropenes as “mini-tags” in the

bioorthogonal tetrazine ligation. The authors primarily focused on the synthesis of several 3-monosubstituted carboxamide cyclopropenes without substitution on the alkene.^[73] Despite undergoing very rapid IEDDA reactions with monoaryl tetrazines, these cyclopropene moieties proved to be highly unstable, degrading overnight at -20 °C which strongly limited their use as bioorthogonal reagents. Therefore, the authors devoted their attention to cyclopropene moieties containing a higher degree of substitution. The outcome of these investigations was the discovery of several 1-methyl-3-substituted cyclopropenes (**17** and **18**, Figure 7) where the introduction of a methyl substituent at the C1 position of the cyclopropene provided significantly enhanced stability with a minimal steric impact.^[73]

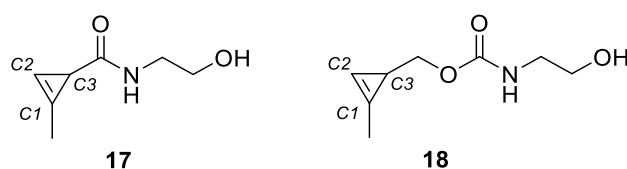


Figure 6. 1-Methyl-3-substituted cyclopropenes with improved stability developed by Devaraj.^[73]

Although cyclopropene **17** displayed improved stability, its reaction with monoaryl tetrazines was measured to occur with a rate constant $k_2 = 0.137 \text{ M}^{-1}\text{s}^{-1}$ in a water/DMSO solution at 37 °C. In an attempt to optimize the kinetics, Devaraj also investigated compound **18**, whose design relied on the hypothesis that removal of the electron-withdrawing carbonyl group at the C3 position may result in enhanced reactivity in the IEDDA reaction, by 1) increasing the HOMO energy of the cyclopropene dienophile and 2) reducing the steric hindrance around the cyclopropene whilst 3) maintaining stability by the presence of the methyl group at the C1 position.

Indeed, reaction of cyclopropene carbamate **18** with a monoaryl tetrazine in aqueous solution at 37 °C was found to occur with an increased rate constant, $k_2 = 13 \text{ M}^{-1}\text{s}^{-1}$.^[73] The application of cyclopropene **18** as a bioorthogonal “mini-tag” was successfully demonstrated in live-cell imaging experiments to visualize the distribution and uptake of cyclopropene-modified phospholipids in breast cancer cells.^[73] However, despite the rate constant of compound **18** being in a similar range

to other biorthogonal reactions, this cyclopropene reacts much slower than other strained alkenes (e.g. *trans*-cyclooctenes) previously investigated in the tetrazine ligation.^[14]

More recently, Devaraj *et al.* reported a thorough study on the development of novel 1-methyl-3-substituted cyclopropenes comprising vinyl, acrylate, acrylamide, amine and amide linkers at the C3 position to evaluate the influence of these substituents electronic properties on the reactivity and stability of the corresponding cyclopropenes in the IEDDA cycloaddition with tetrazines (Table 4).^[72]

Compound number	Cyclopropene structure	k_2 ($M^{-1}s^{-1}$)	Stability
17		4.7×10^{-2}	+-
18		0.37	++
19		0.74	-
20		0.65	++

Table 4. Reactivity (monoaryl tetrazine, DMF/MO PS buffer, pH 7.5, rt) and stability profile of 1-methyl-3-substituted cyclopropenes reported by Devaraj.

++ = stable to aqueous media and cysteine tolerance, +- stable in aqueous media, - = not stable in aqueous media.^[72]

In this study, the authors did not observe a correlation between the cyclopropene reactivity and stability based on the nature of the functional group in the substituent at the cyclopropene C3 position. However, the main outcome of these investigations was the discovery of the amidomethyl-1-methylcyclopropene **20**, which displayed enhanced reactivity in IEDDA cycloadditions ($k_2 = 0.65 M^{-1}s^{-1}$) whilst presenting excellent stability in aqueous media and in presence of thiols. Interestingly, Devaraj *et al.* also noticed that cyclopropene **20** reacted faster with a sterically

hindered *tert*-butyl-substituted tetrazine derivative compared to 5-hydroxy-TCO **10** (1.31×10^{-1} vs. $8.6 \times 10^{-2} \text{ M}^{-1}\text{s}^{-1}$ for **20** and 5-hydroxy-TCO **10**, respectively). This observation revealed that the reactivity of 1-methyl-3-substituted cyclopropenes is minimally impacted by the steric hindrance of the tetrazine substituents.^[72] This is a major difference to *trans*-cyclooctenes, which often display faster kinetics with 6-hydrogen terminated tetrazines but tend to become less reactive when reacting with sterically hindered 3,6-disubstituted tetrazines.^[79]

One of the most recent example of cyclopropenes being used as dienophiles in the tetrazine ligation was reported by Laughlin et al. in 2018.^[80] The authors exploited the sluggish reaction of hindered 3,3-disubstituted cyclopropenes with tetrazines to design 3-*N*-substituted spirocyclopropenes, where the nitrogen is protected with a bulky and light-cleavable protecting group (Figure 7).^[68,69] This renders the cyclopropene unreactive towards IEDDA cycloaddition with tetrazines when the bulky *N*-caging group is present, by sterically preventing the tetrazine from approaching, and reactive once the caging group is removed.

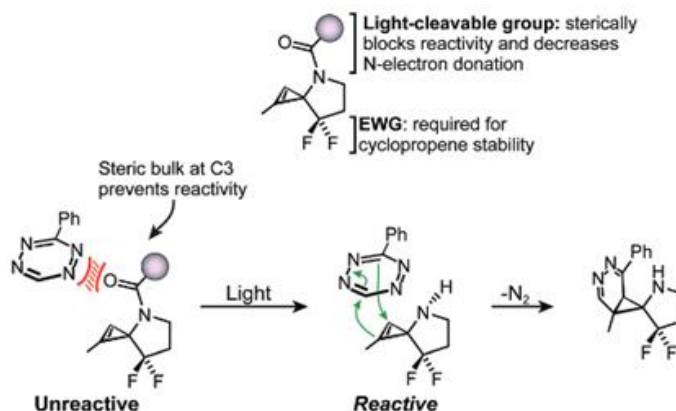


Figure 7. Mode of action of caged cyclopropene developed by Laughlin *et al.*^[80]

Despite the poor second order rate constant of these caged cyclopropenes in the tetrazine ligation ($k_2 = 9.0 \times 10^{-3} \text{ M}^{-1}\text{s}^{-1}$, 3-phenyl-1,2,4,5-tetrazine pyrrolidiny l amide, 1:1 MeCN/aqueous buffer pH 8.8, room temperature), this approach ultimately allows for temporal control of the biorthogonal reactivity.

In the last 20 years, bioorthogonal chemistries have become essential tools in chemical biology, enabling the labelling and study of biomolecules in their native environments, thereby providing significant insights into their structures and functions. Despite dozens of bioorthogonal reactions being reported in the literature, these transformations are not without limitations; each bioorthogonal reaction presents its own strengths and weaknesses. This introduction aimed to give an overview of the principal bioorthogonal reactions utilised in modern chemical biology applications for the covalent modifications of biomolecules. Those reactions are summarized in Figure 8 and are colour-coded based on their second order rate constants. As a general rule of thumb, Kalia and Raines estimated that a bioorthogonal reaction should achieve a rate constant of at least $1 \text{ M}^{-1}\text{s}^{-1}$ to be considered for *in vitro* applications due to low concentrations of specific proteins or other biomolecules in the cellular environment.^[81] Based on this criteria, it is clear then that only a few bioorthogonal reactions appear suitable for the intracellular labelling of biomolecules, explaining the on-going effort for the continuous emergence of novel bioorthogonal reactions with optimised properties to expand the current toolbox available to biological chemists.

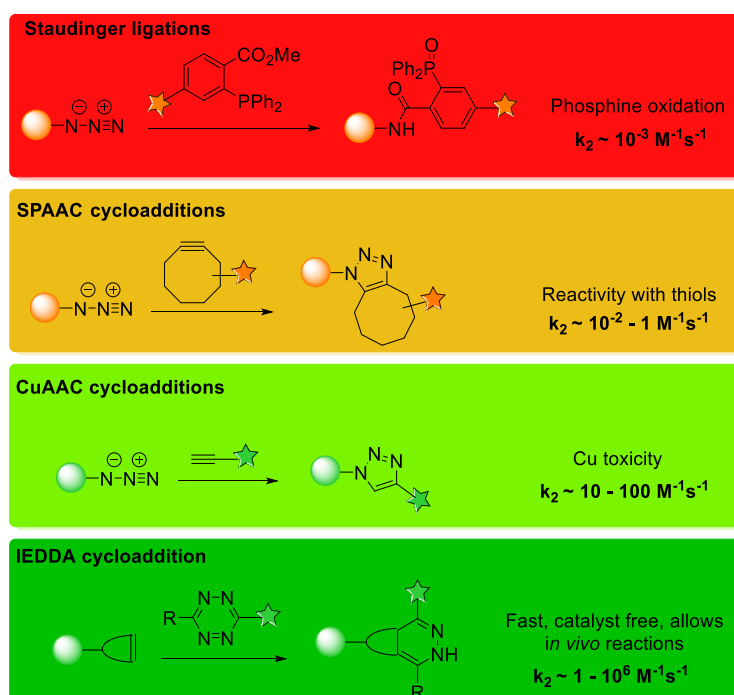


Figure 8. Examples of bioorthogonal reactions and corresponding second-order rate constants.

The intensive efforts to design novel reagents for effective bioorthogonal chemistries and the labelling of biomolecule in complex cellular environments have allowed the development of powerful techniques that can also benefit medicinal chemistry and support the drug discovery process.^[82]

1.2. A Bioorthogonal Strategy for Drug Localisation, Target Identification and Target Occupancy Measurement

Used in combination with imaging techniques, bioorthogonal chemistry approaches have revolutionized the chemical biology field by offering powerful chemical tools to investigate the biological functions of small molecules on a cellular level.^[83] From a medicinal chemistry perspective, the ability to visualize small drug molecules in cellular environments would significantly contribute to the drug development process, notably by providing insights on the subcellular distribution, the site(s) of action, and the interactions with other biomolecules of a small drug molecule of interest.^[84-86] A systematic investigation of these parameters at the preclinical stage could result in a more comprehensive compound characterisation that would ultimately help to better define the phenotype induced by a small drug molecule. Most commonly referred to as (bioorthogonal) chemical probes, these tool compounds are usually designed by chemical functionalisation of a small drug molecule in order to answer key specific biological questions.^[84,87] Recently, Rutkowska *et al.* have developed a strategy based on bioorthogonal chemistry and the IEDDA cycloaddition between *trans*-cyclooctene-labelled probe molecules and tetrazine-tagged reporters to address some of the most challenging aspects of the drug discovery process; namely target/off-target identification, drug localisation and co-localisation with the target as well as measurement of target engagement.^[88] Late stage failures of drug molecule candidates in Phase II or III clinical trials are often caused by off-target effects or lack of evidence of target engagement *in vivo*.^[89] Consequently, this platform represents a powerful method for evaluating target validation early on in the drug development process and could contribute to reduce the attrition rate. The method described by Rutkowska *et al.* relies on the IEDDA reaction of a functionalised chemical probe with

a reporter that allows either pull-down assay for target identification, fluorescence reporting for compound localisation with its target, or measurement of target occupancy *via* competition experiments with an unlabelled substrate (Figure 9).^[88]

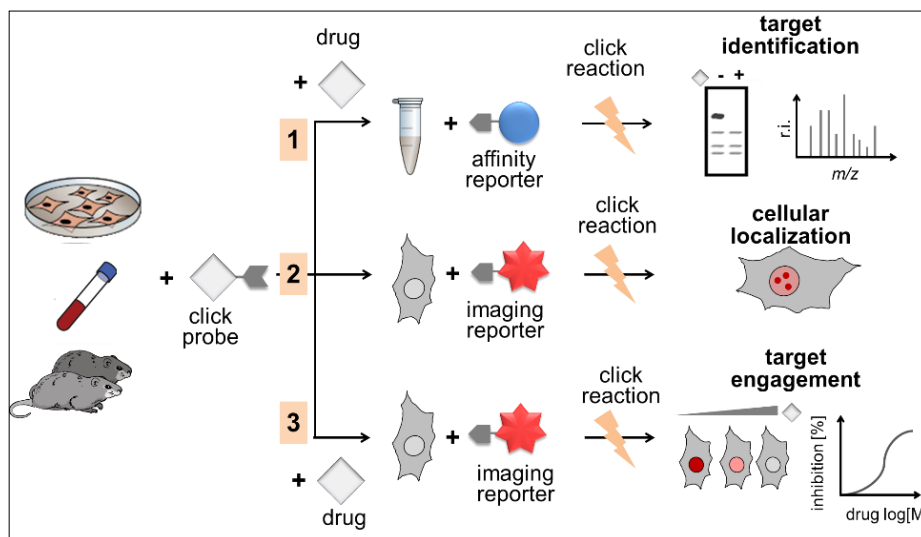


Figure 9. Modular probe strategy based on bioorthogonal chemistry as reported by Rutkowska *et al.*^[88]

More specifically, target identification can be achieved using a biotin-derived bioorthogonal reporter loaded on streptavidin beads reacting with live cells or cell lysates previously incubated with a TCO-labelled chemical probe. Quantitative mass spectrometry is then used to analyse the affinity-captured targets. In addition, cellular localisation and co-localisation with the target can be achieved using a tetrazine-based fluorescent dye as a reporter. Finally, engagement with a cellular target can be measured in a competitive binding assay by observing the reduction of fluorescence signal originating from a TCO-tagged probe bound to the target as increasing concentrations of an unlabelled substrate progressively displace the binding of the tagged probe to the target. Rutkowska *et al.* demonstrated the feasibility of this strategy with a TCO chemical probe (**22**) derived from Olaparib (**21**), a non-covalent inhibitor of the enzyme poly(adenosine diphosphate [ADP]-ribose)polymerase 1 (PARP-1) indicated for the treatment of various ovarian cancers (Figure 10)^[90].

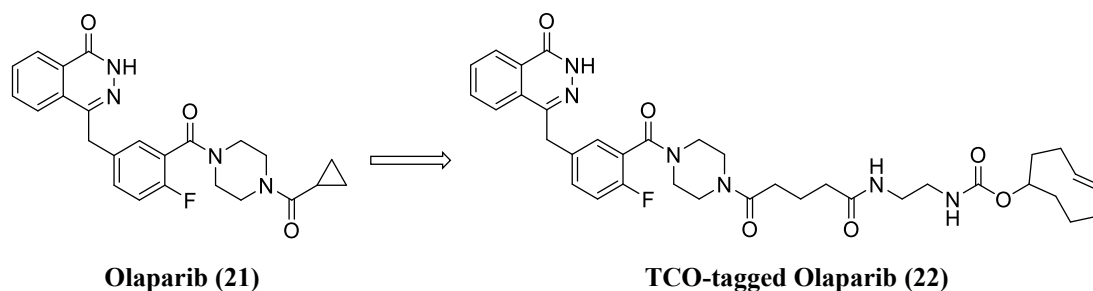


Figure 10. Structures of PARP-1 inhibitor Olaparib and TCO-tagged analogue used in the modular probe assay developed by Rutkowska *et al.*^[88]

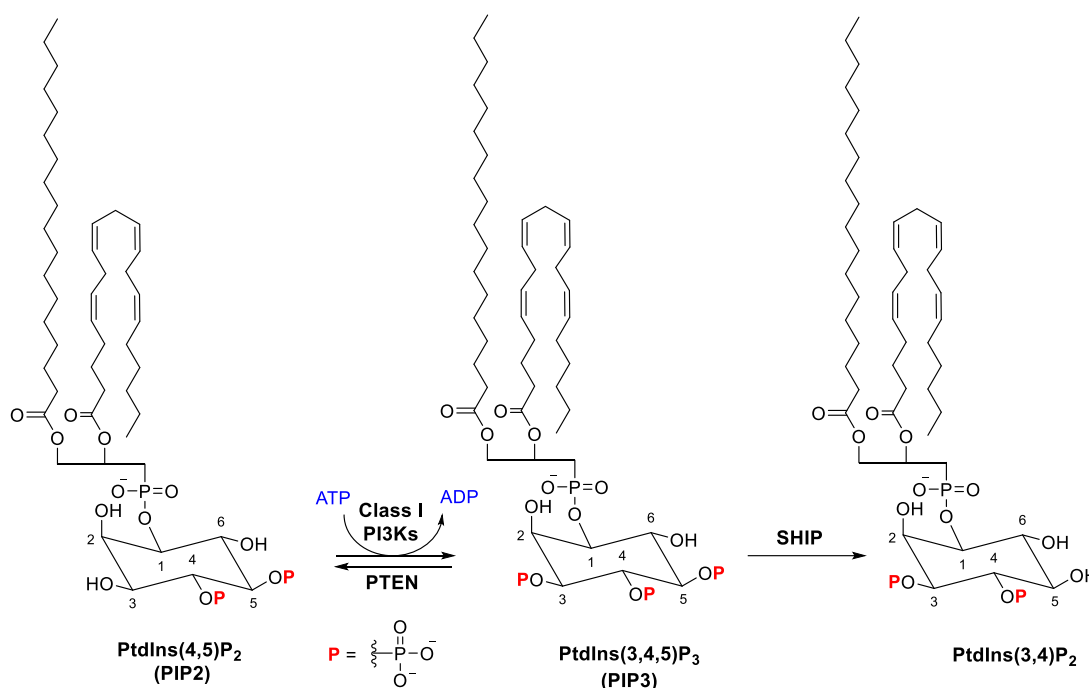
In this thesis, the strategy based on bioorthogonal chemistry reported by Rutkowska *et al.* will be applied to a drug discovery programme investigating inhaled inhibitors of the Phosphoinositide 3-kinase δ (PI3K δ) enzyme in order to determine their localisation in cellular systems and gain a better understanding of their distribution in lung tissues.

1.3. Inhaled PI3K δ Inhibitors for the Treatment of Respiratory Diseases

1.3.1. The PI3K Pathway

Phosphoinositide 3-kinases (PI3Ks) are a family of lipid kinases that catalyse the ATP-dependent phosphorylation of the 3-hydroxy position of the inositol ring of several phosphatidylinositides.^[91,92] Mammalian cells express multiple PI3K proteins that all share a highly conserved kinase domain but differ by their substrate specificity and mode of regulation. Within the PI3K family, the different isoforms can be divided into three classes (Class I, II and III).^[92,93] Class I PI3Ks contains the PI3K α (PI3K α), β (PI3K β), δ (PI3K δ) and γ (PI3K γ) isoforms which are the most extensively studied members of the family.^[92] Class I PI3Ks phosphorylate the 3-position of phosphatidylinositol-(4,5)-diphosphate (referred to as PtdIns(4,5)P₂ or PIP₂) to produce the key signalling molecule phosphatidylinositol-(3,4,5)-triphosphate (PtdIns(3,4,5)P₃ or PIP₃) (Scheme 7).^[94-96] The action of Class I PI3Ks

can be reversed by the phosphatase and tensin homolog (PTEN) protein and by the SH2-containing inositol phosphatases (SHIP1 and SHIP2) that dephosphorylate the 3- and 5-positions of PIP3, respectively (Scheme 7).^[91,97,98]



Scheme 7. Role of PI3 kinases.^[99]

Class I PI3Ks are heterodimeric complexes consisting of a regulatory (or adaptor) subunit and a catalytic subunit.^[95,100] Class I PI3K isoforms can be further divided into two subclasses depending on the nature of their regulatory subunit and their mode of activation.^[92,100] Class I_A PI3Ks includes the PI3K α , PI3K β and PI3K δ isoforms, which are characterised by the association of a p110 catalytic subunit (p110 α , p110 β or p110 δ) and a p85 regulatory subunit.^[93,101,102] Class I_B only comprises the PI3K γ isoform which consists of a p110 γ catalytic subunit and a p101 regulatory subunit.^[103] Class I_A and I_B PI3Ks are activated by receptor tyrosine kinases and G-protein-coupled receptors, respectively.^[103,104] The regulatory subunits of Class I PI3Ks do not possess any intrinsic enzymatic activity, but repress the activity of the catalytic subunits, keeping them inactive in the resting state.^[102]

Activation of the PI3K signalling pathway can occur upon upstream growth-factor stimulation of receptor tyrosine kinases, which results in the recruitment of PI3Ks from the cytosol to the plasma membrane, where PIP2 resides, through the binding of the p85 regulatory subunit to a phosphorylated tyrosine residue on a receptor tyrosine kinase.^[105] This event releases the inhibition of the regulatory subunit on the catalytic subunit and ultimately leads to the phosphorylation of PIP2 to PIP3 (Figure 11).

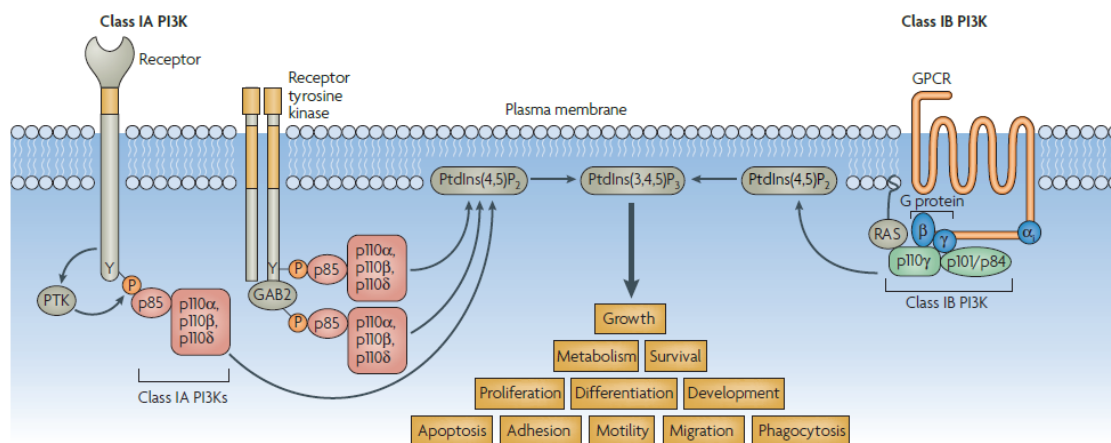


Figure 11. Representation of the activation of the PI3K pathway. Reprinted with permission from Rommel *et al.*^[106] (Copyright 2007 Nature Publishing Group).

PIP3 is a critical second messenger in cells, with several proteins containing a pleckstrin homology (PH) domain able to bind PIP3, that ultimately activates several downstream signalling pathways.^[105] Most notable is the PI3K/Akt/mTOR pathway that is responsible for essential cellular functions including cell growth, metabolism, survival, migration, proliferation, differentiation, and apoptosis.^[98] Finally, the other classes of PI3K enzymes comprise Class II PI3Ks which phosphorylate PtdIns-4-P, and Class III PI3Ks which only phosphorylate PtdIns.^[95]

1.3.2. Class I PI3Ks in Disease

Considerable attention has been given to the Class I PI3K family of kinases, which have been identified as promising therapeutic targets for the treatment of a variety of diseases, caused by abnormal PI3K signalling. Some of these conditions include cancer, chronic inflammation, cardiovascular diseases and metabolic diseases.^[105,107,108] However, Class I PI3Ks are not all similarly expressed throughout the body, and their localisation in specific cell types deeply impacts the disease-relevance of each isoform.^[93,96,109,110] PI3K α and PI3K β are ubiquitously expressed and have been shown to play a key role in cell growth survival and proliferation.^[111] Indeed, mice with knockouts for the genes encoding the p110 α and p110 β subunits were not viable, suffering from impaired embryonic development and early embryonic lethality.^[111] These observations raise serious concerns for the widespread inhibition of the PI3K α and PI3K β isoforms, limiting their investigation to cancer therapy. Indeed, there is evidence that implicates the PI3K pathway in cancer, for example activating mutations in the p110 α catalytic subunit, or mutations resulting in the inactivation of PTEN phosphatase, which both lead to increased cellular levels of PIP3.^[112]

In contrast to PI3K α and PI3K β , expression of the PI3K δ and PI3K γ isoforms is mainly limited to hematopoietic cells with PI3K γ being found in granulocytes, monocytes and macrophages, while PI3K δ is also expressed in B cells and T cells.^[92,93,96,113] Therefore, intensive research has been focused around selective inhibition of PI3K δ and/or PI3K γ , which appear as promising therapeutic targets for the treatment of autoimmune and chronic inflammatory diseases.^[107,113-115]

1.3.3. PI3K δ Inhibition

Dysregulation of the PI3K δ pathway has been observed in people suffering from respiratory diseases whereby an accumulation of inflammatory mediators released by leukocytes ultimately leads to inflammation and airway damage.^[115-117] Therefore, these observations strongly validate PI3K δ inhibition as a promising therapeutic approach for the treatment of asthma and chronic obstructive pulmonary

disease (COPD).^[118] Patients suffering from asthma and COPD can experience episodes of acute inflammation following a viral or bacterial infection known as exacerbations, which frequently results in recurrent hospitalisations and the need for oral steroid treatment, ultimately leading to further lung damage and poor overall prognosis.^[119]

1.3.3.1. Development of Inhaled PI3K δ Inhibitors.

Based on validation of the PI3K δ target for the treatment of respiratory diseases and drawing on institutional expertise in inhaled medicines and devices in our laboratories, a medicinal chemistry project was initiated to develop an inhaled PI3K δ inhibitor. An inhaled delivery route was preferred over oral administration as it would deliver the drug directly to the desired site of action in the lungs, therefore offering the opportunity for quick onset of action, whilst minimizing any systemic effects that may be adverse.^[120-123]

Delivery of drugs by the inhaled route usually require compounds with a specific PK profile. The desired clinical candidate for PI3K δ had to meet various criteria, including: (1) high potency with PI3K δ pIC₅₀ > 9, mainly because of the limitations associated with the inhaler device and the very low dose of drug that it can contain (~ 1 mg); (2) a high selectivity (>100-fold) for PI3K δ over its close isoforms - α , - β , and - γ ; and (3) a low systemic exposure with a moderate-to-high intrinsic clearance along with a low oral bioavailability, since greater than 80% of the dose is swallowed and reaches the gastrointestinal tract following inhalation.^[124]

More specifically, the PI3K δ medicinal chemistry programme initiated in our laboratories aimed at improving the potency and selectivity of the lead compound **30** through structure-based design, and eventually led to the discovery of two inhaled clinical candidates: GSK2269557/nemiralisib and the back-up compound GSK2292767 currently being investigated for their ability to reduce the underlying inflammation causing exacerbations in COPD patients (Figure 12).^[125] Nemiralisib is currently in phase II for the treatment of asthma and COPD whilst GSK2292767 underwent first time in human (FTIH) studies in 2018. The structure-based design

effort conducted in our laboratories that led to the discovery of both clinical candidates is summarized below (Figure 12).

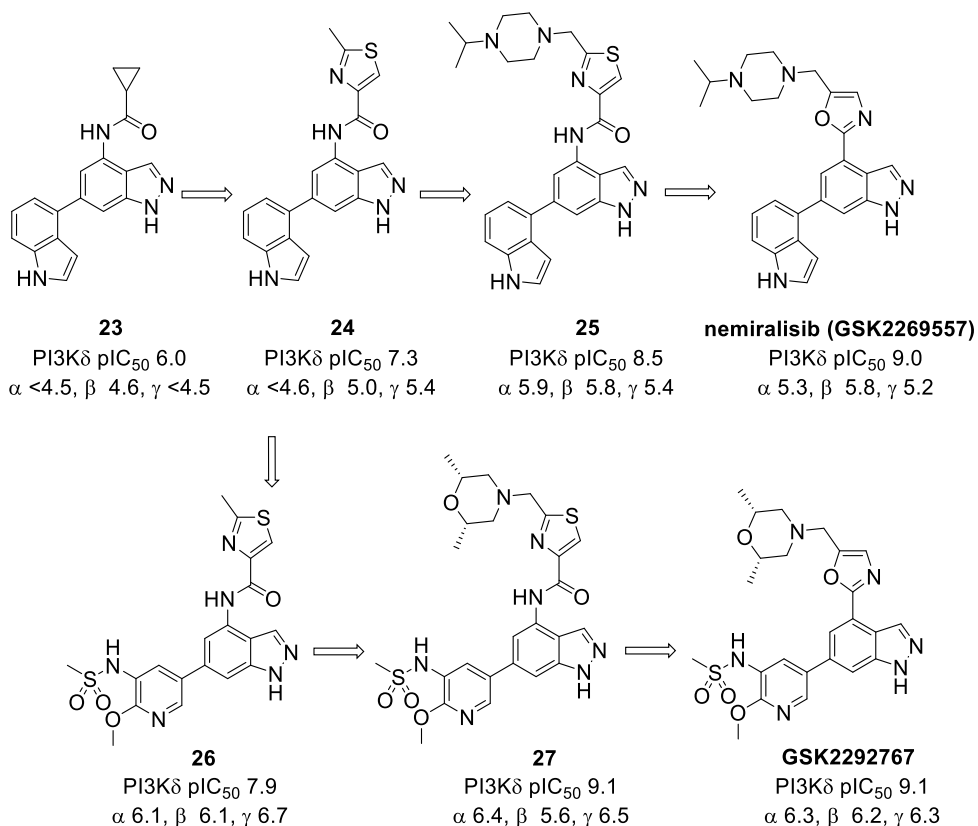


Figure 12. Inhibitor evolution and the discovery of nemiralisib (GSK2269557) and back-up compound GSK2292767.

Lead compound **23**, which contains a cyclopropyl amide substituent at the indazole 4-position was identified from a kinase cross-screening effort and was the first compound discovered to have moderate potency for PI3K δ and selectivity over the other PI3K isoforms. In order to develop PI3K δ inhibitors with enhanced potency and selectivity, SAR studies were conducted on **23** at the two positions of substitution on the indazole core.^[125] First, various amides were investigated at the 4-position whilst keeping the 6-indole substituent unchanged. The introduction of an *ortho*-heteroatom was a major breakthrough since thiazolyl amide **24** increased the PI3K δ potency by 10-fold. It was postulated that the presence of an *ortho*-heteroatom was critical to the activity as it could ensure co-planarity of the amide and indazole core

via an internal hydrogen bond that would enhance the stability of the preferred binding conformation.^[125]

Next, significant investigation was conducted on the 6-position substituent on the indazole, whilst keeping the methylthiazolyl amide of **24** fixed. Although a large array of mono and bicyclic heteroaryl groups were screened in place of the indole, the latter proved to be the best compromise for potency and selectivity.^[125] Following on from this, further optimization was made on the methylthiazolyl amide moiety since modelling suggested that both potency and selectivity could be improved by growing molecules out further through the methyl vector (Figure 12). It was proposed that a lipophilic basic amine, which would be protonated at physiological pH, would come in close proximity to Trp760 (conserved in PI3K α , - β , and - γ), possibly forming a cation- π interaction. This interaction is beneficial in the case of PI3K δ because the adjacent residue to Trp760 is Thr750, forming a hydrophobic pocket known as the “tryptophan shelf”, which is able to accommodate the bulky isopropyl group of **25**.^[125,126] However, in other class I PI3K isoforms, the residue adjacent to the tryptophan is either a lysine or an arginine, larger residues that could clash with the bulky cyclic amine substituent, therefore explaining the enhanced potency and selectivity increase for PI3K δ over analogous class I isoforms α , β , and γ . Compound **25**, which contains a piperazine ring, was found to improve the potency by 10-fold whilst maintaining good levels of selectivity for PI3K δ over other homologous isoforms.

Next, further studies were conducted to design smaller compounds that could interact with Trp760 residue more directly by replacing the methylthiazolyl amide moiety by an appropriate heterocyclic linker. A large range of heterocycles were screened, and oxazole was identified as the best replacement for the methylthiazolyl amide and led to the discovery of nemiralisib/GSK2269557. The back-up clinical candidate GSK2292767 was also identified from the medicinal chemistry programme, whereby the piperazine of nemiralisib was replaced with a *cis*-dimethyl morpholine and the indole was replaced with a pyridine sulfonamide group.

The binding mode of nemiralisib within the active site of PI3K δ was elucidated by X-ray crystallography (Figure 13). The crystal structure demonstrates key interactions with highly conserved regions within the ATP binding pocket of the kinase domain which are very important for the binding of ATP-competitive inhibitors.^[101]

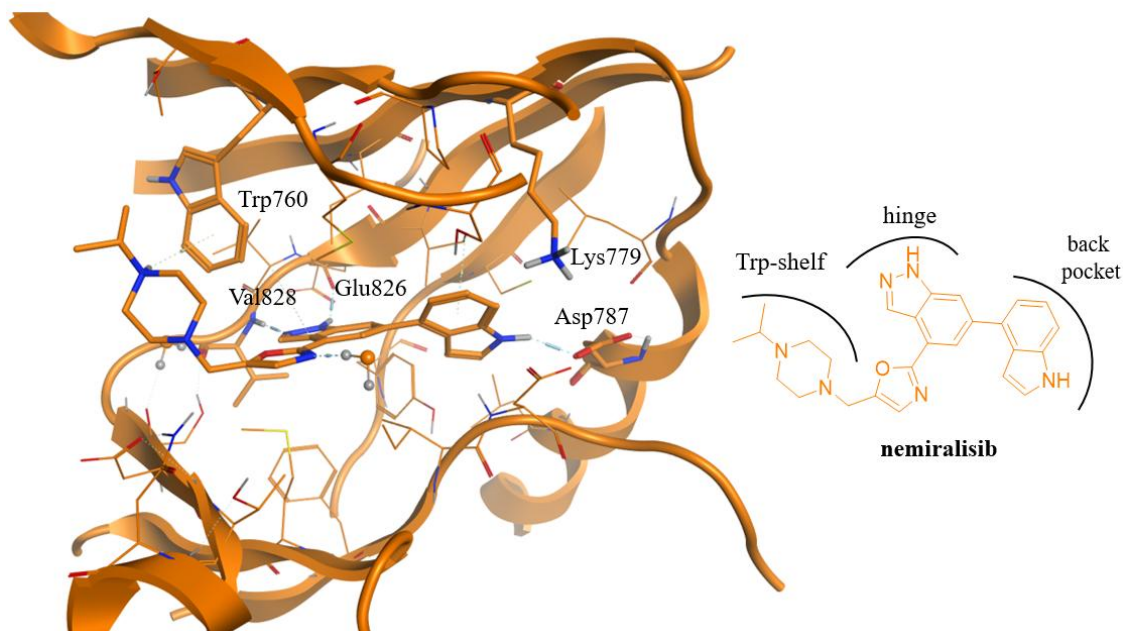


Figure 13. Crystal structure of nemiralisib in the ATP binding site of PI3K δ (PDB 8FVPT).

First, the indazole moiety acts as a binder to the “hinge”, a segment that connects the N-and C-lobes of the kinase domain where the adenine group of ATP establishes hydrogen bonds.^[127] Here, the backbone amide of Val828 in the hinge region makes a characteristic hydrogen bond interaction with the indazole N2, whilst the backbone of carbonyl of Glu826 interacts with the indazole NH. In addition, the indole moiety occupies an area of the kinase domain referred to as the back-pocket (or affinity pocket), a lipophilic pocket that had previously been exploited for the design of PI3K δ inhibitors exhibiting improved potency and selectivity.^[128] More specifically, the indole NH forms a hydrogen bond to the side chain of Asp787 that is responsible for a significant increase in potency. Indeed, a decrease of 2 log units of PI3K δ enzyme potency was observed upon methylation of the indole thereby highlighting the detrimental effect of disrupting this key interaction.^[125] The oxazole

moiety does not display any specific interactions within the ATP active site of the kinase domain and is thought to act as a spacer unit to pack the pendant basic piperazine on the tryptophan shelf which is in close proximity to Trp760 and most likely engages in a π -cation interaction.

The binding mode of the back-up compound GSK2292767 was also investigated by X-ray crystallography with PI3K δ and an overlaid crystal structure with nemiralisib is shown in Figure 14.

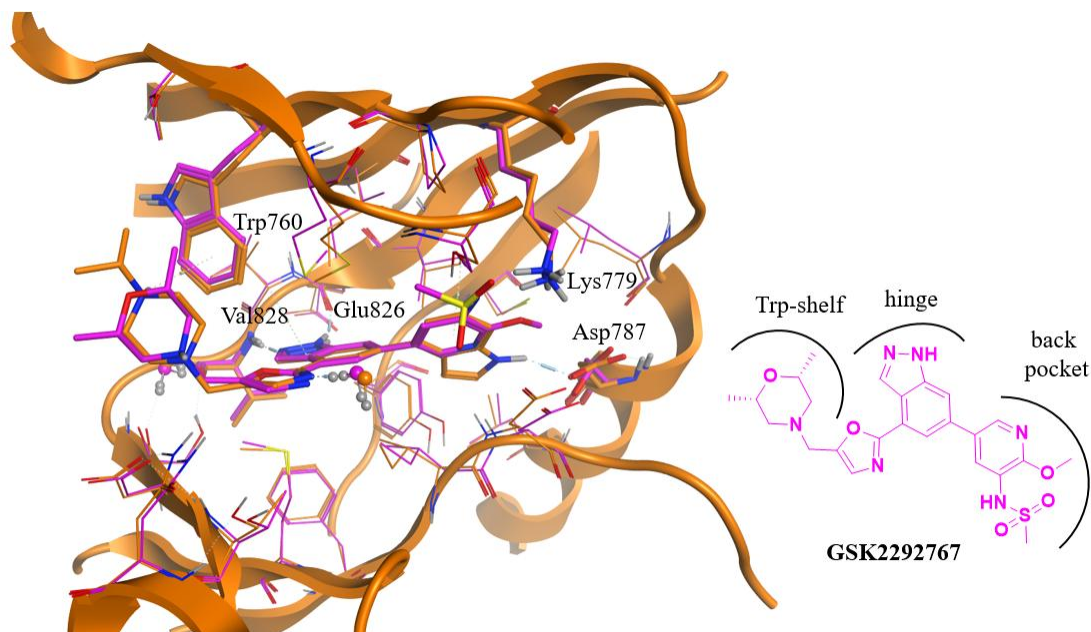
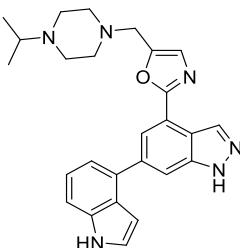
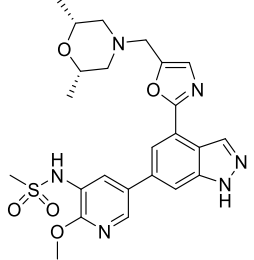


Figure 14. Overlaid crystal structures of nemiralisib (orange) and back-up compound GSK2292767 (magenta) in the ATP binding site of PI3K δ (PDB 5AE9).

Overall, the back-up molecule GSK2292767 adopts an analogous binding mode to nemiralisib, with the indazole moiety engaging in a similar hydrogen bond interactions pattern with the hinge region and the oxazole ring positioning the morpholine moiety against Trp760 (Figure 14). The main difference in the binding mode of the two clinical candidates comes from the nature of the interactions in the back-pocket region of the active site. In comparison to the indole group of nemiralisib engaging in an interaction with Asp797, the sulfonamido oxygen on the 2-methoxypyridine substituent of GSK2292767 forms a hydrogen bond with Lys779. Furthermore, an additional ion pairing interaction is thought to occur between the

protonated Lys779 and the sulfonamide nitrogen, which is acidic ($pK_a = 7.8$) and therefore partially ionised at physiological pH. Finally, GSK2292767 interacts with a water molecule via the pyridyl nitrogen that forms a solvent bridge to Asp787 (water molecule not shown).

The properties of nemiralisib and GSK2292767 are summarised in Table 5 below and will be discussed in more detail throughout this thesis. The inhaled compounds demonstrated a high potency along with a high degree of selectivity for PI3K δ over other Class 1 PI3K isoforms in an enzyme assay (PI3K δ pK_i) and cellular assays in peripheral blood mononuclear cells and human whole blood (PBMC and hWB pIC_{50} , respectively) (Table 5).

Structure		
Compound number	nemiralisib (GSK2269557)	GSK2292767
PI3K δ pK_i (n)	9.9 (4) ^a	10.1 (5) ^a
PI3K α , β , γ pIC_{50} (n)	5.3 (27) ^b , 5.8 (26) ^c , 5.2 (30) ^d	6.3 (17), 6.2 (18), 6.3 (20)
α , β , γ fold selectivity	5012, 1585, 6310	631, 794, 631
PBMC / hWB pIC_{50} (n)	9.6 (5) / 8.9 (3)	9.2 (3) / 8.5 (7)
ChromLogD _{pH7.4} calc./measured	2.8 / 2.5	3.7 / 3.3
cLogP	4.4	2.8
AMP (nm/s, pH 7.4)	230	203 (pH 7.05)
Kinetic / SLF solubility (μ g/mL)	110 / 457 ^e	182 / 4 ^g
Rat/Mouse lung tissue binding (% bound)	99.2 / 97.8	97.9 / 96.3
Mouse blood binding (% bound)	96.7	94.6

*n = number of test occasions included in mean; ^aPI3K δ assay run at a 2 mM ATP concentration; ^bTested <5.3 on one test occasion and <4.6 on one test occasion; ^cTested <4.6 on one test occasion; ^dTested <4.6 on 3 test occasions; ^eHemisuccinate salt, 4h timepoint (micronised material); ^fDid not return a value on one test occasion; ^gFree base, 4h timepoint (crystalline material, micronised).

Table 5. Properties of inhaled PI3K δ inhibitors nemiralisib and GSK2292767.^[125,129]

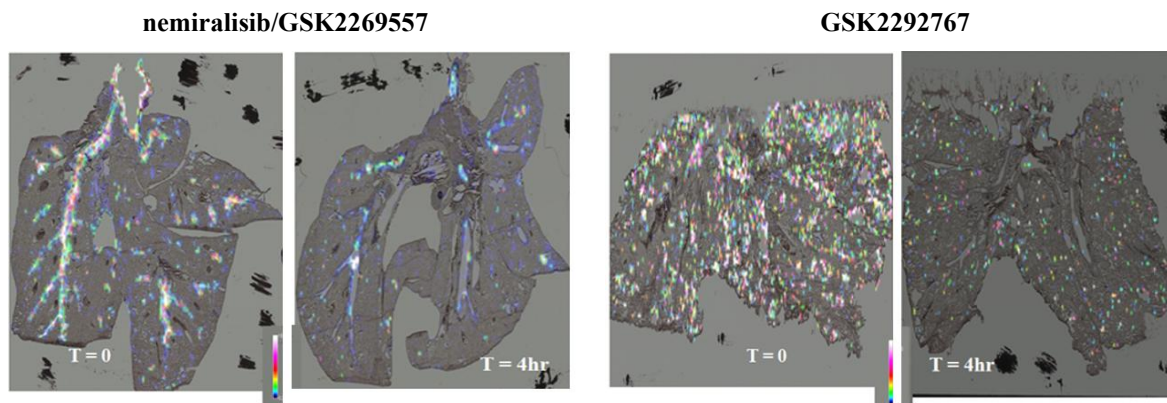
It is essential for inhaled molecules to be retained in the lungs following inhalation to maintain target exposure. Interestingly, nemiralisib and GSK2292767 are hypothesized to achieve retention in the lungs *via* two different mechanisms. First, nemiralisib contains a lipophilic basic amine piperazine ring. Such moieties usually tend to partition into phospholipid membranes, thereby increasing the volume of distribution of the drug molecule and driving increased retention in the lung tissue.^[130,131] This is exemplified with the very high lung tissue binding measured in rat for nemiralisib (99.2% bound, Table 5). In addition, lipophilic molecules containing basic amines that are ionizable at physiological pH can accumulate in specific cellular organelles such as lysosomes, a process referred to as lysosomotropism or lysosomal trapping.^[132] Lysosomes are membrane-bound vesicles localised in the cell cytoplasm and are involved in the degradation of various biomolecules, including proteins and lipids. In addition, lysosomes play a role in numerous cellular processes, such as cell signalling and metabolism.^[133] A characteristic feature of lysosomes is their acidic luminal environment (pH 4-5) which is required for the enzymatic activity of several lysosomal proteases. When lipophilic basic molecules diffuse into the lysosomes, they become protonated due to the acidic environment which restricts their diffusion back into the cytosol.^[134] This sequestration process can result in higher intra-lysosomal compound concentrations relative to those cytoplasm.^[135] Several studies have intended to characterize the physico-chemical properties of small drug molecules on their degree of lysosome entrapment as the cellular responses to such lysosomotropic compounds are still not fully understood. Empirical observations seem to indicate that small molecules with a cLogP value > 2 and a basic pK_a value (i.e pK_a of the conjugated acid) comprised between 6.5 and 11 have a higher propensity for lysosomotropism.

With regard to nemiralisib, its potential sequestration in the lysosomes could constitute a ‘compound reservoir’, which would allow for a slow release of the drug molecule back into the cytosol where it could engage with the PI3K δ target and achieve extended duration of action. Alternatively, GSK2292767 is hypothesised to achieve lung retention through a different mechanism that relies on the low solubility of the compound, as shown by the solubility measured in simulated lung fluids (SLF)

(Table 5). In this case, the low solubility of the compound may result in slow dissolution rates from depots of particulate material into the airway smooth muscles.^[122]

The pharmacokinetic (PK) and pharmacodynamics (PD) profiles of the two inhaled clinical candidates were also investigated to understand the effects of the compounds in the lungs. These studies relied on induced sputum analysis along with measurement of drug concentration in plasma and bronchoalveolar lavages (BAL) from healthy smokers treated with nemiralisib or GSK2292767.^[129] For both compounds, BAL analysis confirmed lung retention at 24 hours as well as higher levels of the drug in the lungs versus plasma. Analysis of induced sputum 3 hours post-dose also demonstrated that both drug molecules achieved target engagement as revealed by the reduced levels of PIP3 proportion, the product of PI3K δ activation.

As part of their clinical development for the treatment of asthma and COPD, the lung distribution of nemiralisib and GSK2292767 following inhaled administration to rats was investigated by MALDI imaging mass spectrometry. Interestingly, in these lung tissue studies the two inhaled clinical candidates exhibit distinct deposition and distribution profiles with nemiralisib being predominantly distributed in the conducting airways whilst GSK2292767 is distributed in the airways and throughout the lung tissue (Figure 15).^[136] Consequently, these observations suggest that the differences in the physico-chemical properties of the two inhaled clinical candidates are likely to influence their lung distribution.



Representative lung section images in rats following inhaled administration. For each compound: Left image - immediately after dosing; Right image - 4 h post dose (n=1 per timepoint). Nemiralisib (succinate salt), single inhaled dose at a dose level of 0.716 mg/kg/day, 60 min exposure period. GSK2292767, single inhaled dose at a dose level of 0.115 mg/kg/day, 60 min exposure period.

Figure 15. Comparison in the MALDI imaging of the lung deposition and distribution profiles for nemiralisib and GSK2292767 following inhaled administration to rats.

Understanding how inhaled molecules distribute in the lungs and the impact of their physico-chemical properties on the lung retention and distribution is essential to design efficacious inhaled therapies. In this context, nemiralisib and GSK2292767 provide a unique opportunity to compare two inhaled drug molecules with distinct lung retention mechanisms. Based on the strategy developed by Rutkowska *et al.*, chemical probes derived from the two inhaled clinical candidates will be synthesised in order to investigate these differences.

1.3.3.2. Orally Administered PI3K δ Inhibitors

Although drug delivery by the inhaled route may offer many advantages compared with oral administration (*e.g.* low dose, weak systemic exposure, improved toxicity profile), patient compliance is essential for successful therapies. Inhaled drug molecules were found to be frequently associated with low patient compliance in comparison to those administered orally.^[137] Taking this into consideration, a

subsequent medicinal chemistry programme was initiated in our laboratory focusing on the development of an oral PI3K δ inhibitor for the treatment of respiratory diseases.

Being a high-value therapeutic target for the treatment of cancers, inflammatory and autoimmune diseases, inhibition of PI3K δ has received significant interest in the recent years, with several PI3K δ inhibitors currently in clinical development. Idelalisib (**28**, Figure 16) was approved by the FDA in 2014 as a first-in class oral PI3K δ inhibitor indicated for the treatment of several haematological malignancies such as CLL (chronic lymphocytic leukemia). More recently, umbralisib **29** received FDA breakthrough therapy designation for the treatment of marginal zone lymphoma. Additional oral PI3K δ inhibitors currently in clinical trials include seletalisib (**30**),^[109,138] developed by UCB for the treatment of mild psoriasis and leniolisib (**31**), developed by Novartis for the treatment of Activated PI3K δ Syndrome.^[139]

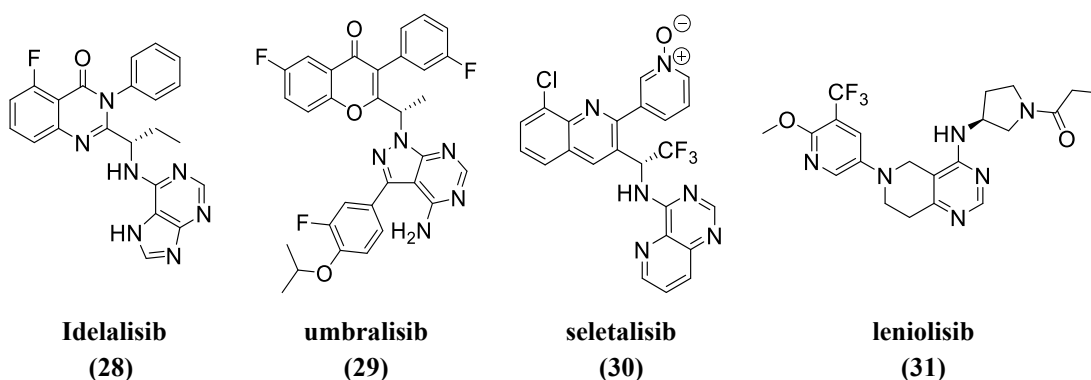
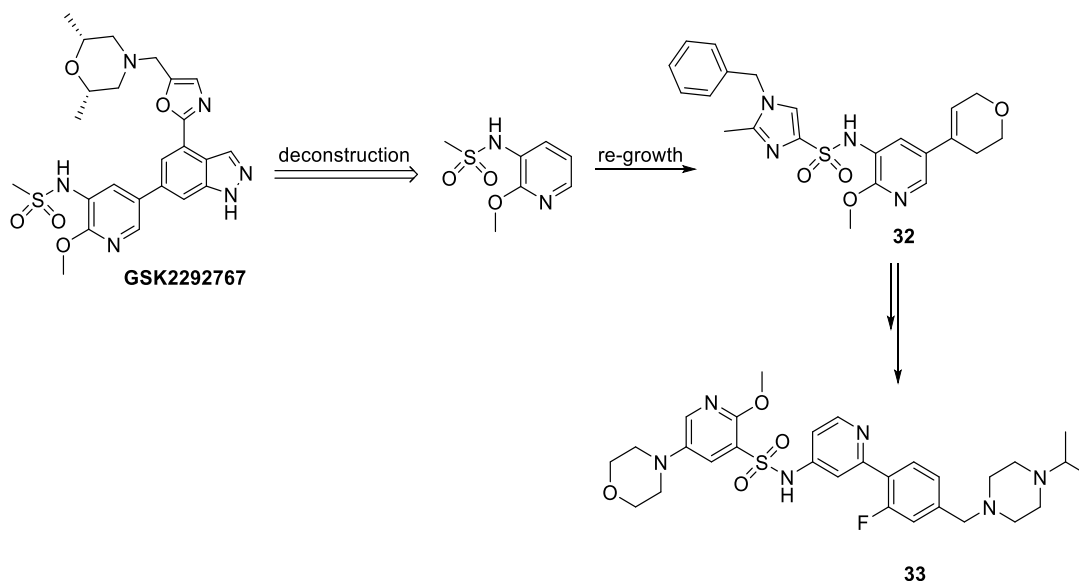


Figure 16. Structures of oral PI3K δ inhibitors.

In our laboratory, the medicinal chemistry programme focusing on the development of an oral PI3K δ inhibitor originated from a deconstruction and regrowth strategy starting from the inhaled clinical candidate GSK2292767.^[140] In this approach, the pyridine-sulfonamide group of GSK2292767 that occupies the back-pocket in the active site of PI3K δ was conserved as a minimal pharmacophore. Then, exploration of novel hinge binders to replace the indazole core of GSK2292767 identified the dihydropyran (as exemplified in compound **32**, Scheme 8) and morpholine moieties as promising alternatives. Additional investigations ultimately led to the discovery of **33** (Scheme 8), a potent PI3K δ inhibitor with a different

chemotype compared to the previously described inhaled molecules and where the pyridine-sulfonamide group is reversed compared to compound **32**.^[141]



Scheme 8. Deconstruction and re-growth approach towards the discovery of compound **33**.

After the discovery of the oral PI3K δ inhibitor **33**, the team was interested in investigating its cellular localization in an imaging assay using a bioorthogonal chemistry strategy, as described above with the modular assay developed by Rutkowska *et al.*^[88] To that end, a TCO-labelled chemical probe **34** derived from **33** was synthesized elsewhere in our laboratories, where the TCO tag was appended to the piperazine moiety (Figure 17).^[142]

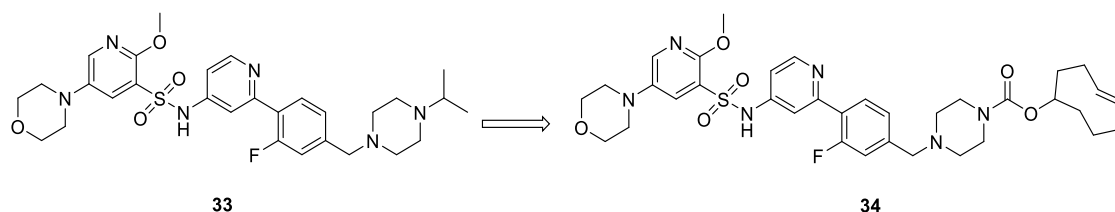
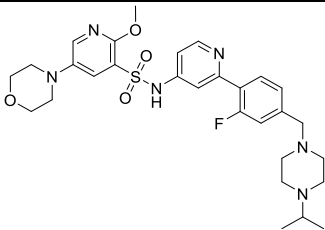
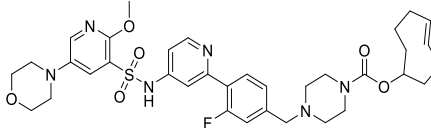


Figure 17. Structures of oral PI3K δ inhibitor **33** and corresponding TCO chemical probes **34**.

The properties of compound **33** and TCO chemical probe **34** are summarized in Table 6 below.

		
Compound number	33	34
PI3K δ p <i>K</i> _i (n)	10.9 (3) ^a	10.1 ^a
PI3K α , β , γ pIC ₅₀ (n)	6.0 (22), 5.3 (22), 5.7 (28)	5.8 (5), 5.8 (5), 6.2 (5)
α , β , γ fold selectivity	1259, 6310, 2512	1000, 1000, 398
hWB pIC ₅₀ (n)	8.2 (47) ^b	7.4 (5)
ChromLogD _{pH7.4} calc./meas.	1.9 / 1.9	6.2 / 6.1
cLogP	4.5	6.6
AMP (nm/s, pH 7.4)	105	483
Kinetic solubility (μg/mL)	≥287	12

*n = number of test occasions included in mean; nt = non tested; ^aPI3K δ assay run at a 2 mM ATP concentration; ^bDid not return a value on one test occasion.

Table 6. Properties of oral PI3K δ inhibitor **33** and corresponding TCO chemical probe **34**.

Compound **33** is a potent PI3K δ inhibitor demonstrating high activity in the enzymatic assay and in human whole blood. Compound **33** is also very selective for PI3K δ with >1000-fold selectivity against other class I PI3K isoforms. The introduction of the TCO moiety had a minimal impact on the enzyme potency of chemical probe **34** compared to the parent **33**. Chemical probe **34** also maintained high whole blood potency (hWB pIC₅₀ 7.4). However, the introduction of the TCO had a significant impact on the lipophilicity of the molecule compared to the parent compound, as shown by the measured ChromLogD_{pH7.4} values (6.1 and 1.9, respectively, Table 6). This chemical probe represented the first tool for profiling in cellular imaging assays that could be compared with probes from the inhaled series of PI3K δ inhibitors.

2. Aims

Nemiralisib and GSK2292767 are both potent inhaled PI3K δ inhibitors currently in clinical development for the treatment of asthma and COPD. The compounds exhibit different physico-chemical properties, and therefore presumably achieve lung retention by dissimilar mechanisms. Although the MALDI imaging studies conducted on the two inhaled clinical candidates provided helpful insights on their lung distribution profiles, this technique does not allow the direct visualization of the compound localization at the single cell level. In this context, being able to visualize the subcellular localization of inhaled drug molecules would be of significant interest from a medicinal chemistry perspective in order to gain a better understanding of their behaviour, especially in the lung following inhalation where there is relatively limited information on optimal drug localisation and lung retention.^[143] This thesis aims to describe the design, synthesis and biological evaluation of optimized chemical probes derived from nemiralisib and GSK2292767 to be used as chemical biology tools in cellular imaging assays. By contrasting two inhaled drug molecules with distinct lung retention mechanisms, this strategy may help to better understand how the molecular properties of inhaled drug molecules influence their cellular distribution in lung tissue.

In addition, PI3K δ being a promising therapeutic target for the treatment of different indications with several compounds currently in clinical trials, a potent and selective chemical probe for PI3K δ would constitute a novel tool for the study of PI3K δ inhibition whilst also enabling direct cellular measurement of target engagement of inhaled and oral PI3K δ inhibitors. Target engagement refers to the ability of a drug molecule to bind to its cellular target in a living system and is either measured directly or deduced from downstream biomarkers of the pathway under study. For PI3K δ , direct target engagement measurement of small molecule inhibitors remains a challenge, mainly because of the difficulties in accessing the site of action and in developing an *in vitro* assay to measure the reduction in cellular levels of PIP3 upon PI3K δ inhibition. Indeed, although reduced levels of PIP3 proportion were measured in induced sputum of healthy volunteers dosed with nemiralisib and

GSK2292767, it is important to mention that PIP3 is not exclusively produced by PI3K δ but also by all the PI3K Class I isoforms.

Despite the repertoire of bioorthogonal reactions having expanded in the last twenty years, the design of bioorthogonal chemical probes with optimal properties in a specific biological system remains a challenging task. Since the inverse-electron demand Diels-Alder reaction between TCO-labelled compounds and tetrazine-tagged reporters had been identified by Rutkowska *et al.* as the most efficient bioorthogonal reaction for their modular imaging and target engagement measurement assays the chemical probes described in this thesis also feature a TCO bioorthogonal tag.^[88] For the design of optimized chemical probes, it is essential that the introduction of TCO tag to the parent compounds should only minimally disrupt their target-ligand interaction in order to maintain sufficient potency and selectivity for PI3K δ . Therefore, to ensure a robust probe-dependent signal in the cellular imaging assay, the designed chemical probes will ideally achieve high enzyme and cellular potency (PI3K δ pIC₅₀ > 8, hWB pIC₅₀ > 7), along with a good selectivity for PI3K δ over the other class I PI3K isoforms (>100 fold). In addition, and as stated by Frye in his guidelines on the design of “high quality chemical probes”,^[144] it is of equal importance that the compounds maintain an appropriate physico-chemical profile, similar to the parent clinical candidates. It is therefore essential to ensure that the designed compounds retain good cellular permeability and solubility to demonstrate their utility as efficient chemical probes. Lastly, the design of these chemical probes will require convergent synthetic routes, ideally enabling late-stage functionalization and introduction of the TCO tag.

Here, the PI3K δ chemical probes meeting the aforementioned requirements will be progressed to the cellular imaging assay. Therefore, the chemical probes will have to undergo efficient IEDDA cycloaddition with tetrazine reporters to observe concentration-dependent fluorescence signals that would allow the visualization of the probe molecules subcellular localisation. If successful, this approach may help to better understand how the parent clinical candidates distribute in the lungs, and how the molecular properties of inhaled drug molecules influence their distribution in living systems.

The design of chemical probes derived from inhaled PI3K δ inhibitors relied on a structure-based approach in order to determine the optimal points of attachment and most suitable linkers to append the TCO tag on nemiralisib and GSK2292767. Indeed, it is essential that the tag only minimally impact binding of the chemical probes to the target in order to maintain good potency and selectivity, whilst also ensuring that the TCO remains accessible for IEDDA reaction with its cycloaddition partner.

2.1. Design of Chemical Probes Derived from Nemiralisib

Starting from the co-crystal structure of nemiralisib in the active site of PI3K δ , vectors projecting towards the solvent were identified and could be exploited for installation of the TCO tag in whilst avoiding steric clashes with the protein. These vectors are highlighted in red in Figure 18 below.

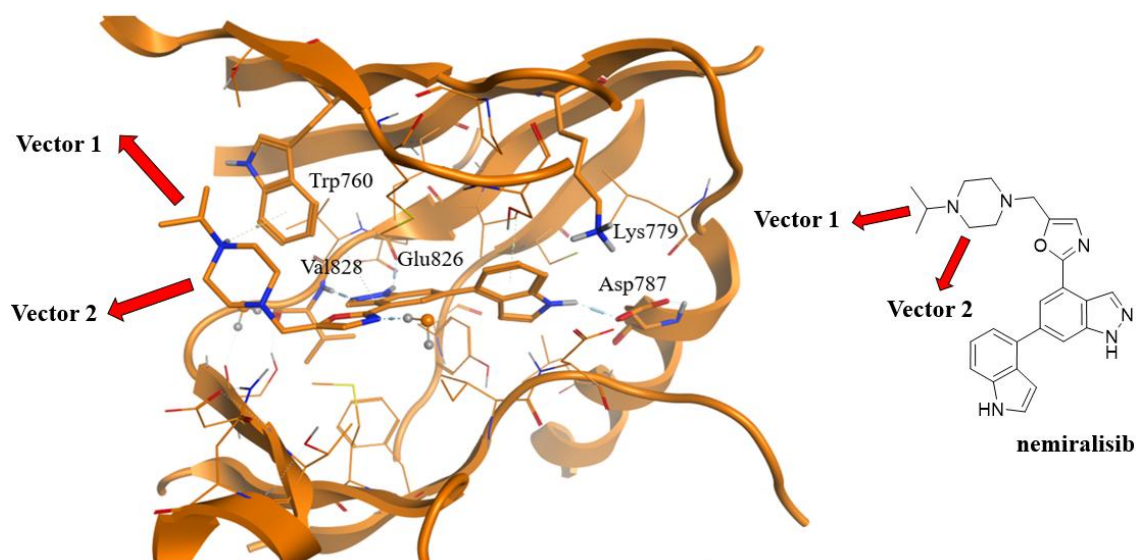


Figure 18. Co-crystal structure of nemiralisib with PI3K δ (PDB 8FVPT) highlighting potential vectors (in red) directing towards the solvent-exposed region.

The co-crystal structure of nemiralisib in the active site of PI3K δ highlighted two potential vectors that could be exploited to project the TCO tag towards the solvent-exposed region: (1) the *N*-isopropyl group on the piperazine and (2) the carbon adjacent to the *N*-isopropyl group on the piperazine. Therefore, the design of several

chemical probes based on the vectors 1 and 2 was initiated. The chemical probes designed from vector 1 are summarised in Figure 19 below.

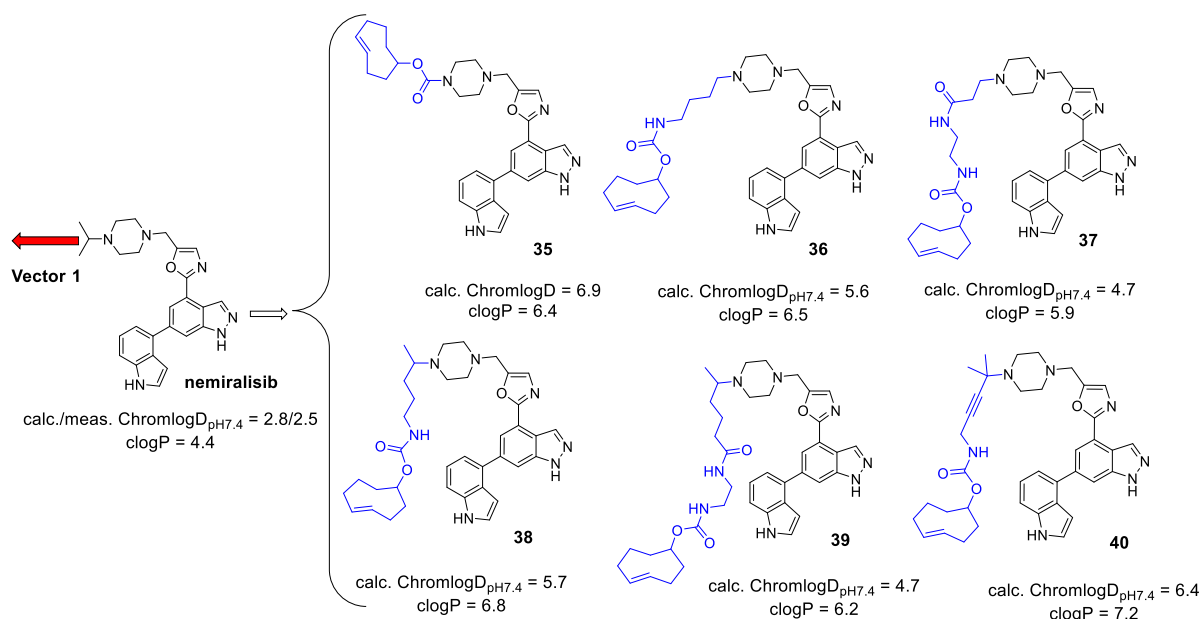


Figure 19. Designed chemical probes derived from nemiralisib, exploring the *N*-isopropyl vector (1) to install the TCO tag.

Within this set of chemical probes, compound **35**, where the *N*-isopropyl moiety on nemiralisib has been removed and the TCO tag is directly appended onto the piperazine via a carbamate group, was designed to assess whether the TCO tag is accommodated in the tryptophan shelf region in the PI3K δ active site. It is interesting to note that the introduction of the TCO group on compound **35** seems to impact significantly the lipophilicity of the molecule compared to nemiralisib, as observed by calculated ChromLogD_{pH7.4} and cLogP values (Figure 19). To balance the contribution of the TCO moiety to the overall lipophilicity of the designed molecules, it was postulated that the introduction of suitable linkers to connect the PI3K δ inhibitor to the TCO tag could help modulating the lipophilicity of the compounds. More specifically, this strategy would rely on the introduction of polar groups (*e.g.* hydrogen bonds donors and acceptors) within the linker to the TCO tag.

For the design of additional chemical probes focusing on vector 1, particular attention was given to the nature of the connective functionality between the nitrogen of the piperazine moiety and the linker to the TCO tag. Indeed, since the potency and selectivity of nemiralisib for PI3K δ is partly driven by a potential π -cation interaction between the lipophilic basic piperazine (predicted to be protonated at physiological pH) and Trp760,^[125] maintaining the basicity of the piperazine in the chemical probes may be essential. In addition, the basic amine of nemiralisib is assumed to play a key role in the lung retention mechanism of the compound, therefore ensuring that the basicity of the piperazine in the chemical probes is maintained may again be important when it comes to visualize the subcellular localisation of the compounds.

Compounds **36** and **37** were designed to assess the minimum linker length required to project the TCO tag into the solvent-exposed region, with compound **36** featuring a 4-carbon linker extending from the nitrogen of the piperazine and compound **37** containing a longer linker with a secondary amide which could reduce the lipophilicity of the molecule (calculated ChromlogD_{pH7.4} = 4.7, Figure 19).

Compounds **38** and **39** were designed to better mimic the isopropyl group of nemiralisib, where the introduction of a methyl group on the linker could potentially make additional hydrophobic interactions in the tryptophan shelf, therefore potentially improving the selectivity of the probes for PI3K δ over other isoforms. Similarly to **36** and **37**, a different linker size was explored to assess the minimum length required to project the TCO tag into the solvent region.

Compound **40** was designed to feature a *gem*-dimethyl moiety, thereby increasing the steric bulk near the tryptophan shelf further. The rationale behind the design of this compound came from the observation that the *tert*-butyl piperazine analogue of nemiralisib remains a very potent and selective PI3K δ inhibitor, reinforcing the fact steric hindrance and hydrophobicity is tolerated in this region of the active site. In compound **40**, the rigid alkyne linker, may also force the remainder of the linker and TCO tag to point towards the solvent-exposed region.

Chemical probes focusing on the carbon adjacent to the *N*-isopropyl group on the piperazine (vector 2) as a potential point of attachment for the TCO tag were also investigated (Figure 20).

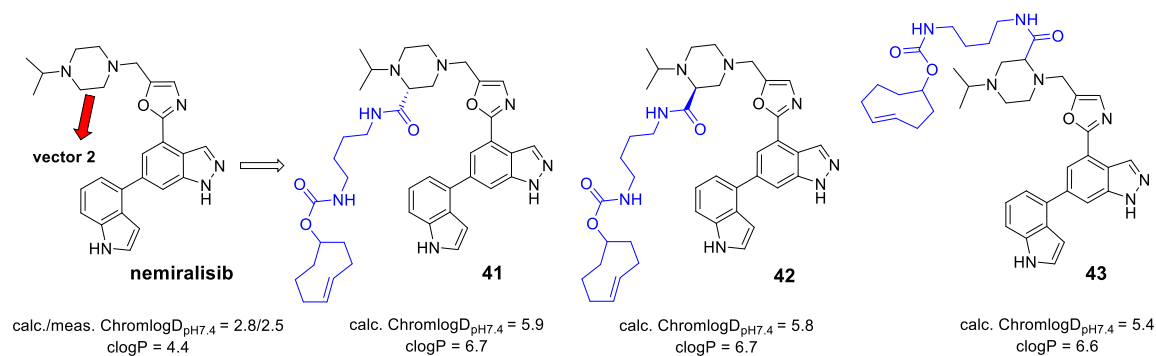


Figure 20. Chemical probes derived from nemiralisib, exploring the carbon adjacent to the *N*-isopropyl group on the piperazine to install the TCO tag (vector 2).

Compounds **41** and **42** contain a chiral piperazine moiety along with an amide group as part as a short carbon linker to the TCO tag. Compound **43**, where the linker is appended to the adjacent carbon on the piperazine was designed as a control to evaluate whether this vector does not extend to the solvent region. These three compounds were initially designed with an amide linker from the piperazine to the TCO tag because of the synthetic tractability of the approach to access the desired molecules, and therefore investigate the suitability of vector 2 as a point of attachment for the TCO tag. However, the amide linker may impact the basicity of the piperazine, and therefore could affect the behaviour of the compounds in a cellular environment which might not be completely representative of the parent compound. Providing that this vector is tolerated to install the TCO tag, additional linkers would then be investigated to maintain the basicity of the piperazine.

2.2. Design of Chemical Probes Derived from GSK2292767

In order to design chemical probes derived from the inhaled clinical candidate GSK2292767, the strategy for installation of the TCO tag focused on the sulfonamide as a point of attachment (Figure 21). The co-crystal structure of GSK2292767 with PI3K δ indicated that this vector may provide access to a solvent-exposed region, and various analogues synthesized in our laboratory showed that larger groups were tolerated at this position.^[141] Similarly to chemical probes derived from nemiralisib, the strategy was to optimize the linker to the TCO tag in order to minimize the lipophilicity of the molecules (Figure 21). Compounds **44** and **45** feature different linker sizes to assess the minimum length required to project the TCO tag into the solvent-exposed region.

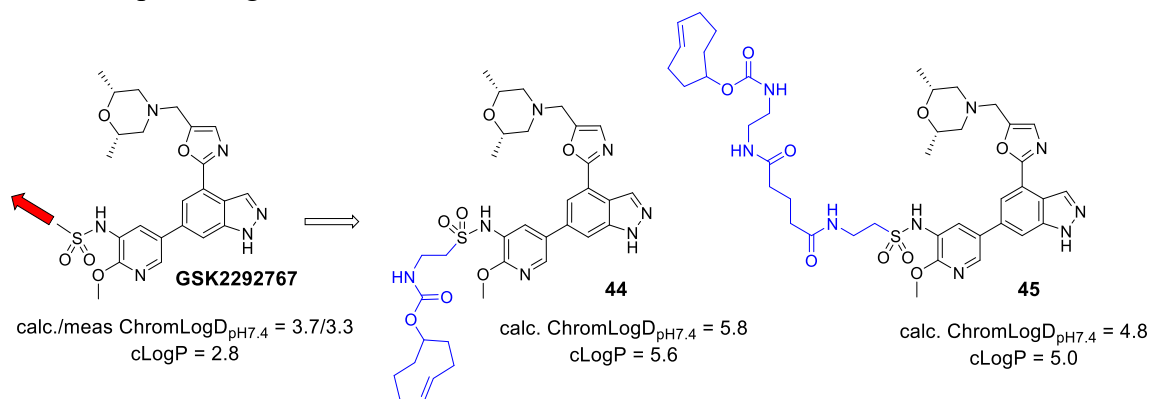


Figure 21. Chemical probes derived from GSK2292767, exploring the sulfonamide vector to install the TCO tag.

3. Results and discussion

Nemiralisib and GSK2292767 share a common indazole-oxazole core but differ by the oxazole-linked pendant amine group and the indazole-linked heterocyclic back-pocket substituent. Therefore, the design of a suitable common intermediate was particularly attractive since it would enable to access chemical probes derived from both inhaled clinical candidates. Retrosynthetic analysis identified novel aldehyde **46** as a promising common intermediate (Figure 22). Indeed, indazole derivative **46** contains an oxazole-linked aldehyde reactive group which would allow the introduction of various functionalised piperazine monomers or *cis*-dimethyl morpholine *via* reductive amination to access chemical probes derived from nemiralisib and GSK2292767, respectively. In addition, the common intermediate **46** features a 6-chloro indazole handle that could be used for the construction of the biaryl bond *via* palladium-catalyzed cross-coupling with functionalized indoles or pyridine-sulfonamides to access chemical probes derived from nemiralisib and GSK2292767, respectively.

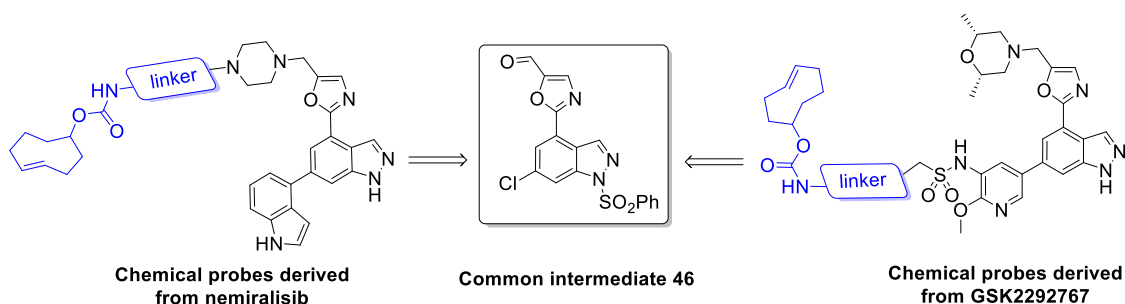
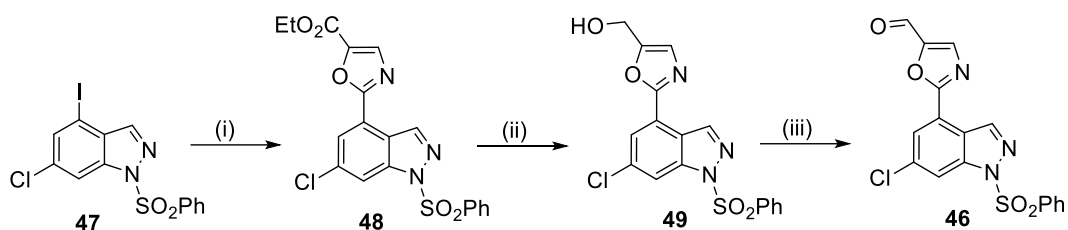


Figure 22. Common intermediate approach for the design of chemical probes derived from nemiralisib and GSK2292767.

The first step in assessing the viability of this approach involved the preparation of the key intermediate **46** (Scheme 10). The synthesis commenced with the benzenesulfonyl protected 6-chloro-4-iodoindazole precursor **47**, available in large quantities in our laboratory.^[145]



Reagents and conditions: (i) ethyl oxazole-5-carboxylate, 1.9 M ZnCl_2 in 2-MeTHF, 1 M LiHMDS in THF, THF, $-10\text{ }^\circ\text{C}$, 1 h; then 6-chloro-4-iodo-1-(phenylsulfonyl)-1*H*-indazole, $\text{Pd}(\text{PPh}_3)_4$ (3 mol%), THF, $60\text{ }^\circ\text{C}$, overnight, 98%; (ii) 1 M DIBAL-H in THF, THF, $0\text{ }^\circ\text{C}$, 3 h, 96%; (iii) DMP, DCM, $0\text{ }^\circ\text{C}$ to rt, 2 h, 73%.

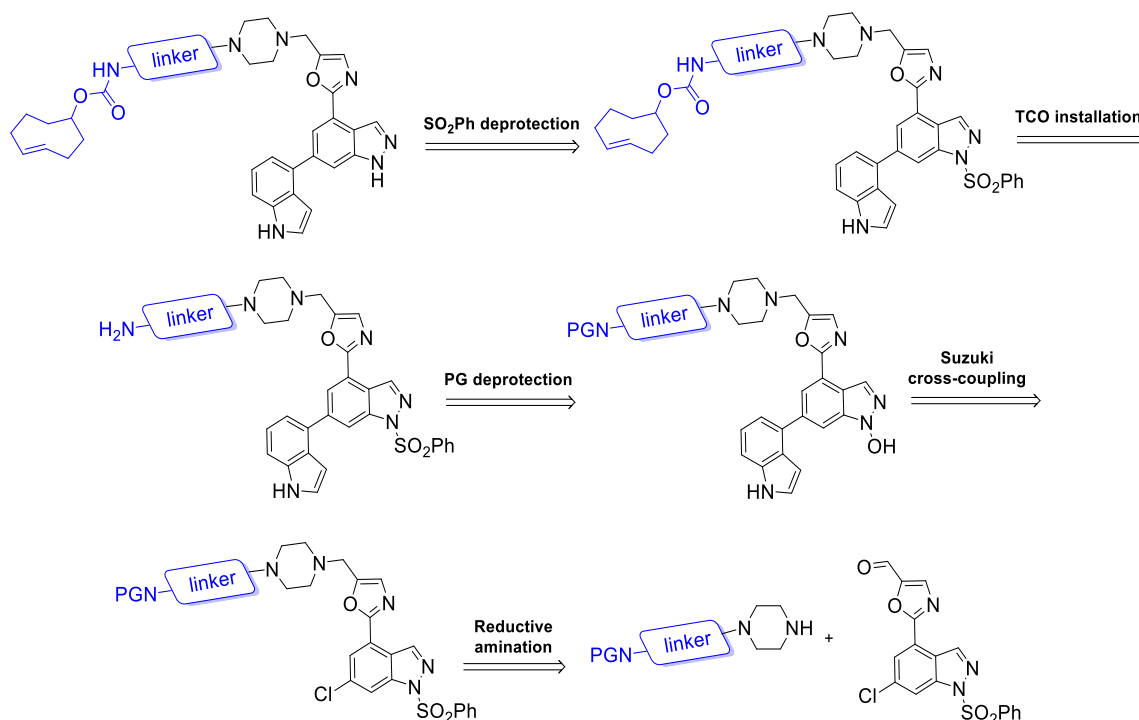
Scheme 9. Synthesis of common intermediate **46**.

The synthesis of compound **48** had been previously reported in our laboratory whereby the indazole-oxazole linkage was formed *via* a Negishi coupling.^[146] Here, ethyl oxazole-5-carboxylate was initially reacted with LiHMDS and ZnCl_2 to form the corresponding organozinc reagent *in situ*. A commercially available 1.9 M anhydrous solution of ZnCl_2 in 2-MeTHF was used in this first step to avoid the use of hygroscopic ZnCl_2 solid, where any trace of moisture could be detrimental to the stability of the organozinc reagent. Using a concentrated solution of ZnCl_2 was also beneficial to lower volumes when this reaction was performed on larger scale (up to 8 g). A homogenous mixture of THF and 2-MeTHF did not seem to impact to reaction. The organozinc reagent generated *in situ* then coupled selectively with the iodine on indazole **47** to afford the desired cross-coupling product **48** in 98% yield. This is in agreement with aryl iodides undergoing oxidative addition more easily than aryl chlorides, which correlates with the relative bond strengths of the C-X bond.^[147] Next, the ethyl ester group on **48** was reduced to the corresponding alcohol **49** with DIBAL-H. Subsequent oxidation mediated by Dess-Martin periodinane afforded the desired aldehyde **46** in a robust and high-yielding 3 step sequence.

With aldehyde **46** in hand, the syntheses of the different chemical probes derived from nemiralisib and GSK2292767 were initiated.

3.1. Synthesis of Chemical Probes Derived from Nemiralisib

The syntheses of chemical probes derived from nemiralisib commenced with the compounds exploring the *N*-isopropyl group on the piperazine (vector 1) as a point of attachment for the TCO tag. The retrosynthetic strategy depicted in Scheme 10 was considered to access these compounds.

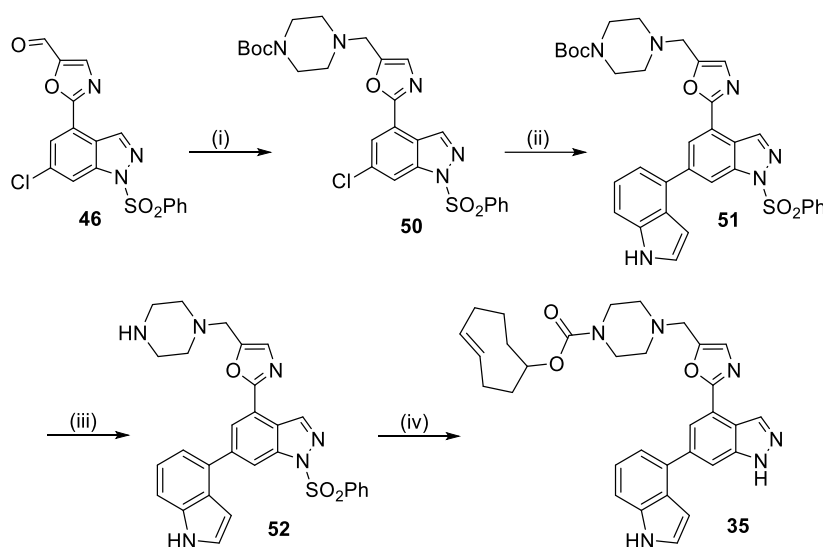


Scheme 10. Retrosynthetic analysis of chemical probes derived from nemiralisib (vector 1).

This retrosynthesis approach relied on the key reductive amination step between novel aldehyde **59** and various functionalised piperazine monomers. Following the reductive amination reaction, a linear sequence of 4 steps was designed to access the desired TCO chemical probes. This involved a Suzuki cross-coupling to install the indole moiety, followed by deprotection of the amino protecting group (PG). In most instances, the selected amino protecting group is phthalimide due to its orthogonality with the benzene sulfonyl protecting group on the indazole, its ease of deprotection with hydrazine, as well as the fact that it has a chromophore to allow for

more facile analysis of the piperazine monomers. In some instances, a Boc protecting group was also chosen due to starting reagent availability. Protecting group removal would then reveal a primary amine to enable late-stage installation of the TCO tag. Finally, removal of the indazole benzene sulfonyl protecting group would yield the desired chemical probes.

The synthesis of the first chemical probe **40** where the TCO tag is directly attached to the piperazine is outlined in Scheme 11 below.



Reagents and conditions: (i) Boc-piperazine, AcOH, DCM, rt, 30 min then STAB, rt, 1 h, 78%; (ii) Indole-4-boronic acid pinacol ester, XPhos Pd G2 (10 mol%), Na₂CO₃, 1,4-dioxane/water (4:1), 90 °C, μ wave, 70 min, 65%; (iii) TFA, DCM, rt, 3 h, 95%; (iv) (*E*)-cyclooct-4-en-1-yl (4-nitrophenyl) carbonate (TCO-PNB ester), DIPEA, DMF, rt, 2h, used crude; then 2 M aq. NaOH, IPA, rt, 30 min, 11% over 2 steps.

Scheme 11. Synthesis of chemical probe **35**.

The synthesis starting with a reductive amination reaction between aldehyde **46** and Boc-piperazine to afford intermediate **50**. Subsequent Suzuki cross-coupling with indole-4-boronic acid pinacol ester mediated by XPhos Pd G2 afforded **51** in 65% yield.

It is well established in palladium-catalysed reactions that aryl chlorides are more challenging substrates to cross-couple in comparison with aryl iodides or aryl bromides due to the high C-Cl bond dissociation energy.^[148] Consequently, aryl

chlorides are intrinsically more reluctant to undergo oxidative addition, the first step of the catalytic cycle in the Suzuki cross-coupling reaction. To overcome this issue, several types of catalyst systems exhibiting higher reactivity were developed and often rely on the introduction of electron-rich phosphine ligands. This was exemplified by Hartwig and co-workers who developed the second-generation pre-catalyst XPhos Pd G2 (Figure 23) that has shown to improve the reactivity of aryl chlorides substrates in palladium-catalysed cross-coupling reactions.^[149]

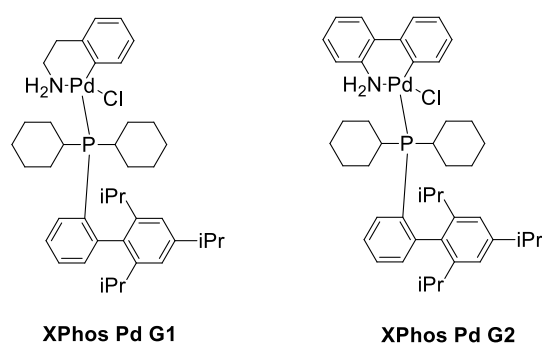


Figure 23. Structure of XPhos Pd pre-catalysts.

The XPhos Pd reagents are classified as pre-catalysts because they readily generate the catalytically active XPhosPd(0) species upon exposure to a base, along with the corresponding indoline or carbazole *via* C-N reductive elimination.^[150] In addition, the enhanced reactivity of XPhos Pd pre-catalysts towards oxidative addition of aryl chloride substrates also arises from the structure of the XPhos ancillary ligand itself. Indeed, the architecture of XPhos and other related dialkyl biaryl monophosphine ligands has been carefully engineered by the choice of suitable substituents that can modulate the reactivity of key steps involved in the catalytic cycle.^[151] For example, the cyclohexyl groups on the phosphorus atom increase the electron density on the palladium centre, thereby facilitating the oxidative addition step. According to Hartwig, the activation of XPhos Pd G1 with weak bases suffered from low reaction rates and required elevated temperatures. A solution was found whereby replacing the aliphatic amine of XPhos Pd G1 by the more acidic 2-aminobiphenyl moiety of XPhos Pd G2 allowed the activation to occur almost instantaneous with weak bases at room temperature.^[149]

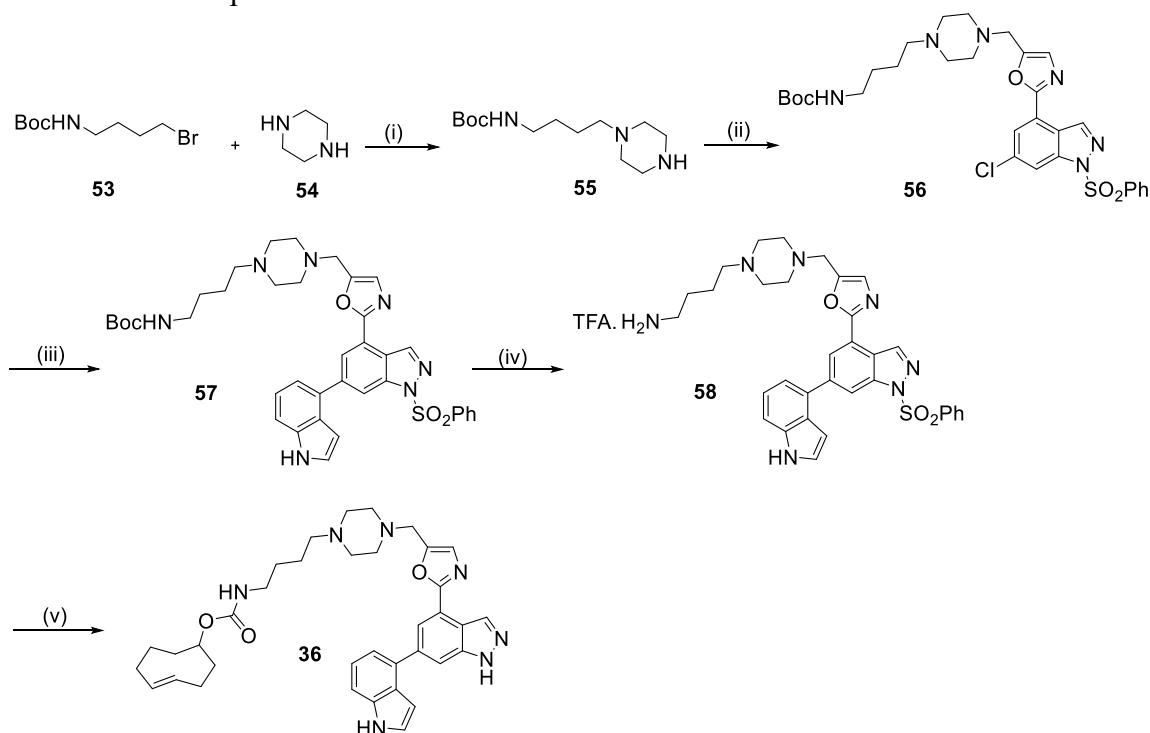
Following the Suzuki coupling, Boc deprotection of compound **51** was successfully carried out with trifluoroacetic acid to afford **52** as a crude material. The latter was then reacted with the commercially available (*E*)-cyclooct-4-en-1-yl-(4-nitrophenyl) carbonate TCO derivative and diisopropylethylamine in DMF to afford the desired carbamate. This intermediate was isolated crude and immediately taken forward in the last step, involving the deprotection of the benzylsulfonyl protecting group under aqueous basic conditions to eventually afford the desired TCO-tagged chemical probe **35**.

The *trans* stereochemistry of the cyclooctene was initially assessed by ¹H NMR. Even though the alkene proton signals appearing as doublet of doublet of doublets (ddd) overlap due to their similar environment within the cyclooctene ring, a coupling constant of 16 Hz that is consistent with a *trans* relationship could be observed. To further confirm the *trans* stereochemistry of the cyclooctene, a model IEDDA cycloaddition with 3,6-dipyridyl-1,2,4,5-tetrazine was conducted by spiking a DMSO solution of the tetrazine reagent to the LCMS vial containing the TCO probe. Upon mixing of the two reagents, the characteristic red-pink purple colour of the tetrazine instantaneously disappeared to give a colourless solution. LCMS analysis revealed the formation of a product whose mass was consistent with the expected ligation product, therefore confirming the integrity of the *trans*-cyclooctene in compound **35**.

In addition, an interesting observation was made when compound **35** was initially purified by mass directed auto preparative HPLC (MDAP) with a water/acetonitrile method containing a formic acid modifier (pH 2-3). These purification conditions resulted in the formation of a second peak on LCMS with the same *m/z*. These observations potentially suggested partial isomerization from the *trans*- to a *cis*-cyclooctene isomer under aqueous acidic conditions. Isolation and NMR analysis of the mixed fractions revealed that the main component was consistent with the desired *trans* isomer. The minor component appeared to have smaller couplings in the alkene multiplets, indicative that it may be a *cis* isomer, however any conclusions remained tentative. As a precaution, all the future chemical probes containing the

trans-cyclooctene group were purified by reverse phase methods with basic modifiers to preserve the integrity of the TCO.

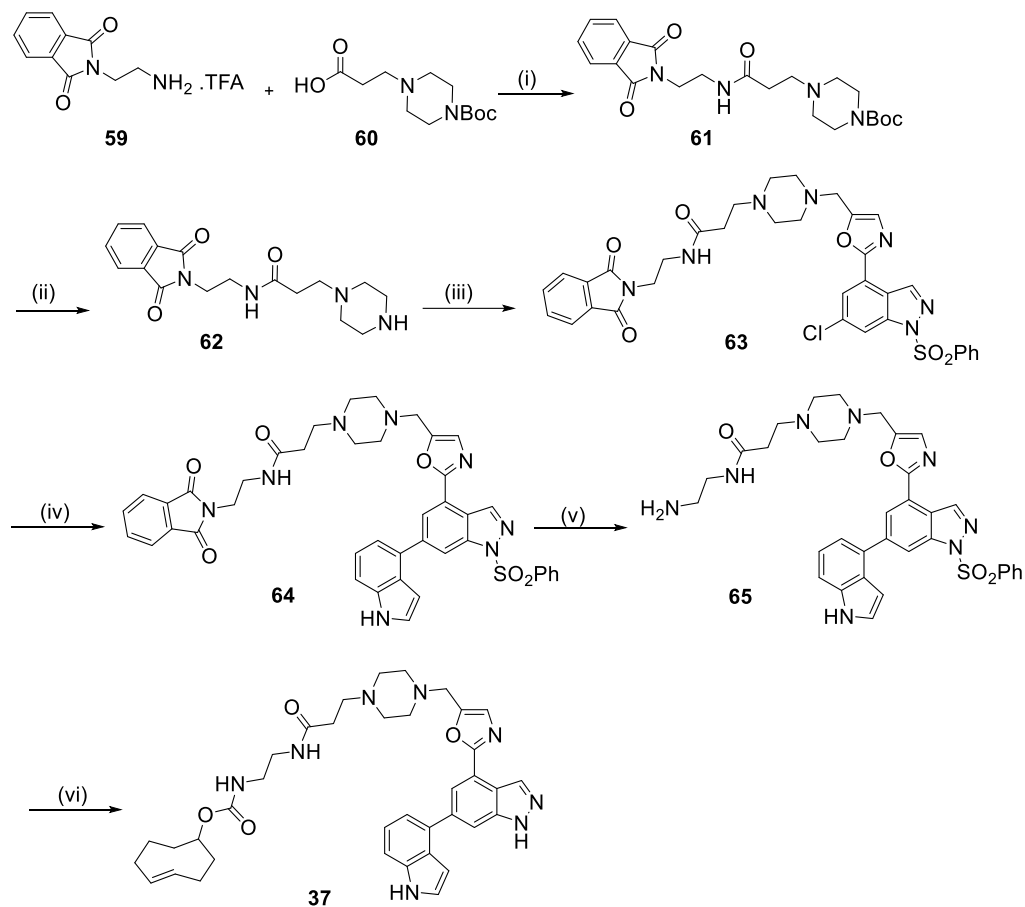
The synthesis of compound **36** containing a short alkyl linker to the TCO tag was initiated (Scheme 13). The synthesis started starting with mono alkylation of piperazine with alkyl bromide **53** to give the key monomer **55**. Subsequent reductive amination with aldehyde **46** gave the desired aryl chloride intermediate **56** that was reacted in a Suzuki reaction to give the corresponding cross-coupled product **57**. Subsequent Boc deprotection revealed the primary amine **58**, which was reacted with TCO-PNB ester to give, after cleavage of the benzenesulfonyl protecting group, the desired chemical probe **36**.



Reagents and conditions: (i) K_2CO_3 , MeCN, rt, 48 h 61%; (ii) **46**, AcOH, DCM, rt, 30 min then STAB, DCM, 1 h, 79%; (iii) indole-4-boronic acid pinacol ester, XPhos Pd G2 (20 mol%), Na_2CO_3 , 1,4-dioxane:water (9:1), 90 °C, μ wave, 1.5 h, 73%; (iv) TFA, DCM, rt, 1.5 h, used crude; (v) TCO-PNB ester, DIPEA, DMF, rt, 1 h, then 1 M aq. NaOH, MeOH, rt, 30 min, 21% over 3 steps.

Scheme 12. Synthesis of chemical probe **36**.

The synthesis of compound **37** featuring a longer linker to the TCO tag is outlined in Scheme 14.



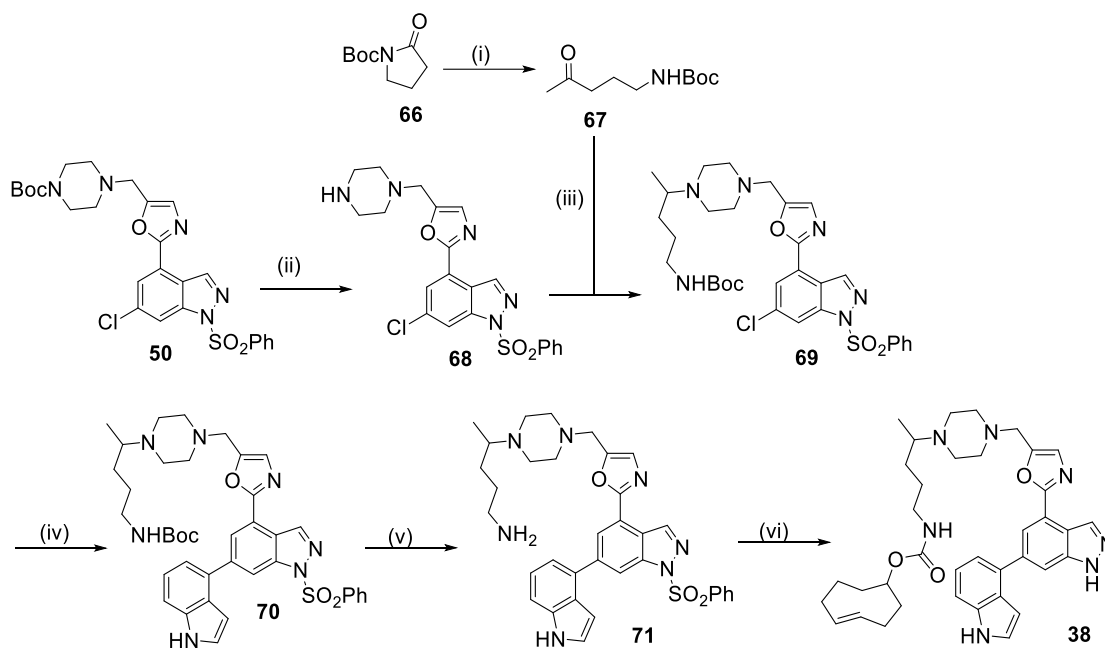
Reagents and conditions: (i) HATU, DIPEA, DCM, rt, overnight, 78%; (ii) TFA, DCM, rt, overnight, used crude; (iii) **46**, AcOH, THF, rt 1 h, then STAB, rt, 2 h, 58%; (iv) 4-Indoleboronic acid pinacol ester, XPhos Pd G2 (10 mol%), Na₂CO₃, 1,4-Dioxane/H₂O (10:1), μ wave, 90 °C, 1 h, 71%; (v) N₂H₄·H₂O, THF, 50 °C, 5.5 h; used crude; (vi) TCO-PNB ester, DIPEA, DMF, rt, 5 h, then 2 M aq NaOH, MeOH, rt, 30 min, 19% after 3 steps.

Scheme 13. Synthesis of chemical probe **37**.

The synthesis started from the commercially available piperazine monomer **60** which underwent amide coupling with the phthalimide-protected ethylene diamine derivative **59** to give the desired intermediate **61**. Subsequent Boc deprotection afforded the key piperazine monomer **62** which underwent reductive amination with aldehyde **46** to give the desired aryl chloride intermediate **63**. Next, compound **63** was subjected to a Suzuki reaction to give the corresponding cross-coupled product **64**.

Subsequent phthalimide deprotection with hydrazine monohydrate revealed the primary amine **65**, which was reacted with TCO-PNB ester to give, after cleavage of the benzene sulfonyl protecting group, the desired chemical probe **37** (Scheme 13).

The synthesis of chemical probe **38** relied on a slightly different approach and involved the key reductive amination reaction between ketone **67** and piperazine derivative **68** (Scheme 14).



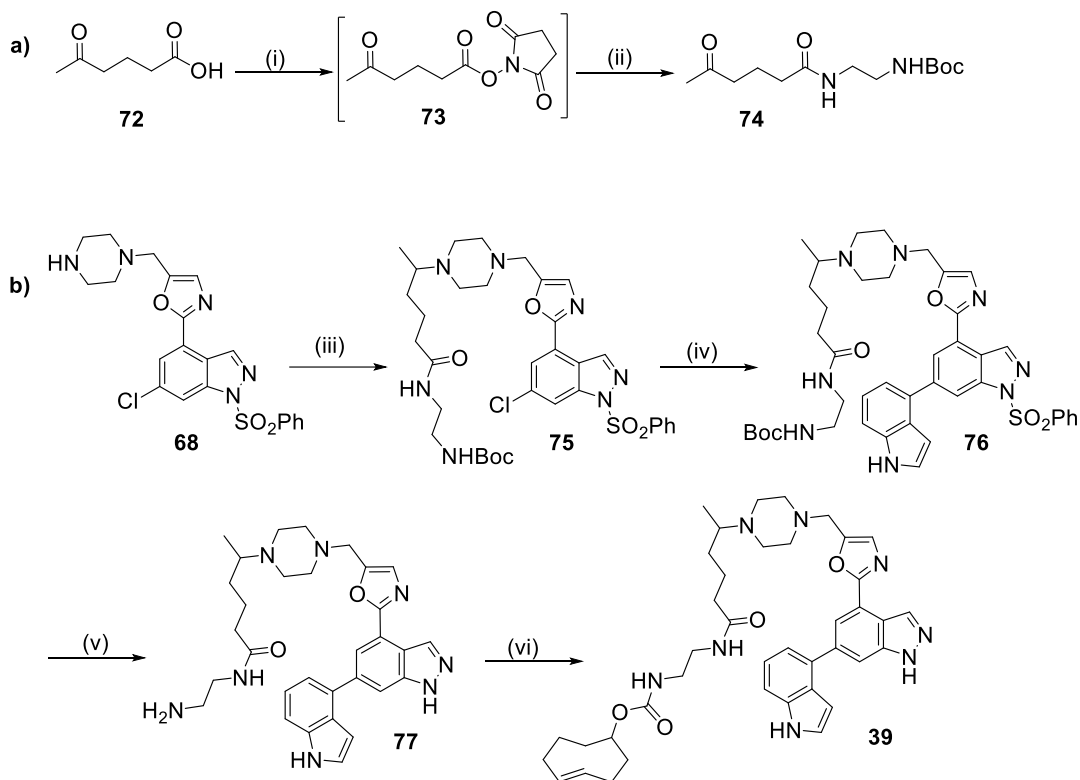
Reagents and conditions: (i) MeMgBr 3 M in Et₂O, THF, 0 °C to rt, overnight, 68%; (ii) TFA, DCM, rt, 2 h, 97%; (iii) AcOH, THF, 45 °C, overnight, then STAB, THF, 45 °C, 2 h, 31%; (iv) indole-4-boronic acid pinacol ester, XPhos Pd G2 (10 mol%), Na₂CO₃, 1,4-Dioxane/H₂O (8:1), μ wave, 90 °C, 1 h, 73%; (v) TFA, DCM, rt, 1.5 h, used crude; (vi) TCO-PNB ester, DIPEA, DMF, rt, 1 h, then 2 M aq NaOH, MeOH, rt, 20 min, 9% over 3 steps.

Scheme 14. Synthesis of chemical probe **38**.

The synthesis of the ketone **67** was conducted in one step from the commercially available *N*-Boc oxopyrrolidine **66** which, upon treatment with methylmagnesium bromide, gave the desired ring-opened ketone. Intermediate **68** was synthesised in one step and involved a Boc deprotection from intermediate **50** previously described for the synthesis of chemical probe **35**. With the two intermediates in hand, ketone **67** and compound **68** were then reacted in a reductive amination step. The transformation proved to be slow, potentially due to steric reasons

rendering the formation of the intermediate iminium species challenging. Indeed, ketones are known to be less reactive substrates compared to aldehydes in reductive amination reactions.^[152] An excess of ketone was used and acetic acid was added in THF at 50 °C to catalyse the formation of the iminium species prior to adding sodium triacetoxyborohydride as the reducing agent. The reaction was monitored by LCMS and worked up at 50% conversion and the desired product was isolated in order to pursue the rest of the synthesis. The aryl chloride **69** was then reacted in a Suzuki coupling to give the biaryl intermediate **70**. Next, Boc deprotection afforded the primary amine **71**, which was subsequently reacted with TCO-PNB ester to give, after benzenesulfonyl deprotection, the desired probe **38**.

The synthesis of the chemical probe **39** was carried out using a very similar approach to chemical probe **38**, relying on a reductive amination between the functionalised ketone **80** and piperazine derivative **57** as key step (Scheme 15).



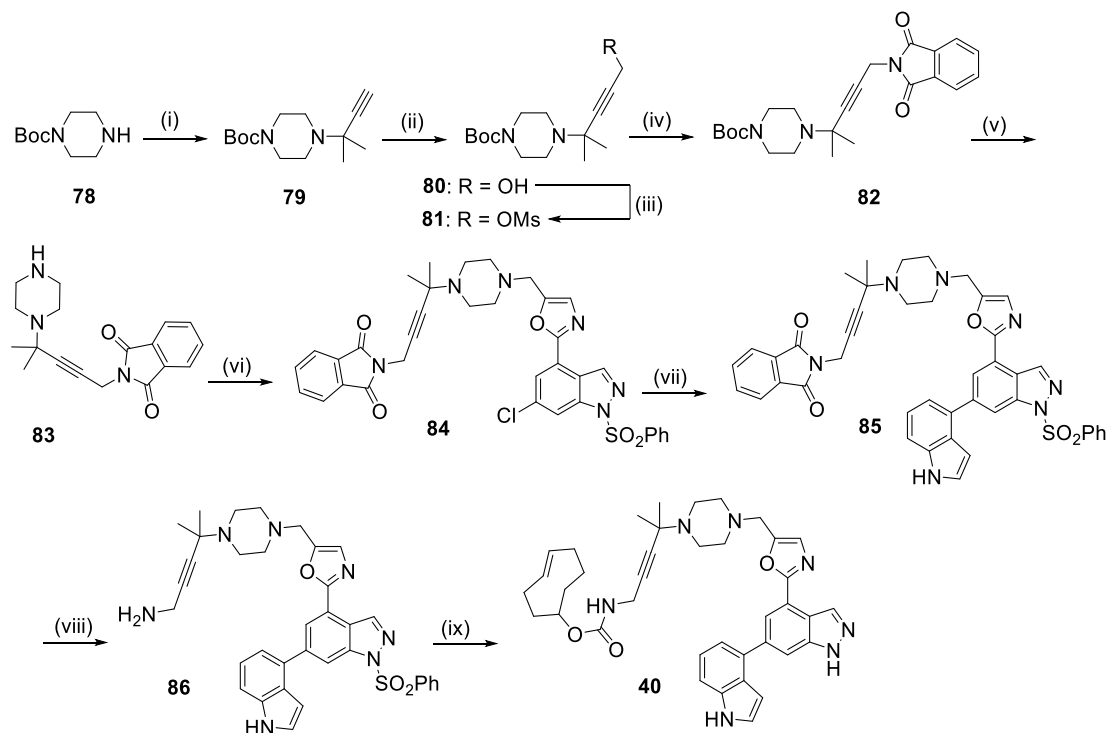
Reagents and conditions: (i) *N,N*-Disuccinimidyl carbonate, Et₃N, DCM, rt, overnight; not isolated (ii) *N*-Boc ethylene diamine, DCM, rt, 3 h, 87%; (iii) **74**, AcOH, THF, 40 °C, 2 h then STAB, 40 °C, 18 h, 55%; (iv) Indole-4-boronic acid pinacol ester, XPhos Pd G2 (30 mol%), Na₂CO₃, 1,4-Dioxane/H₂O (6:1), μ wave, 90 °C, 1.5 h, 63%; (v) TFA, DCM, rt, 1 h, used crude; (vi) TCO-PNB ester, DIPEA, DMF, rt, 1.5 h, then 2 M aq. NaOH, MeOH, rt, 1 h, 9% over 3 steps.

Scheme 15. Synthesis of chemical probe **39**.

The synthesis started from commercially available 4-acetylbutyric acid **72** which was converted to the corresponding activated succinimidyl ester **73** (not isolated) prior to reaction with *N*-Boc ethylene diamine to give the desired ketone **74**. The subsequent key reductive amination reaction with piperazine derivative **68** was slow, even in presence of an excess of ketone, with conversion by LCMS reaching a maximum around 60%. The reaction was stopped and the desired product **75** was isolated in order to pursue the rest of the synthesis. Aryl chloride **75** was then reacted in a Suzuki coupling to afford the biaryl intermediate **76**, which then gave primary amine **77** after subsequent Boc deprotection with TFA. However, isolation of **83** proved to be troublesome as quenching residual TFA with sodium bicarbonate led to

the formation of a solid and several attempts to extract the desired product were unsuccessful as the product remained in the aqueous layer. The aqueous phase was eventually lyophilized and the resulting solid, which contained remaining inorganic impurities, was used crude into the next step to install the TCO tag. Final benzene sulfonyl deprotection gave the desired probe **39** (Scheme 15).

Lastly, the synthesis of chemical probe **40** containing a gem-dimethyl group is depicted in Scheme 16 below.



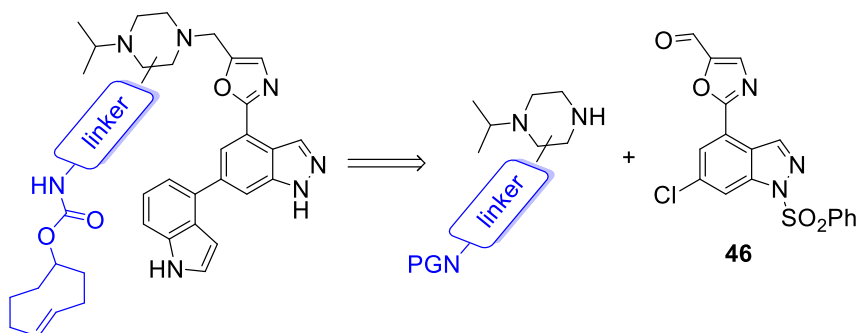
Reagents and conditions: (i) Copper(I) chloride, 3-chloro-3-methyl-1-butyne, Et₃N, THF, rt, 2 h, 71%; (ii) 2 M LDA in THF/hexane, THF, -78 °C, 1 h then paraformaldehyde, THF, -78 °C to rt, overnight, 76%; (iii) Methane sulfonic anhydride, Et₃N, DCM, 0 °C, 2 h, 91%; (iv) Potassium phthalimide salt, DMF, 70 °C, overnight, 57%; (v) TFA, DCM, 3 h, rt, used crude; (vi) **46**, AcOH, STAB, rt, 48 h, 66%; (vii) Indole-4-boronic acid pinacol ester, XPhos Pd G2 (20 mol%), Na₂CO₃, 1,4-Dioxane/H₂O (10:1), μ wave, 90 °C, 1.5 h, 65%; (viii) N₂H₄·H₂O, THF, 45 °C, 5 h then rt overnight, used crude; (ix) TCO-PNB ester, DIPEA, DMF, rt, 1 h, then 1 M aq. NaOH, MeOH, rt, 1 h, 11% over 3 steps.

Scheme 16. Synthesis of chemical probe **40**.

The synthesis commenced with the copper(I) chloride-catalysed alkylation of 1-Boc-piperazine **78** with 3-chloro-3-methyl-1-butyne, which gave the desired propargyl amine **79** according to a procedure described by Murahashi *et al.*^[153] Next,

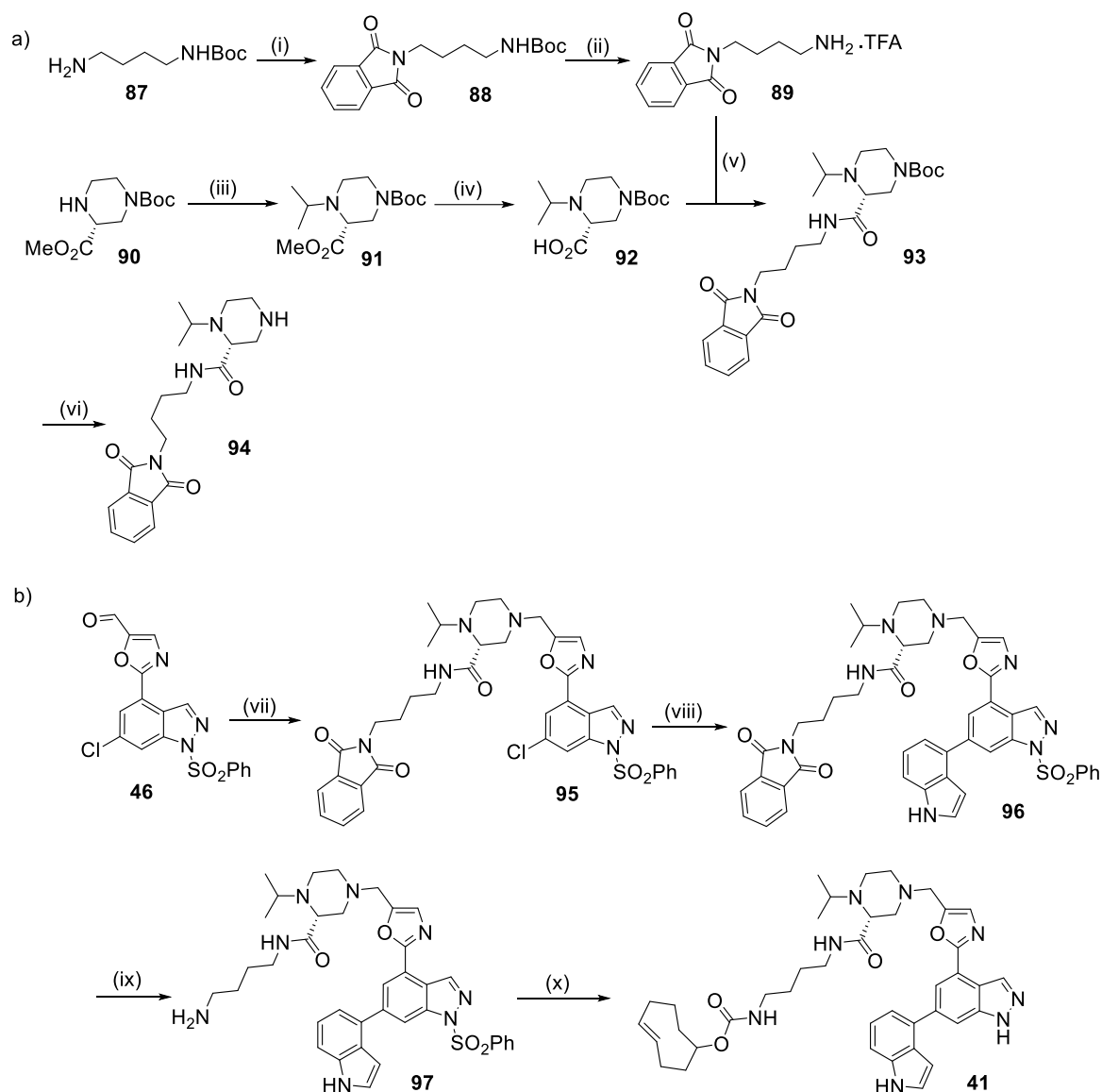
propargyl amine **79** was treated with lithium diisopropylamide (LDA), a strong non-nucleophilic organic base, for deprotonation of the acetylenic proton and *in situ* generation of a lithium acetylide species. Subsequent trapping of the acetylide with paraformaldehyde afforded propargyl alcohol **80**. It was initially assumed that phthalimide-protected propargyl amine **82** could be accessed in one step from propargyl alcohol **80** under Mitsunobu conditions, however the reaction proceeded in poor yield and removal of triphenylphosphine related impurities proved to be challenging. Therefore, a two-step approach was followed whereby propargyl alcohol **80** was converted to mesylate **81**, which was subsequently displaced with potassium phthalimide salt to afford the desired propargyl phthalimide **82** in good yield. Next, compound **82** was treated with TFA to remove the Boc protecting group. Compound **83** started to degrade upon solvent removal on the rotary evaporator after work-up, therefore it was immediately taken forward into the subsequent reductive amination step with aldehyde **46** and this successfully afforded desired compound **84**. Aryl chloride **84** was then reacted in a Suzuki reaction to afford the cross-coupling intermediate **85**. Subsequent deprotection of the phthalimide group with hydrazine monohydrate revealed the primary amine **86** and this was immediately reacted with TCO-PNB ester which, after removal of the benzenesulfonyl protecting group, afforded the desired compound **40**.

The syntheses of the additional chemical probes **41**, **42** and **43** derived from nemiralisib that explore functionalisation from both piperazine carbons followed a similar retrosynthetic strategy and involved a key reductive amination between a functionalised piperazine monomer and aldehyde **46** (Scheme 17).



Scheme 17. Retrosynthesis analysis of chemical probes derived from nemiralisib focusing on piperazine carbons to install the TCO tag (PG = protecting group).

The synthesis of compound **41** is described below (Scheme 18).

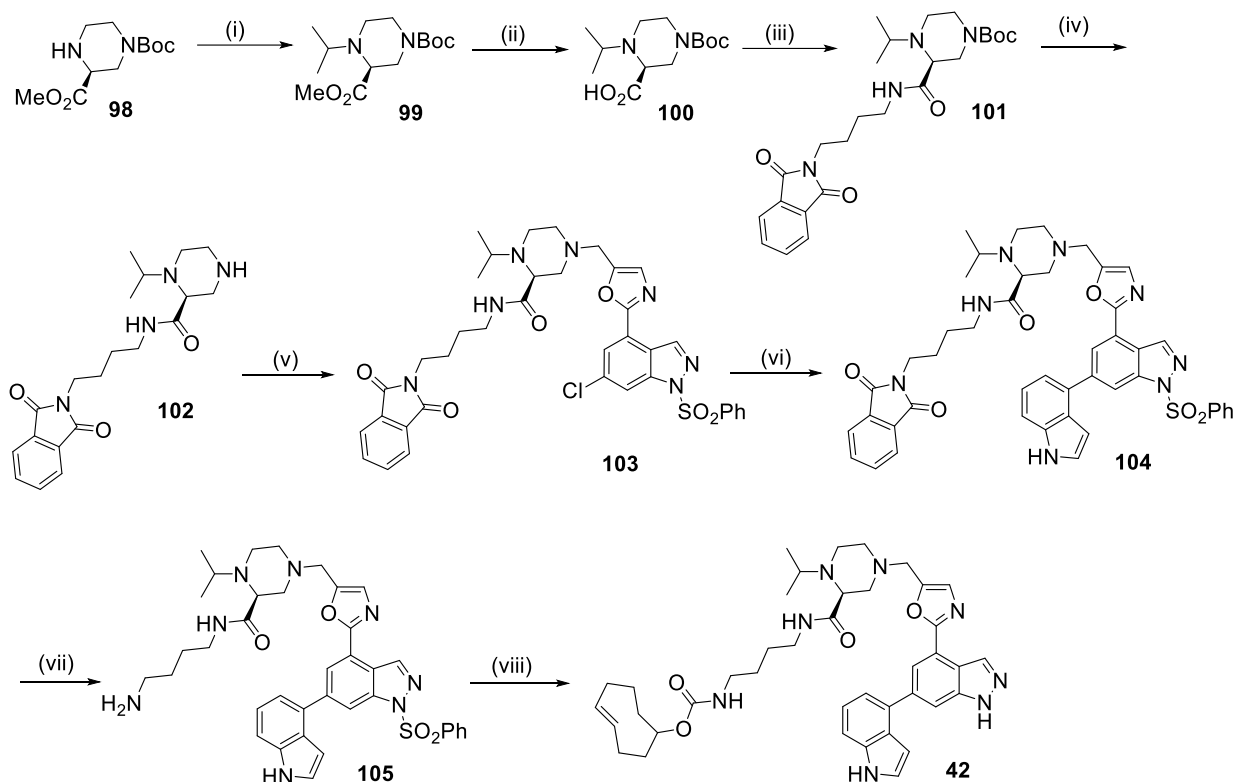


Reagents and conditions: a) (i) Phthalic anhydride, toluene, reflux, 3 h, 92%; (ii) TFA, DCM, rt, overnight, 98%; (iii) Acetone, AcOH, DCM, rt, 20 min then STAB, DCM, 48 h, 82%; (iv) 2 M aq NaOH, MeOH, 0 °C to rt, overnight, 64%; (v) HBTU, HOBt, DIPEA, DMF, rt overnight, 91%; (vi) TFA, DCM, rt, 3 h, 87%; used crude; b) vii) AcOH, DCM, rt, 30 min then STAB, DCM, overnight, 74%; (viii) Indole-4-boronic acid pinacol ester, XPhos Pd G2 (10 mol%), Na₂CO₃, 1,4-Dioxane/H₂O (8:1), μ wave, 90 °C, 1 h, 66%; (ix) N₂H₄·H₂O, THF, 40 °C, overnight; (x) TCO-PNB ester, DIPEA, DMF, 40 °C, 1.5 h, then 2 M aq NaOH, MeOH, rt, 30 min, 24% over 2 steps.

Scheme 18. Synthesis of chemical probe **41**.

The sequence started from the commercially available *N*-Boc protected chiral piperazine **90**, which was subjected to a reductive amination with acetone to install the isopropyl group and intermediate **91**. Next, hydrolysis of ester **91** gave the corresponding carboxylic acid **92**. Isolation of **92** was troublesome as the compound was water-soluble and could not be extracted after solvent removal and pH adjustment to 4-5 with an aqueous HCl solution. The issue was addressed by concentrating the aqueous under reduced pressure and lyophilising to afford a solid that was suspended in DCM and filtered to remove inorganic impurities. The carboxylic acid **92** was subsequently reacted with amine **89**, prepared in two steps from the commercially available amine **87**, in an amide coupling reaction to afford intermediate **93**. Subsequent Boc deprotection gave the key desired piperazine monomer **94**. The piperazine monomer **94** was then coupled to the indazole core in a reductive amination reaction with aldehyde **46** to give aryl chloride **95**. Subsequent Suzuki reaction with indole-4-boronic acid pinacol ester gave the biaryl intermediate **96**. Deprotection of the phthalimide protecting group with hydrazine hydrate afforded the amine **97** which was taken forward for reaction with TCO-PNB ester which gave, upon cleavage of the benzene sulfonyl protecting group, the desired TCO-labelled compound **41**.

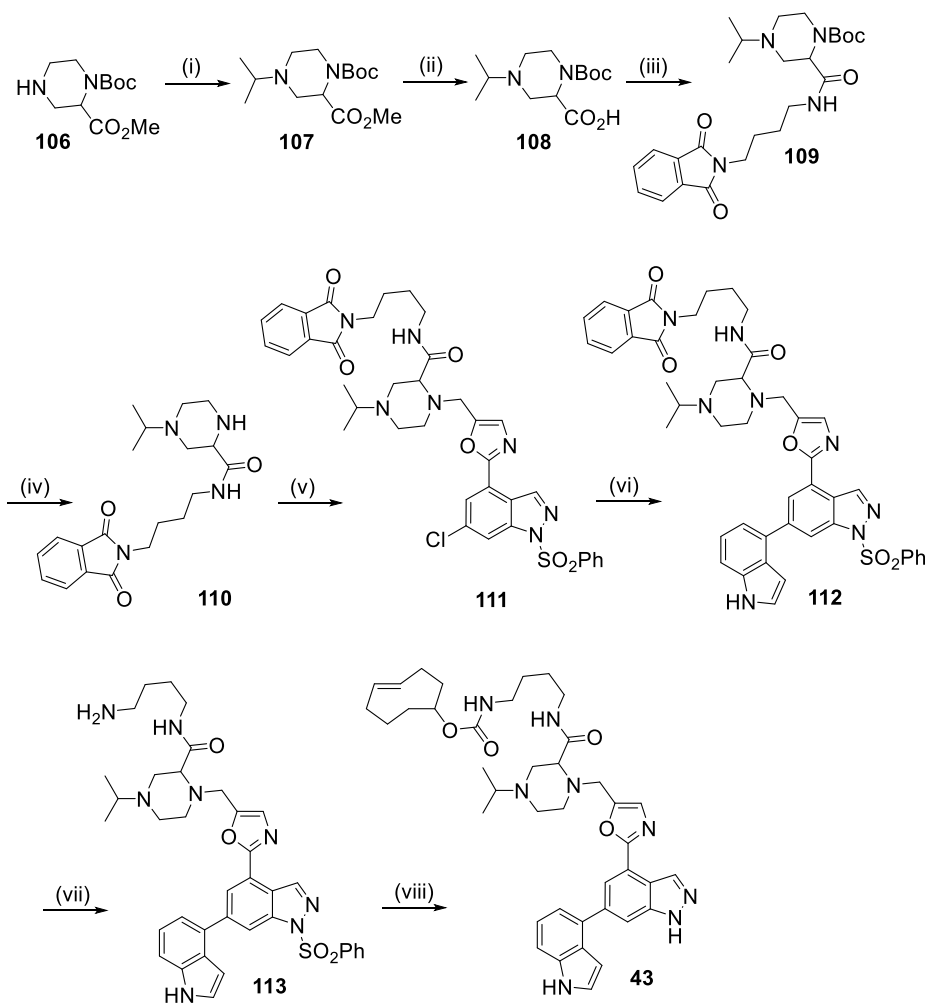
Compound **42** was prepared by an analogous synthetic route to compound **41** using commercially available piperazine monomer **98** with the opposite stereochemistry (Scheme 19).



Reagents and conditions: (i) Acetone, AcOH, DCM, rt, 20 min, then STAB, DCM, rt, overnight, 86%; (ii) 2 M aq NaOH, MeOH, 0 °C to rt, overnight, 83%; (iii) **89**, HBTU, DIPEA, DMF, rt overnight, 69%; (iv) TFA, DCM, rt, 2 h, 88%; (v) **46**, AcOH, DCM, rt, 30 min then STAB, rt, overnight, 23%; (vi) Indole-4-boronic acid pinacol ester, XPhos Pd G2 (2 mol%), Na₂CO₃, 1,4-Dioxane/H₂O (5:1), μ wave, 90 °C, 1 h, 66%; (vii) N₂H₄.H₂O, THF, 45 °C, overnight, used crude; (viii) TCO-PNB ester, DIPEA, DMF, rt, 1.5 h, then 1 M aq NaOH, MeOH, rt, 15 min, 9% over 3 steps.

Scheme 19. Synthesis of chemical probe **42**.

Finally, chemical probe **43** where the linker was appended to the adjacent carbon on the piperazine was synthesized from a racemic piperazine monomer using a similar sequence to the previous probes (Scheme 20).



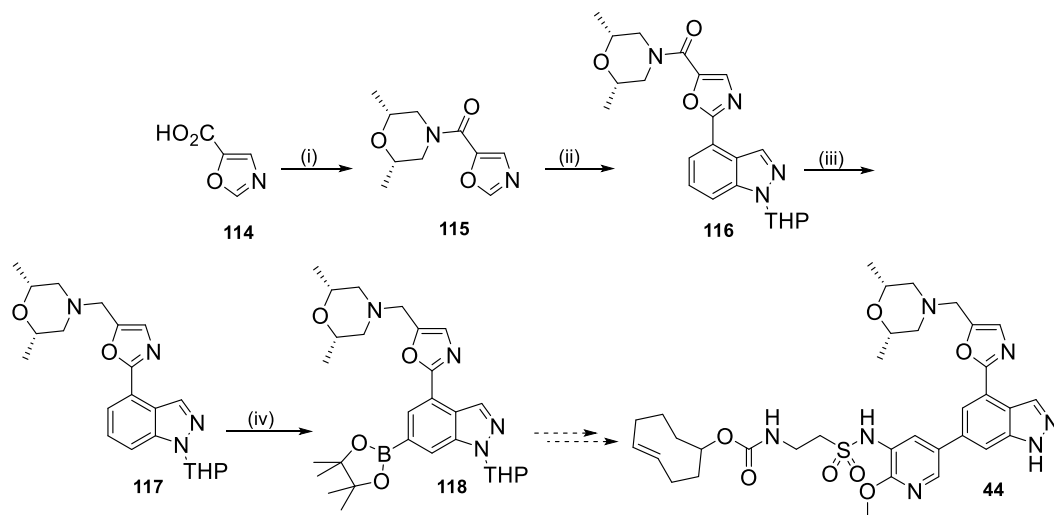
Reagents and conditions: (i) acetone, AcOH, DCM, rt, 30 min then STAB, rt, overnight, 96%; (ii) 2 M aq NaOH, MeOH, 0 °C to rt, overnight, used crude; (iii) **89**, HATU, HOBT, DIPEA, DMF, rt overnight, 70%; (iv) TFA, DCM, rt, 5 h, then 30 °C, 1 h, 99%, used crude; (v) **46**, AcOH, DCM, rt, 30 min then STAB, rt, 1 h, 54%; (vi) indole-4-boronic acid pinacol ester, XPhos Pd G2 (20 mol%), Na₂CO₃, 1,4-Dioxane/H₂O (5:1), μ wave, 90 °C, 1 h 15 min, 81%; (vii) N₂H₄·H₂O, THF, 55 °C, 18 h, 54%; (viii) TCO-PNB ester, DIPEA, DMF, rt, 1 h 45 min, then 2 M aq NaOH, MeOH, rt, 25 min, 39% after 2 steps.

Scheme 20. Synthesis of compound 43.

Having synthesized all of the desired chemical probes derived from nemiralisib, the synthetic effort was then focused on the preparation of chemical probes derived from the second inhaled clinical candidate GSK2292767.

3.2. Synthesis of Chemical Probes derived from GSK2292767

The synthesis of compound **44** was initially investigated following the sequence depicted in Scheme 21, which is inspired from the process route developed elsewhere in our laboratories for the large scale synthesis of the clinical candidate.



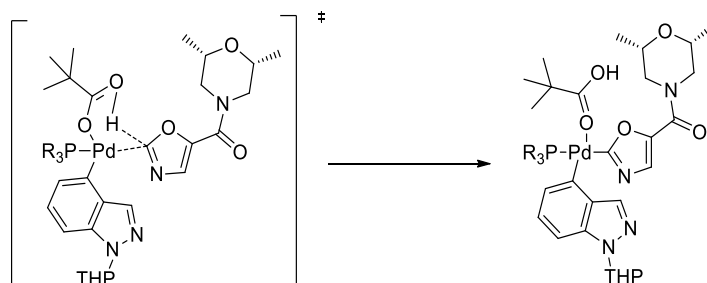
Reagents and conditions: (i) *cis*-2,6-Dimethylmorpholine, T3P[®], DIPEA, EtOAc, rt, overnight, 83%; (ii) 4-chloro-1-(tetrahydro-2*H*-pyran-2-yl)-1*H*-indazole, PdCl₂ (2.8 mol%), XPhos (6 mol%), pivalic acid, K₂CO₃, CPME, 120 °C, μ wave, 2 h, 84%; (iii) 1 M LiAlH₄ in Et₂O, THF, 50 °C, 2 h, 65%; (iv) Pinacolborane, 3,4,7,8-Tetramethyl-1,10-phenanthroline (5 mol%), [Ir(OMe)(1,5-COD)]₂ (2 mol%), THF, 65 °C, overnight, product not isolated.

Scheme 21. Initial approach towards the synthesis of TCO probe **44** derived from GSK2292767.

This synthetic sequence commenced with an amide coupling between oxazole-5-carboxylic acid **114** and *cis*-2,6-dimethylmorpholine mediated by propylphosphonic anhydride (T3P[®]) as coupling agent to afford intermediate **115**. T3P[®] is a widely used coupling agent in peptide bond formation.^[154] Several factors contribute to its attractiveness compared to other coupling reagents include its stability, ease of handling, and the fact that its by-products can be readily removed with an aqueous workup.^[155]

Next, palladium-catalysed direct C-H arylation of oxazole **115** using palladium(II) chloride, XPhos, potassium carbonate and pivalic acid afforded intermediate **116**. The reaction is presumed to proceed *via* a concerted metalation-

deprotonation (CMD) pathway, which means that palladation and deprotonation of the C-H bond occur simultaneously.^[156] In addition, Fagnou *et al.* have identified pivalic acid as a key component of the reaction since the pivalate anion is believed to lower the energy of the C-H bond cleavage (Scheme 22).^[157]

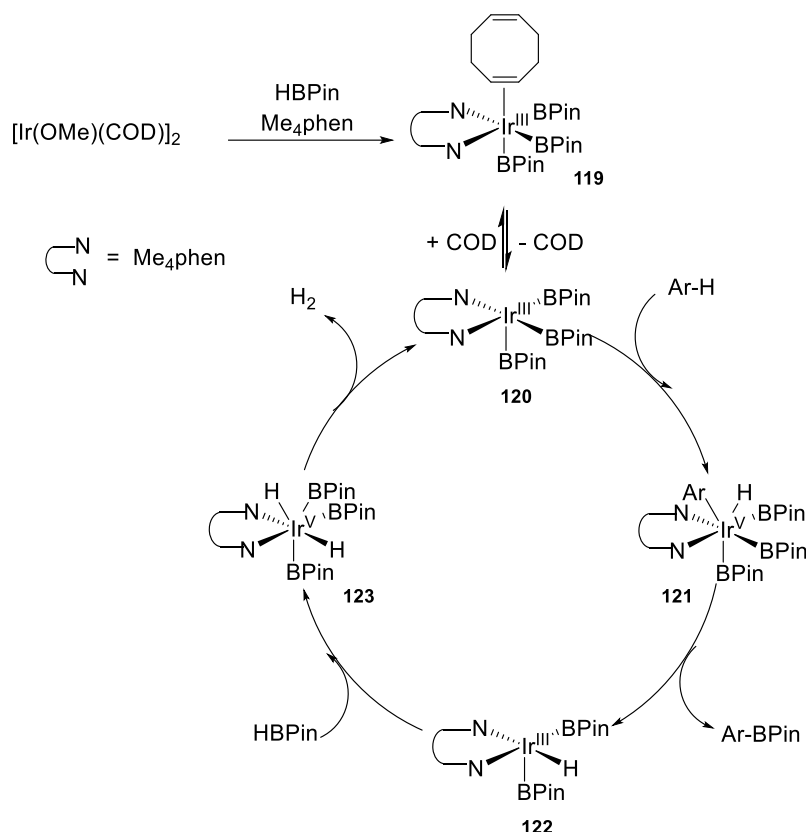


Scheme 22. Transition state for the palladium-catalysed arylation of oxazole **115** in the CMD pathway.

Subsequent amide reduction of compound **116** with LiAlH_4 afforded the corresponding tertiary amine **117**, which was taken forward for an iridium-catalysed C-H borylation reaction.

Arylboronic acids and esters are valuable tools for a variety of transformations in synthetic organic chemistry, most notably the Suzuki cross-coupling reaction.^[158] Arylboronic acids and esters are commonly prepared *via* a precursor containing a reactive handle group such as a halide, as exemplified by the Miyaura borylation.^[159] However, this approach requires an additional synthetic step to access the organoboron reagent from the aryl halide precursor, and therefore explains the significant interest in synthetic organic chemistry for the direct functionalization of aryl C-H bonds to form aryl C-B bonds.^[160,161]

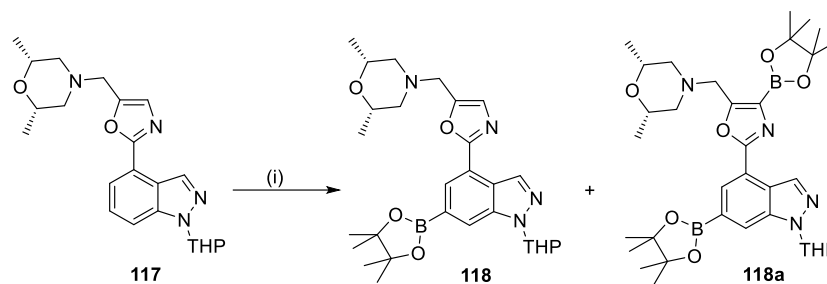
Following on from seminal work by Iverson,^[162] Hartwig reported in 2002 the iridium-catalysed borylation of (hetero)arenes using $[\text{Ir}(\text{OMe})(\text{COD})]_2$ as a catalyst in the presence of B_2Pin_2 or HBPin and a bipyridine ligand (Scheme 23).^[163,164]



Scheme 23. Proposed mechanism for the Ir-catalysed borylation of arenes with HBPIn.^[165]

Mechanistic studies revealed that the reaction proceeds in a $\text{Ir}^{\text{(III/V)}}$ cycle where reversible dissociation of the COD ligand in **119** generates the tris(boryl) $\text{Ir}^{\text{(III)}}$ active catalyst (**120**). Oxidative addition of the arene to **120** yields an $\text{Ir}^{\text{(V)}}$ species (**121**) that undergoes reductive elimination to give the desired arene borylation product and an $\text{Ir}^{\text{(III)}}$ hydride complex (**122**). Oxidative addition of HBPIn to **122** followed by reductive elimination of H_2 eventually regenerates the active catalyst (Scheme 23).^[165]

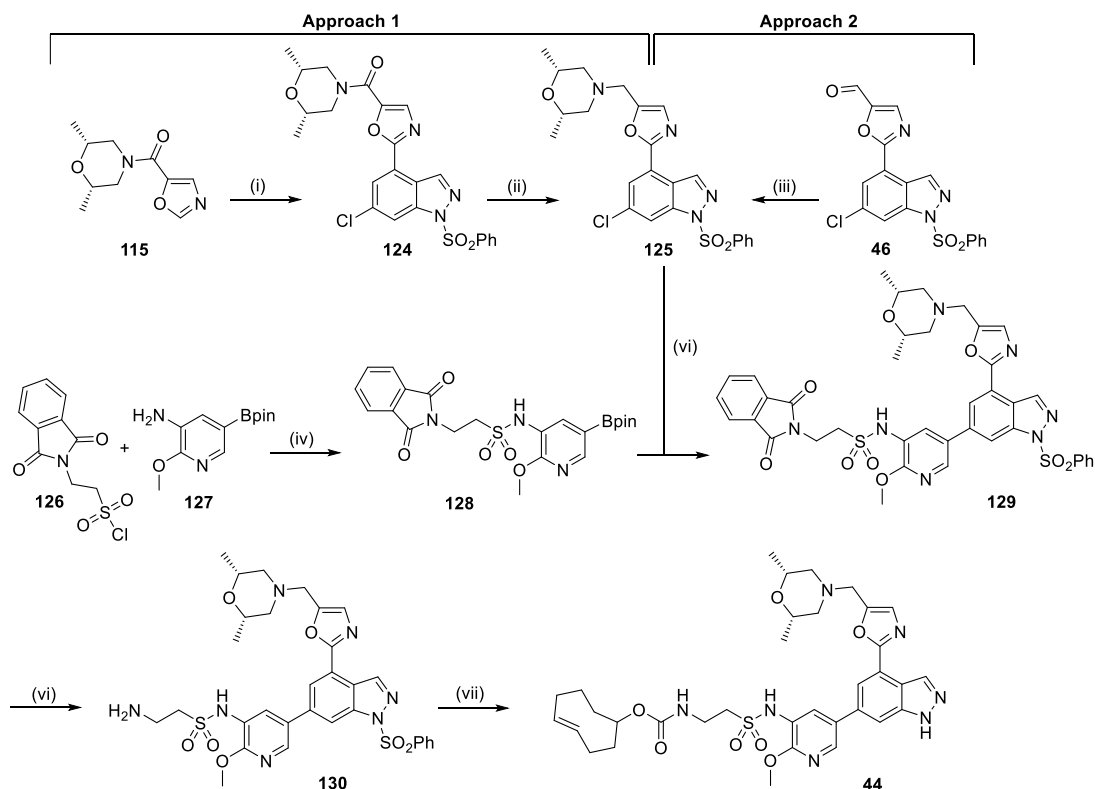
Hartwig also demonstrated that the regioselectivity for the borylation of arenes was controlled almost exclusively by steric effects,^[160] whilst for heteroarenes it was controlled by a combination of electronic and steric effects.^[166] Accordingly, an Ir-catalysed borylation of **117** gave the desired product **118** along with 10% of a bis-borylated compound. Previous work conducted by the process chemistry team elsewhere in our laboratories had identified that the second borylation was occurring on the oxazole to give **118a** (Scheme 23).^[141]



Reagents and conditions: (i) Pinacolborane, 3,4,7,8-Tetramethyl-1,10-phenanthroline (5 mol%), [Ir(OMe)(1,5-cod)]₂ (2 mol%), THF, 65 °C, overnight.

Scheme 24. Iridium-catalysed borylation of **117**.

Purification and isolation of **118** was troublesome since the presence of the side product **118a** prevented its effective recrystallisation from IPA. In addition, attempts to take the crude mixture forward in a Suzuki coupling were not successful. Therefore, this synthetic route was abandoned, especially since the final step of this sequence would have involved an acid-mediated cleavage of the THP protecting group on the indazole, which may not have been compatible with the presence of the *trans*-cyclooctene moiety since previous work had shown isomerisation to the *cis*-isomer could occur under acidic conditions. Therefore, another synthetic route depicted in Scheme 25 was pursued.



Reagents and conditions: (i) 1.9 M ZnCl_2 in 2-MeTHF, 1 M LiHMDS in THF, THF, -20°C , 1.5 h; then 6-chloro-4-iodo-1-(phenylsulfonyl)-1*H*-indazole, $\text{Pd(PPh}_3)_4$ (3 mol%), THF, 65°C , overnight, 77%; (ii) Zn(OAc)_2 , $(\text{EtO})_3\text{SiH}$, THF, 55°C , overnight, 88%; (iii) 2,6-*cis*-Dimethylmorpholine, AcOH, DCM, rt, 1 h, then STAB, DCM, 3 h, 92%; (iv) Pyridine, DMAP, DCM, rt, overnight, 51%; (v) XPhos Pd G2 (20 mol%), Na_2CO_3 , 1,4-Dioxane/Water (7.5:1), μwave , 90°C , 1.5 h, 82%; (vi) $\text{NH}_2\text{NH}_2\cdot\text{H}_2\text{O}$, THF, rt, 2 h, 63%; (vii) TCO-PNB ester, DIPEA, DMF, rt, 1.5 h; then 1 M aq. NaOH, MeOH, rt, 30 min, 26% over 2 steps.

Scheme 25. Synthesis of chemical probe 44.

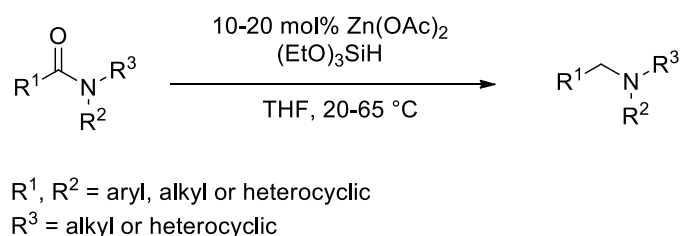
Towards a more convergent approach, the first step of this synthetic route involved a Negishi coupling with a functionalised oxazole moiety already containing the *cis*-dimethyl morpholine group (Approach 1, Scheme 25). Therefore, oxazole **115** was initially reacted with LiHMDS and ZnCl_2 to prepare the corresponding organozinc reagent *in situ* which then underwent the Negishi coupling with the aryl iodide **47** to afford the desired cross-coupling product **124** (Scheme 25).

Next, the reduction of amide **124** to afford the corresponding tertiary amine **125** was investigated. Reduction of the amide functionality is an important transformation in organic synthesis, especially for the pharmaceutical industry since substituted amines are commonly found in biologically active molecules.^[167] Although

efficient reduction of amides can be carried out using stoichiometric amounts of either aluminium or boron hydride reagents, these methods suffer from several drawbacks, including poor functional group tolerance, air and moisture sensitivity and sometimes complicated product isolation and purification procedures.

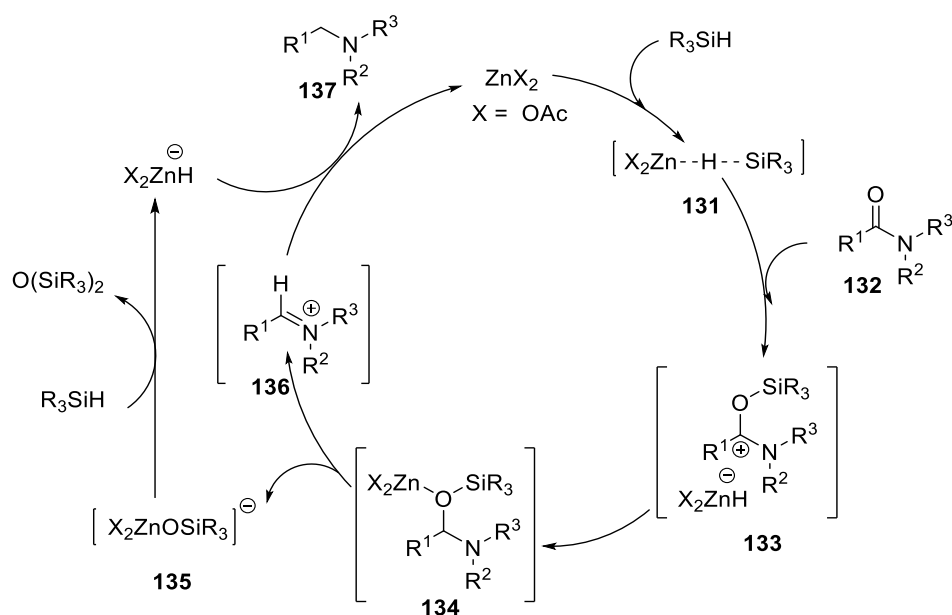
In relation to the current study, the amide reduction step had already been investigated by the process chemistry team in our laboratories on the nemiralisib scaffold.^[168] Although, most of the optimization work had been conducted on compounds featuring THP-protected indazoles, some attention was also given to benzenesulfonyl-protected substrates. It was observed that reductions involving boranes required a large excess of reagents to go to completion, at which point many impurities started to form.^[168] Other reduction methods involving lithium and aluminium hydrides were attempted but did not appear to be compatible with the presence of the benzene sulfonyl protecting group. Therefore, an alternative amide reduction method that would yield the desired tertiary amine **125** in the presence of other reducible functional groups was investigated.

In 2010, Beller *et al.* reported a highly chemoselective protocol for the catalytic reduction of tertiary amides under hydrosilylation conditions using catalytic amounts of Zn(OAc)₂ in combination with triethoxysilane (Scheme 26).^[169]



Scheme 26. Zinc-catalysed chemoselective hydrosilylation of tertiary amides described by Beller.^[169]

The authors proposed the following mechanism for the zinc-catalysed chemoselective hydrosilylation of amides (Scheme 27).



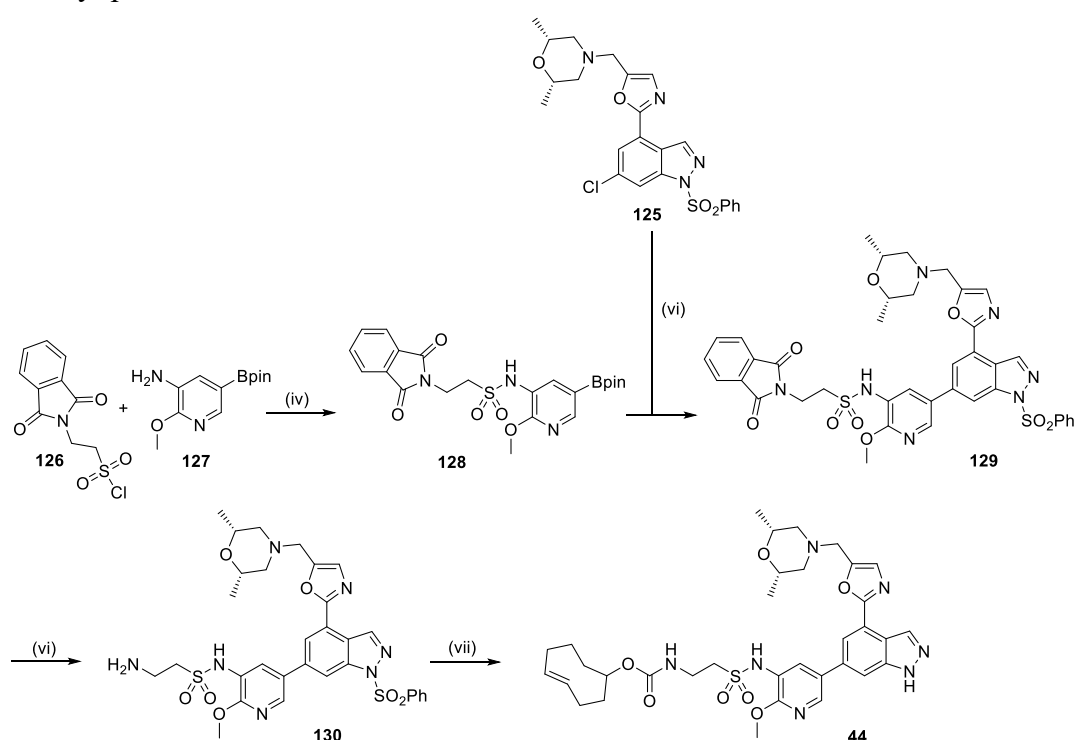
Scheme 27. Proposed reaction mechanism for the zinc-catalyzed chemoselective hydrosilylation of amides under Beller's conditions.^[169]

Zinc(II) acetate is proposed to first activate the silane to form the active species **131**. Then, the carbonyl group of the amide reacts with the active species **131** to generate an *N,O*-acetal intermediate **134** via transition state **134**. Release of the anionic zinc complex **135**, leads to the iminium species **136**. Finally, the anionic zinc ether **135** reacts with another equivalent of silane to convert the iminium ion **136** into the corresponding amine **137** and siloxane.

Here, the reaction conditions developed by Beller were applied for the reduction of the tertiary amide **116** and successfully afforded the desired tertiary amine **125**. However, these conditions showed poor reproducibility in our hands, from clean conversion to the desired product to no conversion at all and therefore were not pursued further. As a more robust strategy, the desired intermediate **125** was successfully prepared via a reductive amination between aldehyde **46** and 2,6-*cis* dimethylmorpholine (Approach 2, Scheme 25).

Meanwhile, the pyridine-sulfonamide pinacol boronic ester **128** was prepared by reacting commercially available sulfonyl chloride **126**, where the nitrogen is protected as a phthalimide group, with the aminopyridine pinacol boronic ester **127** available in large quantities in our laboratory (Scheme 28). Pyridine was selected as a weak base for this transformation as it circumvented the formation of the bis-sulfonamide side-product which was observed by LCMS when triethylamine was used as a base. This is probably due to the relative acidity of the sulfonamide moiety in the product (measured sulfonamide pK_a for GSK2292767 = 7.8).

Next, the pinacol boronic ester **128** was reacted with aryl chloride **125** to afford the biaryl product **129**.



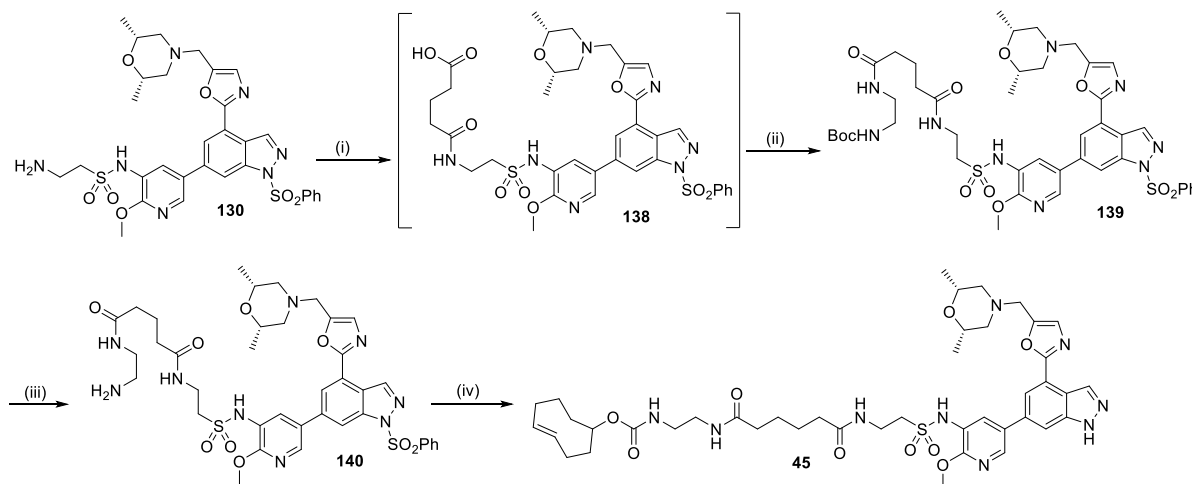
Reagents and conditions: (i) Pyridine, DMAP, DCM, rt, overnight, 51%; (ii) XPhos Pd G2 (20 mol%), Na_2CO_3 , 1,4-Dioxane/Water (7.5:1), μwave , 90 °C, 1.5 h, 82%; (iii) $\text{NH}_2\text{NH}_2 \cdot \text{H}_2\text{O}$, THF, rt, 2 h, 63%; (iv) TCO-PNB ester, DIPEA, DMF, rt, 1.5 h; then 1 M aq. NaOH, MeOH, rt, 30 min, 26% over 2 steps.

Scheme 28. Synthesis of chemical probe **44**.

Subsequent deprotection of the phthalimide protecting group with hydrazine hydrate afforded the primary amine **130**. The final steps involved treatment of **130** with TCO-PNB ester to afford the corresponding carbamate, which gave the TCO

chemical probe **44** after deprotection of the benzenesulfonyl protecting group (Scheme 28).

Once compound **44** was prepared, the synthesis of the remaining chemical probe **45** derived from GSK2292767 was carried out and is described below (Scheme 29).



Reagents and conditions: (i) Glutaric anhydride, Et₃N, DCM, rt, 1.5 h; (ii) *N,N'*-disuccinimidyl carbonate, DCM, rt, 30 min; (iii) Boc ethylene diamine, DCM, rt, 1 h, 90% one pot (3 steps); (iv) TFA, DCM, rt, 2.5 h, used crude; (v) TCO-PNB ester, DIPEA, DMF, rt, 2 h, then 2 M aq NaOH, MeOH, rt, 15 min, 13% over 3 steps.

Scheme 29. Synthesis of chemical probe 45.

The synthesis started with previously synthesised primary amine intermediate **130**, which was reacted with glutaric anhydride to afford the intermediate carboxylic acid **138**. Then, the intermediate carboxylic acid was immediately reacted with *N,N'*-disuccinimidyl carbonate for formation of the corresponding succinimidyl ester that was reacted with *N*-Boc ethylene diamine to give intermediate **151** in an efficient one-pot process. Subsequent *N*-Boc deprotection gave the primary amine **152** that was reacted with the TCO-PNB ester to afford the corresponding carbamate which gave the desired chemical probe **49** after benzene sulfonyl deprotection (Scheme 29).

Once their syntheses completed, the TCO chemical probes derived from nemiralisib and GSK2292767 were screened in several assays for biological characterisation.

3.3. Profiling of TCO Chemical Probes

In order to ensure that the TCO probes have the correct balance of physico-chemical properties, the compounds were profiled in several assays to determine their lipophilicity (measured ChromLogD_{pH7.4}), their kinetic solubility as well as their artificial membrane permeability (AMP).

The intrinsic lipophilicity of a molecule can be described with the logP value, where P represents the partition coefficient of unionised forms of that given molecule between octanol and an aqueous buffer. If a molecule possesses ionisable groups, the lipophilicity can be described with the logD_{pH} value which takes this ionisation into account and reflects the distribution of all species present between the phases for a buffer of known pH (typically physiological pH 7.4). In this thesis, lipophilicity is determined *via* a high-throughput chromatographic method using a reverse phase column, whereby the measured ChromlogD_{pH7.4} is linked to the retention time of the compound of interest.^[170] Lipophilicity can also be predicted using *in silico* packages, although the available methods will have some degree of error. In this thesis, calculated ChromlogD_{pH7.4} is determined using the Global Chromatographic LogD model v9 and cLogP is determined using the Daylight/Biobyte calculation method.^[61,62]

Kinetic solubility measurement is made by determination of the precipitative solubility from a DMSO solution of the compound of interest that is diluted in aqueous buffer at pH 7.4. The amount of compound remaining in solution is detected using either chemiluminescence nitrogen detection (CLND) or charged aerosol detection (CAD) methods.^[171,172] This approach is most suitable for giving a broad indication of low, moderate or high solubility of the compound of interest. The range covered is 1 µg/mL to 500 µg/mL and, with both detection methods, a compound's solubility is considered as low if below 30 µg/mL and high if greater than 200 µg/mL.

Permeability is assessed in a high-throughput assay that measures the speed of permeation of the compound through an artificial phospholipid membrane at pH 7.4.^[173] The rates of permeation range from 0.1 to 2000 nm/s. The permeability

of a compound is considered as low if less than 50 nm/s, and high if greater than 200 nm/s.

In addition of their physico-chemical properties, the TCO chemical probes were screened in biological assays to assess their potency and selectivity for PI3K δ .

3.3.1. Enzyme Potency in TR-FRET Assay

Enzyme potency (PI3K δ pIC₅₀) was determined using a time-resolved fluorescence resonance energy transfer (TR-FRET) biochemical assay.

Fluorescence Resonance Energy Transfer (FRET) is a mechanism that describes the transfer of energy from an excited donor fluorophore molecule to an acceptor molecule. The efficiency of this energy transfer is highly dependent on the distance between the two FRET partners. Successful energy transfer can result in an increase in the fluorescence of the acceptor molecule, which can be measured and quantified relative to a reference and therefore be used to assess interactions between molecules in biological systems.

In this biochemical assay, the percentage of inhibition of a Class 1 PI3K isoform by a compound of interest is assessed by the amount of PIP₃ being generated from PIP₂ as a result of the ATP-mediated PI3K enzymatic activity for that given PI3K isoform. More specifically, the amount of PIP₃ being produced is detected by displacement of a biotinylated-PIP₃ from an energy transfer complex consisting of a Europium (Eu)-labelled anti-glutathione S-transferase (GST) antibody bound to a GST-tagged pleckstrin homology (PH) domain that has a very specific binding affinity for PIP₃, and Streptavidin-Allophycocyanin (APC, a fluorescent protein) (Figure 24).

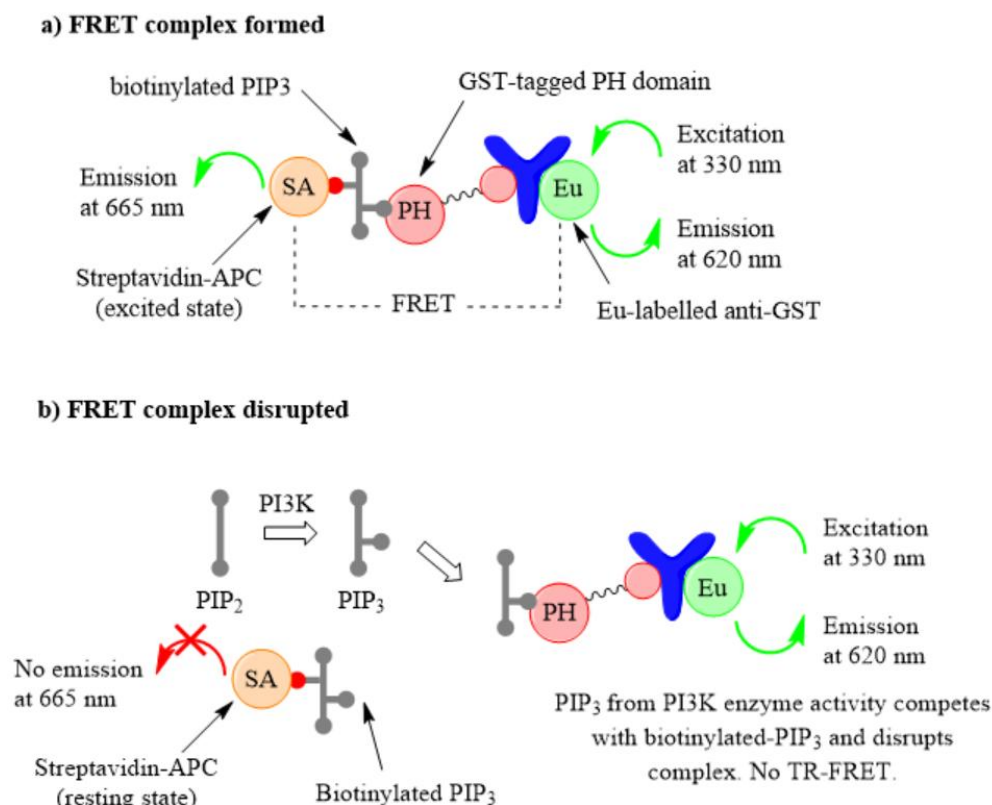


Figure 24. Schematic representation of the PI3K enzyme TR-FRET assay.

For a FRET signal to be observed, the biotinylated-PIP3 must bind to the GST-tagged PH domain. The very high affinity of streptavidin for biotin ensures tight binding of the biotinylated-PIP3 to Streptavidin-APC, allowing the FRET transfer to occur between the Europium (donor) and the APC (receptor) fluorophores. Indeed, excitation of Europium with light at 330 nm triggers an emission at 620 nm that causes an energy transfer to APC, which emits light at 665 nm if the Europium-labelled anti-GST antibody - GST-tagged PH domain - biotinylated PIP3 - Streptavidin-APC complex is intact (a, Figure 24).

However, when a PI3K enzyme produces PIP3 there is a competition between this naturally-formed PIP3 and the biotinylated-PIP3 for binding to the PH domain, therefore disrupting the FRET complex, and consequently reducing the observed fluorescence signal from APC (b, Figure 24). It is the variations in the APC fluorescence signal at 665 nm that is monitored in the FRET assay. Comparison of the APC fluorescence signal obtained in the presence of a PI3K inhibitor of interest to two

reference reactions (one with fully inhibited PI3K using a known pan-PI3K inhibitor, and one without inhibitor) allows determination of the percentage of inhibition, and therefore calculation of a pIC_{50} value. Indeed, full PI3K enzyme inhibition produces no PIP3, therefore no competition with the biotinylated PIP3 for binding to the PH domain, and a full fluorescence signal at 665 nm from APC; whilst no inhibition causes an absence of APC emission due to competition of naturally-formed PIP3 with the biotinylated PIP3 for binding to the PH domain. The assay is run with each of the PI3K α , β , γ and δ enzymes to determine the PI3K δ enzyme potency of each compound of interest as well as their selectivity towards other Class 1 PI3K isoforms. Typically, the assay is run at a concentration of ATP equal to the K_M of the corresponding enzyme, therefore allowing direct pIC_{50} comparison between the different Class I PI3K isoforms. For the most potent PI3K δ inhibitors (PI3K δ $pIC_{50} > 9$) that start to reach the limit of the assay, a more relevant “desensitized” assay that utilises a higher concentration of ATP (2 mM instead of PI3K δ $K_M(ATP) = 80 \mu M$) can be carried out. Then, the Cheng-Prusoff equation allows the calculation of PI3K δ pK_i values, where K_i refers to the binding affinity of the inhibitor.^[174] Unless otherwise noted, the PI3K δ pIC_{50} values reported in this thesis were generated in the assay for which the ATP concentration equals K_M . Since the FRET assay is performed with purified proteins, it may not necessarily reflect the cellular conditions. A competition binding assay known as the lipid kinobead assay was therefore introduced to validate the potency of the most promising chemical probes.

3.3.2. Kinobead Potency in Cell Lysates

Initially established by Bantscheff and co-workers, lipid kinobeads consist of several non-covalent promiscuous ATP-competitive lipid kinase inhibitors immobilised at the surface of a bead matrix for the chemoproteomics profiling of lipid kinase inhibitors of interest.^[175-177] In this assay, cell lysates specifically chosen for their broad coverage of the kinome are pre-incubated with a PI3K δ inhibitor of interest to allow the compound to bind to its target(s) (Figure 25). A kinobead slurry is subsequently added to the lysate mixture for competition binding to PI3K δ to occur

between the PI3K δ inhibitor of interest and the bead-bound kinase inhibitors present in the lysate mix. If the PI3K δ inhibitor is potent and selective, it will occupy the PI3K δ active site and will therefore prevent the binding of the PI3K δ protein to the kinobeads, whilst the non-targeted kinases remain unaffected. After incubation, the beads are gently washed to remove any unbound proteins and the resulting enriched proteins are eluted from the bead matrix and analysed by mass-spectrometry or antibody-based readout.

Dose-dependent competition experiments enable the determination of an inhibition curve and pIC₅₀ value for the PI3K δ inhibitor by measuring the reduction in PI3K δ protein enrichment.

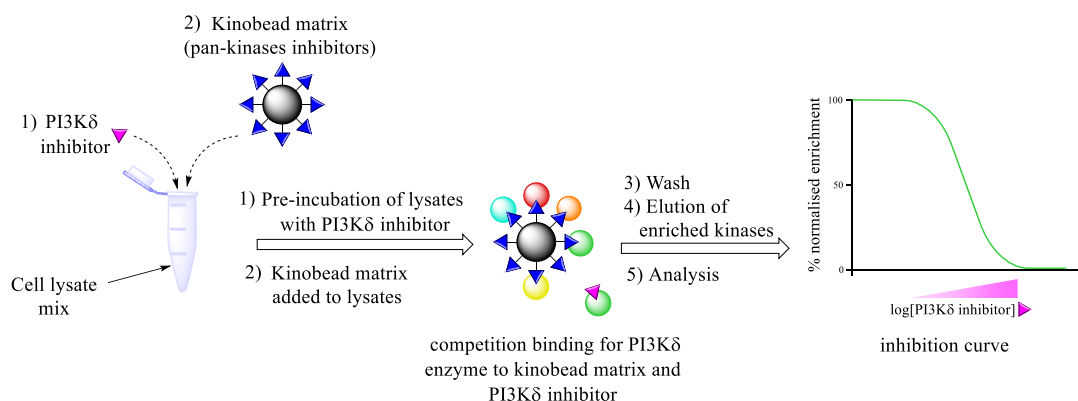


Figure 25. Schematic representation of the Kinobead assay.

One disadvantage of the kinobead assay is that the technique can only be used in cell lysates and not live cells. Therefore, the observed binding profile for the PI3K δ inhibitor may differ from the true engagement profile that the compound would exhibit in live cells as the assay may not take the physico-chemical properties of the PI3K δ inhibitor (e.g. permeability) into consideration. However, it was postulated that the pIC₅₀ value obtained with the kinobead assay for the chemical probes described in this thesis could constitute an informative estimate of their PI3K δ potency in a biologically relevant context. To also address potential membrane permeability issues and activity readout, a whole blood assay was considered for some of the chemical probes.

3.3.3. Human Whole Blood Assay

The cellular potency of TCO probes was assessed in a human whole blood (hWB) assay measuring the secretion reduction of the interferon gamma ($\text{IFN}\gamma$) cytokine following treatment with T-cell stimulating antibody CytoStim in response to $\text{PI3K}\delta$ inhibition.^[125,178] More specifically, CytoStim acts as an artificial superantigen causing an activation of T cells, which start to secrete cytokines, including $\text{IFN}\gamma$, ultimately inducing an inflammatory response.^[179] However, the secretion of $\text{IFN}\gamma$ by T cells was found to be highly sensitive to $\text{PI3K}\delta$ inhibition, a feature that can therefore be reliably exploited to assess the potency of a $\text{PI3K}\delta$ inhibitor by measuring the levels of $\text{IFN}\gamma$ secreted following CytoStim stimulation.^[180]

The human whole-blood assay is based on an Enzyme-Linked Immunosorbent Assay (ELISA) technique and relies on the highly sensitive detection of $\text{IFN}\gamma$ following binding to an anti- $\text{IFN}\gamma$ antibody tagged with an electrochemiluminescent SULFO-TAG (Figure 26). In the first step of the assay, the $\text{PI3K}\delta$ inhibitors of interest are incubated with human whole-blood (hWB) for 1 h prior to CytoStim addition to stimulate the production of cytokines.

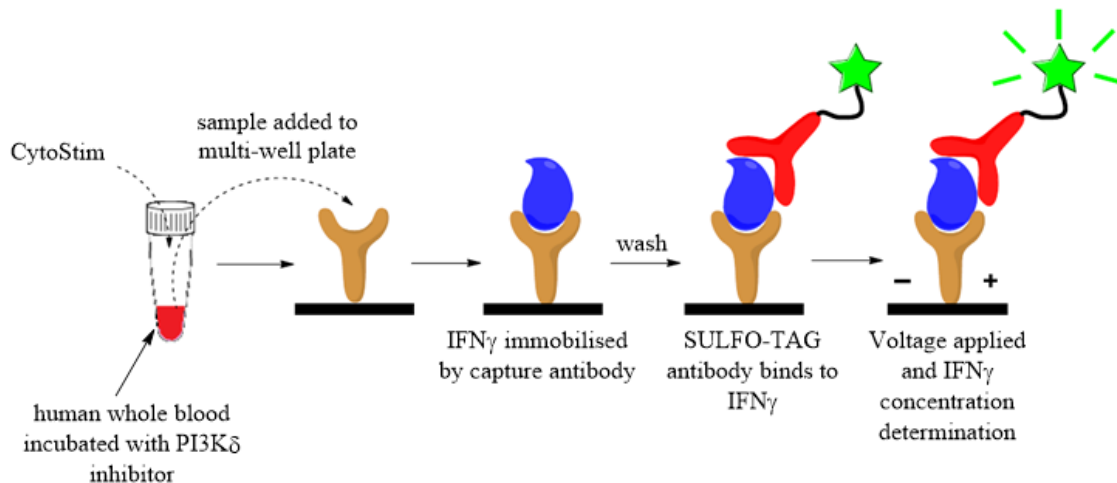


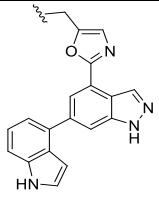
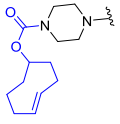
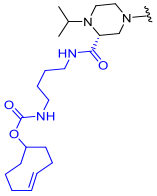
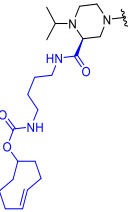
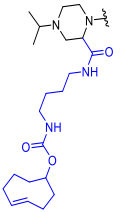
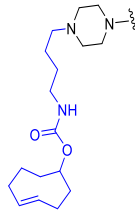
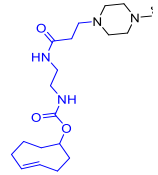
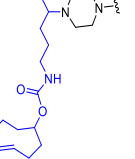
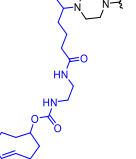
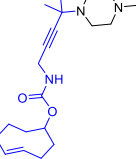
Figure 26. Schematic representation of the enzyme-linked immunosorbent assay (ELISA) human whole blood assay.

The compounds are then incubated for an additional 20 h. Next, an aliquot of this mixture is dispensed onto a conductive multi-well plate where each well contains a capture antibody specific for $\text{IFN}\gamma$. The wells are then washed to remove any

unbound cytokines, and the detection solution containing the SULFO-TAG antibodies is added. The wells are washed again to remove unbound SULFO-TAG antibodies. A voltage is then applied to the plate, which causes the captured SULFO-TAG antibodies to emit light from electron transfer between ruthenium complexes. The intensity of this light can be measured by an automated plate reader to give a quantitative measure of the IFN γ concentration in the sample. Comparing the signal intensity obtained with a calibration curve of samples with known IFN γ concentrations allows the determination of the reduction in the IFN γ secretion in presence of a PI3K δ of interest and the extrapolation of pIC₅₀ for that given compound. It is important to note that potential blood/ plasma protein binding of the chemical probes in a whole blood assay could reduce the free unbound fraction available to engage with PI3K δ target and therefore may not necessarily reflect the PI3K δ potency in an isolated cell line system. This is why the potency of the chemical probes was also assessed in cell lysates using the lipid kinobead.

3.3.4. Properties of Chemical Probes Derived from Nemiralisib

The properties of the chemical probes derived from nemiralisib are presented in Table 7 below.

										
	nemoralisib	35	41	42	43	36	37	38	39	40
PI3Kδ pIC₅₀ (n)	8.5 (4) ^a	6.7 (3)	7.7 (3)	7.6 (2)	6.5 (3)	8.5 (4)	7.9 (4)	8.7 (4)	8.4 (3)	8.1 (5)
PI3Kδ pK_i (n)	9.9 (4) ^a	7.0 (3)	8.0 (3)	7.9 (2)	6.8 (3)	8.8 (4)	8.2 (4)	9.0 (4)	8.7 (3)	8.4 (5)
PI3Kα, β, γ pIC₅₀ (n)	5.3 (27) ^b , 5.8 (26) ^c , 5.2 (30) ^d	5.4 (2) ^f , 5.5 (3), 5.1 (3)	5.2 (1) ^h , 5.2 (2) ^f , <4.5 (3)	<4.1 (2) ^f , 5.4 (1) ^j , 5.8 (1) ^k	5.2 (1) ^h , 4.9 (2) ^f , 5.5 (3)	6.0 (3), 6.1 (3), 6.3 (2) ⁿ	5.5 (3) ^f , 5.5 (4), 5.6 (4)	5.7 (4), 5.9 (4), 5.5 (4)	5.6 (3), 5.7 (3), 5.9 (3)	5.5 (5), 5.7 (4) ^t , 6.2 (5)
α, β, γ selectivity	5012, 1585, 6310	20, 16, 40	316, 316, 1585	3162, 158, 63	20, 40, 10	316, 251, 158	251, 251, 200	1000, 631, 1585	631, 501, 316	398, 251, 79
hWB pIC₅₀ (n)	8.9 (3)	5.5 (3) ^g	6.2 (6) ⁱ	5.8 (2) ^l	4.9 (7) ^m	6.6 (5) ^o	5.4 (7) ^p	6.1 (5) ^q	5.7 (5) ^s	6.5 (2)
Kinobead pIC₅₀ (n)	9.2 (2) ^c	nt	nt	nt	nt	7.6 (2) ^e	nt	7.2 (2) ^r	7.6 (2) ^r	nt
ChromLogD_{pH7.4} calc./measured clogP	2.8 / 2.5 4.4	6.9 / 6.7 6.4	5.9 / 5.9 6.7	5.8 / 6.1 6.7	5.4 / nt 6.6	5.6 / 5.1 6.5	4.7 / 4.4 5.9	5.7 / 5.3 6.8	4.7 / 4.5 6.2	6.4 / 6.4 7.2
AMP (nm/sec, pH 7.4)	230	205	200	260	nt	320	23	230	3	130
Kinetic Solubility (µg/mL)	110	6	1	8	nt	4	11	11	9	6

n = number of test occasions included in mean; nt = non tested; ^aPI3K δ assay run at 2 mM ATP concentration; ^bTested <5.3 on one test occasion and <4.6 on one test occasion; ^cTested <4.6 on one test occasion; ^dTested <4.6 on three test occasions; ^eLipid kinobeads CZK133 / lysate mix HeLa-Jurkat-K-562; ^fTested <4.5 on one test occasion; ^gA batch tested was found to be impure, data not reported; ^hTested <4.5 on two test occasions; ⁱReturned 7.8 on one test occasion, failed to fit a curve on two test occasions; ^jTested <4.1 on one test occasion; ^kTested <4.7 on one test occasion; ^lFailed to fit a curve on four test occasions; ^mFailed to fit a curve on ten test occasions; ⁿTested <5.1 on one test occasions; ^oFailed to fit a curve on five test occasions; ^pFailed to fit a curve on seven test occasions; ^qFailed to fit a curve on one test occasion; ^rLipid kinobeads CZK126 / lysate mix Hut78-MCF7; ^sFailed to fit a curve on 3 test occasions; ^tTested <4.1 on one test occasion.

Table 7. Properties of chemical probes derived from nemiralisib.

Upon screening in the biochemical assay, chemical probe **35** showed a significant drop in enzyme potency compared to nemiralisib. This reduction was thought to result from the large size of the TCO tag potentially clashing with amino acid residues in the active site of PI3K δ . To confirm this hypothesis and evaluate the binding mode of compound **35**, a co-crystal structure with PI3K δ was generated by X-ray crystallography. Unfortunately, no electron density could be observed for the TCO tag, suggesting significant mobility of this group. Given its poor enzyme potency, compound **35** was not screened in the whole blood assay and was not progressed further.

In the biochemical assay, chemical probe **41** achieved a 10-fold increased potency compared to probe **35** and maintained a good selectivity profile for PI3K δ (> 100-fold). However, the cellular potency was moderate (hWB pIC₅₀ = 6.2) and did not quite match the desired potency requirement (PI3K δ pIC₅₀ > 8, hWB pIC₅₀ > 7). In addition, the TCO tag had a significant impact on the lipophilicity of the molecule (ChromLogD_{pH7.4} = 5.9). This was nevertheless reduced compared to chemical probe **39**, probably due to the presence of hydrogen bond donors within the linker.

Next, the chemical probe **42** with the opposite stereochemistry was also screened and showed a similar enzyme potency to probe **41** (PI3K δ pIC₅₀ = 7.6 and 7.7, respectively). This suggested that the stereochemistry at the chiral centre may not be critical for potency.

Compound **43**, which contains a racemic piperazine monomer where the linker extends from the other carbon of the piperazine group, suffered from poor enzyme potency (10-fold decrease compared to compounds **41** and **42**), suggesting as per our hypothesis that this point of attachment was not tolerated and resulted in steric clashes with the surface of the protein.

Overall, the chemical probes derived from nemiralisib where the TCO tag had been installed from vector 1 (*N*-isopropyl vector) displayed enhanced enzyme potency compared from vector 2 (carbon adjacent to the piperazine *N*-isopropyl group).

Indeed, compound **36** with a short alkyl linker displayed a significant increase in enzyme potency (PI3K δ pIC₅₀ = 8.5), over the directly attached TCO of compound **35** and a good selectivity profile for PI3K δ over other isoforms. However, the

increased enzyme potency did not translate to whole blood potency, which was only slightly improved (hWB pIC₅₀ = 6.6) compared to previous chemical probes.

Compound **37**, which displays a longer linker extending from the piperazine nitrogen proved to be 4-fold less potent than compound **36** (PI3Kδ pIC₅₀ = 7.9 and 8.5, respectively) in the enzyme assay but suffered from weak whole blood activity (hWB pIC₅₀ = 5.4). This difference could be rationalized by low permeability that resulted from the presence of an additional hydrogen bond donor within the linker. This implies that the compound is unable to permeate the cell membrane to reach the PI3Kδ target.

In the absence of crystal structures for these chemical probes, compounds **35**, **36** and **37** provided further insights into the linker length required for the TCO tag to access the solvent-exposed region. The results highlighted that a short 4-carbon linker was long enough to avoid any steric clashes with the protein.

Next, chemical probe **38**, which differs structurally from **36** by the introduction of an additional methyl group, proved to be the most potent compound in the enzyme assay (PI3Kδ pIC₅₀ = 8.7). The presence of the additional methyl group had a positive impact on the PI3Kδ selectivity over other PI3K isoforms when compared to compound **36**. This is consistent with the hypothesis that the hydrophobic pocket of PI3Kδ known as the tryptophan shelf is better occupied and since PI3Kδ is able to accommodate bulky substituents in this region, better selectivity is conferred.^[125,126] In addition, the methyl group in **38** had a minimal impact on the lipophilicity of the molecule compared to **36** (ChromLogD_{pH7.4} = 5.1 and 5.3, respectively).

Chemical probe **39**, which is an analogue of compound **38** with a longer linker, displayed high enzyme potency and a good selectivity profile, albeit with reduced selectivity compared to **42**. Similarly to compound **37**, the introduction of a longer linker with hydrogen bond donors resulted in very low permeability, which may explain the modest potency in the whole blood assay.

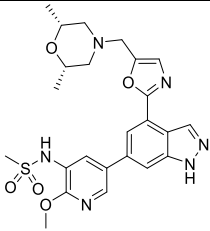
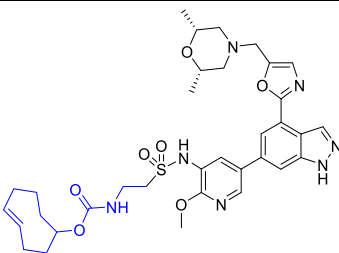
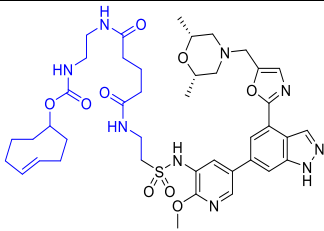
Compound **40**, which contains a rigid *gem*-dimethyl propargyl linker showed a good enzyme potency, however this did not surpass that observed for compounds **38** or **39**. This suggested that the alkyne linker may not properly orient the TCO tag towards the solvent-exposed region as initially proposed. The selectivity profile for PI3Kδ of compound **40** also showed less than a 100-fold selectivity over PI3Kγ. This

level of selectivity would be a concern, since engaging with the non-desired PI3K isoforms when high concentrations of chemical probes are used in the cellular imaging assay could impact data interpretation.

Based on their properties, TCO chemical probes **38** and **39** were selected as the most promising compounds for subsequent evaluation in the cellular imaging assay.

3.3.5. Properties of Chemical Probes Derived from GSK2292767

The properties of the chemical probes derived from GSK2292767 were also investigated and are summarised in Table 8 below.

			
	GSK2292767	44	45
PI3K δ pIC ₅₀ (n)	8.7 (5) ^a	8.2 (5)	8.3 (3)
PI3K δ pK _i (n)	10.1 (5) ^a	8.5 (5)	8.6 (3)
PI3K α , β , γ pIC ₅₀ (n)	6.3 (17), 6.2 (18), 6.3 (20)	5.5 (4) ^d , 5.1 (1) ^e , 6.1 (5)	5.9 (3), 5.5 (3), 6.6 (3)
α , β , γ selectivity (fold)	631, 794, 631	501, 1259, 126	251, 631, 50
hWB pIC ₅₀	8.5 (7)	6.4 (8) ^f	6.4 (14) ^h
Kinobead pIC ₅₀ (n)	9.3 (2) ^b	6.9 (2) ^g	nt
ChromLogD _{pH 7.4} calc./measured	3.7 / 3.3	5.8 / 5.7	4.8 / 4.2
AMP (nm/sec, pH 7.4)	203 (pH 7.05)	295	8
Kinetic / SLF Solubility (μ g/mL)	182 / 4 (free base) ^c	12 / nt	91 / nt

n = number of test occasions included in mean; nt = non tested; ^aPI3K δ assay run at 2 mM ATP concentration; ^bLipid kinobeads CZK133 / lysate mix HeLa-Jurkat-K-562; ^c4 h timepoint (crystalline material); ^dTested <4.5 on one test occasion; ^eTested <4.5 on three test occasions and <4.3 on one test occasion; ^fRanges from 5.7 to 7.1; ^gLipid kinobeads CZK126 / lysate mix Hut78-MCF7; ^hRanges from 5.9 to 6.9, failed to fit a curve on 3 test occasions.

Table 8. Properties of chemical probes derived from GSK2292767.

Compound **44**, which contains a short carbon linker extending from the pyridine sulfonamide vector, maintained high potency and selectivity for PI3K δ in the enzymatic assay. As previously observed with the probes derived from nemiralisib, the introduction of the TCO group had a significant impact on the lipophilicity (ChromLogD_{pH7.4}) of the molecule compared to the parent GSK2292767.

Chemical probe **45**, which contains a longer linker maintained good enzyme potency albeit with an impacted selectivity profile that achieved only 50-fold selectivity over PI3K γ . In addition, the introduction of secondary amides to the linker successfully reduced the lipophilicity of the compound compared to probe **44**, however this resulted in poor permeability.

Based on its properties, TCO chemical probe **44** was selected as the most promising compound for subsequent evaluation in the cellular imaging assay.

3.3.6. Blood Binding of TCO Chemical Probes

For several chemical probes derived from nemiralisib and GSK2292767, a decrease (drop-off) in potency was observed between the enzyme and whole blood assays. This can typically be attributed to a variety of parameters, including low permeability where the compound cannot cross the cell membrane to reach its target, or high blood/plasma protein binding, which reduces the free unbound fraction available to engage with the target.^[181] Alternatively, active efflux mechanisms decreasing the active cell concentration of the compound can also be involved and explain such a drop-off.

The most abundant plasma proteins responsible for binding small drug molecules are human serum albumin (HSA), which tends to bind neutral and acidic molecules (anionic at physiological pH), and α -1-acid glycoprotein (AGP), which typically binds neutral and basic molecules (positively charged at physiological pH).^[182] It is well established that plasma protein binding is correlated to compound lipophilicity, with increased lipophilicity typically associated with increased plasma protein binding.^[183] Since most of the chemical probes derived from nemiralisib and GSK2292767 were shown to be permeable in the artificial membrane permeability

(AMP) assay, it was suggested that the decreased potency observed in the whole blood assay could be attributed to increased plasma protein binding caused by the high lipophilicity of the TCO probes. In our laboratory, HSA and AGP binding are evaluated using an automated gradient HPLC method that utilises chemically bonded plasma protein stationary phases.^[184] Overall, on the set of TCO chemical probes derived from nemiralisib, increased lipophilicity was found to be systematically associated with increased plasma protein binding. This could provide an explanation for the reduced potency in the whole blood assay compared to the enzyme and kinobead assays since the permeability remained high for nearly all chemical probes.

To further verify this hypothesis, a blood protein binding study was initiated in our laboratory on some of the chemical probes.^[185] This also included a measurement of compound stability at a 4 h time point to ensure that the compounds would remain stable in the whole blood assay conditions. These investigations showed that both chemical probes **38** and **41** were stable for a duration of 4 hours at 37 °C in whole blood, albeit the integrity of the *trans*-cyclooctene moiety and its potential isomerisation to its *cis*-isomer was not investigated here.

Blood protein binding studies were conducted using the Rapid Equilibrium Dialysis (RED) technique, a common method to assess the extent to which small drug molecules bind to blood/plasma proteins.^[186] The RED plate is composed of several dialysis inserts which are comprised of two side-by-side chambers, a blood/plasma chamber and a buffer chamber, separated by a dialysis membrane that allows rapid equilibrium.^[187] First, a blood sample matrix is prepared by diluting fresh blood with PBS to which is spiked a solution of compound in an organic solvent (DMSO/MeCN). The matrix sample is then added to the blood chamber and the dialysis buffer (PBS) to the buffer chamber. The plate is then sealed and incubated at 37 °C whilst being agitated for 4 hours to reach equilibrium. After this time, an aliquot from both chambers is taken, processed and submitted to LCMS analysis to determine the unbound fraction (f_u) and the percentage of compound bound to blood proteins (% bound) (Figure 27).

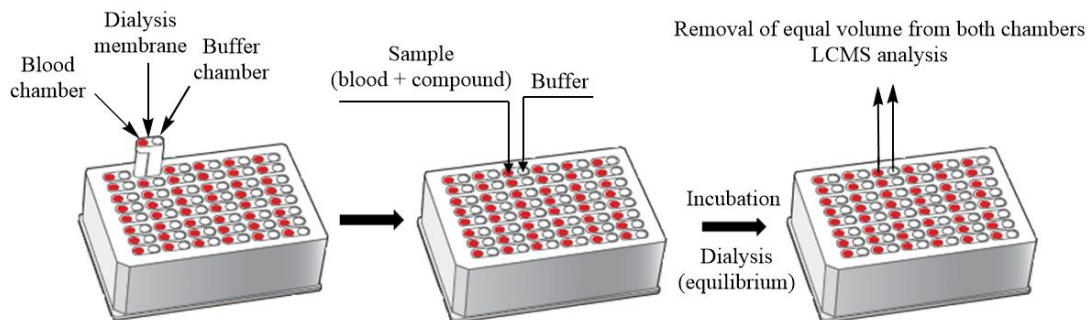


Figure 27. Schematic of the RED (Rapid Equilibrium Dialysis) assay to determine binding to blood/plasma proteins.

Both compounds **38** and **41** were measured to be highly bound (> 99%) to blood proteins, which could therefore explain the very low free fraction available and the moderate potency observed in the whole blood assay. This may also be the case by extension for the other TCO probes as they all share similarly high lipophilicities. These observations highlight the interest of the kinobead assay to assess the potency of the chemical probes. Indeed, most of the chemical probes profiled in the kinobead assay were found to be potent PI3K δ inhibitors (kinobead pIC₅₀ \geq 7) with a level of potency intermediate to the isolated enzyme and the human whole blood assays. Overall, these observations support the hypothesis that the potency drop-off in the human whole blood potency observed for most of the chemical probe could be caused by their lipophilicity and high blood protein binding.

Based on their enzyme and kinobead potency as well as their physico-chemical properties, several TCO chemical probes were selected for subsequent profiling in the cellular imaging assay.

3.4. Cellular Imaging of PI3K δ Chemical probes

The chemical probes derived from each inhaled clinical candidate which were selected for screening in the cellular imaging assay are shown in Figure 28 below.

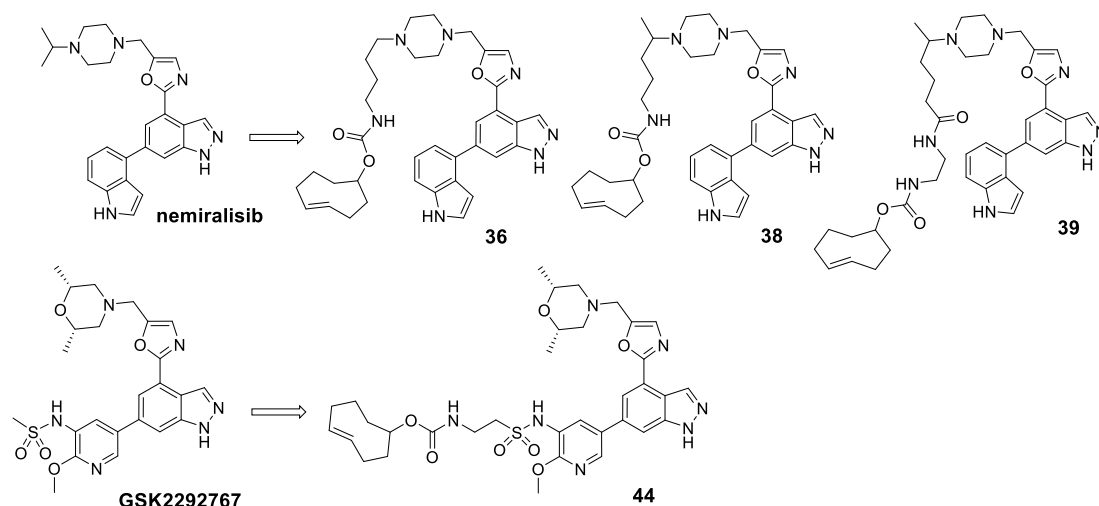


Figure 28. PI3K δ chemical probes investigated in the cellular imaging assay.

Hut78 cells were chosen as an alternative to human Peripheral Blood Mononuclear Cell (PBMCs) for the initial screen of PI3K δ chemical probes in the imaging assay. PBMCs consist of lymphocytes and monocytes that can be extracted from whole blood.^[188] PBMC cells are relevant to PI3K δ inhibition since inflammatory diseases such as asthma and COPD are often multicomponent diseases, involving both airway and systemic inflammation, with several inflammatory biomarkers released by PBMC cells.^[189] In addition, PBMCs are more broadly available than cells from the lungs. On the other hand, Hut78 cells are lymphocytic cells initially isolated from peripheral blood of a male patient with cutaneous T-cell lymphoma.^[190] Similarly to PBMCs, Hut78 cells have a high expression level of PI3K δ compared to other PI3K isoforms and can be cultured, therefore offering the advantage of being readily available, whereas PBMCs need to be extracted from whole blood prior to each experiment, which can present reproducibility issues between each blood donors. In addition, Hut78 cells have a visibly larger cytosol (where PI3K δ is expected to reside)

compared to PBMCs, which might facilitate the visualisation of the cellular localisation of the chemical probes.

The format of the cellular imaging/target engagement assay is depicted in Figure 29 below.^[88]

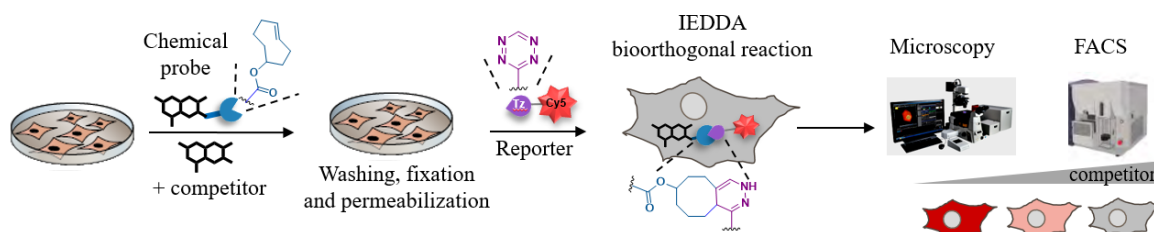


Figure 29. Representation of the cellular imaging and target engagement assay for the visualisation of PI3K δ chemical probes.

Briefly, Hut78 cells are incubated with the TCO-tagged PI3K δ chemical probes (and unlabelled competitors for competition experiments). The cells are then gently washed to remove non-bound chemical probe. The cells subsequently undergo chemical fixation with paraformaldehyde, which reacts with proteins and other cell components to form covalent cross-links. Next, the cells are permeabilized with the surfactant TritonX100 prior to staining with the tetrazine fluorescence dye (tetrazine-Cy5) for the intracellular IEDDA reaction to occur. The cells are then washed again to remove residual Cy5 and fluorescence can be analysed by Fluorescence Activated Cell Sorting (FACS) or confocal microscopy.

Although not fully disclosed in their publication, Rutkowska *et al.* have investigated several fluorescent dyes when optimizing the cellular imaging of the tool chemical probe Olaparib-TCO (**22**) in HeLa cells.^[88] Several factors must be taken into consideration when it comes to selecting a fluorescent dye for cellular imaging applications.^[191,192] First, an excitation wavelength in the red to far-red spectra is usually preferred for cellular imaging, to avoid overlap with autofluorescence of the cells.^[193] Indeed, living cells are known to have an autofluorescence background in the visible region of the spectrum that is caused by the variety of endogenous fluorophores present in the cells, including nucleotides or amino acids which are typically excited by blue/ultraviolet radiation.^[193] Next, the molar extinction coefficient (ϵ), which is a

measure of the light absorbing capacity of a fluorescent dye, is very important and is ultimately linked to the brightness of a dye, with larger molar extinction coefficient resulting in more efficient absorbers dyes.^[191,194] In particular, the brightness of a fluorophore is proportional to the product of the extinction coefficient and the fluorescence quantum yield, which is the ratio between the number of fluorescence photons emitted and the number of photons absorbed.^[191,194,195]

Even though most of their investigations focused on Tetrazine-Cy5 dye (Table 9), Rutkowska *et al.* have also given some attention to fluorogenic tetrazine dyes. The term fluorogenic tetrazines refers to tetrazine-functionalised dyes whose intrinsic fluorescence is quenched through energy transfer by the tetrazine moiety and is only restored upon IEDDA cycloaddition with a dienophile.^[65,196,197] Despite being attractive for live cell imaging applications by potentially offering improved signal-to-noise ratios, the so-called fluorogenic tetrazine ligations are not without limitation. Indeed, most reports of fluorogenic tetrazine dyes are often limited to the imaging of either overexpressed targets or highly abundant cell surface proteins.^[65,196,198] Therefore, fluorogenic dyes might not necessarily provide an advantage over non-fluorogenic dyes when it comes to the cellular imaging of endogenous low expressed intracellular targets such as PI3K δ . Another key factor to take into consideration is the fluorescence ‘turn-on ratio’ which reflects how much brighter the fluorogenic dye becomes once the intrinsic fluorescence of the dye is restored upon IEDDA cycloaddition with a dienophile. In most literature examples, the turn-on ratio is measured in a test tube using DMSO or PBS, which may not truly reflect the cellular conditions in which the dye will be used.^[191,197] Besides, the imaging of low abundant intracellular targets often requires dyes with high brightness (large molar extinction coefficient and high quantum yield), conditions that are not always achieved by fluorogenic dyes as they tend to be less bright than their non-fluorogenic counterparts. An example of a fluorogenic dye investigated by Rutkowska *et al.* is Silicon Rhodamine Tetrazine (SiR-Tetrazine, Table 9).^[199,200] Despite the signal to background ratio being improved with SiR-Tz compared to tetrazine-Cy5 when used on fixed cells, larger quantities of the fluorogenic dye had to be used in this experiment, along with higher laser power, when there is only a 2.5-fold difference in the molar

extinction coefficient of Cy5-Tz and SiR-Tz. Overall, these observations motivated the use of Cy5 for most subsequent cellular imaging experiments.

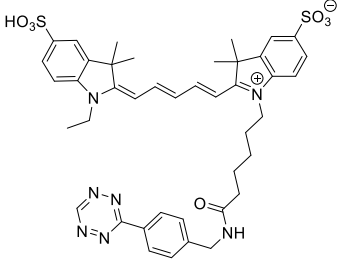
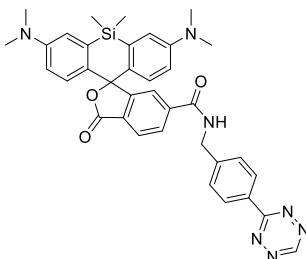
Structure		
Dye Name	3-(p-Benzylamino)-1,2,4,5-tetrazine – Cy5 (Cy5-Tz)	3-(p-Benzylamino)-1,2,4,5-tetrazine – Silicon Rhodamine (SiR-Tz)
MW (g/mol)	826.0	641.8
$\lambda_{\text{Abs/Em}}$ (nm)	649/670 ^[201]	652/674 ^[200]
ϵ (L mmol⁻¹ cm⁻¹)	250 ^[201]	100 ^[200]

Table 9. Properties of tetrazine fluorescent dyes (non-fluorogenic, left and fluorogenic, right).

The FACS technique allows the analysis of the fluorescence resulting from Cy5 by two complementary methods. The first data interpretation method is referred to as “% Cy5-positive cells” and measures the percentage of cells being fluorescently labelled with Cy5. More specifically, a gate for Cy5-positive cells is defined in a FL1-H/FL4-H scatter plot (FL1-H detecting cell autofluorescence and FL4 being a fluorescent channel where the Cy5 signal is detected), and the percentage of Cy5-positive cells amongst all cells is calculated based on the number of events recorded within that gate (Figure 30). In other words, this approach measures the percentage of cells displaying a higher fluorescence than the cells only treated with DMSO (negative control). However, this data interpretation approach does not give any indication on the fluorescence intensity of the fluorescent-labelled cells (i.e. how much brighter than the DMSO control). Therefore, a second approach referred to as “MFI” measures the mean fluorescence intensity of the labelled cells.

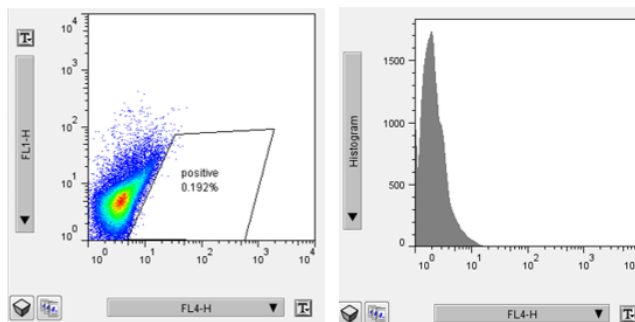


Figure 30. FACS data interpretation methods (left = % Cy5-positive cells, right =MFI).

3.4.1. Synthesis and Selection of Unlabelled PI3K δ Competitors

An important aspect to consider for competition experiments in the imaging assay is the choice of non-labelled (or unmodified) PI3K δ competitor compound used to displace the PI3K δ chemical probe from the active site of the target. A successful competitor should result in decreased fluorescence signals originating from the chemical probe, therefore confirming target engagement of the non-labelled compound and that the observed fluorescence is selective to PI3K δ inhibition. However, if a fluorescence signal remains, this may be an indication that the chemical probes interacts non-specifically with other targets in cells or undergo sequestration in cellular compartments.

It was assumed that the non-labelled PI3K δ inhibitor used as a competitor did not necessarily need to be structurally-related to the chemical probe that was being displaced. This could offer the possibility to use a probe from one compound series of PI3K δ inhibitors and a competitor from another, provided both molecules are potent and selective PI3K δ inhibitors. However, recent unpublished studies by Rutkowska *et al.* revealed that inefficient competition associated with lack of reduced fluorescent signal could be observed when the unmodified competitor displayed either a different binding mode or a different binding site as compared to the chemical probe.^[199] Therefore, where possible, efforts were made to use PI3K δ competitor compounds from the same series as the chemical probe under study.

Because of limitations using the inhaled clinical candidates as competitors for the imaging experiments, close structural analogues were selected (Table 10).

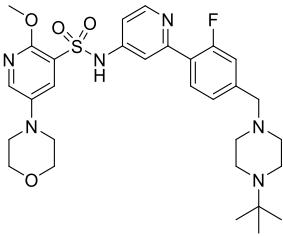
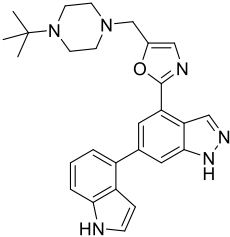
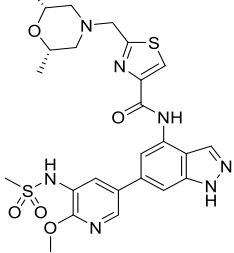
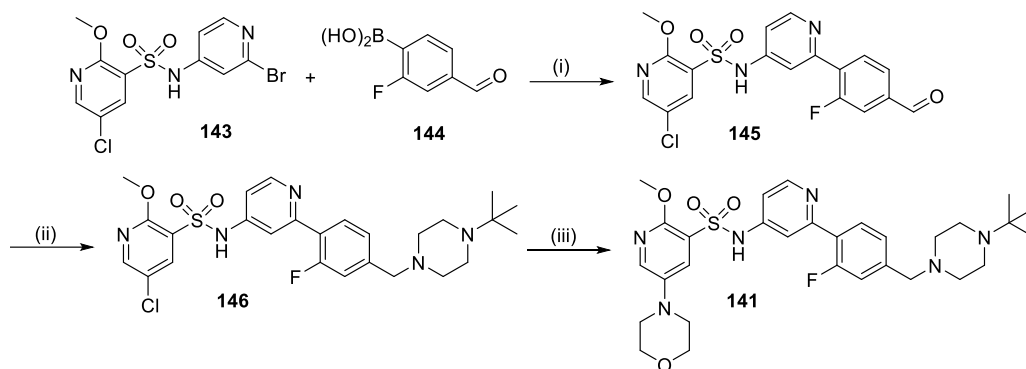
Series	Oral	Inhaled (based on nemiralisib)	Inhaled (based on GSK2292767)
Competitor	 141	 142	 27

Table 10. Structure of PI3K δ competitors used for competition experiments in the cellular imaging/target engagement assay.

For the oral series of PI3K δ inhibitor, the chosen competitor contains a *tert*-butyl piperazine (**141**) instead of the isopropyl piperazine found in the parent compound (**33**). It was reasoned that the introduction of an additional methyl group should minimally impact the physico-chemical properties and that the compound would maintain high potency and selectivity for PI3K δ if the tryptophan shelf is able to accommodate the bulky *tert*-butyl group.^[126] A very similar reasoning was adopted for the inhaled clinical candidate nemiralisib whereby the chosen competitor contains a *tert*-butyl piperazine (**142**). The competitor chosen for the second inhaled clinical candidate GSK2292767 was the thiazolyl amide **27**, previously described in Section 1. The synthesis of competitor **141** is depicted in Scheme 30 below.



Reagents and conditions: (i) (2-Fluoro-4-formylphenyl)boronic acid, K_3PO_4 , Solvias catalyst (13 mol%), EtOH/H₂O (4:1), μ wave, 110 °C, 35 min, 51%; (ii) 1-(*tert*-Butyl)piperazine, AcOH, DCM, rt, 30 min, then STAB, 2 h, 72%; (iii) morpholine, NaOtBu, Pd(OAc)₂ (10 mol%), RuPhos (20 mol%), toluene, 90 °C, 1 h, 3%.

Scheme 30. Synthesis of competitor **141**.

The synthesis started with a Suzuki coupling between 2-bromopyridine **143** and (2-fluoro-4-formylphenyl)boronic acid **144** mediated by Solvias catalyst that contains a bis(2-norbornyl)phosphine ligand. This catalyst was initially reported by Blaser and co-workers, who investigated several combinations of palladacycles and secondary phosphanes with the aim to develop novel catalysts with broad applicability for various palladium cross-coupling reactions.^[202] Next, reductive amination with 1-(*tert*-Butyl)piperazine gave the desired intermediate **146**. Finally, a subsequent Buchwald-Hartwig coupling with morpholine afforded the desired compound **141** in poor yields due to difficulties in isolating the desired product from the corresponding dehalogenated side-product.

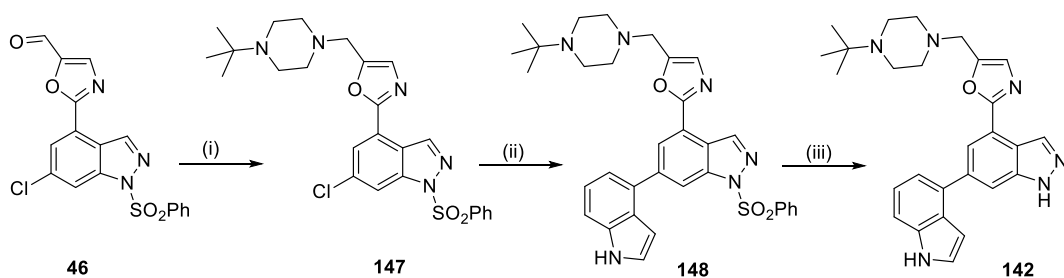
Once its synthesis was complete and prior to its use as a competitor in the imaging assay, the desired *tert*-butyl analogue was profiled in the enzyme, kinobead and human whole blood assays to ensure that it maintained good potency and selectivity for PI3K δ prior. The properties of compound **141** are highlighted in Table 11 below. Overall, compound **141** displayed a very similar potency and selectivity profile compared to the parent compound **33** along with similar physico-chemical properties, therefore confirming its suitability for use as a competitor in the imaging assay.

Compound number	33	141
PI3Kδ pK_i (n)	10.9 (3) ^a	10.6 (2) ^a
PI3Kα, β, γ pIC₅₀ (n)	6.0 (22), 5.3 (22), 5.7 (28)	6.1 (8), 5.4 (8), 5.7 (12)
α, β, γ fold selectivity	1259, 6310, 2512	1000, 5012, 2512
hWB pIC₅₀ (n)	8.2 (47) ^b	8.6 (19) ^c
Kinobead pIC₅₀ (n)	8.6 (4)	8.9 (5)
Meas. ChromLogD_{pH7.4}	1.9	1.9
AMP (nm/s, pH 7.4)	105	122
Kinetic solubility (μg/mL)	≥287	≥295

*n = number of test occasions included in mean; ^aPI3Kδ assay run at a 2 mM ATP concentration; ^bDid not return a value on one test occasion; ^cFailed to fit a curve on one test occasion, Tested >9.8 on one test occasion.

Table 11. Properties of oral PI3Kδ inhibitor **33** and *tert*-butyl analogue **141**.

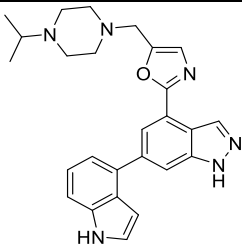
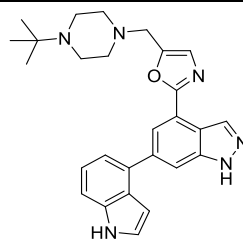
For similar reasons, a suitable nemiralisib analogues contains a *tert*-butyl piperazine. The synthesis of this compound (**142**) is displayed in Scheme 31 below.



Reagents and conditions: (i) 1-*tert*-Butylpiperazine, AcOH, DDCM, rt, 30 min, then STAB, DCM, overnight, 70%; indole-4-boronic acid pinacol ester, XPhos Pd G2 (20 mol%), Na₂CO₃, 1,4-dioxane:water (10:1), 90 °C, μwave, 1 h, 50%; 2 M aqueous NaOH, MeOH, 80 min, 17%.

Scheme 31. Synthesis of competitor **142**.

The synthesis started with a reductive amination between aldehyde **46** and 1-(*tert*-butyl)piperazine to afford desired intermediate **147**. Subsequent Suzuki cross-coupling with indole-4-boronic acid pinacol ester gave the biaryl intermediate **148**, which afforded the desired compound **142** after benzenesulfonyl deprotection (Scheme 31). The properties of compound **142** are highlighted in Table 12 below. Similarly to nemiralisib, the *tert*-butyl piperazine analogue was found to be very potent and selective for PI3K δ (Table 12).

Structure		
Compound number	nemiralisib	142
PI3K δ p <i>K</i> _i (n)	9.9 (4) ^a	9.0 (2)
PI3K α , β , γ pIC ₅₀ (n)	5.3 (27) ^b , 5.8 (26) ^c , 5.2 (30) ^d	4.7 (2), 5.1 (2), 5.3 (2)
α , β , γ fold selectivity	5012, 1585, 6310	10000, 3981, 2512
hWB pIC ₅₀ (n)	8.9 (3)	9.1 (5)
Kinobeard pIC ₅₀ (n)	9.2 (2) ^e	8.5 (1) ^f
Meas. ChromLogD _{pH7.4}	2.5	2.7
AMP (nm/s, pH 7.4)	230	170
Kinetic solubility (μ g/mL)	110	≥ 181

*n = number of test occasions included in mean; ^aPI3K δ assay run at a 2 mM ATP concentration; ^bTested <5.3 on one test occasion and <4.6 on one test occasion; ^cTested <4.6 on one test occasion; ^dTested <4.6 on 3 test occasions; ^eLipid kinobeards CZK133 / lysate mix HeLa-Jurkat-K-562; ^fLipid kinobeards CZK126 / lysate mix Hut78-MCF7.

Table 12. Properties of oral PI3K δ inhibitor nemiralisib and *tert*-butyl analogue **142**.

In addition to the aforementioned competitors, it was suggested that a covalent PI3K δ inhibitor could be used as a competitor in the imaging assay to further investigate the cellular behaviour of some of the chemical probes.

Compound **149** previously developed in our laboratories contains a covalent warhead (highlighted in blue in Figure 31) that selectively targets the kinome-conserved Lysine779 residue.^[203]

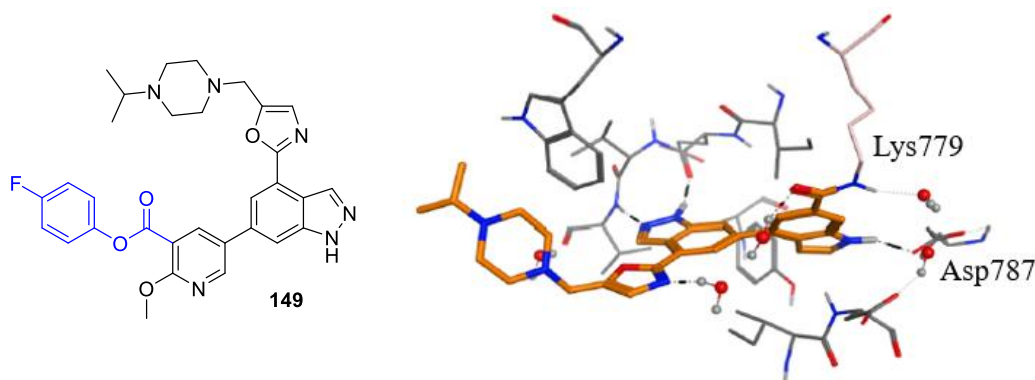


Figure 31. Crystal structure of covalent PI3K δ inhibitor **149** showing electron density from Lys779 onto the ligand.^[203]

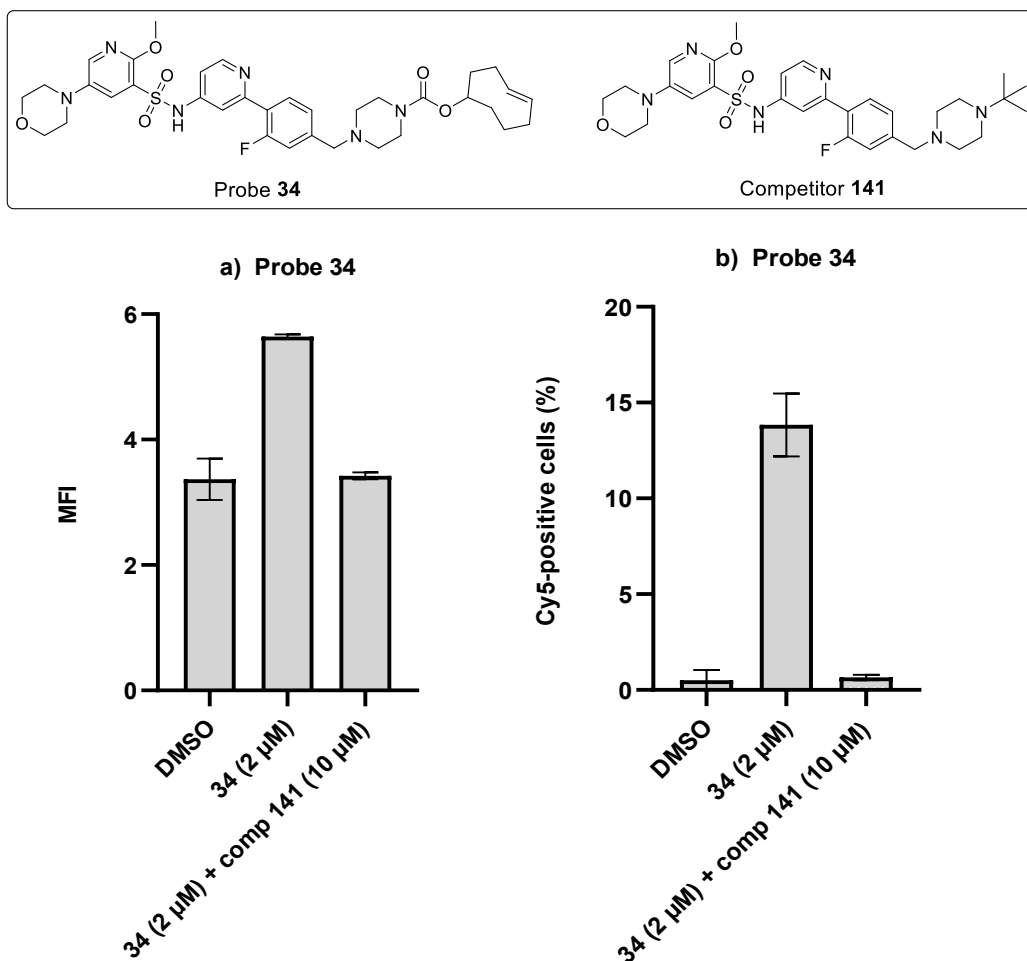
Covalent inhibitors have an advantage over non-covalent ones when the binding mode between the chemical probe and the non-labelled competitor could be different (e.g. irreversible inhibition leading to longer residence time). Pre-incubation of cells with an excess of a covalent inhibitor prior to incubation with the chemical probes would fully occupy the PI3K δ active site and this binding would not be affected by subsequent washing steps or treatment with the chemical probe. Therefore, this is the most efficient way to perform competition experiments.

3.4.2. Imaging Design

The TCO chemical probe **34**, derived from the oral series of PI3K δ inhibitors had previously been investigated in the cellular imaging assay in PBMCs using both FACS and microscopy readouts (unpublished results). In those experiments, the fluorescent signal observed in cells treated with probe **34** proved to be specific for PI3K δ since the chemical probe was successfully competed with the unmodified PI3K δ inhibitor **141** from the same series.

In order to assess the suitability of Hut78 cells as an alternative system to PBMCs to screen the chemical probes derived from nemiralisib and GSK2292767, the cellular imaging of chemical probe **34** was repeated in Hut78 cells with FACS and

microscopy read-out. The results of the FACS experiments are presented in Figure 32 below.



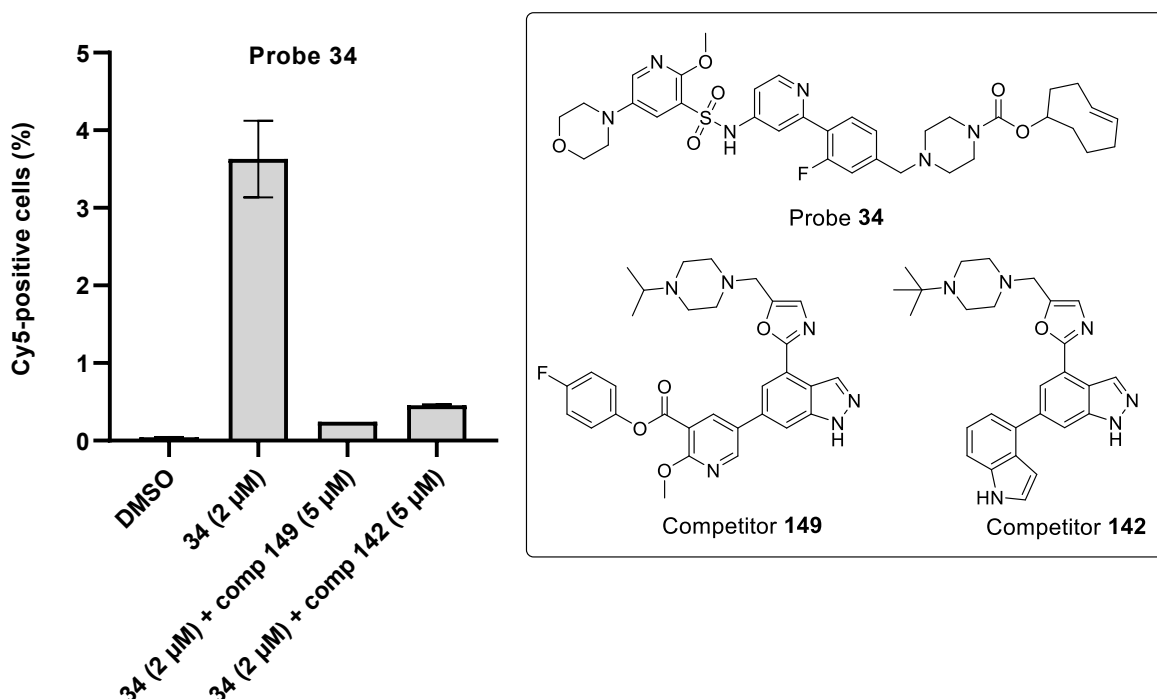
Flow cytometric analysis of Hut78 cells treated for 90 min with DMSO, 2 μ M probe **34**, 2 μ M probe **34** + 10 μ M competitor **141**. After treatment, cells were gently washed to remove unbound probe prior to fixation, permeabilization, and IEDDA reaction with 100 nM Tz-Cy5 for 5 min. Results from one experiment is shown (n=3, STEV). Representative results from at least 2 independent biological replicates; a) Mean Fluorescence Intensity (MFI), b) % Cy5-positive cells.

Figure 32. FACS analysis of fluorescence signal from TCO chemical probe **34**.

FACS analysis of Hut78 cells treated with chemical probe **34** revealed an enhanced fluorescence intensity compared to cells treated with DMSO only (Figure 32a). The fluorescent signal observed in cells treated with DMSO constitutes a small percentage of non-specific background resulting from residual Cy5 dye following the

staining procedure. In addition, successful intracellular competition was observed when cells were simultaneously treated with probe **34** and the structurally related PI3K δ inhibitor **141**, where the fluorescence intensity remains similar to that of the DMSO control (Figure 33). This confirms that the competitor successfully displaced the chemical probe from the PI3K δ active site, and that the TCO probe was ultimately washed away. Overall, these observations support the conclusion that the fluorescent signal resulting from Hut78 cells treated with probe **34** is specific to PI3K δ binding. A similar outcome is shown in Figure 32b that represents the percentage of Hut78 cells fluorescently labelled with Cy5.

Besides, the fluorescent signal resulting from chemical probe **34** was also successfully competed in cells treated with a competitor that did not belong to the oral series of PI3K δ inhibitor, including the non-covalent inhibitor **142** (*tert*-butyl analogue of nemiralisib) from the inhaled series as well as the covalent PI3K δ inhibitor **149** (Figure 33).



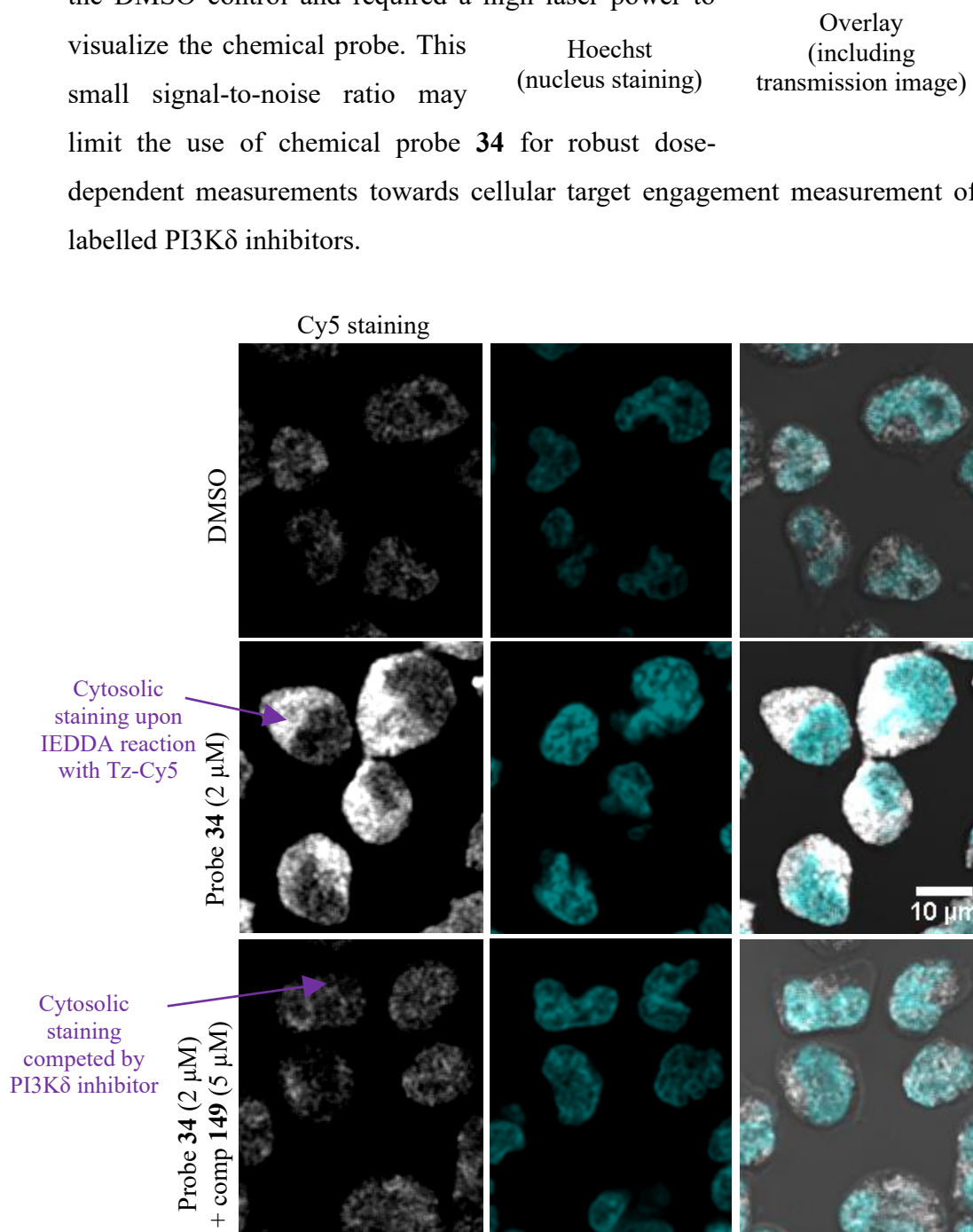
Flow cytometric analysis of Hut78 cells treated for 90 min with DMSO, 2 μ M probe **34**, or 60 min pre-incubation with 5 μ M covalent competitor **149** followed by 90 min 2 μ M probe **34** or 60 min pre-incubation with 5 μ M competitor **142** followed by 90 min 2 μ M probe **34**. After treatment, cells were gently washed to remove unbound probe prior to fixation, permeabilization, and IEDDA reaction with 100 nM Tz-Cy5 for 5 min. Results from one experiment is shown (n=2, STEV). Representative results from at least 2 independent biological replicates.

Figure 33. FACS analysis of fluorescence signal from TCO chemical probe **34** from the oral series of PI3K δ inhibitors in Hut78 cells.

When analysed by microscopy, Hut78 cells treated with chemical probe **34** showed a specific cytosolic signal, which is consistent with the expected cellular localisation of PI3K δ (Figure 34).^[106] For this read-out, an additional staining with a fluorescent dye (Hoechst) was introduced to stain the nucleus of the cells and therefore facilitate the visualisation of the subcellular localisation of the chemical probe.

In alignment with the FACS data, successful competition with PI3K δ inhibitors from the same or different series was observed, for example with the covalent PI3K δ

inhibitor **149** as shown in Figure 34. However, the intensity of the fluorescence observed in Hut78 cells treated with probe **34** was found to be only slightly higher than the DMSO control and required a high laser power to visualize the chemical probe. This small signal-to-noise ratio may limit the use of chemical probe **34** for robust dose-dependent measurements towards cellular target engagement measurement of non-labelled PI3K δ inhibitors.



Hut78 cells treated with 2 μ M probe **34** for 90 min or pre-incubation with 5 μ M covalent competitor **149** for 60 min followed by 90 min incubation with 2 μ M probe **34**. Cells then underwent cytocentrifugation ("cytospin"), followed by fixation, permeabilization, IEDDA reaction with 100 nM

Tz-Cy5 for 5 min. Nuclei were stained with Hoechst. Representative fluorescent images recorded after excitation at 405 nm (Hoechst) and 633 nm (Tz-Cy5). Scale bar 10 μ m.

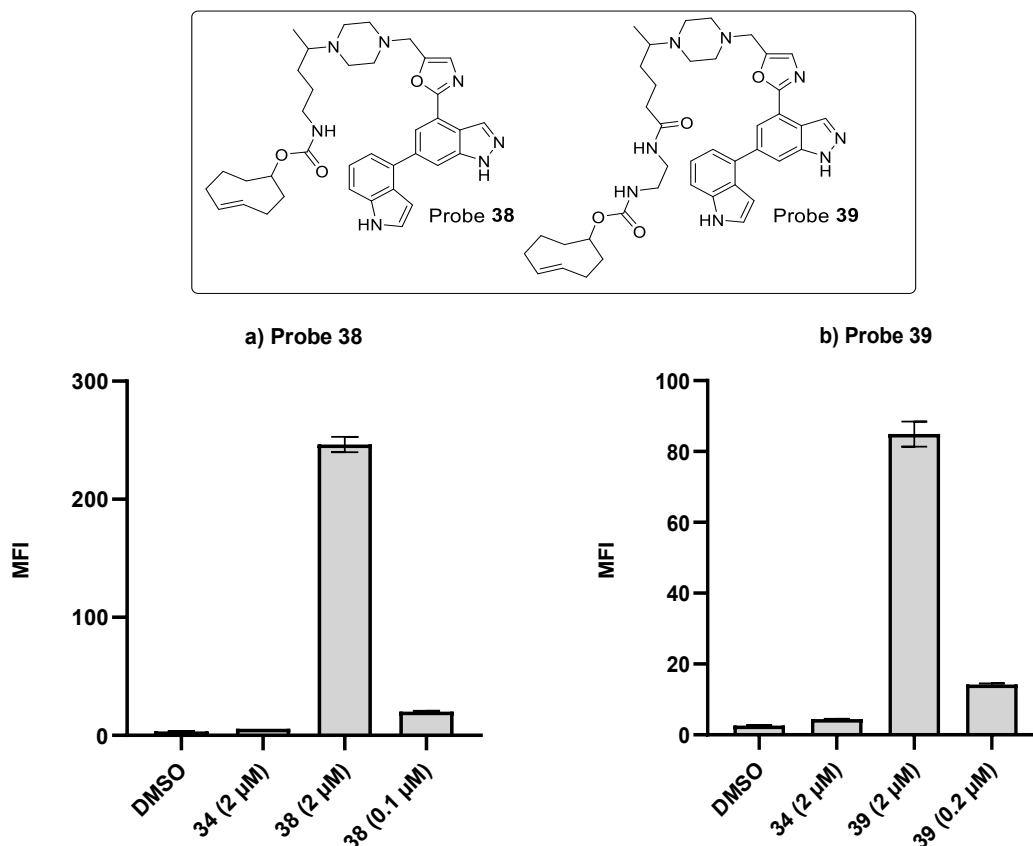
Figure 34. Cellular localisation and competition experiments of TCO chemical probe **34** in Hut78 cells.

Overall, the cellular imaging of chemical probe **34** in Hut78 cells showed similar conclusions to what had previously been observed in PBMCs (i.e. specific but weak cytosolic signal with reproducible competition with several unmodified PI3K δ inhibitors) which confirmed that Hut78 cells were a suitable biological system for the cellular imaging of PI3K δ chemical probes

Based on these observations, the selected PI3K δ chemical probes derived from the inhaled clinical candidates nemiralisib and GSK2292767 were investigated in the cellular imaging assay in Hut78 cells. Since chemical probe **34** derived from the oral series of PI3K δ inhibitor had successfully been imaged in Hut78 cells, it was used as a reference in all subsequent imaging experiments.

3.4.3. Imaging of TCO Chemical Probes Derived from Inhaled PI3K δ Inhibitors

When analysed by FACS, Hut78 cells treated with chemical probes **38** and **39** derived from nemiralisib gave a concentration-dependent fluorescent signal with an intensity that was significantly enhanced compared to the reference chemical probe **34**, even at the lowest concentration tested (Figure 35).

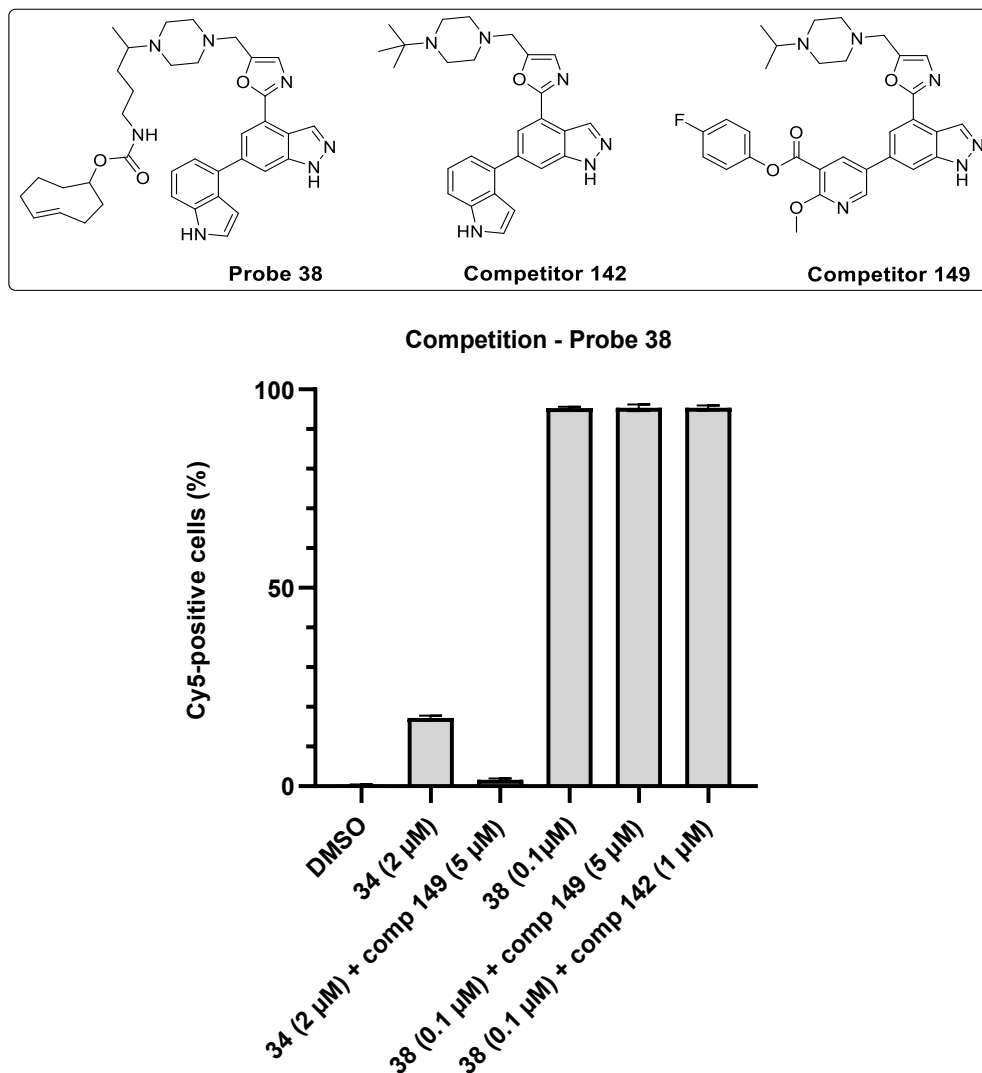


Flow cytometric analysis of Hut78 cells treated for 90 min with DMSO, 2 μM chemical probe **38**, a) 2 and 0.1 μM probe **38**, b) 2 and 0.2 μM chemical probe **39** after treatment, cells were gently washed to remove unbound probe prior to fixation, permeabilization, and IEDDA reaction with 100 nM Tz-Cy5 for 5 min. Results from one experiment is shown (n=3, STEV). Representative results from at least 2 independent biological replicates.

Figure 35. FACS analysis of fluorescence signal from TCO chemical probe **38** and **39** derived from nemiralisib in Hut78 cells.

The fluorescence intensity resulting from the chemical probe **39** was weaker than for chemical **38** when compared at the same concentration (2 μM), which could result from the poor permeability of probe **39** (Table 7, Section 3.3) and impaired crossing through the cell membrane to reach the PI3Kδ target (Figure 35, b). Next, the

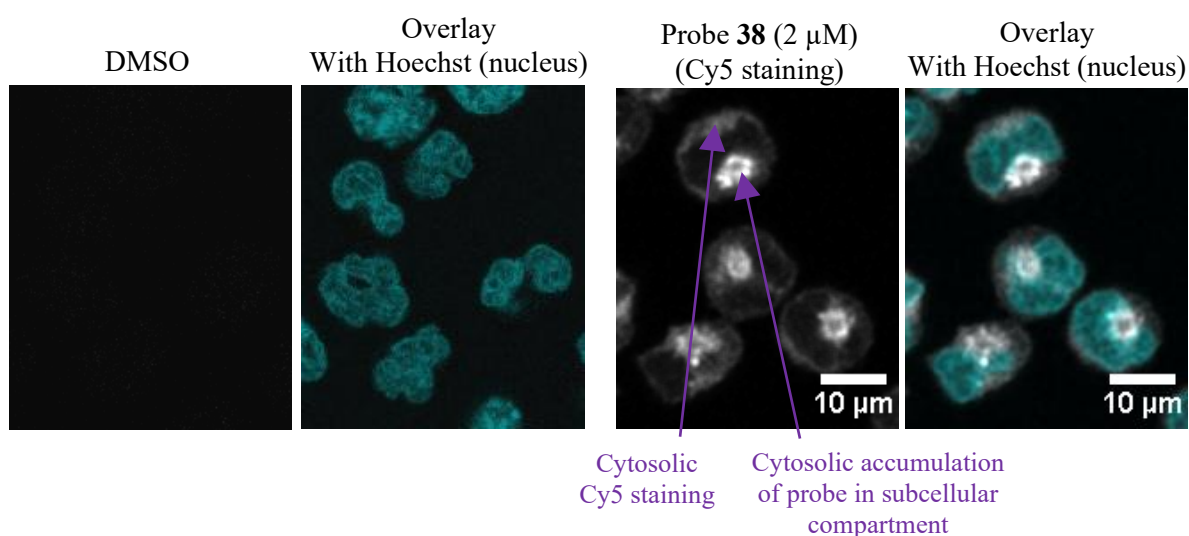
chemical probe **38** derived from nemiralisib was investigated in competition experiments with several PI3K δ inhibitors; both non-covalent and covalent. However, in all cases no competition could be observed by FACS, therefore suggesting that the observed fluorescent signal might also be unspecific (*e.g.* accumulation of the probe) (Figure 36).



Flow cytometric analysis of probe **34**: Hut78 cells treated for 90 min with DMSO, 0.1 μ M probe **38**, 0.1 μ M probe **38** + 1 μ M competitor **142** or 60 min pre-incubation with 5 μ M covalent competitor **149** followed by 90 min incubation with 0.1 μ M probe **38**. Cells subsequently underwent fixation, permeabilization, and IEDDA reaction with 100 nM Tz-Cy5 for 5 min. Results from one experiment is shown (n=2, STEV). Representative results from at least 2 independent biological replicates.

Figure 36. FACS analysis of fluorescence signal from TCO chemical probes **38**.

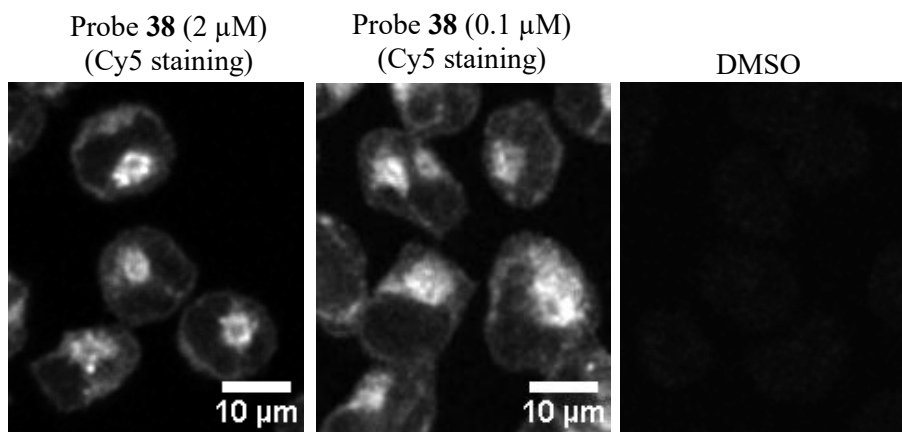
When visualized by confocal microscopy at 2 μ M, the fluorescent signal resulting from chemical probe **38** was not homogeneously distributed across the cytosol, compared to previous observations for probe **34** from the PI3K δ oral series. In this case, in addition to a weak cytosolic staining localized at the periphery of the cells, accumulation of the probe in a specific area of the cytosol that lies adjacent to the nucleus was observed, which could corresponds to specific organelles such as the Golgi and/or the endoplasmic reticulum (ER) (Figure 37).



Hut78 cells treated for 90 min with DMSO or 2 μ M probe **38** before undergoing cyto centrifugation (“cytospin”), followed by fixation, permeabilization, and IEDDA reaction with 100 nM Tz-Cy5 for 5 min. Nuclei were stained with Hoechst. Representative fluorescent images recorded after excitation at 405 nm (Hoechst) and 633 nm (Tz-Cy5). Scale bar 10 μ m.

Figure 37. Cellular localization of TCO chemical probe **38** in Hut78 cells.

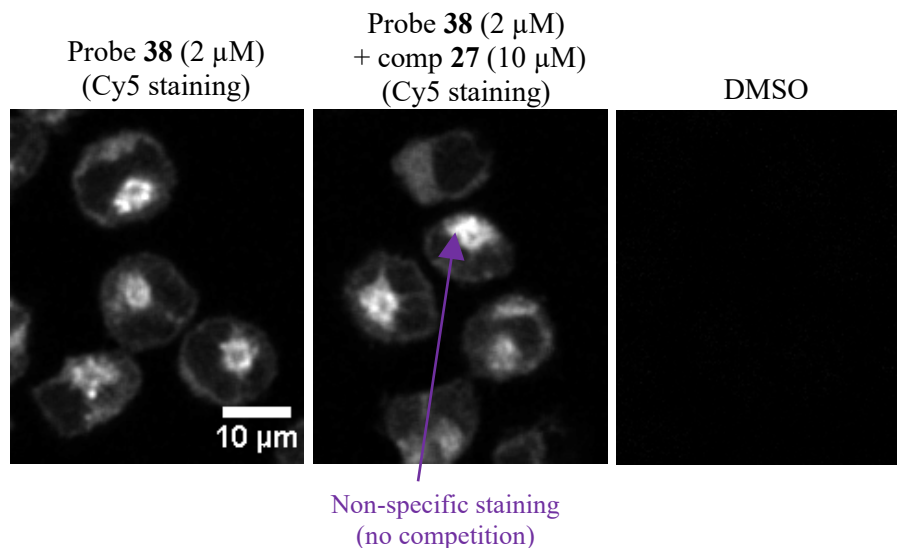
Based on this observation, the imaging experiment of chemical probe **38** was repeated in Hut78 at a reduced concentration (0.1 μ M) to investigate the influence of the concentration on the subcellular localization and accumulation of the compound. When profiled in the imaging assay at a reduced concentration, a less intense fluorescent signal was observed for TCO probe **38** compared to the previous experiment at 2 μ M. However, once again the fluorescent signal was not uniformly distributed throughout the cytosol, with the probe visibly accumulating in an area adjacent to the nucleus (Figure 37).



Hut78 cells treated for 90 min with 2 μ M or 0.1 μ M chemical probe **38** before undergoing cytocentrifugation (“cytospin”), followed by fixation, permeabilization, and IEDDA reaction with 100 nM Tz-Cy5 for 5 min. Representative fluorescent images recorded after excitation at 633 nm (Tz-Cy5). Scale bar 10 μ m.

Figure 38. Comparison of the cellular localisation of TCO chemical probes **38** at two different concentrations in Hut78 cells.

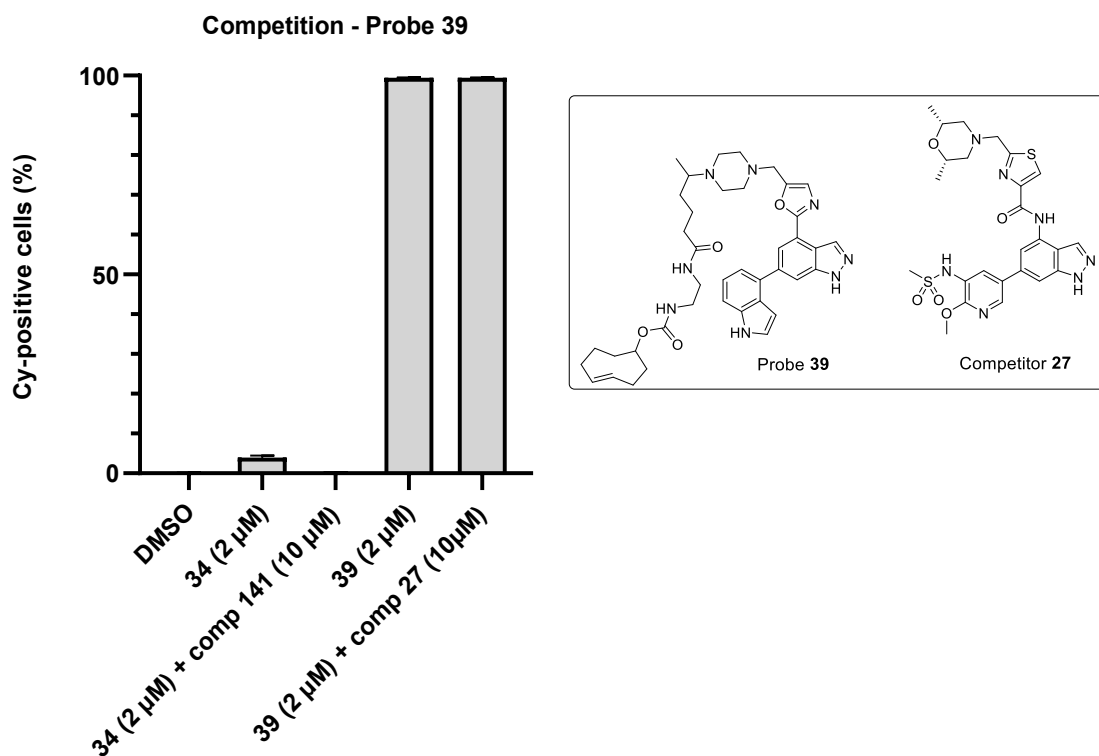
A competition experiment was then intended in Hut78 cells with competitor **27** to further assess the specificity of the fluorescent signal (Figure 39). As previously observed by FACS, no significant competition of the cytosolic signal could be observed by microscopy, with the chemical probe still exhibiting a very strong accumulation in a localized area of the cytosol. This could suggest that the observed staining might be unspecific. However, this does not necessarily exclude the presence of a specific fluorescent signal for PI3K δ , which may be difficult to distinguish from the prevalent unspecific signal.



Hut78 cells treated for 90 min with 2 μM probe **38** or 2 μM probe **38** + 10 μM competitor **27** before undergoing cytocentrifugation (“cytospin”), followed by fixation, permeabilization, and IEDDA reaction with 100 nM Tz-Cy5 for 5 min. Representative fluorescent images recorded after excitation at 633 nm (Tz-Cy5). Scale bar 10 μm.

Figure 39. Cellular localisation and competition experiments of chemical probe **38** in Hut78 cells.

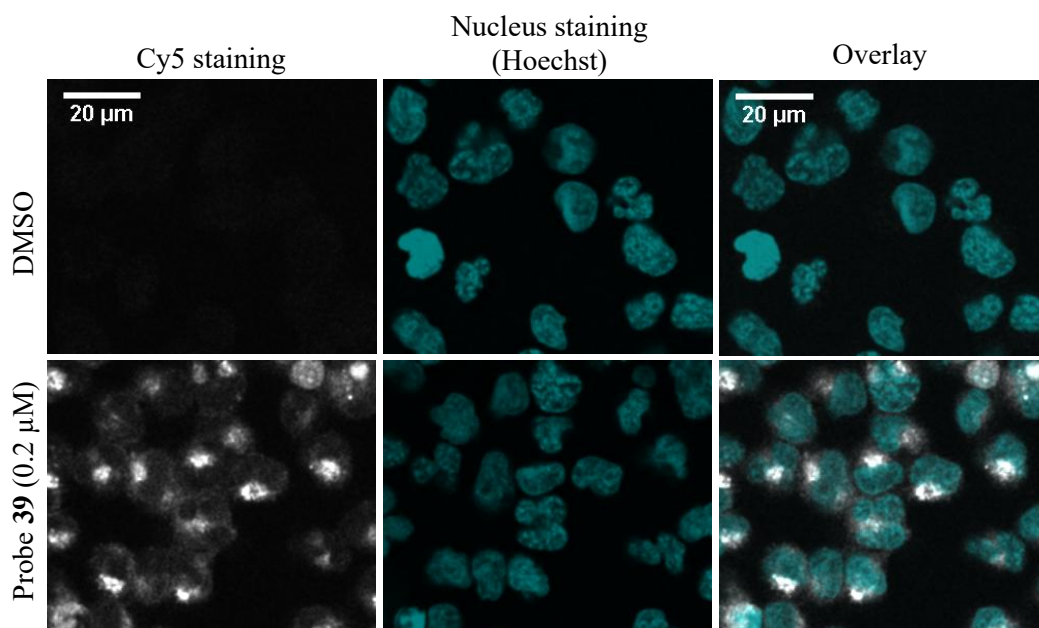
Despite the low permeability of chemical probe **39**, additional experiments were carried out to investigate potential differences in compound accumulation and subcellular distribution in comparison with probe **38**. FACS analysis of Hut78 cells treated with chemical probe **39** showed absence of competition in presence of inhaled PI3Kδ competitor **27**, again suggesting non-specific accumulation (Figure 40).



Hut78 cells treated for 90 min with 2 μ M probe **34**, 2 μ M probe **34** + 10 μ M competitor **141**, 2 μ M probe **39** or 2 μ M probe **39** + 10 μ M competitor **27**. Cells subsequently underwent fixation, permeabilization, and IEDDA reaction with 100 nM Tz-Cy5 for 5 min. Results from one experiment is shown (n=3, STEV). Representative results from at least 2 independent biological replicates.

Figure 40. FACS analysis of fluorescence signal from TCO chemical probes **39** in Hut78 cells.

When investigated by microscopy, Hut78 cells treated with chemical probe **39** (0.2 μ M) showed a very similar outcome to cells treated with probe **38**, with the probe localizing in the cytosol and a prevalent accumulation in subcellular compartments (Figure 41). In this experiment a very low laser power (0.4%) was needed to detect low concentration of the probe, therefore highlighting the extent of probe accumulation (i.e. by comparison, chemical probe **34** from the oral series of PI3K δ inhibitors usually requires a laser power of around 10% to be visualised by confocal microscopy).



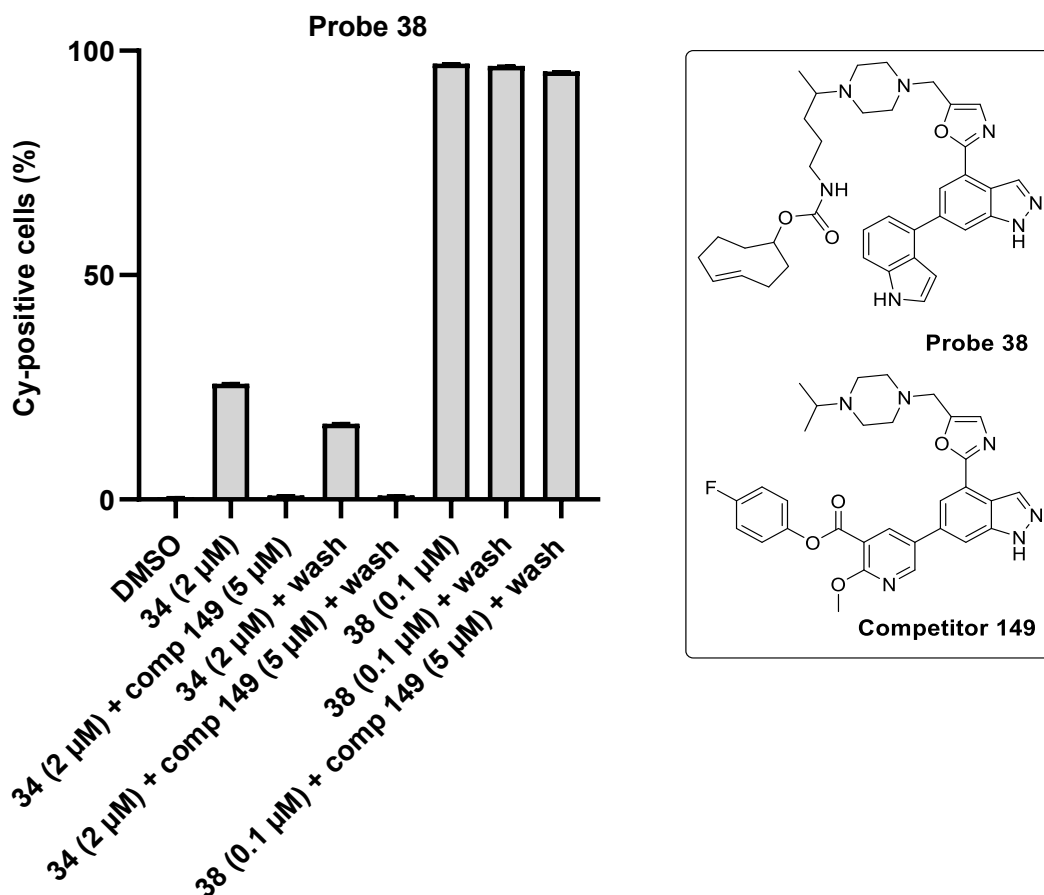
Hut78 cells treated for 90 min with DMSO or 0.2 μ M chemical probe **39** before undergoing cytocentrifugation (“cytospin”), followed by fixation, permeabilization and IEDDA reaction with 100 nM Tz-Cy5 for 5 min. Nuclei were stained with Hoechst. Representative fluorescent images recorded after excitation at 405 nm (Hoechst) and 633 nm (Tz-Cy5). Scale bar 20 μ m.

Figure 41. Cellular localisation of chemical probe **39** in Hut78 cells.

To further understand the accumulation of the chemical probes derived from nemiralisib observed in the cytosol of Hut78 cells, an additional washing step with cell media was implemented after incubation with the chemical probes and before the fixation procedure. It was hypothesized that this additional washing step could help to reduce the unspecific signal by removing chemical probe not bound to PI3K δ .

When investigated by FACS, cells treated with the reference probe **34** from the oral series of PI3K δ and subsequently washed with media gave a weaker fluorescent signal compared to those which did not undergo washing (Figure 42). Therefore, the introduction of this additional washing step prior to fixation reduced the signal intensity, suggesting that the probe had been partially washed away. Nevertheless,

However, in both cases successful competition was observed with the covalent PI3K δ inhibitor **149**, as previously observed for that chemical probe.

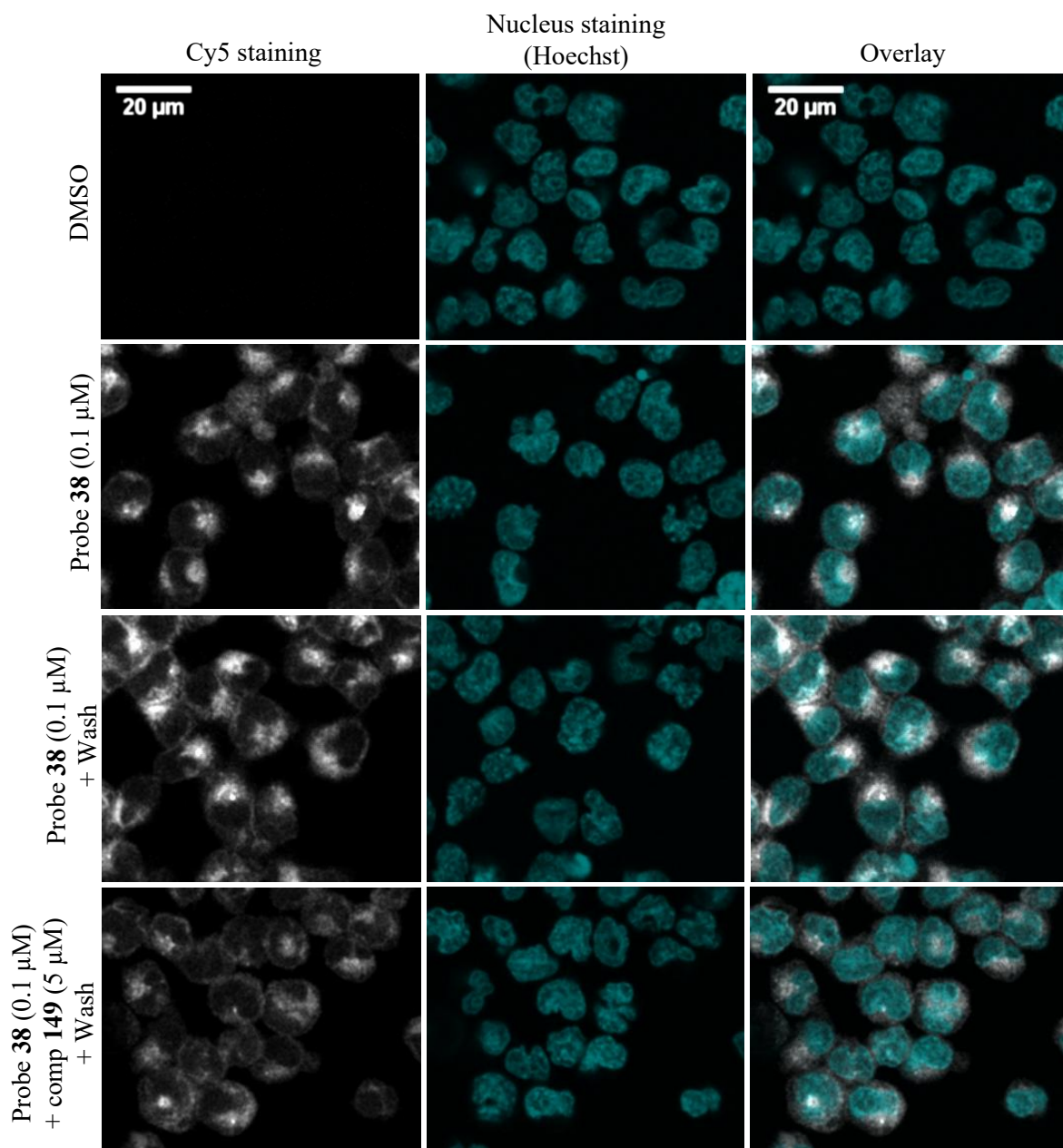


Hut78 cells treated for 90 min with DMSO, 2 μ M probe **34**, 0.1 μ M probe **38** or 60 min pre-incubation with 5 μ M covalent competitor **149** followed by 90 min incubation with 2 μ M probe **34** or 0.1 μ M probe **38**. Cells subsequently underwent fixation, permeabilization, and IEDDA reaction with 100 nM Tz-Cy5 for 5 min. When indicated, cells were washed with cell media before fixation. Results from one experiment is shown (n=2, STEV). Representative results from at least two independent biological replicates.

Figure 42. FACS analysis of fluorescence signal from TCO chemical probes **38** in Hut78 cells.

In the case of Hut78 cells treated chemical probe **38** derived from nemiralisib, the implementation of the additional washing step with media did not impact the

fluorescent signal in comparison with cells that did not undergo washing. In both cases no significant competition could be observed with the covalent PI3K δ inhibitor **149** (Figure 42). Similarly, when investigated by microscopy the implementation of the additional washing step did not seem to significantly reduce the fluorescent signal in Hut78 cells (Figure 43).



Hut78 cells treated for 90 min with DMSO or 0.1 μM chemical probe **38** or or 60 min pre-incubation with 5 μM covalent competitor **149** followed by 90 min incubation with 0.1 μM probe **38** before undergoing cytocentrifugation (“cytospin”), followed by fixation, permeabilization and IEDDA reaction with 100 nM Tz-Cy5 for 5 min. Nuclei were stained with Hoechst. When indicated, cells were

washed will cell media before fixation. Representative fluorescent images recorded after excitation at 405 nm (Hoechst) and 633 nm (Tz-Cy5). Scale bar 20 μm .

Figure 43. Cellular localisation of chemical probe **38** in Hut78 cells assessing the influence of a washing step with media before fixation on compound accumulation.

Based on the observed subcellular localization of the TCO chemical probes derived from nemiralisib in Hut78, it was proposed that the compounds could accumulate in specific organelles in the vicinity of the nucleus such as the Golgi apparatus and the endoplasmic reticulum (ER).

The endoplasmic reticulum (ER) is an organelle localized in the cytosol of eukaryotic cells. It can be divided in two functionally distinct structures, the rough endoplasmic reticulum (RER) and the smooth endoplasmic reticulum (SER) (Figure 44). The RER is contiguous with the nuclear envelope and is constituted of a network of flattened, membrane-enclosed sacs known as cisternae. The RER plays a major role in the synthesis, modification and transport of proteins. The SER consists of a network of tubules and plays a key role in the synthesis of phospholipids, which are major components of the plasma and internal membranes. The RER and SER are interconnected, and the proteins synthesized by the rough ER can move into the SER to be subsequently targeted to other organelles such as the Golgi apparatus (Figure 44).

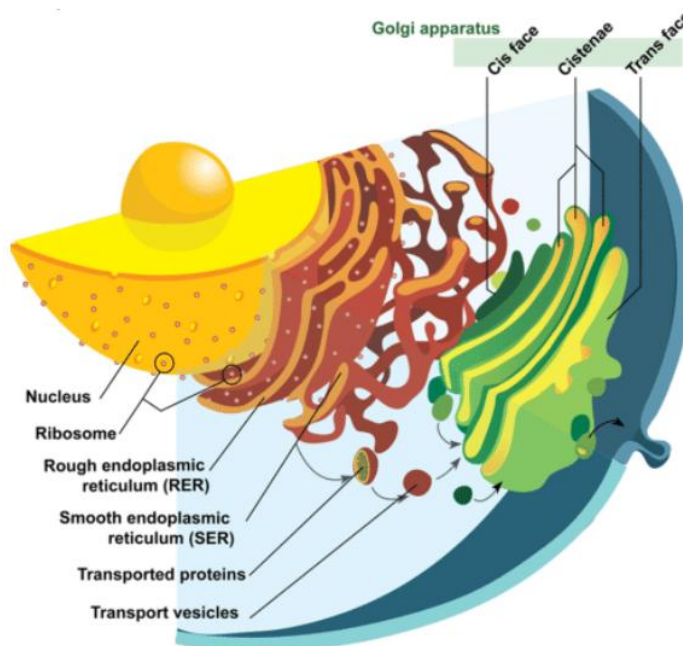


Figure 44. Schematic representation of the cell structure highlighting the endoplasmic reticulum (ER) and the Golgi apparatus.^[204]

The Golgi apparatus, sometimes also referred to as the Golgi complex, is another important organelle in eukaryotic cells that consists of flattened sacs called cisternae stacked in a semicircular formation (Figure 44). Each cisterna has a membrane that separates it from the cytoplasm of the cell and most cisternae differ in structure, composition, and function. Cargo proteins and phospholipids enter the Golgi at the *cis* face of the stack, which is closely associated with the ER, and depart from the *trans* face (Figure 44). As they progress through the Golgi cisternae layers, cargo proteins undergo various modifications such as glycosylation. The *trans*-most cisternae are designated as the *trans*-Golgi network (TGN) and are responsible for packaging cargo proteins *via* secretory vesicles for delivery to their intended destinations. In addition, the Golgi apparatus is known to be an acidic organelle with a pH decreasing along the *cis-trans* axis of the Golgi stack from pH 6.7 (*cis*-Golgi) to pH 6.0 at the *trans*-Golgi network.^[205]

Due to their properties and membrane-rich composition, unspecific accumulation of small molecules has previously been observed in those organelles, particularly lipophilic or basic amines-containing molecules.^[206,207]

To confirm the nature of the organelles in which the chemical probes derived from nemiralisib are accumulating, additional imaging experiments were carried out. To that aim, wheat germ agglutinin (WGA)-Alexa Fluor 488 was used as an additional dye to stain cellular membranes and facilitate the visualisation of ER and Golgi structures in Hut78 cells.^[208] As discussed above, several proteins localized in the Golgi are glycosylated, therefore lectins (sugar-binding proteins) such as wheat germ agglutinin functionalised with a fluorophore are well established dyes to stain the Golgi apparatus.^[209] In addition, the Alexa Fluor 488 dye exhibits a bright green fluorescence with an excitation/emission maxima of 495/519 nm that is distinct from Tetrazine-Cy5 and Hoechst and its fluorescence is not sensitive to pH, therefore explaining its widespread applications in fixed and permeabilised cells.

Hut78 cells treated with chemical probe **38** derived from nemiralisib were primarily stained with tetrazine Cy5 and subsequently underwent simultaneous staining with Hoechst and WGA-Alexa Fluor 488. The results of this multi-staining procedure are shown in Figure 45.

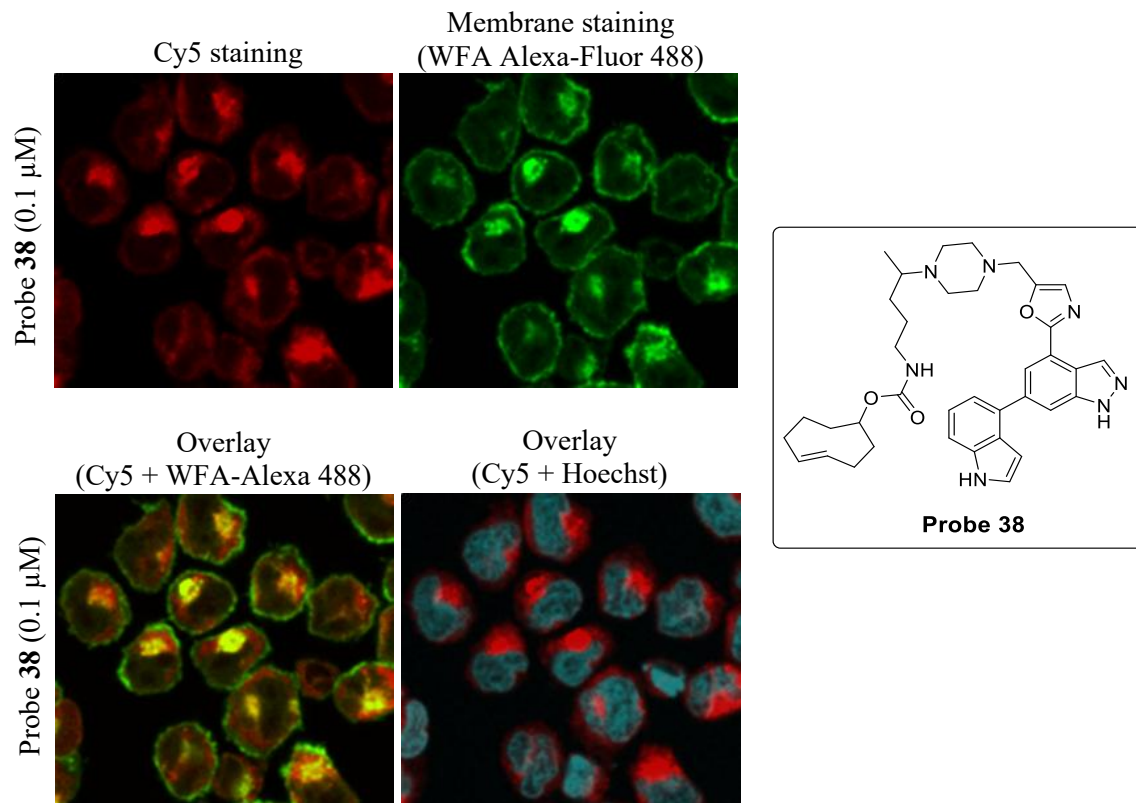
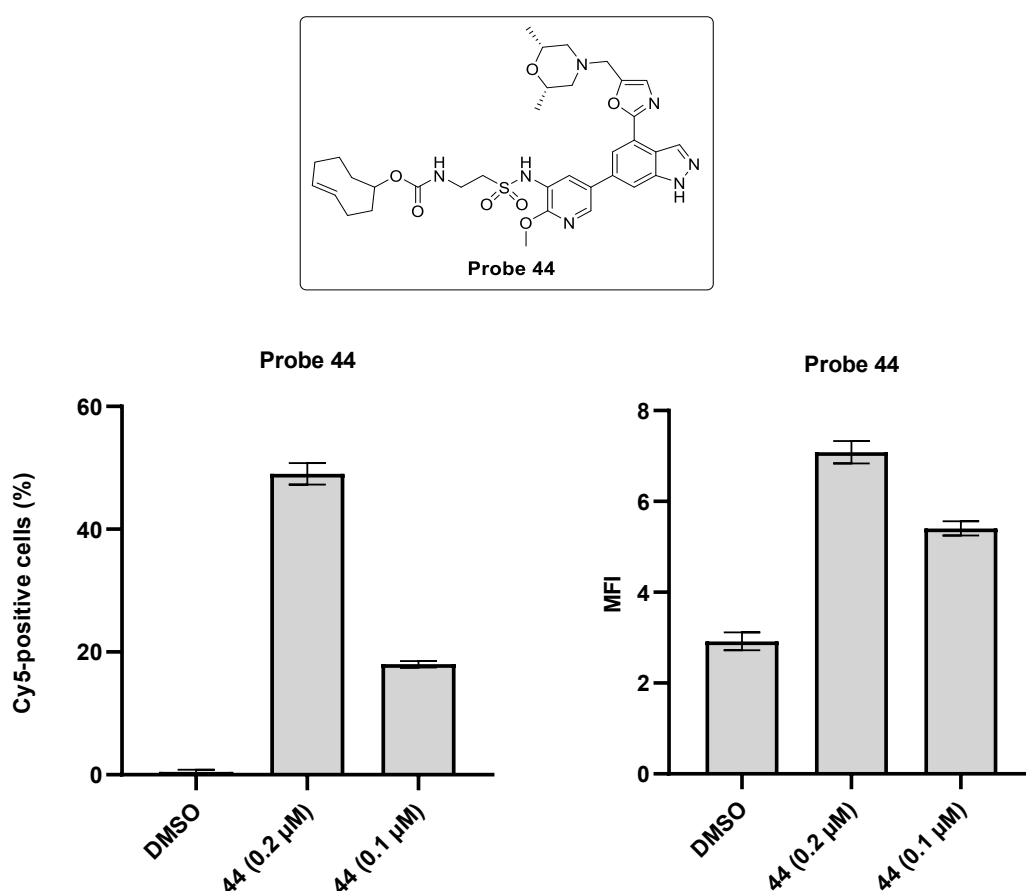


Figure 45. Multi staining procedure of chemical probe **38** in Hut78 cells with Tetrazine-Cy5, Hoechst and Alexa-Fluor 488.

In this experiment, Hut78 cells treated with chemical probe **38** showed once again a weak cytosolic staining and a strong accumulation in a subcellular compartment that lies in close vicinity to the nucleus as judged by the Cy5 and Hoechst staining (top left and bottom right panel). The Cy5 staining correlates well with the WGA Alexa-Fluor 488 staining as indicated by the co-localised yellow fluorescent signal, therefore clearly demonstrating that chemical probe **38** accumulates in membrane-rich organelles (Golgi/ER). A similar outcome was also observed with the less permeable chemical probe **39** derived from nemiralisib.

Next, the TCO chemical probe derived from the other inhaled PI3K δ inhibitor GSK2292767 was investigated in the imaging assay in Hut78 cells. The chemical probe **34** from the oral series of PI3K δ inhibitors was used for comparison.

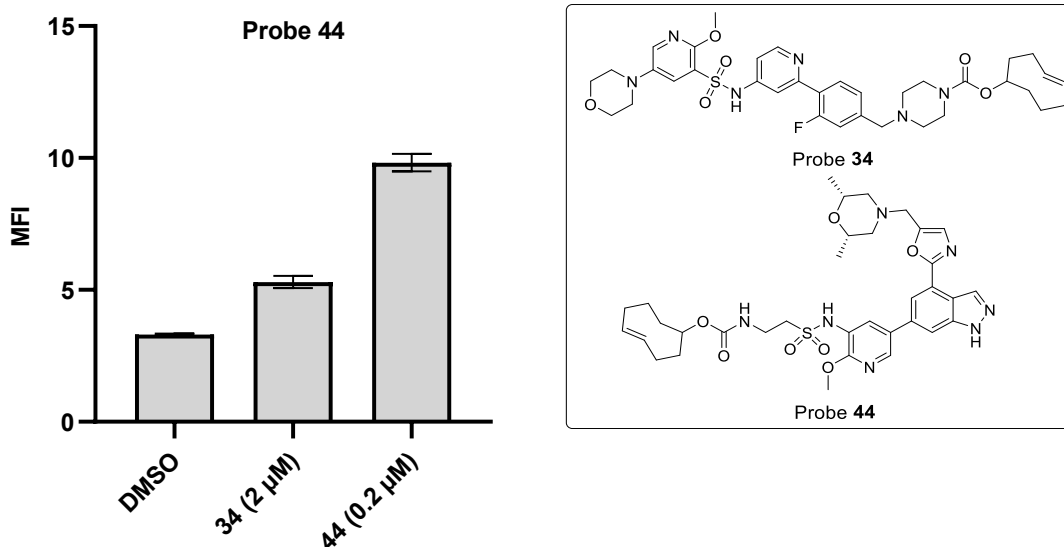
By FACS, a concentration-dependent signal was observed for Hut78 cells treated with chemical probe **44** at 0.2 μ M and 0.1 μ M (Figure 46).



Hut78 cells treated for 90 min with DMSO, 0.2 μ M probe **44** or 0.1 μ M probe **44**. Cells subsequently underwent fixation, permeabilization and IEDDA reaction with 100 nM Tz-Cy5 for 5 min. Results from one experiment is shown (n=3, STEV). Representative results from at least two independent biological replicates.

Figure 46. FACS analysis of chemical probe **44** derived from GSK2292767 in Hut78 cells.

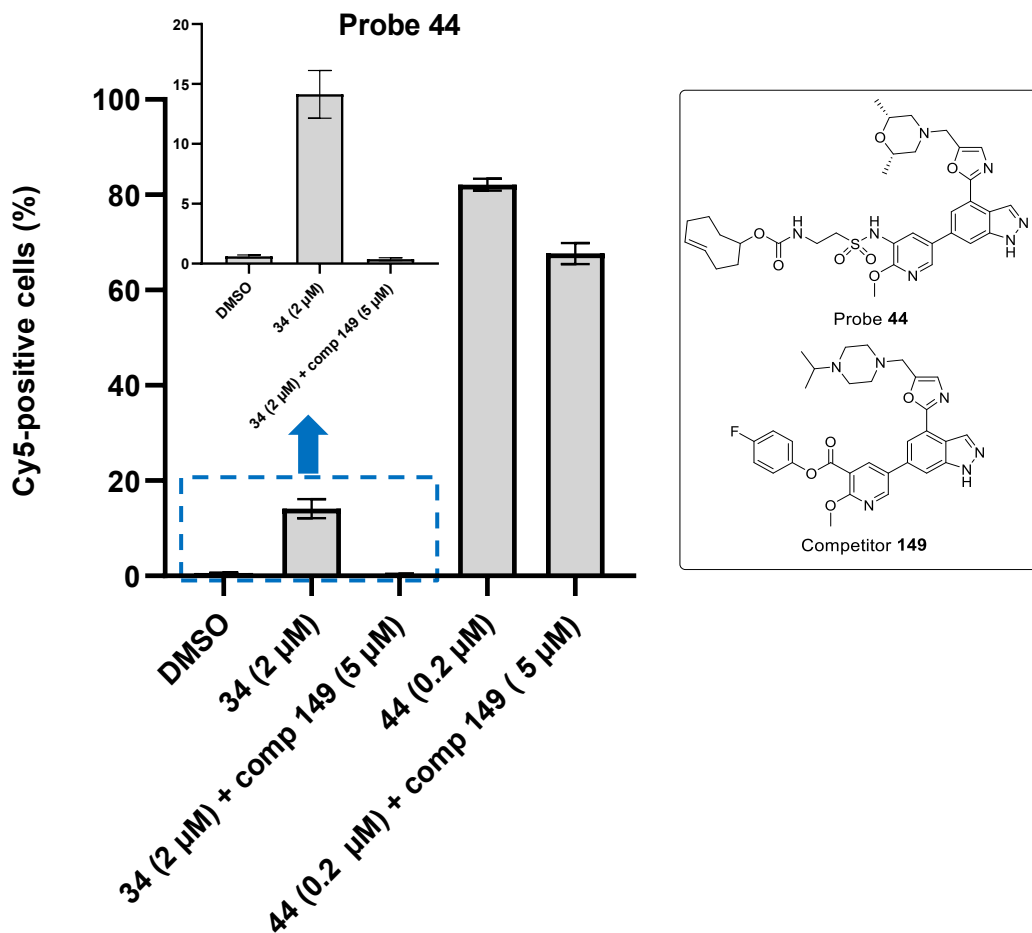
In addition, the fluorescent signal observed in Hut78 cells treated with chemical **44** (0.2 μ M) was more intense than the signal observed for the reference probe **34** from the oral series of PI3K δ inhibitors (2 μ M) despite being screened at a significantly reduced concentration (Figure 47).



Hut78 cells treated for 90 min with DMSO, 2 μ M probe **34** or 0.2 μ M probe **44**. Cells subsequently underwent fixation, permeabilization and IEDDA reaction with 100 nM Tz-Cy5 for 5 min. Results from one experiment is shown (n=3, STEV). Representative results from at least two independent biological replicates.

Figure 47. FACS comparison of TCO chemical probes **34** and **44**.

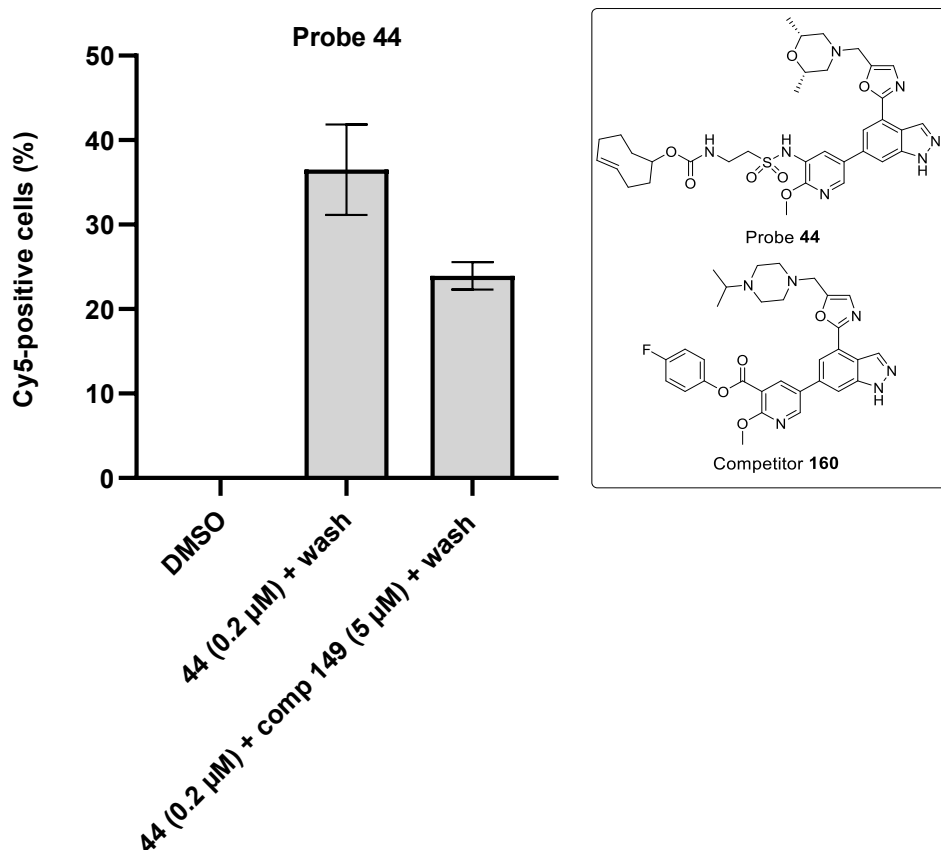
Following on from this, a competition experiment was carried out whereby Hut78 cells were first incubated with the covalent PI3K δ inhibitor **149** and subsequently treated with chemical probe **44** (Figure 48). A partial competition of the fluorescent signal was observed, which indicates that the major part of the fluorescence signal might be unspecific (i.e. non-specific binding of the probe in cells).



Hut78 cells treated for 90 min with DMSO, 2 μ M probe **34** or 0.2 μ M probe **44** or 60 min pre-incubation with 5 μ M covalent competitor **149** followed by 90 min treatment with 2 μ M probe **34** or 0.2 μ M probe **44**. After treatment, cells were submitted for fixation, permeabilization, and IEDDA reaction with 100 nM Tz-Cy5 for 5 min. Results from one experiment is shown (n=3, STEV). Representative results from at least 2 independent biological replicates.

Figure 48. FACS analysis of the competition experiment for chemical probe **44** in Hut78 cells.

As previously considered for chemical probes derived from nemiralisib, the impact of a washing step with media prior to fixation was investigated with chemical probe **44** with the aim to reduce the non-specific signal (Figure 49).



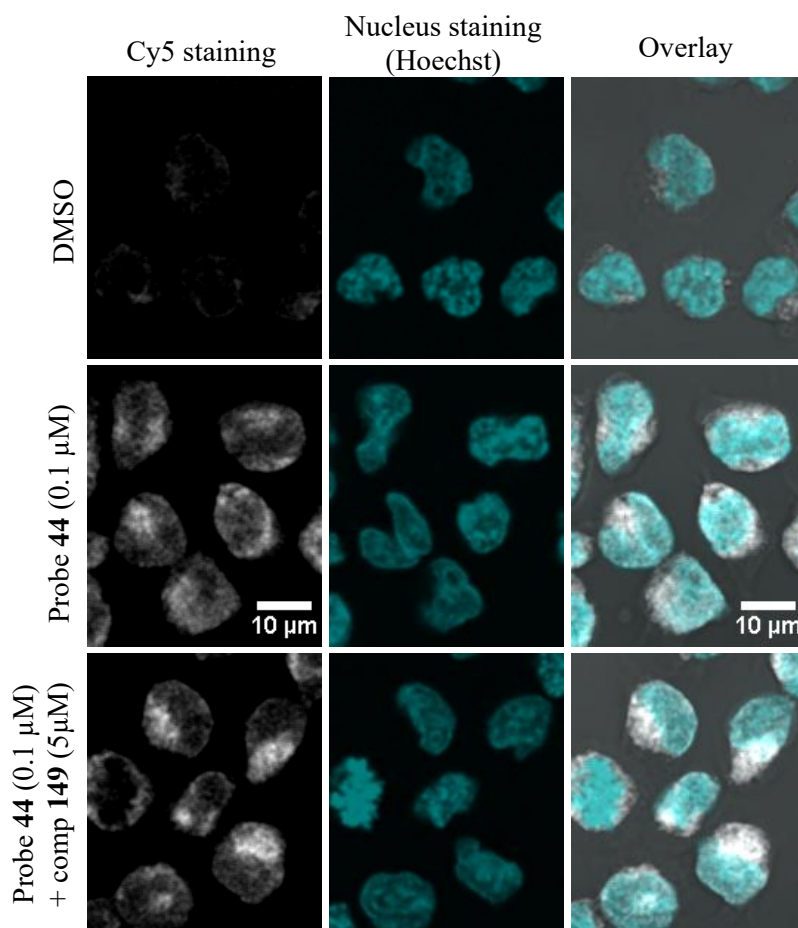
Hut78 cells treated for 90 min with DMSO or 0.2 μ M probe **44** or 60 min pre-incubation with 5 μ M covalent competitor **149** followed by 90 min treatment with 0.2 μ M probe **44**. After treatment, cells were submitted for fixation, permeabilization, and IEDDA reaction with 100 nM Tz-Cy5 for 5 min. Results from one experiment is shown (n=3, STEV). Where indicated, cells were washed with media before fixation. Percentage of observed competition varied between biological replicates.

Figure 49. FACS analysis of competition experiments for probe **44**, assessing the influence of washing step with media on the fluorescent signal.

Here, the introduction of a washing step with media after incubation of the cells with the covalent competitor and probe **44** reduced the fluorescent signal compared to cells which did not undergo that additional wash (Figures 48 and 49), therefore suggesting that the chemical probe might have been partially washed out. The

additional washing step did not have a significant impact on the non-specific signal since still only partial competition was observed in the presence of the covalent PI3K δ inhibitor **149**. This suggests that, in addition to specific binding, accumulation of the probe in cells may also be occurring (Figure 49).

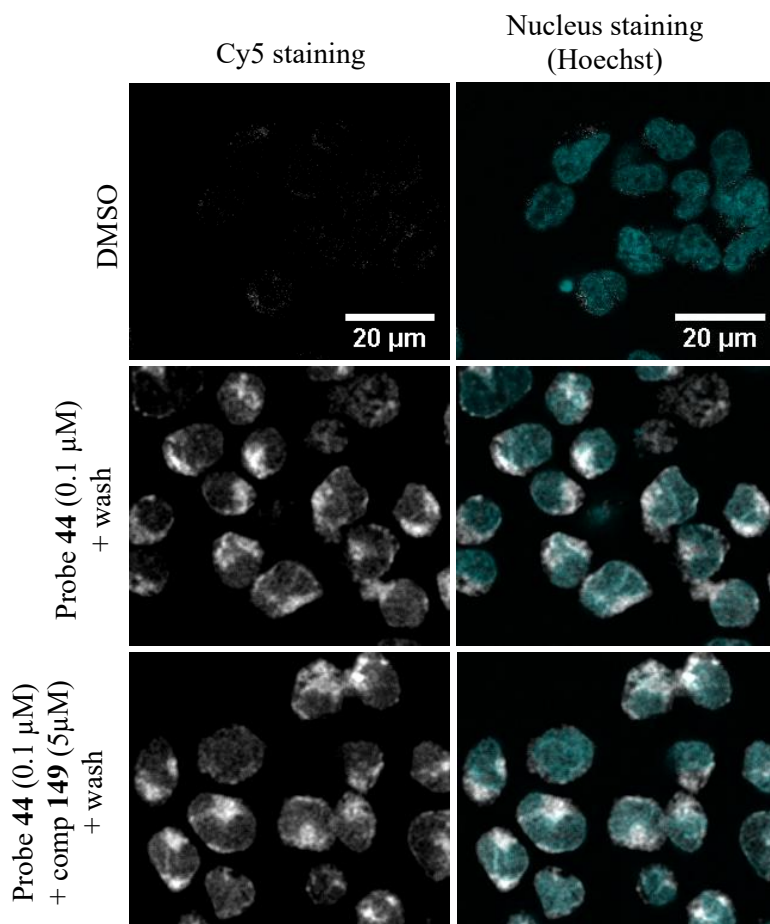
The cellular localisation of chemical probe **44** in Hut78 cells was also investigated (Figure 50).



Hut78 cells treated for 90 min with DMSO or probe 0.1 μ M probe **44** or pre-incubated for 60 min with 5 μ M covalent competitor **149** followed by 90 min treatment with 0.1 μ M probe **44**. Cells subsequently underwent cytocentrifugation (“cytospin”), followed by fixation, permeabilization, and IEDDA reaction with 100 nM Tz-Cy5 for 5 min. Nuclei were stained with Hoechst. Representative fluorescent images recorded after excitation at 405 nm (Hoechst) and 633 nm (Tz-Cy5). Scale bar 10 μ m.

Figure 50. Cellular localization and competition experiments of chemical probe **44** derived from GSK2292767 in Hut78 cells.

When visualised by confocal microscopy, Hut78 cells treated with chemical probe **44** derived from GSK2292767 showed a fluorescent signal localized in the cytosol (Figure 50). Although the staining for probe **44** was distributed more homogenously across the cytosol compared to the previously investigated chemical probes **38** and **39** derived from nemiralisib, a milder accumulation could also be observed in a localized area of the cytosol. In addition, no significant competition of the fluorescent signal could be detected when cells were treated with the covalent PI3K δ inhibitor **149** (Figure 50), suggesting that the staining is mainly unspecific. However, it is important to note that a higher laser power (12%) for Cy5 was required in order to visualize the fluorescent signal compared to probes **38** and **39** derived from nemiralisib (0.4%), which confirms that the compound accumulation observed for probe **44** is less pronounced. The influence of the washing step with media after incubation with the probe and before fixation was also investigated by microscopy in order to assess any differences on the subcellular localization and/or accumulation of the probe (Figure 51).



Hut78 cells pre-incubated for 60 min with 5 μ M covalent competitor **149** and then treated for 90 min with 0.1 μ M probe **44** before undergoing cytocentrifugation (“cytospin”), followed by fixation, permeabilization, and IEDDA reaction with 100 nM Tz-Cy5 for 5 min. Nuclei were stained with Hoechst. Representative fluorescent images recorded after excitation at 405 nm (Hoechst) and 633 nm (Tz-Cy5). Scale bar 20 μ m. Where indicated, cells were washed with media before fixation.

Figure 51. Cellular localization of chemical probe **44** derived from GSK2292767 in Hut78 cells, investigating the influence of a washing step with media before fixation.

The fluorescence signal observed in Hut78 cells treated with probe **44** and subsequently washed with media appeared relatively uniform across the cytosol but absence of competition was observed in presence of the covalent PI3K δ inhibitor **149**, confirming that the staining is mainly unspecific.

3.4.4. Imaging Conclusions of TCO Probes in Hut78 Cells

Overall, visualisation by microscopy of the subcellular localisation of PI3K δ chemical probes revealed different localisation patterns and varying degrees of accumulation across the different series. Interestingly, distinct behaviour was also observed within probes derived from the inhaled series (from nemiralisib or GSK2292767). These differences in cellular localisation and degrees of accumulation are summarised below and depicted in Figure 52, where a representative image of the subcellular localisation of a chemical probe from each series at the same concentration and with the same laser power is shown:

- Oral series: A specific cytosolic staining that can be successfully competed with non-covalent and covalent PI3K δ inhibitors was observed for chemical probe **34**, albeit with limited signal-to-noise ratio compared to DMSO control.
- Nemiralisib inhaled: A significant accumulation in membrane-rich organelles such as ER/Golgi was observed for chemical probes **38** and **39**, in addition to a weaker cytosolic staining. No competition of the fluorescent signal could be observed with either covalent or non-covalent PI3K δ inhibitors.
- GSK2292767 inhaled: Compared to chemical probes **38** and **39** derived from nemiralisib, a fluorescence signal visibly more homogeneously distributed across the cytosol was observed for probe **44**, along with a lower degree of accumulation but absence of significant competition.

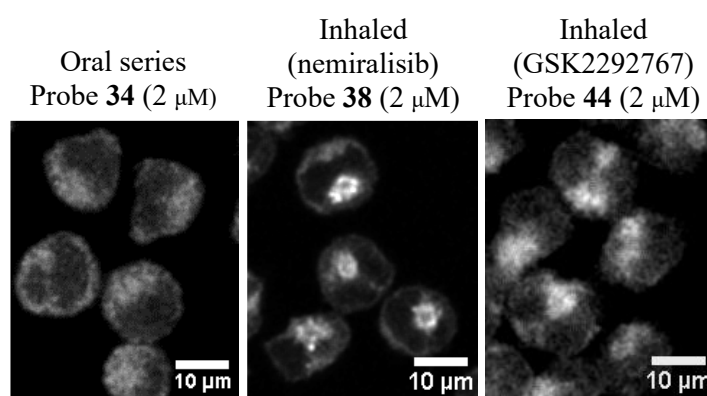
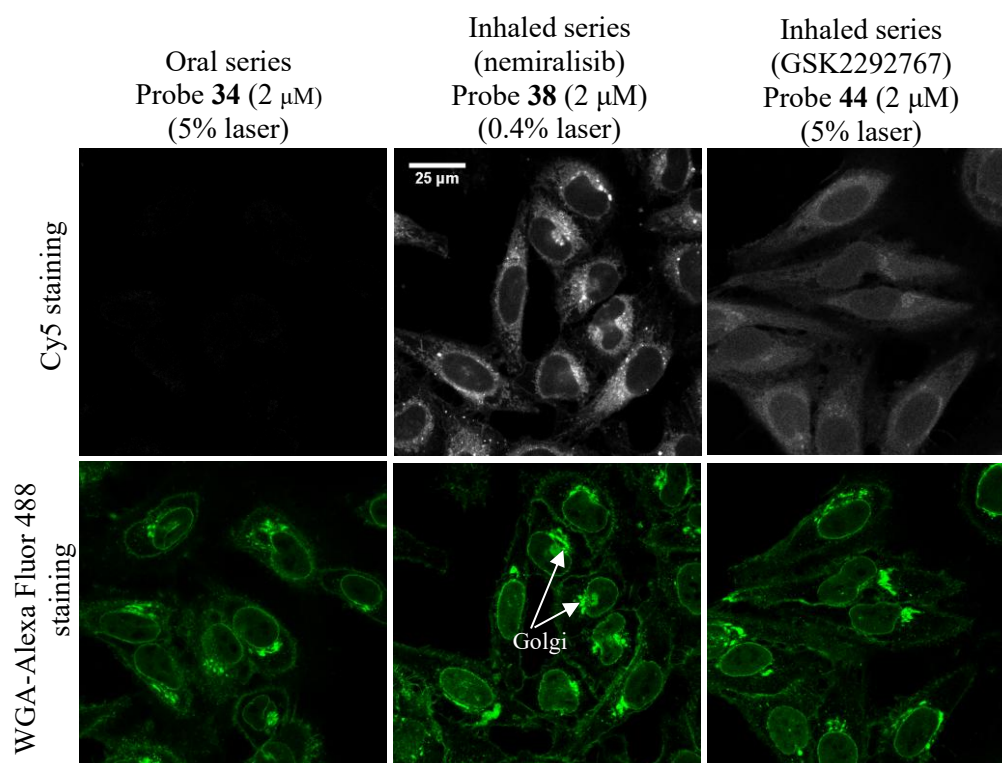


Figure 52. Representative image of the subcellular localisation of TCO chemical probes from each series of PI3K δ inhibitors: probe **34**, oral series (left); probe **38**, nemiralisib inhaled (middle); probe **44**, GSK2292767 inhaled probe (right).

Given their potency measured in the kinobead assay (Table 13), it is likely that the TCO chemical probes engage with PI3K δ in a cellular context, however this signal might not be detected in the competition experiments if the non-specific binding overcomes the specific binding to the target. In other words, the TCO chemical probes are likely to bind to PI3K δ in Hut78 cells, however the compounds may also bind non-specifically and therefore accumulate in various membrane-rich and acidic subcellular compartments. This subcellular sequestration may also explain why the additional washing step with media before fixation did not improve competition experiments.

Additional experiments were conducted in order to evaluate the specificity of the fluorescent signal resulting from the TCO probes. One experiment included investigating the cellular behaviour of a TCO probe derived from each series of PI3K δ inhibitors in an imaging assay that would involve HeLa cells as an alternative cell line to Hut78 cells.

HeLa cells are an immortalized cell line, originally derived from a patient suffering from cervical cancer, which are now extensively used in research due to their stable growth.^[210] In addition, HeLa cells have a significantly lower expression level of PI3K δ compared to Hut78 or PBMC cells, therefore evaluating whether the compounds would be prone to accumulation in such a cellular system, independently of the PI3K δ target, was of significant interest. HeLa cells are also visibly structurally larger than Hut78 or PBMC cells, which may aid visualisation of the subcellular localisation of the TCO probes. Similar to previous imaging experiments, in Hut78 cells, wheat germ agglutinin (WGA)-Alexa488 was used as an additional dye to stain cellular membranes and aid visualisation of Golgi/ER structures in HeLa cells Figure 53).^[208]



HeLa cells were treated for 90 min with 2 μ M chemical probes **34**, **38** or **44** following by fixation, permeabilization, and IEDDA reaction with 100 nM Tz-Cy5 for 5 min. Membranes were stained with Wheat Germ Agglutinin (WGA)-Alexa Fluor 488. Representative fluorescent images recorded after excitation at 488 nm (Alexa488) and 633 nm (Tz-Cy5).

Figure 53. Cellular localisation of TCO chemical probes **34**, **38** and **44** derived from each series of PI3K δ inhibitors in HeLa cells.

In this imaging assay, all three chemical probes were screened at the same concentration (2 μ M) for comparison. HeLa cells treated with chemical probe **34** derived from the oral series of PI3K δ inhibitor did not show any fluorescent signal (Figure 53). This suggests that, in the absence of the PI3K δ target that is not expressed in this cell line, the probe has been successfully washed out and therefore is not available to react with Tetrazine-Cy5. Overall, this further confirms the selectivity of chemical probe **34** for PI3K δ .

However, chemical probes **38** and **44**, derived from the inhaled clinical candidates nemiralisib and GSK2292767, respectively, showed a very distinct cellular behaviour. Indeed, HeLa cells treated with chemical probe **38** displayed a cytosolic

staining for Cy5 with more pronounced accumulation in the Golgi based on the co-localised signal with WGA-Alexa Fluor 488 (Figure 53). Furthermore, the very low laser power (0.4%) used to visualise the chemical probe further highlights the degree of accumulation of that compound. In addition to a pronounced accumulation in the Golgi, staining for Cy5 was also visualised in smaller vesicles that may be lysosomes (Figure 53).

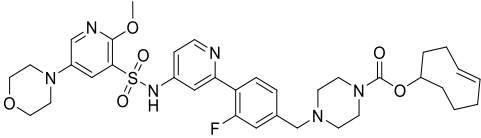
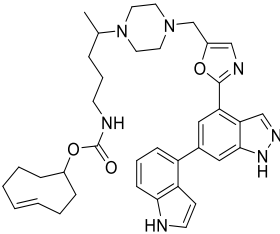
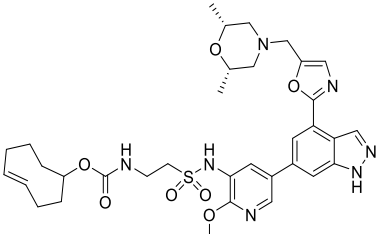
On the other hand, HeLa cells treated with chemical probe **44** derived from GSK2292767 gave a weaker Cy5 staining that was relatively more homogeneously distributed throughout the cytosol, albeit with some degree of accumulation visible in the Golgi. However, the laser power in this case (5%) was higher than the one used for visualisation of chemical probe **38** derived from nemiralisib (0.4%), which further confirms previous observations on the lower degree of accumulation of probe **44**.

Overall, the outcome of this imaging experiment in HeLa cells was in agreement with previous observations in Hut78 cells where chemical probe **38** also demonstrated a greater extent of accumulation in membrane-rich subcellular organelles compared to probe **44**. In addition, this imaging experiment in HeLa cells confirms that the subcellular localization of the chemical probes derived from the inhaled clinical candidates (and even more so of probe **38** derived from nemiralisib) is independent from binding to PI3K δ .

3.4.5. Imaging of TCO Chemical Probes in HeLa Cells to Investigate Compound Accumulation

The differences observed in the subcellular localisation of the chemical probes and their accumulation could be due to the presence of the TCO tag and its impact on the physico-chemical properties of the compounds, namely increased lipophilicity and lower solubility, compared to the parent PI3K δ inhibitors. Whilst it is well established that increased compound lipophilicity can be correlated with non-specific binding in cells, for example by binding to membranes and other cellular proteins, this hypothesis alone does not support the observed outcome of the imaging experiments. Here, the TCO chemical probes from each series of PI3K δ inhibitors investigated in the imaging

assay exhibit increased lipophilicity (measured $\text{ChromLogD}_{\text{pH}7.4} > 5$, Table 13) compared to the parent compound from which they are derived ($1.9 < \text{measured ChromLogD}_{\text{pH}7.4} < 3.3$, Tables 5 and 6, Section 1.3.3). However, within this set of chemical probes, the most lipophilic compound is probe **34** from the oral series of PI3K δ inhibitors ($\text{ChromLogD}_{\text{pH}7.4}$, Table 13). Unlike chemical probes **38** and **44** derived from nemiralisib and GSK2292767 respectively, probe **34** displayed a homogeneous cytosolic signal when visualised by confocal microscopy in Hut78 cells and the signal was successfully competed with several PI3K δ inhibitors. In addition, despite all three chemical probes exhibiting low solubility (Table 13), distinct differences were observed in the subcellular localisation of the compounds. Overall, these observations suggest that the accumulation observed in membrane-rich organelles such as ER and Golgi for the TCO probes derived from the inhaled clinical candidates (even more so for probes **38** and **39** derived from nemiralisib) might not be driven by the TCO tag and its impact on the physico-chemical properties of the chemical probes. This may be a reflection of the cellular behaviour of the parent compounds.

Structure			
Compound number	34	38	44
PI3K δ pIC ₅₀ (n)	8.8 (8)	8.7 (4)	8.2 (5)
PI3K α , β , γ pIC ₅₀ (n)	5.8 (5), 5.8 (5), 6.2 (5)	5.7 (4), 5.9 (4), 5.5 (4)	5.4 (4) ^b , 5.1 (1) ^c , 6.1 (5)
α , β , γ fold selectivity	1000, 1000, 398	1000, 631, 1585	501, 1259, 126
Kinobead pIC ₅₀ (n)	7.1 (2) ^a	7.2 (2) ^a	6.9 (2) ^a
Measured ChromLogD _{pH7.4}	6.1	5.3	5.7
AMP (nm/s, pH 7.4)	483	230	295
Kinetic solubility (μ g/mL)	12	11	12

*n = number of test occasions included in mean; ^aLipid kinobeasfs CZK126 / lysate mix Hut78-MCF7; ^bTested <4.5 on one test occasion; ^cTested <4.5 on three test occasions and <4.3 on one test occasion.

Table 13. Summary of the properties of TCO chemical probes from each series of PI3K δ inhibitors.

Nemiralisib contains a basic amine which is hypothesised to play an important role in the lung retention mechanism of the compound. This could potentially occur *via* intracellular non-specific binding and/or intracellular sequestration in acidic organelles. Therefore, these potential non-specific binding and sequestration processes may also occur for the corresponding TCO probes, which could explain the accumulation in membrane-rich organelles such as the ER and Golgi and the absence of competition by the non-labelled PI3K δ inhibitors observed in the imaging assay. Additional sequestration of the chemical probes could occur in lysosomes due to their acidic environment, however their relatively small size (0.1-1.2 μ m) renders any conclusion tentative at this stage. LysoTracker fluorescent dyes were considered to label acidic organelles such as lysosomes and confirm sequestration of the chemical probes in these subcellular compartments.^[211] More specifically, LysoTracker dyes consist of a fluorophore linked to a weak base partially protonated at physiological pH, therefore allowing selective targeting to acidic organelles. However, the LysoTracker dyes have been mostly designed to be used for live cell imaging experiments according to the supplier and may not be compatible with fixed procedures.^[212]

The strong accumulation in membrane-rich and acidic subcellular organelles demonstrated by chemical probes **38** and **39** may indicate that this non-specific binding is a mechanism by which the inhaled clinical candidate constitutes a subcellular “compound reservoir” that could contribute to its retention in the lungs. This may explain the MALDI lung deposition of nemiralisib, which was predominantly localised in the upper airways, in that the non-specific binding of the compound driven by the basic amine protonated at physiological pH may result in the compound staying at the site of deposition after inhaled administration. More specifically, it could be possible that non-specific binding of nemiralisib and sequestration in epithelial cells’ subcellular organelles lining the upper airway constitute a compound reservoir and prevent nemiralisib from distributing evenly throughout the lung tissues. In addition, the composition of the upper airways is different from other part of the lung, as it contains more mucus and phospholipids resulting in much thicker lung lining in comparison to the alveoli that contain more protein and less phospholipids.^[122]

In contrast to nemiralisib, GSK2292767 contains a morpholine moiety which is less basic than the piperazine of nemiralisib ($pK_a = 5.5$ and 8.1 , respectively). Consistently, a slightly more uniform cytosolic signal was observed for probe **44** derived from GSK2292767. A higher laser power was also required to visualize chemical probe **44** which also indicates that the compound is less prone to accumulation compared to probes **38** and **39** derived from nemiralisib.

These hypotheses are based on the TCO-modified versions of the inhaled clinical candidates, for which the physico-chemical properties have been modified compared to the parent molecules. Therefore, drawing conclusions on whether the subcellular localization of the TCO chemical probes observed in the imaging assay is a true reflection of the parent compounds' behaviours remains challenging. It may be possible that this sequestration in subcellular organelles could also occur for the inhaled PI3K δ clinical candidates due to some of their intrinsic properties, such as their ionisation state.

To address this hypothesis, it was envisioned that TCO chemical probes derived from nemiralisib where the basicity of the piperazine nitrogen atoms would be attenuated whilst maintaining good potency and selectivity for PI3K δ could be designed and screened in the imaging assay.

The first step of this approach consisted in designing and synthesizing a structurally related analogue of nemiralisib where the basicity of the piperazine ring would be disrupted or attenuated. Towards that aim, compound **150** featuring an oxopiperazine moiety was envisioned (Figure 54) and its synthesis is outlined below (Scheme 32).

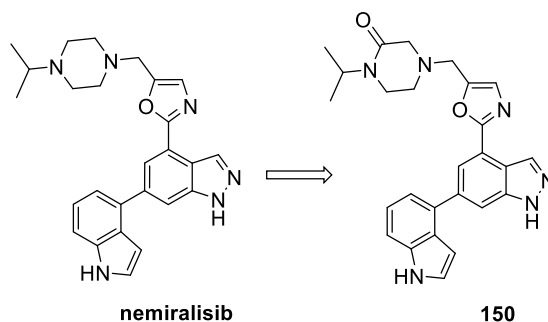
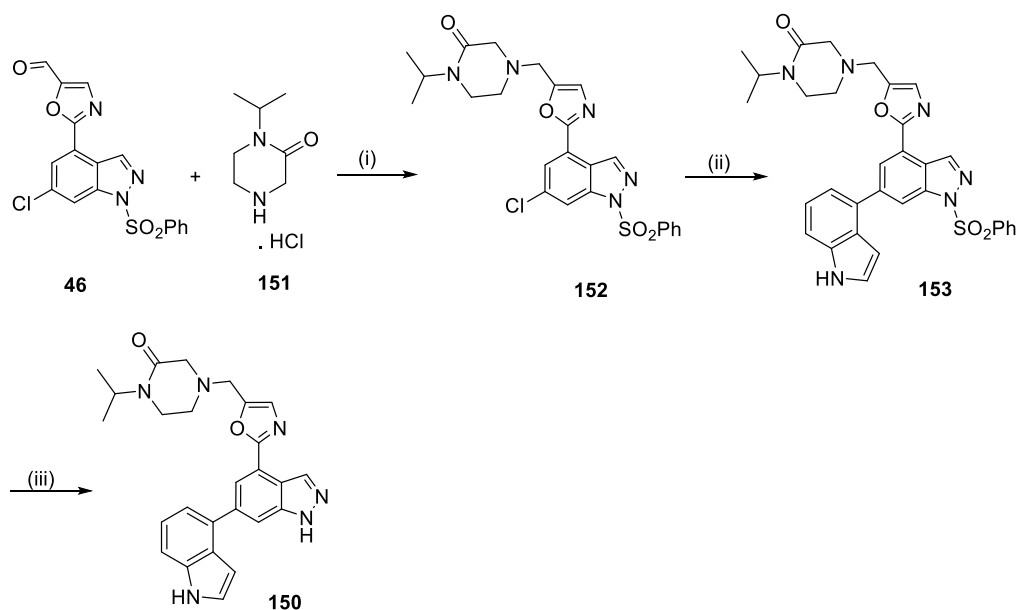


Figure 54. Structure of oxopiperazine analogue of nemiralisib.

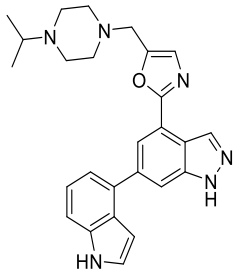
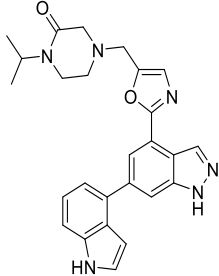


Reagents and conditions: (i) **151**, Et₃N, DCM, rt, 5 min then **46**, AcOH, rt, 30 min followed by STAB, 1 h, 73%; (ii) Indole-4-boronic acid pinacol ester, XPhos Pd G2 (20 mol%), Na₂CO₃, 1,4-dioxane/water (9:1), 90 °C, μ wave, 1 h, 82%; (iii) 1 M aqueous NaOH, MeOH, rt, 30 min, 37%.

Scheme 32. Synthesis of oxopiperazine analogue of nemiralisib **150**.

The synthesis started with a reductive amination reaction between aldehyde **46** and commercially available 1-isopropylpiperazin-2-one, hydrochloride (**151**) to give the desired intermediate **152**. Subsequent Suzuki coupling successfully afforded the biaryl intermediate **153**, which gave the desired compound **150** after deprotection of the benzenesulfonyl group (Scheme 32).

Compound **150** was subsequently profiled in the PI3K δ enzyme and human whole blood assays to ensure that the oxopiperazine motif was tolerated. The properties of compound **150** are summarized in Table 14 below.

Structure		
Compound number	nemiralisib	150
PI3K δ p <i>K</i> _i (n)	9.9 (4) ^a	10.6 (1) ^a
PI3K α , β , γ p <i>I</i> C ₅₀ (n)	5.3 (27) ^b , 5.8 (26) ^c , 5.2 (30) ^d	5.1 (5), 5.4 (5), 6.0 (5)
α , β , γ fold selectivity	5012, 1585, 6310	5012, 2512, 631
hWB p <i>I</i> C ₅₀ (n)	8.9 (3)	8.1 (2)
AMP (nm/s, pH 7.4)	230	73
Kinetic solubility (μ g/mL)	110	15

*n = number of test occasions included in mean; ^aPI3K δ assay run at a 2 mM ATP concentration; ^bTested <5.3 on one test occasion and <4.6 on one test occasion; ^cTested <4.6 on one test occasion; ^dTested <4.6 on 3 test occasions.

Table 14. Properties of nemiralisib and oxopiperazine analogue **150**.

Overall, oxopiperazine compound **150** was found to be a highly potent PI3K δ inhibitor maintaining good selectivity for PI3K δ over other Class I PI3K isoforms, albeit with approximately a 10-fold selectivity drop towards PI3K γ . However, the replacement of the piperazine moiety with an oxopiperazine had an impact on the physico-chemical properties with compound **150** exhibiting moderate permeability and lower solubility compared to nemiralisib.

The p*K*_a of the oxopiperazine N4 nitrogen in compound **150** was then investigated and compared to the p*K*_a of the most basic piperazine nitrogen in

nemiralisib in order to assess the suitability of **150** to act as a nemiralisib surrogate with attenuated basicity. Therefore, predicted pK_a values were obtained using the ChemAxon pK_a prediction model and these predictions were compared to the measured pK_a values for those compounds (Figure 55).

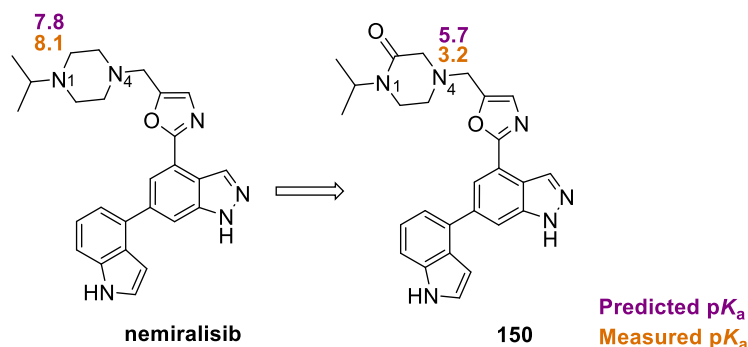


Figure 55. Predicted and measured pK_a values of basic nitrogen atoms in nemiralisib and oxopiperazine analogue **150**.

The measured pK_a values were determined using a spectrophotometric (UV-metric) titration method. Briefly, a 10 mM DMSO solution of the sample is prepared and subsequently titrated with acid or base whilst UV/vis spectra are collected. Provided that the compound possesses a chromophore near the ionizable group and that the UV spectra of the neutral and ionized species are different, the pK_a of the sample can be determined by measuring the absorbance of the solution at different pH values.

The most basic piperazine nitrogen in nemiralisib (N1) was measured with a pK_a = 8.1, which correlates well with the predicted value (pK_a = 7.8) (Figure 55). The N4 nitrogen in compound **150** was measured to have a pK_a = 3.2, therefore confirming that the oxopiperazine motif disrupted the basicity of the compound, whilst maintaining good potency and selectivity for PI3K δ .

Based on these observations, the oxopiperazine motif was then incorporated into TCO chemical probe **154** (Figure 56), for direct comparison with probe **36** previously described in this thesis. An additional TCO probe featuring an exocyclic amide group (**155**) was also selected to provide another comparison.

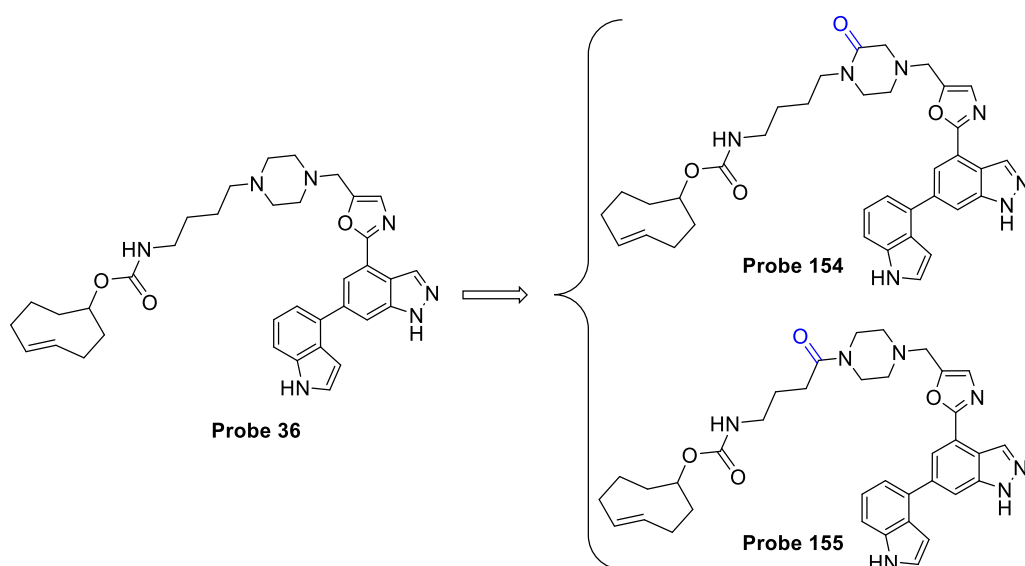
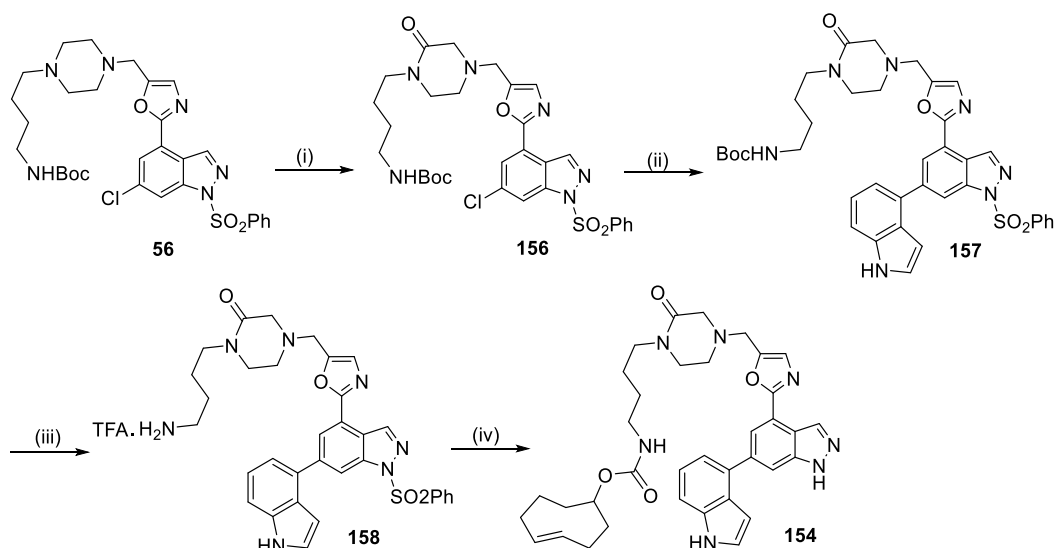


Figure 56. Structure of TCO chemical probes **154** and **155** derived from probe **36**.

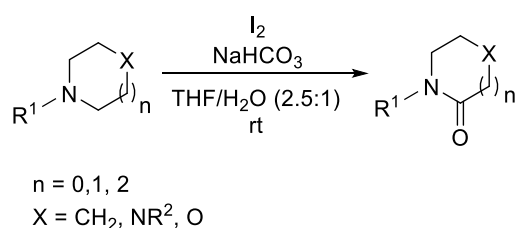
The synthesis of oxopiperazine TCO probe **154** is described below (Scheme 33). Initial attempts to access intermediate **156** by *N*-alkylation with various *N*-protected-4-bromobutan-1-amine derivatives of an oxopiperazine precursor were unsuccessful. Therefore, an alternative approach was considered and relied on the formation of the oxopiperazine moiety directly from the corresponding piperazine intermediate **56** (previously prepared for the synthesis of TCO chemical probe **36**) using a selective late-stage C-H oxidation reaction described by Griffiths *et al.* (Scheme 33).^[213]



Reagents and conditions: (i) I_2 , $NaHCO_3$, THF/ H_2O (2.5:1), rt, 45 min, 54%; (ii) Indole-4-boronic acid pinacol ester, XPhos Pd G2 (20 mol%), Na_2CO_3 , 1,4-dioxane/water (5:1), 90 °C, μ wave, 1 h, 55%; (iii) TFA, DCM, rt, 1.5 h, used crude; (iv) DIPEA, DMF, rt, 5 min followed by TCO-PNB ester, rt, 1.5 h, used crude. Then 1 M aqueous NaOH, MeOH, rt, 1 h, 18% over 3 steps.

Scheme 33. Synthesis of oxopiperazine TCO chemical probe **154**.

The metal-free procedure developed by Griffiths *et al.* uses mild conditions and exhibits a good functional group tolerance which contributes to its attractiveness for the late-stage chemoselective α -oxidation of cyclic tertiary amines to the corresponding lactams.^[213] More specifically, the reaction uses molecular iodine as an oxidant and sodium bicarbonate as a weak base (Scheme 34).



Scheme 34. Late-stage chemoselective oxidation of cyclic amines to the corresponding lactams described by Griffiths *et al.*^[213]

According to the authors, oxidation occurring selectively at the endocyclic position results from the preferred formation of an endocyclic iminium species from a *N*-iodoammonium intermediate due to a more effective anti-periplanar E2-elimination of

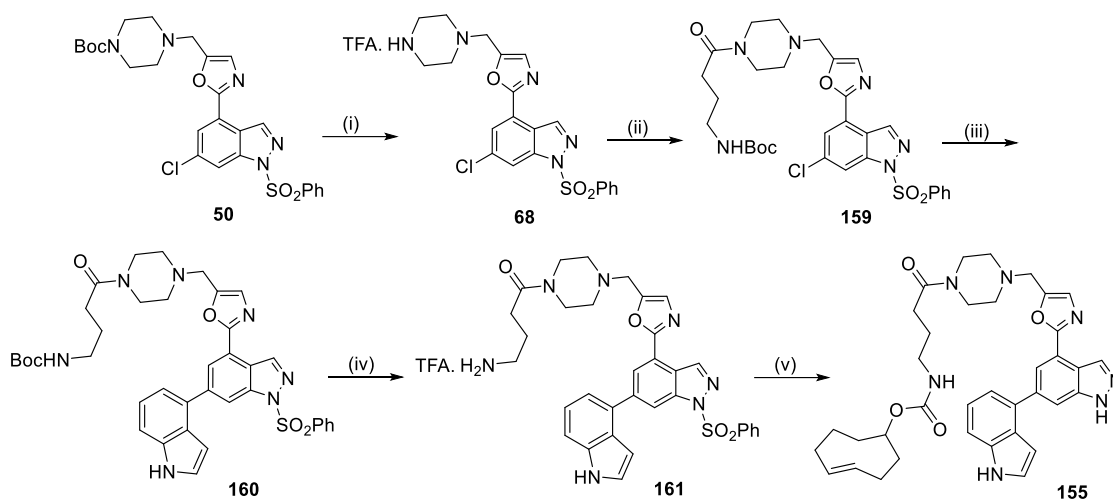
the N–I and endocyclic C–H α bonds in comparison to the exocyclic position (*e.g.* R¹ = CH₂R) that can freely rotate.

In the case of piperazine substrates which contain more than just one set of α -C–H protons, over-oxidation can occur and result in the formation of bis-lactams products. However, preferential oxidation of the endocyclic methylene group adjacent to the more electron-rich piperazine nitrogen is typically observed.^[213]

Therefore, the reaction of compound **56** under these conditions should favour oxidation of the endocyclic methylene unit on the piperazine to form the corresponding 2-oxopiperazine.

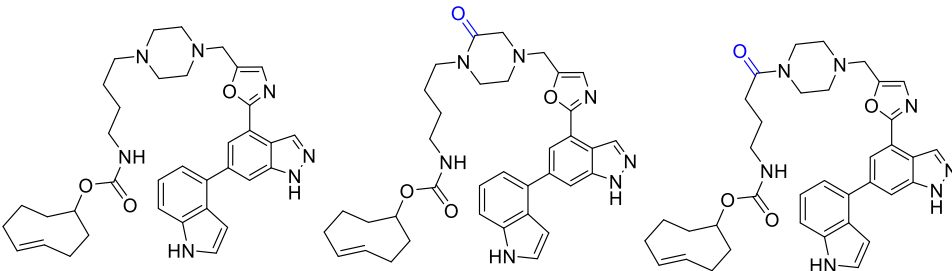
LCMS analysis of the crude reaction mixture showed the formation of a major peak whose mass was consistent with an oxidation product, and no impurities consistent with over-oxidation side-products were observed. NMR analysis of the isolated product confirmed oxidation had occurred at the predicted endocyclic position, affording the desired oxopiperazine product **156**. Next, Suzuki coupling gave the biaryl intermediate **157** that then underwent Boc deprotection to give the crude primary amine **158** as the corresponding TFA salt. Subsequent treatment with TCO PNB ester and deprotection of the benzenesulfonyl group afforded the desired oxopiperazine TCO probe **154**.

The additional TCO chemical probe **155** featuring an exocyclic amide was synthesized following a sequence depicted in Scheme 35. The sequence started with Boc deprotection of previously described intermediate **50** to give the crude corresponding TFA salt that was taken forward in an amide coupling reaction with γ -(Boc-amino)butyric acid (Boc-GABA-OH) mediated by HATU to give **159**. Subsequent Suzuki cross coupling with indole-4-boronic acid pinacol ester afforded to the desired intermediate **160** that then underwent Boc deprotection to give the crude primary amine **161** as the corresponding TFA salt. Reaction of **161** with TCO PNB ester and deprotection of the benzenesulfonyl group afforded the desired TCO probe **155**.



Scheme 35. Synthesis of TCO chemical probe **155.**

Once their syntheses complete, the properties of the chemical probes **154** and **155** were determined and compared to the reference probe **36** (Table 15).

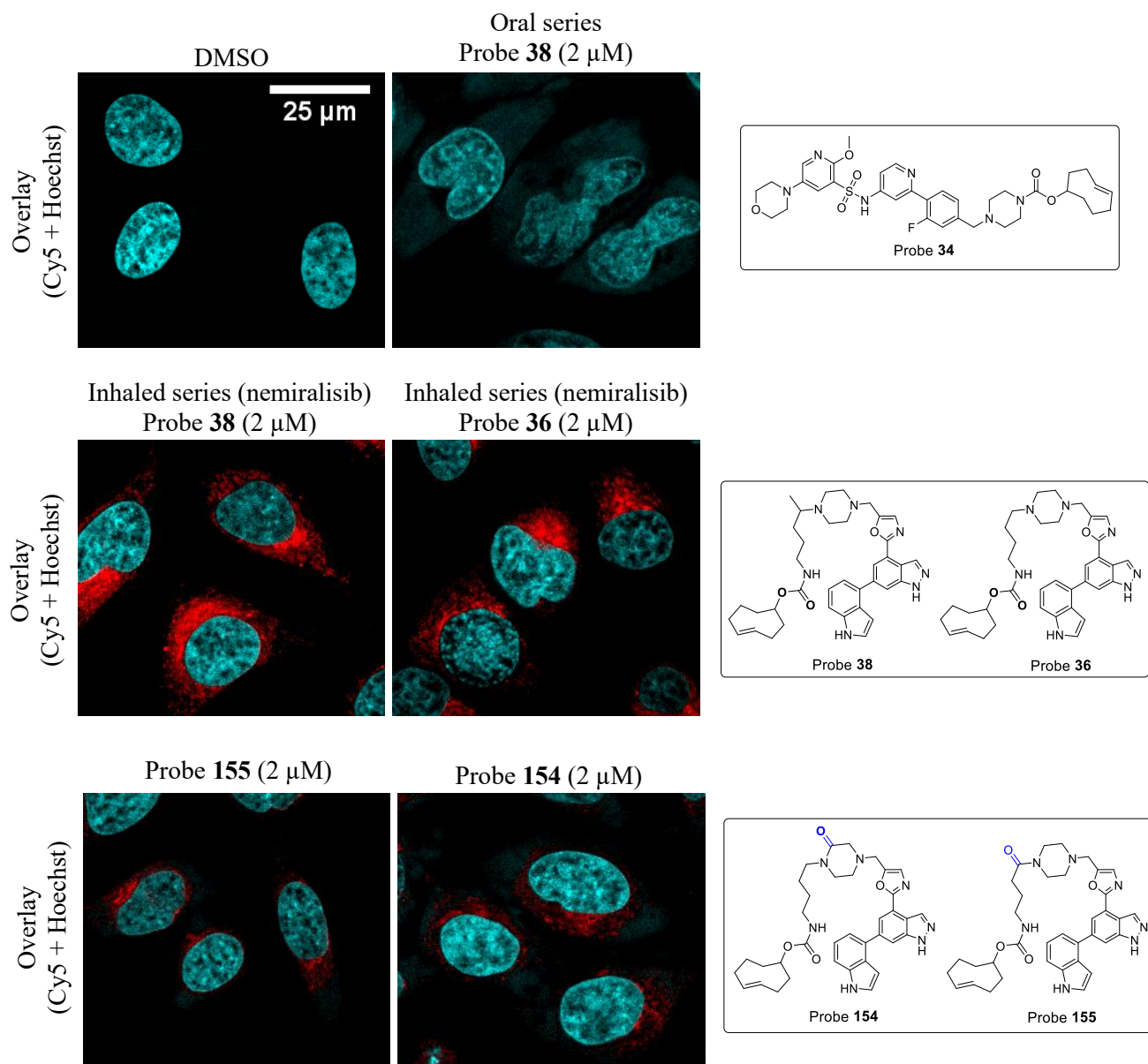
Structure			
Compound number	36	154	155
PI3K δ pIC ₅₀ (n)	8.5 (4)	7.4 (6)	7.2 (6)
PI3K α , β , γ pIC ₅₀ (n)	6.0 (3), 6.1 (3), 6.3 (2) ^a	5.7 (3), 5.9 (3), 6.1 (2)	5.4 (3), 5.7 (3), 6.2 (3)
α , β , γ fold selectivity	316, 251, 159	50, 32, 20	63, 32, 10
Kinobead pIC ₅₀ (n)	7.6 (2) ^b	7.0 (2) ^b	6.8 (2) ^b
meas.ChromLogD _{pH7.4}	5.1	5.0	4.9
AMP (nm/s, pH 7.4)	320	133	71
Kinetic solubility (μ g/mL)	4	1	1

*n = number of test occasions included in mean; ^aTested <5.1 on one test occasion; ^bLipid kinobeads CZK133 / lysate mix HeLa-Jurkat-K-562.

Table 15. Properties of TCO chemical probes **154**, **155** and reference probe **36**.

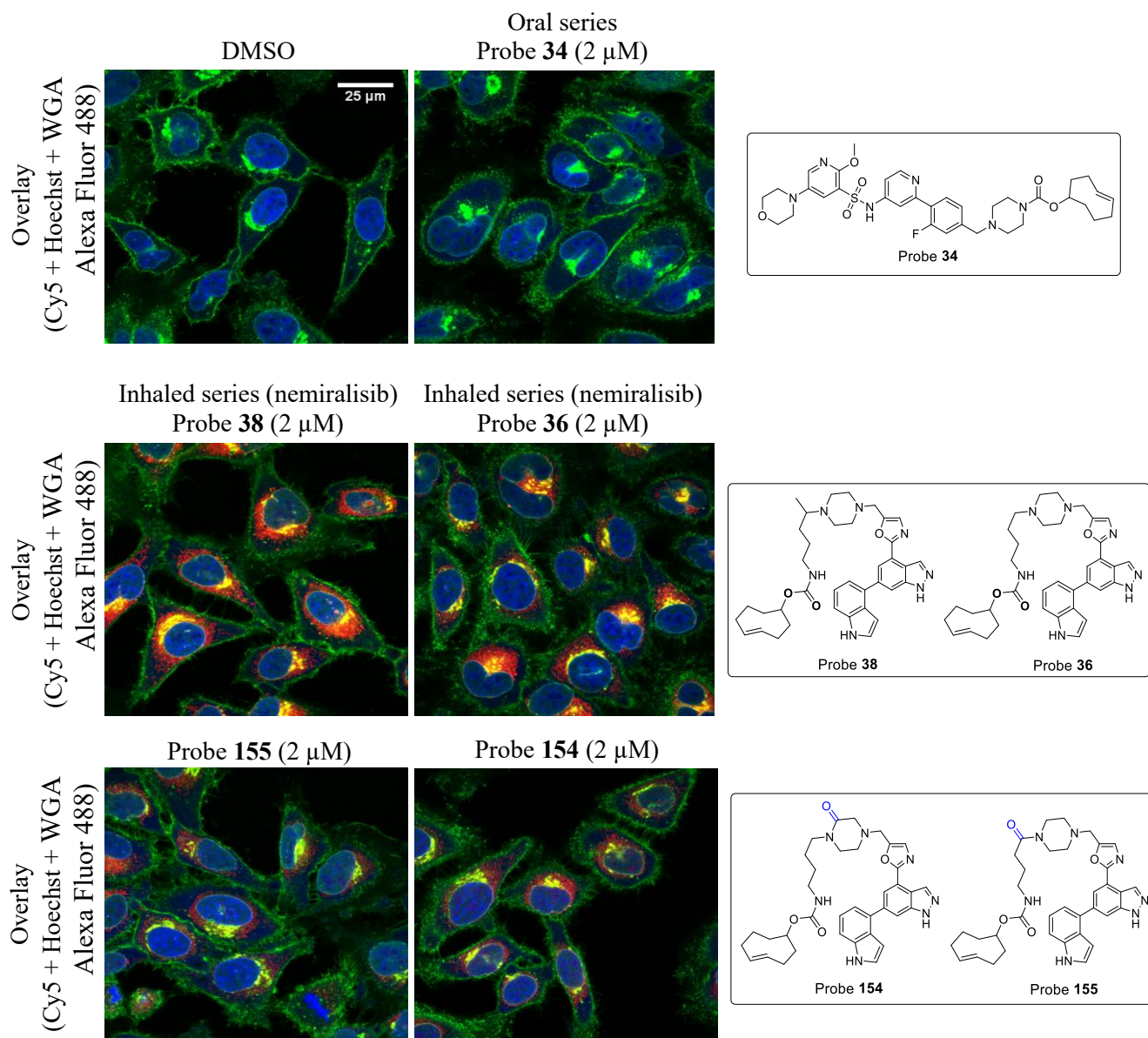
Despite the oxopiperazine analogue of nemiralisib (**150**) maintaining good potency and selectivity for PI3K δ , the introduction of the oxopiperazine motif in the TCO probe **154** displayed a 12-fold decrease in enzyme potency compared to the reference probe **36** (PI3K δ pIC₅₀ = 7.4 and 8.5, respectively), which therefore caused a drop in selectivity towards the other Class I PI3K isoforms (≤ 50 fold). However, probe **154** remained a potent compound in the kinobead assay with only a 4-fold drop in potency relative to the reference probe **36** (kinobead pIC₅₀ = 7.0 and 7.6, respectively). Similarly, TCO probe **155** exhibited a 20-fold drop in PI3K δ enzyme potency relative to the reference probe **36** (PI3K δ pIC₅₀ = 7.2 and 8.5, respectively) but the compound remained relatively potent in the kinobead assay (kinobead pIC₅₀ = 6.8).

Based on these results, TCO chemical probes **154** and **155** were then profiled in the imaging assay. The imaging experiment was carried out in HeLa cells, a cell line not expressing the target, to directly address the specificity of the staining and the extent of accumulation independently of the presence of the PI3K δ (Figure 57 and Figure 58).



HeLa cells were treated for 60 min with DMSO, 2 μM chemical probes **34**, **36**, **38**, **154** and **155** then washing with PBS before fixation, permeabilization, and IEDDA reaction with 100 nM Tz-Cy5 for 7 min. Nuclei were stained with Hoechst. Representative fluorescent images recorded after excitation at 405 nm (Hoechst) and 633 nm (Tz-Cy5, 0.3% laser power). Scale bar 25 μm .

Figure 57. Cellular imaging of TCO chemical probes **34**, **36**, **38**, **154** and **155** in HeLa cells.



HeLa cells were treated for 60 min with DMSO, 2 μ M chemical probes **34**, **36**, **38**, **154** and **155** then washing with PBS before fixation, permeabilization, and IEDDA reaction with 100 nM Tz-Cy5 for 7 min. Nuclei were stained with Hoechst. Membranes were stained with WGA Alexa-Fluor 488. Representative fluorescent images recorded after excitation at 405 nm (Hoechst), 488 nm (WGA Alexa-Fluor 488) and 633 nm (Tz-Cy5, 0.3% laser power). Scale bar 25 μ m.

Figure 58. Cellular imaging of TCO chemical probes **34**, **36**, **38**, **154** and **155** in HeLa cells.

In this experiment, the staining observed in HeLa cells treated with the less basic probes **154** and **155** was compared to the staining in cells treated with the basic probes **36** and **38**, as well as probe **34** from the oral series of PI3K δ inhibitors.

Similar to previous observations in Hut78 and HeLa, no fluorescent signal for Cy5 could be observed for probe **34**, suggesting that the compound has been washed out in the absence of the PI3K δ target (Figure 57 and Figure 58). For the basic chemical probes **38** derived from nemiralisib, a fluorescent signal was observed in the cytosol of HeLa cells. Yellow staining indicative of co-localization between Cy5 and WGA-Alexa Fluor 488 showed the probe localizing in the membrane-rich Golgi organelle, and around the nucleus which could be consistent with the ER (Figure 58). Chemical probe **36** that shares very similar properties relative to probe **38** behaved very similarly to probe **38** with a strong accumulation in the cytosol of HeLa cells and co-localization in the Golgi and ER (Figure 57 and Figure 58). The very low laser power (0.3%) further highlights the degree of accumulation observed for these two compounds. Interestingly, HeLa cells treated with the less basic probes **154** and **155** showed a fluorescent signal localized in the Golgi and ER which was significantly reduced compared to the accumulation observed for **36** and **38** (Figure 57 and Figure 58). These results support the hypothesis that the basicity of the piperazine ring on probes derived from nemiralisib could be driving their subcellular localization.

Overall, the basic piperazine ring present in chemical probes **36**, **38** (and **39** previously described) derived from nemiralisib seems to contribute to the non-specific binding of the compounds observed in membrane-rich and acidic organelles. It may be possible that these intracellular accumulation and sequestration processes also occur for nemiralisib in epithelial cells constituting the lining of the upper airway when the compound is administered. Therefore, this might prevent nemiralisib from distributing evenly throughout the lung tissues and could rationalise the lung deposition of the compound observed in rats by MALDI imaging (Section 1, Figure 15). Consequently, these intracellular “compound reservoirs” could contribute to the lung retention mechanism of the compound. Indeed, target engagement at 24 h was observed for nemiralisib following bronchioalveolar lavages.^[129] This could be due to an equilibrium whereby the non-specifically bound fraction of nemiralisib in subcellular compartments would progressively diffuse back in the cytosol where it could be available to interact with PI3K δ and drive sufficient duration of action. In addition, independently of the potential intracellular accumulation of nemiralisib, the

very high potency of the compound measured in enzyme, kinobead PMBC and human whole blood assays may imply that a very low unbound fraction of the compound free in the cytosol is enough to achieve efficacy. The lower basicity of the morpholine ring of GSK2292767 may explain why the corresponding chemical probes displayed a more homogenous cytosolic staining and were less prone to accumulation, as indicated by the lower laser power required to visualise the compounds.

Overall, this further strengthens the hypothesis that the strategy based on bioorthogonal chemistry and the IEDDA reaction is a suitable technique to investigate the subcellular localization of chemical probes derived from PI3K δ inhibitors.

4. NanoSIMS Imaging

The cellular imaging of PI3K δ probes derived from inhaled compounds nemiralisib and GSK2292767 highlighted different subcellular localisation for these compounds, along with varying degrees of non-specific accumulation in Hut78 and HeLa cells. Although this subcellular localisation may not be driven by the TCO tag and its influence on the physico-chemical properties of the functionalised chemical probes, it remains unclear if it is a true reflection of the cellular behaviour of the inhaled parent molecules. Therefore, methodologies that enable the visualization of compound subcellular localization without any significant changes to its structure and physico-chemical properties would be of significant interest. More specifically, a complementary imaging technique that would involve labelling a biomolecule with a tag that would minimally impact the physico-chemical properties whilst still allowing the visualisation of the inhaled PI3K δ inhibitors at the subcellular level would help to further validate the observations and hypotheses established in Section 3.

Secondary ion mass spectrometry imaging (SIMS) has experienced a considerable development over the last few years with the emergence of novel methodologies that allow single-cell resolution analysis.^[214-216] Amongst these techniques is nanoscale secondary ion mass spectrometry (NanoSIMS), which has become an increasingly utilized method for the imaging of biomolecules at the subcellular level.^[217]

The concept of NanoSIMS remains similar to other secondary ion mass spectrometry methods. Briefly, the surface of a sample of interest is progressively scanned and sputtered with a highly focused primary ion beam which leads to the ejection of secondary ions (atomic and molecular species) (Figure 59). The ionized particles are then accelerated into a magnetic sector mass analyzer where they are separated by mass to charge ratio (m/z).^[218] This is a consequence of the curved trajectory of a charged particle travelling in a magnetic field, with the curvature varying with the m/z of the ion. Therefore, after passing through the magnetic sector analyzer, ions with different m/z ratios will be separated and will emerge at different locations before eventually reaching the detectors. An interesting feature of the NanoSIMS instrument is that it is composed of 7 moveable detectors, therefore allowing the detection of up to 7 different secondary ions from the same spot of the sample surface (Figure 59).

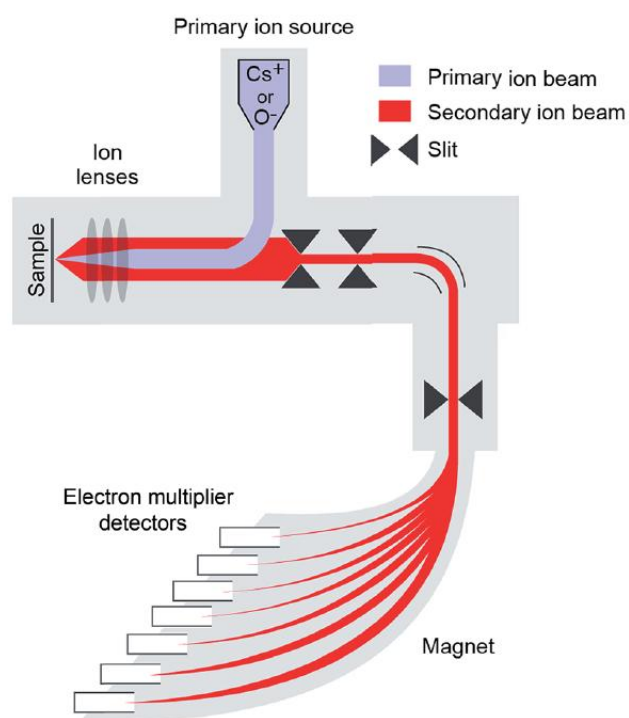


Figure 59. Schematic representation of the NanoSIMS instrument. Reprinted with permission from Steinhauser *et al.*^[219] (Copyright 2019, The Royal Society of Chemistry).

By progressively scanning the surface of the sample whilst recording its positions, the focused primary ion beam allows the generation of an ion map that indicates the distribution and the signal intensity of each ion across the scanned area. In addition, depth profiling allows the analysis of the three-dimensional composition of the sample from a series of consecutive two-dimensional ion maps.^[217]

The NanoSIMS instrument offers several imaging configurations, therefore making it a versatile technique that can be suitable for different applications depending on the questions that need to be addressed. One possible application of the NanoSIMS technique is the analysis a biological sample and the quantification of a specific mass of interest within cells and subcellular structures. This can be done *via* the measurement of the chemical composition of the sample. For example, detection of phosphorus (^{31}P) can help to delineate the nucleus borders due to the high phosphate content within the chromatin. The nitrogen element is also typically detected as the CN^- ion.

The highly-energetic primary ion beam required for NanoSIMS imaging often leads to extensive fragmentation of the organic molecules present at the surface of the sample, which consequently limits molecular information.^[220] Therefore, a common strategy to allow the detection of specific biomolecules within a biological sample relies on a labelling process whereby an atom which is naturally not present, or is present in very low concentrations, in the surrounding environment is incorporated onto the molecule of interest.^[221] For example, ^{19}F -enriched organic molecules have been successfully detected by SIMS imaging techniques.^[221] Alternatively, stable isotopes such as ^{15}N , which accounts for 0.64% of the nitrogen isotopic abundance, is the optimum labelling atom of choice. This NanoSIMS configuration, often referred to as isotope ratio measurements, enables the detection of a stable isotope-labelled biomolecule by measuring isotopic enrichment in comparison with the background isotopic ratio.^[220] Typically for those experiments, the NanoSIMS instrument is configured so that two of the detectors capture two different isotopes of a given element (e.g. $^{12}\text{C}^{14}\text{N}$ and $^{12}\text{C}^{15}\text{N}$).

The efficiency of the NanoSIMS analysis and the quality of the images generated can be dependent on the sample preparation. Therefore, it is crucial that the sample

preparation preserves the integrity of the biological sample and the spatial distribution of the biomolecule of interest. Most common sample preparation protocols for NanoSIMS imaging rely on chemical fixation and freeze-drying techniques, therefore ensuring that the sample does not contain any volatile substances such as water. This is particularly important because the NanoSIMS principle relies on the acceleration of ionized particles in a magnetic field under a high vacuum, which therefore requires that the sample withstand such vacuum.

Another important aspect to consider during sample preparation is the conductivity of the sample. This is due to the net charge deposition onto the sample following bombardment with the primary ion beam. Therefore, the sample should be coated with a thin conductive layer to remove the excess charges. This can be overcome by mounting the biological sample on a silicon chip which are commonly used due to their conductivity properties.

Additional features of the NanoSIMS instrument that contribute to its attractiveness include high sensitivity, high spatial resolution (down to 50 nm) as well as high mass resolution ($M/\Delta M > 10\,000$), thereby enabling the accurate visualisation of the distribution of elements at a subcellular level.^[217] The mass resolution characterises the ability to distinguish two species of slightly different m/z and is expressed as the ratio of the mass being measured (M) and the resolvable mass difference between the two species (ΔM). This high mass resolution provided by the NanoSIMS instrument is essential for the effective detection of ions with very close masses. This is particularly true for the analysis of biological samples enriched in ^{15}N as the instrument must be able to resolve the molecular ion $^{12}\text{C}^{15}\text{N}^-$ from the molecular ions $^{13}\text{C}^{14}\text{N}^-$ which both have a molecular weight of approximately 27 Daltons and that could be ejected from the surface of the sample simultaneously.

In the case of inhaled PI3K δ inhibitors, a NanoSIMS imaging strategy was conducted to investigate the subcellular localization of oral and inhaled PI3K δ inhibitors in HeLa and Hut78 cells. The results of these NanoSIMS investigations may help to validate the outcome of the bioorthogonal TCO chemical probes visualised by fluorescence microscopy. In addition, such a collaborative approach could explore the potentials and/or limitations of these two orthogonal imaging techniques.

In a first instance, fluorine-labelling was selected for the design of labelled-molecules due to the synthetic tractability of fluorine incorporation compared to other stable isotopes. Since the TCO chemical probe derived from nemiralisib showed the most accumulation in Hut78 and HeLa cells (Section 3), it was reasoned that a fluorine-containing analogue of nemiralisib could be designed and profiled by NanoSIMS to initially assess the suitability of this technique for the visualisation of compound subcellular localization.

Previous SAR studies conducted in our laboratory on the nemiralisib scaffold demonstrated that substitution at the 6-position of the indole with fluorine was tolerated and was associated with a slight increase in PI3K δ potency, whilst maintaining a good selectivity profile over the other Class I PI3K isoforms.^[125] Based on these observations, the fluorine analogue **162** was designed as a nemiralisib surrogate for NanoSIMS imaging (Figure 60).

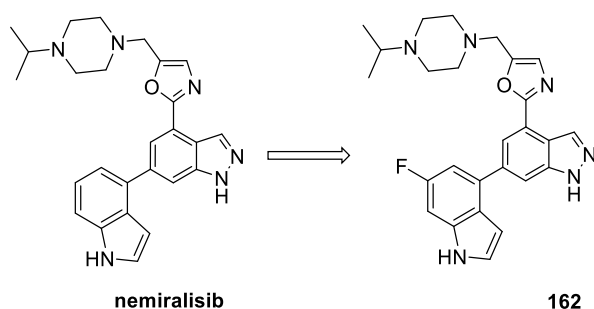
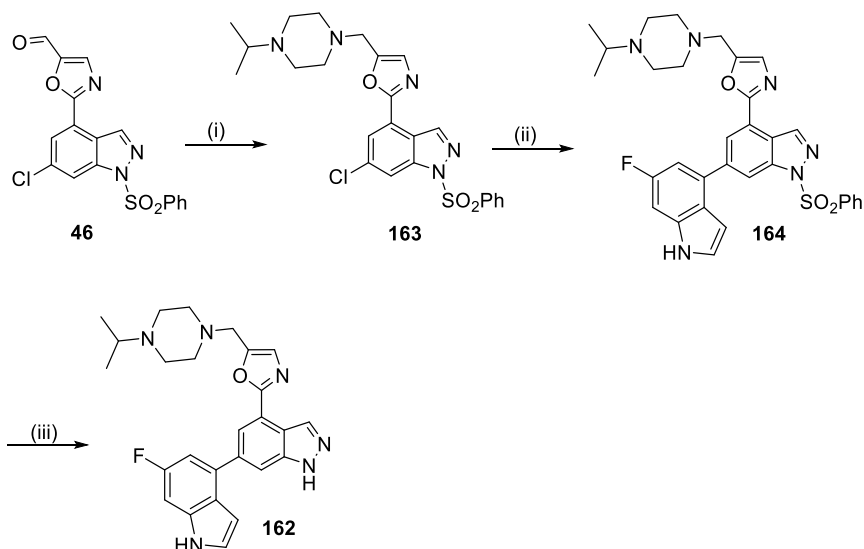


Figure 60. fluorine analogue of nemiralisib **162**.

The synthesis of compound **162** is depicted in Scheme 36 below.

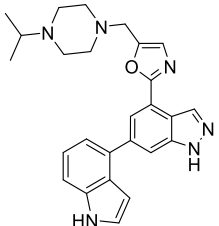
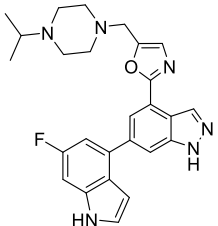


Reagents and conditions: (i) 1-Isopropylpiperazine, AcOH, DCM, rt, 30 min then STAB, DCM, rt, 1 h, 87%; (ii) 6-Fluoroindole-4-boronic acid pinacol ester, XPhos Pd G2 (20 mol%), Na₂CO₃, 1,4-dioxane/water (9:1), 90 °C, μ wave, 1 h, 74%; (iii) 1 M aqueous NaOH, MeOH, rt, 110 min, 53%.

Scheme 36. Synthesis of fluorine analogue of nemiralisib **162**.

The synthesis started with a reductive amination reaction between aldehyde **46** and 1-isopropylpiperazine to give intermediate **163**. Subsequent Suzuki cross-coupling with commercially available 6-fluoroindole-4-boronic acid pinacol ester afforded intermediate **164**, which successfully gave the desired fluorine analogue **162** after benzenesulfonyl deprotection.

Next, fluorine analogue **162** was biologically profiled to ensure that it would maintain similar properties to nemiralisib prior to its utilization as a surrogate in the NanoSIMS imaging experiment. Overall, compound **162** displayed a very similar profile to nemiralisib with slightly enhanced PI3K δ potency, a good selectivity profile for other PI3K isoforms and a mild increase in compound lipophilicity (Table 16).

Structure		
Compound number	nemiralisib	162
PI3K δ pKi (n)	9.9 (4) ^a	10.8 (1) ^a
PI3K α , β , γ pIC ₅₀ (n)	5.3 (27) ^b , 5.8 (26) ^c , 5.2 (30) ^d	5.2 (2), 5.8 (2), 6.1 (2)
α , β , γ fold selectivity	5012, 1585, 6310	31623, 7943, 3981
Kinobead pIC ₅₀ (n)	9.2 (2) ^e	9.0 (2) ^e
Meas. ChromLogD _{pH7.4}	2.5	3.2
AMP (nm/s, pH 7.4)	230	310
Kinetic solubility (μ g/mL)	110	136

*n = number of test occasions included in mean; ^aPI3K δ assay run at a 2 mM ATP concentration; ^bTested <5.3 on one test occasion and <4.6 on one test occasion; ^cTested <4.6 on one test occasion; ^dTested <4.6 on 3 test occasions; ^eLipid kinobeads CZK133 / Lysate mix HeLa-Jurkat-K-562.

Table 16. Properties of fluorine analogue of nemiralisib **162**.

Based on its optimized properties, the fluorine analogue of nemiralisib **162** was then investigated by NanoSIMS imaging in HeLa cells. More specifically, HeLa cells were grown on a silicon chip and subsequently treated with compound **162** (5 μ M). The cells were then washed three times with PBS, freeze dried and analysed by NanoSIMS (Figure 61).

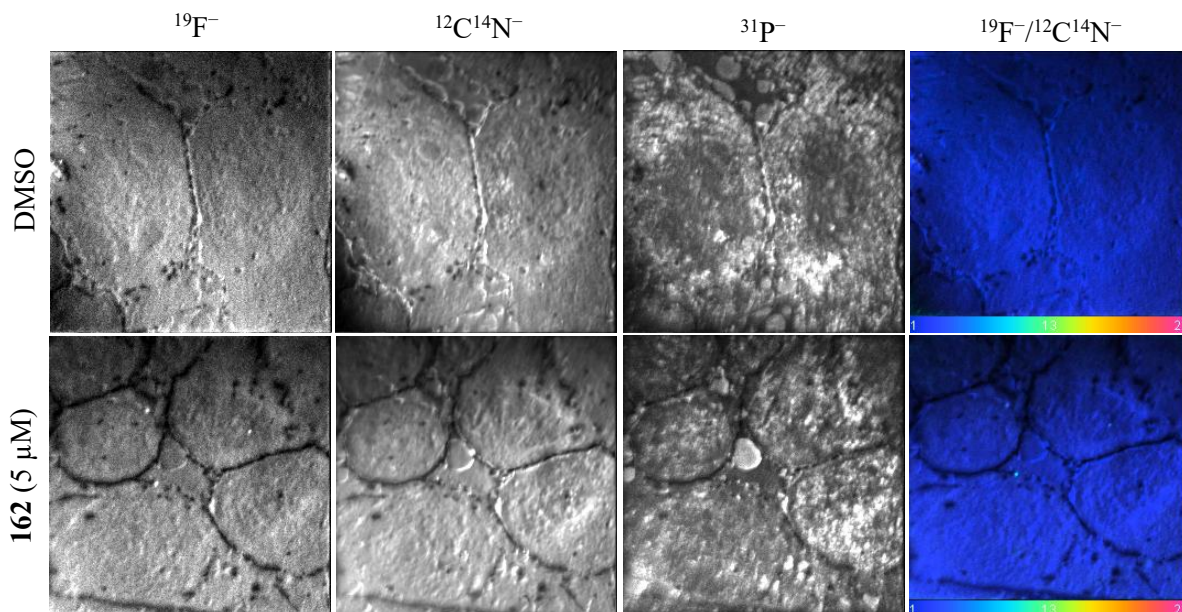


Figure 61. Visualization of HeLa cells treated with compound **162** (5 μ M, 2 h) by NanoSIMS imaging. $^{19}\text{F}^-$, $^{12}\text{C}^{14}\text{N}^-$, $^{31}\text{P}^-$ secondary ions are shown (greyscale). The value of the $^{19}\text{F}^-/^{12}\text{C}^{14}\text{N}^-$ ratio is represented on a colour scale. Scale bar 10 μ m.

In this experiment, detection of the $^{12}\text{C}^{14}\text{N}^-$ secondary ions was used to detect the cell contours whilst $^{31}\text{P}^-$ ions delineates the nucleus. However, the $^{19}\text{F}^-/^{12}\text{C}^{14}\text{N}^-$ ratio did not allow the visualization of $^{19}\text{F}^-$ enrichment in the cytosol as the intensity proved to be similar to the one of cells treated with DMSO (control). Therefore, the use of the fluorine analogue **162** did not allow to confirm the accumulation of the compound in HeLa cells, a cell line not expressing the PI3K δ target, and any conclusion remained tentative. Since compound **162** only contained one fluorine atom, the sensitivity of the NanoSIMS instrument might not allow to differentiate between the fluorine intensity coming from the compound and the environmental fluorine background.

The next approach focused on ^{15}N as an alternative labelling strategy. ^{15}N accounts for 0.64% of the nitrogen isotopic abundance, therefore making it an ideal candidate for labeling. In addition, ^{15}N would not impact the physico-chemical properties of the compounds. Therefore, it was reasoned that a ^{15}N analogue of the two

inhaled clinical candidates nemiralisib and GSK2292767 would be designed, along with a ^{15}N analogue of the oral PI3K δ inhibitor **33** for comparison.

Due to the limited availability of ^{15}N -containing building blocks that can be sourced commercially from most common suppliers, it was envisioned that the most tractable synthetic approach would involve a *de novo* syntheses of a ^{15}N -labelled isopropylpiperazine and a *cis*-2,6-dimethylmorpholine. Therefore, the three ^{15}N -labelled PI3K δ inhibitors depicted in Figure 62 were selected.

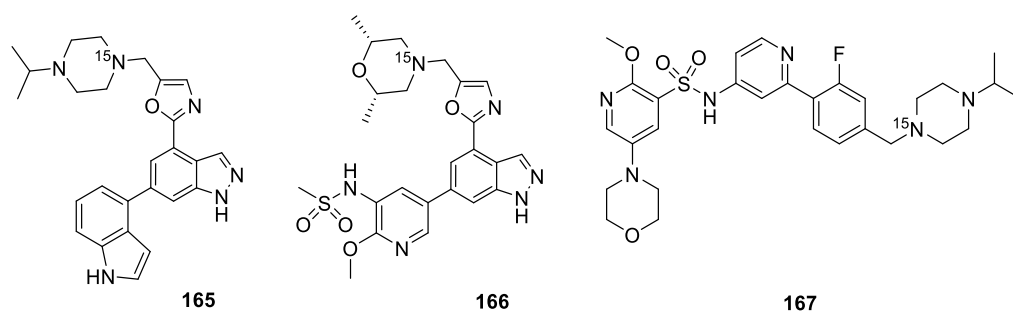
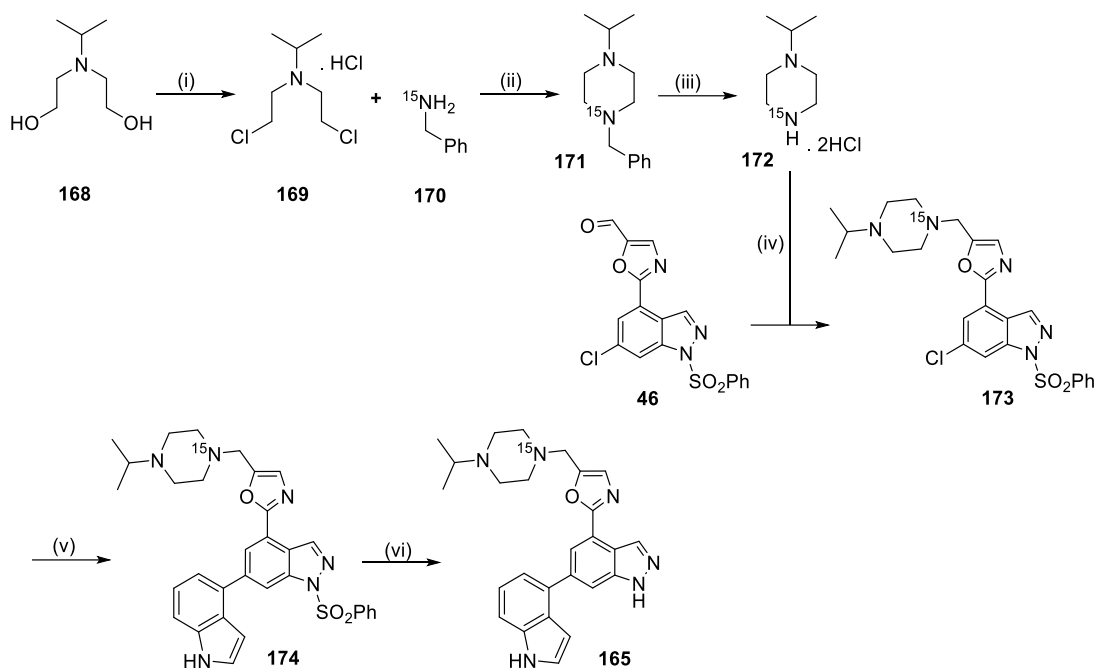


Figure 62. Structures of ^{15}N -analogues of nemiralisib, GSK2292767 and oral PI3K δ inhibitor **33**.

In addition, a ^{15}N -labelled isopropylpiperazine monomer could be utilized for the syntheses of both ^{15}N -nemiralisib (**165**) and ^{15}N oral PI3K δ inhibitor **167** (Figure 62), therefore optimizing the efficiency of this approach. Overall, this synthetic strategy would allow the late-stage installation a ^{15}N -labelled piperazine or morpholine monomer *via* a robust reductive amination reaction employing intermediates previously described in this thesis.

The synthesis of the ^{15}N -nemiralisib analogue is described below (Scheme 37)



Reagents and conditions: (i) SOCl_2 , DCM, rt, overnight, 96% (crude); (ii) DIPEA, acetonitrile, 120°C , μwave , 1 h, 81%; (iii) 5% Pd/C, H_2 , 1,1,2-trichloroethane, MeOH, 50°C , H-Cube[®] (5 bar, 1 mL/min), used crude; (iv) Et_3N , DCM, rt, 5 min then **46**, AcOH, DCM, rt, 30 min followed by STAB, DCM, rt, 30 min, 35% over 2 steps; (v) Indole-4-boronic acid pinacol ester, XPhos Pd G2 (20 mol%), Na_2CO_3 , 1,4-dioxane/water (10:1), 90°C , μwave , 1 h, 64%; (vi) 1 M aqueous NaOH, MeOH, rt, 80 min, 39%.

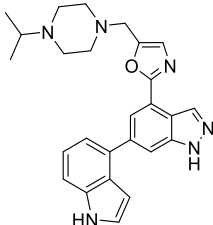
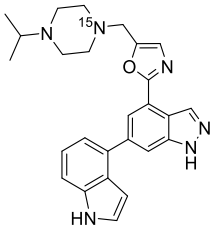
Scheme 37. Synthesis of ^{15}N -nemiralisib analogue **165**.

The synthesis started with chlorination of the commercially available diethanolamine derivative **168** with thionyl chloride to give the corresponding nitrogen mustard **169**. Cyclisation with commercially available ^{15}N -benzylamine (**170**) was successfully carried out in the microwave to afford the desired benzyl-protected ^{15}N -labelled piperazine **171**. Next, N-debenzylation of **171** was conducted using hydrogenolysis conditions described by Wang and Hu.^[222] These conditions rely on a synergistic system whereby Pd-C catalyzes the C-Cl bond cleavage of 1,1,2-trichloroethane in a monodehydrochlorination step that releases HCl *in situ*, facilitating the subsequent catalytic hydrogenolysis of the benzylamine to directly yield the corresponding amine hydrochloride. This approach appears particularly

advantageous for the *N*-debenzylation of volatiles or low-molecular weight amines that can be therefore be more easily isolated as solid crystal hydrochlorides.^[222]

Here, the conditions developed by Wang and Hu were utilized for the *N*-debenzylation of **171** and successfully afforded the crude dihydrochloride piperazine **172** that was immediately taken forward in a reductive amination reaction with aldehyde **46** to give intermediate **173**. Subsequent Suzuki cross-coupling afforded the desired intermediate **174**, which gave the ¹⁵N-nemiralisib analogue **165** after benzenesulfonyl deprotection.

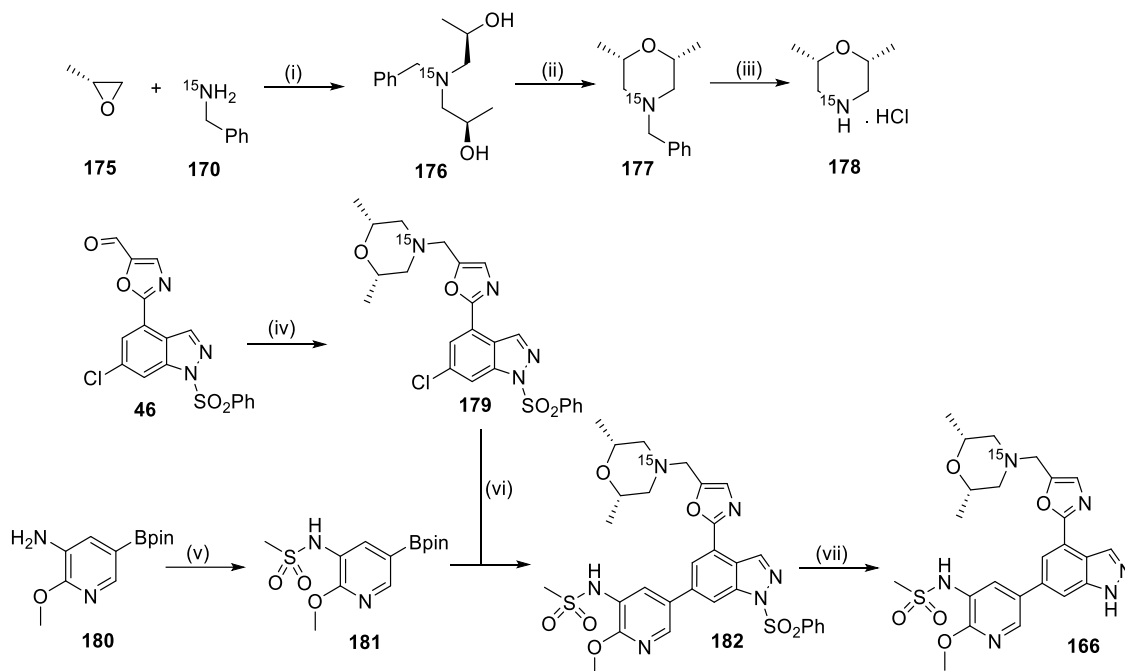
The ¹⁵N-nemiralisib analogue **165** was then profiled to confirm its properties would remain very similar to nemiralisib (Table 17).

Structure		
Compound number	nemiralisib	¹⁵ N-nemiralisib (165)
PI3Kδ p <i>K</i> _i (n)	9.9 (4) ^a	9.9 (3) ^a
PI3Kα, β, γ p <i>IC</i> ₅₀ (n)	5.3 (27) ^b , 5.8 (26) ^c , 5.2 (30) ^d	5.0 (3), 5.2 (3), 5.4 (3)
α, β, γ fold selectivity	5012, 1585, 6310	3162, 1995, 1259
Kinobead p <i>IC</i> ₅₀ (n)	9.2 (2) ^e	9.1 (2) ^e

*n = number of test occasions included in mean; ^aPI3Kδ assay run at a 2 mM ATP concentration; ^bTested <5.3 on one test occasion and <4.6 on one test occasion; ^cTested <4.6 on one test occasion; ^dTested <4.6 on 3 test occasions; ^eLipid kinobeads CZK133 / Lysate mix HeLa-Jurkat-K-562.

Table 17. Properties of ¹⁵N-nemiralisib (**165**).

The synthesis of the ^{15}N -GSK2292767 analogue (**166**) is described in Scheme 38 below.

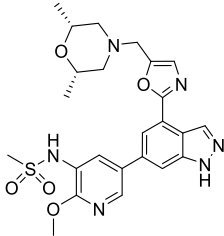
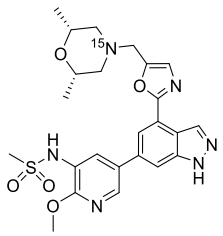


Reagents and conditions: (i) MeOH, 60 °C, overnight, 79%; (ii) H₂SO₄, H₂O, 130 °C, μ wave, 80 min, 88%; (iii) 5% Pd/C, H₂, 1,1,2-trichloroethane, MeOH, 35 °C, H-Cube[®] (1 bar, 1 mL/min), 68%; (iv) **178**, Et₃N, DCM, rt, 5 min then **46**, AcOH, DCM, rt, 1 h followed by STAB, DCM, rt, 1 h, 61%; (v) MsCl, DMAP, pyridine, DCM, rt, 59%; (vi) XPhos Pd G2 (20 mol%), Na₂CO₃, 1,4-dioxane/water (10:1), 90 °C, μ wave, 1 h, 77%; (vii) 1 M aqueous NaOH, MeOH, rt, 1 h, 23%.

Scheme 38. Synthesis of ^{15}N -GSK2292767 (**165**)

The synthesis started with ring opening of chiral (*R*)-(+)-Propylene oxide (**175**) with ^{15}N -benzylamine (**170**) to give intermediate **176**. Subsequent microwave-assisted cyclization mediated by concentrated sulfuric acid successfully afforded the desired ^{15}N -labelled 2,6-*cis*-dimethylmorpholine **177**. NMR studies confirmed the *cis*-relationship. Next, *N*-debenzylation using Wang and Hu conditions previously described successfully gave morpholine **178** as the hydrochloride salt.^[222] The morpholine was taken forward in a reductive amination reaction with aldehyde **46** to give the desired intermediate **179**. Subsequent Suzuki cross-coupling with pinacol boronic ester **181**, prepared in one step from **180**, gave the desired intermediate **182**. Finally, deprotection of the benzenesulfonyl group on **182** afforded the desired ^{15}N -GSK2292767 analogue **166**.

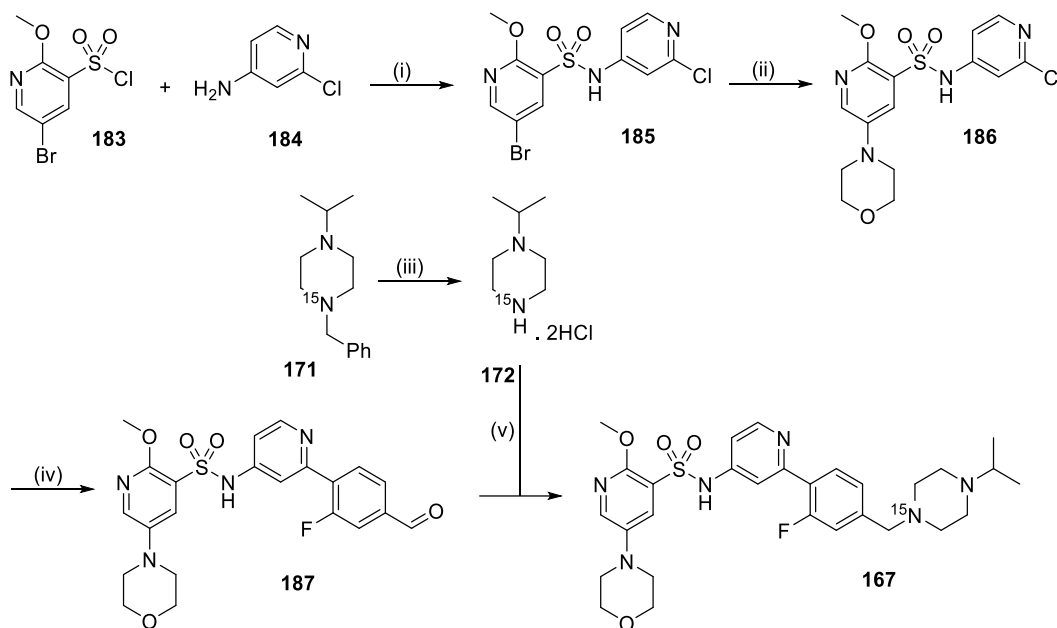
The properties of ^{15}N -GSK2292767 (**166**) are summarized in Table 18 below.

Structure		
Compound number	GSK2292767A	^{15}N -GSK2292767 (166)
PI3K δ pKi (n)	10.1 (5) ^a	10.6 (3) ^a
PI3K α , β , γ pIC ₅₀ (n)	6.3 (17), 6.2 (18), 6.3 (20)	6.5 (3), 6.3 (3), 7.2 (3)
α , β , γ fold selectivity	631, 794, 631	398, 631, 79
Kinobead pIC ₅₀ (n)	9.3 (2) ^b	9.5 (2) ^b

*n = number of test occasions included in mean; ^aPI3K δ assay run at a 2 mM ATP concentration; ^bLipid kinobeads CZK133 / Lysate mix HeLa-Jurkat-K-562.

Table 18. Properties of ^{15}N -GSK2292767 (**166**)

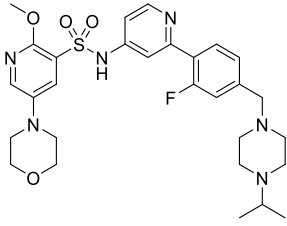
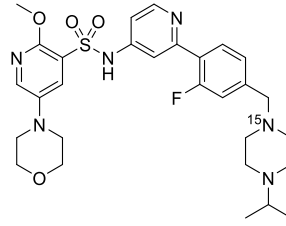
The synthesis of compound **167**, the ^{15}N -labelled analogue of the oral PI3K δ inhibitor **33** was then carried out and is depicted in Scheme 39 below.



Reagents and conditions: (i) pyridine, 0 °C, 2 h, overnight, 68%; (ii) morpholine, CuI (0.2 mol%), 2-isobutyrylcyclohexan-1-one (0.6 mol%), K₂CO₃, DMSO, 110 °C, 29%; (iii) 5% Pd/C, H₂, 1,1,2-trichloroethane, MeOH, 50 °C, H-Cube[®] (5 bar, 1 mL/min), used crude; (iv) (2-fluoro-4-formylphenyl)boronic acid, XPhos Pd G2 (20 mol%), Na₂CO₃, 1,4-dioxane/water (9:1), 90 °C, μ wave, 75 min, 72%; (iv) Et₃N, DCM, rt, 5 min then **187**, AcOH, DCM, rt, 30 min followed by STAB, DCM, rt, overnight, 34%.

Scheme 39. Synthesis of ^{15}N -labelled oral PI3K δ inhibitor **167**.

The synthesis started with the formation of sulfonamide **185** by reacting sulfonyl chloride **183** (available in our laboratories) with 2-chloropyridin-4-amine **184**. Intermediate **185** was then reacted in an Ullmann coupling reaction with morpholine to access compound **186**. Subsequent Suzuki cross-coupling with (2-fluoro-4-formylphenyl)boronic acid afforded aldehyde intermediate **187**. Next, *N*-debenzylation of ^{15}N -labelled piperazine **171** successfully gave the isopropyl piperazine **172** as the dihydrochloride salt. Finally, reductive amination with aldehyde **187** afforded the desired ^{15}N -labelled oral PI3K δ inhibitor **167**. The properties of **167** are summarized in Table 19 below.

Structure		
Compound number	33	167
PI3K δ pKi (n)	10.9 (3) ^a	10.3 (3) ^a
PI3K α , β , γ pIC ₅₀ (n)	6.0 (22), 5.3 (22), 5.7 (28)	5.9 (3), 5.5 (3), 6.3 (3)
α , β , γ fold selectivity	1259, 6310, 2512	794, 1995, 316
Kinobead pIC ₅₀ (n)	8.6 (4)	9.4 (2)

*n = number of test occasions included in mean; ^aPI3K δ assay run at a 2 mM ATP concentration.

Table 19. Properties of ¹⁵N-labelled PI3K δ inhibitor **167**.

Overall, all three isotope-labelled compounds ¹⁵N-nemiralisib (**165**), ¹⁵N-GSK2292767 (**166**) and **167** displayed very similar properties compared to the parent molecules.

Since TCO chemical probes derived from nemiralisib showed strong accumulation in HeLa cells, ¹⁵N-nemiralisib (**165**) was the first compound to be screened by NanoSIMS imaging. HeLa cells were grown on a silicon chip, subsequently treated with ¹⁵N-nemiralisib **165** at various concentrations (0.5, 1, 5 and 20 μ M). The cells were then washed three times with PBS, freeze dried and analysed by NanoSIMS (Figure 63).

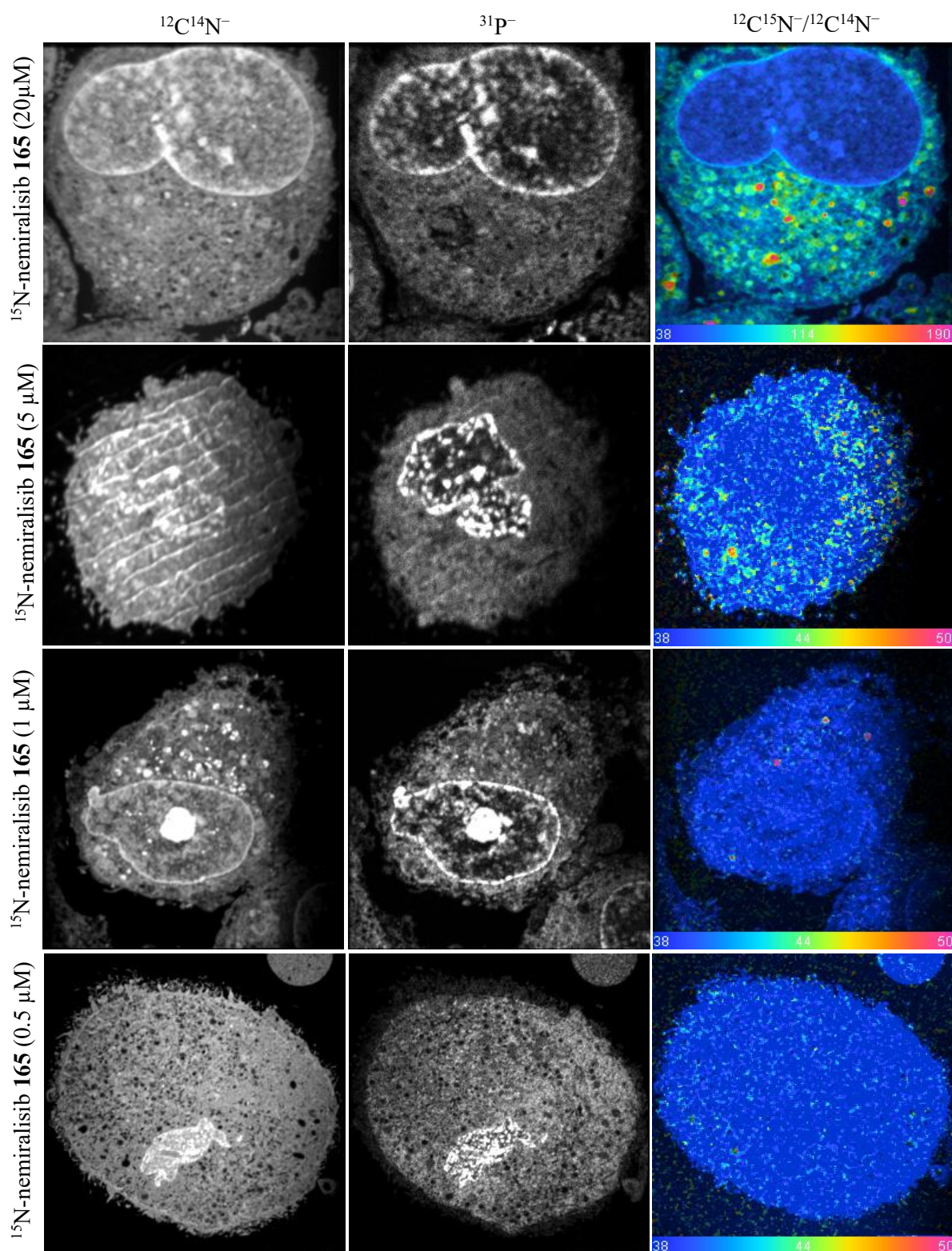


Figure 63 Visualization of HeLa cells treated with ^{15}N -nemiralisib (**165**) by NanoSIMS imaging (0.5, 1, 5 and 20 μM , 2 h). $^{12}\text{C}^{14}\text{N}^-$, $^{31}\text{P}^-$ secondary ions are shown (greyscale). The $^{12}\text{C}^{15}\text{N}^- / ^{12}\text{C}^{14}\text{N}^-$ ratio allows the direct visualisation of ^{15}N enrichment and the value of the ratio is represented on a colour scale: dark blue on the left represents the natural ratio whilst a shift in colour to the right indicates enrichment in ^{15}N . At high concentration (20 μM), signal is also observed in the nucleus.

Visualization of ^{15}N -nemiralisib (**165**) in HeLa cells showed a concentration-dependent signal with ^{15}N enrichment as demonstrated by “hotspots” in the cytoplasm compared to the DMSO control ($^{12}\text{C}^{15}\text{N}^-/^{12}\text{C}^{14}\text{N}^-$ ratio). This demonstrates that ^{15}N -nemiralisib (**165**) tends to accumulate in the cytosol of HeLa cells in the absence of the PI3K δ target. NanoSIMS images also indicates higher ^{15}N enrichment in close vicinity to the nucleus, which could correspond to specific subcellular organelles such as the ER and Golgi apparatus. These observations for ^{15}N -nemiralisib (**165**) demonstrates the cellular behaviour of nemiralisib which has a propensity to accumulate in the cytosol, independently of the binding to the target, potentially due to its basicity therefore forming a “compound reservoir”. These results are in agreement with previous observations of the TCO chemical probes derived from nemiralisib which showed accumulation in acidic and membrane-rich subcellular organelles.

Next, the three compounds ^{15}N -nemiralisib (**165**), ^{15}N -GSK2292767 (**166**) and ^{15}N -oral PI3K δ inhibitor (**167**) were investigated in HeLa cells at the same concentration (5 μM) to assess their subcellular localization and potential accumulation (Figure 64).

^{15}N -GSK2292677 (**166**) could be detected in the cytosol of HeLa cells, however the ^{15}N enrichment and signal intensity was visibly reduced compared to ^{15}N -nemiralisib (**165**). This demonstrates that the compound is accumulating to a lesser extend compared to ^{15}N -nemiralisib. Finally, the ^{15}N -oral PI3K δ inhibitor (**167**) showed a signal intensity which was very similar to the DMSO control, therefore suggesting that the compound is not accumulating. These observations strongly align with the imaging by confocal microscopy of the corresponding TCO probes in HeLa cells (Section 3.4.4).

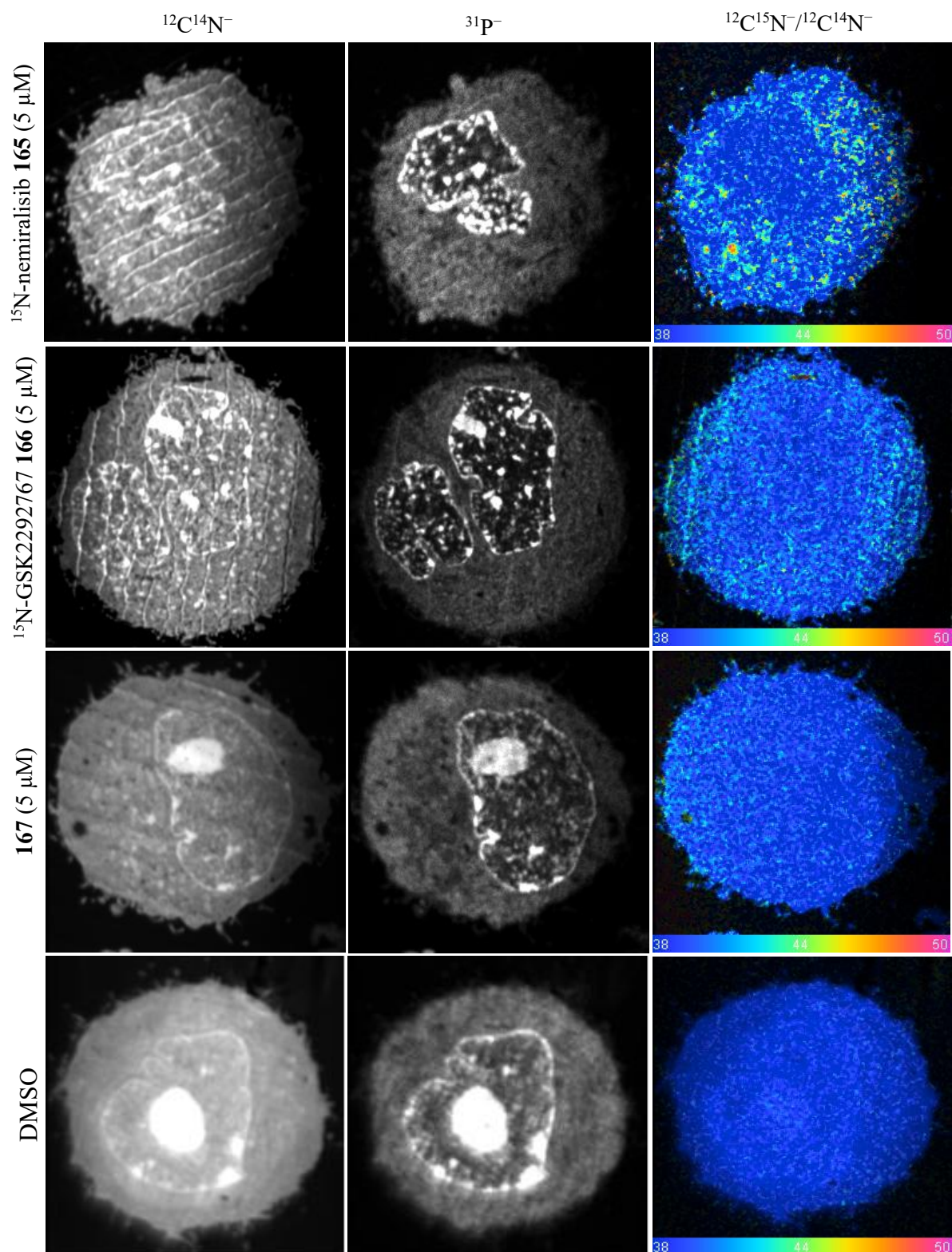


Figure 64. Visualization of HeLa cells treated with DMSO, ^{15}N -nemiralisib (**165**), ^{15}N -GSK2292767 (**166**) or **167** by NanoSIMS imaging (5 μM , 2 h). $^{12}\text{C}^{14}\text{N}^-$, $^{31}\text{P}^-$ secondary ions are shown (greyscale). The $^{12}\text{C}^{15}\text{N}^- / ^{12}\text{C}^{14}\text{N}^-$ ratio is represented on a colour scale: dark blue on the left represents the natural ratio whilst a shift in colour to the right indicates enrichment in ^{15}N .

Overall, these results confirmed that the TCO bioorthogonal probes and the fluorescence microscopy approach is a suitable technique for the visualization of compound subcellular localization. This also suggests that the TCO tag is unlikely to impact the subcellular localization of the compounds to which it is attached.

NanoSIMS is a powerful imaging technique which exhibits good sensitivity, high spatial resolution and high mass resolution. Based on these features, NanoSIMS imaging is a complementary approach to the bioorthogonal chemical probes and the fluorescence microscopy strategy for the visualization of compounds at the subcellular level. Each technique requires the installation of a labeling moiety on the biomolecule of interest prior to imaging. The TCO tag can be installed from commercially available reagents on a biomolecule of interest, for example from a primary amine handle. In addition, the TCO tag has a significant impact on the physico-chemical properties of the biomolecules to which it is attached, especially by increasing their lipophilicity and reducing their solubility. On the other hand, labeling of biomolecules with stable isotopes such as ^{15}N for NanoSIMS imaging has a minimal impact on the properties of the compound. However, this requires a more challenging synthetic effort often associated with a bespoke synthesis due to the limited commercially available ^{15}N -labelled starting materials. Several additional factors may also limit the widespread utilization of NanoSIMS as a routine imaging technique. The first limitation is the lower sensitivity of this method. High degree of accumulation in distinct compartments is usually necessary to enable visualization of small molecules. Moreover, it is frequently advised to increase the labeling to several atoms for efficient detection. Next, the parameters of the NanoSIMS instruments often need to be fine-tuned for effective acquisition when moving across the sample surface, therefore the requisite expertise and the analysis of several samples can be challenging and require up to several weeks of continuous analysis. This is an important factor to take into consideration when designing experiments, and a major difference to fluorescence microscopy imaging which can be conducted within a few hours. The last limitation is the instrument accessibility and cost associated. In 2018, there were 42 instruments installed worldwide that are currently commercially produced by only one company (CAMECA).

5. Cyclopropenes as “Mini-Tags”

Despite its prevalence as a bioorthogonal reagent in IEDDA reaction with tetrazines, the *trans*-cyclooctene moiety is not without limitation, some of which include its large structural size, lipophilicity and potential isomerization to the unreactive *cis*-cyclooctene. Therefore, there has been a significantly growing interest over the last few years to optimise the tagging strategy by considering alternative strained alkenes as bioorthogonal tags.

Cyclopropene derivatives have been proposed as ‘mini-tags’ and have received much interest in the context of bioorthogonal reactions.^[69,71,73,223] Owing to their small sizes and lower lipophilicity compared to *trans*-cyclooctenes, cyclopropenes are less likely to disrupt target-ligand interactions whilst also ensuring minimal variation in the physico-chemical properties of the chemical probes compared to the parent molecules. Therefore, providing they successfully undergo IEDDA reaction with tetrazines, the use of cyclopropene-tagged chemical probes would be of significant interest for direct comparison with TCO for the visualisation of compound cellular localisation.

The suitability of cyclopropenes as bioorthogonal tags in the IEDDA reaction with tetrazines had previously been investigated by Rutkowska *et al.* through the synthesis of chemical probe **188** (Olaparib-cyclopropene 1) (Figure 65).^[142] The compound was designed to provide a direct comparison with the TCO-tagged Olaparib analogue **22**, a tool compound that has been extensively investigated and successfully used to visualise the subcellular localization of PARP1 in cells.^[88]

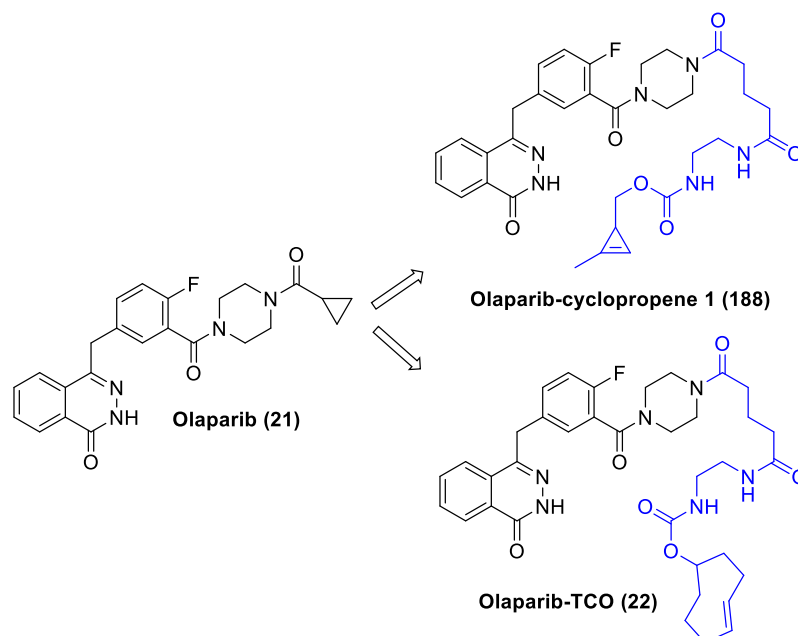


Figure 65. Structure of Olaparib-cyclopropene 1 chemical probe (**188**) designed by Rutkowska *et al.* for direct comparison with Olaparib-TCO (**22**).

However, when investigated in a cellular imaging assay in HeLa cells, the Olaparib-cyclopropene probe 1 (**188**) did not allow visualization of the cellular localisation of PARP1.^[199] Despite several concentrations of tetrazine-Cy5 dye being investigated along with extended reaction times to favour the tetrazine ligation, no fluorescent staining of probe bound to target was observed. It was suggested that this could result from the slower kinetics of cyclopropenes in the tetrazine ligation compared to TCO.

The cyclopropene moiety **18** used as a bioorthogonal tag in compound **188** was one of the first monomers investigated by Devaraj (Figure 66).

^[73] More recent studies focusing on the development of novel 1-methyl-3-substituted cyclopropenes led to the discovery of monomer **20**, one of the most reactive cyclopropenes in IEDDA reaction with tetrazines to date ($k_2 = 0.65 \text{ M}^{-1}\text{s}^{-1}$).

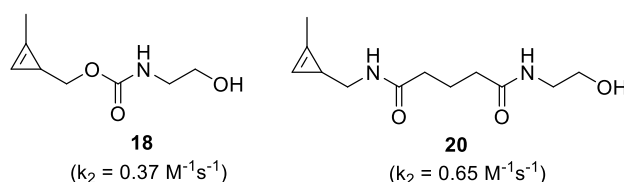


Figure 66. Structures of cyclopropene monomers developed by Devaraj.^[73]

Therefore, the suitability of cyclopropene monomer **20** to act as an optimized bioorthogonal tag was assessed by designing a chemical probe derived from Olaparib referred to as Olaparib-cyclopropene 2 (**189**) (Figure 67).

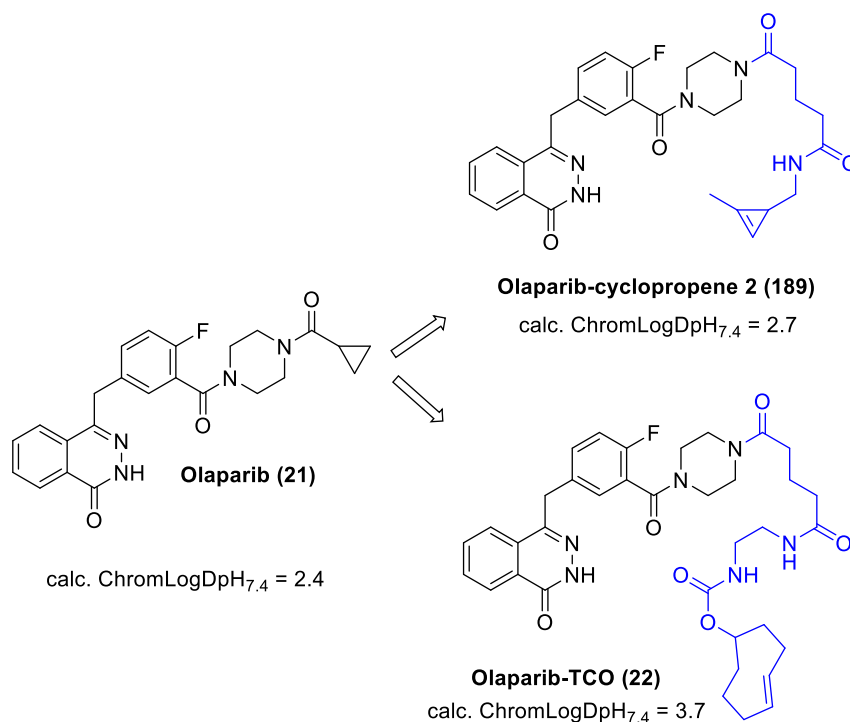
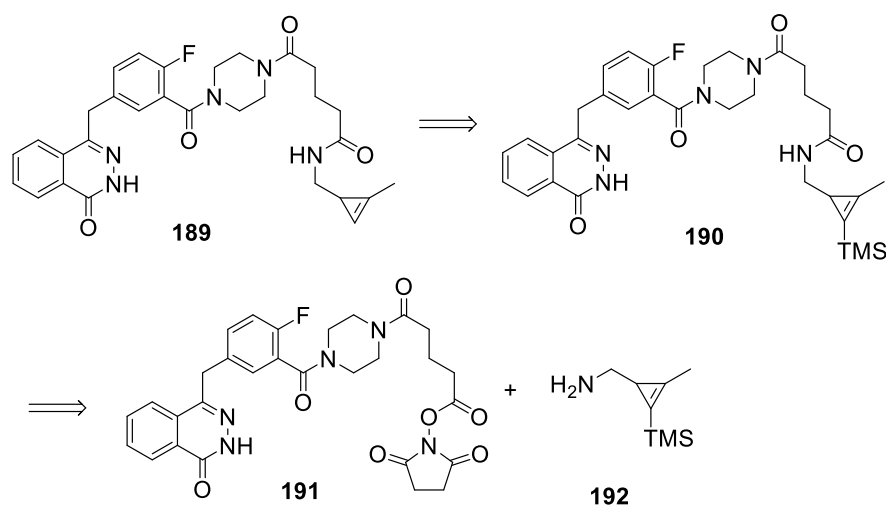


Figure 67. Structure of novel Olaparib-cyclopropene probe 2 (**189**).

Calculated $\text{ChromLogD}_{\text{pH}7.4}$ values were also considered to assess the impact the cyclopropene moiety on the lipophilicity of **189** compared to the TCO probe (**22**) and the parent compound Olaparib. The lipophilicity of chemical probe **189** was calculated to be slightly higher compared to Olaparib and significantly lower than the TCO probe, therefore confirming the interest for cyclopropenes to minimally impact the physico-chemical properties of the compounds to which they are attached (Figure 67).

Provided that the Olaparib-cyclopropene probe 2 (**189**) successfully undergoes the tetrazine ligation with Tz-Cy5 in and allows the visualisation of the cellular localization of PARP1, this cyclopropene bioorthogonal reagent could be subsequently installed on the inhaled clinical candidates for the cellular imaging of PI3K δ inhibitors.

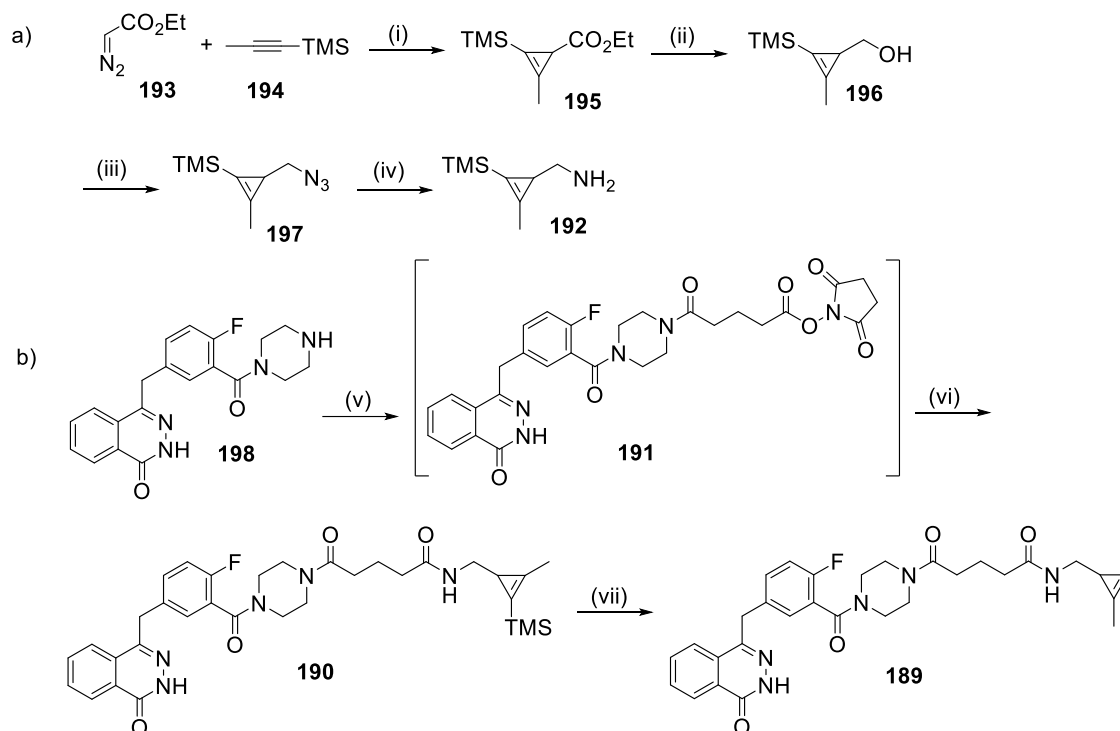
The retrosynthesis considered to access chemical probe Olaparib-cyclopropene 2 (**189**) is outlined in Scheme 40 below.



Scheme 40. Retrosynthesis analyses for the synthesis of chemical probe Olaparib-cyclopropene **189**.

The retrosynthetic approach relied on the reaction between a *N*-hydroxysuccinimide (NHS) ester-functionalised Olaparib intermediate **191** that would react with the TMS-protected cyclopropene amine **192**, previously reported by Devaraj.^[72] Removal of the cyclopropene TMS protecting group on **190** would then yield the desired Olaparib-cyclopropene 2 chemical probe (**189**).

The forward synthetic route to access chemical probe **189** is depicted in Scheme 41 below.



Reagents and conditions: a) (i) $\text{Rh}_2(\text{OAc})_4$ (1.25 mol%), syringe pump addition (1.5 mL/h), neat, rt, then 18 h, rt, 68%; (ii) DIBAL-H 1.5 M in DCM, Et_2O , 0 °C, 3 h, 85%; (iii) DPPA, DBU, THF, 0 °C to rt, overnight, used crude; (iv) PPh_3 , THF/ H_2O (5:1), rt, overnight, 51% over 2 steps (used crude); b) (v) Glutaric anhydride, Et_3N , DCM, rt, 2 h, then DSC, rt, 30 min, not isolated; (vi) **192**, DCM, 2 h 82%; (vii) TBAF 2.0 M in THF, THF, rt, 3 h, 85%.

Scheme 41. Synthesis of Olaparib-cyclopropene chemical probe **189**.

The synthesis commenced with a rhodium-catalysed cyclopropenation reaction between ethyl diazoacetate (**193**) and trimethylsilylpropyne (**194**) to yield the cyclopropene ester intermediate **195**.^[224] Since the initial reports in 1973,^[225] the decomposition of diazo compounds using dirhodium(II) tetraacetate catalyst to form transient rhodium carbenoid species has found a wide range of applications in synthetic organic chemistry, including C-H bonds insertions, cyclopropanation and cyclopropenation reactions.^[226-228]

Despite being very versatile reagents, diazo compounds are highly reactive species, which can limit their practical use in synthetic organic chemistry.^[229] This is exemplified by diazomethane, the simplest member of the family, which is extremely sensitive and explosive.^[230] Nonetheless, the stability of diazo compounds can be

enhanced by the presence of electron-withdrawing carbonyl groups, enabling further delocalization of the electron density, as is the case with commercially available ethyl diazoacetate.^[229]

Dirhodium(II) tetraacetate is an air-stable catalyst that exhibits a “paddle wheel” structure, whereby a dirhodium(II) core is surrounded by four equatorial μ_2 -acetoxy bridging ligands (Figure 68).^[231,232] Within the complex, each rhodium possesses a vacant axial coordination site (L, Figure 68) opposite the Rh-Rh axis that can be involved in the diazo decomposition.^[233]

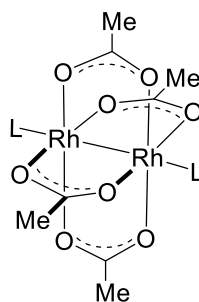
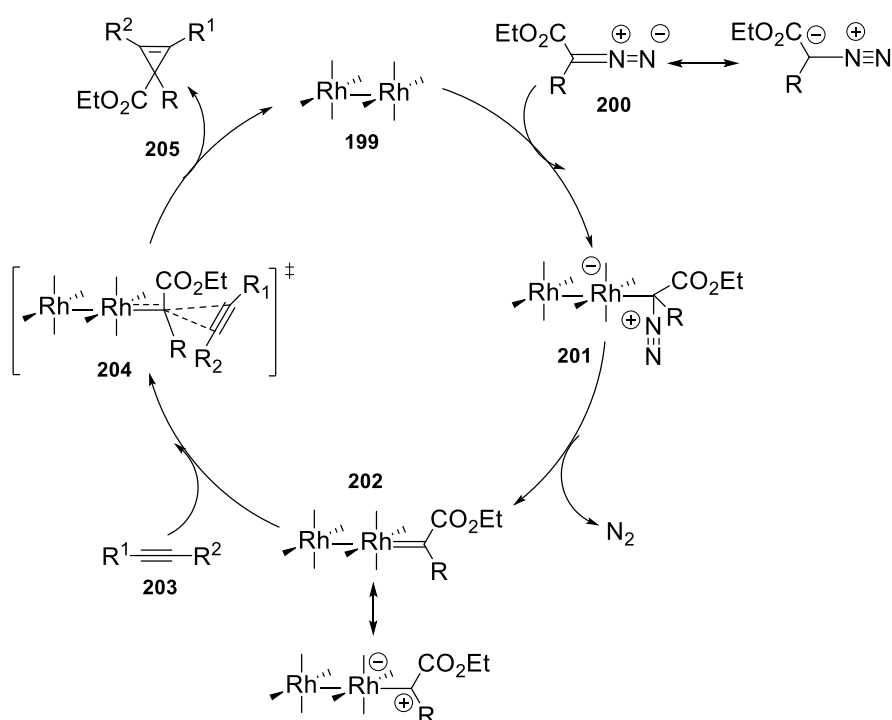


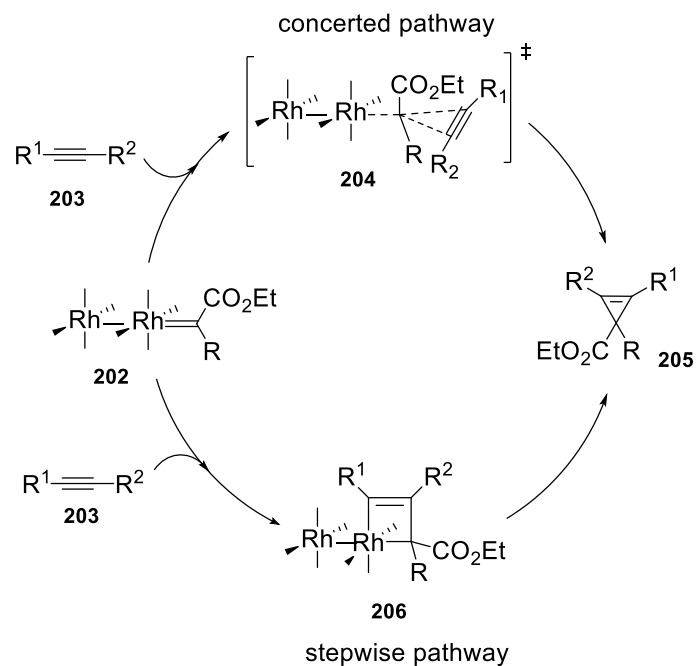
Figure 68. Paddle wheel structure of dirhodium(II) tetraacetate catalyst.
(L = vacant axial coordination site).

It was demonstrated that complexation of the negatively polarized carbon of the diazo compound (**200**) to the axial site of the rhodium catalyst (**199**) leads to the formation of a zwitterionic metal alkyl complex **201**, with subsequent irreversible extrusion of N₂ to generate a transient electrophilic rhodium(II) carbenoid species **202** (Scheme 42).^[234-236] It is believed that only one of the rhodium atoms acts as a diazo binding site.^[237] The second rhodium atom can accept electron density, thereby enhancing the electrophilicity of the carbenoid moiety and promoting subsequent addition of the alkyne (**203**) and generation of the product (Scheme 42).^[233]



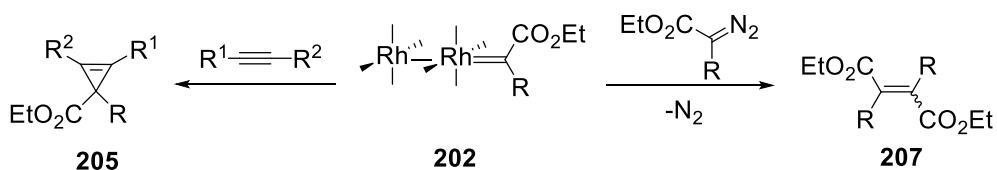
Scheme 42. Mechanism for the rhodium-catalysed cyclopropanation reaction *via* a rhodium carbenoid species. Ligands are omitted for clarity.

Despite the prevalence of rhodium carbenoid chemistry, mechanistic information on their reaction with alkynes to form cyclopropenes is scarce and often inferred from their reaction with alkenes for cyclopropane formation,^[238] for which more extensive mechanistic studies have been conducted.^[227,228,239] The most prevalent pathway for dirhodium(II) tetracarboxylate catalysts involves a concerted mechanism where the alkyne attacks the electropositive rhodium carbenoid carbon directly to form the desired cyclopropene product *via* a three-membered ring transition state (204, Scheme 42).^[228,239,240] However, an alternative stepwise mechanism involving a rhodium metallacycle (206, Scheme 43) that subsequently undergoes a reductive elimination to form the cyclopropene product cannot be totally excluded.^[241]



Scheme 43. Alternative stepwise pathway for reaction of rhodium carbenoid with alkynes. Ligands are omitted for clarity.

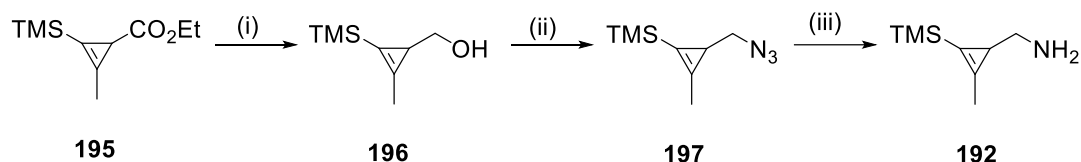
An important aspect that can significantly impact the yield of rhodium-catalysed cyclopropanation reactions is the competitive formation of diazo compound dimers (**207**) which can occur if there is competition between the alkyne and the diazo compound for reaction with the rhodium carbenoid species (Scheme 44).^[242]



Scheme 44. Side reaction leading to the formation of dimers of diazo compounds.

In order to minimize the formation of this side product, cyclopropanation reactions are typically conducted with an excess of alkyne reagent and a very slow addition of the diazo compound.^[226] In the current study, the cyclopropanation was carried out neat with a slow syringe pump addition (< 1 mL/h) of ethyl diazoacetate to a mixture of trimethylsilylpropyne and rhodium catalyst. Because of the highly volatile

character of minimally substituted cyclopropenes, the reaction mixture was purified directly by normal phase silica gel column chromatography and the desired fractions were carefully concentrated on a rotary evaporator at room temperature to afford the desired cyclopropene ester **195** (Scheme 45).

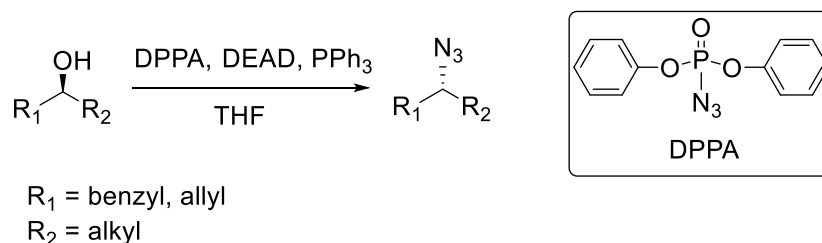


Reagents and conditions: (i) DIBAL-H 1.5 M in DCM, Et₂O, 0 °C, 3 h, 85%; (ii) DPPA, DBU, THF, 0 °C to rt, overnight, used crude; (iii) PPh₃, THF/H₂O (5:1), rt, overnight, used crude.

Scheme 45. Synthesis of cyclopropene amine **192**.

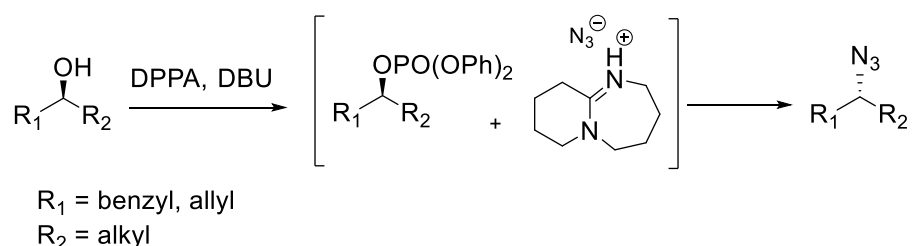
Subsequent reduction of the ester moiety in **195** successfully afforded the desired cyclopropene alcohol **196** (Scheme 45). Once cyclopropene alcohol **196** was isolated, synthesis of the cyclopropene amine **192** was carried out and was accessed *via* the intermediate azide **197** (Scheme 45).

Given their versatility and the wide variety of organic reactions in which they are involved, the direct conversion of alcohols into their corresponding azides is a major functional group transformation in synthetic chemistry.^[15,26] Amongst these direct conversion methods, Mitsunobu displacement using diphenyl phosphorazidate (DPPA) as the azide source has been shown to successfully allow the conversion of alkyl, benzylic and allylic alcohols into their corresponding azides.^[243,244] Under these conditions, a substrate alcohol is reacted with diethyl azodicarboxylate (DEAD) and triphenyl phosphine prior to the addition of DPPA as the azide source (Scheme 46).



Scheme 46. Direct conversion of alcohols into azides under Mitsunobu conditions.^[244]

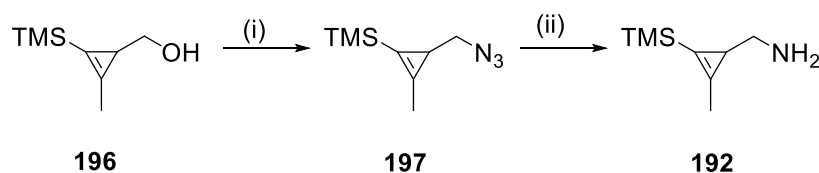
However, this approach can sometimes be limited by the formation of the corresponding olefin by-product resulting from an elimination process as well as difficulties in removing triphenylphosphine oxide.^[245] Further optimisation in the direct conversion of alcohols to azides came from Thompson *et al.* who reported a method that solely uses DPPA and 1,8-diazabicyclo[5.4.0]undec-7-ene (DBU) (Scheme 47).^[245] Mechanistically, a two-step process is involved, the alcohol is converted into the corresponding phosphate intermediate that can subsequently be displaced by the azide ion generated *in situ* present as an organic-soluble DBU salt.^[245]



Scheme 47. Direct conversion of alcohols into azides as described by Thompson.^[245]

There are several aspects that contribute to the attractiveness of the approach developed by Thompson, including cleaner reaction profiles and simplified product isolation compared with other Mitsunobu displacement methods. Indeed, the DBU salt of diphenylphosphate formed during the reaction is water soluble and can be easily removed with an aqueous work-up.^[245] Excess DBU can also be removed with an acidic work-up, yielding crude reaction mixtures that only contain the desired azide and residual traces of DPPA.

Here, the approach developed by Thompson successfully enabled the synthesis of cyclopropene azide **197** which was used crude in the subsequent Staudinger reduction (Scheme 48).^[72]

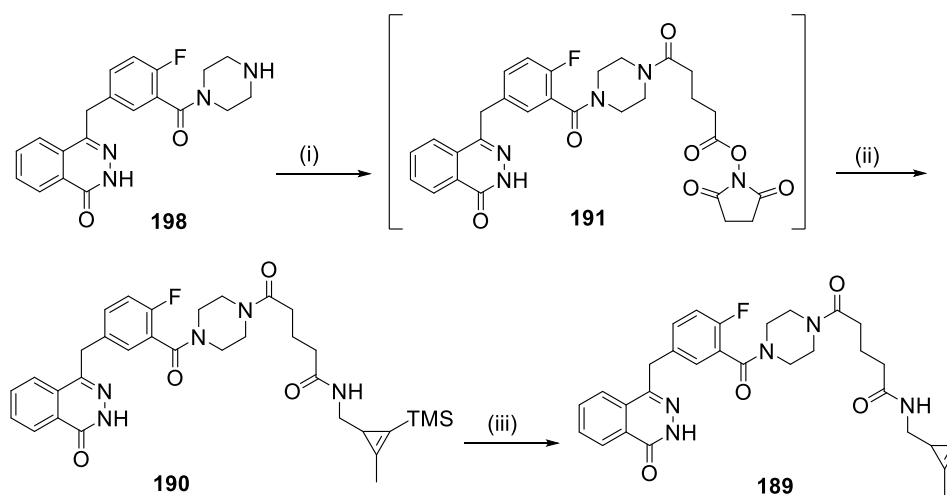


Reagents and conditions: (i) DIBAL-H 1.5 M in DCM, Et₂O, 0 °C, 3 h, 85%; (ii) DPPA, DBU, THF, 0 °C to rt, overnight, used crude; (iii) PPh₃, THF/H₂O (5:1), rt, overnight, 51% over 2 steps (used crude).

Scheme 48. Synthesis of cyclopropene amine **192**.

The Staudinger reduction is the reaction between an organic azide and triphenylphosphine to produce an iminophosphorane intermediate (sometimes also referred as phosphinimine) and subsequent hydrolysis to form a primary amine.^[19] This reaction allows the reduction of azides to amines under very mild conditions and therefore offers an alternative for the reduction of organic azides containing functional groups sensitive to hydrogenation conditions.^[246]

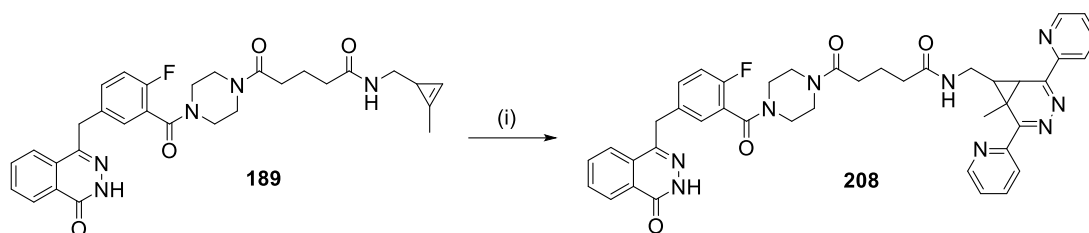
Here, the Staudinger reduction of azide **197** with triphenylphosphine in a THF/water mixture successfully afforded the desired cyclopropene amine **192**. Both the cyclopropene azide and amine intermediates proved to be particularly volatile and the amine was not amenable to long-term storage. Therefore, crude cyclopropene amine **192** was immediately taken forward and reacted with the functionalised Olaparib NHS-ester intermediate **191** in a one pot process (Scheme 49). More specifically, Olaparib precursor **198** was reacted with glutaric anhydride to give the corresponding carboxylic acid. In the same pot, *N,N'*-disuccinimidyl carbonate was added to convert the carboxylic acid to the NHS ester **191** to which was added cyclopropene amine **192**. Final deprotection of the TMS group with TBAF, afforded the Olaparib-cyclopropene 2 chemical probe **189** (Scheme 49).



Reagents and conditions: (i) Glutaric anhydride, Et₃N, DCM, rt, 2 h, then DSC, rt, 30 min, not isolated; (ii) **192**, DCM, 2 h 82%; (vii) TBAF 2.0 M in THF, THF, rt, 3 h, 85%.

Scheme 49. Final steps towards the synthesis of Olaparib-cyclopropene 2 (**189**).

Once **189** was prepared, its reactivity in a model IEDDA reaction with 3,6-dipyridyl-1,2,4,5-tetrazine (**12**) was investigated (Scheme 50).

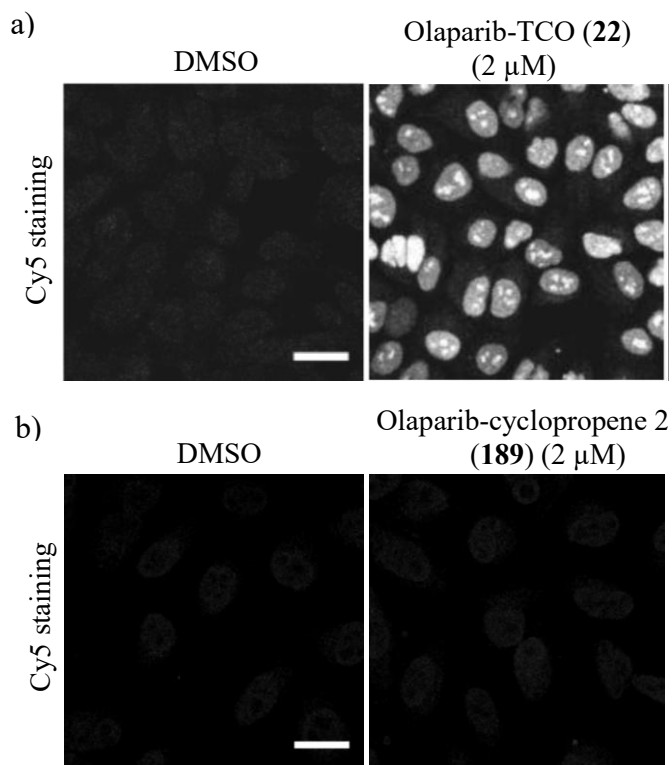


Reagents and conditions: (i) 3,6-Dipyridyl-1,2,4,5-tetrazine (**12**), MeOH, rt, 15 min, 45%.

Scheme 50. Model IEDDA reaction of Olaparib-cyclopropene **189** with 3,6-dipyridyl-1,2,4,5-tetrazine.

Upon addition of the 3,6-dipyridyl-1,2,4,5-tetrazine, the characteristic red/pink colour of the tetrazine progressively disappeared to give a pale yellow solution. The reaction was monitored by LCMS after 15 min and indicated the conversion of the cyclopropene starting material **189** to a major peak whose mass was consistent with the expected cycloadduct. NMR analysis of the isolated product showed a complex mixture of signals, which could be attributable to a mixture of rotamers and diastereoisomers of the diazanorcaradiene product **208**. Overall, this gave supporting evidence that the cyclopropene moiety effectively underwent IEDDA reaction with the tetrazine.

Based on these observations, Olaparib-cyclopropene 2 chemical probe (**189**) was profiled in a cellular imaging assay in HeLa cells to assess its ability to undergo IEDDA reaction with Tz-Cy5 in a cellular context (Figure 69).



- a) HeLa cells treated for 60 min with DMSO or 2 μ M Olaparib-TCO (**22**) followed by fixation, permeabilization, and IEDDA reaction with 100 nM Tz-Cy5 for 5 min. Scale bar 25 μ m.
- b) HeLa cells treated for 60 min with DMSO or 2 μ M Olaparib-TCO (**22**) followed by fixation, permeabilization, and IEDDA reaction with 200 nM Tz-Cy5 for 10 min. Scale bar 25 μ m.

Figure 69. Visualisation of Olaparib-cyclopropene 2 (**189**) chemical probe in HeLa cells.

However, the probe did not allow the visualization of the cellular localization of the Olaparib target, PARP1. Indeed, similarly to what had been observed for Olaparib-cyclopropene probe 1 (**188**),^[199] the staining from the tetrazine-Cy5 observed in HeLa cells treated with probe **189** (2 μ M) was of similar intensity to the DMSO control. Despite increased concentrations of dye being used along with extended staining reaction time (up to 30 minutes), the fluorescent signal was no different to the DMSO control. Consequently, although cyclopropene **20** showed increased reactivity with tetrazines compared to **18** in Devaraj studies,^[72] introduction of this monomer on chemical probe **189** was not suitable for the visualization of the subcellular localization of PARP1 in HeLa cells. Therefore, the TCO tag appears to remain an optimal bioorthogonal reagent for cellular imaging experiment.

Several studies have been conducted by Houk to elucidate the differences in reactivity of cyclopropene and *trans*-cyclooctene in IEDDA cycloadditions with tetrazines using the distortion/interaction model.^[247-249]

The distortion/interaction model, also referred to as the activation strain model, was initially developed by Houk, as a tool to analyse the activation barriers of bimolecular reactions and has been applied to several types of reactions, including cycloadditions.^[247] In this energy decomposition model, the activation energy ($\Delta E^\ddagger_{\text{act}}$) of a bimolecular reaction is expressed as the sum of the distortion energy ($\Delta E^\ddagger_{\text{dist}}$) and the interaction energy ($\Delta E^\ddagger_{\text{int}}$) as summarized in the equation below:

$$\Delta E^\ddagger_{\text{act}} = \Delta E^\ddagger_{\text{dist}} + \Delta E^\ddagger_{\text{int}}$$

The distortion energy (also called activation strain) corresponds to the energy required to distort the reactants from their ground-state geometries to the transition state geometries. Consequently, the distortion energy is characterized by the rigidity of the reactants' structures and usually depends on the strength of the bonds being broken or the flexibility of the bond angles being distorted to achieve the transition state geometry. Therefore, the distortion energy term can be further divided into the individual contributions coming from each of the reactants involved in the reaction being investigated; typically for a cycloaddition reaction $\Delta E^\ddagger_{\text{dist}} = \Delta E^\ddagger_{\text{dist_4e}} + \Delta E^\ddagger_{\text{dist_2e}}$ for the diene and dienophile partners, respectively. The sign of the distortion energy term is generally positive, implying that it is a destabilizing factor that contributes to increasing the activation barrier of the reaction.

The interaction energy ($\Delta E^\ddagger_{\text{int}}$) arises from the orbital overlap between the distorted reactants in the transition state and therefore depends on their mutual orientation as they approach each other. As a consequence, the interaction energy for a cycloaddition reaction is directly related to the HOMO-LUMO interactions as described by the frontier molecular orbital theory. The sign of the interaction energy is generally negative, suggesting that it is a stabilizing factor that counteracts the distortion energy and therefore contributes to the reduction of the reaction activation energy. The distortion/interaction model is illustrated in Figure 70 with the IEDDA reaction between 1,2,3,4-tetrazine and ethylene as an example.^[248] The solid black line

in Figure 70 represents the potential energy along the reaction coordinate for this cycloaddition.

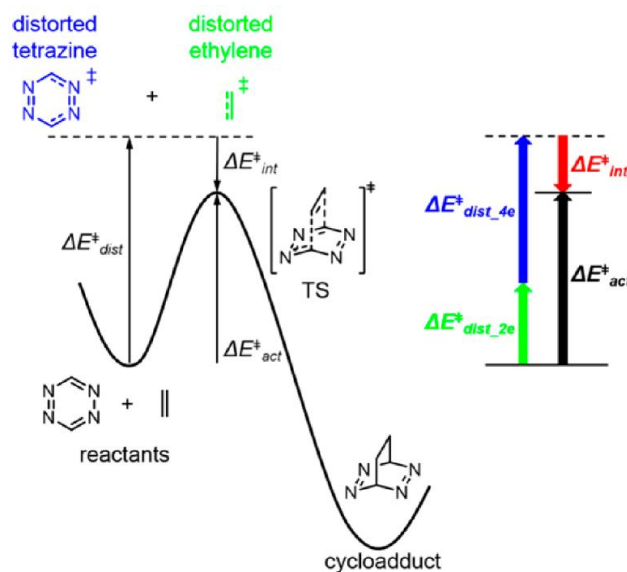


Figure 70. Representation of the distortion/interaction model for the IEDDA reaction of 1,2,4,5-tetrazine and ethylene.^[248] Reprinted with permission from Houk *et al.*^[248]

(Copyright 2014 American Chemical Society).

Seminal studies undertaken by Sauer focusing on the reactivity of cyclopropenes and other strained alkenes as dienophiles in IEDDA cycloadditions with tetrazines were previously discussed in this thesis.^[68] They revealed that the reactivity of cyclic alkenes (from cyclopropene to cyclohexene) decreased as the ring size increased, with the exception of *trans*-cyclooctene which was the most reactive cycloalkene. This reactivity pattern had initially been attributed to strain release. However, if ring strain was controlling the reactivity of cycloalkenes in IEDDA cycloadditions, the difference between the strain energy (*SE*) of the cycloalkenes and the strain energy of the corresponding cycloalkanes (ΔSE) should correlate with the rate constants. The ΔSE of cycloalkenes under study shown in Table 20 suggest that cyclopropenes would be more reactive than *trans*-cyclooctene in IEDDA cycloaddition with tetrazines ($\Delta SE = 27.7$ and 5.7 , respectively). However, for a given tetrazine, *trans*-cyclooctene usually displays higher second order rate constant (k_2) compared to cyclopropene, therefore suggesting that strain release does not only account for the reactivity of strained alkenes in IEDDA reactions.

Cycloalkene	SE	Cycloalkane	SE	ΔSE
Cyclopropene	55.2	Cyclopropane	27.5	27.7
<i>Trans</i> -cyclooctene	17.9	Cyclooctane	12.2	5.7

Table 20. Strain energies (*SE*, in kcal/mol) of cycloalkenes and cycloalkanes.^[248,249]

When applied to the IEDDA reaction of several cycloalkenes with tetrazines, the distortion/interaction model showed an increase in the distortion energy of the cycloalkenes as the ring size increased (from cyclopropene to cyclohexene) whilst the interaction energy remained fairly constant across the series.^[249] These results suggest that the increase in the cycloalkene distortion energy required to achieve the transition state geometry accounts for the increased activation barrier observed from cyclopropene to cyclohexene. In the case of *trans*-cyclooctene, the distortion energy required to achieve the transition state geometry was found to be lower than for cyclopropene due to the compound already being pre-distorted in the ground state. Consequently, *trans*-cyclooctene has an extremely early transition state that further lowers the activation barrier and explains its high reactivity in IEDDA reaction with tetrazines compared to other cycloalkenes.^[248]

Additional studies aiming to further elucidate the reactivity of strained alkenes in IEDDA have been focusing on the influence of 1,2,4,5-tetrazines substituents on the reaction rates of cycloadditions with *trans*-cyclooctene. Due to a unique ring system consisting of an heterocycle with four nitrogen atoms, 1,2,4,5-tetrazines are electron deficient dienes possessing low-lying vacant orbitals. According to the Frontier Molecular Orbital Theory, the interaction between the LUMO of the tetrazine and the HOMO of the cycloalkene is the main factor that contributes to the reactivity of the IEDDA cycloaddition. Therefore, the energy of the 1,2,4,5-tetrazine LUMO orbital can be further lowered by the introduction of electron-withdrawing groups, resulting in a smaller HOMO-LUMO energy gap and ultimately an increase in reactivity. Alternatively, the presence of electron-donating groups raises the energy of the LUMO orbital, resulting in a decrease in reactivity.

In 2011, Hilderbrand and co-workers undertook a comprehensive investigation of the influence of substituents on the second-order rate constants of a variety of 1,2,4,5-tetrazines with various cycloalkenes using DFT calculations.^[79] Those studies revealed that 1,2,4,5-tetrazines substituted with electron donating groups were indeed less reactive than those functionalised with electron-withdrawing groups. For example, comparison of 3,6-dimethyl-1,2,4,5-tetrazine and 3,6-bis(trifluoromethyl)-1,2,4,5-tetrazine showed that the more electron-deficient tetrazine tend to have had stronger interaction energies compared to the more electron-rich ones, arising from the favourable interaction between the tetrazine LUMO and cycloalkene HOMO frontier orbitals. This results in lower activation energies and earlier transition states for electron-deficient tetrazines. Those studies also showed that the tetrazine distortion energies vary depending on the electronic nature of the substituents and tend to decrease for electron-deficient tetrazines where the transition state is relatively early. However, these differences in distortion energies are not as significant as the difference in interaction energies, which appears to mostly account for the differences in activation barriers.

These observations were later confirmed in a thorough study from Devaraj *et al.* who showed that the electronic nature of the substituents at the C3 and C6 position of the 1,2,4,5-tetrazines can significantly impact both their stability in biological media and reactivity with cycloalkenes in IEDDA reactions.^[72] In this study, 1,2,4,5-tetrazines substituted with electron-donating groups were found to be highly stable, albeit displaying slower reaction rates compared to those substituted with electron-withdrawing group that displayed lower stability in biological media but faster reaction rates.

Using the distortion/interaction model, Devaraj showed that unlike *trans*-cyclooctene, the distortion energy required for cyclopropene was not very sensitive to the steric hindrance of the tetrazine substituents. Therefore, it was suggested that the larger size of *trans*-cyclooctene may limit the approach of 1,2,4,5-tetrazines decorated with sterically bulky substituents.

Finally, Devaraj also reported a comparison study of second-order rate constants of cyclopropene monomer **20** and *trans*-cyclooctene with selected tetrazines.

It was confirmed that tetrazine substituents could be used to tune the reactivity of cycloalkenes in IEDDA reactions, however mono- and disubstituted tetrazines tend to react 2-3 orders of magnitude faster with *trans*-cyclooctene than with 1-methyl-3-substituted cyclopropene **20**.^[72]

Based on these observations and the challenges associated with modifying the 1-methyl-3-substituted cyclopropene scaffold, it was reasoned that investigating additional 1,2,4,5-tetrazines bearing electron-withdrawing groups and comparing their reactivity with chemical probe Olaparib-cyclopropene **2** (**189**) would be of significant interest. Provided that a tetrazine with enhanced reactivity compared to that of the mono-substituted tetrazine moiety present in tetrazine-Cy5 is identified, coupling to the Cy5 fluorescent dye would result in a novel fluorophore that may enable the visualization of the subcellular localization of the Olaparib-cyclopropene **2** chemical probes in HeLa cells. The 1,2,4,5-tetrazines considered in this study are depicted in Figure 71.

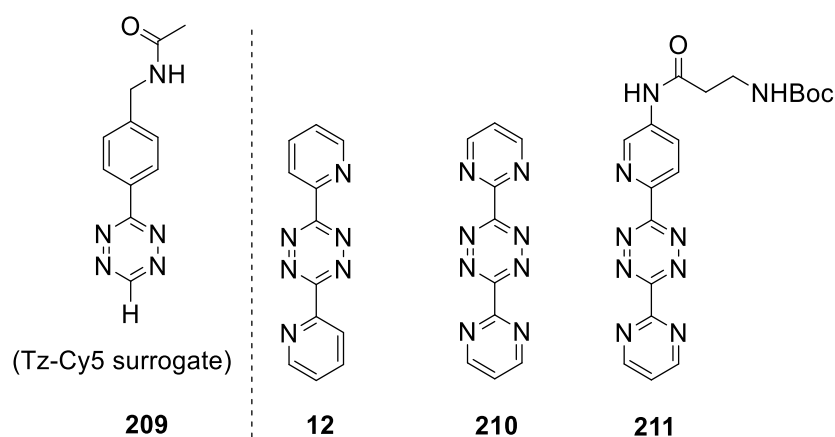
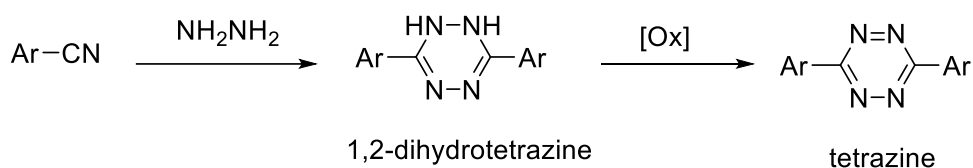


Figure 71. 1,2,4,5-Tetrazines considered for reactivity comparison with 1,2,4,5-tetrazine **209** (Tetrazine-Cy5 surrogate)

1,2,4,5-Tetrazine **209** is a mono-substituted tetrazine that contains an acetamide group designed as a surrogate for Tetrazine-Cy5. 3,6-Dipyridyl- and -dipyrimidyl-1,2,4,5-tetrazines (**12** and **210**, respectively) have previously been described and are commonly used in kinetics studies with cycloalkenes.^[250] Finally, 1,2,4,5-Tetrazines

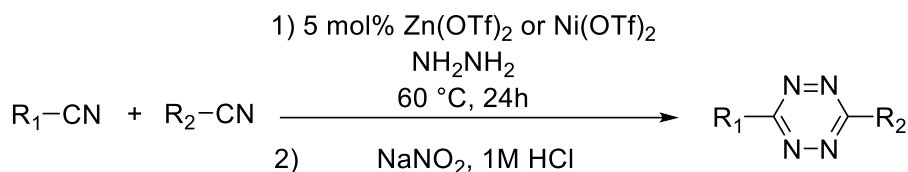
211 was designed to incorporate a Boc-protected primary amine group that would provide a handle for potential subsequent functionalisation with Cy5. The syntheses of these tetrazines are described in more details below.

A common synthetic route to access 1,2,4,5- tetrazines is the original Pinner synthesis described at the end of the 19th century.^[251] In this approach, the 1,2,4,5-tetrazine is formed in two steps, involving condensation of an aromatic nitrile with hydrazine to form a 1,2-dihydrotetrazine that subsequently oxidized to the corresponding tetrazine (Scheme 51).^[251,252]



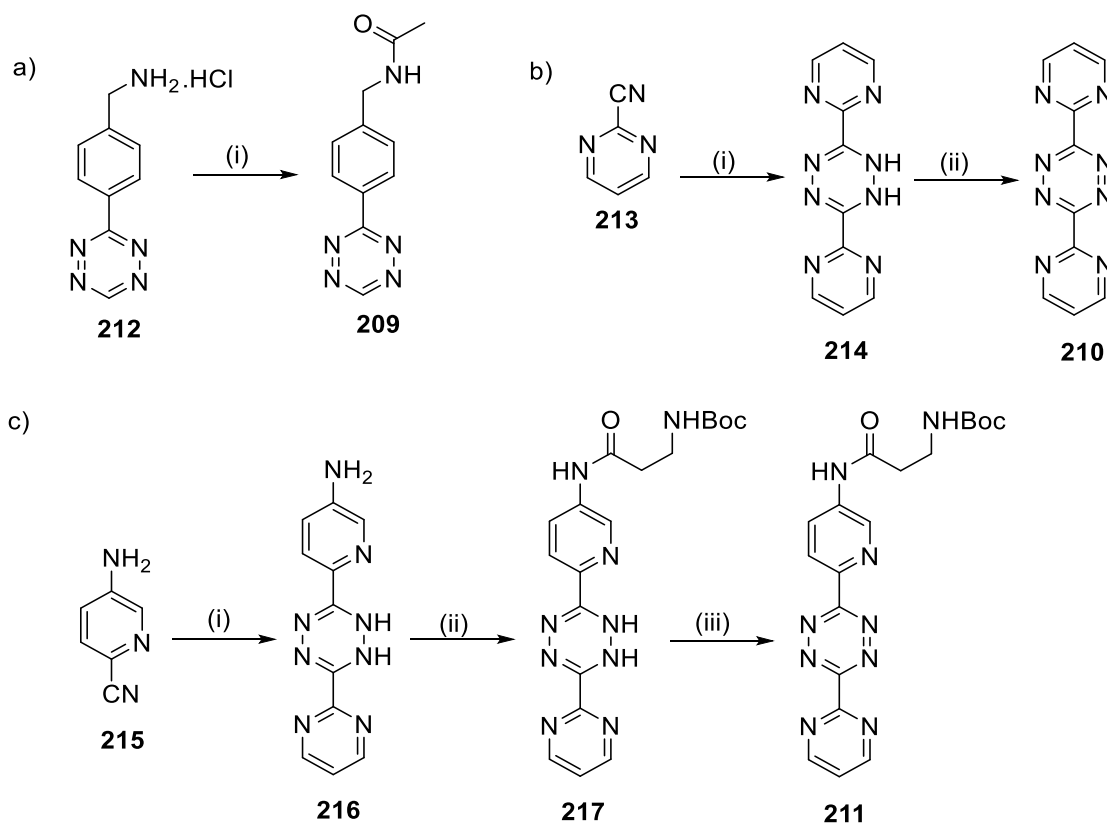
Scheme 51. Original Pinner synthesis of 1,2,4,5-tetrazines.^[251]

Despite being useful for the synthesis of symmetrical 1,2,4,5-tetrazines, this approach has limitations for the synthesis of asymmetric tetrazines for which a statistical mixture of products is obtained, rendering purification and isolation challenging. In addition, this approach is limited to aromatic nitriles, as aliphatic nitriles are unreactive and alkyl tetrazines are usually obtained in very low yields.^[50] In 2012, Devaraj and co-workers reported a novel Lewis acid-catalysed one-pot synthesis of 1,2,4,5-tetrazines using nickel or zinc triflate, allowing the formation of 1,2,4,5-tetrazines from aliphatic nitriles (Scheme 52).^[253]



Scheme 52. Lewis acid-catalysed synthesis of 1,2,4,5-tetrazines reported by Devaraj.^[253]

1,2,4,5-Tetrazine **209** (Tetrazine-Cy5 surrogate) was accessed in one step by treatment of commercially available (4-(1,2,4,5-tetrazin-3-yl)phenyl)methanamine hydrochloride **212** with acetic anhydride (Scheme 53, a).



Reagent and conditions: a) (i) DIPEA, Ac₂O, DCM, rt, 30 min, 78%; b) (i) NH₂NH₂·H₂O, HCl 37%, THH, reflux, overnight, 55%; (ii) NaNO₂, AcOH, rt, 20 min, 30%; c) (i) **213**, NH₂NH₂·H₂O, 90 °C, overnight, 27%; (ii) Boc-β-Ala-OH, DMAP, EDCI, DMF, rt, 2 h, 50%; (iii) NaNO₂, AcOH, rt, 30 min, 58%.

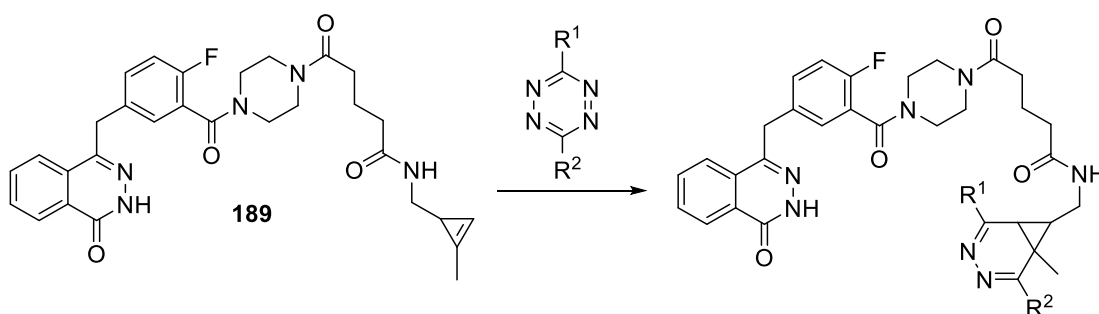
Scheme 53. Syntheses of 1,2,4,5-tetrazines **209**, **210** and **211**.

3,6-Dypirymidyl-1,2,4,5-tetrazine **210** was accessed following the classical two-step sequence, starting with condensation of hydrazine hydrate onto pyrimidine-2-carbonitrile **213** to afford the corresponding 1,2-dihydrotetrazine **214** followed by oxidation to the 1,2,4,5-tetrazine using sodium nitrite in acetic acid (Scheme 53, b).

Finally, synthesis of 1,2,4,5-tetrazine **211** started with condensation of hydrazine hydrate in a 1:1 mixture of 5-aminopyrimidine-2-carbonitrile **215** and pyrimidine-2-carbonitrile **213**

to give a statistical mixture of dihydrotetrazines from which **216** was isolated. Subsequent amide coupling with Boc- β -Ala-OH afforded the dihydrotetrazine **217** which was oxidized to the corresponding 1,2,3,4-tetrazine **211** (Scheme 53, c). Interestingly, oxidation of dihydrotetrazine **217** with a small excess of sodium nitrite (1.2 equivalents) in acetic acid also led to formation of a *N*-nitrosoamide tetrazine as a side-product (3:1 ratio), where nitrosation occurred on the Boc-protected nitrogen.

Once their syntheses completed, the second-order rate constants for IEDDA reaction between the different 1,2,4,5-tetrazines and chemical probe Olaparib-cyclopropene **2** were investigated (Scheme 54).



Scheme 54. Second-order rate constants determination of IEDDA reaction of Olaparib-cyclopropene **2** chemical probe (**189**) with different 1,2,4,5-tetrazines. Only one isomer of diazanocaradiene product is depicted.

It is well established for IEDDA reaction between tetrazines and cycloalkenes that the initial [4+2] cycloaddition step can be considered as the rate-determining step according to DFT calculations.^[254] Therefore, the reaction rates of IEDDA cycloaddition can be determined by monitoring the decay of the characteristic red/pink colour of the tetrazine over time in the presence of excess cycloalkenes (pseudo first order conditions).

The UV-vis absorption spectra of 1,2,4,5-tetrazines typically shows two characteristic maxima, a stronger one at around 320 nm and a weaker one at around 520 nm, the latter one being responsible for the characteristic colour of the compound. The UV-vis absorption spectrum of 3,6-dipyridyl-1,2,4,5-tetrazine (2 mM) in a 1:1 acetonitrile/PBS mixture is shown below in Figure 72 and highlights the weaker absorption maxima at 520 nm.

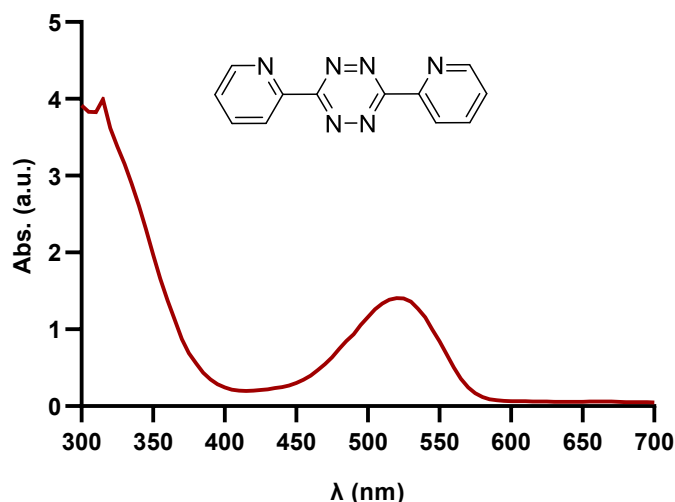


Figure 72. UV-vis absorption spectrum of 3,6-dipyridyl-1,2,4,5-tetrazine (1:1 acetonitrile/PBS, 2 mM).

Since the diazanocaradiene product **208** resulting from the IEDDA reaction of Olaparib-cyclopropene 2 probe (**189**) and 3,6-dipyridyl-1,2,4,5-tetrazine (**12**) appeared yellowish in colour, it was reasoned that the weaker absorption maximum at 520 nm would be selected for these kinetics experiments in order to avoid interference with potentially absorbing IEDDA products at 320 nm.

For the kinetic experiments, reaction mixtures consisting of Olaparib-cyclopropene 2 (**189**) and the different 1,2,4,5-tetrazines in 1:1 MeCN/PBS (total volume = 100 μ L) were prepared in separate wells of a 96-well plate at 25 $^{\circ}$ C so that a final concentration of 1 mM tetrazine and 10, 13 and 17 mM of **189** was achieved. Immediately after the 1,2,4,5-tetrazines solution being added to the well to initiate the IEDDA cycloaddition, the progress of the reaction was monitored by recording the decay of the tetrazines absorbance with a microplate reader for 2 minutes (2 seconds interval) at a wavelength of 520 nm. The pseudo-first order rate constants (K_{obs}) were then determined by linear fit of $\ln([A]/[A_0])$ against reaction time using the pseudo-first order rate equation: $A = A_0 \cdot \exp(-k \cdot [\mathbf{189}] \cdot t)$ where A = absorbance at time t , A_0 = initial absorbance, $k \cdot [\mathbf{189}]$ = pseudo-first order rate constant (K_{obs}), t = time.

This procedure was repeated three times for each concentration of Olaparib-cyclopropene 2. The second-order rate constants (k_2) were eventually obtained by

plotting the pseudo-first order rate constant (K_{obs}) against the concentration of Olaparib-cyclopropene 2 (**189**) (Figure 73).

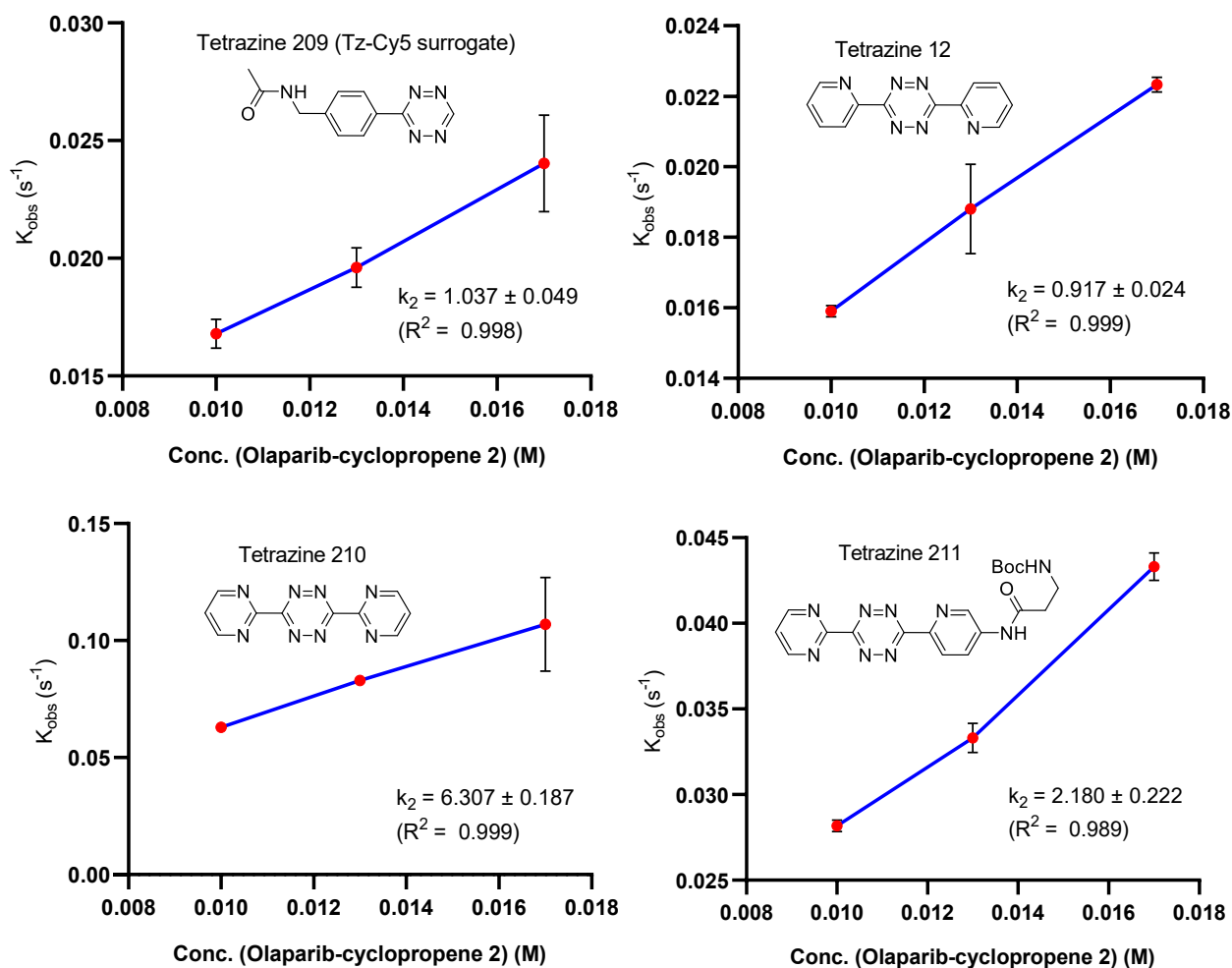


Figure 73. Second-order rate constant (k_2) determination of Olaparib-cyclopropene 2 (**189**) reacted with several 1,2,4,5-tetrazines.

The second-order rate constants (k_2) of the various 1,2,4,5-tetrazines investigated in this study are summarised in Table 21 below.

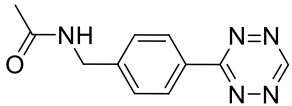
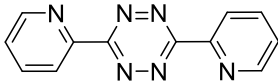
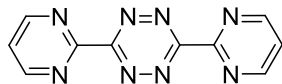
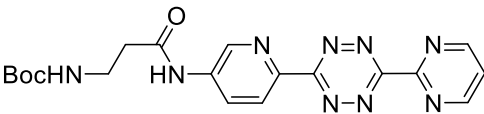
Compound number	Tetrazine Structure	k_2 ($\text{M}^{-1}\text{s}^{-1}$)
209		1.037 ± 0.049
12		0.917 ± 0.024
210		6.307 ± 0.187
211		2.180 ± 0.022

Table 21. Second-order rate constant (k_2) of Olaparib-cyclopropene **2** (**162**) reacted with different 1,2,4,5-tetrazines.

In this experiment, 1,2,4,5-Tetrazine **209** designed as a surrogate for Tetrazine-Cy5 displayed a second-order rate constant $k_2 = 1.037 \pm 0.049$, which is in a similar range to the second-order rate constants reported by Devaraj for cyclopropene monomer **20** with other mono-substituted 1,2,4,5-tetrazine.^[72] 3,6-Dipyridyl-1,2,4,5-tetrazine **12** displayed relatively similar reactivity ($k_2 = 0.917 \pm 0.024$), which is consistent with previous observations that mono-substituted tetrazines can participate in IEDDA reactions with similar kinetics than di-substituted tetrazines depending on the nature of the electron-withdrawing group. 3,6-Dipyrimidyl-1,2,4,5-tetrazine (**210**) bearing the most electron-withdrawing substituents showed the highest reactivity ($k_2 = 6.307 \pm 0.187$). Finally, 1,2,4,5-tetrazine **211** showed intermediate reactivity ($k_2 = 2.180 \pm 0.022$). Whilst the second-order rate constants determined in this experiment are in agreement with those reported in the literature for 1-methyl-3-substituted cyclopropenes, reactions with the most reactive tetrazines **210** and **211** are still 3 orders of magnitude slower than rate-constants typically observed for *trans*-cyclooctene derivatives.^[72]

However, as 1,2,4,5-tetrazine **211** displayed a 2-fold increase in reactivity compared to the 1,2,4,5-tetrazine **209** and possesses a handle for subsequent functionalisation, coupling to Cy5 to design a novel more reactive fluorophore could be considered to reinvestigate the cellular imaging of chemical probe **189** in HeLa cells.

Besides the rate constant, another important aspect to consider when dealing with bioorthogonal reagents is their stability in biological media. It has been previously reported that more reactive 1,2,4,5-tetrazines substituted with electron-withdrawing groups are susceptible to decomposition in aqueous environments.^[79] This was observed in the kinetic experiment previously described whereby a solution of 3,6-dipyrimidyl-1,2,4,5-tetrazine in 1:1 acetonitrile/PBS went from a characteristic purple colour to yellowish solution over approximately 1 h, therefore indicating degradation of the 1,2,4,5-tetrazine ring. Overall, this stability concern restricts the utility of electron-deficient 1,2,4,5-tetrazines in biological applications and further reinforces the challenge in finding a suitable balance between reactivity and stability in biological media for bioorthogonal reagents

6. Conclusion

The use of bioorthogonal chemistry approaches to tag biomolecules in their native environment has received considerable interest over the last two decades. Significant progress has been made on the discovery and optimisation of bioorthogonal reactions. Amongst these, the tetrazine ligation between *trans*-cyclooctene (TCO) tagged-substrates and tetrazine reporters has become one of the most widespread transformation for the cellular imaging of biomolecules. Given their unique features, bioorthogonal chemical probes can be utilised in a drug discovery context to interrogate the biological functions of small molecule ligands on a cellular level. The programme of research described in this thesis focused on the design, synthesis and biological evaluation of novel TCO-tagged chemical probes derived from nemiralisib and GSK2292767, two inhaled PI3K δ inhibitors currently being investigated for the treatment of asthma and COPD.

Using a structure-based design approach, several chemical probes were prepared by identifying suitable vectors and linkers to install the TCO tag on the parent compounds. The syntheses of these chemical probes required the design of efficient synthetic routes, allowing for the late-stage installation of the TCO tag. For this purpose, a synthetic route based on a novel aldehyde common intermediate was designed to access chemical probes derived from both nemiralisib and GSK2292767 *via* a key reductive amination reaction.

Based on their potency in the enzymatic and cell lysate-based binding assays, chemical probes were selected for subsequent profiling in a cellular imaging assay in Hut78 and HeLa cells. The IEDDA reaction between the TCO-tagged compounds and a fluorescent tetrazine dye successfully enabled the visualisation of the subcellular localization of the PI3K δ chemical probes. Interestingly, distinct cellular behaviours were observed for each series of chemical probes. Chemical probe **34** derived from the oral series of PI3K δ inhibitor displayed a specific cytosolic staining that could successfully be competed with various unmodified PI3K δ inhibitors. To date, and to the best of our knowledge, compound **34** remains the first effective PI3K δ chemical probe ever developed for cellular imaging purposes. On the other hand, chemical probes derived from the inhaled clinical candidate nemiralisib showed a significant

accumulation in membrane-rich and acidic subcellular compartments, identified as the endoplasmic reticulum and Golgi apparatus. Finally, a chemical probe derived from GSK2292767 was also prone to accumulation in similar subcellular compartments, however to a much lesser extent than chemical probes derived from nemiralisib. This cellular behaviour was shown to be independent from PI3K δ as a similar accumulation outcome was observed in HeLa cells, which do not express the target. This indicates that the observed accumulation was not driven by the target but rather by the physico-chemical properties of the molecules such as their ionisation state. Indeed, attenuating the basicity of the piperazine ring of TCO probes derived from nemiralisib with an oxopiperazine motif significantly reduced the accumulation observed in HeLa cells.

Taken together, these findings suggest that, despite being very lipophilic, the TCO tag is very unlikely to be responsible for the observed subcellular aggregation of the compounds. Rather, these different cellular behaviours may reflect the inherent subcellular localisation of the inhaled clinical candidates. This can be explained for nemiralisib for which the basicity of the compound had been suggested to play a key role in its lung retention mechanism *via* intracellular non-specific binding and/or sequestration in acidic organelles. Therefore, this approach has proven to be a very powerful strategy to visualise the subcellular localization of the compounds and successfully enabled the validation of the hypothesis that this observed subcellular localization is solely resulting from the inherent properties of the inhaled clinical candidates.

To finally confirm the conclusions drawn on the TCO chemical probes and to ensure that these conclusions hold true for unmodified versions of the compounds, an orthogonal imaging technique based on NanoSIMS was chosen. This technique requires the design and synthesis of ^{15}N -labelled analogues of the inhaled and oral PI3K δ inhibitors in order to further study their subcellular localization. The NanoSIMS investigations corroborated the outcome of the fluorescence microscopy approach as accumulation of ^{15}N -nemiralisib was detected in the cytosol of HeLa cells. Therefore, this intracellular accumulation and sequestration processes may occur for nemiralisib in the epithelial cells constituting the lining of the upper airway after inhalation and

could rationalise the lung deposition of the compound observed by MALDI imaging in rats. The chemical probes described in thesis have been pivotal in further understanding the lung retention mechanism of drug molecules administered by inhalation for the treatment of a disease of considerable societal need. This approach seems to have a big potential in supporting successful design of future efficacious inhaled therapies, whilst providing new selective tools that can contribute to the further study of the PI3K δ target. This is of significant interest as several PI3K δ inhibitors for delivery by both the inhaled and oral routes are currently in clinical development. In addition, due to high sequence and structure similarities between isoforms of the PI3K family, the development of selective antibodies for imaging-based assays that could help to gain a better understanding of the mode of action of those proteins remains very challenging. Consequently, the TCO probes designed, synthesized and investigated in the course of this work are first in class example that this problem can be overcome by bioorthogonal chemical probes.

These investigations also helped to gain a better insight in the advantages and limitations of two orthogonal imaging techniques. The TCO tag has a significant impact on the physico-chemical properties of the biomolecules to which it is attached, especially by increasing their lipophilicity and reducing their solubility. On the other hand, labeling of biomolecules with stable isotopes such as ^{15}N for NanoSIMS imaging has a minimal impact on the properties of the compound. However, this requires a more challenging synthetic effort often associated with a bespoke synthesis due to the limited commercially available ^{15}N -labelled starting materials. Several other factors that may limit the widespread utilization of NanoSIMS as a routine imaging technique include cost, instrument accessibility and time required for measurement and analysis which can take up to several days. This is a major difference to the fluorescence microscopy based imaging assays which are more broadly available and can be conducted within a few hours.

In order to reduce the potential negative effect of lipophilic TCO group, additional investigations towards the development of novel and alternative bioorthogonal reagents in the tetrazine ligation have focused on cyclopropenes “mini-tags”. A cyclopropene-containing bioorthogonal chemical probe derived from

Olaparib (PARP1 inhibitor) was designed and compared to its TCO analogue. Although the cyclopropene tag successfully reduced the lipophilicity of the compound in comparison with the TCO-analogue, the Olaparib-cyclopropene probe did not enable the visualization of the subcellular localization of PARP1. This is probably a consequence from the slower kinetics of cyclopropenes in IEDDA reactions compared to TCO. Further studies to improve the rate of reaction of this transformation relied on the design of 1,2,4,5-tetrazines substituted with electron-withdrawing groups and led the path to potential novel fluorophores. Thus, the alternative cyclopropene “mini-tag” for IEDDA reaction has not proven to be useful for the effective subcellular localization of the compound, therefore confirming the significant advantage of the chosen TCO strategy, whilst emphasizing a need to further develop small and reactive bioorthogonal reagents.

7. Future Work

The multidisciplinary aspect and the orthogonal imaging techniques described in this thesis open several pertinent avenues to follow in future work.

First, in addition to HeLa cells, NanoSIMS imaging of the ^{15}N -labelled PI3K δ inhibitors in Hut78 cells, a cell line expressing the target, could help to further validate the conclusions regarding the subcellular accumulation of nemiralisib. For example, quantification of ^{15}N ratios and comparison between HeLa and Hut78 cells may provide further insights into the degree of accumulation of the compound across different spatial localizations of the cytosol.

Another aspect for future work opportunities rely on the optimization of the cellular imaging assay for the visualization of bioorthogonal chemical probes by fluorescence microscopy. The investigation of novel TCO derivatives (e.g. *trans*-cyclooctene containing heteroatoms) may help to improve the physico-chemical properties of the chemical probes to which they are attached. The design of novel alternative handles and linkers to the TCO tag could also be considered.

Cyclopropenes are also promising “mini-tag” for the cellular imaging of biomolecules *via* bioorthogonal chemistry approaches. To date, their application has been mainly limited to the visualization of highly abundant cell surfaces proteins due to slower kinetics in the IEDDA reaction compared to TCO. Investigations conducted in this thesis have highlighted more reactive 1,2,4,5-tetrazines in comparison with Tetrazine-Cy5. Therefore, coupling of these novel 1,2,4,5-tetrazines to the Cy5 dye may result in novel fluorophores with increased reactivity for the cellular imaging of endogenous intracellular targets such as PI3K δ .

Finally, investigations around novel fluorogenic 1,2,4,5-tetrazines that only fluoresce upon IEDDA reaction with a dienophile could be considered to further improve live cells imaging experiments.

8. Experimental

8.1. General Chemistry Experimental Data Methods

Solvents and Reagents:

All sensitive reactions were performed in oven-dried glassware under a positive pressure of nitrogen unless otherwise noted. Solvents (anhydrous) and reagents were purchased from commercial suppliers or obtained from GlaxoSmithKline's internal compound storage and used as received without further purification. Where materials were synthesized in-house, full procedures or literature references to procedures are provided.

Chromatography:

Thin-layer chromatography (TLC) using plastic-backed 50 precoated silica plates (particle size 0.2 mm). Spots were detected by ultraviolet (UV) (254 nm) light and/or by staining with a potassium permanganate solution followed by gentle heating. Automated normal phase column chromatography on silica gel was performed using a CombiFlash[®] Teledyne ISCO system with RediSep[®] cartridges. Automated reverse phase chromatography was carried out using a CombiFlash[®] Teledyne ISCO system with SNAP KP-C18-HS cartridges.

Liquid Chromatography Mass Spectrometry (LCMS):

Reactions were monitored by LCMS using a Waters Acquity Ultra Performance system equipped with an Acquity UPLC CSH C18 column (50 mm x 2.1 mm, 1.7 μ m packing diameter) and using alternate-scan positive and negative electrospray. Analytes were detected as a summed UV wavelength of 210 – 350 nm. Two liquid phase methods were used:

- **Method A – Low pH** - Injection volume: 0.3 μ L, 40 °C, 1 mL/min flow rate. Gradient elution with the eluents as (A) H₂O containing 0.1% volume/volume

(v/v) formic acid and (B) acetonitrile. Gradient conditions are summarized below.

Time (min)	%A	%B
0	97	3
1.5	5	95
1.9	5	95
2.0	97	3

- **Method B – High pH** - Injection volume: 0.3 μ L, 40 $^{\circ}$ C, 1 mL/min flow rate. Gradient elution with the eluents as (A) 10 mM ammonium bicarbonate in water adjusted to pH 10 with ammonia and (B) acetonitrile. Gradient conditions are summarized below.

Time (min)	%A	%B
0	97	3
0.05	97	3
1.5	5	95
1.90	5	95
2	97	3

Nuclear magnetic resonance (NMR) spectroscopy:

Proton (^1H), carbon (^{13}C) and fluorine (^{19}F) spectra were recorded at 25 $^{\circ}$ C (unless otherwise noted) on a Bruker Spectrospin 400-Ultrashield spectrometer (^1H = 400 MHz, ^{13}C = 101 MHz, ^{19}F = 376 MHz). Chloroform-*d* (CDCl_3), DMSO-*d*₆ (DMSO) and Methanol-*d*₄ (MeOD) were used as the NMR solvents. The ^1H NMR chemical shifts are reported as δ values in ppm downfield from tetramethylsilane and are referenced relative to the chemical shift of CHCl_3 (δ = 7.26 ppm), DMSO (δ = 2.50 ppm) or MeOH (δ = 3.31 ppm), unless otherwise noted. Coupling constants (*J*) are reported in Hz with the signal multiplicities designated as singlet (s), doublet (d), triplet (t), quartet (q), quintuplet (quint.), septet (sept.), multiplet (m), broad singlet

(bs) and combination thereof. ^{13}C NMR chemical shifts are reported as δ values in ppm and are referenced from the central peak of the carbon resonance of the solvent: CDCl_3 $\delta = 77.16$ ppm, DMSO $\delta = 39.52$ ppm and MeOH $\delta = 49.00$ ppm.

Infrared (IR) spectroscopy:

IR spectra were recorded using a Perkin Elmer Spectrum 1 machine. Absorption maxima (ν_{max}) are reported in wavenumbers (cm^{-1}) to the nearest whole number.

Microwave reactions:

Microwave reactions were performed in a Biotage[®] Initiator system.

Mass Directed Automated Preparative HPLC purification:

Mass directed automated preparative HPLC purification was performed on a Waters Acquity Ultra Performance system using alternate-scan positive and negative electrospray and a summed UV wavelength of 210–350 nm. The methods used are described below:

- **Method A:** Xselect CSH C18 column (150 mm x 30 mm, 5 μm packing diameter). Injection volume: 1 mL, ambient temperature, 40 mL/min flow rate. Gradient elution with the eluents as (A) 10 mM ammonium bicarbonate adjusted to pH 10 with ammonia and (B) acetonitrile. Gradient conditions are summarized below.

Time (min)	%A	%B
0	50	50
1	50	50
20	1	99
20.5	1	99
25	1	99

- **Method B:** Xselect CSH C18 column (150 mm x 30 mm, 5 µm packing diameter). Injection volume: 1 mL, ambient temperature, 40 mL/min flow rate. Gradient elution with the eluents as (A) 10 mM ammonium bicarbonate adjusted to pH 10 with ammonia and (B) acetonitrile. Gradient conditions are summarized below.

Time (min)	%A	%B
0	70	30
1	70	30
20	15	85
20.5	1	99
25	1	99

- **Method C:** Xselect CSH C18 column (150 mm x 30 mm, 5 µm packing diameter). Injection volume: 1 mL, ambient temperature, 40 mL/min flow rate. Gradient elution with the eluents as (A) 10 mM ammonium bicarbonate adjusted to pH 10 with ammonia and (B) acetonitrile. Gradient conditions are summarized below.

Time (min)	%A	%B
0	85	15
1	85	15
20	45	55
20.5	1	99
25	1	99

- **Method D:** Xselect CSH C18 column (150 mm x 30 mm, 5 µm packing diameter). Injection volume: 1 mL, ambient temperature, 40 mL/min flow rate. Gradient elution with the eluents as (A) 10 mM ammonium bicarbonate adjusted to pH 10 with ammonia and (B) acetonitrile. Gradient conditions are summarized below.

Time (min)	%A	%B
0	100	0
3	100	0
22	75	25
22.5	75	25
23	1	99
27	1	99

- **Method E:** Xselect CSH C18 column (150 mm x 30 mm, 5 µm packing diameter). Injection volume: 1 mL, ambient temperature, 40 mL/min flow rate. Gradient elution with the eluents as (A) 0.1% v/v solution of formic acid in water and (B) 0.1% v/v solution of formic Acid in acetonitrile. Gradient conditions are summarized below.

Time (min)	%A	%B
0	85	15
1	85	15
20	45	55
20.5	1	99
25	1	99

Preparative HPLC:

The methods for the Preparative HPLC used for the purification of compounds are described below:

- **Method A:** Xselect CSH C18 column (100 mm x 30 mm, 5 µm packing diameter). Ambient temperature, 40 mL/min flow rate. Gradient elution with the eluents as (A) H₂O containing 0.1% volume/volume (v/v) formic acid and (B) acetonitrile.
- **Method B:** Xselect CSH C18 column (100 mm x 30 mm, 5 µm packing diameter). Ambient temperature, 40 mL/min flow rate. Gradient elution with the eluents as (A) 10 mM ammonium bicarbonate in water adjusted to pH 10 with ammonia solution and (B) acetonitrile.
- **Method C:** CSH C18 column (150 mm x 30 mm, 5 µm packing diameter). Ambient temperature, 30 mL/min flow rate. Gradient elution with the eluents as (A) 10 mM ammonium bicarbonate in water adjusted to pH 10 with ammonia solution and (B) acetonitrile. Varied volumes injections (typically 500 µL). Gradient conditions are summarized below.

Time (min)	%A	%B
0	60	40
4	60	40
20	30	70
21	30	70
21.1	1	99
25.1	1	99
25.1	50	50
30	50	50

- **Method D:** CSH C18 column (150 mm x 30 mm, 5 μ m packing diameter). Ambient temperature, 40 mL/min flow rate. Gradient elution with the eluents as (A) 10 mM ammonium bicarbonate in water adjusted to pH 10 with ammonia solution and (B) acetonitrile. Varied volumes injections (typically 1 mL). Gradient conditions are summarized below.

Time (min)	%A	%B
0	70	30
4	70	30
4.5	70	30
20	50	50
21	50	50
23	1	99
25	1	99

- **Method E:** CSH C18 column (150 mm x 30 mm, 5 μ m packing diameter). Ambient temperature, 40 mL/min flow rate. Gradient elution with the eluents as (A) 10 mM ammonium bicarbonate in water adjusted to pH 10 with ammonia solution and (B) acetonitrile. Varied volumes injections (typically 500 μ L). Gradient conditions are summarized below.

Time (min)	%A	%B
0	70	30
4	70	30
4.5	70	30
20	20	80
21.5	20	80
22	1	99
25	1	99

- **Method F:** CSH C18 column (150 mm x 30 mm, 5 μ m packing diameter). Ambient temperature, 40 mL/min flow rate. Gradient elution with the eluents as (A) 10 mM ammonium bicarbonate in water adjusted to pH 10 with ammonia solution and (B) acetonitrile. Varied volumes injections (typically 1 mL). Gradient conditions are summarized below.

Time (min)	%A	%B
0	70	30
4	70	30
4.5	70	30
20	20	80
21	20	80
23	5	95
25	5	95

- **Method G:** CSH C18 column (150 mm x 30 mm, 5 μ m packing diameter). Ambient temperature, 40 mL/min flow rate. Gradient elution with the eluents as (A) 10 mM ammonium bicarbonate in water adjusted to pH 10 with ammonia solution and (B) acetonitrile. Varied volumes injections (typically 1 mL). Gradient conditions are summarized below.

Time (min)	%A	%B
0	100	0
4	100	0
4.5	100	0
20	50	50
21.5	50	50
22	1	99
25	1	99

High Resolution Mass Spectrometry (HRMS):

HRMS analysis were conducted on a Waters XEVO G2-XS quadrupole time-of-flight (QToF) mass spectrometer instrument. LCMS analysis has been carried out using one of the following methods:

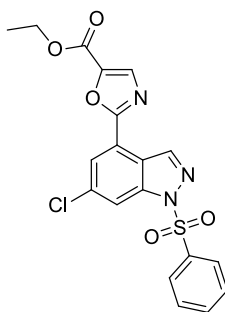
- **Method A – 10 min formic for confirmation:** Ionisation mode: Positive Electrospray. Acquity UPLC CSH C18 column (100 mm x 2.1 mm, 1.7 µm packing diameter) at 50 °C, 0.8 mL/min flow rate. Gradient elution with the eluents as (A) H₂O containing 0.1% volume/volume (v/v) formic acid and (B) acetonitrile. The UV detection was a summed signal from wavelength of 210 nm to 350 nm. Injection volume: 0.2 µL. The gradient employed is summarised below:

Time (min)	%A	%B
0	97	3
8.5	0	100
9.0	0	100
9.5	97	3
10	97	3

- **Method B – 20 min High pH for confirmation:** Ionisation mode: Positive Electrospray. Acquity UPLC BEH C18 column (100 mm x 2.1 mm, 1.7 µm packing diameter) at 50 °C, 0.8 mL/min flow rate. Gradient elution with the eluents as (A) 10 mM ammonium bicarbonate in water adjusted to pH 10 with ammonia solution and (B) acetonitrile. The UV detection was a summed signal from wavelength of 210 nm to 500 nm. Injection volume: 0.2 µL. The gradient employed is summarised below:

Time (min)	%A	%B
0	99	1
0.5	99	1
17	10	90
18.5	10	90
19	99	1
20	99	1

8.2. General Experimental Procedures

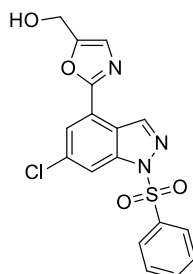


Ethyl 2-(6-chloro-1-(phenylsulfonyl)-1*H*-indazol-4-yl)oxazole-5-carboxylate (48)^[125]

To a stirred solution of ethyl oxazole-5-carboxylate (2.85 g, 20.18 mmol) in dry THF (30 mL) cooled to -10 °C was added zinc(II) chloride 1.9 M in 2-MeTHF (29.4 mL, 55.90 mmol). Then, LiHMDS 1.5 M in THF (18.6 mL, 27.90 mmol) was added over 10 min. The resulting solution was stirred under N₂ at -10°C for 1 h after which a solution of 6-chloro-4-iodo-1-(phenylsulfonyl)-1*H*-indazole (6.50 g, 15.53 mmol) in THF (50 mL) was added followed by a solution of Pd(PPh₃)₄ (0.54 g, 0.47 mmol) in THF (5 mL). The atmosphere in the flask was purged by 3 nitrogen/vacuum cycles. The reaction mixture was then heated to 60 °C overnight, after which the mixture had turned dark brown. The reaction was cooled to room temperature and quenched by the slow addition of a saturated aqueous NH₄Cl solution (80 mL). EtOAc (120 mL) was added and the phases were separated. The aqueous was extracted with EtOAc (3 x 100 mL). The combined organic extracts were washed with brine (200 mL), dried by passing through a hydrophobic frit and concentrated under reduced pressure. The residue was triturated with IPA (80 mL) and the solid was isolated by vacuum filtration. The solid was washed with more IPA (100 mL) and dried in a vacuum oven (40°C) overnight to afford the title compound as a beige solid (6.59 g, 98% yield).

LCMS (Method A): t_R = 1.45 Min, $[M+H]^+$ = 432.14, purity 100%; ¹H NMR (400 MHz, Chloroform-*d*) δ 8.92 (d, J = 0.9 Hz, 1H), 8.38 (dd, J = 1.7, 0.9 Hz, 1H), 8.11 (d, J = 1.7 Hz, 1H), 8.04 – 7.99 (m, 2H), 7.89 (s, 1H), 7.64 – 7.58 (m, 1H), 7.54 – 7.46 (m, 2H), 4.43 (q, J = 7.1 Hz, 2H), 1.42 (t, J = 7.1 Hz, 3H); ¹³C NMR (101 MHz,

Chloroform-*d*) δ 160.9, 157.5, 143.1, 141.4, 141.3, 137.3, 136.0, 135.4, 134.8, 129.6, 127.9, 124.5, 121.6, 120.6, 116.0, 62.0, 14.4; $\nu_{\max}(\text{neat})$: 3102, 2292, 1723, 1601, 1563, 1386, 1297, 1258, 1148, 1070, 926, 727 cm^{-1} ; HRMS (Method A): calcd. for $\text{C}_{19}\text{H}_{14}\text{N}_3\text{O}_5\text{SCl}$ $[\text{M}+\text{H}]^+$ 432.0421; found 432.0420.

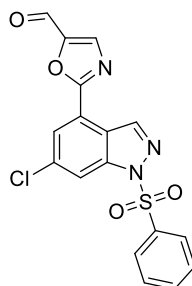


(2-(6-chloro-1-(phenylsulfonyl)-1*H*-indazol-4-yl)oxazol-5-yl)methanol (49)^[125]

To a stirred solution of ethyl 2-[6-chloro-1-(phenylsulfonyl)-1*H*-indazol-4-yl]-1,3-oxazole-5-carboxylate (2.22 g, 5.14 mmol) in THF (30 mL) cooled to 0 °C was added DIBAL-H 1 M in THF (18.0 mL, 17.99 mmol) slowly over 10 mins. Upon complete addition, the reaction mixture was stirred at 0 °C for 3 h. The reaction was then quenched by the slow addition of MeOH (20 mL), followed by a saturated aqueous solution of Rochelle's salt (50 mL). The mixture was stirred at room temperature for 20 mins. The mixture was then partitioned between EtOAc (80 mL) and water (50 mL). The layers were separated and the aqueous phase was extracted with EtOAc (4 x 80 mL). The combined organic extracts were dried by passing through a hydrophobic frit and concentrated under reduced pressure. The crude material was triturated with IPA (60 mL). The solids were isolated by vacuum filtration and dried under vacuum (40 °C) overnight to afford the title compound as a beige solid (1.92 g, 96% yield).

LCMS (Method A): t_R = 1.16 Min, $[\text{M}+\text{H}]^+$ = 390.15, purity 100%; ^1H NMR (400 MHz, $\text{DMSO}-d_6$) δ 8.97 (d, J = 0.9 Hz, 1H), 8.24 (dd, J = 1.7, 0.9 Hz, 1H), 8.06 – 8.00 (m, 2H), 7.88 (d, J = 1.7 Hz, 1H), 7.82 – 7.70 (m, 1H), 7.69 – 7.59 (m, 2H), 7.33 (d, J = 0.9 Hz, 1H), 5.55 (t, J = 5.9 Hz, 1H), 4.59 (d, J = 5.9 Hz, 2H); ^{13}C (101 MHz, $\text{DMSO}-d_6$) δ 157.1, 154.0, 141.4, 140.7, 136.0, 135.4, 134.9, 130.0, 127.4, 125.9, 122.3, 121.5, 120.5, 113.7, 53.5; $\nu_{\max}(\text{neat})$: 3274, 3103, 2854, 1596, 1580, 1547, 1452, 1447, 1392,

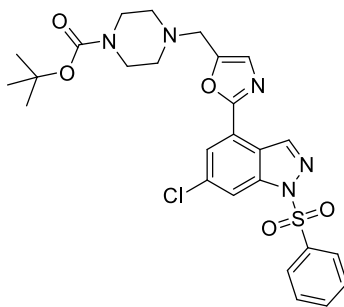
1098, 1043, 721 cm^{-1} ; HRMS (Method A): calcd. for $\text{C}_{17}\text{H}_{13}\text{N}_3\text{O}_4\text{SCl}$ $[\text{M}+\text{H}]^+$ 390.0315; found 390.0312.



2-(6-chloro-1-(phenylsulfonyl)-1*H*-indazol-4-yl)oxazole-5-carbaldehyde (46)

To a suspension of (2-(6-chloro-1-(phenylsulfonyl)-1*H*-indazol-4-yl)oxazol-5-yl)methanol (2.17 g, 5.57 mmol) in DCM (30 mL) cooled to 0 °C was added Dess-Martin periodinane (3.07 g, 7.24 mmol) in one fraction upon which all solid particles went into solution. The reaction was stirred at room temperature under N_2 atmosphere for 2 h. The reaction mixture was then diluted with more DCM (40 mL), transferred to a separatory funnel and washed with a saturated aqueous solution of sodium bicarbonate (2 x 60 mL). The organic layer was dried by passing through a hydrophobic frit. Florisil was added and solvents were removed under reduced pressure to adsorb the compound. Purification was carried out by automated column chromatography on silica gel eluting with 0-60% EtOAc/cyclohexane over 18 CV. The product-containing fractions were concentrated under reduced pressure to afford the title compound as a light yellow solid (1.58 g, 73% yield).

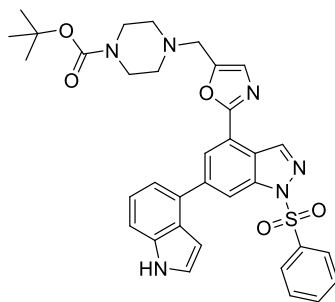
LCMS (Method A): t_{R} = 1.28 Min, $[\text{M}+\text{H}]^+ = 388.15$, purity 99%; ^1H NMR (400 MHz, Chloroform-*d*) δ 9.89 (s, 1H), 8.93 (d, $J = 0.9$ Hz, 1H), 8.42 (dd, $J = 1.6, 0.9$ Hz, 1H), 8.12 (d, $J = 1.6$ Hz, 1H), 8.06 – 7.98 (m, 3H), 7.65 – 7.60 (m, 1H), 7.55 – 7.48 (m, 2H); ^{13}C NMR (101 MHz, Chloroform-*d*) δ 176.3, 162.1, 149.9, 141.4, 141.1, 138.6, 137.2, 136.0, 134.9, 129.6, 127.9, 125.0, 121.8, 120.0, 116.6; ν_{max} (neat): 3092, 2848, 1696, 1596, 1563, 1447, 1380, 1181, 1075, 921, 727 cm^{-1} ; HRMS (Method A): calcd. for $\text{C}_{17}\text{H}_{11}\text{ClN}_3\text{O}_4\text{S}$ $[\text{M}+\text{H}]^+$ 388.0159; found 388.0156.



***tert*-Butyl-4-((2-(6-chloro-1-(phenylsulfonyl)-1*H*-indazol-4-yl)oxazol-5-yl)methyl)piperazine-1-carboxylate (50)**

To a stirred suspension of 2-(6-chloro-1-(phenylsulfonyl)-1*H*-indazol-4-yl)oxazole-5-carbaldehyde (501 mg, 1.29 mmol) in DCM (10 mL) was added 1-Boc piperazine (481 mg, 2.58 mmol) followed by acetic acid (37 μ L, 0.65 mmol). The reaction mixture was stirred at room temperature for 30 min after which sodium triacetoxymethylborohydride (411 mg, 1.94 mmol) was added in one portion. The reaction mixture was stirred for an additional hour at room temperature. The reaction was then partitioned between DCM (40 mL) and a saturated aqueous sodium bicarbonate solution (40 mL). The layers were separated and the aqueous phase was further extracted with DCM (3 x 40 mL). The combined organics layers were dried by passing through a hydrophobic frit and concentrated under reduced pressure. The crude material was dissolved in a minimum amount of DCM and purified by automated column chromatography on silica gel eluting with 10-80% EtOAc/cyclohexane over 18 CV. The product-containing fractions were concentrated under reduced pressure to afford the title compound as a white solid (551 mg, 76% yield)

LCMS (Method A): t_R = 1.10 Min, $[M+H]^+$ = 558.17, purity 98%; 1H NMR (400 MHz, Chloroform-*d*) δ 8.90 (d, J = 0.9 Hz, 1H), 8.33 – 8.28 (m, 1H), 8.05 – 7.97 (m, 2H), 7.95 (d, J = 1.6 Hz, 1H), 7.64 – 7.56 (m, 1H), 7.53 – 7.46 (m, 2H), 7.13 (s, 1H), 3.70 (s, 2H), 3.45 (t, J = 5.0 Hz, 4H), 2.47 (t, J = 5.0 Hz, 4H), 1.44 (s, 9H); ^{13}C NMR (101 MHz, Chloroform-*d*) δ 158.7, 154.6, 149.6, 141.6, 141.3, 137.2, 135.8, 134.5, 129.4, 127.9, 127.7, 123.2, 121.6, 121.2, 114.5, 79.8, 55.6, 55.5, 43.5, 28.4; ν_{max} (neat): 3122, 2986, 2832, 1683, 1533, 1430, 1378, 1170, 1128, 1078, 855, 560 cm^{-1} ; HRMS (Method A): calcd. for $C_{26}H_{29}N_5O_5SCl$ $[M+H]^+$ 558.1578; found 558.1576.

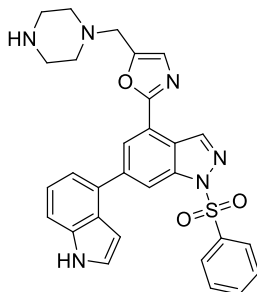


***tert*-Butyl-4-((2-(6-(1*H*-indol-4-yl)-1-(phenylsulfonyl)-1*H*-indazol-4-yl)oxazol-5-yl)methyl)piperazine-1-carboxylate (51)**

tert-Butyl-4-((2-(6-chloro-1-(phenylsulfonyl)-1*H*-indazol-4-yl)oxazol-5-yl)methyl)piperazine-1-carboxylate (200 mg, 0.36 mmol), indole-4-boronic acid pinacol ester 4 (174 mg, 0.72 mmol), XPhos Pd G2 (28 mg, 0.04 mmol), sodium carbonate (91 mg, 0.86 mmol) were charged in a microwave vial and suspended in 1,4-dioxane/water (4:1, 5 mL). The atmosphere in a vial was purged with 3 vacuum/nitrogen cycles and the reaction mixture was stirred at 90 °C for 70 minutes in the microwave. The reaction was partitioned between EtOAc (15 mL) and water (10 mL), the layers were separated and the aqueous phase was further extracted with EtOAc (2 x 15 mL). The combined organic extracts were washed with brine (20 mL), dried by passing through a hydrophobic frit and concentrated under reduced pressure. The crude material was dissolved in a minimum amount of DCM and purified by automated column chromatography on silica gel eluting with 10-100% EtOAc/cyclohexane over 30 CV. The product-containing fractions were concentrated under reduced pressure to afford the title compound as a white solid (149 mg, 65% yield).

LCMS (Method A): t_R = 1.08 Min, $[M+H]^+$ = 639.32, purity 100%; 1H NMR (400 MHz, Chloroform-*d*) δ 8.99 (d, J = 0.9 Hz, 1H), 8.63 (dd, J = 1.3, 0.9 Hz, 1H), 8.49 (bs, 1H), 8.36 (d, J = 1.3 Hz, 1H), 8.07 – 7.96 (m, 2H), 7.61 – 7.54 (m, 1H), 7.54 – 7.49 (m, 1H), 7.49 – 7.42 (m, 2H), 7.40 – 7.32 (m, 3H), 7.15 (s, 1H), 6.80 – 6.74 (m, 1H), 3.73 (s, 2H), 3.52 – 3.36 (m, 4H), 2.55 – 2.37 (m, 4H), 1.44 (s, 9H); ^{13}C NMR (101 MHz, Chloroform-*d*) δ 160.0, 154.7, 149.0, 143.1, 141.9, 141.5, 137.6, 136.4, 134.3, 132.6, 129.3, 127.7, 127.6, 126.2, 125.3, 124.1, 122.4, 121.7, 120.7, 120.5,

114.3, 111.5, 101.6, 79.8, 52.5, 55.4, 43.4, 28.4; $\nu_{\text{max}}(\text{neat})$: 3276, 3094, 2974, 2820, 1681, 1385, 1242, 1168, 1133, 1088, 997, 585 cm^{-1} ; HRMS (Method A): calcd. for $\text{C}_{34}\text{H}_{34}\text{N}_6\text{O}_5\text{S}$ $[\text{M}+\text{H}]^+$ 639.2389; found 639.2399.



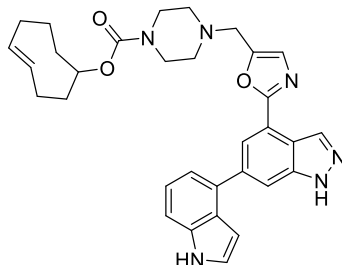
2-(6-(1H-indol-4-yl)-1-(phenylsulfonyl)-1H-indazol-4-yl)-5-(piperazin-1-ylmethyl)oxazole (52)

To a stirred solution of *tert*-butyl-4-((2-(6-(1H-indol-4-yl)-1-(phenylsulfonyl)-1H-indazol-4-yl)oxazol-5-yl)methyl)piperazine-1-carboxylate (100 mg, 0.16 mmol) in DCM (5 mL) was added trifluoroacetic acid (1.5 mL) and the mixture was stirred at room temperature for 3 h. Volatiles were removed under reduced pressure and the residue was partitioned between DCM (15 mL) and a saturated aqueous sodium bicarbonate solution (15 mL). The layers were separated and the aqueous phase was further extracted with DCM (2 x 15 mL). The combined organic extracts were washed with brine (10 mL), dried by passing through a hydrophobic frit and concentrated under reduced pressure to afford the crude material as a light brown solid (80 mg, 95% yield) which was used in the next step without further purification.

The reaction was repeated on a 98 mg scale and an aliquot was purified by Mass Directed Automated Preparative HPLC (Method E) for characterisation.

LCMS (Method B): t_R = 1.15 Min, MH^+ = 539.14, purity 98%; ^1H NMR (400 MHz, Methanol- d_4) δ 8.97 (d, J = 0.9 Hz, 1H), 8.59 (dd, J = 1.3, 0.9 Hz, 1H), 8.34 (d, J = 1.3 Hz, 1H), 8.04 – 7.98 (m, 2H), 7.70 – 7.64 (m, 1H), 7.59 – 7.47 (m, 3H), 7.40 (d, J = 3.2 Hz, 1H), 7.32 – 7.21 (m, 3H), 6.66 (dd, J = 3.2, 1.0 Hz, 1H), 3.82 (s, 2H), 3.04 (t, J = 5.1 Hz, 4H), 2.68 (t, J = 5.1 Hz, 4H). 2H not observed (exchangeable); ^{13}C NMR (101 MHz, Methanol- d_4) δ 161.5, 150.4, 145.2, 142.8, 138.5, 138.4, 135.9, 132.9, 130.7, 129.1, 128.6, 127.4, 127.0, 125.1, 122.8, 122.6, 121.8, 120.7, 115.2, 113.04,

112.97, 101.1, 52.9, 52.2, 45.5; ν_{max} (neat): 3257, 2821, 1594, 1375, 1172, 1090, 993, 894, 729, 684 cm^{-1} ; HRMS (Method A): calcd. for $\text{C}_{29}\text{H}_{27}\text{N}_6\text{O}_3\text{S}$ $[\text{M}+\text{H}]^+$ 539.1865; found 539.1864.



(*E*)-cyclooct-4-en-1-yl 4-((2-(6-(1*H*-indol-4-yl)-1*H*-indazol-4-yl)oxazol-5-yl)methyl)piperazine-1-carboxylate (35)

TCO installation:

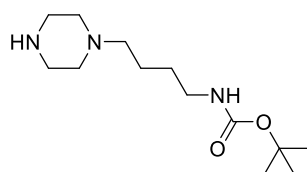
To a stirred solution of 2-(6-(1*H*-indol-4-yl)-1-(phenylsulfonyl)-1*H*-indazol-4-yl)-5-(piperazin-1-ylmethyl)oxazole (80 mg, 0.15 mmol) in DMF (4 mL) was added (*E*)-cyclooct-4-en-1-yl (4-nitrophenyl) carbonate (48 mg, 0.16 mmol) and DIPEA (78 μL , 0.45 mmol). The reaction mixture was stirred for 2 h at room temperature under an atmosphere of N_2 . The reaction was then partitioned between EtOAc (10 mL) and water (10 mL). The layers were separated and the aqueous phase was extracted with EtOAc (3 x 15 mL). The combined organic extracts were washed with a 5% LiCl aqueous solution (3 x 15 mL) then dried by passing through a hydrophobic frit and concentrated under reduced pressure.

Benzenesulfonyl deprotection:

The residue was immediately suspended in IPA (3 mL) and a 2 M aqueous NaOH solution (1 mL) was added. The reaction was stirred at room temperature for 30 min after which IPA was removed under reduced pressure. The reaction mixture was partitioned between EtOAc (10 mL) and water (10 mL). The layers were separated and the aqueous was further extracted with EtOAc (2 x 10 mL). The combined organic extracts were dried by passing through a hydrophobic frit and concentrated under reduced pressure. The crude material was purified by Mass Directed Automated Preparative HPLC (Method A). The product-containing fractions were concentrated

under reduced pressure to approximately 5 mL which were lyophilized overnight to afford the title compound as a white solid (9 mg, 11% yield over 2 steps).

LCMS (Method B): t_R = 1.24 Min, $[M+H]^+$ = 551.21, purity 98%; 1H NMR (600 MHz, Chloroform-*d*) δ 10.39 (bs, 1H), 8.82 (d, J = 0.9 Hz, 1H), 8.43 (bs, 1H), 8.27 (d, J = 1.3 Hz, 1H), 7.88 (dd, J = 1.3, 0.9 Hz, 1H), 7.50 - 7.43 (m, 1H), 7.34 - 7.31 (m, 1H), 7.32 - 7.30 (m, 1H), 7.32 - 7.29 (m, 1H), 7.21 (s, 1H), 6.75 (ddd, J = 3.0, 2.0, 0.8 Hz, 1H), 5.56 (ddd, J = 16.0, 10.5, 2.9 Hz, 1H), 5.52 (ddd, J = 15.8, 10.5, 3.5 Hz, 1H), 4.99 - 4.91 (m, 1H), 3.79 (s, 2H), 3.59 (bs, 4H), 2.60 (t, J = 5.0 Hz, 4H), 2.34 - 2.28 (m, 1H), 2.33 - 2.27 (m, 1H), 2.32 - 2.25 (m, 1H), 2.27 - 2.23 (m, 1H), 2.15 - 2.10 (m, 1H), 1.89 - 1.80 (m, 1H), 1.82 - 1.77 (m, 1H), 1.70 - 1.63 (m, 1H), 1.52 - 1.42 (m, 1H), 1.24 - 1.17 (m, 1H); ^{13}C NMR (101 MHz, Chloroform-*d*) δ 161.3, 154.9, 148.4, 141.3, 140.4, 136.3, 135.8, 135.1, 133.5, 131.9, 127.7, 126.3, 124.9, 122.4, 121.9, 120.2, 120.0, 119.0, 111.3, 110.8, 101.9, 70.8, 52.5, 52.5 (2C), 43.8 (2C), 41.1, 34.3, 32.6, 30.3, 28.3; ν_{max} (neat): 3265, 2927, 2858, 1673, 1440, 1340, 1245, 987, 754 cm^{-1} ; HRMS (Method A): calcd. for $C_{32}H_{35}N_6O_3$ $[M+H]^+$ 551.2770; found 551.2769

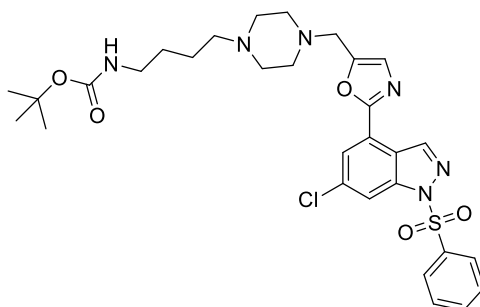


***tert*-Butyl (4-(piperazin-1-yl)butyl)carbamate (55)**

To a stirred solution of piperazine (0.95 g, 11.04 mmol) in acetonitrile (30 mL) was added 4-(Boc-amino)butyl bromide (1.21 g, 4.80 mmol) followed by potassium carbonate (1.33 g, 9.60 mmol). The reaction mixture was stirred at room temperature for 48 h. Acetonitrile was removed under reduced pressure. The crude residue was partitioned between DCM (30 mL) and water (30 mL). The layers were separated and the aqueous was further extracted with DCM (3 x 50 mL). The combined organics were dried by passing through a hydrophobic frit and concentrated under reduced pressure. The residue was taken in a minimum amount of DCM and purified by automated column chromatography on silica gel eluting with 0-40% (MeOH + 1%

Et₃N)/DCM over 20 CV. The product containing fractions were identified by TLC (DCM/MeOH 8:2, KMnO₄ stain) and concentrated under reduced pressure to afford the title compound as a colourless oil (755 mg, 61% yield).

¹H NMR (400 MHz, Chloroform-*d*) δ 5.52 (bs, 1H), 3.03 – 2.88 (m, 2H), 2.75 (q, *J* = 4.4 Hz, 4H), 2.35 – 2.20 (m, 4H), 2.18 (q, *J* = 5.3 Hz, 2H), 1.49 (bs, 1H), 1.43 – 1.31 (m, 4H), 1.29 (s, 9H); ¹³C NMR (101 MHz, Chloroform-*d*) δ 156.0, 78.5, 58.6, 54.4, 45.8, 40.4, 28.4, 27.9, 24.0; ν_{max}(DCM): 3319, 3214, 2937, 2803, 1696, 1524, 1447, 1170 cm⁻¹; HRMS (Method B): calcd. for C₁₃H₂₈N₃O₂ [M+H]⁺ 258.2182; found 258.2185.

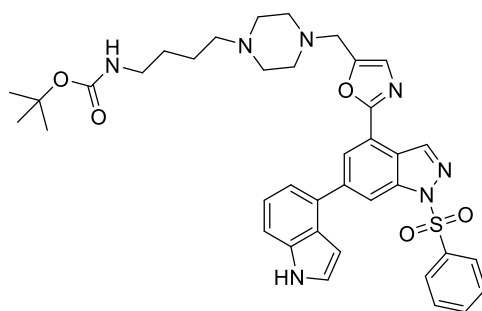


***tert*-Butyl (4-(4-((2-(6-chloro-1-(phenylsulfonyl)-1*H*-indazol-4-yl)oxazol-5-yl)methyl)piperazin-1-yl)butyl)carbamate (56)**

To a stirred suspension of 2-(6-chloro-1-(phenylsulfonyl)-1*H*-indazol-4-yl)oxazole-5-carbaldehyde (600 mg, 1.55 mmol) in DCM (4 mL) was added a solution of *tert*-butyl (4-(piperazin-1-yl)butyl)carbamate (478 mg, 1.86 mmol) in DCM (8 mL) followed by acetic acid (44 μL, 0.77 mmol). The reaction mixture was stirred at room temperature for 30 min after which sodium triacetoxyborohydride (426 mg, 2.01 mmol) was added in one portion. The reaction mixture was stirred for an additional hour at room temperature. The reaction was then partitioned between DCM (30 mL) and a saturated aqueous sodium bicarbonate solution (40 mL). The layers were separated and the aqueous was further extracted with DCM (3 x 40 mL). The combined organics were dried by passing through a hydrophobic frit and concentrated under reduced pressure. The crude was taken in a minimum amount of DCM and purified by automated column chromatography on silica gel eluting with 0-25% MeOH/EtOAc over 18 CV. The

product containing fractions were concentrated under reduced pressure to afford the title compound as a white solid (767 mg, 79% yield).

LCMS (Method A): $t_R = 0.93$ Min, $[M+H]^+ = 629.32$, purity 100%; 1H NMR (400 MHz, Chloroform-*d*) δ 8.89 (d, $J = 0.9$ Hz, 1H), 8.29 (dd, $J = 1.7, 0.9$ Hz, 1H), 8.03 – 7.97 (m, 2H), 7.94 (d, $J = 1.7$ Hz, 1H), 7.62 – 7.55 (m, 1H), 7.53 – 7.43 (m, 2H), 7.12 (s, 1H), 5.05 (bs, 1H), 3.69 (s, 2H), 3.13 – 3.04 (m, 2H), 2.66 – 2.42 (m, 8H), 2.39 – 2.32 (m, 2H), 1.54 – 1.45 (m, 4H), 1.42 (s, 9H); ^{13}C NMR (101 MHz, Chloroform-*d*) δ 158.7, 156.1, 150.0, 141.8, 141.4, 137.4, 135.9, 134.7, 129.5, 128.0, 127.8, 123.4, 121.8, 121.3, 114.6, 79.1, 58.0, 53.0, 52.7, 52.4, 40.6, 28.6, 28.0, 24.3; $\nu_{max}(\text{neat})$: 3108, 2937, 2820, 1685, 1585, 1524, 1447, 1380, 1164, 1065, 920, 727 cm^{-1} ; HRMS (Method A): calcd. for $C_{30}H_{38}ClN_6O_5S$ $[M+H]^+ 629.2313$; found 629.2323.

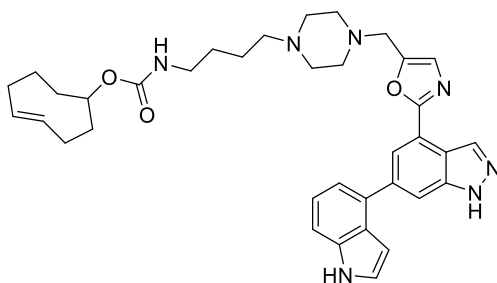


***tert*-Butyl (4-(4-((2-(6-(1*H*-indol-4-yl)-1-(phenylsulfonyl)-1*H*-indazol-4-yl)oxazol-5-yl)methyl)piperazin-1-yl)butyl)carbamate (57)**

In a microwave vial was added *tert*-butyl (4-(4-((2-(6-chloro-1-(phenylsulfonyl)-1*H*-indazol-4-yl)oxazol-5-yl)methyl)piperazin-1-yl)butyl)carbamate (222 mg, 0.35 mmol), 4-(4,4,5,5-tetramethyl-1,3,2-dioxaborolan-2-yl)-1*H*-indole (172 mg, 0.71 mmol), XPhos Pd G2 (56 mg, 0.071 mmol) and sodium carbonate (112 mg, 1.06 mmol). Solids were suspended in 1,4-dioxane (4.5 mL) and water (0.5 mL). The vial was sealed and purged with 3 vacuum/nitrogen cycles and subsequently heated at 90 °C in the microwave for 1 h. More pinacol boronic ester (86 mg, 1 equiv.) was added along with more XPhos Pd G2 (55 mg, 0.2 equiv.). The vial was sealed again and heated in the microwave at 90 °C for an additional 30 min. The reaction was partitioned between EtOAc (30 mL) and water (30 mL). The layers were separated and the

aqueous was extracted with EtOAc (3 x 30 mL). The combined organic extracts were dried by passing through a hydrophobic frit and concentrated under reduced pressure. The residue was dissolved in a minimum amount of DCM and purified by automated column chromatography on silica gel eluting 0-25% MeOH/EtOAc over 18 CV. The product containing fractions were concentrated under reduced pressure to afford the title compound as light orange solid (183 mg, 73% yield).

LCMS (Method A): t_R = 0.95 Min, $[M+H]^+$ = 710.29, purity 97%; 1H NMR (400 MHz, Chloroform-*d*) δ 8.99 (d, J = 0.9 Hz, 1H), 8.70 (bs, 1H), 8.62 (dd, J = 1.3, 0.9 Hz, 1H), 8.35 (d, J = 1.3 Hz, 1H), 8.07 – 7.99 (m, 2H), 7.61 – 7.53 (m, 1H), 7.52 – 7.48 (m, 1H), 7.48 – 7.43 (m, 2H), 7.37 – 7.31 (m, 3H), 7.14 (s, 1H), 6.78 – 6.74 (m, 1H), 5.09 (bs, 1H), 3.71 (s, 2H), 3.18 – 2.97 (m, 2H), 2.68 – 2.40 (m, 8H), 2.40 – 2.29 (m, 2H), 1.56 – 1.46 (m, 4H), 1.42 (s, 9H); ^{13}C NMR (101 MHz, Chloroform-*d*) δ 160.1, 156.2, 149.5, 143.2, 142.1, 141.7, 137.7, 136.5, 134.4, 132.8, 129.4, 127.7, 126.4, 125.5, 124.2, 122.4, 121.8, 120.9, 120.6, 114.4, 111.6, 101.8, 79.1, 58.0, 53.0, 52.7, 52.5, 40.6, 28.6, 28.1, 24.4; ν_{max} (neat): 3412, 3313, 2975, 2931, 2809, 1691, 1602, 1508, 1447, 1369, 1242, 1170, 727 cm^{-1} ; HRMS (Method A): calcd. for $C_{38}H_{44}N_7O_5S$ $[M+H]^+$ 710.3125; found 710.3109.



(*E*)-cyclooct-4-en-1-yl (4-(4-((2-(6-(1*H*-indol-4-yl)-1*H*-indazol-4-yl)oxazol-5-yl)methyl)piperazin-1-yl)butyl)carbamate (36)

Boc deprotection:

To a stirred solution of *tert*-butyl (4-(4-((2-(6-(1*H*-indol-4-yl)-1-(phenylsulfonyl)-1*H*-indazol-4-yl)oxazol-5-yl)methyl)piperazin-1-yl)butyl)carbamate (134 mg, 0.19 mmol) in DCM (6 mL) was added TFA (2 mL). The reaction was stirred at room temperature for 90 min. Volatiles were then removed under reduced pressure and the

crude was suspended in dioxane (5 mL) and solvents were removed under reduced pressure. This was repeated twice to remove TFA traces to give the crude title compound as the TFA salt which was used immediately in the following step without further purification.

LCMS (Method B): t_R = 1.31 Min, $[M+H]^+$ = 610.24, 100%.

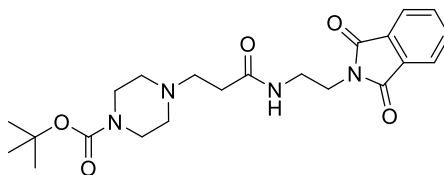
TCO installation:

The crude 4-(4-((2-(6-(1*H*-indol-4-yl)-1-(phenylsulfonyl)-1*H*-indazol-4-yl)oxazol-5-yl)methyl)piperazin-1-yl)butan-1-amine, TFA salt **65** was dissolved in DMF (7 mL). To the previous solution was added DIPEA (331 μ L, 1.89 mmol) and the reaction was stirred at room temperature for 5 min. Then, (*E*)-cyclooct-4-en-1-yl (4-nitrophenyl) carbonate (83 mg, 0.28 mmol) was added and the reaction mixture turned yellow in colour. The reaction was stirred at room temperature for 1 h. The reaction was then partitioned between EtOAc (20 mL) and water (20 mL). The layers were separated, and the aqueous phase was extracted with EtOAc (3 x 20 mL). The combined organic extracts were washed with a 5% LiCl aqueous solution (3 x 30 mL) then dried by passing through a hydrophobic frit and concentrated under reduced pressure. ¹⁵N

Benzenesulfonyl deprotection:

The crude residue was immediately dissolved in MeOH (5 mL) and 1 M aqueous NaOH solution (1 mL) was added. The reaction mixture was stirred at room temperature for 30 min. MeOH was removed under reduced pressure and the residue was partitioned between EtOAc (15 mL) and water (15 mL). The layers were separated and the aqueous was further extracted with EtOAc (3 x 20 mL). The combined organics extracts were dried by passing through a hydrophobic frit and concentrated under reduced pressure. The crude was taken in MeOH/DMSO (1:1, 3 mL) and purified by preparative HPLC (Method B) eluting with 30-65% acetonitrile/10 mM ammonium bicarbonate in water over 35 min (3 x 1 mL injection). The product containing fractions were combined and concentrated under reduced pressure to approximately 10 mL which were lyophilized to afford the title compound as a white solid (25 mg, 21% yield over 3 steps).

LCMS (Method B): $t_R = 1.21$ Min, $[M+H]^+ = 622.47$, purity 97%; 1H NMR (600 MHz, Methanol- d_4) δ 8.69 (d, $J = 0.9$ Hz, 1H), 8.23 (dd, $J = 1.3, 0.9$ Hz, 1H), 7.95 (d, $J = 1.3$ Hz, 1H), 7.45 (dd, $J = 6.9, 2.2$ Hz, 1H), 7.33 (d, $J = 3.2$ Hz, 1H), 7.28 – 7.21 (m, 3H), 6.67 (d, $J = 3.2$ Hz, 1H), 5.63 (ddd, $J = 15.5, 11.2, 3.6$ Hz, 1H), 5.49 (ddd, $J = 15.5, 11.2, 3.4$ Hz, 1H), 4.79 – 4.75 (m, 1H), 3.80 (s, 2H), 3.14 – 3.04 (m, 2H), 2.76 – 2.39 (m, 8H), 2.34 (dt, $J = 22.1, 5.9$ Hz, 3H), 2.27 – 2.14 (m, 3H), 2.02 (d, $J = 12.2$ Hz, 1H), 1.86 – 1.75 (m, 1H), 1.75 – 1.67 (m, 1H), 1.68 – 1.58 (m, 1H), 1.58 – 1.41 (m, 5H), 1.24 – 1.16 (m, 1H). 3H not observed (exchangeable); ^{13}C NMR (151 MHz, Methanol- d_4) δ 163.0, 158.8, 150.2, 143.1, 142.3, 138.4, 136.5, 135.5, 134.2, 132.7, 128.9, 127.7, 126.6, 122.9, 122.8, 120.8, 120.6, 119.7, 113.2, 112.3, 101.6, 71.4, 59.3, 53.9, 53.4, 52.9, 42.1, 41.6, 35.4, 33.9, 41.0, 29.2, 29.0, 24.8; ν_{max} (neat): 3418, 3269, 2931, 2810, 1441, 1696, 1519, 1441, 1342, 1259, 932, 760 cm^{-1} ; HRMS (Method B): calcd. for $C_{36}H_{44}N_7O_3$ $[M+H]^+ 622.3506$; found 622.3508.

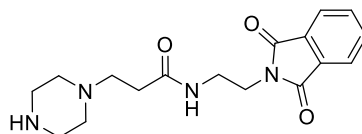


***tert*-Butyl 4-(3-((2-(1,3-dioxoisindolin-2-yl)ethyl)amino)-3-oxopropyl)piperazine-1-carboxylate (61)**

To a stirred suspension of 3-(4-(*tert*-butoxycarbonyl)piperazin-1-yl)propanoic acid (607 mg, 2.35 mmol), 2-(2-aminoethyl)isoindoline-1,3-dione.TFA salt (751 mg, 2.47 mmol) and HATU (1.34 g, 3.52 mmol) in DCM (10 mL) was added DIPEA (1.6 mL, 9.40 mmol) upon which solids went into solution and reaction mixture turned slightly yellow. The reaction was stirred at room temperature under an atmosphere of N_2 overnight. The reaction was partitioned between DCM (20 mL) and a saturated aqueous sodium bicarbonate solution (20 mL). The layers were separated and the aqueous was further extracted with DCM (3 x 30 mL). The combined organic extracts were dried by passing through a hydrophobic frit. Florisil was added and solvents were removed under reduced pressure to adsorb material. Purification was carried out by automated column chromatography on silica gel eluting with 0-12%

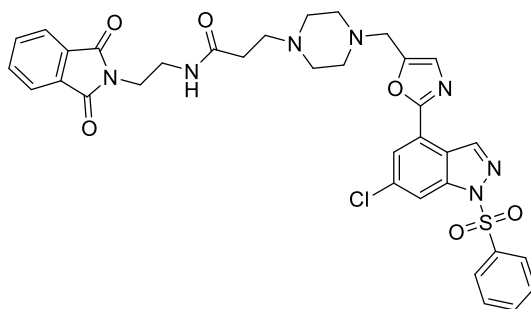
MeOH/EtOAc over 20 CV. The product-containing fractions were concentrated under reduced pressure and dried on a high vacuum line overnight to afford a pale yellow solid (0.78 g, 78% yield, estimated 70% pure). The compound was used in the next step without further purification.

LCMS (Method A): $t_R = 0.61$ Min, $[M+H]^+ = 431.21$.



***N*-(2-(1,3-Dioxoisindolin-2-yl)ethyl)-3-(piperazin-1-yl)propanamide (62)**

To a stirred solution of *tert*-butyl 4-(3-((2-(1,3-dioxoisindolin-2-yl)ethyl)amino)-3-oxopropyl)piperazine-1-carboxylate (390 mg, 0.91 mmol) in DCM (10 mL) was added TFA (1.5 mL) and the reaction was stirred at room temperature under N₂ atmosphere overnight. Volatiles were removed under reduced pressure. The crude residue was then taken in MeOH (5 mL), loaded on a 5 g Flash NH₂ cartridge and eluted with more MeOH (20 mL). The filtrate was concentrated under reduced pressure to about 5 mL which were loaded again on the cartridge and eluted with MeOH (20 mL). The filtrate was concentrated under reduced pressure to afford the crude title compound as a yellow oil (396 mg) which was used in the next step without further purification.

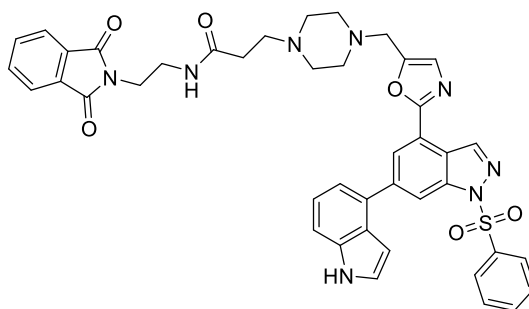


3-(4-((2-(6-chloro-1-(phenylsulfonyl)-1*H*-indazol-4-yl)oxazol-5-yl)methyl)piperazin-1-yl)-*N*-(2-(1,3-dioxisoindolin-2-yl)ethyl)propanamide (63)

To a stirred suspension of 2-(6-chloro-1-(phenylsulfonyl)-1*H*-indazol-4-yl)oxazole-5-carbaldehyde (302 mg, 0.78 mmol) in THF (2 mL) was added a solution of crude *N*-(2-(1,3-dioxisoindolin-2-yl)ethyl)-3-(piperazin-1-yl)propanamide (396 mg, 0.84 mmol) in THF (6 mL). To the previous mixture was added acetic acid (48 μ L, 0.84 mmol) and the reaction mixture was stirred at room temperature under an atmosphere of N₂ for 1 h. STAB (178 mg, 0.84 mmol) was then added in one portion and more THF (2 mL) was added. The reaction was stirred at room temperature for 2 h. The reaction was partitioned between EtOAc (30 mL), a saturated aqueous sodium bicarbonate solution (20 mL) and water (25 mL). The layers were separated and the aqueous was further extracted with EtOAc (5 x 40 mL). The combined organic extracts were dried by passing through a hydrophobic frit. Florisil was added and solvents were removed under reduced pressure to adsorb the compound. Purification was carried out by automated column chromatography on silica gel eluting with 0-60% (3:1 EtOAc/EtOH)/cyclohexane over 20 CV and then 0-45% MeOH/EtOAc over 20 CV. The product-containing fractions were combined and concentrated under reduced pressure and dried on a high vacuum to afford the title compound as a colourless oil which turned into an off-white sticky solid under vacuum (343 mg, 58% yield).

LCMS (Method A): t_R = 0.89 Min, $[M+H]^+ = 702.16$, purity 98%; ¹H NMR (400 MHz, Chloroform-*d*) δ 8.86 (d, J = 0.9 Hz, 1H), 8.25 (dd, J = 1.7, 0.9 Hz, 1H), 8.18 (t, J = 6.0 Hz, 1H), 8.00 – 7.94 (m, 2H), 7.90 (d, J = 1.7 Hz, 1H), 7.82 – 7.75 (m, 2H), 7.72 – 7.65 (m, 2H), 7.62 – 7.54 (m, 1H), 7.51 – 7.43 (m, 2H), 7.05 (s, 1H), 3.84 – 3.70 (m, 2H), 3.55 (s, 2H), 3.55 – 3.46 (m, 2H), 2.54 (t, J = 6.1 Hz, 2H), 2.52 – 2.33 (m, 8H),

2.28 (t, $J = 6.1$ Hz, 2H); ^{13}C NMR (101 MHz, Chloroform- d) δ 172.6, 168.4, 158.6, 149.8, 141.6, 141.3, 137.2, 135.8, 134.7, 134.1, 132.0, 129.5, 127.9, 127.7, 123.3, 123.2, 121.7, 121.2, 114.5, 53.6, 52.9, 52.3, 52.2, 38.1, 37.9, 32.1; $\nu_{\text{max}}(\text{neat})$: 3097, 2942, 2820, 1773, 712, 1630, 1585, 1469, 1380, 1170, 1098, 921, 724 cm^{-1} ; HRMS (Method A): calcd. for $\text{C}_{34}\text{H}_{33}\text{ClN}_7\text{O}_6\text{S}$ $[\text{M}+\text{H}]^+$ 702.1902; found 702.1888.

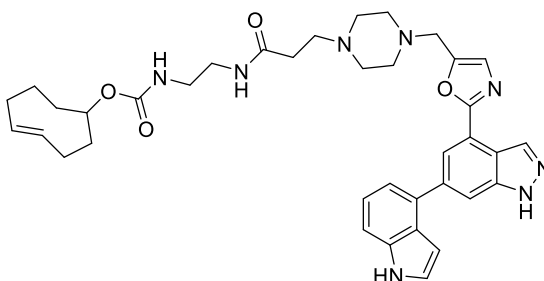


3-(4-((2-(6-(1*H*-indol-4-yl)-1-(phenylsulfonyl)-1*H*-indazol-4-yl)oxazol-5-yl)methyl)piperazin-1-yl)-*N*-(2-(1,3-dioxoisindolin-2-yl)ethyl)propanamide (64)

In a microwave vial were added 4-(4,4,5,5-tetramethyl-1,3,2-dioxaborolan-2-yl)-1*H*-indole (106 mg, 0.44 mmol), sodium carbonate (115 mg, 1.09 mmol), XPhos Pd G2 (29 mg, 0.036 mmol) and a solution of 3-(4-((2-(6-chloro-1-(phenylsulfonyl)-1*H*-indazol-4-yl)oxazol-5-yl)methyl)piperazin-1-yl)-*N*-(2-(1,3-dioxoisindolin-2-yl)ethyl)propanamide (255 mg, 0.36 mmol) in 1,4-dioxane (5 mL). Water (0.5 mL) was added and the vial was sealed and purged with 3 vacuum/nitrogen cycles. The vial was then heated at 90 °C in the microwave for 1 h. The reaction was partitioned between EtOAc (30 mL) and water (20 mL). The layers were separated and the aqueous was extracted with EtOAc (3 x 30 mL). The combined organic extracts were dried by passing through a hydrophobic frit. Florisil was added and solvents were removed under reduced pressure to adsorb the compound. Purification was carried out by automated column chromatography on silica gel eluting with 0-40% MeOH/EtOAc over 20 CV. The product containing fractions were combined and concentrated under reduced pressure to afford the title compound as a dark yellow oil (202 mg, 71% yield).

LCMS (Method A): $t_{\text{R}} = 0.91$ Min, $[\text{M}+\text{H}]^+ = 783.19$, purity 96%; ^1H NMR (400 MHz, Chloroform- d) δ 8.98 (d, $J = 0.9$ Hz, 1H), 8.62 (dd, $J = 1.3, 0.9$ Hz, 1H), 8.33 (d, $J =$

1.3 Hz, 1H), 8.22 (bs, 1H), 8.06 – 8.00 (m, 2H), 7.82 – 7.76 (m, 2H), 7.70 – 7.63 (m, 2H), 7.59 – 7.54 (m, 1H), 7.51 – 7.43 (m, 3H), 7.38 – 7.31 (m, 3H), 7.08 (s, 1H), 6.78 – 6.73 (m, 1H), 3.80 – 3.73 (m, 2H), 3.61 – 3.57 (m, 2H), 3.56 – 3.47 (m, 2H), 2.56 (t, $J = 6.1$ Hz, 2H), 2.54 – 2.35 (m, 8H), 2.31 (t, $J = 6.1$ Hz, 2H). 1H not observed (exchangeable); ^{13}C NMR (101 MHz, Chloroform- d) δ 172.8, 168.4, 160.1, 149.3, 143.2, 142.0, 141.7, 137.7, 136.5, 134.4, 134.2, 132.7, 132.1, 129.5, 127.8, 127.7, 126.4, 125.5, 124.1, 123.4, 122.5, 121.8, 120.9, 120.6, 114.5, 111.6, 101.7, 53.6, 52.8, 52.3, 52.2, 38.1, 38.0, 32.1; ν_{max} (neat): 3274, 3053, 2942, 2815, 1768, 1707, 1652, 1430, 1386, 1176, 727, 716 cm^{-1} ; HRMS (Method A): calcd. for $\text{C}_{42}\text{H}_{39}\text{N}_8\text{O}_6\text{S}$ $[\text{M}+\text{H}]^+$ 783.2713; found 783.2701.



(*E*)-cyclooct-4-en-1-yl (2-(3-(4-((2-(6-(1*H*-indol-4-yl)-1*H*-indazol-4-yl)oxazol-5-yl)methyl)piperazin-1-yl)propanamido)ethyl)carbamate (37)

Phthalimide deprotection:

To a stirred solution of 3-(4-((2-(6-(1*H*-indol-4-yl)-1-(phenylsulfonyl)-1*H*-indazol-4-yl)oxazol-5-yl)methyl)piperazin-1-yl)-*N*-(2-(1,3-dioxoisindolin-2-yl)ethyl)propanamide (172 mg, 0.22 mmol) in THF (4 mL) was added hydrazine hydrate (25 μL , 0.33 mmol) and the reaction mixture was stirred at room temperature for 2 h under N_2 . More hydrazine hydrate (3 μL) was added and the reaction was heated to 50 $^{\circ}\text{C}$ and stirred for an additional 3.5 h. The reaction was cooled to room temperature and acetone (2 mL) was added. The mixture was stirred at room temperature for 15 min after which volatiles were removed under reduced pressure. The crude mixture was let overnight at room temperature after which the crude showed 20% of an impurity consistent with cleavage of the benzene sulfonyl protecting group.

The crude residue was taken in MeOH (3 mL) and 2 mL of this solution were immediately taken forward to the next step.

TCO installation:

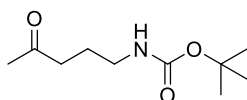
This reaction was conducted using the 2 mL solution of crude **72** in MeOH (2 mL) which were concentrated under reduced pressure and dissolved in DMF (4 mL). To the previous solution was added (*E*)-cyclooct-4-en-1-yl (4-nitrophenyl) carbonate (32 mg, 0.11 mmol) and DIPEA (35 μ L, 0.20 mmol) and the reaction mixture was stirred at room temperature under N₂ atmosphere. After 1 h, more (*E*)-cyclooct-4-en-1-yl (4-nitrophenyl) carbonate (35 mg, 0.12 mmol) and DIPEA (39 μ L, 0.22 mmol) were added and the reaction was stirred at room temperature for an additional 4 h. The reaction was partitioned between EtOAc (10 mL) and water (10 mL). The layers were separated and the aqueous was further extracted with EtOAc (3 x 15 mL). The combined organics extracts were washed with a 5% aqueous LiCl solution (15 mL), dried by passing through a hydrophobic frit and concentrated under reduced pressure.

Benzenesulfonyl deprotection:

The crude was immediately taken in MeOH (4 mL) and an aqueous solution of 2 M NaOH was added (1 mL). The reaction was stirred at room temperature for 30 min, after which solvents were removed under reduced pressure. The residue was taken up in MeOH/DMSO (1:1, 4 mL) which were purified by MDAP (Method B) (4 x 1 mL injection). The product-containing fractions were combined and concentrated under reduced pressure to about 5 mL which were lyophilized overnight to a white solid (56 mg) which still contained impurities. 40 mg were dissolved in DMSO (10 mL) and purified by preparative HPLC (Method D, 1 mL injections). The product-containing fractions were evaporated *in vacuo* and transferred into a 20 mL vial using DCM (3 x 10 mL) which was removed under a stream of nitrogen. The compound was then taken up in MeCN/water (1:1, 6 mL) which were lyophilized to afford the title compound as a white solid (28 mg, 19% over 3 steps).

LCMS (Method B): t_R = 1.02 Min, $[M+H]^+$ = 665.51, purity 96%; ¹H NMR (700 MHz, Methanol-*d*₄) δ 8.68 (s, 1H), 8.22 (s, 1H), 7.95 (s, 1H), 7.45 (d, J = 7.5 Hz, 1H), 7.33

(d, $J = 3.1$ Hz, 1H), 7.28 (s, 1H), 7.25 – 7.21 (m, 2H), 6.66 (d, $J = 3.1$ Hz, 1H), 5.61 (ddd, $J = 15.4, 11.3, 3.6$ Hz, 1H), 5.46 (ddd, $J = 15.4, 11.3, 3.6$ Hz, 1H), 4.79 – 4.74 (m, 1H), 3.84 (s, 2H), 3.29 – 3.22 (m, 2H), 3.21 – 3.14 (m, 2H), 2.82 – 2.62 (m, 10H), 2.44 – 2.39 (m, 2H), 2.35 – 2.26 (m, 1H), 2.23 – 2.12 (m, 3H), 2.04 – 1.97 (m, 1H), 1.83 – 1.74 (m, 1H), 1.74 – 1.65 (m, 1H), 1.66 – 1.57 (m, 1H), 1.57 – 1.47 (m, 1H), 1.23 – 1.12 (m, 1H). 4H not observed (exchangeable); ^{13}C NMR (176 MHz, Methanol- d_4) δ 174.3, 162.9, 158.8, 149.9, 142.8, 142.1, 138.3, 136.3, 135.4, 134.1, 132.6, 128.9, 127.6, 126.5, 122.7, 120.6, 120.4, 119.6, 113.0, 112.2, 101.4, 71.5, 54.9, 53.4, 52.9 (2C), 52.5, 41.9, 41.3, 40.5, 35.2, 33.7, 33.3, 30.8, 29.0; ν_{max} (neat): 3405, 3277, 2927, 2817, 1695, 1652, 1548, 1437, 1339, 1265, 1157, 752 cm^{-1} ; HRMS (Method A): calcd. for $\text{C}_{37}\text{H}_{45}\text{N}_8\text{O}_4$ $[\text{M}+\text{H}]^+$ 665.3564; found 665.3562.

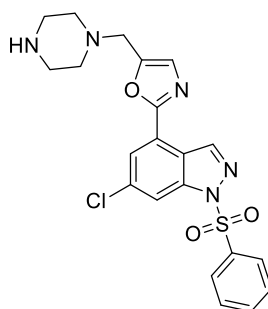


***tert*-Butyl (4-oxopentyl)carbamate (67)**

To a stirred solution of *tert*-butyl 2-oxopyrrolidine-1-carboxylate (5.01 g, 27.0 mmol) in dry THF (50 mL) cooled to 0 °C was added methylmagnesium bromide 3 M in Et₂O (12.6 mL, 37.9 mmol) dropwise under N₂ atmosphere. Upon complete addition, the mixture was allowed to warm to room temperature and was stirred overnight. The reaction was then quenched by the addition of water (100 mL). The reaction was extracted with EtOAc (3 x 100 mL). The combined organic extracts were dried by passing through a hydrophobic frit and concentrated under reduced pressure. The residue was taken in a minimum amount of DCM and purified by automated column chromatography on silica gel eluting with 0-60% EtOAc/cyclohexane over 20 CV. The product-containing fractions were identified by TLC (cyclohexane/EtOAc 6:4, KMnO₄ stain) and were concentrated under reduced pressure to afford the title compound as a pale yellow oil (3.68 g, 67% yield).

^1H NMR (400 MHz, Methanol- d_4) δ 3.02 (t, $J = 6.9$ Hz, 2H), 2.50 (t, $J = 7.2$ Hz, 2H), 2.13 (s, 3H), 1.69 (tt, $J = 7.2, 6.9$ Hz, 2H), 1.43 (s, 9H). 1H not observed exchangeable; ^{13}C NMR (101 MHz, Chloroform- d) δ 208.4, 156.2, 79.3, 40.9, 40.1, 30.1, 28.5, 24.3.

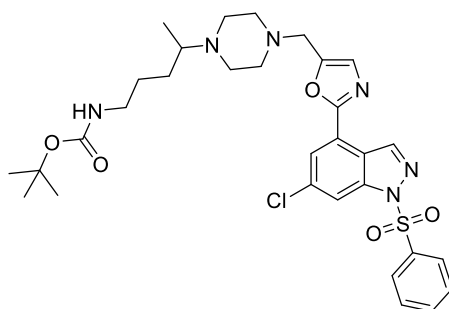
$\nu_{\max}(\text{neat})$: 3363, 2977, 2931, 1690, 1518, 1450, 1392, 1365, 1162 cm^{-1} ; HRMS (Method A): calcd. for $\text{C}_{10}\text{H}_{19}\text{NO}_3\text{Na}$ $[\text{M}+\text{Na}]^+$ 224.1263; found 224.1261.



2-(6-chloro-1-(phenylsulfonyl)-1H-indazol-4-yl)-5-(piperazin-1-ylmethyl)oxazole (68)

To a stirred solution of *tert*-butyl 4-((2-(6-chloro-1-(phenylsulfonyl)-1H-indazol-4-yl)oxazol-5-yl)methyl)piperazine-1-carboxylate (1.61 g, 2.89 mmol) in DCM (25 mL) was added TFA (4 mL) and the reaction mixture was stirred at room temperature for 2 h. Volatiles were then removed under reduced pressure. The crude was dissolved in DCM (15 mL) and quenched by the slow addition of a saturated aqueous sodium bicarbonate solution (25 mL). The biphasic mixture was diluted with more DCM (60 mL) and more aqueous sodium bicarbonate solution (60 mL) was added. The layers were separated and the aqueous layer was further extracted with DCM (3 x 60 mL). The combined organics were dried by passing through a hydrophobic frit and concentrated under reduced pressure. The residue was dried on a high vacuum line overnight to afford the title compound as a pale yellow solid (1.28 g, 97% yield).

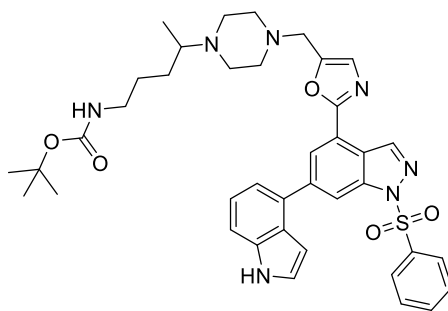
LCMS (Method B): t_R = 1.16 Min, $[\text{M}+\text{H}]^+$ = 458.20, purity 100%; ^1H NMR (400 MHz, Methanol- d_4) δ 8.89 (s, 1H), 8.53 (bs, 1H), 8.30 (dd, J = 1.7, 0.9 Hz, 1H), 8.05 – 7.99 (m, 2H), 7.93 (d, J = 1.7 Hz, 1H), 7.71 – 7.65 (m, 1H), 7.60 – 7.54 (m, 2H), 7.30 (s, 1H), 3.92 – 3.78 (m, 2H), 3.26 – 3.11 (m, 4H), 2.84 – 2.70 (m, 4H); ^{13}C NMR (101 MHz, Methanol- d_4) δ 160.0, 151.0, 142.52, 142.45, 138.2, 137.0, 136.2, 130.8, 129.4, 128.8, 124.1, 122.9, 122.4, 115.5, 52.6, 50.9, 45.0; $\nu_{\max}(\text{neat})$: 3424, 3117, 2835, 1676, 1584, 1446, 1378, 1171, 1090, 921, 725 cm^{-1} ; HRMS (Method A): calcd. for $\text{C}_{21}\text{H}_{21}\text{ClN}_5\text{O}_3\text{S}$ $[\text{M}+\text{H}]^+$ 458.1054; found 458.1058.



***tert*-Butyl (4-(4-((2-(6-chloro-1-(phenylsulfonyl)-1*H*-indazol-4-yl)oxazol-5-yl)methyl)piperazin-1-yl)pentyl)carbamate (69)**

To a stirred solution of 2-(6-chloro-1-(phenylsulfonyl)-1*H*-indazol-4-yl)-5-(piperazin-1-ylmethyl)oxazole (660 mg, 1.44 mmol) in anhydrous THF (20 mL) was added *tert*-butyl (4-oxopentyl)carbamate (1.16 g, 5.77 mmol) followed by acetic acid (41 μ L, 0.72 mmol). The reaction was stirred overnight under N₂ atmosphere at 45 °C. STAB (397 mg, 1.87 mmol) was then added in one portion and the reaction mixture was stirred at 45 °C for 2 h. The reaction was cooled to room temperature and partitioned between EtOAc (40 mL) and a saturated aqueous sodium bicarbonate solution (30 mL). The layers were separated and the aqueous was further extracted with EtOAc (3 x 40 mL). The combined organic layers were dried by passing through a hydrophobic frit and concentrated under reduced pressure. The crude residue was taken in a minimum amount of DCM and purified by automated column chromatography on silica gel eluting with 0-25% MeOH/EtOAc over 20 CV. The product-containing fractions were combined and concentrated under reduced pressure. The residue was then dried on a high vacuum line overnight to afford the title compound as a yellow solid (291 mg, 31% yield).

LCMS (Method A): t_R = 0.95 Min, $[M+H]^+$ = 643.40, purity 100%; ¹H NMR (400 MHz, DMSO-*d*₆) δ 8.94 (d, J = 0.9 Hz, 1H), 8.27 (dd, J = 1.7, 0.9 Hz, 1H), 8.07 – 8.01 (m, 2H), 7.91 (d, J = 1.7 Hz, 1H), 7.80 – 7.73 (m, 1H), 7.67 – 7.61 (m, 2H), 7.35 (s, 1H), 6.72 (bs, 1H), 3.71 (s, 2H), 2.90 – 2.81 (m, 2H), 2.49 – 2.23 (m, 9H), 1.46 – 1.34 (m, 4H), 1.33 (s, 9H), 0.87 (d, J = 6.4 Hz, 3H); ¹³C NMR (101 MHz, DMSO-*d*₆) δ 157.3, 155.5, 150.7, 141.3, 140.7, 136.0, 135.4, 134.9, 130.0, 127.7, 127.4, 122.4, 121.5, 120.5, 113.7, 57.8, 57.7, 57.6, 52.4, 51.3, 47.4, 30.0, 28.2, 26.4, 13.8; HRMS (Method A): calcd. for C₃₁H₄₀ClN₆O₅S $[M+H]^+$ 643.2469; found 643.2457.

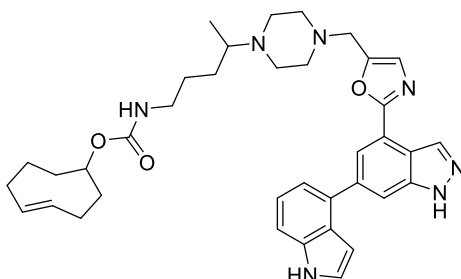


***tert*-Butyl (4-(4-((2-(6-(1*H*-indol-4-yl)-1-(phenylsulfonyl)-1*H*-indazol-4-yl)oxazol-5-yl)methyl)piperazin-1-yl)pentyl)carbamate (70)**

To a microwave vial was added 4-(4,4,5,5-tetramethyl-1,3,2-dioxaborolan-2-yl)-1*H*-indole (84 mg, 0.35 mmol), sodium carbonate (91 mg, 0.86 mmol) and XPhos Pd G2 (23 mg, 0.029 mmol). Then a solution of *tert*-butyl (4-(4-((2-(6-chloro-1-(phenylsulfonyl)-1*H*-indazol-4-yl)oxazol-5-yl)methyl)piperazin-1-yl)pentyl)carbamate (185 mg, 0.29 mmol) in 1,4-dioxane (4 mL) was added, followed by water (0.5 mL). The vial was sealed and the atmosphere was purged by 3 vacuum/nitrogen cycles. The vial was heated in the microwave for 1 h at 90 °C. The reaction was partitioned between EtOAc (20 mL) and water (15 mL). The layers were separated and the aqueous was further extracted with EtOAc (3 x 20 mL). The combined organics extracts were dried by passing through a hydrophobic frit. Florisil was added and solvents were removed under reduced pressure. Purification was carried out by automated column chromatography on silica gel eluting with 0-30% MeOH/EtOAc over 22 CV. The product-containing fractions were combined and concentrated under reduced pressure to afford the title compound as a beige solid (151 mg, 72% yield).

LCMS (Method A): t_R = 0.96 Min, $[M+H]^+ = 724.30$, purity 94%; 1H NMR (400 MHz, Chloroform-*d*) δ 8.99 (d, $J = 0.9$ Hz, 1H), 8.62 (dd, $J = 1.3, 0.9$ Hz, 1H), 8.61 (bs, 1H), 8.35 (d, $J = 1.3$ Hz, 1H), 8.05 – 8.00 (m, 2H), 7.60 – 7.53 (m, 1H), 7.52 – 7.43 (m, 3H), 7.37 – 7.32 (m, 3H), 7.13 (s, 1H), 6.84 – 6.67 (m, 1H), 5.07 (bs, 1H), 3.70 (s, 2H), 3.14 – 3.01 (m, 2H), 2.66 – 2.43 (m, 9H), 1.59 – 1.45 (m, 4H), 1.41 (s, 9H), 0.94 (d, $J = 6.4$ Hz, 3H); ^{13}C NMR (101 MHz, $CDCl_3$) δ 160.1, 156.2, 149.5, 143.2, 142.1, 141.7, 137.8, 136.5, 134.4, 132.8, 129.4, 127.8, 127.7, 126.4, 125.4, 124.2, 122.5,

121.8, 121.0, 120.6, 114.4, 111.6, 101.8, 79.0, 58.4, 53.3, 52.6, 47.8, 40.9, 31.5, 28.6, 27.0, 14.0; ν_{\max} (neat): 3274, 2937, 2815, 1707, 1607, 1513, 1447, 1380, 1159, 1087, 965, 721 cm^{-1} ; HRMS (Method B): calcd. for $\text{C}_{39}\text{H}_{46}\text{N}_7\text{O}_5\text{S}$ $[\text{M}+\text{H}]^+$ 724.3281; found 724.3290.



(*E*)-cyclooct-4-en-1-yl (4-(4-((2-(6-(1*H*-indol-4-yl)-1*H*-indazol-4-yl)oxazol-5-yl)methyl)piperazin-1-yl)pentyl)carbamate (**38**)

Boc deprotection:

To a stirred solution of *tert*-butyl 4-(4-((2-(6-(1*H*-indol-4-yl)-1-(phenylsulfonyl)-1*H*-indazol-4-yl)oxazol-5-yl)methyl)piperazin-1-yl)pentyl)carbamate (114 mg, 0.16 mmol) in DCM (4 mL) was added TFA (1 mL). The resulting solution was stirred at room temperature under N_2 for 1.5 h. Volatiles were then removed under reduced pressure. The residue was partitioned between DCM (15 mL) and a saturated aqueous sodium bicarbonate solution (10 mL). The layers were separated and the aqueous was further extracted with DCM (3 x 10 mL). The combined organic extracts were dried by passing through a hydrophobic frit and concentrated under reduced pressure to afford the crude primary amine as a beige solid which was used immediately in the following step without further purification.

TCO installation:

To a stirred solution of crude 4-(4-((2-(6-(1*H*-indol-4-yl)-1-(phenylsulfonyl)-1*H*-indazol-4-yl)oxazol-5-yl)methyl)piperazin-1-yl)pentan-1-amine in DMF (4 mL) was added (*E*)-cyclooct-4-en-1-yl (4-nitrophenyl) carbonate (50 mg, 0.17 mmol) and DIPEA (55 μL , 0.31 mmol). The reaction was stirred at room temperature for 1 h under an atmosphere of N_2 . The reaction was partitioned between EtOAc (10 mL) and water

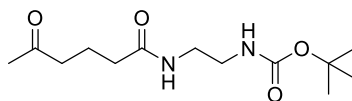
(10 mL). The layers were separated and the aqueous was extracted with EtOAc (3 x 10 mL). The combined organics were washed with a 5% aqueous LiCl solution (20 mL), dried by passing through a hydrophobic frit and concentrated under reduced pressure.

Benzenesulfonyl deprotection:

The crude was immediately taken in MeOH (4 mL) and a 2 M aqueous NaOH solution (1 mL) was added. The reaction was stirred at room temperature for 20 min. MeOH was removed under reduced pressure. The residue was partitioned between EtOAc (10 mL) and water (10 mL). The layers were separated and the aqueous was further extracted with EtOAc (3 x 10 mL). The combined organic extracts were dried by passing through a hydrophobic frit and concentrated under reduced pressure. The residue was taken up in MeOH/DMSO (1:1, 2 mL) and 1 mL of this solution was purified by Mass Directed Auto Preparative HPLC (Method A). The purification failed to remove impurities. The product-containing fractions were combined and concentrated under reduced pressure. The residue was taken in water/MeCN (1:1, 6 mL) which were lyophilised to afford a white solid (15 mg). The compound was dissolved in DMSO (3 mL) and purified by preparative HPLC (Method E). The desired fractions were combined, partially concentrated under reduced pressure and lyophilized. The compound was taken up in MeCN/water (1:1, 6 mL) and lyophilized once more to afford the title compound as a white fluffy solid (10 mg, 9% yield over 3 steps).

LCMS (Method B): t_R = 1.26 Min, $[M+H]^+$ = 636.34, purity 98%; 1H NMR (600 MHz, DMSO- d_6) δ 8.71 (d, J = 0.9 Hz, 1H), 8.25 (d, J = 1.3 Hz, 1H), 7.95 (dd, J = 1.3, 0.9 Hz, 1H), 7.51 – 7.45 (m, 1H), 7.35 (d, J = 3.2 Hz, 1H), 7.30 (s, 1H), 7.28 – 7.23 (m, 2H), 6.68 (dd, J = 3.2, 1.0 Hz, 1H), 5.65 – 5.62 (m, 1H), 5.49 – 5.42 (m, 1H), 4.78 – 4.74 (m, 1H), 3.84 (s, 2H), 3.22 – 3.03 (m, 2H), 2.75 – 2.50 (m, 11H), 2.40 – 2.25 (m, 1H), 2.25 – 2.13 (m, 3H), 2.09 – 1.97 (m, 1H), 1.85 – 1.67 (m, 1H), 1.68 – 1.43 (m, 3H), 1.40 – 1.28 (m, 2H), 1.22 – 1.14 (m, 1H), 1.03 (d, J = 6.4 Hz, 3H); ^{13}C NMR (151 MHz, Methanol- d_4) δ 162.9, 158.7, 150.1, 142.1, 138.3, 136.3, 135.3, 134.1, 132.6, 128.8, 127.6, 126.4, 122.72, 122.66, 120.7, 120.4, 119.6, 113.0, 112.2, 101.5, 71.3,

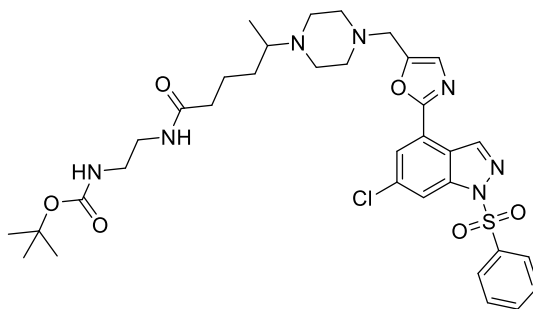
60.0, 54.8, 53.8, 52.8, 49.6, 42.0, 41.7, 35.2, 33.7, 31.2, 30.8, 29.0, 28.2, 14.7; HRMS: calcd. for C₃₇H₄₆N₇O₃ [M+H]⁺ 636.3662; found 636.3674.



***tert*-Butyl (2-(5-oxohexanamido)ethyl)carbamate (74)**

To a stirred solution of 5-oxohexanoic acid (0.98 g, 7.53 mmol) in anhydrous DCM (50 mL) cooled to 0 °C was added triethylamine (1.04 mL, 7.61 mmol) followed by *N,N*-disuccinimidyl carbonate (2.51 g, 9.79 mmol) portion wise over 5 min. After a few minutes all solids particles went into solution. The solution was stirred at room temperature overnight, after which a solution of *N*-Boc-ethylenediamine (2.17 g, 13.55 mmol) in DCM (10 mL) was added. The reaction mixture was washed with water (2 x 80 mL). The organic layer was dried by passing through a hydrophobic frit and concentrated under reduced pressure. The crude was dissolved in a minimum amount of DCM and purified by automated column chromatography on silica gel eluting with 0-80% (3:1 EtOAc/EtOH)/cyclohexane over 16 CV. The product-containing fractions were identified by TLC (cyclohexane/(3:1 EtOAc/EtOH) 2:8, KMnO₄ stain) and concentrated under reduced pressure to afford the title compound as a white solid (1.78 g, 87% yield).

¹H NMR (400 MHz, DMSO-*d*₆) δ 7.74 (t, *J* = 5.7 Hz, 1H), 6.70 (t, *J* = 5.7 Hz, 1H), 3.06 (td, *J* = 6.5, 5.7 Hz, 2H), 2.96 (td, *J* = 6.5, 5.7 Hz, 2H), 2.40 (t, *J* = 7.3 Hz, 2H), 2.05 (s, 3H), 2.03 (t, *J* = 7.6 Hz, 3H), 1.66 (tt, *J* = 7.6, 7.3 Hz, 2H), 1.36 (s, 9H); ¹³C NMR (101 MHz, DMSO) δ 208.0, 171.9, 155.6, 77.6, 42.0, 39.7, 38.7, 34.5, 29.6, 28.2, 19.4; HRMS (Method A): calcd. for C₁₃H₂₄N₂O₄Na [M+Na]⁺ 295.1634; found 295.1632; ν_{max}(neat): 3356, 3326, 2939, 1709, 1676, 1642, 1523, 1277, 1161, 864, 623 cm⁻¹.



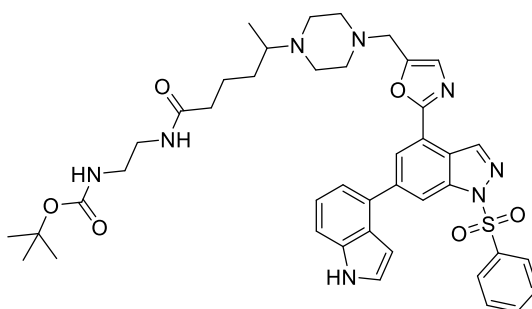
***tert*-Butyl (2-(5-(4-((2-(6-chloro-1-(phenylsulfonyl)-1*H*-indazol-4-yl)oxazol-5-yl)methyl)piperazin-1-yl)hexanamido)ethyl)carbamate (75)**

To a stirred suspension of 2-(6-chloro-1-(phenylsulfonyl)-1*H*-indazol-4-yl)-5-(piperazin-1-ylmethyl)oxazole (400 mg, 0.87 mmol) in THF (12 mL) was added *tert*-butyl (2-(5-oxohexanamido)ethyl)carbamate (714 mg, 2.62 mmol) and acetic acid (25 μ L, 0.44 mmol). The reaction mixture was stirred at 40 °C under an atmosphere of N₂ for 2 h after which STAB (278 mg, 1.31 mmol) was added in one portion. The reaction was then stirred at 40 °C for 18 h. More *tert*-butyl (2-(5-oxohexanamido)ethyl)carbamate (475 mg, 2 equiv.) were added along with more acetic acid (25 μ L). The reaction was stirred at 40 °C for 48 h. The reaction mixture was cooled to room temperature and then partitioned between EtOAc (30 mL) and a saturated aqueous sodium bicarbonate solution (25 mL). The layers were separated and the aqueous was extracted with EtOAc (3 x 25 mL) and then DCM (2 x 25 mL). The combined organic extracts were dried by passing through a hydrophobic frit. Florisil was added and solvents were removed under reduced pressure to adsorb the compound. Purification was carried out by automated column chromatography on silica gel eluting with 0-80% (3:1 EtOAc/ MeOH)/cyclohexane over 20 CV. The product-containing fractions were combined and concentrated under reduced pressure to afford the title compound as a yellow oil (341 mg, 55% yield).

The reaction was repeated on 80 mg scale and was purified by Mass Directed Automated Preparative HPLC (Method E) for characterisation.

LCMS (Method A): t_R = 0.92 Min, $[M+H]^+$ = 714.28, purity 100%; ¹H NMR (400 MHz, Chloroform-*d*) δ 8.90 (d, J = 0.9 Hz, 1H), 8.30 (dd, J = 1.7, 0.9 Hz, 1H), 8.04 – 7.97 (m, 2H), 7.95 (d, J = 1.7 Hz, 1H), 7.64 – 7.55 (m, 1H), 7.53 – 7.44 (m, 2H), 7.12

(s, 1H), 6.32 (s, 1H), 5.06 (s, 1H), 3.73 – 3.64 (m, 2H), 3.38 – 3.30 (m, 2H), 3.29 – 3.19 (m, 2H), 2.79 – 2.57 (m, 9H), 2.17 (t, $J = 7.0$ Hz, 2H), 1.74 – 1.54 (m, 3H), 1.42 (s, 9H), 1.38 – 1.26 (m, 1H), 1.03 (d, $J = 6.5$ Hz, 3H); ^{13}C NMR (101 MHz, Chloroform- d) δ 173.6, 158.8, 157.1, 149.8, 141.8, 141.4, 137.4, 135.9, 134.7, 129.5, 128.1, 127.8, 123.4, 121.8, 121.3, 114.6, 79.8, 59.1, 52.42, 52.36, 47.8, 40.8, 40.5, 36.5, 32.7, 28.5, 22.7, 13.9; ν_{max} (neat): 3308, 2973, 2818, 1700, 1648, 1590, 1449, 1376, 1174, 1095, 925, 726 cm^{-1} ; HRMS (Method A): calcd. for $\text{C}_{34}\text{H}_{45}\text{ClN}_7\text{O}_6\text{S}$ $[\text{M}+\text{H}]^+$ 714.2841; found 714.2851.

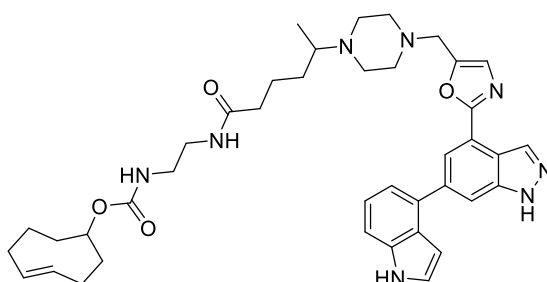


***tert*-Butyl (2-(5-(4-((2-(6-(1*H*-indol-4-yl)-1-(phenylsulfonyl)-1*H*-indazol-4-yl)oxazol-5-yl)methyl)piperazin-1-yl)hexanamido)ethyl)carbamate (76)**

To a microwave vial was added 4-(4,4,5,5-tetramethyl-1,3,2-dioxaborolan-2-yl)-1*H*-indole (142 mg, 0.58 mmol), XPhos Pd G2 (71 mg, 0.090 mmol), sodium carbonate (142 mg, 1.34 mmol) and a solution of *tert*-butyl (2-(5-(4-((2-(6-chloro-1-(phenylsulfonyl)-1*H*-indazol-4-yl)oxazol-5-yl)methyl)piperazin-1-yl)hexanamido)ethyl)carbamate (320 mg, 0.45 mmol) in 1,4-dioxane (6 mL). Water (1 mL) was added. The vial was sealed and the atmosphere was purged with 3 vacuum/nitrogen cycles. The vial was heated in the microwave for 1 h at 90 °C. More pinacol boronic ester (109 mg, 1 equiv.) and XPhos Pd G2 (36 mg, 0.1 equiv.) were added. The atmosphere was purged again with 3 vacuum/nitrogen cycles and the reaction was heated in the microwave for an additional 30 min at 90 °C. The reaction was partitioned between EtOAc (25 mL) and water (25 mL). The layers were separated and the aqueous was further extracted with EtOAc (3 x 20 mL). The combined organic extracts were dried by passing through a hydrophobic frit. Florisil was added and solvents were removed under reduced pressure. Purification was carried out by

automated column chromatography on silica gel eluting with 0-40% MeOH/EtOAc over 20 CV. The product-containing fractions were combined and concentrated under reduced pressure to afford the title compound as a brown oil (225 mg, 63% yield).

LCMS (Method A): t_R = 0.93 Min, $[M+H]^+$ = 795.53, purity 98%; 1H NMR (400 MHz, Chloroform-*d*) δ 8.99 (d, J = 0.9 Hz, 1H), 8.91 (bs, 1H), 8.62 (dd, J = 1.3, 0.9 Hz, 1H), 8.34 (d, J = 1.3 Hz, 1H), 8.05 – 7.99 (m, 2H), 7.59 – 7.52 (m, 1H), 7.52 – 7.42 (m, 3H), 7.37 – 7.30 (m, 3H), 7.13 (s, 1H), 6.84 – 6.66 (m, 1H), 6.30 (bs, 1H), 5.02 (bs, 1H), 3.69 (s, 2H), 3.38 – 3.29 (m, 2H), 3.29 – 3.19 (m, 2H), 2.67 – 2.48 (m, 10H), 2.16 (t, J = 7.4 Hz, 2H), 1.71 – 1.48 (m, 2H), 1.42 (s, 9H), 1.36 – 1.25 (m, 1H), 0.97 (d, J = 6.5 Hz, 3H); ^{13}C NMR (101 MHz, Chloroform-*d*) δ 173.8, 160.0, 157.1, 149.4, 143.2, 142.1, 141.6, 137.7, 136.6, 134.4, 132.7, 129.4, 127.7, 126.4, 125.5, 124.2, 122.4, 121.8, 120.9, 120.5, 114.3, 111.6, 101.6, 79.8, 58.9, 52.5, 48.0, 40.8, 40.5, 36.7, 33.0, 28.5, 25.0, 22.9, 14.1; ν_{max} (neat): 3305, 2971, 2817, 1692, 1644, 1538, 1450, 1367, 1265, 1172, 1090, 895, 726 cm^{-1} ; HRMS (Method A): calcd. for $C_{42}H_{51}N_8O_6S$ $[M+H]^+$ 795.3652; found 795.3654.



(*E*)-cyclooct-4-en-1-yl (2-(5-(4-((2-(6-(1*H*-indol-4-yl)-1*H*-indazol-4-yl)oxazol-5-yl)methyl)piperazin-1-yl)hexanamido)ethyl)carbamate (43)

Boc deprotection:

To a stirred solution of *tert*-butyl (2-(5-(4-((2-(6-(1*H*-indol-4-yl)-1-(phenylsulfonyl)-1*H*-indazol-4-yl)oxazol-5-yl)methyl)piperazin-1-yl)hexanamido)ethyl)carbamate (215 mg, 0.27 mmol) in DCM (8 mL) was added TFA (1.5 mL). The resulting solution was stirred at room temperature under N_2 atmosphere for one hour. Volatiles were removed under reduced pressure. The crude was partitioned between DCM (15 mL)

and a saturated aqueous sodium bicarbonate solution (15 mL). A solid crashed out upon addition of the aqueous sodium bicarbonate solution. The biphasic mixture was stirred at room temperature for 15 min after which it was transferred to a separatory funnel. More aqueous sodium bicarbonate (30 mL) was added along with more DCM (20 mL). The layers were separated and the aqueous was extracted with DCM (2 x 30 mL). The combined organic extracts were dried by passing through a hydrophobic frit and concentrated under reduced pressure. Most of the product remained in the aqueous layer. The aqueous layer was concentrated under reduced pressure and the residue was taken in water/MeCN (1:1, 6 mL) which were lyophilized to afford the crude primary amine as a grey solid.

TCO installation:

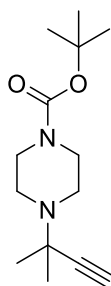
To a stirred solution of crude primary amine in DMF (5 mL) was added (*E*)-cyclooct-4-en-1-yl (4-nitrophenyl) carbonate (79 mg, 0.27 mmol) and DIPEA (52 μ L, 0.30 mmol) upon which the reaction turned yellow in colour. The reaction was stirred at room temperature for 1.5 h. The reaction was partitioned between EtOAc (20 mL) and water (20 mL). The layers were separated and the aqueous was further extracted with EtOAc (3 x 20 mL). The combined organic extracts were washed with a 5% aqueous LiCl solution (2 x 20 mL), dried by passing through a hydrophobic frit and concentrated under reduced pressure.

Benzene sulfonyl deprotection:

The crude was immediately dissolved in MeOH (5 mL) and a 2 M aqueous NaOH solution (0.5 mL) was added. The reaction was stirred at room temperature for 1 h. MeOH was removed under reduced pressure and the residue was partitioned between EtOAc (15 mL) and water (15 mL). The layers were separated and the aqueous was further extracted with EtOAc (3 x 15 mL). The combined organic extracts were washed with brine (25 mL), dried by passing through a hydrophobic frit and concentrated under reduced pressure. The crude was taken in MeOH/DMSO (1:1, 3 mL) and purified by Mass Directed Automated Preparative HPLC (Method B, 3 x 1 mL injection). The product-containing fractions were concentrated under reduced

pressure. The residue was dissolved in water/acetonitrile (1:1, 6 mL) which were lyophilized to afford a white solid (26 mg). The compound still contained impurities. 23 mg were dissolved in DMSO (8 mL) which were purified by preparative HPLC (Method F). The desired fractions were combined and concentrated under reduced pressure. The residue was taken in MeCN/water (1:1, 6 mL) and freeze-dried to afford the title compound as a white solid (9% yield over 3 steps).

LCMS (Method B): $t_R = 1.09$ Min, $[M+H]^+ = 707.49$, purity 95%; 1H NMR (600 MHz, Methanol- d_4) δ 8.69 (s, 1H), 8.24 (d, $J = 1.2$ Hz, 1H), 7.95 (s, 1H), 7.49 – 7.43 (m, 1H), 7.34 (d, $J = 3.2$ Hz, 1H), 7.30 – 7.18 (m, 3H), 6.67 (d, $J = 3.2$ Hz, 1H), 5.62 (ddd, $J = 15.3, 11.2, 3.7$ Hz, 1H), 5.47 (ddd, $J = 15.4, 11.2, 3.4$ Hz, 1H), 4.80 – 4.75 (m, 1H), 3.82 (s, 2H), 3.29 – 3.14 (m, 4H), 2.77 – 2.56 (m, 9H), 2.36 – 2.25 (m, 1H), 2.24 – 2.14 (m, 5H), 2.05 – 1.98 (m, 1H), 1.83 – 1.74 (m, 1H), 1.75 – 1.67 (m, 1H), 1.67 – 1.47 (m, 5H), 1.36 – 1.25 (m, 1H), 1.23 – 1.14 (m, 1H), 1.04 (d, $J = 6.5$ Hz, 3H). 4H not observed (exchangeable); ^{13}C NMR (151 MHz, Methanol- d_4) δ 176.3, 162.9, 158.8, 150.0, 142.9, 142.1, 138.3, 136.3, 135.4, 134.1, 132.8, 132.5, 128.8, 127.6, 126.4, 122.70, 122.66, 120.6, 120.4, 119.6, 113.0, 112.2, 101.5, 71.5, 60.3, 53.5, 52.7, 49.6, 42.0, 41.4, 40.5, 35.2, 33.7, 30.8, 29.0, 24.0, 14.52, 14.51; $\nu_{max}(\text{neat})$: 3277, 2927, 2823, 1695, 1646, 1541, 1449, 1339, 1265, 1118, 1039, 996, 757 cm^{-1} ; HRMS (Method B): calcd. for $C_{40}H_{51}N_8O_4$ $[M+H]^+ 707.4033$; found 707.4040.

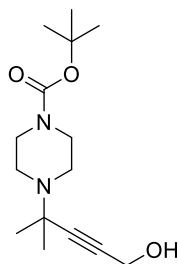


***tert*-Butyl 4-(2-methylbut-3-yn-2-yl)piperazine-1-carboxylate (79)**

To a stirred solution of 1-Boc-piperazine (3.50 g, 18.79 mmol) in THF (30 mL) was added 3-chloro-3-methylbut-1-yne (2.74 mL, 24.43 mmol) followed by triethylamine (3.54 mL, 25.40 mmol). To the previous solution was added copper(I) chloride (0.15 g, 1.50 mmol). The reaction mixture started to become thicker. More THF (15 mL)

was added. The reaction was stirred at room temperature for 2 h after which water (50 mL) and 1 M aqueous HCl (35 mL) were added. The reaction mixture was concentrated under reduced pressure remove most of the THF. The aqueous was then washed with EtOAc (60 mL). The layers were separated and the aqueous was made slightly basic (pH 8) by the addition of a saturated aqueous sodium bicarbonate solution (100 mL). The aqueous phase was then extracted with EtOAc (3 x 100 mL). The combined organic extracts were dried by passing through a hydrophobic frit and concentrated under reduced pressure to afford the crude title compound as a beige solid (3.38 g, 71% yield)

^1H NMR (400 MHz, Chloroform-*d*) δ 3.56 – 3.37 (m, 4H), 2.64 – 2.46 (m, 4H), 2.28 (s, 1H), 1.46 (s, 9H), 1.39 (s, 6H); ^{13}C NMR (101 MHz, Chloroform-*d*) δ 154.8, 85.6, 79.7, 71.7, 54.1, 46.9, 43.7, 28.6, 27.8; ν_{max} (neat): 3227, 2083, 2825, 1682, 1450, 1411, 1361, 1239, 1168, 1122 cm^{-1} .

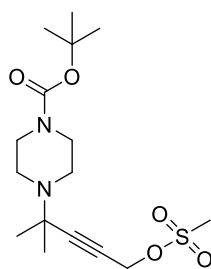


***tert*-Butyl 4-(5-hydroxy-2-methylpent-3-yn-2-yl)piperazine-1-carboxylate (80)**

To a stirred solution of *tert*-butyl 4-(2-methylbut-3-yn-2-yl)piperazine-1-carboxylate (2.50 g, 9.91 mmol) in dry THF (30 mL) cooled to -78 °C was added LDA 2.0 M in THF/hexane (6.4 mL, 12.88 mmol) slowly under N₂ atmosphere. Upon complete addition, the reaction was stirred at -78 °C for 1 h and then a suspension of paraformaldehyde (0.89 g, 29.70 mmol) in THF (10 mL) was added. The reaction was then allowed to warm to room temperature overnight. The reaction was then quenched with a saturated aqueous ammonium chloride solution (60 mL) and extracted with EtOAc (3 x 70 mL). The combined organics extracts were dried by passing through a hydrophobic frit and concentrated under reduced pressure. The crude residue was dissolved in a minimum amount of DCM and purified by automated column chromatography on silica gel eluting with 0-25% MeOH/DCM over 16 CV. The

product containing fractions were identified by TLC (DCM/MeOH, 8:2, KMnO₄ stain) and concentrated under reduced pressure to afford the title compound as an orange oil (2.14 g, 76% yield).

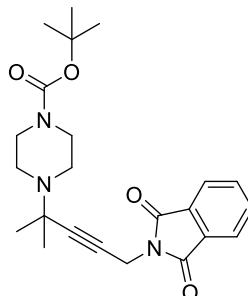
¹H NMR (400 MHz, Chloroform-*d*) δ 4.28 (s, 2H), 3.53 – 3.37 (m, 4H), 2.60 – 2.51 (m, 4H), 1.80 (bs, 1H), 1.46 (s, 9H), 1.38 (s, 6H); ¹³C NMR (101 MHz, Chloroform-*d*) δ 154.8, 87.4, 82.4, 79.8, 54.3, 51.2, 46.9, 44.0, 28.6, 27.6; ν_{max}(DCM): 3430, 2981, 2859, 2820, 1696, 1419, 1364, 1054, 1009 cm⁻¹; HRMS (Method A): calcd. for C₁₅H₂₇N₂O₃ [M+H]⁺ 283.2022; found 283.2024.



***tert*-Butyl 4-(2-methyl-5-((methylsulfonyl)oxy)pent-3-yn-2-yl)piperazine-1-carboxylate (81)**

To a stirred solution of *tert*-butyl 4-(5-hydroxy-2-methylpent-3-yn-2-yl)piperazine-1-carboxylate (630 mg, 2.23 mmol) in dry DCM (15 mL) cooled to 0 °C was added methane sulfonic anhydride (505 mg, 2.90 mmol) followed by triethylamine (466 μL, 3.35 mmol). The reaction was stirred at 0 °C for 2 h under N₂ atmosphere. The reaction was partitioned between DCM (30 mL) and water (30 mL) and the layers were separated. The aqueous was further extracted with DCM (3 x 25 mL). The combined organic extracts were dried by passing through a hydrophobic frit and concentrated under reduced pressure. The residue was dissolved in a minimum amount of DCM and purified by automated column chromatography on silica gel eluting with 0-20% MeOH/DCM over 18 CV. The product-containing fractions were concentrated under reduced pressure to afford the title compound as a colourless oil (733 mg, 91% yield). Compound was not amenable to long term storage and was used immediately in the subsequent step.

^1H NMR (400 MHz, Chloroform-*d*) δ 4.87 (s, 2H), 3.44 (t, J = 5.1 Hz, 4H), 3.09 (s, 3H), 2.55 (t, J = 5.1 Hz, 4H), 1.46 (s, 9H), 1.39 (s, 6H); ^{13}C NMR (101 MHz, Chloroform-*d*) δ 154.8, 92.0, 79.8, 76.2, 58.0, 54.4, 47.0, 43.9, 39.0, 28.6, 27.4.

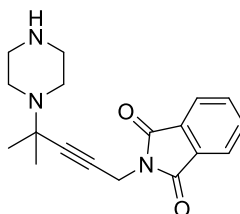


***tert*-Butyl 4-(5-(1,3-dioxoisindolin-2-yl)-2-methylpent-3-yn-2-yl)piperazine-1-carboxylate (82)**

To a stirred solution of *tert*-butyl 4-(2-methyl-5-((methylsulfonyl)oxy)pent-3-yn-2-yl)piperazine-1-carboxylate (2.50 g, 6.94 mmol) in DMF (30 mL) was added phthalimide potassium salt (1.93 g, 10.4 mmol) and the reaction was stirred overnight at 70 °C under N_2 atmosphere. After a few minutes, reaction became very thick and more DMF (20 mL) was added. The reaction was cooled to room temperature, partitioned between EtOAc (150 mL) and water (200 mL) and the layers were separated. The aqueous was further extracted with EtOAc (3 x 150 mL). The combined organics were washed with a 5% aqueous LiCl solution (2 x 150 mL) and then washed with an 0.5 M aqueous NaOH solution (2 x 150 mL). The organic layer was then dried by passing through a hydrophobic frit and concentrated under reduced pressure. The crude residue was dissolved in a minimum amount of DCM and purified by automated column chromatography on silica gel eluting with 0-60% (3:1 EtOAc/EtOH)/cyclohexane over 18 CV. The product containing fractions were concentrated under reduced pressure to afford the title compound as a yellow oil which still contained impurities. The residue was dissolved in MeOH/DMSO (1:1, 8 mL) and purified by automated reverse phase chromatography on C18 silica eluting with 40-70% acetonitrile/water 10 mM ammonium bicarbonate over 18 CV. The product containing fractions were concentrated under reduced pressure to remove most of the acetonitrile and the aqueous was then extracted with DCM (4 x 100 mL). The

combined organics were dried by passing through a hydrophobic frit and concentrated under reduced pressure. The residue was dried on a high vacuum line overnight to afford the title compound as a pale yellow solid (1.62 g, 57% yield).

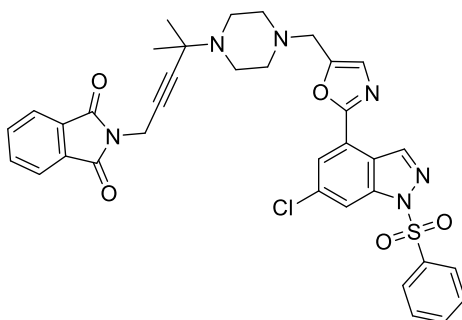
LCMS (Method B): $t_R = 1.23$ Min, $[M+H]^+ = 412.33$, purity 100%; 1H NMR (400 MHz, Chloroform-*d*) δ 7.97 – 7.82 (m, 2H), 7.78 – 7.66 (m, 2H), 4.45 (s, 2H), 3.45 – 3.34 (m, 4H), 2.52 (t, $J = 5.2$ Hz, 4H), 1.44 (s, 8H), 1.32 (s, 6H); ^{13}C NMR (101 MHz, Chloroform-*d*) δ 167.2, 154.8, 134.2, 132.2, 123.6, 85.1, 79.6, 77.3, 54.1, 46.8, 44.0, 28.6, 27.5, 27.4; $\nu_{max}(\text{neat})$: 2975, 2920, 2831, 1768, 1724, 1691, 1425, 1358, 1253, 1081, 948, 727 cm^{-1} ; HRMS (Method A): calcd. for $C_{23}H_{30}N_3O_4$ $[M+H]^+ 412.2236$; found 412.2236.



2-(4-Methyl-4-(piperazin-1-yl)pent-2-yn-1-yl)isoindoline-1,3-dione (83)

To a stirred solution of *tert*-butyl 4-(5-(1,3-dioxoisoindolin-2-yl)-2-methylpent-3-yn-2-yl)piperazine-1-carboxylate (709 mg, 1.72 mmol) in DCM (12 mL) was added TFA (3 mL) and the reaction mixture was stirred at room temperature for 3 h. Volatiles were then removed under reduced pressure. The crude was dissolved in DCM (20 mL) and quenched by slow addition of a saturated aqueous sodium bicarbonate solution (25 mL). The biphasic mixture was transferred to a separatory funnel and diluted with more DCM (50 mL) and more aqueous sodium bicarbonate solution (40 mL). The layers were separated and the aqueous was further extracted with DCM (3 x 30 mL). The combined organics were dried by passing through a hydrophobic frit and concentrated under reduced pressure removal to afford the crude title compound as a yellow solid (602 mg). The compound started to degrade extremely quickly upon solvent removal and was used immediately into the subsequent step.

LCMS (Method B): $t_R = 0.82$ Min, $[M+H]^+ = 312.21$, purity 71%.

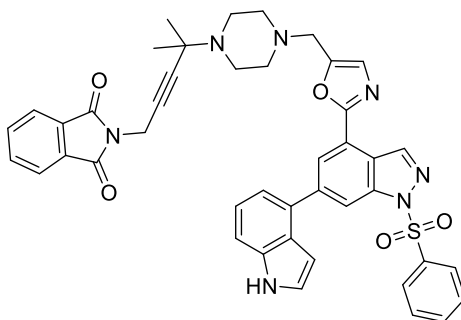


2-(4-(4-((2-(6-chloro-1-(phenylsulfonyl)-1*H*-indazol-4-yl)oxazol-5-yl)methyl)piperazin-1-yl)-4-methylpent-2-yn-1-yl)isoindoline-1,3-dione (84)

To a stirred solution of crude 2-(4-methyl-4-(piperazin-1-yl)pent-2-yn-1-yl)isoindoline-1,3-dione (596 mg, 1.34 mmol) in DCM (12 mL) was added 2-(6-chloro-1-(phenylsulfonyl)-1*H*-indazol-4-yl)oxazole-5-carbaldehyde (400 mg, 1.03 mmol), acetic acid (29 μ L, 0.52 mmol) followed by STAB (328 mg, 1.55 mmol). The reaction mixture was stirred at room temperature under N_2 atmosphere for 48 h. The reaction was partitioned between DCM (60 mL) and a saturated aqueous sodium bicarbonate solution (60 mL). The layers were separated and the aqueous phase was further extracted with DCM (3 x 70 mL). The combined organic extracts were dried by passing through a hydrophobic frit and concentrated under reduced pressure. The residue was taken in a minimum amount of DCM and purified by automated column chromatography on silica gel eluting with 0-10% MeOH/EtOAc over 16 CV. The product containing fractions were concentrated under reduced pressure. The residue was dried on a high vacuum line overnight to afford the title compound as a pale yellow solid (464 mg, 66% yield).

LCMS (Method A): t_R = 0.96 Min, $[M+H]^+$ = 683.30, purity 100%; 1H NMR (400 MHz, Chloroform-*d*) δ 8.92 (d, J = 0.9 Hz, 1H), 8.31 (dd, J = 1.7, 0.9 Hz, 1H), 8.04 – 7.99 (m, 2H), 7.96 (d, J = 1.7 Hz, 1H), 7.89 – 7.83 (m, 2H), 7.75 – 7.69 (m, 2H), 7.64 – 7.57 (m, 1H), 7.54 – 7.46 (m, 2H), 7.12 (s, 1H), 4.46 (s, 2H), 3.70 (s, 2H), 2.75 – 2.53 (m, 8H), 1.32 (s, 6H); ^{13}C NMR (101 MHz, Chloroform-*d*) δ 167.2, 158.7, 150.0, 141.8, 141.4, 137.4, 136.0, 134.7, 134.3, 132.3, 129.5, 128.1, 127.8, 123.6, 123.4, 121.9, 121.3, 114.6, 85.2, 77.4, 54.1, 53.1, 52.3, 46.8, 27.5, 27.3; ν_{max} (DCM): 3095,

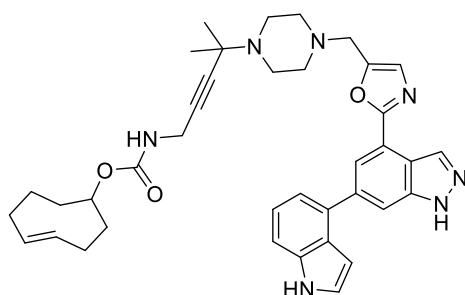
2930, 2818, 1717, 1589, 1536, 1468, 1381, 1291, 1342, 924, 727 cm^{-1} ; HRMS (Method A): calcd. for $\text{C}_{35}\text{H}_{32}\text{ClN}_6\text{O}_5\text{S}$ $[\text{M}+\text{H}]^+$ 683.1843; found 683.1843.



2-(4-(4-((2-(6-(1*H*-Indol-4-yl)-1-(phenylsulfonyl)-1*H*-indazol-4-yl)oxazol-5-yl)methyl)piperazin-1-yl)-4-methylpent-2-yn-1-yl)isoindoline-1,3-dione (85)

In a microwave vial were charged 2-(4-(4-((2-(6-chloro-1-(phenylsulfonyl)-1*H*-indazol-4-yl)oxazol-5-yl)methyl)piperazin-1-yl)-4-methylpent-2-yn-1-yl)isoindoline-1,3-dione (436 mg, 0.64 mmol), 4-(4,4,5,5-tetramethyl-1,3,2-dioxaborolan-2-yl)-1*H*-indole (310 mg, 1.28 mmol), XPhos Pd G2 (100 mg, 0.13 mmol) and sodium carbonate (203 mg, 1.92 mmol). Solids were suspended in 1,4-dioxane (10 mL) and water (1 mL). The vial was sealed and purged with 3 vacuum/nitrogen cycles and subsequently heated at 90 °C in the microwave for 75 mins after which more 4-(4,4,5,5-tetramethyl-1,3,2-dioxaborolan-2-yl)-1*H*-indole (310 mg, 1.28 mmol) and XPhos Pd G2 (100 mg, 0.13 mmol) were added. The vial was sealed and purged with 3 vacuum/nitrogen cycles again and subsequently heated at 90 °C in the microwave for an additional 15 min. The reaction was partitioned between EtOAc (60 mL) and water (60 mL), the layers were separated, and the aqueous was extracted with EtOAc (3 x 60 mL). The combined organic extracts were dried by passing through a hydrophobic frit and concentrated under reduced pressure. The residue was dissolved in a minimum amount of DCM and purified by automated column chromatography on silica gel eluting with 0-15% MeOH/EtOAc over 18 CV. The product-containing fractions were concentrated under reduced pressure to afford the title compound as a yellow solid (315 mg, 65% yield).

LCMS (Method A): t_R = 0.97 Min, $[M+H]^+$ = 764.37, purity 97%; 1H NMR (400 MHz, Chloroform- d) δ 8.99 (d, J = 0.9 Hz, 1H), 8.64 (bs, 1H), 8.63 – 8.61 (m, 1H), 8.35 (d, J = 1.3 Hz, 1H), 7.87 – 7.81 (m, 2H), 7.72 – 7.65 (m, 2H), 7.60 – 7.53 (m, 1H), 7.53 – 7.41 (m, 3H), 7.38 – 7.30 (m, 3H), 7.13 (s, 2H), 6.79 – 6.73 (m, 1H), 4.44 (s, 2H), 3.75 – 3.67 (m, 2H), 2.78 – 2.47 (m, 9H), 1.31 (s, 6H); ^{13}C NMR (101 MHz, Chloroform- d) δ 167.2, 160.0, 149.4, 143.2, 142.1, 141.7, 137.7, 136.5, 134.4, 134.2, 132.8, 132.2, 129.4, 127.8, 127.7, 126.4, 125.5, 124.2, 123.6, 122.5, 121.8, 121.0, 120.6, 114.3, 111.5, 101.9, 85.3, 77.4, 54.1, 53.1, 52.3, 46.7, 27.5, 27.4; ν_{max} (DCM): 3416, 2981, 2923, 2817, 1771, 1724, 1601, 1389, 1449, 1342, 1210, 1177, 1117, 944 cm^{-1} ; HRMS (Method A): calcd. for $C_{43}H_{38}N_7O_5S$ $[M+H]^+$ 764.2655; found 764.2661.



(*E*)-Cyclooct-4-en-1-yl (4-(4-((2-(6-(1*H*-indol-4-yl)-1*H*-indazol-4-yl)oxazol-5-yl)methyl)piperazin-1-yl)-4-methylpent-2-yn-1-yl)carbamate (44)

Phthalimide deprotection:

To a stirred solution of 2-(4-(4-((2-(6-(1*H*-indol-4-yl)-1-(phenylsulfonyl)-1*H*-indazol-4-yl)oxazol-5-yl)methyl)piperazin-1-yl)-4-methylpent-2-yn-1-yl)isoindoline-1,3-dione (304 mg, 0.40 mmol) in Tetrahydrofuran (THF) (10 mL) was added hydrazine monohydrate (42 μ L, 0.56 mmol) and the reaction mixture was stirred at room temperature under N_2 atmosphere for 1 h. The reaction mixture was then warmed to 45 $^{\circ}C$ and stirred for an additional 90 min. Hydrazine monohydrate (40 μ L) was added and the reaction mixture was stirred at 45 $^{\circ}C$ for an additional hour. Hydrazine monohydrate (20 μ L, 0.53 mmol) was added and the reaction mixture was stirred at 45 $^{\circ}C$ for an additional 90 min. The reaction was then cooled to room temperature and stirred overnight. Volatiles were removed under reduced pressure to afford the crude

primary amine as a pale pink solid. The crude was immediately taken forward in the next step without any further purification.

TCO installation:

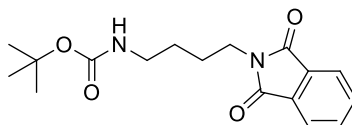
To a stirred solution of crude 4-(4-((2-(6-(1*H*-indol-4-yl)-1-(phenylsulfonyl)-1*H*-indazol-4-yl)oxazol-5-yl)methyl)piperazin-1-yl)-4-methylpent-2-yn-1-amine **91** in DMF (6 mL) was added (*E*)-cyclooct-4-en-1-yl (4-nitrophenyl) carbonate (85 mg, 0.29 mmol) followed by DIPEA (61 μ L, 0.35 mmol). The reaction was stirred at room temperature for 30 min. More (*E*)-cyclooct-4-en-1-yl (4-nitrophenyl) carbonate (78 mg, 0.27 mmol) and DIPEA (47 μ L, 0.27 mmol) were added and the reaction was stirred at room temperature under for an additional 30 min. The reaction mixture was partitioned between EtOAc (20 mL) and water (20 mL). The layers were separated and the aqueous phase was further extracted with EtOAc (3 x 20 mL). The combined organic extracts were washed with a 5% aqueous LiCl solution (3 x 30 mL). The organics were dried by passing through a hydrophobic frit and concentrated under reduced pressure. The crude was dissolved in a minimum amount of DCM and purified by automated column chromatography on silica gel eluting with 0-20% MeOH/EtOAc. The product containing fractions were concentrated under reduced pressure to afford the benzene sulfonyl intermediate as a yellow oil (376 mg) which still contained impurities.

Benzenesulfonyl deprotection:

The compound was immediately dissolved in MeOH (5 mL) and a 1 M aqueous NaOH solution (1 mL) was added. The reaction mixture was stirred at room temperature for 1 h. Solvent was removed under reduced pressure and the residue was partitioned between EtOAc (15 mL) and water (15 mL). The layers were separated and the aqueous was further extracted with EtOAc (3 x 15 mL). The combined organics extracts were dried by passing through a hydrophobic frit and concentrated under reduced pressure. The crude was taken in MeOH/DMSO (1:1, 1 mL) and purified by Mass Directed Automated Preparative HPLC (Method B). The product-containing fraction was concentrated under reduced pressure to remove most of the acetonitrile

and then lyophilised to afford the title compound as an off-white solid (26.9 mg, 11% yield over 3 steps).

LCMS (Method B): $t_R = 1.25$ Min, $[M+H]^+ = 646.46$, purity 99%; 1H NMR (600 MHz, Methanol- d_4) δ 8.70 (s, 1H), 8.23 (d, $J = 1.2$ Hz, 1H), 7.95 (s, 1H), 7.47 – 7.43 (m, 1H), 7.33 (d, $J = 3.1$ Hz, 1H), 7.27 (s, 1H), 7.25 – 7.22 (m, 2H), 6.67 (d, $J = 3.1$ Hz, 1H), 5.65 – 5.51 (m, 1H), 5.36 (ddd, $J = 15.5, 11.3, 3.3$ Hz, 1H), 4.76 – 4.70 (m, 1H), 3.97 – 3.80 (m, 2H), 3.77 (s, 2H), 2.83 – 2.59 (m, 8H), 2.21 – 2.05 (m, 3H), 2.06 – 1.90 (m, 1H), 1.81 – 1.60 (m, 2H), 1.61 – 1.40 (m, 2H), 1.34 (s, 6H), 1.12 – 1.06 (m, 1H). 3H not observed (exchangeable); ^{13}C NMR (151 MHz, Methanol- d_4) δ 163.3, 158.6, 150.5, 143.2, 142.5, 138.4, 136.6, 135.9, 134.5, 132.9, 129.2, 128.0, 126.8, 123.13, 123.09, 121.1, 120.8, 120.1, 113.3, 112.6, 101.9, 84.9, 82.7, 72.2, 55.8, 54.2, 53.1, 48.0, 42.2, 35.6, 34.0, 31.6, 31.1, 29.4, 28.2; $\nu_{max}(\text{neat})$: 3270, 2927, 2832, 2817, 1701, 1618, 1504, 1340, 1217, 1173, 1122, 1042, 942, 750 cm^{-1} ; HRMS (Method A): calcd. for $C_{38}H_{43}N_7O_3$ $[M+H]^+ 646.3506$; found 646.3502.

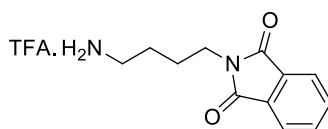


***tert*-Butyl (4-(1,3-dioxoisindolin-2-yl)butyl)carbamate (88)**

To a stirred solution of *tert*-butyl (4-aminobutyl)carbamate (2.91 g, 15.46 mmol) in toluene (40 mL) was added phthalic anhydride (2.29 g, 15.46 mmol) and the reaction mixture was stirred under reflux using a Dean–Stark trap for 3 h. After 3 h, the reaction mixture was cooled to room temperature and toluene was removed under reduced pressure. The residue was diluted with DCM (80 mL), washed with a 0.5 M aqueous HCl (60 mL), water (60 mL) and then a saturated aqueous sodium bicarbonate solution (60 mL). The organic layer was then dried by passing through a hydrophobic frit and concentrated under reduced pressure to afford the title compound as a white solid which was dried in a vacuum oven (40 °C) for 48 h (4.53 g, 92% yield).

LCMS (Method A): $t_R = 1.09$ Min, $[M+Na]^+ = 341.09$, purity 100%; 1H NMR (400 MHz, Chloroform- d) δ 7.86 – 7.82 (m, 2H), 7.74 – 7.67 (m, 2H), 4.55 (bs, 1H), 3.70

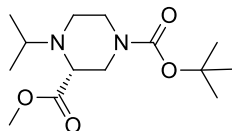
(t, $J = 7.1$ Hz, 2H), 3.16 (q, $J = 6.4$ Hz, 2H), 1.78 – 1.63 (m, 2H), 1.59 – 1.48 (m, 2H), 1.43 (s, 9H); ^{13}C NMR (101 MHz, Chloroform- d) δ 168.4, 156.0, 134.0, 132.2, 123.3, 79.2, 40.1, 37.6, 28.4, 27.5, 26.0; ν_{max} (neat): 3374, 2950, 1704, 1681, 1528, 1438, 1399, 1271, 1171, 1052, 718, 530 cm^{-1} ; HRMS (Method A): calcd. for $\text{C}_{17}\text{H}_{22}\text{N}_2\text{O}_4\text{Na}$ $[\text{M}+\text{Na}]^+$ 341.1477; found 341.1476.



2-(4-Aminobutyl)isoindoline-1,3-dione, trifluoroacetic acid salt (89)

To a stirred solution of *tert*-butyl (4-(1,3-dioxoisoindolin-2-yl)butyl)carbamate (4.41 g, 13.85 mmol) in DCM (25 mL) was added TFA (4 mL). The reaction was stirred at room temperature under N_2 atmosphere for 2.5 h. 2 mL TFA were added and the reaction was stirred overnight. Volatiles were removed under reduced pressure; the crude residue was taken in dioxane (2 x 10 mL) and solvent were removed under reduced pressure. The crude was dried under vacuum for 3 h to afford a light orange oil to which was added Et_2O (20 mL) which led to a white solid precipitating out. The solid particles were isolated by vacuum filtration and washed with more Et_2O (40 mL). The solid was dried under vacuum to afford the crude title compound (TFA salt) as a white solid (4.50 g, 98%).

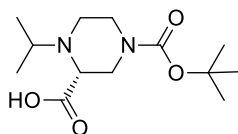
LCMS (Method A): $t_{\text{R}} = 0.36$ Min, $[\text{M}+\text{H}]^+ = 219.21$, purity 95%; ^1H NMR (400 MHz, DMSO- d_6) δ 7.91 – 7.79 (m, 7H), 3.61 (t, $J = 6.5$ Hz, 2H), 2.89 – 2.74 (m, 2H), 1.71 – 1.61 (m, 2H), 1.61 – 1.50 (m, 2H); ^{13}C NMR (101 MHz, DMSO- d_6) δ 168.0, 134.4, 131.6, 123.0, 38.4, 36.8, 25.0, 24.5; ^{19}F NMR (376 MHz, DMSO- d_6) δ -73.95; ν_{max} (neat): 3406, 3098, 2933, 2870, 1771, 1706, 1615, 1550, 1469, 1127, 720 cm^{-1} ; HRMS (Method A): calcd. for $\text{C}_{12}\text{H}_{15}\text{N}_2\text{O}_2$ $[\text{M}+\text{H}]^+$ 219.1134; found 219.1134.



(*R*)-1-*tert*-Butyl 3-methyl 4-isopropylpiperazine-1,3-dicarboxylate (91)

To a stirred solution of 1-(*tert*-butyl) 3-methyl (*R*)-piperazine-1,3-dicarboxylate (3.01 g, 12.3 mmol) in DCM (12 mL) was added acetone (7.3 mL, 99.0 mmol) and acetic acid (353 μ L, 6.16 mmol). The resulting mixture was stirred at room temperature under N_2 atmosphere for 20 min after which STAB (3.13 g, 14.8 mmol) was added in one portion. The reaction was stirred at room temperature for 48 h. The reaction was partitioned between DCM (20 mL) and a saturated aqueous sodium bicarbonate solution. The layers were separated and the aqueous was extracted with DCM (2 x 45 mL). The combined organic extracts were dried by passing through a hydrophobic frit. Florisil was added and the solvent was removed under reduced pressure to adsorb the compound. Purification was carried out by automated column chromatography on silica gel eluting with 10-70% EtOAc/cyclohexane over 20 CV. The product-containing fractions were identified by TLC (cyclohexane/EtOAc 3:7 $KMnO_4$ stain) and concentrated under reduced pressure to afford the title compound as an orange oil (2.91 g, 82% yield).

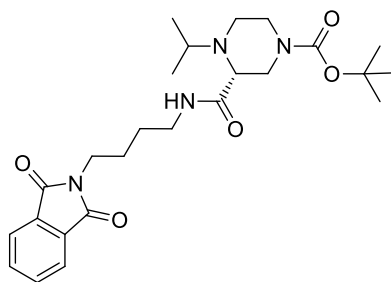
1H NMR (400 MHz, Chloroform-*d*) δ 3.70 (s, 3H), 3.65 – 3.53 (m, 2H), 3.55 – 3.35 (m, 3H), 3.01 – 2.84 (m, 2H), 2.51 – 2.33 (m, 1H), 1.43 (s, 9H), 1.10 (d, J = 6.5 Hz, 3H), 0.96 (d, J = 6.5 Hz, 3H); ^{13}C NMR (101 MHz, Chloroform-*d*) δ 172.4, 154.4, 80.0, 60.4, 51.8 (2C), 46.7, 43.5, 42.8, 28.5, 21.1, 16.8; ν_{max} (DCM): 2979, 2864, 1738, 1697, 1419, 1366, 1293, 1158, 1125, 869, 759 cm^{-1} .



(*R*)-4-(*tert*-Butoxycarbonyl)-1-isopropylpiperazine-2-carboxylic acid (92)

To a stirred solution of 1-(*tert*-butyl) 3-methyl (*R*)-4-isopropylpiperazine-1,3-dicarboxylate (1.16 g, 4.05 mmol) in methanol (12 mL) cooled to 0 °C was added sodium hydroxide 2 M in water (12.2 mL, 24.30 mmol) and the reaction mixture was allowed to warm to room temperature and was stirred overnight under an atmosphere of N₂. Methanol was removed under reduced pressure and the pH of aqueous was adjusted to 4-5 with a 2 M aqueous HCl solution (~10 mL). The aqueous was concentrated under reduced pressure to about 5 mL which were lyophilized overnight. The obtained solid (1.7 g) was suspended in DCM (15 mL) and filtered by vacuum filtration. The solid was washed with more DCM (30 mL) and EtOAc (20 mL). The filtrate was concentrated under reduced pressure to afford the title compound as a pale orange solid (0.71 g, 64% yield).

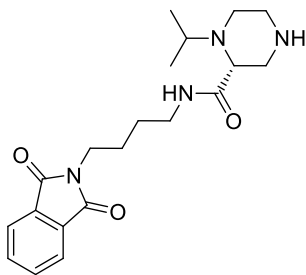
¹H NMR (400 MHz, Chloroform-*d*) 4.53 – 4.35 (m, 1H), 4.28 – 4.06 (m, 1H), 4.00 (sept, *J* = 6.7 Hz, 1H), 3.69 – 3.55 (m, 1H), 3.74 – 3.51 (m, 1H), 3.51 – 3.33 (m, 2H), 3.33 – 3.17 (m, 1H), 2.87 – 2.65 (m, 1H), 1.46 (s, 9H), 1.43 (d, *J* = 6.7 Hz, 3H), 1.26 (d, *J* = 6.7 Hz, 3H). 1H not observed (exchangeable); ¹³C NMR (101 MHz, Chloroform-*d*) δ 167.9, 153.8, 81.4, 64.5, 55.4, 45.1, 43.2, 40.3, 28.4, 18.5, 15.1; ν_{max}(neat): 2984, 2859, 2204, 1691, 1424, 1173, 1110, 1052, 758, 607, 554 cm⁻¹.



(*R*)-tert-Butyl 3-((4-(1,3-dioxoisindolin-2-yl)butyl)carbamoyl)-4-isopropylpiperazine-1-carboxylate (93)

To a stirred solution of (*R*)-4-(*tert*-butoxycarbonyl)-1-isopropylpiperazine-2-carboxylic acid (531 mg, 1.95 mmol) in DMF (10 mL) was added HBTU (815 mg, 2.15 mmol), HOBT hydrate (382 mg, 2.15 mmol), DIPEA (1.4 mL, 7.80 mmol) and 2-(4-aminobutyl)isoindoline-1,3-dione.TFA salt (777 mg, 2.34 mmol). The resulting solution was stirred at room temperature under N₂ atmosphere overnight. The reaction mixture was partitioned between EtOAc (20 mL) and water (15 mL) and the layers were separated. The aqueous phase was further extracted with EtOAc (3 x 20 mL). The combined organic extracts were washed with a 5% aqueous LiCl solution (3 x 20 mL) and dried by passing through a hydrophobic frit. Florisil was added and solvents were removed under reduced pressure to adsorb the compound. Purification was carried out by automated column chromatography on silica gel eluting with 20-90% EtOAc/cyclohexane over 20 CV. The product-containing fractions were combined and concentrated under reduced pressure. The residue was dried on a high vacuum line overnight to afford the title compound as a white fluffy solid (842 mg, 91% yield).

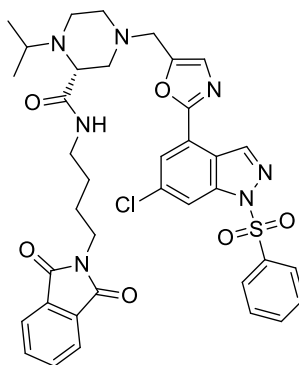
LCMS (Method A): t_R = 0.71 Min, $[M+H]^+$ = 473.26, purity 100%; ¹H NMR (400 MHz, Chloroform-*d*) δ 7.87 – 7.80 (m, 2H), 7.74 – 7.68 (m, 2H), 7.01 (bs, 1H), 3.93 – 3.75 (m, 2H), 3.70 (t, J = 7.1 Hz, 2H), 3.43 – 3.14 (m, 3H), 3.11 – 2.98 (m, 1H), 2.91 (sept, J = 6.5 Hz, 1H), 2.82 – 2.70 (m, 2H), 2.56 (dd, J = 13.2, 9.9 Hz, 1H), 1.78 – 1.65 (m, 2H), 1.62 – 1.49 (m, 2H), 1.43 (s, 9H), 1.09 (d, J = 6.7 Hz, 3H), 0.96 (d, J = 6.5 Hz, 3H); ¹³C NMR (101 MHz, Chloroform-*d*) δ 172.4, 168.5, 154.7, 134.1, 132.3, 123.4, 80.2, 62.6, 52.1, 45.4, 43.4, 41.7, 38.7, 37.6, 28.5, 27.2, 26.2, 20.6, 15.5; ν_{max} (neat): 3332, 2971, 1771, 1707, 1664, 1397, 1366, 1137, 838, 720, 557, 530 cm⁻¹; HRMS (Method A): calcd. for C₂₅H₃₇N₄O₅ $[M+H]^+$ 473.2764; found 473.2766.



(R)-N-(4-(1,3-Dioxisoindolin-2-yl)butyl)-1-isopropylpiperazine-2-carboxamide (94)

To a stirred solution of *tert*-butyl (*R*)-3-((4-(1,3-dioxisoindolin-2-yl)butyl)carbamoyl)-4-isopropylpiperazine-1-carboxylate (798 mg, 1.69 mmol) in DCM (8 mL) was added TFA (2 mL) and the resulting mixture was stirred at room temperature under an atmosphere of N₂ for 3 h. Volatiles were then removed under reduced pressure. The crude residue was partitioned between DCM (10 mL) and a saturated aqueous sodium bicarbonate solution (15 mL). The layers were separated and the aqueous was extracted with DCM (3 x 20 mL). The combined organic extracts were washed with brine (30 mL) and dried by passing through a hydrophobic frit to afford the crude title compound as a yellow oil (549 mg, 87% yield).

LCMS (Method B): *t*_R = 0.80 Min, [M+H]⁺ = 373.21, purity 95%; ¹H NMR (400 MHz, Chloroform-*d*) δ 7.87 – 7.79 (m, 2H), 7.74 – 7.66 (m, 2H), 6.99 (bs, 1H), 3.70 (t, *J* = 7.1 Hz, 2H), 3.39 – 3.21 (m, 1H), 3.21 – 3.12 (m, 3H), 3.03 – 2.95 (m, 1H), 2.89 (sept, *J* = 6.7 Hz, 1H), 2.83 – 2.70 (m, 3H), 2.60 (bs, 1H), 2.46 – 2.37 (m, 1H), 1.77 – 1.66 (m, 2H), 1.62 – 1.51 (m, 2H), 1.08 (d, *J* = 6.7 Hz, 3H), 0.97 (d, *J* = 6.7 Hz, 3H); ¹³C NMR (101 MHz, Chloroform-*d*) δ 172.7, 168.5, 134.1, 132.3, 123.4, 63.8, 51.6, 49.6, 45.6, 42.9, 38.5, 37.7, 27.2, 26.2, 21.1, 15.0; *v*_{max}(DCM): 3277, 2963, 2859, 1769, 1711, 1649, 1533, 1398, 1052, 847, 717 cm⁻¹; HRMS (Method A): calcd. for C₂₀H₂₉N₄O₃ [M+H]⁺ 373.2240; found 373.2244.

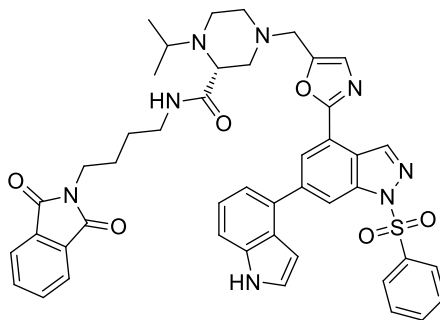


(R)-4-((2-(6-Chloro-1-(phenylsulfonyl)-1*H*-indazol-4-yl)oxazol-5-yl)methyl)-*N*-(4-(1,3-dioxisoindolin-2-yl)butyl)-1-isopropylpiperazine-2-carboxamide (95)

To a stirred suspension of 2-(6-chloro-1-(phenylsulfonyl)-1*H*-indazol-4-yl)oxazole-5-carbaldehyde (250 mg, 0.65 mmol) in DCM (5 mL) was added (*R*)-*N*-(4-(1,3-dioxisoindolin-2-yl)butyl)-1-isopropylpiperazine-2-carboxamide (288 mg, 0.77 mmol) and acetic acid (18 μ L, 0.32 mmol). The resulting mixture was stirred at room temperature under an atmosphere of N₂ for 30 min after which STAB (178 mg, 0.84 mmol) was added. The reaction was stirred at room temperature under an atmosphere of N₂ overnight. The reaction was partitioned between DCM (15 mL) and a saturated aqueous sodium bicarbonate solution (10 mL). The layers were separated, the aqueous was extracted with DCM (3 x 15 mL). The combined organic extracts were dried by passing through a hydrophobic frit. Florisil was added and the solvent was removed under reduced pressure to adsorb the compound. Purification was carried out by automated column chromatography on silica gel eluting with 0-30% MeOH/EtOAc over 20 CV. The product-containing fractions were concentrated under reduced pressure to afford the title compound as a pale yellow solid (354 mg, 74% yield).

LCMS (Method A): t_R = 0.93 Min, $[M+H]^+$ = 744.18, purity 95%; ¹H NMR (400 MHz, Chloroform-*d*) δ 8.88 (d, J = 0.9 Hz, 1H), 8.29 (dd, J = 1.6, 0.9 Hz, 1H), 8.03 – 7.97 (m, 2H), 7.91 (d, J = 1.6 Hz, 1H), 7.85 – 7.76 (m, 2H), 7.72 – 7.64 (m, 2H), 7.63 – 7.54 (m, 1H), 7.54 – 7.45 (m, 2H), 7.13 (s, 1H), 6.96 (bs, 1H), 3.72 – 3.60 (m, 4H), 3.39 – 3.18 (m, 3H), 2.97 – 2.83 (m, 2H), 2.78 – 2.71 (m, 2H), 2.62 – 2.53 (m, 1H), 2.40 – 2.26 (m, 2H), 1.78 – 1.62 (m, 2H), 1.60 – 1.47 (m, 2H), 1.06 (d, J = 6.7 Hz, 3H), 0.96 (d, J = 6.5 Hz, 3H); ¹³C NMR (101 MHz, CDCl₃) δ 172.3, 168.4, 158.8,

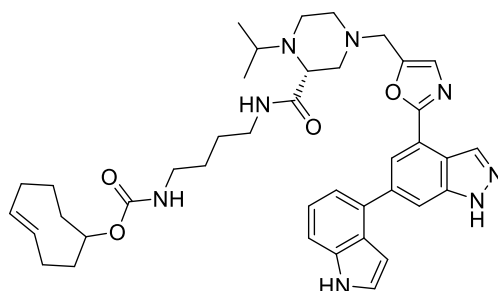
149.5, 141.8, 141.4, 137.4, 135.9, 134.7, 134.1, 132.2, 129.5, 128.2, 127.8, 123.3, 121.7, 121.3, 114.6, 63.0, 56.3, 52.7, 52.3, 51.1, 42.1, 38.5, 37.6, 27.2, 26.2, 21.2, 15.2; ν_{max} (neat): 3219.9, 3068, 2979, 1707, 1643, 1371, 1167, 921, 722, 607, 560 cm^{-1} ; HRMS (Method A): calcd. for $\text{C}_{37}\text{H}_{39}\text{N}_7\text{O}_6\text{S}\text{Cl}$ $[\text{M}+\text{H}]^+$ 744.2371; found 744.2371.



(*R*)-4-((2-(6-(1*H*-Indol-4-yl)-1-(phenylsulfonyl)-1*H*-indazol-4-yl)oxazol-5-yl)methyl)-*N*-(4-(1,3-dioxoisindolin-2-yl)butyl)-1-isopropylpiperazine-2-carboxamide (96)

In a microwave vial was charged indole-4-boronic acid pinacol ester (122 mg, 0.50 mmol), XPhos Pd G2 (33 mg, 0.04 mmol) and sodium carbonate (132 mg, 1.25 mmol). A suspension of (*R*)-4-((2-(6-chloro-1-(phenylsulfonyl)-1*H*-indazol-4-yl)oxazol-5-yl)methyl)-*N*-(4-(1,3-dioxoisindolin-2-yl)butyl)-1-isopropylpiperazine-2-carboxamide (310 mg, 0.42 mmol) in 1,4-dioxane (4 mL) was added to the flask along with water (0.5 mL). The vial was sealed and the atmosphere was purged by 3 vacuum/nitrogen cycles. The reaction was heated in the microwave at 90 °C for 1 h. The reaction was then partitioned between water (15 mL) and EtOAc (20 mL), the layers were separated and the aqueous was extracted with EtOAc (3 x 20 mL). The combined organic layers were dried by passing through a hydrophobic frit and concentrated under reduced pressure. The residue was re-suspended in DCM and Florisil was added. Solvents were removed under reduced pressure to adsorb the compound. Purification was carried out by automated column chromatography on silica gel eluting with 0-30% MeOH/EtOAc over 25 CV. The product-containing fractions were concentrated under reduced pressure to afford the title compound as a light yellow solid (226 mg, 66% yield).

LCMS (Method A): $t_R = 0.95$ Min, $[M+H]^+ = 825.34$, purity 96%; 1H NMR (400 MHz, Chloroform-*d*) δ 8.97 (d, $J = 0.9$ Hz, 1H), 8.67 (bs, 1H), 8.61 (dd, $J = 1.3, 0.9$ Hz, 1H), 8.31 (d, $J = 1.3$ Hz, 1H), 8.07 – 7.98 (m, 2H), 7.83 – 7.74 (m, 2H), 7.70 – 7.63 (m, 2H), 7.60 – 7.53 (m, 1H), 7.52 – 7.42 (m, 3H), 7.38 – 7.29 (m, 3H), 7.14 (s, 1H), 6.98 (bs, 1H), 6.78 – 6.72 (m, 1H), 3.69 (s, 2H), 3.61 (t, $J = 7.2$ Hz, 2H), 3.35 – 3.22 (m, 2H), 3.22 – 3.10 (m, 1H), 2.97 – 2.83 (m, 2H), 2.78 – 2.69 (m, 2H), 2.62 – 2.51 (m, 1H), 2.40 – 2.31 (m, 2H), 1.68 – 1.57 (m, 2H), 1.54 – 1.41 (m, 2H), 1.04 (d, $J = 6.7$ Hz, 3H), 0.96 (d, $J = 6.7$ Hz, 3H); ^{13}C NMR (101 MHz, $CDCl_3$) δ 172.4, 168.4, 160.1, 148.9, 143.2, 142.1, 141.7, 137.7, 136.5, 134.4, 134.1, 132.7, 132.2, 129.4, 128.0, 127.7, 126.4, 125.5, 124.2, 123.3, 122.5, 121.8, 120.8, 120.6, 114.4, 111.6, 101.8, 63.0, 56.3, 52.5, 52.3, 51.1, 42.1, 38.4, 37.6, 27.2, 26.2, 21.2, 15.4; $\nu_{max}(neat)$: 3268, 2965, 2828, 2833, 1766, 1709, 1655, 1610, 1535, 1373, 1172, 1091, 729 cm^{-1} ; HRMS (Method A): calcd. for $C_{45}H_{45}N_8O_6S$ $[M+H]^+ 825.3183$; found 825.3192.



(*E*)-cyclooct-4-en-1-yl 4-((*R*)-4-((2-(6-(1*H*-indol-4-yl)-1*H*-indazol-4-yl)oxazol-5-yl)methyl)-1-isopropylpiperazine-2-carboxamido)butyl)carbamate (41)

Phthalimide deprotection:

To a stirred solution of (*R*)-4-((2-(6-(1*H*-indol-4-yl)-1-(phenylsulfonyl)-1*H*-indazol-4-yl)oxazol-5-yl)methyl)-*N*-(4-(1,3-dioxoisindolin-2-yl)butyl)-1-isopropylpiperazine-2-carboxamide (194 mg, 0.24 mmol) in THF (4 mL) was added hydrazine hydrate (36 μ L, 0.47 mmol). The reaction mixture was stirred at room temperature for 3 h under N_2 atmosphere. Reaction was then warmed to 40 $^{\circ}C$ and stirred overnight. More hydrazine hydrate (18 μ L, 0.24 mmol) was added and the reaction was stirred at 40 $^{\circ}C$ for an additional 4 h. The reaction was cooled to room temperature. Acetone (1 mL) was added and the reaction was stirred at room

temperature for 15 min. Volatiles were removed under reduced pressure. The residue was taken up in EtOH (5 mL), the precipitate was filtered by vacuum filtration and washed with more EtOH (15 mL). The filtrate was concentrated under reduced pressure to give the crude title compound as a brown solid (108 mg) which was used directly into the next step.

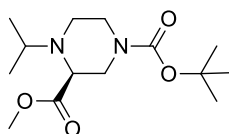
TCO installation:

To a stirred solution of crude (*R*)-4-((2-(6-(1*H*-indol-4-yl)-1-(phenylsulfonyl)-1*H*-indazol-4-yl)oxazol-5-yl)methyl)-*N*-(4-aminobutyl)-1-isopropylpiperazine-2-carboxamide (74 mg, 0.11 mmol) in DMF (3 mL) was added (*E*)-cyclooct-4-en-1-yl (4-nitrophenyl) carbonate (34 mg, 0.12 mmol) and DIPEA (47 μ L, 0.27 mmol). The reaction mixture was stirred at 40 °C for 1.5 h under an atmosphere of N₂. Then, the reaction mixture was cooled to room temperature, partitioned between EtOAc (10 mL) and water (8 mL). The layers were separated and the aqueous was extracted with EtOAc (3 x 10 mL). The combined organics were washed with a 5% aqueous LiCl solution (3 x 15 mL), dried by passing through a hydrophobic frit and concentrated under reduced pressure.

Benzenesulfonyl deprotection:

The crude residue was immediately suspended in MeOH (3 mL) and a 2 M aqueous NaOH solution (0.5 mL) was added. The reaction mixture was stirred at room temperature for 30 min. Methanol was then removed under reduced pressure. The crude was partitioned between EtOAc (5 mL) and water (5 mL). The layers were separated and the aqueous was extracted with more EtOAc (3 x 5 mL). The combined organic extracts were dried by passing through a hydrophobic frit and concentrated under reduced pressure. The residue was suspended in MeOH/DMSO (1:1, 2 mL) and purified by Mass Directed Automated Preparative HPLC (Method A, 2 x 1 mL injection). The product-containing fractions were partially concentrated under reduced pressure and lyophilized to give the title compound as a white solid (18 mg, 24% over 2 steps).

LCMS (Method B): $t_R = 1.22$, $[M+H]^+ = 707.58$, purity 100%; 1H NMR (400 MHz, Methanol- d_4) δ 8.67 (s, 1H), 8.23 (d, $J = 1.2$ Hz, 1H), 7.95 (dd, $J = 1.2, 1.0$ Hz, 1H), 7.48 – 7.44 (m, 1H), 7.34 (d, $J = 3.2$ Hz, 1H), 7.27 (s, 1H), 7.26 – 7.22 (m, 2H), 6.69 – 6.65 (m, 1H), 5.68 – 5.56 (m, 1H), 5.54 – 5.43 (m, 1H), 4.76 (s, 1H), 3.88 – 3.73 (m, 2H), 3.28 (d, $J = 3.3$ Hz, 1H), 3.24 – 3.07 (m, 2H), 3.07 – 2.98 (m, 1H), 2.96 – 2.80 (m, 5H), 2.60 – 2.49 (m, 1H), 2.50 – 2.38 (m, 2H), 2.38 – 2.25 (m, 1H), 2.20 (d, $J = 14.2$ Hz, 3H), 2.01 (d, $J = 11.9$ Hz, 1H), 1.87 – 1.52 (m, 3H), 1.50 – 1.34 (m, 4H), 1.28 – 1.14 (m, 2H), 1.09 (d, $J = 6.7$ Hz, 3H), 0.94 (d, $J = 6.7$ Hz, 3H). 4H not observed (exchangeable); ^{13}C NMR (101 MHz, Methanol- d_4) δ 174.1, 162.9, 158.7, 150.0, 142.9, 142.1, 138.3, 136.3, 135.3, 134.1, 132.5, 128.8, 127.6, 126.5, 122.7 (2C), 120.6, 120.4, 119.6, 113.0, 112.2, 101.5, 71.2, 64.8, 57.2, 53.5, 52.6, 51.7, 42.9, 42.0, 41.2, 39.8, 35.2, 33.7, 30.8, 29.0, 28.4, 27.7, 21.1, 14.3; $\nu_{max}(\text{neat})$: 3269, 2929, 1655, 1523, 1439, 1340, 1218, 1034, 945, 755, 554 cm^{-1} ; HRMS (Method A): calcd. for $C_{40}H_{51}N_8O_4$ $[M+H]^+ 707.4033$; found 707.4032.

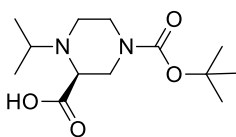


(S)-1-*tert*-Butyl 3-methyl 4-isopropylpiperazine-1,3-dicarboxylate (99)

To a stirred solution of 1-(*tert*-butyl) 3-methyl (*S*)-piperazine-1,3-dicarboxylate (3.05 g, 12.49 mmol) in DCM (12 mL) was added acetone (7.34 mL, 100 mmol) and acetic acid (357 μL , 6.24 mmol). The resulting mixture was stirred at room temperature under N_2 atmosphere for 20 min after which STAB (3.18 g, 14.98 mmol) was added in one portion. The reaction was stirred overnight at room temperature. The reaction was partitioned between DCM (20 mL) and a saturated aqueous sodium bicarbonate solution. The layers were separate and the aqueous was extracted with DCM (2 x 45 mL). The combined organic extracts were dried by passing through a hydrophobic frit. Florisil was added and the solvent was removed under reduced pressure to adsorb the compound. Purification was carried out by automated column chromatography on silica gel eluting with 10-70% EtOAc/cyclohexane over 20 CV. The product-containing fractions were identified by TLC (cyclohexane/EtOAc 3:7 $KMnO_4$ stain)

and concentrated under reduced pressure to afford the title compound as an orange oil (3.07 g, 86% yield).

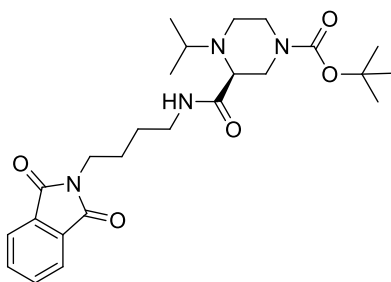
^1H NMR (400 MHz, Chloroform-*d*) δ 3.63 (s, 3H), 3.58 – 3.48 (m, 2H), 3.42 – 3.29 (m, 3H), 2.97 – 2.76 (m, 2H), 2.42 – 2.31 (m, 1H), 1.36 (s, 9H), 1.03 (d, J = 6.6 Hz, 3H), 0.88 (d, J = 6.6 Hz, 3H); ^{13}C NMR (101 MHz, Chloroform-*d*) δ 172.2, 154.2, 79.8, 60.1, 51.69, 51.65, 46.6, 43.7, 42.7, 28.3, 20.9, 16.8; ν_{max} (DCM): 2971, 2870, 1741, 1695, 1456, 1365, 1286, 1161 cm^{-1} ; HRMS (Method A): calcd. for $\text{C}_{14}\text{H}_{27}\text{N}_2\text{O}_4$ $[\text{M}+\text{H}]^+$ 287.1971; found 287.1971.



(*S*)-4-(*tert*-Butoxycarbonyl)-1-isopropylpiperazine-2-carboxylic acid (100)

To a stirred solution of 1-(*tert*-butyl) 3-methyl (*S*)-4-isopropylpiperazine-1,3-dicarboxylate (2.17 g, 7.58 mmol) in MeOH (20 mL) cooled to 0 °C was added a 2 M aqueous NaOH solution (18.9 mL, 37.90 mmol) and the reaction mixture was allowed to warm to room temperature and was stirred overnight under an atmosphere of N_2 . Methanol was removed under reduced pressure and the pH of aqueous was adjusted to 4-5 with a 2 M aqueous HCl solution (~15mL). The aqueous was concentrated under reduced pressure to about 5 mL which were lyophilized overnight. The solid obtained was suspended in DCM (20 mL) and filtered by vacuum filtration. The solid was washed with more DCM (50 mL). The filtrate was concentrated under reduced pressure to afford the title compound as a beige solid (1.72 g, 83% yield).

^1H NMR (400 MHz, Chloroform-*d*) δ 4.51 – 4.35 (m, 1H), 4.24 – 4.07 (m, 1H), 4.07 – 3.93 (m, 1H), 3.70 – 3.58 (m, 1H), 3.58 – 3.20 (m, 3H), 2.89 – 2.72 (m, 1H), 1.46 (s, 9H), 1.43 (d, J = 6.7 Hz, 3H), 1.26 (d, J = 6.7 Hz, 3H); ν_{max} (DCM): 3485, 2976, 2928, 1691, 1628, 1422, 1365, 1156 cm^{-1} ; HRMS (Method A): calcd. for $\text{C}_{13}\text{H}_{25}\text{N}_2\text{O}_4$ $[\text{M} + \text{H}]^+$ 273.1814; found 273.1812.

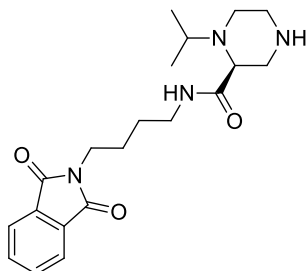


(S)-tert-Butyl 3-((4-(1,3-dioxoisindolin-2-yl)butyl)carbamoyl)-4-isopropylpiperazine-1-carboxylate (101)

To a stirred solution of (S)-4-(tert-butoxycarbonyl)-1-isopropylpiperazine-2-carboxylic acid (402 mg, 1.476 mmol) in DMF (8 mL) was added 2-(4-aminobutyl)isoindoline-1,3-dione, TFA salt (589 mg, 1.77 mmol), HBTU (672 mg, 1.77 mmol), HOBT hydrate (323 mg, 1.77 mmol) and DIPEA (0.77 mL, 4.43 mmol). The reaction mixture was stirred overnight under an atmosphere of N₂. The reaction was partitioned between EtOAc (20 mL) and water (20 mL). The layers were separated and the aqueous was extracted with EtOAc (3 x 30 mL). The combined organic layers were then washed with a 5% aqueous LiCl solution (3 x 30 mL). The organic layer was dried by passing through a hydrophobic frit. Florisil was added and the solvent was removed under reduced pressure to adsorb the compound. Purification was carried out by automated column chromatography on silica gel eluting with 10-100% EtOAc/cyclohexane over 20 CV. The product-containing fractions were concentrated under reduced pressure. The residue was then dried on a high vacuum line overnight to afford the title compound as pale yellow fluffy solid (481 mg, 69% yield).

LCMS (Method A): t_R = 0.70 Min, $[M+H]^+$ = 473.28, purity 100%; ¹H NMR (400 MHz, Chloroform-*d*) δ 7.85 – 7.79 (m, 2H), 7.74 – 7.67 (m, 2H), 7.02 (s, 1H), 3.91 – 3.74 (m, 2H), 3.70 (t, J = 7.1 Hz, 2H), 3.39 – 3.14 (m, 4H), 3.10 – 2.97 (m, 1H), 2.89 (sept, J = 6.7 Hz, 1H), 2.81 – 2.70 (m, 1H), 2.61 – 2.48 (m, 1H), 1.76 – 1.64 (m, 2H), 1.61 – 1.49 (m, 2H), 1.42 (s, 9H), 1.08 (d, J = 6.7 Hz, 3H), 0.95 (d, J = 6.7 Hz, 3H); ¹³C NMR (101 MHz, Chloroform-*d*) δ 172.4, 168.5, 154.7, 134.1, 132.3, 123.4, 80.1, 62.6, 52.0, 45.4, 43.2, 41.7, 38.6, 37.6, 28.5, 27.2, 26.2, 20.6, 15.5; ν_{max} (neat): 2971,

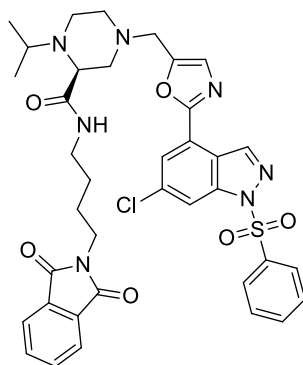
2939, 2864, 1712, 1667, 1527, 1396, 1167, 1138, 843, 721 cm^{-1} ; HRMS (Method A): calcd. for $\text{C}_{25}\text{H}_{37}\text{N}_4\text{O}_5$ $[\text{M}+\text{H}]^+$ 473.2764; found 473.2763.



(S)-N-(4-(1,3-Dioxisoindolin-2-yl)butyl)-1-isopropylpiperazine-2-carboxamide (102)

To a stirred solution of *tert*-butyl (*S*)-3-((4-(1,3-dioxisoindolin-2-yl)butyl)carbamoyl)-4-isopropylpiperazine-1-carboxylate (420 mg, 0.89 mmol) in DCM (6 mL) was added TFA (2 mL) and the resulting solution was stirred at room temperature under N_2 atmosphere for 2 h. Volatiles were then removed under reduced pressure. The crude was partitioned between DCM (15 mL) and a saturated aqueous sodium bicarbonate solution (15 mL). The layers were separated and the aqueous phase was extracted with DCM (3 x 20 mL). The combined organic extracts were dried by passing through a hydrophobic frit and concentrated under reduced pressure to afford the crude title compound as an orange oil (290 mg, 88% yield). The product was not amenable to long term storage and was used immediately in the subsequent step.

LCMS (Method A): t_R = 0.53 Min, $[\text{M}+\text{H}]^+$ = 373.22, purity 100%; ^1H NMR (400 MHz, Chloroform-*d*) δ 7.82 – 7.71 (m, 2H), 7.68 – 7.60 (m, 2H), 6.88 (bs, 1H), 3.64 (t, J = 7.1 Hz, 2H), 3.36 – 3.14 (m, 2H), 3.14 – 3.02 (m, 2H), 2.93 – 2.85 (m, 1H), 2.80 (sept, J = 6.7 Hz, 1H), 2.74 – 2.60 (m, 3H), 2.30 (ddd, J = 11.4, 10.0, 3.2 Hz, 1H), 1.74 – 1.56 (m, 2H), 1.55 – 1.44 (m, 2H), 1.01 (d, J = 6.7 Hz, 3H), 0.89 (d, J = 6.7 Hz, 3H). 1H not observed (exchangeable).

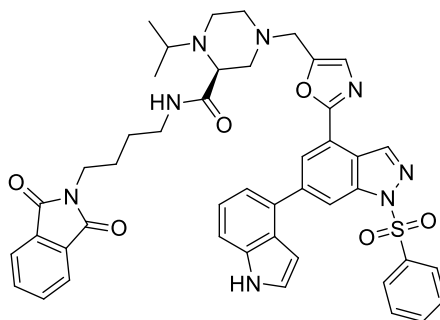


(S)-4-((2-(6-Chloro-1-(phenylsulfonyl)-1*H*-indazol-4-yl)oxazol-5-yl)methyl)-*N*-(4-(1,3-dioxisoindolin-2-yl)butyl)-1-isopropylpiperazine-2-carboxamide (103)

To a stirred solution of 2-(6-chloro-1-(phenylsulfonyl)-1*H*-indazol-4-yl)oxazole-5-carbaldehyde (360 mg, 0.93 mmol) in dry DCM (10 mL) was added (*S*)-*N*-(4-(1,3-dioxisoindolin-2-yl)butyl)-1-isopropylpiperazine-2-carboxamide (415 mg, 1.11 mmol) and acetic acid (27 μ L, 0.46 mmol). The reaction was stirred at room temperature for 30 min after which STAB (295 mg, 1.39 mmol) was added in one portion. The reaction was stirred overnight at room temperature under N₂ atmosphere. The reaction was partitioned between DCM (20 mL) and a saturated aqueous sodium bicarbonate solution (15 mL). The layers were separated and the aqueous was further extracted with DCM (3 x 15 mL). The combined organic extracts were dried by passing through a hydrophobic frit. Florisil was added and solvents were removed under reduced pressure to adsorb the compound. Purification was carried out by automated column chromatography on silica gel eluting with 0-20% MeOH/EtOAc over 20 CV. The product-containing fractions were concentrated under reduced pressure to afford the title compound as a white solid (156 mg, 23% yield).

LCMS (Method A): t_R = 0.95 Min, $[M+H]^+$ = 744.21, purity 98%; ¹H NMR (400 MHz, Chloroform-*d*) δ 8.88 (d, J = 0.9 Hz, 1H), 8.29 (dd, J = 1.7, 0.9 Hz, 1H), 8.05 – 7.96 (m, 2H), 7.91 (d, J = 1.7 Hz, 1H), 7.86 – 7.76 (m, 2H), 7.73 – 7.64 (m, 2H), 7.64 – 7.54 (m, 1H), 7.54 – 7.44 (m, 2H), 7.14 (s, 1H), 6.94 (bs, 1H), 3.73 – 3.58 (m, 4H), 3.39 – 3.16 (m, 3H), 2.98 – 2.85 (m, 2H), 2.79 – 2.72 (m, 2H), 2.63 – 2.52 (m, 1H), 2.39 – 2.25 (m, 2H), 1.77 – 1.63 (m, 2H), 1.60 – 1.48 (m, 2H), 1.06 (d, J = 6.6 Hz, 3H), 0.97 (d, J = 6.6 Hz, 3H); ¹³C NMR (101 MHz, Chloroform-*d*) δ 172.4, 168.4,

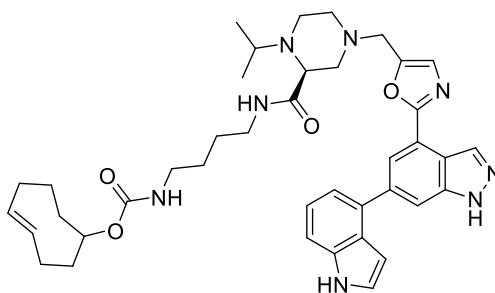
158.8, 149.5, 141.8, 141.4, 137.4, 135.9, 134.7, 134.1, 132.2, 129.6, 128.2, 127.8, 123.39, 123.32, 121.8, 121.3, 114.7, 63.0, 56.4, 52.3, 51.1, 42.1, 38.8, 38.5, 37.7, 27.2, 26.2, 21.3, 15.2; ν_{max} (neat): 3064, 2969, 2813, 1771, 1713, 1646, 1378, 1289, 1182, 925, 720 cm^{-1} ; HRMS (Method A): calcd. for $\text{C}_{37}\text{H}_{39}\text{ClN}_7\text{O}_6\text{S}$ $[\text{M}+\text{H}]^+$ 744.2371; found 744.2365.



(S)-4-((2-(6-(1H-Indol-4-yl)-1-(phenylsulfonyl)-1H-indazol-4-yl)oxazol-5-yl)methyl)-N-(4-(1,3-dioxoisindolin-2-yl)butyl)-1-isopropylpiperazine-2-carboxamide (104)

To a microwave vial was added (S)-4-((2-(6-chloro-1-(phenylsulfonyl)-1H-indazol-4-yl)oxazol-5-yl)methyl)-N-(4-(1,3-dioxoisindolin-2-yl)butyl)-1-isopropylpiperazine-2-carboxamide (259 mg, 0.35 mmol), 4-(4,4,5,5-tetramethyl-1,3,2-dioxaborolan-2-yl)-1H-indole (102 mg, 0.42 mmol), XPhos Pd G2 (5.5 mg, 6.96 μmol) and sodium carbonate (111 mg, 1.04 mmol). Solids were dissolved in 1,4-dioxane (5 mL) and water (0.5 mL) was added. The vial was sealed and purged with 3 vacuum/nitrogen cycles. The reaction was heated in the microwave for 1 h at 90 $^{\circ}\text{C}$. The reaction was then partitioned between EtOAc (25 mL) and water (25 mL). The layers were separated and the aqueous was further extracted with EtOAc (3 x 20 mL). The combined organic extracts were dried by passing through a hydrophobic frit. Florisil was added and solvents were removed under reduced pressure. The compound was purified by automated column chromatography on silica gel eluting with 0-30% MeOH/EtOAc over 20 CV. The product-containing fractions were concentrated under reduced pressure to afford the title compound as a beige solid (189 mg, 66% yield).

LCMS (Method A): t_R = 0.96 Min, $[M+H]^+$ = 825.49, purity 96%; 1H NMR (400 MHz, Chloroform- d) δ 8.97 (d, J = 0.8 Hz, 1H), 8.61 (dd, J = 1.3, 0.8 Hz, 1H), 8.58 (bs, 1H), 8.31 (d, J = 1.3 Hz, 1H), 8.06 – 7.99 (m, 2H), 7.83 – 7.75 (m, 2H), 7.71 – 7.62 (m, 2H), 7.60 – 7.54 (m, 1H), 7.52 – 7.42 (m, 3H), 7.36 – 7.31 (m, 3H), 7.14 (s, 1H), 6.97 (bs, 1H), 6.77 – 6.74 (m, 1H), 3.69 (s, 2H), 3.61 (t, J = 7.2 Hz, 2H), 3.37 – 3.22 (m, 3H), 2.97 – 2.82 (m, 2H), 2.78 – 2.67 (m, 2H), 2.61 – 2.52 (m, 1H), 2.40 – 2.28 (m, 2H), 1.72 – 1.56 (m, 2H), 1.55 – 1.42 (m, 2H), 1.04 (d, J = 6.6 Hz, 3H), 0.94 (d, J = 6.6 Hz, 3H); ^{13}C NMR (101 MHz, $CDCl_3$) δ 172.4, 168.4, 160.2, 148.9, 143.2, 142.1, 141.7, 137.7, 136.5, 134.4, 134.1, 132.8, 132.2, 129.5, 128.0, 127.8, 126.4, 125.5, 124.2, 123.3, 122.5, 121.8, 120.9, 120.7, 114.4, 111.6, 101.8, 63.0, 56.3, 52.5, 52.3, 51.2, 42.1, 38.5, 37.6, 27.2, 26.2, 21.2, 15.4; ν_{max} (neat): 3278, 2939, 2822, 1770, 1709, 1538, 1467, 1395, 1654, 1372, 1175, 726 cm^{-1} ; HRMS (Method A): calcd. for $C_{45}H_{45}N_8O_6S$ $[M+H]^+$ 825.3183; found 825.3174.



(*E*)-Cyclooct-4-en-1-yl (4-((*S*)-4-((2-(6-(1*H*-indol-4-yl)-1*H*-indazol-4-yl)oxazol-5-yl)methyl)-1-isopropylpiperazine-2-carboxamido)butyl)carbamate (42)

Phthalimide deprotection:

To a stirred solution of (*S*)-4-((2-(6-(1*H*-indol-4-yl)-1-(phenylsulfonyl)-1*H*-indazol-4-yl)oxazol-5-yl)methyl)-*N*-(4-(1,3-dioxoisindolin-2-yl)butyl)-1-isopropylpiperazine-2-carboxamide (180 mg, 0.22 mmol) in THF (5 mL) was added hydrazine hydrate (25 μ L, 0.33 mmol). The reaction was stirred at 45 °C under N_2 atmosphere for 3 h. Hydrazine monohydrate (50 μ L, 0.66 mmol) was added and the reaction was stirred at 45 °C for an additional 2 h. Hydrazine monohydrate (100 μ L, 1.32 mmol) was added and the reaction was stirred overnight at 45 °C. The reaction was cooled to room temperature and acetone (5 mL) was added. The mixture was stirred at room temperature for 15 min after which solvents were removed under reduced pressure to

afford the crude primary amine as a brown oil which was used immediately in the subsequent step.

TCO installation:

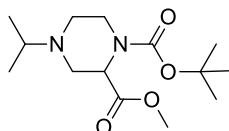
To a stirred solution of crude (*S*)-4-((2-(6-(1*H*-indol-4-yl)-1-(phenylsulfonyl)-1*H*-indazol-4-yl)oxazol-5-yl)methyl)-*N*-(4-aminobutyl)-1-isopropylpiperazine-2-carboxamide in DMF (4 mL) was added (*E*)-cyclooct-3-en-1-yl (4-nitrophenyl) carbonate (70 mg, 0.24 mmol) followed by DIPEA (76 μ L, 0.44 mmol). The mixture was stirred at room temperature under N₂ atmosphere for 1.5 h. The reaction was partitioned between EtOAc (20 mL) and water (10 mL). The layers were separated and the aqueous was further extracted with EtOAc (3 x 20 mL). The combined organic extracts were washed with a 5% aqueous LiCl solution (2 x 20 mL), then dried by passing through a hydrophobic frit and concentrated under reduced pressure.

Benzenesulfonyl deprotection:

The crude intermediate was immediately dissolved in MeOH (4 mL). To the previous solution was added a 1 M aqueous NaOH solution (0.5 mL) and the reaction was stirred at room temperature for 15 min. 0.5 mL of 1 M aqueous NaOH were added and the reaction was stirred at room temperature for an additional 20 min. Methanol was removed under reduced pressure. The residue was partitioned between EtOAc (15 mL) and water (15 mL). The layers were separated and the aqueous was further extracted with EtOAc (3 x 15 mL). The combined organic extracts were dried by passing through a hydrophobic frit and concentrated under reduced pressure. The crude was taken in MeOH/DMSO (1:1, 2 mL) and purified by Mass Directed Automated Preparative HPLC (Method B, 2 x 1 mL injection). The product-containing fractions were concentrated under reduced pressure. The residue was taken in MeCN/H₂O (1:1, 6 mL) and lyophilized to give the title compound as a white solid (14.3 mg, 9% over 3 steps).

LCMS (Method B): t_R = 1.20 Min, $[M+H]^+$ = 707.48, purity 100%; ¹H NMR (400 MHz, Methanol-*d*₄) δ 8.67 (d, J = 1.0 Hz, 1H), 8.22 (d, J = 1.3 Hz, 1H), 7.95 (dd, J = 1.3, 1.0 Hz, 1H), 7.47 – 7.44 (m, 1H), 7.33 (d, J = 3.2 Hz, 1H), 7.28 – 7.26 (m, 1H), 7.25 – 7.21 (m, 2H), 6.66 (dd, J = 3.2, 1.0 Hz, 1H), 5.68 – 5.57 (m, 1H), 5.53 – 5.42

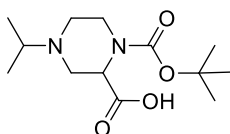
(m, 1H), 4.76 – 4.74 (m, 1H), 3.80 (s, 2H), 3.28 – 3.22 (m, 1H), 3.23 – 3.06 (m, 2H), 3.06 – 2.96 (m, 2H), 2.97 – 2.78 (m, 4H), 2.59 – 2.49 (m, 1H), 2.49 – 2.38 (m, 2H), 2.38 – 2.24 (m, 1H), 2.24 – 2.12 (m, 3H), 2.08 – 1.96 (m, 1H), 1.85 – 1.49 (m, 4H), 1.47 – 1.36 (m, 4H), 1.33 – 1.14 (m, 1H), 1.08 (d, $J = 6.7$ Hz, 3H), 0.95 (d, $J = 6.7$ Hz, 3H). 4H not observed (exchangeable); ^{13}C NMR (101 MHz, Methanol- d) δ 174.2, 163.0, 150.0, 142.1, 138.3, 136.3, 135.5, 134.1, 132.6, 129.6, 128.8, 127.6, 126.5, 122.8, 122.7, 120.7, 120.4, 119.6, 113.0, 112.2, 106.4, 101.5, 71.3, 64.8, 57.2, 53.5, 52.7, 51.8, 43.0, 42.0, 41.3, 39.8, 35.3, 33.8, 30.9, 29.0, 28.4, 27.7, 21.1, 14.4; ν_{max} (neat): 3273, 2928, 2859, 1692, 1660, 1517, 1441, 1341, 1259, 1120, 989, 754 cm^{-1} ; HRMS (Method A): calcd. for $\text{C}_{40}\text{H}_{51}\text{N}_8\text{O}_4$ $[\text{M}+\text{H}]^+$ 707.4033; found 707.4028.



1-*tert*-Butyl 2-methyl 4-isopropylpiperazine-1,2-dicarboxylate (107)

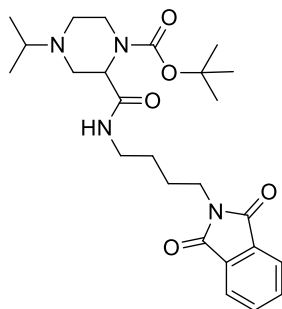
To a stirred solution of 1-(*tert*-butyl) 2-methyl piperazine-1,2-dicarboxylate (3.24 g, 13.26 mmol) in DCM (20 mL) was added acetone (7.90 mL, 106 mmol) and acetic acid (379 μL , 6.63 mmol). The resulting solution was stirred at room temperature under an atmosphere of N_2 for 30 min after which STAB (4.22 g, 19.89 mmol) was added portion wise over 10 min. The reaction was stirred overnight under N_2 atmosphere. The reaction was partitioned between DCM (20 mL) and a saturated aqueous sodium bicarbonate solution (40 mL). The layers were separated and the aqueous was extracted with DCM (3 x 50 mL). The combined organic extracts were dried by passing through a hydrophobic frit. Florisil was added and solvents were removed under reduced pressure to adsorb the compound. Purification was carried out by automated column chromatography on silica gel eluting with 0-70% EtOAc/cyclohexane over 20 CV. The product-containing fractions were identified by TLC (cyclohexane/EtOAc 4:6, KMnO_4 stain) and concentrated under reduced pressure to afford the title compound as a colourless oil (3.64 g, 96% yield).

^1H NMR (400 MHz, Chloroform-*d*) (1:1 mixture of rotamers) δ 4.76 – 4.70 (m, 0.5H), 4.59 – 4.51 (m, 0.5H), 3.93 – 3.81 (m, 0.5H), 3.81 – 3.63 (m, 0.5H), 3.74 (s, 3H), 3.36 – 3.26 (m, 1H), 3.25 – 3.15 (m, 0.5H), 3.15 – 3.04 (m, 0.5H), 2.77 – 2.58 (m, 2H), 2.38 – 2.21 (m, 2H), 1.47 (s, 4.5H), 1.44 (s, 4.5H), 1.01 (d, J = 6.5 Hz, 3H), 0.96 (d, J = 6.5 Hz, 3H); ^{13}C NMR (101 MHz, Chloroform-*d*) (1:1 mixture of rotamers) δ 171.8, 171.5, 156.0, 155.5, 80.2, 56.0, 54.8, 54.4, 52.1, 49.0, 48.81, 42.6, 41.6, 28.4, 19.1, 17.0; ν_{max} (DCM): 2968, 2815, 1751, 1698, 1455, 1365, 1169, 1115, 972 cm^{-1} ; HRMS (Method A): calcd. for $\text{C}_{14}\text{H}_{27}\text{N}_2\text{O}_4$ $[\text{M}+\text{H}]^+$ 287.1971; found 287.1972.



1-(*tert*-Butoxycarbonyl)-4-isopropylpiperazine-2-carboxylic acid (108)

To a stirred solution of 1-(*tert*-butyl) 2-methyl 4-isopropylpiperazine-1,2-dicarboxylate (3.36 g, 11.73 mmol) in MeOH (25 mL) cooled to 0 °C was added a 2 M aqueous NaOH solution (23.5 mL, 46.90 mmol). The reaction mixture was allowed to warm to room temperature and was stirred overnight under an atmosphere of N_2 . MeOH was removed under reduced pressure and the pH of the aqueous was adjusted to 4-5 with a 2 M aqueous HCl solution (~20 mL). The aqueous was concentrated under reduced pressure to about 10 mL which were lyophilized overnight. The solid obtained was suspended in DCM (25 mL) and filtered by vacuum filtration. The solid was washed with more DCM (50 mL). The solid was suspended in DCM + 10% MeOH (30 mL), sonicated and then filtered again. The filtrate was concentrated under reduced pressure to afford the crude title compound as a white solid (3.52 g). The compound was used immediately in the subsequent step without further purification.

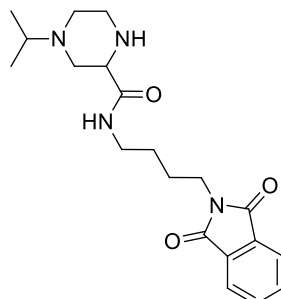


***tert*-Butyl 2-((4-(1,3-dioxisoindolin-2-yl)butyl)carbamoyl)-4-isopropylpiperazine-1-carboxylate (109)**

To a stirred solution of 1-(*tert*-butoxycarbonyl)-4-isopropylpiperazine-2-carboxylic acid (1.51 g, 5.54 mmol) in DMF (20 mL) was added 2-(4-aminobutyl)isoindoline-1,3-dione TFA salt (2.03 g, 6.10 mmol), HATU (2.53 g, 6.65 mmol) and DIPEA (3.9 mL, 22.18 mmol) upon which all solids particles went into solution. Then, HOBt hydrate (1.48 g, 8.32 mmol) was added and the reaction was stirred overnight at room temperature under N₂ atmosphere. The reaction mixture was partitioned between EtOAc (40 mL) and water (30 mL). The biphasic mixture was transferred to a separatory funnel and a saturated aqueous sodium bicarbonate solution (20 mL) was added. The layers were separated and the aqueous phase was further extracted with EtOAc (4 x 50 mL). The combined organic extracts were washed with a 5% aqueous LiCl solution (2 x 30 mL) and dried by passing through a hydrophobic frit. Florisil was added and solvents were removed under reduced pressure to adsorb the compound. Purification was carried out by automated column chromatography on silica gel eluting with 0-50% (3:1 EtOAc/EtOH)/cyclohexane over 20 CV. The product-containing fractions were combined and concentrated under reduced pressure to afford the title compound as a colourless oil (1.82 g, 70% yield).

LCMS (Method A): t_R = 0.70 Min, $[M+H]^+ = 473.24$, purity 96%; ¹H NMR (400 MHz, Chloroform-*d*) δ 7.85 – 7.79 (m, 2H), 7.73 – 7.67 (m, 2H), 6.79 (bs, 1H), 4.60 – 4.48 (m, 1H), 4.08 – 3.89 (m, 1H), 3.69 (t, J = 7.1 Hz, 2H), 3.45 – 3.21 (m, 3H), 3.07 – 2.95 (m, 1H), 2.76 – 2.66 (m, 2H), 2.32 – 2.17 (m, 2H), 1.76 – 1.65 (m, 2H), 1.60 – 1.48 (m, 2H), 1.45 (s, 9H), 1.00 (d, J = 6.6 Hz, 3H), 0.96 (d, J = 6.6 Hz, 3H); ¹³C NMR (101 MHz, Chloroform-*d*) δ 170.3, 168.5, 155.1, 134.0, 132.3, 123.3, 80.9, 55.7, 54.6,

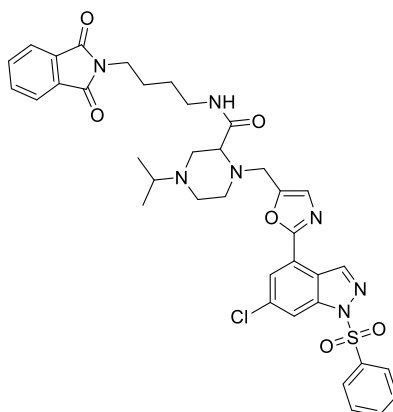
48.7, 48.4, 41.7, 38.9, 38.7, 37.6, 28.5, 27.2, 27.1, 26.2, 18.6, 17.5; ν_{max} (DCM): 2931, 2809, 1768, 1707, 1657, 1535, 1436, 1392, 1358, 1169, 721 cm^{-1} ; HRMS (Method A): calcd. for $\text{C}_{25}\text{H}_{37}\text{N}_4\text{O}_5$ $[\text{M}+\text{H}]^+$ 473.2764; found 473.2770.



***N*-(4-(1,3-Dioxoisindolin-2-yl)butyl)-4-isopropylpiperazine-2-carboxamide
(110)**

To a stirred solution of *tert*-butyl 2-((4-(1,3-dioxoisindolin-2-yl)butyl)carbamoyl)-4-isopropylpiperazine-1-carboxylate (1.62 g, 3.43 mmol) in DCM (15 mL) was added TFA (2 mL). The reaction was stirred at room temperature under N_2 atmosphere for 2 h after which 1 mL additional TFA was added and the reaction was stirred at room temperature for another 2 h. 1 mL of TFA was added again and the reaction was stirred at room temperature for an additional 2 h. 1 mL of TFA was added and the reaction was stirred for 90 min at 32 °C. The reaction was then cooled to room temperature. Volatiles were removed under reduced pressure. The residue was partitioned between DCM (30 mL) and a saturated aqueous sodium bicarbonate solution (25 mL). The layers were separated and the aqueous was extracted with DCM (3 x 50 mL). The combined organic extracts were dried by passing through a hydrophobic frit and concentrated under reduced pressure to afford the crude title compound as a yellow oil (1.26 g, 99% yield). The product was used directly in the next step without further purification.

LCMS (Method A): t_{R} = 0.49 Min, $[\text{M}+\text{H}]^+$ = 373.21, purity 100%.

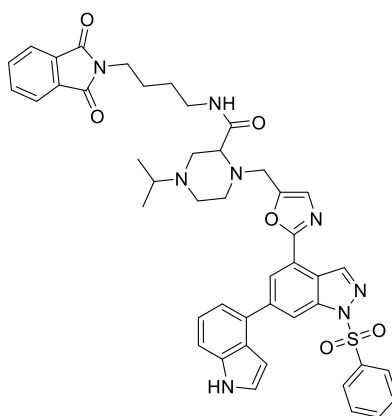


1-((2-(6-Chloro-1-(phenylsulfonyl)-1*H*-indazol-4-yl)oxazol-5-yl)methyl)-*N*-(4-(1,3-dioxoisindolin-2-yl)butyl)-4-isopropylpiperazine-2-carboxamide (111)

To a stirred suspension of 2-(6-chloro-1-(phenylsulfonyl)-1*H*-indazol-4-yl)oxazole-5-carbaldehyde (685 mg, 1.77 mmol) in DCM (10 mL) was added a solution of *N*-(4-(1,3-dioxoisindolin-2-yl)butyl)-4-isopropylpiperazine-2-carboxamide (724 mg, 1.94 mmol) in DCM (5 mL) followed by acetic acid (51 μ L, 0.88 mmol). The reaction mixture was stirred at room temperature under an atmosphere of N₂ for 30 min after which STAB (562 mg, 2.65 mmol) was added in one portion. The reaction was stirred at room temperature under N₂ for 1 h. The reaction was partitioned between DCM (30 mL) and a saturated aqueous sodium bicarbonate solution (30 mL). The layers were separated and the aqueous phase was extracted with DCM (3 x 40 mL). The combined organic extracts were dried by passing through a hydrophobic frit and Florisil was added and solvents were removed under reduced pressure to adsorb the compound. Purification was carried out by automated column chromatography on silica gel using 0-100% EtOAc/cyclohexane over 12 CV and then 0-30% MeOH/EtOAc over 20 CV. The product-containing fractions were concentrated under reduced pressure to afford the title compound as a light yellow solid (703 mg, 54% yield).

LCMS (Method A): t_R = 0.94 Min, $[M+H]^+$ = 744.20, purity 97%; ¹H NMR (400 MHz, Chloroform-*d*) δ 8.89 (d, J = 0.9 Hz, 1H), 8.25 (dd, J = 1.7, 0.9 Hz, 1H), 8.06 – 7.99 (m, 2H), 7.86 (d, J = 1.7 Hz, 1H), 7.75 – 7.66 (m, 2H), 7.64 – 7.56 (m, 3H), 7.54 – 7.45 (m, 2H), 7.17 (s, 1H), 3.82 – 3.66 (m, 4H), 3.47 (s, 1H), 3.39 – 3.24 (m, 1H), 3.25 – 3.11 (m, 1H), 2.96 – 2.87 (m, 1H), 2.87 – 2.81 (m, 1H), 2.77 – 2.62 (m, 2H), 2.61 –

2.51 (m, 1H), 2.51 – 2.41 (m, 2H), 1.84 – 1.70 (m, 2H), 1.70 – 1.58 (m, 2H), 1.02 (d, $J = 6.7$ Hz, 6H). 1H not observed (exchangeable); ^{13}C NMR (101 MHz, Chloroform-*d*) δ 170.9, 168.3, 158.7, 149.7, 141.8, 141.3, 137.4, 135.8, 134.7, 134.0, 132.1, 129.6, 128.3, 127.9, 123.16, 123.13, 121.7, 121.2, 114.6, 64.7, 54.6, 51.5, 50.1, 50.0, 48.4, 38.5, 37.6, 27.4, 26.4, 18.4, 18.3; ν_{max} (neat): 3064, 2975, 2826, 1768, 1707, 1668, 1591, 1535, 1447, 1392, 1176, 727 cm^{-1} ; HRMS (Method A): calcd. for $\text{C}_{37}\text{H}_{39}\text{ClN}_7\text{O}_6\text{S}$ $[\text{M}+\text{H}]^+$ 744.2371; found 744.2374.

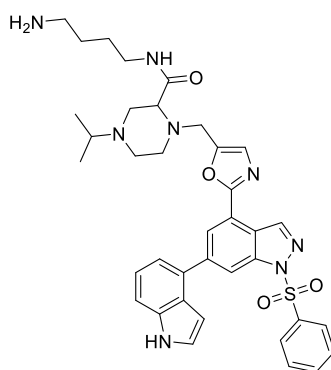


1-((2-(6-(1*H*-Indol-4-yl)-1-(phenylsulfonyl)-1*H*-indazol-4-yl)oxazol-5-yl)methyl)-*N*-(4-(1,3-dioxisoindolin-2-yl)butyl)-4-isopropylpiperazine-2-carboxamide (112)

In a microwave vial were added 1-((2-(6-chloro-1-(phenylsulfonyl)-1*H*-indazol-4-yl)oxazol-5-yl)methyl)-*N*-(4-(1,3-dioxisoindolin-2-yl)butyl)-4-isopropylpiperazine-2-carboxamide (700 mg, 0.94 mmol), 4-(4,4,5,5-tetramethyl-1,3,2-dioxaborolan-2-yl)-1*H*-indole (297 mg, 1.22 mmol), sodium carbonate (299 mg, 2.82 mmol) and XPhos Pd G2 (148 mg, 0.19 mmol). Solids were suspended in 1,4-dioxane (10 mL) and water (2 mL). The vial was sealed and purged with 3 vacuum/nitrogen cycles. The vial was heated at 90 °C in the microwave for 75 mins. The reaction was partitioned between EtOAc (30 mL) and water (20 mL), the layers were separated and the aqueous was extracted with EtOAc (3 x 50 mL). The combined organic extracts were dried by passing through a hydrophobic frit. Florisil was added and solvents were removed under reduced pressure to adsorb the compound. Purification was carried out by automated column chromatography on silica gel eluting with 0-100% EtOAc/cyclohexane over 12 CV and then 0-30% MeOH/EtOAc over 20 CV. The

product containing fractions were concentrated under reduced pressure to afford the title compound as a dark yellow solid (625 mg, 81% yield).

LCMS (Method A): t_R = 0.94 Min, $[M+H]^+ = 825.26$, purity 96%; 1H NMR (400 MHz, Chloroform-*d*) δ 8.99 (d, J = 0.9 Hz, 1H), 8.87 (bs, 1H), 8.57 (dd, J = 1.3, 0.9 Hz, 1H), 8.27 (d, J = 1.3 Hz, 1H), 8.07 – 8.00 (m, 2H), 7.73 – 7.67 (m, 2H), 7.61 – 7.54 (m, 3H), 7.54 – 7.43 (m, 3H), 7.36 – 7.32 (m, 1H), 7.32 – 7.28 (m, 2H), 7.17 (s, 1H), 6.75 – 6.69 (m, 1H), 3.85 – 3.62 (m, 2H), 3.57 (t, J = 7.1 Hz, 2H), 3.40 – 3.31 (m, 1H), 3.31 – 3.21 (m, 1H), 3.21 – 3.15 (m, 1H), 2.96 – 2.88 (m, 1H), 2.89 – 2.80 (m, 1H), 2.75 – 2.60 (m, 2H), 2.55 – 2.46 (m, 1H), 2.47 – 2.32 (m, 2H), 1.70 – 1.57 (m, 2H), 1.57 – 1.44 (m, 2H), 1.00 (dd, J = 6.5, 2.5 Hz, 6H). 1H not observed (exchangeable); ν_{max} (neat): 3053, 2964, 2820, 1613, 1774, 1707, 1535, 1447, 1375, 1170, 721 cm^{-1} ; HRMS: calcd. for $C_{45}H_{45}N_8O_6S$ $[M+H]^+ 825.3183$; found 825.3179.

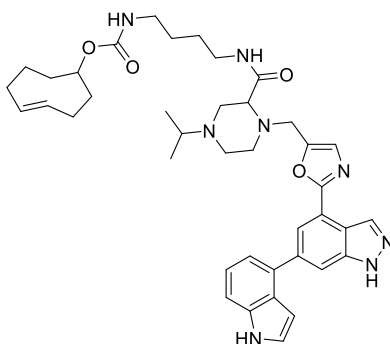


1-((2-(6-(1*H*-Indol-4-yl)-1-(phenylsulfonyl)-1*H*-indazol-4-yl)oxazol-5-yl)methyl)-*N*-(4-aminobutyl)-4-isopropylpiperazine-2-carboxamide (113)

To a stirred solution of 1-((2-(6-(1*H*-indol-4-yl)-1-(phenylsulfonyl)-1*H*-indazol-4-yl)oxazol-5-yl)methyl)-*N*-(4-(1,3-dioxoisindolin-2-yl)butyl)-4-isopropylpiperazine-2-carboxamide (411 mg, 0.50 mmol) in THF (5 mL) was added hydrazine hydrate (57 μ L, 0.75 mmol) and the reaction was stirred at 55 $^{\circ}C$ under N_2 atmosphere overnight. Hydrazine hydrate (57 μ L, 0.75 mmol) was added and the reaction was stirred at 55 $^{\circ}C$ for 5.5 h. More hydrazine hydrate (15 μ L, 0.20 mmol) was added and the reaction was stirred at 55 $^{\circ}C$ for an additional 1.5 h. The reaction was then cooled to room temperature and acetone (5 mL) was added. The mixture was stirred at room

temperature for 10 min. Solvents were removed under reduced pressure and the residue was dissolved in DCM. Florisil was added and solvents were removed under reduced pressure to adsorb the compound. Purification was carried out by automated column chromatography on silica gel eluting with 0-50% MeOH/EtOAc. The desired product was not eluted and the column was flushed with MeOH + 1% Et₃N. The product-containing fractions were concentrated under reduced pressure to afford the title compound as a yellow solid (186 mg, 54% yield). The compound was immediately used in the subsequent step.

LCMS (Method B): t_R = 1.17 Min, $[M+H]^+$ = 695.30, purity 94%.



(*E*)-Cyclooct-4-en-1-yl (4-(1-((2-(6-(1*H*-indol-4-yl)-1*H*-indazol-4-yl)oxazol-5-yl)methyl)-4-isopropylpiperazine-2-carboxamido)butyl)carbamate (43)

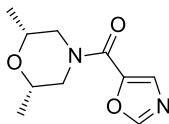
TCO installation:

To a stirred solution of 1-((2-(6-(1*H*-indol-4-yl)-1-(phenylsulfonyl)-1*H*-indazol-4-yl)oxazol-5-yl)methyl)-*N*-(4-aminobutyl)-4-isopropylpiperazine-2-carboxamide (133 mg, 0.19 mmol) in DMF (5 mL) was added (*E*)-cyclooct-3-en-1-yl (4-nitrophenyl) carbonate (56 mg, 0.19 mmol) and DIPEA (67 μ L, 0.38 mmol). The reaction was stirred at room temperature under N₂ for 105 min. The reaction was partitioned between EtOAc (20 mL) and water (15 mL). The layers were separated and the aqueous was extracted with EtOAc (3 x 15 mL). The combined organics were washed with a 5% aqueous LiCl solution (2 x 15 mL), dried by passing through a hydrophobic frit and concentrated under reduced pressure.

Benzenesulfonyl deprotection:

The crude was immediately suspended in MeOH (5 mL) and a 2 M aqueous NaOH solution (1 mL, 2.00 mmol) was added. The reaction was stirred at room temperature for 25 min. Solvents were removed under reduced pressure. The crude was partitioned between EtOAc (15 mL) and water (15 mL). The layers were separated and the aqueous was further extracted with EtOAc (3 x 15 mL). The combined organic extracts were dried by passing through a hydrophobic frit and concentrated under reduced pressure. The residue was taken in MeOH/DMSO (1:1, 3 mL) and purified by MDAP (Method B, 3 x 1 mL injection). The product-containing fractions were concentrated under reduced pressure. The residue was taken in acetonitrile/water (1:1, 6 mL) and lyophilised to afford the title compound as a white solid (53 mg, 39% yield over 2 steps).

LCMS (Method B): t_R = 1.19 Min, $[M+H]^+$ = 707.51, purity 100%; 1H NMR (400 MHz, Methanol- d_4) δ 8.70 (s, 1H), 8.23 (d, J = 1.3 Hz, 1H), 7.95 (d, J = 1.3 Hz, 1H), 7.52 – 7.43 (m, 1H), 7.34 (d, J = 3.2 Hz, 1H), 7.30 – 7.18 (m, 3H), 6.67 (dd, J = 3.3, 0.9 Hz, 1H), 5.66 – 5.55 (m, 1H), 5.54 – 5.42 (m, 1H), 4.78 – 4.71 (m, 1H), 4.01 – 3.71 (m, 2H), 3.29 – 3.24 (m, 2H), 3.24 – 3.13 (m, 1H), 3.12 – 2.97 (m, 4H), 2.97 – 2.87 (m, 1H), 2.87 – 2.77 (m, 1H), 2.75 – 2.62 (m, 1H), 2.62 – 2.51 (m, 1H), 2.51 – 2.36 (m, 2H), 2.36 – 2.11 (m, 4H), 2.05 – 1.95 (m, 1H), 1.87 – 1.54 (m, 3H), 1.54 – 1.38 (m, 4H), 1.26 – 1.13 (m, 1H), 1.03 (d, J = 6.5 Hz, 6H). 4H not observed (exchangeable); ν_{max} (neat): 3262, 2928, 2854, 1690, 1662, 1520, 1452, 1338, 1124, 942, 754 cm^{-1} ; HRMS (Method A): calcd. for $C_{40}H_{51}N_8O_4$ $[M+H]^+$ 707.4033; found 707.4028.

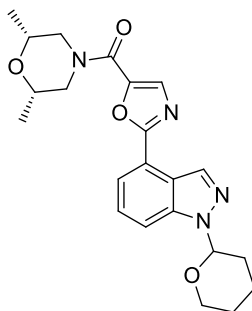


((2R,6S)-2,6-Dimethylmorpholino)(oxazol-5-yl)methanone (115)

To a suspension of oxazole-5-carboxylic acid (5.25 g, 46.40 mmol) in EtOAc (60 mL) were added sequentially DIPEA (16.2 mL, 92.75 mmol) upon which the solid went into solution and T3P[®] (50 wt. % in EtOAc, 33.2 mL, 55.70 mmol). Then, (2R,6S)-

2,6-dimethylmorpholine (8.63 mL, 69.60 mmol) was added and the resulting solution was stirred at room temperature overnight. The reaction mixture was washed with water (2 x 50 mL). The organic phase was dried by passing through a hydrophobic frit and concentrated under reduced pressure. The residue was triturated with cyclohexane (30 mL). The solids were isolated by vacuum filtration and dried under vacuum (40 °C) to give the title compound as a white solid (8.07 g, 83% yield).

LCMS (Method A): t_R = 0.59 min, $[M+H]^+$ = 211.07; 1H NMR (400 MHz, DMSO- d_6) δ 8.44 (s, 1H), 7.64 (s, 1H), 4.40 – 3.95 (m, 2H), 3.62 – 3.46 (m, 2H), 3.04 – 2.52 (m, 2H), 1.14 (d, J = 6.2 Hz, 6H); ^{13}C NMR (101 MHz, DMSO- d_6) δ 156.6, 153.1, 144.0, 130.3, 71.2, 49.2, 18.4; $\nu_{max}(neat)$: 3105, 2969, 2877, 1618, 1589, 1493, 1436, 1373, 1276, 1168, 1083, 980, 837, 746 cm^{-1} ; HRMS (Method A): calcd. for $C_{10}H_{15}N_2O_3$ $[M+H]^+$ 211.1083; found 211.1084.

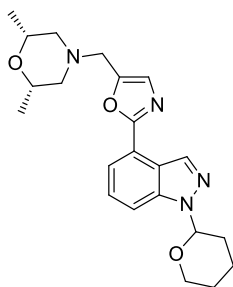


((2*R*,6*S*)-2,6-Dimethylmorpholino)(2-(1-(tetrahydro-2*H*-pyran-2-yl)-1*H*-indazol-4-yl)oxazol-5-yl)methanone (116)

4-chloro-1-(tetrahydro-2*H*-pyran-2-yl)-1*H*-indazole (4.00 g, 16.90 mmol), ((2*R*,6*S*)-2,6-dimethylmorpholino)(oxazol-5-yl)methanone (4.26 g, 20.28 mmol), pivalic acid (1.04 g, 10.14 mmol), palladium(II) chloride (84 mg, 0.47 mmol), XPhos (0.48 g, 1.01 mmol) and potassium carbonate (3.97 g, 28.70 mmol) were split between two microwave vials, dissolved in CPME (20 mL in each vial, 40 mL total) and heated in the microwave for 2 h at 120 °C. The combined reaction mixtures were partitioned between DCM (150 mL) and water (100 mL). The layers were separated and the aqueous phase was further extracted with DCM (2 x 50 mL). The combined organic extracts were washed with brine (150 mL), dried by passing through a hydrophobic

frit and concentrated under reduced pressure. The residue was triturated with MeOH (30 mL). The solids were collected by vacuum filtration, washed with more MeOH (2 x 20 mL) and dried under vacuum to afford the title compound as a grey solid (5.86 g, 84% yield).

LCMS (Method A): t_R = 1.12 Min, $[M+H]^+$ = 411.31, purity 98%; 1H NMR (400 MHz, DMSO- d_6) δ 8.58 (d, J = 0.9 Hz, 1H), 8.00 (dd, J = 8.5, 0.7 Hz, 1H), 7.97 (s, 1H), 7.91 (dd, J = 7.3, 0.7 Hz, 1H), 7.62 (dd, J = 8.5, 7.3 Hz, 1H), 5.96 (dd, J = 9.6, 2.4 Hz, 1H), 4.38 – 4.18 (m, 2H), 3.94 – 3.86 (m, 1H), 3.83 – 3.73 (m, 1H), 3.67 – 3.56 (m, 2H), 3.15 – 2.57 (m, 2H), 2.47 – 2.39 (m, 1H), 2.11 – 1.97 (m, 2H), 1.84 – 1.68 (m, 1H), 1.65 – 1.55 (m, 2H), 1.15 (d, J = 6.2 Hz, 6H); ^{13}C NMR (101 MHz, DMSO- d_6) δ 160.6, 156.5, 144.1, 139.8, 133.1, 132.9, 126.5, 120.8, 120.3, 118.4, 113.9, 84.1, 71.2, 66.6, 28.9, 24.7, 22.1, 18.5; ν_{max} (neat): 2969, 2934, 2855, 1644, 1533, 1441, 1418, 1276, 1089, 1043, 923, 798, 727 cm^{-1} ; HRMS (Method A): calcd. for $C_{22}H_{27}N_4O_4$ $[M+H]^+$ 411.2032; found 411.2025.

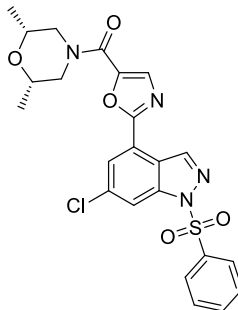


(2R,6S)-2,6-Dimethyl-4-((2-(1-(tetrahydro-2H-pyran-2-yl)-1H-indazol-4-yl)oxazol-5-yl)methyl)morpholine (117)

To a stirred solution of ((2R,6S)-2,6-dimethylmorpholino)(2-(1-(tetrahydro-2H-pyran-2-yl)-1H-indazol-4-yl)oxazol-5-yl)methanone (1.00 g, 2.44 mmol) in anhydrous THF (20 mL) was added $LiAlH_4$ 1 M in Et_2O (7.3 mL, 7.31 mmol) dropwise. Upon complete addition, the resulting solution was heated to 50 °C for 2 h. The reaction was cooled to room temperature and then to 0 °C and carefully quenched by the slow addition of EtOAc (10 mL). The reaction was partitioned between EtOAc (20 mL) and a saturated aqueous Rochelle's salt solution (30 mL). The resulting biphasic mixture was stirred at 0 °C for 30 min. The layers were separated and the aqueous phase was

further extracted with EtOAc (2 x 25mL). The combined organic extracts were dried by passing through a hydrophobic frit and concentrated under reduced pressure. The crude material was dissolved in a minimum amount of DCM and purified by automated column chromatography on silica gel eluting with 20-100% EtOAc/cyclohexane over 20 CV. The product-containing fractions were concentrated under reduced pressure to afford the title compound as a yellow oil (0.63 g, 65% yield).

LCMS (Method A): t_R = 0.66 Min, $[M+H]^+ = 397.40$, purity 94%; 1H NMR (400 MHz, Chloroform-*d*) δ 8.69 (s, 1H), 7.87 (dd, J = 7.3, 0.8 Hz, 1H), 7.67 (dd, J = 8.4, 0.8 Hz, 1H), 7.43 (dd, J = 8.4, 7.3 Hz, 1H), 7.12 (s, 1H), 5.75 (dd, J = 9.2, 2.7 Hz, 1H), 4.05 – 3.95 (m, 1H), 3.75 – 3.68 (m, 3H), 3.67 (s, 2H), 2.83 – 2.72 (m, 2H), 2.63 – 2.47 (m, 1H), 2.22 – 2.01 (m, 2H), 1.93 – 1.82 (m, 2H), 1.81 – 1.57 (m, 3H), 1.13 (d, J = 6.3 Hz, 6H); ^{13}C NMR (101 MHz, Chloroform-*d*) δ 161.1, 160.6, 148.5, 140.0, 134.5, 127.5, 126.3, 121.4, 120.3, 112.4, 85.6, 71.7, 67.4, 59.0, 52.5, 29.5, 25.1, 22.5, 19.2; ν_{max} (neat): 2969, 2849, 1669, 1612, 1555, 1452, 1316, 1271, 1080, 1040, 914, 790 cm^{-1} ; HRMS (Method A): calcd. for $C_{22}H_{29}N_4O_3$ $[M+H]^+ 397.2240$; found 397.2235.

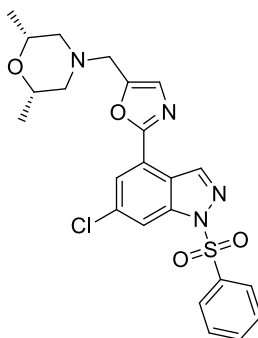


(2-(6-Chloro-1-(phenylsulfonyl)-1*H*-indazol-4-yl)oxazol-5-yl)((2*R*,6*S*)-2,6-dimethylmorpholino)methanone (124)

To a stirred solution of ((2*R*,6*S*)-2,6-dimethylmorpholino)(oxazol-5-yl)methanone (4.50 g, 21.40 mmol) in THF (20 mL) cooled to -20 °C was added zinc chloride 1.9 M in 2-MeTHF (31.2 mL, 59.20 mmol). Then, LiHMDS 1.0 M in THF (29.6 mL, 29.60 mmol) was added slowly over 15 min. The resulting solution was stirred under N_2 at -20 °C for 90 min after which a solution of 6-chloro-4-iodo-1-(phenylsulfonyl)-1*H*-indazole (6.89 g, 16.46 mmol) and $Pd(PPh_3)_4$ (0.57 g, 0.49 mmol) in THF (40 mL) was

added. The reaction solution mixture was degassed with three vacuum/nitrogen cycles and then heated to 65°C under N₂ atmosphere for 5 h. More Pd(PPh₃)₄ (0.57 g, 0.03 equiv.) was added and the reaction was stirred overnight under N₂ at 65°C. The reaction was then cooled to room temperature and quenched by the slow addition of a saturated aqueous NH₄Cl solution (80 mL). The phases were separated and the aqueous was extracted with EtOAc (3 x 150 mL). The combined organic extracts were washed with brine (80 mL), dried by passing through a hydrophobic frit and concentrated under reduced pressure. The residue was suspended in a minimum amount of DCM and purified by automated column chromatography on silica gel eluting with 0-80% EtOAc/cyclohexane over 20 CV. Some material was lost when compound was loaded on the column and impurities co-eluted with desired product. The product-containing fractions were concentrated under reduced pressure and the residue was triturated with IPA (50 mL). The solid was isolated by vacuum filtration and washed with more IPA (2 x 50 mL). The solid was dried under vacuum to afford the title compound as an off-white solid (6.35 g, 77% yield).

LCMS (Method A): t_R = 1.33 Min, $[M+H]^+ = 500.95$, purity 98%; ¹H NMR (400 MHz, Chloroform-*d*) δ 8.89 (d, J = 0.9 Hz, 1H), 8.37 (dd, J = 1.7, 0.9 Hz, 1H), 8.06 – 7.98 (m, 2H), 7.98 (d, J = 1.7 Hz, 1H), 7.67 (s, 1H), 7.64 – 7.58 (m, 1H), 7.55 – 7.42 (m, 2H), 4.71 – 3.90 (m, 2H), 3.66 (dq, J = 10.7, 6.2, 2.5 Hz, 2H), 3.31 – 2.41 (m, 2H), 1.24 (d, J = 6.2 Hz, 6H); ¹³C NMR (101 MHz, Chloroform-*d*) δ 158.4, 156.1, 144.1, 140.4, 140.2, 136.3, 135.0, 133.8, 132.4, 128.6, 126.9, 123.0, 120.5, 119.7, 114.7, 71.1, 48.7, 17.9; ν_{max} (neat): 3111, 2969, 2867, 1618, 1533, 1447, 1373, 1282, 1167, 1083, 929, 718 cm⁻¹; HRMS (Method A): calcd. for C₂₃H₂₂ClN₄O₅S $[M+H]^+ 501.0999$; found 501.1003.



(2*R*,6*S*)-4-((2-(6-chloro-1-(phenylsulfonyl)-1*H*-indazol-4-yl)oxazol-5-yl)methyl)-2,6-dimethylmorpholine (125)

Approach 1:

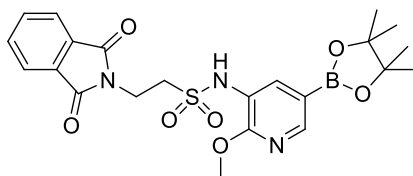
To a stirred suspension of Zn(OAc)₂ (0.11 g, 0.60 mmol) in anhydrous THF (2 mL) was added triethoxysilane (3.3 mL, 17.97 mmol). The mixture was degassed with 3 vacuum/nitrogen cycles and stirred for 30 minutes at room temperature. Then a suspension of (2-(6-chloro-1-(phenylsulfonyl)-1*H*-indazol-4-yl)oxazol-5-yl)((2*R*,6*S*)-2,6 dimethylmorpholino)methanone (1.50 g, 2.99 mmol) in THF (15 mL) was added to the vial and the mixture was stirred at 45 °C under N₂. The reaction mixture was opened to air, Zn(OAc)₂ (110 mg, 0.60 mmol) and triethoxysilane (3.3 mL, 17.97 mmol) were added and the reaction was warmed to 55 °C and stirred overnight under N₂. The reaction mixture was cooled to room temperature, partitioned between EtOAc (20 mL) and water (15 mL) and the layers were separated. The aqueous phase was extracted with EtOAc (2 x 15 mL) and the combined organic extracts were washed with brine, dried by passing through a hydrophobic frit and concentrated under reduced pressure. The crude material was triturated with IPA (15 mL), the solids were collected by vacuum filtration, washed with more IPA and dried in a vacuum oven (40 °C) overnight to afford the title compound as a beige solid (1.28 g, 88% yield).

Approach 2:

To a stirred solution of 2-(6-chloro-1-(phenylsulfonyl)-1*H*-indazol-4-yl)oxazole-5-carbaldehyde (1.00 g, 2.58 mmol) in DCM (20 mL) was added (2*R*,6*S*)-2,6-dimethylmorpholine (0.45 g, 3.87 mmol) and acetic acid (74 µL, 1.29 mmol). The reaction was stirred at room temperature under for 1 h after which sodium triacetoxyborohydride (0.82 g, 3.87 mmol) was added in one portion. The reaction was

stirred at room temperature for another 3 h. The reaction was partitioned between DCM (30 mL) and a saturated aqueous sodium bicarbonate solution (50 mL). The layers were separated and the aqueous was further extracted with DCM (3 x 40 mL). The combined organic extracts were dried by passing through a hydrophobic frit and concentrated under reduced pressure. The residue oil dissolved in a minimum amount of DCM and purification was carried out by silica gel chromatography eluting with 50-80% petrol ether 40-60/EtOAc gradient 50-80%. The product-containing fractions were combined and concentrated under reduced pressure to afford the title compound as a pale yellow solid (1.16 g, 92% yield).

LCMS (Method A): t_R = 0.94 Min, $[M+H]^+$ = 486.96, purity 99%; 1H NMR (400 MHz, Chloroform-*d*) δ 8.91 (d, J = 0.9 Hz, 1H), 8.31 (dd, J = 1.7, 0.9 Hz, 1H), 8.05 – 7.98 (m, 2H), 7.96 (d, J = 1.7 Hz, 1H), 7.65 – 7.56 (m, 1H), 7.54 – 7.44 (m, 2H), 7.14 (s, 1H), 3.78 – 3.71 (m, 2H), 3.66 (s, 2H), 2.76 (dd, J = 10.6, 1.8 Hz, 2H), 1.85 (app. t, J = 10.6 Hz, 2H), 1.15 (d, J = 6.4 Hz, 6H); ^{13}C NMR (151 MHz, Chloroform-*d*) δ 158.8, 149.8, 141.8, 141.4, 137.4, 136.0, 134.7, 129.5, 128.1, 127.8, 123.4, 121.8, 121.3, 114.7, 71.7, 59.1, 55.6, 19.2; ν_{max} (neat): 2969, 2786, 1592, 1542, 1449, 1376, 607, 563 cm^{-1} ; HRMS (Method A): calcd. for $C_{23}H_{24}ClN_4O_4S$ $[M+H]^+$ 487.1207; found 487.1207.

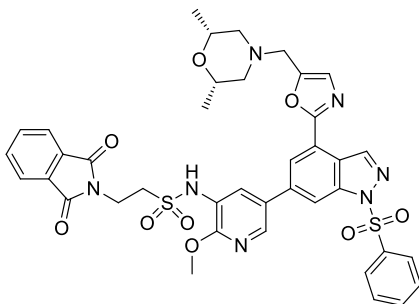


2-(1,3-Dioxoisindolin-2-yl)-N-(2-methoxy-5-(4,4,5,5-tetramethyl-1,3,2-dioxaborolan-2-yl)pyridin-3-yl)ethane-1-sulfonamide (128)

To a stirred solution of 2-methoxy-5-(4,4,5,5-tetramethyl-1,3,2-dioxaborolan-2-yl)pyridin-3-amine (5.70 g, 22.79 mmol) in dry DCM (30 mL) cooled to 0 °C was added pyridine (2.8 mL, 34.20 mmol) followed by 2-(1,3-dioxoisindolin-2-yl)ethane-1-sulfonyl chloride (7.48 g, 27.30 mmol). Finally, DMAP (0.28 g, 2.28 mmol) was added and the resulting solution was allowed to warm to room temperature and was stirred overnight under N_2 . The reaction mixture was washed with water (2 x 150 mL)

and dried by passing through a hydrophobic frit. Florisil was added and the solvent was removed under reduced pressure to adsorb the compound. Purification was carried out by automated column chromatography on silica gel eluting with 0-60% EtOAc/cyclohexane over 20 CV. The product-containing fractions were combined and concentrated under reduced pressure. The residue was dried on a high vacuum line overnight to afford the title compound as a beige solid under vacuum (5.62 g, 51% yield).

LCMS (Method A): t_R = 1.18 Min, $[M+H]^+$ = 488.12 (58%) and t_R = 0.76 Min, $[M+H]^+$ = 406.09 (37%), consistent with hydrolysis to the corresponding boronic acid on the LCMS; 1H NMR (400 MHz, Chloroform-*d*) δ 8.30 (d, J = 1.6 Hz, 1H), 8.06 (d, J = 1.6 Hz, 1H), 7.88 – 7.82 (m, 2H), 7.77 – 7.69 (m, 2H), 7.11 (bs, 1H), 4.17 (t, J = 6.3 Hz, 2H), 4.05 (s, 3H), 3.43 (t, J = 6.3 Hz, 2H), 1.32 (s, 12H); ^{13}C NMR (101 MHz, Chloroform-*d*) δ 168.1, 156.9, 149.9, 134.4, 134.4, 132.0, 123.7, 120.4, 84.2, 54.3, 48.7, 32.7, 25.0. 1C not observed (C-B); ν_{max} (neat): 2979, 1776, 1724, 1601, 1397, 1373, 1326, 1255, 1141, 1085, 972, 722 cm^{-1} ; HRMS (Method A): calcd. for $C_{22}H_{27}BN_3O_7S$ $[M+H]^+$ 488.1663; found 488.1666.

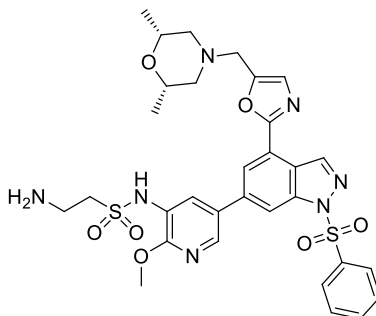


***N*-(5-(4-(5-(((2*R*,6*S*)-2,6-dimethylmorpholino)methyl)oxazol-2-yl)-1-(phenylsulfonyl)-1*H*-indazol-6-yl)-2-methoxypyridin-3-yl)-2-(1,3-dioxoisindolin-2-yl)ethane-1-sulfonamide (129)**

In a microwave vial were added (2*R*,6*S*)-4-((2-(6-chloro-1-(phenylsulfonyl)-1*H*-indazol-4-yl)oxazol-5-yl)methyl)-2,6-dimethylmorpholine (1.44 g, 2.96 mmol), 2-(1,3-dioxoisindolin-2-yl)-*N*-(2-methoxy-5-(4,4,5,5-tetramethyl-1,3,2-dioxaborolan-2-yl)pyridin-3-yl)ethane-1-sulfonamide (1.73 g, 3.55 mmol), Xphos Pd G2 (0.47 g,

0.59 mmol) and sodium carbonate (0.94 g, 8.87 mmol) which were suspended in 1,4-dioxane (15 mL) and water (2 mL). The vial was sealed, purged with 3 vacuum/nitrogen cycles and heated at 90 °C in the microwave for 1.5 h. The reaction was partitioned between EtOAc (80 mL) and water (60 mL). The layers were separated and the aqueous phase was extracted with EtOAc (3 x 80 mL). The combined organic extracts were dried by passing through a hydrophobic frit and concentrated under reduced pressure. The residue was taken in DCM, Florisil was added and solvents were removed under reduced pressure to adsorb the compound. Purification was carried out by automated column chromatography on silica gel eluting with 0-70% (3:1 EtOAc/EtOH)/cyclohexane over 16 CV. The product-containing fractions were concentrated under reduced pressure to afford the title compound as a light brown solid (1.98 g, 82% yield).

LCMS (Method A): t_R = 0.95 Min, $[M+H]^+$ = 812.13, purity 95%; 1H NMR (400 MHz, Chloroform-*d*) δ 8.96 (d, J = 0.9 Hz, 1H), 8.38 (dd, J = 1.4, 0.9 Hz, 1H), 8.29 (d, J = 2.2 Hz, 1H), 8.11 (d, J = 2.2 Hz, 1H), 8.10 (d, J = 1.4 Hz, 1H), 8.06 – 7.99 (m, 2H), 7.90 – 7.80 (m, 2H), 7.78 – 7.68 (m, 2H), 7.62 – 7.53 (m, 1H), 7.53 – 7.43 (m, 2H), 7.36 (bs, 1H), 7.14 (s, 1H), 4.24 (t, J = 6.1 Hz, 2H), 4.13 (s, 3H), 3.74 – 3.64 (m, 2H), 3.68 (s, 2H), 3.51 (t, J = 6.1 Hz, 2H), 2.80 – 2.72 (m, 2H), 1.86 (app. t, J = 10.6 Hz, 2H), 1.14 (d, J = 6.3 Hz, 6H); ^{13}C NMR (101 MHz, Chloroform-*d*) δ 168.1, 159.7, 154.8, 149.5, 141.9, 141.6, 141.5, 141.4, 139.1, 137.5, 134.6, 134.5, 131.9, 130.2, 129.5, 127.9, 127.8, 123.8, 122.2, 121.6, 121.2, 112.8, 71.7, 59.1, 54.6, 52.6, 49.1, 32.8, 19.2; ν_{max} (neat): 2980, 2934, 2872, 2809, 2245, 1772, 1713, 1607, 1390, 1339, 1141, 1082, 908, 719 cm^{-1} ; HRMS (Method A): calcd. for $C_{39}H_{38}N_7O_9S_2$ $[M+H]^+$ 812.2172; found 812.2166.

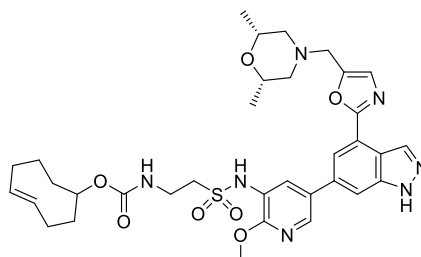


2-Amino-N-(5-(4-(5-(((2R,6S)-2,6-dimethylmorpholino)methyl)oxazol-2-yl)-1-(phenylsulfonyl)-1H-indazol-6-yl)-2-methoxypyridin-3-yl)ethane-1-sulfonamide (130)

To a stirred solution of *N*-(5-(4-(5-(((2R,6S)-2,6-dimethylmorpholino)methyl)oxazol-2-yl)-1-(phenylsulfonyl)-1H-indazol-6-yl)-2-methoxypyridin-3-yl)-2-(1,3-dioxoisindolin-2-yl)ethane-1-sulfonamide (1.90 g, 2.34 mmol) in THF (15 mL) was added hydrazine hydrate (0.36 mL, 4.68 mmol) under N₂ atmosphere. The reaction was stirred at room temperature for 2 h. Acetone (10 mL) was added and the reaction was stirred at room temperature for 15 min. Volatiles were removed under reduced pressure. The residue was partitioned between EtOAc (30 mL) and water (30 mL). The layers were separated and the aqueous phase was extracted with EtOAc (3 x 60 mL). The combined organic extracts were washed with brine (100 mL), dried by passing through a hydrophobic frit and concentrated under reduced pressure. The crude was re-suspended in a minimum amount of DCM, Florisil was added and solvents were removed under reduced pressure to adsorb the compound. Purification was carried out by automated column chromatography on silica gel eluting with 0-25% (MeOH+1% Et₃N)/DCM over 18 CV. The product-containing fractions were concentrated under reduced pressure to afford the title compound as a light yellow solid (1.01 g, 63% yield).

LCMS (Method B): *t_R* = 0.94 Min, [M+H]⁺ = 682.44, purity 98%; ¹H NMR (400 MHz, Chloroform-*d*) δ 8.96 (d, *J* = 0.9 Hz, 1H), 8.38 (dd, *J* = 1.5, 0.9 Hz, 1H), 8.28 (d, *J* = 2.3 Hz, 1H), 8.13 (d, *J* = 2.3 Hz, 1H), 8.12 (d, *J* = 1.5 Hz, 1H), 8.04 – 7.99 (m, 2H), 7.61 – 7.54 (m, 1H), 7.52 – 7.44 (m, 2H), 7.14 (s, 1H), 4.09 (s, 3H), 3.74 – 3.62 (m, 4H), 3.34 – 3.26 (m, 4H), 2.80 – 2.68 (m, 2H), 1.85 (app. t, *J* = 10.6 Hz, 2H), 1.14 (d,

$J = 6.2$ Hz, 6H). 3H not observed (exchangeable); ^{13}C NMR (101 MHz, Chloroform-*d*) δ 159.7, 154.7, 149.5, 141.9, 141.7, 140.8, 139.3, 137.5, 134.6, 130.2, 129.5, 127.9, 127.8, 127.5, 122.17, 122.15, 121.8, 121.5, 112.7, 71.7, 59.1, 55.0, 54.5, 52.6, 37.1, 19.2; ν_{max} (neat): 3374, 2969, 2869, 2813, 1600, 1469, 1459, 1383, 1173, 1139, 1079, 835, 724 cm^{-1} ; HRMS (Method A): calcd. for $\text{C}_{31}\text{H}_{36}\text{N}_7\text{O}_7\text{S}_2$ $[\text{M}+\text{H}]^+$ 682.2118; found 682.2120.



(*E*)-Cyclooct-4-en-1-yl(2-(*N*-(5-(4-(5-(((2*R*,6*S*)-2,6-dimethylmorpholino)methyl)oxazol-2-yl)-1*H*-indazol-6-yl)-2-methoxypyridin-3-yl)sulfamoyl)ethyl)carbamate (44)

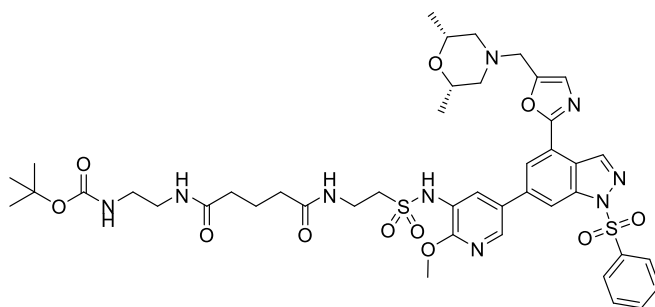
TCO installation:

To a stirred solution of 2-amino-*N*-(5-(4-(5-(((2*R*,6*S*)-2,6-dimethylmorpholino)methyl)oxazol-2-yl)-1-(phenylsulfonyl)-1*H*-indazol-6-yl)-2-methoxypyridin-3-yl)ethane-1-sulfonamide (111 mg, 0.16 mmol) in DMF (5 mL) was added (*E*)-cyclooct-4-en-1-yl (4-nitrophenyl) carbonate (52 mg, 0.18 mmol) followed by DIPEA (57 μL , 0.33 mmol). The reaction was stirred at room temperature under N_2 atmosphere for 1.5 h. More (*E*)-cyclooct-4-en-1-yl (4-nitrophenyl) carbonate (15 mg, 0.3 equiv.) was added and the reaction was stirred at room temperature for an additional 30 min. The reaction was partitioned between EtOAc (20 mL) and water (20 mL). The layers were separated and the aqueous phase was extracted with EtOAc (3 x 15 mL). The combined organic extracts were washed with a 5% aqueous LiCl solution (2 x 25 mL), dried by passing through a hydrophobic frit and concentrated under reduced pressure.

Benzene sulfonyl deprotection:

The crude was immediately taken in MeOH (5 mL). To the previous solution was added a 1 M aqueous NaOH solution (0.5 mL, 0.50 mmol). The reaction was stirred at room temperature for 30 min under N₂ atmosphere. The reaction was partitioned between EtOAc (20 mL) and water (20 mL). The layers were separated and the aqueous was further extracted with EtOAc (3 x 20 mL). The combined organic extracts were dried by passing through a hydrophobic frit and concentrated under reduced pressure. The residue was taken up in MeOH/DMSO (1:1, 3 mL) and purified by preparative HPLC (Method B) eluting with 25-55% acetonitrile/(water + 10 mM ammonium bicarbonate) (3 x 1 mL injection). The product-containing fractions were combined and partly concentrated under reduced pressure to remove acetonitrile. The aqueous was then extracted with EtOAc (3 x 20 mL). The combined organic extracts were dried by passing through a hydrophobic frit and concentrated under reduced pressure. The residue was taken up in acetonitrile/water (1:1, 8 mL) and lyophilised to afford the title compound as a white solid (29 mg, 26% over 2 steps).

LCMS (Method B): t_R = 1.00 Min, $[M+H]^+$ = 694.17, purity 100%; ¹H NMR (600 MHz, Chloroform-*d*) δ 8.82 (d, J = 0.9 Hz, 1H), 8.33 (d, J = 2.2 Hz, 1H), 8.14 – 8.10 (m, 1H), 8.08 (d, J = 1.4 Hz, 1H), 7.71 (dd, J = 1.4, 0.9 Hz, 1H), 7.27 (s, 1H), 7.22 (bs, 1H), 5.63 – 5.56 (m, 2H), 5.51 (bs, 1H), 4.98 – 4.92 (m, 1H), 4.15 (s, 3H), 3.88 – 3.74 (m, 6H), 3.47 – 3.39 (m, 2H), 2.96 – 2.89 (m, 2H), 2.40 – 2.22 (m, 3H), 2.15 – 2.09 (m, 1H), 2.04 – 1.96 (m, 2H), 1.93 – 1.84 (m, 1H), 1.84 – 1.76 (m, 1H), 1.74 – 1.64 (m, 1H), 1.60 – 1.47 (m, 1H), 1.25 (d, J = 6.3 Hz, 6H), 1.28 – 1.22 (m, 1H). 2H not observed (exchangeable); ¹³C NMR (151 MHz, Chloroform-*d*) δ 160.9, 156.3, 154.5, 149.0, 141.4, 141.2, 136.2, 135.7, 135.5, 131.8, 130.7, 129.9, 127.9, 127.6, 121.0, 120.8, 119.5, 109.9, 71.8, 71.1, 59.1, 54.5, 52.6, 52.3, 41.1, 35.9, 34.3, 32.8, 30.0, 28.1, 19.3; ν_{max} (neat): 3372, 3249, 2933, 2959, 1699, 1486, 1407, 1259, 1141, 1081, 866 cm⁻¹; HRMS (Method A): calcd. for C₃₄H₄₄N₇O₇S $[M+H]^+$ 694.3023; found 694.3039.

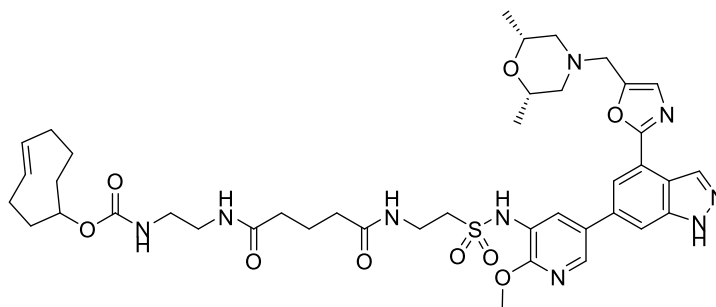


***tert*-Butyl (2-(5-((2-(*N*-(5-(4-(5-(((2*R*,6*S*)-2,6-dimethylmorpholino)methyl)oxazol-2-yl)-1-(phenylsulfonyl)-1*H*-indazol-6-yl)-2-methoxypyridin-3-yl)sulfamoyl)ethyl)amino)-5-oxopentanamido)ethyl)carbamate (139)**

To a stirred solution of 2-amino-*N*-(5-(4-(5-(((2*R*,6*S*)-2,6-dimethylmorpholino)methyl)oxazol-2-yl)-1-(phenylsulfonyl)-1*H*-indazol-6-yl)-2-methoxypyridin-3-yl)ethane-1-sulfonamide (92 mg, 0.14 mmol) in DCM (8 mL) was added glutaric anhydride (22 mg, 0.19 mmol) and triethylamine (19 μ L, 0.14 mmol). The reaction was stirred at room temperature for 1.5 h. To the previous reaction mixture was then added *N,N'*-disuccinimidyl carbonate (45 mg, 0.18 mmol) and the reaction was stirred at room temperature for 30 min. To the previous reaction mixture was then added a solution of *tert*-butyl (2-aminoethyl)carbamate (43 mg, 0.27 mmol) in DCM (2 mL) and the reaction was stirred at room temperature for an additional hour. The reaction was partitioned between DCM (20 mL) and water (20 mL). The layers were separated and the aqueous phase was further extracted with DCM (3 x 20 mL). The combined organic extracts were dried by passing through a hydrophobic frit and concentrated under reduced pressure. The residue was dissolved in a minimum amount of DCM and purified by automated column chromatography on silica gel eluting with 0-20% MeOH/DCM over 18 CV. The product-containing fractions were combined and concentrated under reduced pressure to afford the title compound as a pale yellow solid (114 mg, 90% yield).

LCMS (Method B): t_R =1.00 Min, $[M+H]^+ = 938.60$, purity 99%; 1H NMR (400 MHz, Chloroform-*d*) δ 8.95 (d, $J = 0.9$ Hz, 1H), 8.39 (dd, $J = 1.3, 0.9$ Hz, 1H), 8.34 (d, $J = 2.3$ Hz, 1H), 8.12 (d, $J = 1.3$ Hz, 1H), 8.10 (d, $J = 2.3$ Hz, 1H), 8.05 – 7.98 (m, 2H), 7.62 – 7.54 (m, 1H), 7.53 – 7.45 (m, 2H), 7.14 (s, 1H), 6.99 (bs, 1H), 6.63 (bs, 1H), 5.14 (bs, 1H), 4.11 (s, 3H), 3.89 – 3.79 (m, 2H), 3.79 – 3.61 (m, 4H), 3.41 – 3.35 (m,

4H), 3.34 – 3.23 (m, 2H), 2.76 (dd, $J = 10.6, 1.8$ Hz, 2H), 2.31 – 2.19 (m, 4H), 2.05 – 1.94 (m, 2H), 1.85 (app. t, $J = 10.6$ Hz, 2H), 1.43 (s, 9H), 1.14 (d, $J = 6.3$ Hz, 6H). 1H not observed (exchangeable); ^{13}C NMR (101 MHz, Chloroform- d) δ 173.5, 173.3, 159.5, 157.2, 155.4, 149.4, 141.8, 141.7, 141.6, 139.0, 137.3, 134.5, 130.0, 129.5, 129.4, 127.8, 127.6, 122.0, 121.9, 121.4, 121.0, 112.6, 80.0, 71.6, 59.0, 54.4, 53.4, 52.4, 51.7, 40.7, 40.0, 34.9, 34.5, 28.4, 21.3, 19.1; ν_{max} (neat): 3068, 2975, 2821, 1652, 1501, 1449, 1384, 1337, 1252, 1173, 1141, 1082, 725 cm^{-1} ; HRMS (Method A): calcd. for $\text{C}_{43}\text{H}_{56}\text{N}_9\text{O}_{11}\text{S}_2$ $[\text{M}+\text{H}]^+$ 938.3541; found 938.3543.



(*E*)-Cyclooct-4-en-1-yl (2-(5-((2-(*N*-(5-(4-(5-(((2*R*,6*S*)-2,6-dimethylmorpholino)methyl)oxazol-2-yl)-1*H*-indazol-6-yl)-2-methoxypyridin-3-yl)sulfamoyl)ethyl)amino)-5-oxopentanamido)ethyl)carbamate (45)

Boc deprotection:

To a stirred solution of *tert*-butyl (2-(5-((2-(*N*-(5-(4-(5-(((2*S*,6*R*)-2,6-dimethylmorpholino)methyl)oxazol-2-yl)-1-(phenylsulfonyl)-1*H*-indazol-6-yl)-2-methoxypyridin-3-yl)sulfamoyl)ethyl)amino)-5-oxopentanamido)ethyl)carbamate (150 mg, 0.16 mmol) in DCM (5 mL) was added TFA (1.5 mL) and the resulting solution was stirred at room temperature under N_2 atmosphere for 2.5 h. Volatiles were then removed under reduced pressure. The crude was partitioned between DCM (15 mL) and a saturated aqueous sodium bicarbonate solution (15 mL). The layers were separated and the aqueous phase was extracted with DCM (3 x 20 mL). The combined organic extracts were dried by passing through a hydrophobic frit and concentrated under reduced pressure to afford the crude primary amine (138 mg) as a yellow oil.

TCO installation:

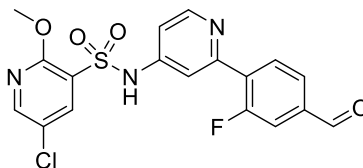
The crude was immediately dissolved in DMF (5 mL). To the previous solution was added (*E*)-cyclooct-4-en-1-yl (4-nitrophenyl) carbonate (51 mg, 0.18 mmol) and DIPEA (56 μ L, 0.32 mmol). The reaction mixture was stirred at room temperature for 2 h under N₂ atmosphere. The reaction was partitioned between EtOAc (10 mL) and water (10 mL). The layers were separated and the aqueous phase was extracted with EtOAc (3 x 10 mL). The combined organics were washed with a 5% LiCl solution (20 mL), dried by passing through a hydrophobic frit and concentrated under reduced pressure.

Benzenesulfonyl deprotection:

The crude was immediately dissolved in MeOH (5 mL). To the previous solution was added a 2.0 M NaOH aqueous solution in water (1.5 mL, 3.00 mmol). The reaction was stirred at room temperature for 15 min. Solvents were removed under reduced pressure. The residue was partitioned between EtOAc (10 mL) and water (10 mL). The layers were separated and the aqueous phase was further extracted with EtOAc (3 x 10 mL). The combined organic extracts were dried by passing through a hydrophobic frit and concentrated under reduced pressure. The residue was taken up in MeOH/DMSO (1:1, 2 mL). 1 mL of this solution was purified by preparative HPLC (Method G). The product-containing fractions were combined, partially evaporated under reduced pressure and lyophilized. The residue was taken up in MeCN/water (1:1, 8 mL) and lyophilized again to afford the title compound as a white solid (18 mg, 13% over 3 steps).

LCMS (Method B): t_R = 0.87 Min, $[M+H]^+$ = 850.39, purity 100%; ¹H NMR (600 MHz, DMSO-*d*₆) δ 13.48 (bs, 1H), 9.62 (bs, 1H), 8.58 (s, 1H), 8.39 (d, J = 2.3 Hz, 1H), 7.98 (d, J = 2.3 Hz, 1H), 7.95 (bs, 1H), 7.93 (d, J = 1.3 Hz, 1H), 7.87 (s, 1H), 7.74 (bs, 1H), 7.35 (s, 1H), 6.89 (bs, 1H), 5.61 – 5.50 (m, 1H), 5.46 – 5.36 (m, 1H), 4.22 – 4.16 (m, 1H), 3.99 (s, 3H), 3.74 (s, 2H), 3.64 – 3.55 (m, 2H), 3.54 – 3.45 (m, 2H), 3.29 – 3.26 (m, 2H), 3.10 – 3.00 (m, 2H), 3.00 – 2.93 (m, 2H), 2.81 (dd, J = 10.6, 1.8 Hz, 2H), 2.29 – 2.17 (m, 3H), 2.06 – 1.99 (m, 4H), 1.94 – 1.80 (m, 4H), 1.78 (app. t, J = 10.6 Hz, 2H), 1.72 – 1.64 (m, 2H), 1.64 – 1.53 (m, 2H), 1.53 – 1.45 (m, 1H),

1.04 (d, $J = 6.3$ Hz, 6H); ^{13}C NMR (151 MHz, $\text{DMSO-}d_6$) δ 172.0, 171.8, 159.9, 156.3, 155.8, 149.2, 141.1, 140.5, 134.9, 134.8, 133.6, 132.5, 130.7, 129.5, 127.5, 121.8, 119.6, 118.4, 117.9, 110.0, 79.1, 70.9, 58.3, 53.8, 51.4, 51.3, 40.6, 40.1, 39.9, 38.6, 38.1, 34.7, 33.7, 32.1, 30.5, 21.2, 18.9; $\nu_{\text{max}}(\text{neat})$: 3291, 2934, 2859, 1690, 1649, 1544, 1486, 1334. 1253. 1138, 1081, 996 cm^{-1} ; HRMS (Method B): calcd. for $\text{C}_{41}\text{H}_{56}\text{N}_9\text{O}_9\text{S}$ $[\text{M}+\text{H}]^+$ 850.3922; found 850.3912.

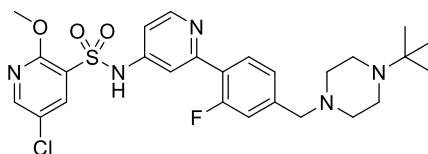


5-Chloro-*N*-(2-(2-fluoro-4-formylphenyl)pyridin-4-yl)-2-methoxypyridine-3-sulfonamide (145)

To a microwave vial was added *N*-(2-bromopyridin-4-yl)-5-chloro-2-methoxypyridine-3-sulfonamide (1.03 g, 2.72 mmol), (2-fluoro-4-formylphenyl)boronic acid (0.91 g, 5.44 mmol), tripotassium phosphate (1.73 g, 8.16 mmol) and Solvias catalyst (2'-(Dimethylamino)-2-biphenyl-palladium(II) chloride Dinorbornylphosphine complex) (198 mg, 0.35 mmol). Solids were suspended in ethanol (8 mL) and water (2 mL). The vial was sealed and the atmosphere was purged with 3 nitrogen/vacuum cycles. The reaction was heated in the microwave for 35 min at 110 °C. The reaction mixture was filtered through celite and eluted with MeOH (150 mL). The filtrate was concentrated under reduced pressure. The residue was taken in a minimum amount of DCM and Florisil was added. The solvent was removed under reduced pressure to adsorb the compound. Purification was carried out by automated column chromatography on silica gel eluting with 0-20% MeOH/DCM over 20 CV. The product-containing fractions were combined and concentrated under reduced pressure to afford the title compound as an orange solid (585 mg, 51% yield).

LCMS (Method A): $t_R = 1.00$ Min, $[\text{M}+\text{H}]^+ = 422.07$, purity 93%; ^1H NMR (400 MHz, $\text{Chloroform-}d$) δ 10.02 (d, $J = 1.8$ Hz, 1H), 8.54 (d, $J = 5.6$ Hz, 1H), 8.30 – 8.24 (m, 2H), 8.19 – 8.11 (m, 1H), 7.75 (dd, $J = 8.0, 1.5$ Hz, 1H), 7.65 (dd, $J = 11.1, 1.5$ Hz,

1H), 7.58 – 7.54 (m, 1H), 7.09 (dd, $J = 5.6, 2.2$ Hz, 1H), 4.09 (s, 3H). 1H not observed (exchangeable); ^{13}C NMR (101 MHz, Chloroform- d) δ 190.7, 160.8 (d, $J = 253.1$ Hz), 157.9, 153.2, 151.03, 150.93, 144.9, 140.0, 138.5 (d, $J = 6.8$ Hz), 132.2 (d, $J = 12.5$ Hz), 132.1 (d, $J = 2.2$ Hz), 126.2 (d, $J = 3.3$ Hz), 124.6, 121.8, 116.5 (d, $J = 24.0$ Hz), 114.3 (d, $J = 10.6$ Hz), 112.6, 55.3; ^{19}F NMR (376 MHz, Chloroform- d) δ -115.23 – -115.55 (m); ν_{max} (neat): 3086, 2957, 1693, 1614, 1499, 1458, 1300, 1139, 1069, 763, 601 cm^{-1} ; HRMS (Method A): calcd. for $\text{C}_{18}\text{H}_{14}\text{ClFN}_3\text{O}_4\text{S}$ $[\text{M}+\text{H}]^+$ 422.0378; found 422.0384.

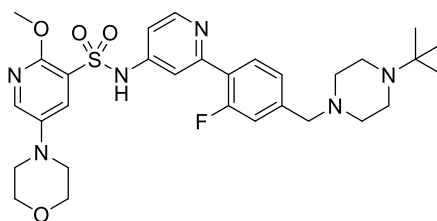


***N*-(2-(4-((4-(*tert*-butyl)piperazin-1-yl)methyl)-2-fluorophenyl)pyridin-4-yl)-5-chloro-2-methoxypyridine-3-sulfonamide (146)**

To a stirred solution of 5-chloro-*N*-(2-(2-fluoro-4-formylphenyl)pyridin-4-yl)-2-methoxypyridine-3-sulfonamide (1.75 g, 3.53 mmol in DCM (15 mL) was added a solution of 1-(*tert*-butyl)piperazine (1.01 g, 7.06 mmol) in DCM (5 mL) followed by acetic acid (101 μL , 1.77 mmol). The reaction was stirred at room temperature for 30 min after which sodium triacetoxyborohydride (1.12 g, 5.30 mmol) was added in one portion. The reaction was stirred at room temperature for 2 h. The reaction mixture was partitioned between DCM (100 mL) and a saturated sodium bicarbonate solution (100 mL). The layers were separated and the aqueous phase was further extracted with DCM (3 x 80 mL). The combined organic extracts were dried by passing through a hydrophobic frit and concentrated under reduced pressure. The residue was dissolved in a minimum amount of DCM and purified by automated normal phase chromatography on silica gel eluting with 0-20% MeOH/DCM over 20 CV. The product-containing fractions were combined and concentrated under reduced pressure to afford the title compound as a pale yellow solid (1.39 g, 72% yield).

LCMS (Method B): $t_{\text{R}} = 0.82$ Min, $[\text{M}+\text{H}]^+ = 548.14$, purity 99%; ^1H NMR (400 MHz, DMSO- d_6) δ 8.35 (d, $J = 2.6$ Hz, 1H), 8.21 (d, $J = 6.0$ Hz, 1H), 8.19 (bs, 1H), 8.16 (d,

$J = 2.6$ Hz, 1H), 7.80 – 7.73 (m, 1H), 7.31 – 7.27 (m, 1H), 7.25 – 7.23 (m, 1H), 7.23 – 7.19 (m, 1H), 6.89 (dd, $J = 5.9, 2.2$ Hz, 1H), 3.86 (s, 3H), 3.57 (s, 2H), 2.95 – 2.78 (m, 4H), 2.62 – 2.51 (m, 4H), 1.14 (s, 9H); ^{13}C NMR (101 MHz, DMSO- d_6) δ 162.1 (d, $J = 280.9$ Hz), 158.2, 153.8 (d, $J = 11.3$ Hz), 150.7, 147.8, 147.7, 141.3 (d, $J = 7.7$ Hz), 138.1, 130.5 (d, $J = 2.7$ Hz), 126.5, 125.0, 124.9 (d, $J = 2.7$ Hz), 122.6, 116.1 (d, $J = 22.8$ Hz), 114.6 (d, $J = 7.8$ Hz), 113.3, 60.3, 57.6, 54.2, 51.5, 45.5, 24.8; ^{19}F NMR (376 MHz, DMSO- d_6) δ -116.39 – -118.79 (m); ν_{max} (neat): 3019, 2769, 1624, 1574, 1471, 1329, 1220, 1292, 1102, 1001, 868 cm^{-1} ; HRMS (Method B): calcd. for $\text{C}_{26}\text{H}_{32}\text{ClFN}_5\text{O}_3\text{S}$ $[\text{M}+\text{H}]^+$ 548.1898; found 548.1899.

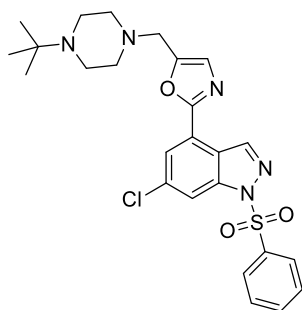


***N*-(2-(4-((4-(*tert*-butyl)piperazin-1-yl)methyl)-2-fluorophenyl)pyridin-4-yl)-2-methoxy-5-morpholinopyridine-3-sulfonamide (141)**

In an oven-dried microwave vial was added *N*-(2-(4-((4-(*tert*-butyl)piperazin-1-yl)methyl)-2-fluorophenyl)pyridin-4-yl)-5-chloro-2-methoxypyridine-3-sulfonamide (424 mg, 0.77 mmol), RuPhos (72 mg, 0.16 mmol), palladium(II) acetate (17 mg, 0.077 mmol) and sodium *tert*-butoxide (387 mg, 4.02 mmol). The vial was sealed and solids were dissolved in toluene (10 mL). Morpholine (0.14 mL, 1.63 mmol) was then added and the atmosphere in the vial was purged with 3 vacuum/nitrogen cycles. The vial was heated thermally to 90 °C for 1 h. The reaction mixture was cooled down to room temperature, filtered through celite and eluted with MeOH (200 mL). The filtrate was concentrated under reduced pressure, dissolved in DMSO/MeOH (1:1, 6 mL) and purified by automated reverse phase chromatography eluting with 5-25% MeCN + 0.1% Formic acid/ Water + 0.1% Formic acid. The product-containing fractions were concentrated under reduced pressure to remove most of the acetonitrile. The remaining aqueous was partitioned between EtOAc (50 mL) and a saturated aqueous sodium bicarbonate solution (30 mL). The layers were separated and the aqueous was further

extracted with EtOAc (3 x 50 mL). The combined organic extracts were dried by passing through a hydrophobic frit and concentrated under reduced pressure. The product was dissolved in DMSO/MeOH (1:5 mL, 6 mL) and the solids were isolated by vacuum filtration. The solid was washed with more MeOH (10 mL) and dried under vacuum. The solid was then dissolved in MeCN/water (1:1, 6 mL) and freeze-dried overnight to afford the title compound as a white solid (12 mg, 3%).

LCMS (Method B): t_R = 0.72 Min, $[M+H]^+$ = 599.23, purity 100%; 1H NMR (400 MHz, DMSO- d_6) δ 8.30 (d, J = 5.7 Hz, 1H), 8.02 (d, J = 3.0 Hz, 1H), 7.83 (d, J = 3.0 Hz, 1H), 7.80 – 7.73 (m, 1H), 7.40 – 7.35 (m, 1H), 7.23 – 7.17 (m, 2H), 6.95 (dd, J = 5.7, 2.2 Hz, 1H), 3.83 (s, 3H), 3.78 – 3.67 (m, 4H), 3.52 (s, 2H), 3.09 – 3.01 (m, 4H), 2.70 – 2.58 (m, 4H), 2.49 – 2.35 (m, 4H), 1.05 (s, 9H). 1H not observed (exchangeable); ^{13}C NMR (101 MHz, DMSO- d_6) δ 159.5 (d, J = 248.6 Hz), 153.1, 151.7, 149.1, 148.9, 142.0, 141.9, 138.0, 130.4 (d, J = 2.7 Hz), 127.5, 125.0, 124.80 (d, J = 2.7 Hz), 122.5, 116.0, (d, J = 23.0 Hz), 113.1 (d, J = 9.5 Hz), 112.1, 65.9, 60.7, 54.7, 53.7, 52.7, 48.9, 45.3, 25.3; ^{19}F NMR (376 MHz, DMSO- d_6) δ -117.11 – -117.30 (m); ν_{max} (neat): 2968, 2817, 1625, 1589, 1476, 1304, 1273, 1119, 1002, 957, 872 cm^{-1} ; HRMS (Method A): calcd. for $C_{30}H_{40}FN_6O_4S$ $[M+H]^+$ 599.2816; found 599.2818.

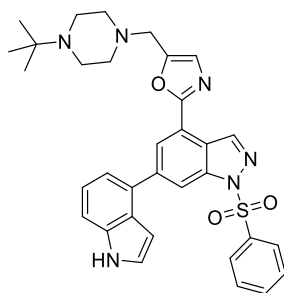


5-((4-(*tert*-Butyl)piperazin-1-yl)methyl)-2-(6-chloro-1-(phenylsulfonyl)-1*H*-indazol-4-yl)oxazole (147)

To a stirred suspension of 2-(6-chloro-1-(phenylsulfonyl)-1*H*-indazol-4-yl)oxazole-5-carbaldehyde (300 mg, 0.77 mmol) in DCM (8 mL) was added 1-(*tert*-butyl)piperazine (330 mg, 2.32 mmol) and acetic acid (22 μ L, 0.39 mmol). The reaction mixture was stirred for 30 min at room temperature under nitrogen after which sodium triacetoxyborohydride (246 mg, 1.16 mmol) was added in one portion. The reaction

was then stirred at room temperature overnight. The reaction was partitioned between DCM (20 mL) and a saturated aqueous sodium bicarbonate solution (20 mL). The layers were separated and the aqueous phase was further extracted with DCM (3 x 20 mL). The combined organic extracts were dried by passing through a hydrophobic frit. Florisil was added and the solvent was removed under reduced pressure to adsorb the compound. Purification was carried out by automated column chromatography on silica gel eluting with 0-30% MeOH/EtOAc over 20 CV. The product-containing fractions were combined and concentrated under reduced pressure to afford the title compound as a beige solid (279 mg, 70% yield).

LCMS (Method A): $t_R = 0.85$ Min, $[M+H]^+ = 514.20$, 100% purity; 1H NMR (400 MHz, Chloroform-*d*) δ 8.91 (d, $J = 0.9$ Hz, 1H), 8.31 (dd, $J = 1.7, 0.9$ Hz, 1H), 8.05 – 7.99 (m, 2H), 7.96 (d, $J = 1.7$ Hz, 1H), 7.65 – 7.57 (m, 1H), 7.55 – 7.44 (m, 2H), 7.13 (s, 1H), 3.71 (s, 2H), 2.79 – 2.43 (m, 8H), 1.08 (s, 9H); ^{13}C NMR (101 MHz, Chloroform-*d*) δ 158.7, 150.3, 141.8, 141.5, 137.4, 136.0, 134.7, 129.6, 128.1, 127.8, 123.4, 121.8, 121.3, 114.6, 53.8, 52.4, 45.7, 26.0; $\nu_{max}(\text{neat})$: 3080, 2973, 2810, 1586, 1447, 1377, 1290, 1204, 1173, 1069, 923 cm^{-1} ; HRMS (Method A): calcd. for $C_{25}H_{29}ClN_5O_3S$ $[M+H]^+ 514.1680$; found 514.1705.

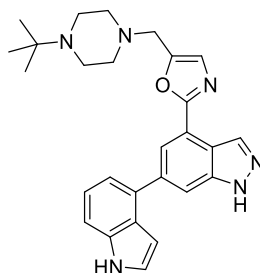


2-(6-(1H-Indol-4-yl)-1-(phenylsulfonyl)-1H-indazol-4-yl)-5-((4-(tert-butyl)piperazin-1-yl)methyl)oxazole (148)

To a microwave vial was added 5-((4-(*tert*-butyl)piperazin-1-yl)methyl)-2-(6-chloro-1-(phenylsulfonyl)-1H-indazol-4-yl)oxazole (239 mg, 0.47 mmol), indole-4-boronic acid pinacol ester (136 mg, 0.56 mmol), XPhos Pd G2 (7 mg, 9.30 μmol) and sodium carbonate (148 mg, 1.40 mmol). Solids were dissolved in 1,4-dioxane (5 mL) and

water (0.5 mL) was added. The vial was sealed and the atmosphere was purged with 3 vacuum/nitrogen cycles. The reaction was heated in the microwave for 1 h at 90 °C. The reaction was partitioned between EtOAc (25 mL) and water (25 mL). The layers were separated and the aqueous phase was further extracted with EtOAc (3 x 20 mL). The combined organic extracts were dried by passing through a hydrophobic frit. Florisil was added and the solvent was removed under reduced pressure to adsorb the compound. Purification was carried out by automated column chromatography on silica gel eluting with 0-30% MeOH/EtOAc over 20 CV. The product-containing fractions were combined and concentrated under reduced pressure to afford the title compound a beige solid (139 mg, 50% yield).

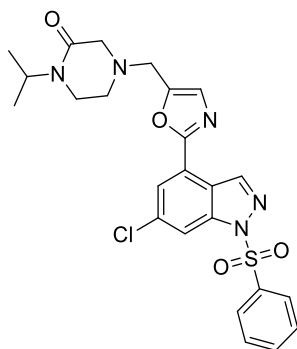
LCMS (Method A): t_R = 0.87 Min, $[M+H]^+$ = 595.45, purity 100%; 1H NMR (400 MHz, DMSO- d_6) δ 11.45 (bs, 1H), 8.99 (d, J = 0.9 Hz, 1H), 8.50 (dd, J = 1.3, 0.9 Hz, 1H), 8.25 (d, J = 1.3 Hz, 1H), 8.06 – 7.94 (m, 2H), 7.78 – 7.72 (m, 1H), 7.67 – 7.60 (m, 2H), 7.58 – 7.52 (m, 2H), 7.34 – 7.26 (m, 3H), 6.67 – 6.53 (m, 1H), 3.69 (s, 2H), 2.48 – 2.38 (m, 8H), 0.94 (s, 9H); ^{13}C NMR (101 MHz, DMSO- d_6) δ 158.5, 150.2, 142.9, 141.6, 141.1, 136.5, 136.3, 135.2, 131.0, 130.0, 127.4, 127.2, 126.8, 125.5, 122.9, 121.5, 120.7, 120.5, 119.4, 112.9, 112.2, 99.5, 53.0, 52.9, 51.2, 45.1, 25.6; ν_{max} (neat): 3253, 2963, 1604, 1532, 1450, 1371, 1278, 1172, 1093, 966, 727 cm^{-1} ; HRMS (Method A): calcd. for $C_{33}H_{35}N_6O_3S$ $[M+H]^+$ 595.2491.; found 595.2529.



2-(6-(1*H*-indol-4-yl)-1*H*-indazol-4-yl)-5-((4-(*tert*-butyl)piperazin-1-yl)methyl)oxazole (142)

To a stirred suspension of 2-(6-(1*H*-indol-4-yl)-1-(phenylsulfonyl)-1*H*-indazol-4-yl)-5-((4-(*tert*-butyl)piperazin-1-yl)methyl)oxazole (98 mg, 0.17 mmol) in MeOH (5 mL) was added sodium hydroxide 2.0 M in water (1 mL). The reaction was stirred at room temperature for 20 min. More sodium hydroxide 2.0 M in water (1 mL) was added and reaction was stirred for an additional hour at room temperature. MeOH was removed under reduced pressure. The crude was partitioned between EtOAc (15 mL) and water (15 mL). The layers were separated and the aqueous phase was further extracted with EtOAc (3 x 15 mL). The combined organic extracts were dried by passing through a hydrophobic frit and concentrated under reduced pressure. The crude was dissolved in MeOH/DMSO (1:1, 2 mL) and purified by Mass Directed Automated Preparative HPLC (Method C). The product-containing fractions were concentrated under reduced pressure. The residue was dissolved in MeCN/water (1:1, 6 mL) and freeze-dried to afford the title compound as a white solid (12.5 mg, 17% yield).

LCMS (Method B), t_R = 1.04 Min, $[M+H]^+$ = 455.33, purity 99%; 1H NMR (600 MHz, Methanol- d_4) δ 8.69 (s, 1H), 8.24 (s, 1H), 7.95 (s, 1H), 7.48 – 7.42 (m, 1H), 7.33 (d, J = 3.2 Hz, 1H), 7.29 – 7.19 (m, 3H), 6.67 (dd, J = 3.2, 1.0 Hz, 1H), 3.79 (s, 2H), 2.85 – 2.54 (m, 8H), 1.07 (s, 9H). 2H not observed (exchangeable); ^{13}C NMR (151 MHz, Methanol- d_4) δ 162.9, 150.0, 143.0, 142.1, 138.3, 135.3, 134.1, 128.8, 127.6, 126.4, 122.7, 122.6, 120.6, 120.4, 119.6, 113.0, 112.2, 101.5, 55.2, 53.9, 52.7, 46.3, 25.8; HRMS (Method A): calcd. for $C_{27}H_{31}N_6O$ $[M+H]^+$ 455.2559; found 455.2563.

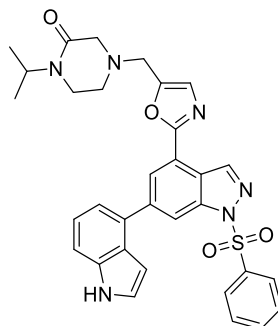


4-((2-(6-Chloro-1-(phenylsulfonyl)-1*H*-indazol-4-yl)oxazol-5-yl)methyl)-1-isopropylpiperazin-2-one (152)

To a stirred suspension of 1-isopropylpiperazin-2-one, hydrochloride (90 mg, 0.50 mmol) in DCM (6 mL) was added triethylamine (70 μ L, 0.50 mmol). The reaction mixture was stirred at room temperature for 5 min and sonicated for a few seconds upon which all solids went into solution. Then, 2-(6-chloro-1-(phenylsulfonyl)-1*H*-indazol-4-yl)oxazole-5-carbaldehyde (150 mg, 0.39 mmol) was added in one portion followed by acetic acid (11 μ L, 0.19 mmol). The reaction was stirred at room temperature for 30 min after which sodium triacetoxyborohydride (123 mg, 0.58 mmol) was added in one portion. The reaction mixture was stirred for an additional hour at room temperature. The reaction was partitioned between DCM (20 mL) and a saturated aqueous sodium bicarbonate solution (20 mL). The layers were separated and the aqueous was further extracted with DCM (3 x 25 mL). The combined organics were dried by passing through a hydrophobic frit and concentrated under reduced pressure. The crude residue was taken in a minimum amount of DCM and purified by automated column chromatography on silica gel eluting with 0-25% MeOH/EtOAc over 18 CV. The product containing fractions were concentrated under reduced pressure to afford the title compound as a colourless oil (145 mg, 73% yield).

LCMS (Method A): t_R = 1.20 Min, MH^+ = 514.29, purity 99%; 1H NMR (400 MHz, Chloroform-*d*) δ 8.87 (d, J = 0.9 Hz, 1H), 8.27 (dd, J = 1.7, 0.9 Hz, 1H), 8.00 – 7.94 (m, 2H), 7.90 (d, J = 1.7 Hz, 1H), 7.60 – 7.54 (m, 1H), 7.50 – 7.42 (m, 2H), 7.15 (s, 1H), 4.81 (sept, J = 6.8 Hz, 1H), 3.73 (s, 2H), 3.26 – 3.17 (m, 4H), 2.79 – 2.70 (m, 2H), 1.09 (d, J = 6.8 Hz, 6H); ^{13}C NMR (101 MHz, Chloroform-*d*) δ 165.6, 158.9,

148.7, 141.6, 141.3, 137.2, 135.8, 134.7, 129.5, 128.3, 127.7, 123.3, 121.5, 121.2, 114.7, 57.0, 51.2, 49.4, 43.7, 39.7, 19.1; ν_{max} (neat): 3126, 3071, 2974, 1636, 1585, 1491, 1448, 1378, 1172, 1076, 855 cm^{-1} ; HRMS (Method B): calcd. for $\text{C}_{24}\text{H}_{25}\text{ClN}_5\text{O}_4\text{S}$ $[\text{M}+\text{H}]^+$ 514.1316; found 514.1321.

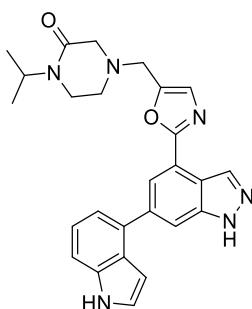


4-((2-(6-(1*H*-indol-4-yl)-1-(phenylsulfonyl)-1*H*-indazol-4-yl)oxazol-5-yl)methyl)-1-isopropylpiperazin-2-one (153)

A microwave vial was charged with 4-((2-(6-chloro-1-(phenylsulfonyl)-1*H*-indazol-4-yl)oxazol-5-yl)methyl)-1-isopropylpiperazin-2-one (135 mg, 0.26 mmol), indole-4-boronic acid pinacol ester (128 mg, 0.53 mmol), XPhos Pd G2 (41 mg, 0.053 mmol) and sodium carbonate (84 mg, 0.79 mmol). Solids were suspended in 1,4-dioxane (4.5 mL) and water (0.5 mL). The vial was sealed and purged with 3 vacuum/nitrogen cycles and subsequently heated at 90 °C in the microwave for 1 h. The reaction mixture was partitioned between EtOAc (20 mL) and water (20 mL). The layers were separated and the aqueous phase was extracted with EtOAc (3 x 20 mL). The combined organic extracts were dried by passing through a hydrophobic frit and concentrated under reduced pressure. The residue was dissolved in a minimum amount of DCM and purified by automated column chromatography on silica gel eluting with 0-20% MeOH/EtOAc over 18 CV. The product-containing fractions were combined and concentrated under reduced pressure to afford the title compound as a beige solid (128 mg, 82% yield).

LCMS (Method B): t_{R} = 1.22 Min, $[\text{M}+\text{H}]^+$ = 595.37, purity 89%; ^1H NMR (400 MHz, Chloroform-*d*) δ 8.99 (d, J = 0.9 Hz, 1H), 8.69 (bs, 1H), 8.63 (dd, J = 1.3, 0.9 Hz, 1H), 8.35 (d, J = 1.3 Hz, 1H), 8.06 – 8.01 (m, 2H), 7.60 – 7.53 (m, 1H), 7.53 – 7.42 (m,

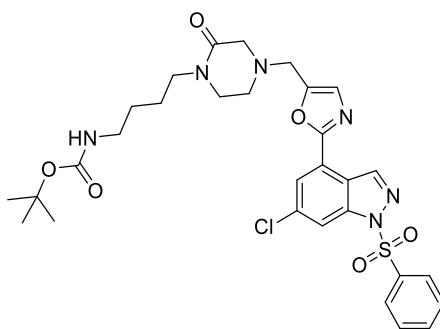
3H), 7.37 – 7.31 (m, 3H), 7.18 (s, 1H), 6.78 – 6.73 (m, 1H), 4.84 (sept, $J = 6.8$ Hz, 1H), 3.79 – 3.72 (m, 2H), 3.27 – 3.20 (m, 4H), 2.80 – 2.72 (m, 2H), 1.10 (d, $J = 6.8$ Hz, 6H); ^{13}C NMR (101 MHz, Chloroform- d) δ 165.7, 160.4, 148.2, 143.2, 142.0, 141.7, 137.7, 136.6, 134.4, 132.7, 129.5, 128.2, 127.8, 126.4, 125.5, 124.3, 122.5, 121.8, 120.7, 120.6, 114.6, 111.6, 101.7, 57.1, 51.2, 49.4, 43.8, 39.8, 19.2; ν_{max} (neat): 3248, 2977, 1644, 1604, 1447, 1370, 1343, 1307, 1182, 1091, 757 cm^{-1} ; HRMS (Method B): calcd. for $\text{C}_{32}\text{H}_{31}\text{N}_6\text{O}_4\text{S}$ $[\text{M}+\text{H}]^+$ 595.2127; found 595.2129.



4-((2-(6-(1H-indol-4-yl)-1H-indazol-4-yl)oxazol-5-yl)methyl)-1-isopropylpiperazin-2-one (150)

To a stirred suspension of 4-((2-(6-(1H-indol-4-yl)-1-(phenylsulfonyl)-1H-indazol-4-yl)oxazol-5-yl)methyl)-1-isopropylpiperazin-2-one (102 mg, 0.17 mmol) in MeOH (5 mL) was added sodium hydroxide 1.0 M in water (1.5 mL) upon which all solids went into solution. The reaction mixture was stirred at room temperature for 30 min. MeOH was removed under reduced pressure and the residue was partitioned between EtOAc (15 mL) and water (15 mL). The layers were separated and the aqueous was further extracted with EtOAc (3 x 15 mL). The combined organics extracts were dried by passing through a hydrophobic frit and concentrated under reduced pressure. The crude was dissolved in MeOH/DMSO (1:1, 1 mL) and purified by Mass Directed Automated Preparative HPLC (Method C). The product-containing fractions were concentrated under reduced pressure to remove most of the acetonitrile. The aqueous was then extracted with EtOAc (3 x 20 mL). The combined organics extracts were dried by passing through a hydrophobic frit and concentrated under reduced pressure. The residue was dissolved in MeCN/water (1:1, 8 mL) and freeze-dried overnight to afford the title compound as a white solid (29 mg, 37% yield).

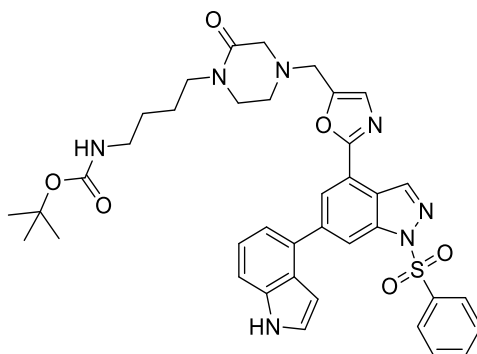
LCMS (Method B): $t_R = 0.93$ Min, $[M+H]^+ = 455.34$, purity 100%; 1H NMR (400 MHz, Methanol- d_4) δ 8.67 (d, $J = 1.0$ Hz, 1H), 8.22 (d, $J = 1.3$ Hz, 1H), 7.94 (dd, $J = 1.3, 1.0$ Hz, 1H), 7.48 – 7.41 (m, 1H), 7.32 (d, $J = 3.2$ Hz, 1H), 7.29 (s, 1H), 7.26 – 7.18 (m, 2H), 6.66 (dd, $J = 3.2, 1.0$ Hz, 1H), 4.70 (sept, $J = 6.8$ Hz, 1H), 3.84 (s, 2H), 3.30 – 3.24 (m, 4H), 2.85 – 2.79 (m, 2H), 1.11 (d, $J = 6.8$ Hz, 6H). 2H not observed (exchangeable); ^{13}C NMR (101 MHz, Methanol- d_4) δ 168.2, 163.0, 149.6, 142.8, 142.1, 138.3, 135.4, 134.1, 128.8, 127.6, 126.4, 122.7, 122.6, 120.6, 120.4, 119.6, 113.0, 112.2, 101.5, 57.5, 51.5, 50.0, 45.7, 41.0, 19.1; HRMS (Method B): calcd. for $C_{26}H_{27}N_6O_2$ $[M+H]^+ 455.2195$; found 455.2193.



***tert*-Butyl (4-(4-((2-(6-chloro-1-(phenylsulfonyl)-1*H*-indazol-4-yl)oxazol-5-yl)methyl)-2-oxopiperazin-1-yl)butyl)carbamate (156)**

To a stirred solution of *tert*-butyl (4-(4-((2-(6-chloro-1-(phenylsulfonyl)-1*H*-indazol-4-yl)oxazol-5-yl)methyl)piperazin-1-yl)butyl)carbamate (405 mg, 0.644 mmol) in THF (18 mL) and water (7.2 mL) was added sodium bicarbonate (541 mg, 6.44 mmol) followed by iodine (1.23 mg, 4.83 mmol). The reaction was stirred at room temperature for 45 min. The reaction was quenched by the addition of a saturated aqueous sodium thiosulfate solution (15 mL). The reaction mixture was partitioned between EtOAc (50 mL) and water (50 mL). The layers were separated and the aqueous was extracted with EtOAc (3 x 50 mL). The combined organic extracts were dried by passing through a hydrophobic frit and concentrated under reduced pressure. The crude was dissolved in a minimum amount of DCM and purified by automated column chromatography on silica gel eluting with 0-25% MeOH/EtOAc over 18 CV. The product-containing fractions were combined and concentrated under reduced pressure to afford the title compound as a yellow oil (225 mg, 54% yield).

LCMS (Method A): $t_R = 1.28$ Min, $[M+H]^+ = 643.24$, purity 100%; 1H NMR (400 MHz, Chloroform- d) δ 8.89 (d, $J = 0.9$ Hz, 1H), 8.30 (dd, $J = 1.6, 0.9$ Hz, 1H), 8.02 – 7.97 (m, 2H), 7.92 (d, $J = 1.6$ Hz, 1H), 7.63 – 7.55 (m, 1H), 7.52 – 7.45 (m, 2H), 7.16 (s, 1H), 4.63 (bs, 1H), 3.82 – 3.67 (m, 2H), 3.40 – 3.30 (m, 4H), 3.22 (s, 2H), 3.16 – 3.07 (m, 2H), 2.81 – 2.74 (m, 2H), 1.61 – 1.51 (m, 2H), 1.51 – 1.43 (m, 2H), 1.41 (s, 9H); ^{13}C NMR (101 MHz, Chloroform- d) δ 166.3, 159.0, 156.2, 148.7, 141.7, 141.4, 137.3, 135.91, 134.7, 129.5, 128.4, 127.8, 123.4, 121.5, 121.3, 114.8, 79.3, 56.8, 51.2, 49.4, 46.5, 46.1, 40.2, 28.5, 27.4, 24.2; ν_{max} (neat): 3328, 2974, 2931, 2917, 1700, 1637, 1537, 1502, 1449, 1380, 1291, 1174, 1093, 924. cm^{-1} ; HRMS (Method A): calcd. for $C_{30}H_{36}ClN_6O_6S$ $[M+H]^+ 643.2106$; found 643.2101.

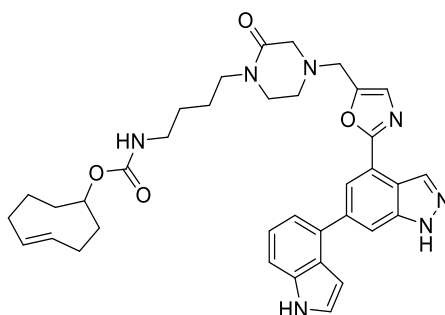


***tert*-Butyl (4-(4-((2-(6-(1*H*-indol-4-yl)-1-(phenylsulfonyl)-1*H*-indazol-4-yl)oxazol-5-yl)methyl)-2-oxopiperazin-1-yl)butyl)carbamate (157)**

To a microwave vial was added *tert*-butyl (4-(4-((2-(6-chloro-1-(phenylsulfonyl)-1*H*-indazol-4-yl)oxazol-5-yl)methyl)-2-oxopiperazin-1-yl)butyl)carbamate (288 mg, 0.45 mmol), indole-4-boronic acid pinacol ester (218 mg, 0.90 mmol), XPhos Pd G2 (71 mg, 0.090 mmol) and sodium carbonate (142 mg, 1.34 mmol). The solids were suspended in 1,4-dioxane (5 mL) and water (1 mL). The vial was sealed and the atmosphere was purged with 3 nitrogen/vacuum cycles. The vial was heated in the microwave at 90 °C for 1 h. The reaction mixture was partitioned between EtOAc (30 mL) and water (30 mL). The layers were separated and the aqueous phase was further extracted with EtOAc (3 x 30 mL). The combined organic extracts were dried by passing through a hydrophobic frit and concentrated under reduced pressure. The crude was dissolved in a minimum amount of DCM and purified by automated column

chromatography on silica gel eluting with 0-25% MeOH/EtOAc over 20 CV. The product-containing fractions were combined and concentrated under reduced pressure to afford the title compound as a light brown solid (178 mg, 55% yield). The compound was immediately taken forward in the following step.

LCMS (Method A): t_R = 1.26 Min, $[M+H]^+$ = 724.25, purity 95%.



(*E*)-Cyclooct-4-en-1-yl (4-(4-((2-(6-(1*H*-indol-4-yl)-1*H*-indazol-4-yl)oxazol-5-yl)methyl)-2-oxopiperazin-1-yl)butyl)carbamate (154)

Boc deprotection:

To a stirred solution of *tert*-butyl (4-(4-((2-(6-(1*H*-indol-4-yl)-1-(phenylsulfonyl)-1*H*-indazol-4-yl)oxazol-5-yl)methyl)-2-oxopiperazin-1-yl)butyl)carbamate (172 mg, 0.24 mmol) in DCM (8 mL) was added TFA (1 mL). The reaction was stirred at room temperature for 1.5 h. Volatiles were removed under reduced pressure, the crude was suspended in toluene (2 x 8 mL) and solvents were removed under reduced pressure to afford the crude TFA salt as a brown solid. The crude was immediately taken forward in the next step.

TCO installation:

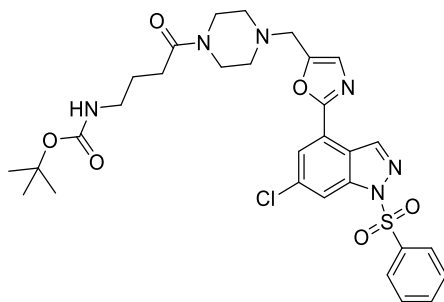
To a stirred solution of crude 4-((2-(6-(1*H*-indol-4-yl)-1-(phenylsulfonyl)-1*H*-indazol-4-yl)oxazol-5-yl)methyl)-1-(4-aminobutyl)piperazin-2-one, trifluoroacetic acid salt in DMF (6 mL) was added DIPEA (0.33 mL, 1.90 mmol). The reaction mixture was stirred at room temperature for 5 min after which (*E*)-cyclooct-4-en-1-yl (4-nitrophenyl) carbonate (76 mg, 0.26 mmol) was added in one portion. The reaction was stirred at room temperature for 1.5 h. The reaction mixture was partitioned between EtOAc (25 mL) and water (25 mL). The layers were separated and the

aqueous was further extracted with EtOAc (3 x 30 mL). The combined organic extracts were washed with a 5% aqueous LiCl solution (2 x 50 mL), dried by passing through a hydrophobic frit and concentrated under reduced pressure to afford the crude material as a yellow oil which was immediately taken forward in the next step.

Benzenesulfonyl deprotection:

To a stirred suspension of the crude (*E*)-cyclooct-4-en-1-yl (4-(4-((2-(6-(1*H*-indol-4-yl)-1-(phenylsulfonyl)-1*H*-indazol-4-yl)oxazol-5-yl)methyl)-2-oxopiperazin-1-yl)butyl)carbamate (184 mg, 0.24 mmol) in MeOH (6 mL) was added sodium hydroxide 1 M in water (1 mL) and the reaction mixture was stirred at room temperature for 1 h. MeOH was removed under reduced pressure and the residue was partitioned between EtOAc (20 mL) and water (20 mL). The layers were separated and the aqueous phase was further extracted with EtOAc (3 x 20 mL). The combined organic extracts were washed with brine (50 mL), dried by passing through a hydrophobic frit and concentrated under reduced pressure. The crude was dissolved in MeOH/DMSO (1:1, 2 mL) and purified by Mass Directed Automated Preparative HPLC (Method B, 2 x 1 mL injection). The product-containing fractions were freeze-dried to afford the title compound as a white solid (26.8 mg, 18% yield over 3 steps).

LCMS (Method B): t_R = 1.10 Min, $[M+H]^+$ = 636.33, purity 100%; 1H NMR (400 MHz, Methanol- d_4) δ 8.66 (d, J = 0.9 Hz, 1H), 8.21 (d, J = 1.3 Hz, 1H), 7.94 (dd, J = 1.3, 0.9 Hz, 1H), 7.49 – 7.41 (m, 1H), 7.33 (d, J = 3.2 Hz, 1H), 7.28 (s, 1H), 7.26 – 7.19 (m, 2H), 6.66 (dd, J = 3.3, 0.9 Hz, 1H), 5.68 – 5.52 (m, 1H), 5.50 – 5.34 (m, 1H), 4.78 – 4.66 (m, 1H), 3.84 (s, 2H), 3.42 – 3.33 (m, 4H), 3.24 (s, 2H), 3.18 – 3.02 (m, 2H), 2.87 – 2.78 (m, 2H), 2.37 – 2.22 (m, 1H), 2.22 – 2.08 (m, 3H), 2.04 – 1.95 (m, 1H), 1.82 – 1.63 (m, 2H), 1.63 – 1.37 (m, 6H), 1.18 – 1.08 (m, 1H). 3H not observed (exchangeable); ^{13}C NMR (101 MHz, Methanol- d_4) δ 168.8, 163.0, 158.7, 149.5, 142.9, 142.1, 138.3, 136.3, 135.4, 134.1, 132.5, 128.9, 127.6, 126.5, 122.7, 122.6, 120.6, 120.4, 119.6, 113.0, 112.2, 101.5, 71.2, 57.2, 51.4, 49.9, 47.5, 47.1, 41.9, 41.2, 35.2, 33.7, 30.8, 29.0, 28.2, 25.0; ν_{max} (neat): 3270, 2929, 2859, 1693, 1634, 1504, 1436, 1341, 1268, 1123, 987, 754 cm^{-1} ; HRMS (Method B): calcd. for $C_{36}H_{42}N_7O_4$ $[M+H]^+$ 636.3298; found 636.3290.

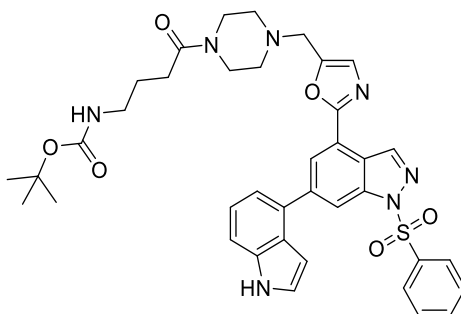


***tert*-Butyl (4-(4-((2-(6-chloro-1-(phenylsulfonyl)-1*H*-indazol-4-yl)oxazol-5-yl)methyl)piperazin-1-yl)-4-oxobutyl)carbamate (159)**

To a stirred solution of 2-(6-chloro-1-(phenylsulfonyl)-1*H*-indazol-4-yl)-5-(piperazin-1-ylmethyl)oxazole, trifluoroacetic acid salt (564 mg, 0.99 mmol) in DMF (8 mL) was added DIPEA (861 μ L, 4.93 mmol). The reaction mixture was stirred at room temperature for 5 min after which Boc-GABA-OH (401 mg, 1.97 mmol) and HATU (562 mg, 1.48 mmol) were added. The reaction mixture was stirred at room temperature for 1 h. The reaction was then partitioned between EtOAc (30 mL) and water (30 mL). The layers were separated and the aqueous was further extracted with EtOAc (3 x 30 mL). The combined organic extracts were washed with a 5% aqueous LiCl solution (2 x 50 mL), dried by passing through a hydrophobic frit and concentrated under reduced pressure. The residue was dissolved in a minimum amount of DCM and purified by automated column chromatography on silica gel eluting with 0-20% MeOH/EtOAc over 18 CV. The product-containing fractions were combined and concentrated under reduced pressure to afford the title compound as a light yellow solid (513 mg, 84% yield).

LCMS (Method B): t_R = 1.32 Min, $[M+H]^+$ = 643.25, purity 99%; 1H NMR (400 MHz, Chloroform-*d*) δ 8.88 (s, 1H), 8.28 (s, 1H), 8.04 – 7.96 (m, 2H), 7.92 (d, J = 1.6 Hz, 1H), 7.62 – 7.56 (m, 1H), 7.53 – 7.44 (m, 2H), 7.22 (s, 1H), 4.83 (bs, 1H), 3.92 (s, 2H), 3.79 – 3.50 (m, 4H), 3.17 – 3.07 (m, 2H), 2.84 – 2.71 (m, 4H), 2.35 (t, J = 7.1 Hz, 2H), 1.85 – 1.71 (m, 2H), 1.40 (s, 9H); ^{13}C NMR (101 MHz, Chloroform-*d*) δ 171.3, 162.8, 159.4, 156.5, 141.7, 141.3, 137.3, 136.0, 134.8, 129.6, 129.3, 127.8, 123.6, 121.4, 121.3, 114.9, 79.5, 52.3, 51.9, 44.7, 40.3, 30.2, 28.5, 25.4; ν_{max} (neat):

3344, 2971, 2934, 1697, 1645, 1536, 1448, 1380, 1251, 1170, 1093, 922, 835 cm^{-1} ;
 HRMS (Method A): calcd. for $\text{C}_{30}\text{H}_{36}\text{ClN}_6\text{O}_6\text{S}$ $[\text{M}+\text{H}]^+$ 643.2106; found 643.2111.

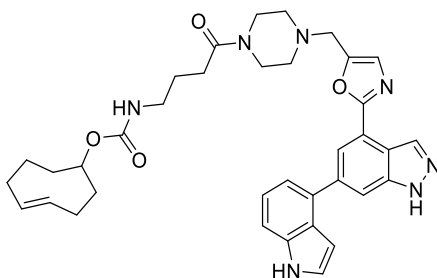


***tert*-Butyl (4-(4-((2-(6-(1*H*-indol-4-yl)-1-(phenylsulfonyl)-1*H*-indazol-4-yl)oxazol-5-yl)methyl)piperazin-1-yl)-4-oxobutyl)carbamate (160)**

To a microwave vial was added *tert*-butyl (4-(4-((2-(6-chloro-1-(phenylsulfonyl)-1*H*-indazol-4-yl)oxazol-5-yl)methyl)piperazin-1-yl)-4-oxobutyl)carbamate (480 mg, 0.75 mmol), indole-4-boronic acid pinacol ester (363 mg, 1.49 mmol), XPhos Pd G2 (117 mg, 0.15 mmol) and sodium carbonate (237 mg, 2.24 mmol). The solids were suspended in dioxane (8 mL) and water (1 mL). The vial was sealed and the atmosphere was purged with 3 nitrogen/vacuum cycles. The vial was heated in the microwave at 90°C for 1 h. The reaction mixture was partitioned between EtOAc (40 mL) and water (40 mL). The layers were separated and the aqueous phase was further extracted with EtOAc (3 x 40 mL). The combined organic extracts were dried by passing through a hydrophobic frit and concentrated under reduced pressure. The residue was dissolved in a minimum amount of DCM and purified by automated column chromatography on silica gel eluting with 0-25% MeOH/EtOAc over 20 CV. The product-containing fractions were combined and concentrated under reduced pressure to afford the title compound as a pale yellow solid (391 mg, 72% yield).

LCMS (Method A): t_R = 1.28 Min, $[\text{M}+\text{H}]^+$ = 724.28, purity 95%; ^1H NMR (400 MHz, Chloroform-*d*) δ 8.99 (d, J = 0.9 Hz, 1H), 8.63 (dd, J = 1.3, 0.9 Hz, 1H), 8.35 (d, J = 1.3 Hz, 1H), 8.05 – 7.99 (m, 2H), 7.61 – 7.53 (m, 1H), 7.53 – 7.49 (m, 1H), 7.49 – 7.43 (m, 2H), 7.38 – 7.33 (m, 3H), 7.15 (s, 1H), 6.78 – 6.74 (m, 1H), 4.75 (bs, 1H), 3.73 (s, 2H), 3.68 – 3.39 (m, 4H), 3.22 – 3.06 (m, 2H), 2.59 – 2.47 (m, 4H), 2.32 (t, J

= 7.3 Hz, 2H), 1.90 – 1.66 (m, 2H), 1.41 (s, 9H); ^{13}C NMR (101 MHz, Chloroform-*d*) δ 171.0, 160.3, 156.3, 148.9, 143.2, 142.0, 141.7, 137.7, 136.6, 134.4, 132.8, 129.5, 128.0, 127.8, 126.4, 125.5, 124.2, 122.5, 121.8, 120.8, 120.6, 114.5, 111.6, 101.8, 79.3, 52.8, 52.5, 41.6, 40.4, 30.6, 28.6, 25.6; ν_{max} (neat): 3296, 2929, 1692, 1623, 1506, 1448, 1361, 1249, 1170, 1088, 998 752 cm^{-1} ; HRMS (Method A): calcd. for $\text{C}_{38}\text{H}_{42}\text{N}_7\text{O}_6\text{S}$ $[\text{M}+\text{H}]^+$ 724.2917; found 724.2917.



(*E*)-Cyclooct-4-en-1-yl (4-(4-((2-(6-(1*H*-indol-4-yl)-1*H*-indazol-4-yl)oxazol-5-yl)methyl)piperazin-1-yl)-4-oxobutyl)carbamate (155)

Boc deprotection:

To a stirred solution of *tert*-butyl (4-(4-((2-(6-(1*H*-indol-4-yl)-1-(phenylsulfonyl)-1*H*-indazol-4-yl)oxazol-5-yl)methyl)piperazin-1-yl)-4-oxobutyl)carbamate (231 mg, 0.32 mmol) in DCM (7 mL) was added TFA (1.5 mL). The reaction was stirred at room temperature for 1 h. Volatiles were then removed under reduced pressure. The crude was suspended in toluene (2 x 8 mL) and solvents were removed under reduced pressure to afford crude TFA salt of the amine as a yellow oil, which was immediately taken forward in the next step.

TCO installation:

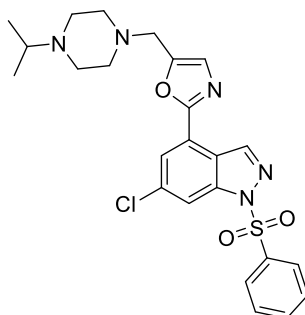
To a stirred solution of crude 1-(4-((2-(6-(1*H*-indol-4-yl)-1-(phenylsulfonyl)-1*H*-indazol-4-yl)oxazol-5-yl)methyl)piperazin-1-yl)-4-aminobutan-1-one, trifluoroacetic acid salt in DMF (8 mL) was added DIPEA (556 μL , 3.19 mmol). The reaction mixture was stirred at room temperature for 5 min after which (*E*)-cyclooct-4-en-1-yl (4-nitrophenyl) carbonate (102 mg, 0.35 mmol) was added in one portion. The reaction was stirred at room temperature for 1 h. The reaction mixture was partitioned between

EtOAc (25 mL) and water (25 mL). The layers were separated and the aqueous was further extracted with EtOAc (3 x 30 mL). The combined organic extracts were washed with a 5% aqueous LiCl solution (2 x 50 mL), dried by passing through a hydrophobic frit and concentrated under reduced pressure to afford the crude compound as a yellow oil which was immediately taken forward in the next step.

Benzenesulfonyl deprotection:

To a stirred suspension of crude (*E*)-cyclooct-4-en-1-yl (4-(4-((2-(6-(1*H*-indol-4-yl)-1-(phenylsulfonyl)-1*H*-indazol-4-yl)oxazol-5-yl)methyl)piperazin-1-yl)-4-oxobutyl)carbamate (247 mg, 0.32 mmol) in MeOH (6 mL) was added sodium hydroxide 1 M in water (1 mL) and the reaction mixture was stirred at room temperature for 1 h. MeOH was removed under reduced pressure and the residue was partitioned between EtOAc (20 mL) and water (20 mL). The layers were separated and the aqueous phase was further extracted with EtOAc (3 x 20 mL). The combined organic extracts were dried by passing through a hydrophobic frit and concentrated under reduced pressure. The crude was dissolved in MeOH/DMSO (1:1, 2 mL) and purified by Mass Directed Automated Preparative (Method B, 2 x 1 mL injection). The product-containing fractions were freeze-dried to afford the title compound as a white solid (30.1 mg, 15% yield over 3 steps).

LCMS (Method B): t_R = 1.09 Min, $[M+H]^+$ = 636.34, purity 99%; 1H NMR (400 MHz, Methanol- d_4) δ 8.67 (d, J = 0.9 Hz, 1H), 8.22 (d, J = 1.2 Hz, 1H), 7.98 – 7.90 (m, 1H), 7.49 – 7.42 (m, 1H), 7.34 (d, J = 3.2 Hz, 1H), 7.26 (s, 1H), 7.25 – 7.19 (m, 2H), 6.66 (dd, J = 3.2, 0.9 Hz, 1H), 5.70 – 5.54 (m, 1H), 5.50 – 5.39 (m, 1H), 4.79 – 4.70 (m, 1H), 3.69 – 3.48 (m, 4H), 3.18 – 3.01 (m, 2H), 2.62 – 2.54 (m, 5H), 2.39 (t, J = 7.5 Hz, 2H), 2.36 – 2.23 (m, 1H), 2.23 – 2.09 (m, 4H), 2.07 – 1.95 (m, 1H), 1.86 – 1.43 (m, 6H), 1.24 – 1.09 (m, 1H). 3H not observed (exchangeable); ^{13}C NMR (101 MHz, Methanol- d_4) δ 173.4, 162.9, 158.7, 150.1, 142.8, 142.1, 138.3, 136.3, 135.4, 134.1, 132.7, 132.6, 128.7, 127.6, 126.5, 122.7, 120.6, 120.4, 119.6, 112.9, 112.2, 101.5, 71.3, 53.7, 53.4, 52.7, 46.6, 42.6, 41.9, 41.1, 35.2, 33.7, 31.1, 30.8, 29.0, 26.7; ν_{max} (neat): 3264, 2934, 2854, 1695, 1622, 1545, 1513, 1438, 1340, 1259, 1216, 1121, 991 cm^{-1} ; HRMS (Method B): calcd. for $C_{36}H_{42}N_7O_4$ $[M+H]^+$ 636.3298; found 636.3306.

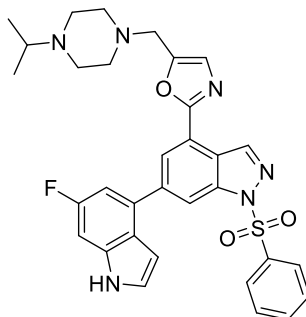


2-(6-Chloro-1-(phenylsulfonyl)-1*H*-indazol-4-yl)-5-((4-isopropylpiperazin-1-yl)methyl)oxazole (163)^[146]

To a stirred suspension of 2-(6-chloro-1-(phenylsulfonyl)-1*H*-indazol-4-yl)oxazole-5-carbaldehyde (226 mg, 0.58 mmol) in DCM (10 mL) was added 1-isopropylpiperazine (112 mg, 0.87 mmol) followed by acetic acid (17 μ L, 0.29 mmol). The reaction mixture was stirred at room temperature for 30 min after which sodium triacetoxyborohydride (161 mg, 0.76 mmol) was added in one portion. The reaction mixture was stirred at room temperature for 1 h. More 1-isopropyl piperazine (112 mg, 1.5 equiv.) was added and the reaction was stirred for an additional 30 min at room temperature. More sodium triacetoxyborohydride (161 mg, 1.3 equiv.) was added and the reaction was stirred at room temperature for an additional 30 min. The reaction was partitioned between DCM (30 mL) and a saturated aqueous sodium bicarbonate solution (30 mL). The layers were separated and the aqueous was further extracted with DCM (3 x 20 mL). The combined organic extracts were dried by passing through a hydrophobic frit and concentrated under reduced pressure. The residue was dissolved in a minimum amount of DCM and purified by automated column chromatography on silica gel eluting with 0-25% MeOH/EtOAc over 16 CV. The product-containing fractions were combined and concentrated under reduced pressure to afford the title compound as a pale yellow solid (254 mg, 87% yield).

LCMS (Method A): t_R = 0.83 Min, MH^+ = 500.20, purity 100%; 1H NMR (400 MHz, DMSO- d_6) δ 8.94 (d, J = 0.9 Hz, 1H), 8.27 (dd, J = 1.7, 0.9 Hz, 1H), 8.07 – 8.00 (m, 2H), 7.91 (d, J = 1.7 Hz, 1H), 7.82 – 7.72 (m, 1H), 7.70 – 7.58 (m, 2H), 7.35 (s, 1H), 3.70 (s, 2H), 2.61 (sept, J = 6.5 Hz, 1H), 2.48 – 2.40 (m, 8H), 0.93 (d, J = 6.5 Hz, 6H); ^{13}C NMR (101 MHz, DMSO- d_6) δ 157.3, 150.7, 141.3, 140.7, 136.0,

135.4, 134.9, 130.0, 127.7, 127.4, 122.4, 121.5, 120.5, 113.7, 53.6, 52.4, 51.3, 47.8, 18.1; ν_{max} (neat): 3064, 2965, 2811, 1586, 1540, 1467, 1446, 1377, 1290, 1173, 1069, 923 cm^{-1} ; HRMS (Method A): calcd. for $\text{C}_{24}\text{H}_{27}\text{ClN}_5\text{O}_3\text{S}$ $[\text{M}+\text{H}]^+$ 500.1523; found 500.1525.

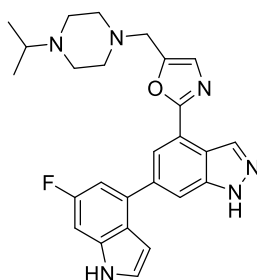


2-(6-(6-Fluoro-1H-indol-4-yl)-1-(phenylsulfonyl)-1H-indazol-4-yl)-5-((4-isopropylpiperazin-1-yl)methyl)oxazole (163)

In a microwave vial was added 2-(6-chloro-1-(phenylsulfonyl)-1H-indazol-4-yl)-5-((4-isopropylpiperazin-1-yl)methyl)oxazole (100 mg, 0.20 mmol), 6-fluoro-4-indole boronic pinacol ester (63 mg, 0.24 mmol), XPhos Pd G2 (32 mg, 0.04 mmol) and sodium carbonate (64 mg, 0.60 mmol). The solids were suspended in 1,4-dioxane (4.5 mL) and water (0.5 mL). The vial was sealed and purged with 3 vacuum/nitrogen cycles. The vial was heated in the microwave at 90 °C for 1 h. The reaction mixture was partitioned between EtOAc (20 mL) and water (20 mL). The layers were separated and the aqueous phase was extracted with EtOAc (3 x 20 mL). The combined organic extracts were dried by passing through a hydrophobic frit and concentrated under reduced pressure. The residue was taken in a minimum amount of DCM and purified by automated column chromatography on silica gel eluting with 0-35% MeOH/EtOAc over 18 CV. The product-containing fractions were combined and concentrated under reduced pressure to afford the title compound as a pale brown solid (88 mg, 74% yield).

LCMS (Method A): t_R = 0.90 Min, $[\text{M}+\text{H}]^+$ = 599.23, purity 100%; ^1H NMR (400 MHz, $\text{DMSO}-d_6$) δ 11.50 (bs, 1H), 8.99 (d, J = 0.9 Hz, 1H), 8.50 (dd, J = 1.3, 0.9 Hz, 1H), 8.22 (d, J = 1.3 Hz, 1H), 8.05 – 8.00 (m, 2H), 7.78 – 7.71 (m, 1H), 7.67 – 7.60 (m, 2H), 7.53 (dd, J = 3.2, 2.3 Hz, 1H), 7.36 – 7.30 (m, 2H), 7.22 (dd, J = 10.0, 2.3 Hz, 1H), 6.62 – 6.52 (m, 1H), 3.69 (s, 2H), 2.55 (sept, J = 6.5 Hz, 1H), 2.48 – 2.34 (m,

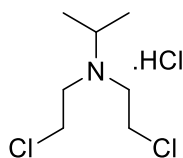
8H), 0.90 (d, $J = 6.5$ Hz, 6H); ^{13}C NMR (101 MHz, DMSO- d_6) δ 158.6 (d, $J = 234.3$ Hz), 158.4, 150.3, 141.5, 140.9, 136.3 (d, $J = 12.8$ Hz), 136.3, 136.2, 135.2, 131.9 (d, $J = 9.9$ Hz), 130.0, 127.5, 127.4, 127.2, 122.9, 122.5, 120.9, 120.6, 113.2, 107.6 (d, $J = 25.7$ Hz), 99.7, 97.9 (d, $J = 25.6$ Hz), 53.4, 52.5, 51.3, 47.8, 18.1; ^{19}F NMR (376 MHz, DMSO- d_6) δ -120.10 – -123.65 (m); ν_{max} (neat): 3319, 2970, 2812, 1613, 1541, 1451, 1380, 1341, 1174, 1131, 1095, 961 cm^{-1} ; HRMS (Method): calcd. for $\text{C}_{32}\text{H}_{32}\text{FN}_6\text{O}_3\text{S}$ $[\text{M}+\text{H}]^+$ 599.2241; found 599.2239.



2-(6-(6-Fluoro-1H-indol-4-yl)-1H-indazol-4-yl)-5-((4-isopropylpiperazin-1-yl)methyl)oxazole (162)

To a stirred suspension of 2-(6-(6-fluoro-1H-indol-4-yl)-1-(phenylsulfonyl)-1H-indazol-4-yl)-5-((4-isopropylpiperazin-1-yl)methyl)oxazole (76 mg, 0.13 mmol) in MeOH (4 mL) was added sodium hydroxide 1.0 M in water (1 mL) and the reaction was stirred at room temperature for 20 min. More 1 M aqueous NaOH (1 mL) was added and the reaction was stirred at room temperature for an additional hour. Another 1 mL of 1 M aqueous NaOH was added and the reaction was stirred at room temperature for an additional 30 min. MeOH was removed under reduced pressure. The crude was partitioned between EtOAc (15 mL) and water (10 mL). The layers were separated and the aqueous was further extracted with EtOAc (3 x 15 mL). The combined organic extracts were dried by passing through a hydrophobic frit and concentrated under reduced pressure. The residue was dissolved in MeOH/DMSO (1:1, 1 mL) and purified by Mass Directed Automated Preparative (Method B). The product-containing fraction was freeze-dried to afford the title compound as a white solid (31 mg, 53% yield).

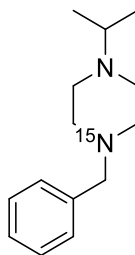
LCMS (Method B): $t_R = 1.01$ Min, $[M+H]^+ = 459.23$, purity 98%; 1H NMR (400 MHz, DMSO- d_6) δ 13.48 (bs, 1H), 11.41 (bs, 1H), 8.61 (d, $J = 0.9$ Hz, 1H), 8.06 (d, $J = 1.3$ Hz, 1H), 7.93 (dd, $J = 1.3, 0.9$ Hz, 1H), 7.50 – 7.39 (m, 1H), 7.32 (s, 1H), 7.30 – 7.24 (m, 1H), 7.12 (dd, $J = 10.8, 2.9$ Hz, 1H), 6.64 – 6.53 (m, 1H), 3.73 (s, 2H), 2.58 (sept, $J = 6.5$ Hz, 1H), 2.48 – 2.39 (m, 8H), 0.93 (d, $J = 6.5$ Hz, 6H); ^{13}C NMR (101 MHz, DMSO) δ 160.4, 159.2 (d, $J = 229.4$ Hz), 157.6, 149.5, 141.0, 137.7, 136.2 (d, $J = 13.0$ Hz), 133.4 (d, $J = 9.9$ Hz), 127.2, 126.8, 126.7, 122.6, 119.7, 119.2, 118.3, 111.6, 107.2 (d, $J = 25.3$ Hz), 100.1, 97.1 (d, $J = 25.6$ Hz), 53.5, 52.5, 51.4, 47.9, 18.2; ^{19}F NMR (376 MHz, DMSO- d_6) δ -116.21 – -125.88 (m); $\nu_{max}(neat)$: 3165, 2964, 1817, 2356, 1611, 1611, 1586, 1417, 1384, 1331, 1258, 1168, 1108, 914 cm^{-1} ; HRMS (Method A): calcd. for $C_{26}H_{28}FN_6O$ $[M+H]^+ 459.2309$; found 459.2296.



***N,N*-Bis(2-chloroethyl)propan-2-amine, hydrochloride salt (169)**

To a stirred solution of 2,2'-(isopropylazanediyl)bis(ethan-1-ol) (1.62 g, 11.00 mmol) in DCM (10 mL) was added thionyl chloride (2.41 mL, 33.00 mmol) and the reaction was stirred at room temperature overnight. Volatiles were removed under reduced pressure. Toluene (2 x 10 mL) was added and solvents were removed under reduced pressure to afford the crude title compound as a pale yellow solid (2.32 g, 96% yield). The product was used in the next step without further purification.

1H NMR (400 MHz, Methanol- d_4) δ 4.03 (t, $J = 6.4$ Hz, 4H), 3.89 (sept, $J = 6.7$ Hz, 1H), 3.73 – 3.59 (m, 5H), 1.42 (d, $J = 6.7$ Hz, 6H); ^{13}C NMR (101 MHz, Methanol- d_4) δ 59.6, 53.3, 38.7, 16.7; $\nu_{max}(neat)$: 2986, 2405, 1467, 1383, 1285, 1129, 988, 750 cm^{-1} .



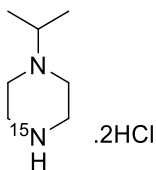
1-Benzyl-4-isopropylpiperazine-1-¹⁵N (171)

To a microwave vial was added *N,N*-bis(2-chloroethyl)propan-2-amine, hydrochloride (515 mg, 2.34 mmol). The vial was sealed and solids were suspended in anhydrous acetonitrile (2.5 mL). Then, benzylamine-¹⁵N (383 μ L, 3.50 mmol) was added followed by DIPEA (1.22 mL, 7.00 mmol). The vial was heated in the microwave at 120 °C for 1 h. Acetonitrile was removed under reduced pressure and the crude was partitioned between DCM (50 mL), water (20 mL) and a saturated aqueous sodium bicarbonate solution (30 mL). The layers were separated and the aqueous was further extracted with DCM (3 x 40 mL). The combined organic extracts were dried by passing through a hydrophobic frit and concentrated under reduced pressure. The crude was dissolved in a minimum amount of DCM and purified by automated column chromatography on silica gel eluting with 0-20% (MeOH + 1% Et₃N)/DCM over 20 CV. The product-containing fractions were combined and concentrated under reduced pressure to afford the title compound as an orange oil (416 mg, 81% yield).

LCMS (Method B): t_R = 0.98 Min, $[M+H]^+$ = 220.29, 100% purity; ¹H NMR (400 MHz, Chloroform-*d*) δ 7.50 – 7.18 (m, 5H), 3.53 (s, 2H), 2.72 – 2.62 (m, 1H), 2.61 – 2.40 (m, 8H), 1.06 (d, J = 6.7 Hz, 6H); ¹³C NMR (101 MHz, Chloroform-*d*) δ 138.3, 129.4, 128.3, 127.1, 63.27 (d, J = 3.8 Hz), 54.6, 53.58 (d, J = 3.4 Hz), 48.9, 18.8.

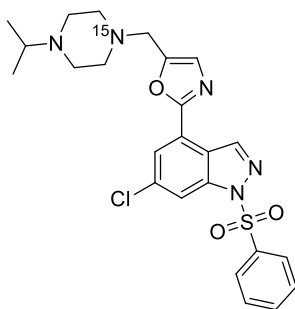
HRMS (Method A): calcd. for C₁₄H₂₃N¹⁵N $[M+H]^+$ 220.1832; found 220.1838.

ν_{max} (neat): 2964, 2806, 2763, 1495, 1453, 1177, 1010, 806, 736 cm⁻¹.



1-Isopropylpiperazine-4-¹⁵N, dihydrochloride (172)

A solution of 1-benzyl-4-isopropylpiperazine-1-¹⁵N (226 mg, 1.03 mmol) and 1,1,2-trichloroethane (0.21 mL, 2.27 mmol) in MeOH (20 mL) was hydrogenated on a H-Cube[®] at 50 °C, 5 bar and a flow rate of 1 mL/min. After the first pass, more 1,1,2-trichloroethane (0.11 mL, 1.1 equiv.) was added and the solution was hydrogenated again using the same conditions. After the second pass, 1,1,2-trichloroethane (0.11 mL, 1.1 equiv) was added and the solution was hydrogenated using the same conditions. After the third pass, more 1,1,2-trichloroethane (0.11 mL, 1.1 equiv.) was added and the solution was hydrogenated using the same condition as above. The solution was then concentrated under reduced pressure to afford the crude title compound as a pale brown oil which was immediately taken forward in the next step.

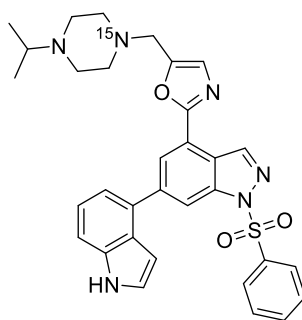


2-(6-Chloro-1-(phenylsulfonyl)-1*H*-indazol-4-yl)-5-((4-isopropylpiperazin-1-yl)-1-¹⁵N)methyl)oxazole (173)

To a stirred solution of 1-isopropylpiperazine-4-¹⁵N, dihydrochloride (208 mg, 1.03 mmol) in DCM (8 mL) was added triethylamine (287 µL, 2.06 mmol) and the reaction was stirred at room temperature for 5 min. To the previous reaction mixture was added 2-(6-chloro-1-(phenylsulfonyl)-1*H*-indazol-4-yl)oxazole-5-carbaldehyde (279 mg, 0.72 mmol) followed by acetic acid (29 µL, 0.52 mmol). The reaction mixture was stirred at room temperature for 30 min after which sodium triacetoxyborohydride (284

mg, 1.34 mmol) was added in one portion. The reaction mixture was stirred at room temperature for an additional 30 min. The reaction was partitioned between DCM (30 mL) and a saturated aqueous sodium bicarbonate solution (30 mL). The layers were separated and the aqueous was further extracted with DCM (3 x 30 mL). The combined organic extracts were dried by passing through a hydrophobic frit and concentrated under reduced pressure. The residue was dissolved in a minimum amount of DCM and purified by automated column chromatography on silica gel eluting with 0-25% MeOH/EtOAc over 18 CV. The product-containing fractions were combined and concentrated under reduced pressure to afford the title compound as a pale yellow solid (179 mg, 35% yield over 2 steps)

LCMS (Method A): $t_R = 0.83$ Min, $[M+H]^+ = 501.16$, 100% purity; 1H NMR (400 MHz, Chloroform- d) δ 8.90 (d, $J = 0.9$ Hz, 1H), 8.30 (dd, $J = 1.7, 0.9$ Hz, 1H), 8.05 – 7.98 (m, 2H), 7.95 (d, $J = 1.7$ Hz, 1H), 7.64 – 7.55 (m, 1H), 7.53 – 7.43 (m, 2H), 7.12 (s, 1H), 3.70 (s, 2H), 2.66 (sept, $J = 6.5$ Hz, 1H), 2.61 – 2.52 (m, 8H), 1.03 (d, $J = 6.5$ Hz, 6H); ^{13}C NMR (101 MHz, Chloroform- d) δ 158.7, 150.07 (d, $J = 1.6$ Hz), 141.8, 141.4, 137.4, 135.9, 134.7, 129.5, 128.0, 127.8, 123.4, 121.8, 121.3, 114.6, 54.5, 53.21 (d, $J = 3.5$ Hz), 52.48 (d, $J = 3.9$ Hz), 48.6, 18.7; ν_{max} (neat): 3062, 2964, 2808, 1596, 1540, 1448, 1377, 1266, 1172, 1070, 923 cm^{-1} ; HRMS (Method A): calcd. for $C_{24}H_{27}ClN_4^{15}NO_3S$ $[M+H]^+ 501.1493$; found 501.1494.

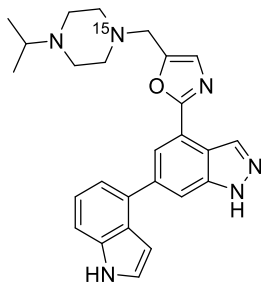


2-(6-(1H-indol-4-yl)-1-(phenylsulfonyl)-1H-indazol-4-yl)-5-((4-isopropylpiperazin-1-yl-1- ^{15}N)methyl)oxazole (174)

To a microwave vial were added 2-(6-chloro-1-(phenylsulfonyl)-1H-indazol-4-yl)-5-((4-isopropylpiperazin-1-yl-1- ^{15}N)methyl)oxazole (135 mg, 0.27 mmol), indole-4-

boronic acid pinacol ester (131 mg, 0.54 mmol), XPhos Pd G2 (42 mg, 0.054 mmol) and sodium carbonate (86 mg, 0.81 mmol). The solids were suspended in 1,4-dioxane (4.5 mL) and water (0.5 mL). The vial was sealed and purged with 3 vacuum/nitrogen cycles. The vial was heated in the microwave at 90 °C for 1 h. The reaction mixture was partitioned between EtOAc (30 mL) and water (25 mL). The layers were separated and the aqueous phase was extracted with EtOAc (3 x 25 mL). The combined organic extracts were dried by passing through a hydrophobic frit and concentrated under reduced pressure. The residue was taken in a minimum amount of DCM and purified by automated column chromatography on silica gel eluting with 0-30% MeOH/EtOAc over 20 CV. The product containing fractions were combined and concentrated under reduced pressure to afford the title compound as a pale brown solid (101 mg, 64% yield).

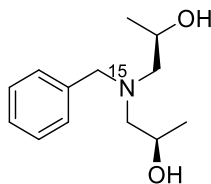
LCMS (Method A): t_R = 0.87 Min, $[M+H]^+$ = 582.34, 100% purity; 1H NMR (400 MHz, DMSO- d_6) δ 11.45 (bs, 1H), 8.99 (d, J = 0.9 Hz, 1H), 8.50 (dd, J = 1.3, 0.9 Hz, 1H), 8.25 (d, J = 1.3 Hz, 1H), 8.03 – 7.98 (m, 2H), 7.79 – 7.72 (m, 1H), 7.68 – 7.60 (m, 2H), 7.59 – 7.56 (m, 1H), 7.55 – 7.53 (m, 1H), 7.35 – 7.26 (m, 3H), 6.69 – 6.52 (m, 1H), 3.70 (s, 2H), 2.56 (sept, J = 6.5 Hz, 1H), 2.48 – 2.35 (m, 8H), 0.91 (d, J = 6.5 Hz, 6H); ^{13}C NMR (101 MHz, DMSO- d_6) δ 158.5, 150.2, 142.9, 141.6, 141.1, 136.5, 136.3, 135.2, 131.0, 130.0, 127.5, 127.2, 126.8, 125.5, 123.0, 121.5, 120.7, 120.5, 119.4, 113.0, 112.2, 99.5, 53.5, 52.47 (d, J = 3.0 Hz), 51.32 (d, J = 3.8 Hz), 47.8, 18.2. ν_{max} (neat): 3093, 2961, 2922, 1638, 1542, 1450, 1381, 1340, 1183, 1087, 1056, 951 cm^{-1} ; HRMS (Method A): calcd. for $C_{32}H_{33}N_5^{15}NO_3S$ $[M+H]^+$ 582.2305; found 582.2303.



2-(6-(1*H*-indol-4-yl)-1*H*-indazol-4-yl)-5-((4-isopropylpiperazin-1-yl-1-¹⁵N)methyl)oxazole (165)

To a stirred suspension of 2-(6-(1*H*-indol-4-yl)-1-(phenylsulfonyl)-1*H*-indazol-4-yl)-5-((4-isopropylpiperazin-1-yl-1-¹⁵N)methyl)oxazole (74 mg, 0.13 mmol) in MeOH (5 mL) was added sodium hydroxide 1.0 M in water (1 mL) and the reaction mixture was stirred at room temperature for 1 h. More sodium hydroxide 1.0 M in water (0.5 mL) was added and the reaction was stirred at room temperature for an additional 20 min. MeOH was removed under reduced pressure and the residue was partitioned between EtOAc (25 mL) and water (25 mL). The layers were separated and the aqueous was further extracted with EtOAc (3 x 25 mL). The combined organic extracts were dried by passing through a hydrophobic frit and concentrated under reduced pressure. The crude was dissolved in MeOH/DMSO (1:1, 1 mL) and purified by Mass Directed Automated Preparative HPLC (Method C). The product-containing fractions were freeze dried to afford the title compound as a white solid (22 mg, 39% yield).

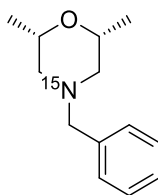
LCMS (Method B): t_R = 0.99 Min, $[M+H]^+$ = 442.32, 100% purity; ¹H NMR (700 MHz, DMSO-*d*₆) δ 13.42 (bs, 1H), 11.35 (bs, 1H), 8.59 (d, J = 0.9 Hz, 1H), 8.07 (d, J = 1.3 Hz, 1H), 7.90 (dd, J = 1.3, 0.9 Hz, 1H), 7.49 – 7.47 (m, 1H), 7.47 – 7.45 (m, 1H), 7.31 (s, 1H), 7.26 – 7.21 (m, 2H), 6.62 – 6.57 (m, 1H), 3.72 (s, 2H), 2.58 (sept, J = 6.5 Hz, 1H), 2.49 – 2.39 (m, 8H), 0.93 (d, J = 6.5 Hz, 6H); ¹³C NMR (176 MHz, DMSO-*d*₆) δ 160.0, 149.4, 141.2, 139.0, 136.4, 133.5, 132.3, 127.2, 126.2, 125.7, 121.4, 119.9, 119.1, 119.0, 118.0, 111.3, 99.9, 53.5, 52.51 (d, J = 3.5 Hz), 51.43 (d, J = 3.9 Hz), 47.9, 18.1; ν_{max} (neat): 3195, 2966, 2822, 1617, 1543, 1456, 1383, 1341, 1281, 1178, 1128 1026. 1003 cm⁻¹; HRMS (Method A): calcd. for C₂₆H₂₉N₅¹⁵NO $[M+H]^+$ 442.2373; found 442.2373.



(2*R*,2'*R*)-1,1'-(Benzylazanediy-¹⁵N)bis(propan-2-ol) (176)

To a stirred solution of benzylamine-¹⁵N (356 μ L, 3.25 mmol) in MeOH (5 mL) was added (*R*)-(+)-propylene oxide (524 μ L, 7.49 mmol) and the reaction mixture was stirred at 60 °C overnight. MeOH was removed under reduced pressure. The residue was dissolved in a minimum amount of DCM and purified by automated column chromatography on silica gel eluting with 0-50% (3:1 EtOAc/EtOH + 1% Et₃N)/Cyclohexane over 20 CV. The product-containing fractions were combined and concentrated under reduced pressure to afford the title compound as a colourless oil (580 mg, 79% yield).

LCMS (Method B): t_R = 0.93 Min, $[M+H]^+$ = 225.15, 99% purity; ¹H NMR (400 MHz, Chloroform-*d*) δ 7.42 – 7.20 (m, 5H), 3.93 – 3.83 (m, 3H), 3.54 (d, J = 13.6 Hz, 1H), 2.92 (bs, 2H), 2.51 – 2.44 (m, 4H), 1.12 (d, J = 6.2 Hz, 6H); ¹³C NMR (101 MHz, CDCl₃) δ 138.6, 129.1, 128.7, 127.5, 64.20 (d, J = 2.4 Hz), 62.30 (d, J = 5.1 Hz), 59.99 (d, J = 4.9 Hz), 20.44 (d, J = 1.8 Hz); ν_{max} (DCM): 3371, 2971, 2807, 1495, 1452. 1413, 1374, 1330, 1269, 1062, 1045, 954 cm⁻¹; HRMS (Method B): calcd. for C₁₃H₂₂¹⁵NO₂ $[M+H]^+$ 225.1621; found 225.1622.

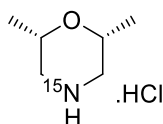


(2*S*,6*R*)-4-Benzyl-2,6-dimethylmorpholine-4-¹⁵N (177)

A microwave vial was charged with (2*R*,2'*R*)-1,1'-(Benzylazanediy-¹⁵N)bis(propan-2-ol) (405 mg, 1.81 mmol) and suspended in water (0.5 mL). Sulfuric acid 99.99% (577 μ L, 10.83 mmol) was added. The vial was sealed and heated in the microwave at

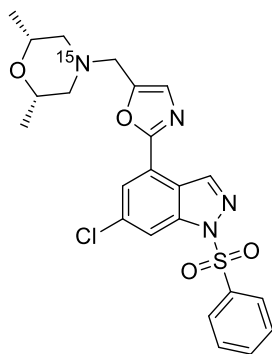
130 °C for 1 h. More sulfuric acid (190 µL, 2 equiv.) was added and the vial was heated in the microwave at 130 °C for an additional 20 min. The reaction mixture was partitioned between EtOAc (60 mL) and a 1 M aqueous NaOH solution so that the pH of the aqueous phase reached 8-9. The layers were separated and the aqueous phase was further extracted with EtOAc (3 x 50 mL). The combined organic layers were dried by passing through a hydrophobic frit and concentrated under reduced pressure. The residue was dissolved in a minimum amount of DCM and purified by automated column chromatography on silica gel eluting with 0-40% EtOAc/cyclohexane over 20 CV. The product-containing fractions were combined and concentrated under reduced pressure to afford the title compound as a colourless oil (326 mg, 88% yield).

LCMS (Method B): t_R = 1.08 Min, $[M+H]^+$ = 207.20, 100% purity; 1H NMR (600 MHz, Chloroform-*d*) δ 7.30 – 7.18 (m, 5H), 3.68 – 3.62 (m, 2H), 3.43 (s, 2H), 2.65 (dd, J = 10.6, 1.8 Hz, 2H), 1.71 (app. t, J = 10.6 Hz, 2H), 1.09 (d, J = 6.4 Hz, 6H); ^{13}C NMR (151 MHz, Chloroform-*d*) δ 138.08 (d, J = 1.9 Hz), 129.31 (d, J = 1.2 Hz), 128.4, 127.2, 71.86 (d, J = 1.3 Hz), 63.20 (d, J = 4.2 Hz), 59.63 (d, J = 3.3 Hz), 19.29 (d, J = 2.1 Hz); ν_{max} (DCM): 3028, 2972, 2930, 2868, 2770, 1497, 1455, 1376, 1355, 1323, 1143, 1084 1060 cm^{-1} ; HRMS (Method A): calcd. for $C_{13}H_{20}^{15}NO$ $[M+H]^+$ 207.1515; found 207.1514.



(2*S*,6*R*)-2,6-Dimethylmorpholine-4- ^{15}N , hydrochloride (178)

A solution of (2*S*,6*R*)-4-benzyl-2,6-dimethylmorpholine-4- ^{15}N (273 mg, 1.32 mmol) and 1,1,2-trichloroethane (135 µL, 1.456 mmol) in MeOH (20 mL) was hydrogenated on a H-Cube[®] at 35 °C, 1 bar and a flow rate of 1 mL/min. The solution was concentrated under reduced pressure. Et₂O (8 mL) was added and the mixture was sonicated for a few seconds upon which a white solid precipitated out. The solid was isolated by vacuum filtration to afford the title compound as a white solid (138 mg, 68%, yield). The compound was immediately taken forward in the following step.

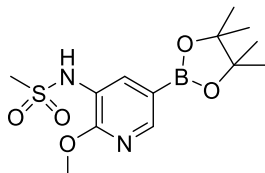


(2*R*,6*S*)-4-((2-(6-Chloro-1-(phenylsulfonyl)-1*H*-indazol-4-yl)oxazol-5-yl)methyl)-2,6-dimethylmorpholine-4-¹⁵N (179)

To a stirred solution of (2*S*,6*R*)-2,6-dimethylmorpholine-4-¹⁵N, hydrochloride (108 mg, 0.71 mmol) in DCM (8 mL) was added triethylamine (99 μ L, 0.71 mmol) and the reaction was stirred at room temperature for 5 min. To the previous reaction mixture was added 2-(6-chloro-1-(phenylsulfonyl)-1*H*-indazol-4-yl)oxazole-5-carbaldehyde (250 mg, 0.65 mmol) followed by acetic acid (18 μ L, 0.32 mmol). The reaction mixture was stirred at room temperature for 1 h after which sodium triacetoxyborohydride (205 mg, 0.97 mmol) was added in one portion. The reaction mixture was stirred at room temperature for an additional hour. The reaction was partitioned between DCM (30 mL) and a saturated aqueous sodium bicarbonate solution (30 mL). The layers were separated and the aqueous phase was further extracted with DCM (3 x 30 mL). The combined organic extracts were dried by passing through a hydrophobic frit and concentrated under reduced pressure. The residue was dissolved in a minimum amount of DCM and purified by automated column chromatography on silica gel eluting with 0-20% MeOH/EtOAc over 18 CV. The product-containing fractions were combined and concentrated under reduced pressure to afford the title compound as a pale yellow solid (191 mg, 61% yield).

LCMS (Method A): t_R = 0.94 Min, $[M+H]^+$ = 488.26, 100% purity; ¹H NMR (400 MHz, Chloroform-*d*) δ 8.91 (d, J = 0.9 Hz, 1H), 8.31 (dd, J = 1.6, 0.9 Hz, 1H), 8.04 – 7.99 (m, 2H), 7.96 (d, J = 1.6 Hz, 1H), 7.62 – 7.59 (m, 1H), 7.54 – 7.44 (m, 2H), 7.14 (s, 1H), 3.77 – 3.67 (m, 2H), 3.66 (s, 2H), 2.75 (dd, J = 10.6, 1.8 Hz, 2H), 1.85 (app. t, J = 10.6 Hz, 2H), 1.15 (d, J = 6.3 Hz, 6H); ¹³C NMR (101 MHz, Chloroform-*d*) δ

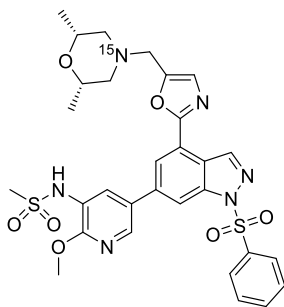
158.8, 149.8, 141.8, 141.4, 137.4, 136.0, 134.7, 129.5, 128.1, 127.8, 123.4, 121.8, 121.3, 114.7, 71.7, 59.12 (d, $J = 3.3$ Hz), 52.53 (d, $J = 4.2$ Hz), 19.22 (d, $J = 2.2$ Hz); ν_{max} (neat): 2971, 1606, 1496, 1458, 1445, 1400, 1384, 1318, 1178, 1146, 1075, 1011 cm^{-1} ; HRMS (Method B): calcd. for $\text{C}_{23}\text{H}_{24}\text{ClN}_3^{15}\text{NO}_4\text{S}$ $[\text{M}+\text{H}]^+$ 488.1177; found 488.1180.



***N*-(2-Methoxy-5-(4,4,5,5-tetramethyl-1,3,2-dioxaborolan-2-yl)pyridin-3-yl)methanesulfonamide (181)**

To a stirred solution of 2-methoxy-5-(4,4,5,5-tetramethyl-1,3,2-dioxaborolan-2-yl)pyridin-3-amine (800 mg, 3.20 mmol) in DCM (10 mL) cooled to 0 °C was added DMAP (39 mg, 0.32 mmol), followed by pyridine (388 μL , 4.80 mmol) and methanesulfonyl chloride (498 μL , 6.40 mmol). The reaction was stirred overnight and let to warm to room temperature. The reaction mixture was diluted with DCM (60 mL) and washed with water (50 mL). The organic phase was dried by passing through a hydrophobic frit and concentrated under reduced pressure. The residue was dissolved in a minimum amount of DCM and purified by automated column chromatography on silica gel eluting with 0-60% EtOAc/cyclohexane over 18 CV. The product-containing fractions were combined and concentrated under reduced pressure to afford the title compound as a beige solid (623 mg, 59% yield).

LCMS (Method A): $t_{\text{R}} = 1.02$ Min, $[\text{M}+\text{H}]^+ = 329.12$ (67%) and $t_{\text{R}} = 0.47$ Min, $[\text{M}+\text{H}]^+ = 247.10$ (31%), consistent with hydrolysis to the corresponding boronic acid on the LCMS; ^1H NMR (400 MHz, Chloroform- d) δ 8.30 (d, $J = 1.7$ Hz, 1H), 8.03 (d, $J = 1.7$ Hz, 1H), 6.70 (bs, 1H), 4.02 (s, 3H), 3.00 (s, 3H), 1.31 (s, 12H); ^{13}C NMR (101 MHz, Chloroform- d) δ 156.7, 149.5, 133.4, 120.9, 84.2, 54.3, 39.9, 25.0. 1C not observed (C-B); ν_{max} (neat): 3263, 2978, 1603, 1572, 1292, 1356, 1324, 1138, 1104, 1005, 970 cm^{-1} ; HRMS (Method A): calcd. for $\text{C}_{13}\text{H}_{22}\text{BN}_2\text{O}_5\text{S}$ $[\text{M}+\text{H}]^+$ 329.1342; found 329.1345

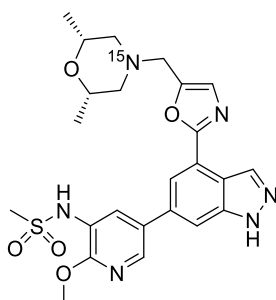


***N*-(5-(4-(5-(((2*R*,6*S*)-2,6-Dimethylmorpholino-4-¹⁵N)methyl)oxazol-2-yl)-1-(phenylsulfonyl)-1*H*-indazol-6-yl)-2-methoxypyridin-3-yl)methanesulfonamide (182)**

In a microwave vial was added (2*R*,6*S*)-4-((2-(6-chloro-1-(phenylsulfonyl)-1*H*-indazol-4-yl)oxazol-5-yl)methyl)-2,6-dimethylmorpholine-4-¹⁵N (165 mg, 0.34 mmol), *N*-(2-methoxy-5-(4,4,5,5-tetramethyl-1,3,2-dioxaborolan-2-yl)pyridin-3-yl)methanesulfonamide (222 mg, 0.68 mmol), XPhos Pd G2 (53 mg, 0.068 mmol) and sodium carbonate (108 mg, 1.01 mmol). The solids were suspended in 1,4-dioxane (5 mL) and water (0.5 mL) was added. The vial was sealed and purged with 3 vacuum/nitrogen cycles. The vial was heated in the microwave at 90 °C for 1 h. The reaction mixture was partitioned between EtOAc (30 mL) and water (35 mL). The layers were separated and the aqueous phase was extracted with EtOAc (3 x 30 mL). The combined organic extracts were dried by passing through a hydrophobic frit and concentrated under reduced pressure. The residue was dissolved in a minimum amount of DCM and purified by automated column chromatography on silica gel eluting with 0-20% MeOH/EtOAc over 20 CV. The product-containing fractions were combined and concentrated under reduced pressure to afford the title compound as a pale yellow solid (170 mg, 77% yield).

LCMS (Method A): t_R = 0.85 Min, $[M+H]^+$ = 654.36, 100% purity; ¹H NMR (400 MHz, Chloroform-*d*) δ 8.97 (d, J = 0.9 Hz, 1H), 8.40 (dd, J = 1.4, 0.9 Hz, 1H), 8.31 (d, J = 2.3 Hz, 1H), 8.12 (d, J = 1.4 Hz, 1H), 8.11 (d, J = 2.3 Hz, 1H), 8.05 – 7.98 (m, 2H), 7.63 – 7.55 (m, 1H), 7.53 – 7.45 (m, 2H), 7.15 (s, 1H), 6.82 (bs, 1H), 4.11 (s, 3H), 3.76 – 3.60 (m, 4H), 3.09 (s, 3H), 2.77 (dd, J = 10.6, 1.8 Hz, 2H), 1.86 (app. t, J = 10.6 Hz, 2H), 1.14 (d, J = 6.3 Hz, 6H).

^{13}C NMR (101 MHz, Chloroform- d) δ 159.7, 154.7, 149.6, 141.9, 141.7, 141.1, 139.2, 137.5, 134.6, 130.3, 129.6, 128.0, 127.8, 127.1, 122.21, 122.18, 121.63, 121.59, 112.8, 71.7, 59.12 (d, J = 3.3 Hz), 54.56 (d, J = 4.0 Hz), 40.2, 19.23 (d, J = 1.9 Hz); ν_{max} (neat): 2976, 1607, 1498, 1458, 1446, 1399, 1384, 1319, 1178, 1146, 1076 cm^{-1} ; HRMS (Method B): calcd. for $\text{C}_{30}\text{H}_{33}\text{N}_5^{15}\text{NO}_7\text{S}_2$ $[\text{M}+\text{H}]^+$ 654.1930; found 654.1820.

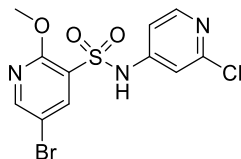


***N*-(5-(4-(5-(((2*R*,6*S*)-2,6-Dimethylmorpholino-4- ^{15}N)methyl)oxazol-2-yl)-1*H*-indazol-6-yl)-2-methoxypyridin-3-yl)methanesulfonamide (166)**

To a stirred suspension of *N*-(5-(4-(5-(((2*R*,6*S*)-2,6-dimethylmorpholino-4- ^{15}N)methyl)oxazol-2-yl)-1-(phenylsulfonyl)-1*H*-indazol-6-yl)-2-methoxypyridin-3-yl)methanesulfonamide (140 mg, 0.21 mmol) in MeOH (5 mL) was added sodium hydroxide 1 M in water (1 mL) and the reaction mixture was stirred at room temperature for 1 h. MeOH was removed under reduced pressure and the residue was partitioned between EtOAc (25 mL) and water (25 mL). The layers were separated and the aqueous phase was further extracted with EtOAc (3 x 25 mL). The combined organic extracts were dried by passing through a hydrophobic frit and concentrated under reduced pressure. The crude was dissolved in MeOH/DMSO (1:1, 2 mL) and purified by Mass Directed Automated Preparative HPLC (Method C, 2 x 1 mL injection). The product-containing fractions were freeze dried to afford the title compound as a white solid (26 mg, 24% yield).

LCMS (Method B): t_{R} = 0.77 Min, $[\text{M}+\text{H}]^+$ = 514.13, 100% purity; ^1H NMR (400 MHz, DMSO- d_6) δ 13.48 (bs, 1H), 9.40 (bs, 1H), 8.58 (d, J = 1.0 Hz, 1H), 8.39 (d, J = 2.3 Hz, 1H), 7.98 (d, J = 2.3 Hz, 1H), 7.93 (d, J = 1.4 Hz, 1H), 7.88 (dd, J = 1.4, 0.9 Hz, 1H), 7.35 (s, 1H), 3.99 (s, 3H), 3.74 (s, 2H), 3.66 – 3.50 (m, 2H), 3.10 (s,

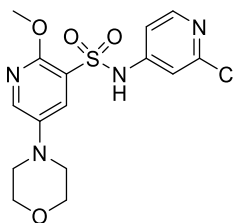
3H), 2.80 (dd, $J = 10.6, 1.4$ Hz, 2H), 1.78 (app. t, $J = 10.6$ Hz, 2H), 1.04 (d, $J = 6.3$ Hz, 6H); ^{13}C NMR (101 MHz, DMSO) δ 159.9, 156.3, 149.2, 141.1, 140.5, 134.9, 133.6, 130.5, 129.5, 127.5, 121.9, 119.6, 118.3, 117.9, 110.0, 70.9, 58.29 (d, $J = 3.5$ Hz), 53.8, 51.31 (d, $J = 3.9$ Hz), 40.7, 18.90 (d, $J = 2.1$ Hz); $\nu_{\text{max}}(\text{neat})$: 3200, 2971, 2811, 1606, 1489, 1409, 1331, 1170, 1253, 1143. 1078, 948 cm^{-1} ; HRMS (Method B): calcd. for $\text{C}_{24}\text{H}_{29}\text{N}_5^{15}\text{NO}_5\text{S}$ $[\text{M}+\text{H}]^+$ 514.1998; found 514.1884.



5-Bromo-*N*-(2-chloropyridin-4-yl)-2-methoxypyridine-3-sulfonamide (185)

To a stirred solution of 5-bromo-2-methoxypyridine-3-sulfonyl chloride (2.73 g, 9.53 mmol) in pyridine (9.25 mL, 114 mmol) cooled to 0 °C was added 2-chloropyridin-4-amine (1.23 g, 9.53 mmol) and the reaction mixture was stirred at 0 °C for 2 h. Pyridine was removed under reduced pressure. The residue was dissolved in DCM and Florisil was added. Solvents were removed under reduced pressure to adsorb the compound. Purification was carried out by automated column chromatography on silica gel eluting with 0-30% EtOAc/Cyclohexane over 25 CV. The product-containing fractions were combined and concentrated under reduced pressure to afford the title compound as a yellow solid (2.45 g, 68% yield).

LCMS (Method A): $t_{\text{R}} = 0.67$ Min, $[\text{M}+\text{H}]^+ = 377.89$, 100% purity; ^1H NMR (400 MHz, Chloroform- d) δ 8.40 (d, $J = 2.3$ Hz, 1H), 8.36 (d, $J = 2.3$ Hz, 1H), 8.23 (d, $J = 5.9$ Hz, 1H), 7.09 (d, $J = 1.9$ Hz, 1H), 7.00 (dd, $J = 5.9, 1.9$ Hz, 1H), 4.06 (s, 3H). 1H not observed (exchangeable); ^{13}C NMR (101 MHz, Chloroform- d) δ 158.3, 153.5, 152.7, 150.7, 146.2, 142.2, 122.1, 112.9, 111.8, 111.7, 55.4; $\nu_{\text{max}}(\text{neat})$: 3110, 2897, 1594, 1550, 1465, 1410, 1395, 1348, 1298, 1233, 1163, 1143, 1073 cm^{-1} ; HRMS (Method A): calcd. for $\text{C}_{11}\text{H}_{10}\text{BrClN}_3\text{O}_3\text{S}$ $[\text{M}+\text{H}]^+$ 377.9315; found 377.9317.



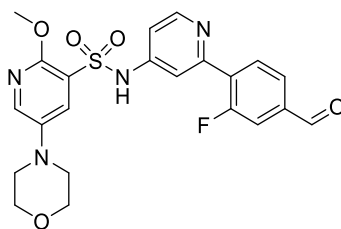
***N*-(2-Chloropyridin-4-yl)-2-methoxy-5-morpholinopyridine-3-sulfonamide (186)**

To an oven-dried microwave vial was added 5-bromo-*N*-(2-chloropyridin-4-yl)-2-methoxypyridine-3-sulfonamide (1.02 g, 2.69 mmol), potassium carbonate (1.12 g, 8.08 mmol) and copper(I) iodide (0.10 g, 0.54 mmol). Solids were suspended in DMSO (12 mL). The vial was sealed and 2-isobutyrylcyclohexan-1-one (0.17 mL, 1.62 mmol) was added followed by morpholine (1.41 mL, 16.16 mmol). The atmosphere in the vial was purged with 5 vacuum/nitrogen cycles. The vial was heated thermally to 110 °C overnight. The reaction was diluted with EtOAc (50 mL), filtered through celite and eluted with more EtOAc (200 mL). This was transferred to a separatory funnel and water (200 mL) was added. The layers were separated and the aqueous layer was made acidic (pH 4-5) by the addition of a 1 M aqueous HCl solution (approximately 10 mL). The aqueous was extracted again with EtOAc (3 x 80 mL). The combined organic extracts were washed with brine (250 mL), dried by passing through a hydrophobic frit and concentrated under reduced pressure. The residue was dissolved in DCM and florisil was added. Solvents were removed under reduced pressure to adsorb the compound. Purification was carried out by automated column chromatography on silica gel eluting with 0-60% EtOAc/cyclohexane over 22 CV. The product-containing fractions were combined and concentrated under reduced pressure to afford the title compound as a beige solid (301 mg, 29% yield).

LCMS (Method B): t_R = 0.55 Min, $[M+H]^+$ = 385.04, 100% purity; 1H NMR (400 MHz, Chloroform-*d*) δ 8.17 (d, J = 5.6 Hz, 1H), 8.10 (bs, 1H), 7.96 (d, J = 3.0 Hz, 1H), 7.82 (d, J = 3.0 Hz, 1H), 7.07 (d, J = 2.0 Hz, 1H), 6.94 (dd, J = 5.6, 2.0 Hz, 1H), 4.02 (s, 3H), 3.94 – 3.79 (m, 4H), 3.16 – 3.06 (m, 4H); ^{13}C NMR (101 MHz, Chloroform-*d*) δ 153.4, 152.6, 150.5, 146.6, 142.6, 140.1, 128.6, 120.3, 112.9, 112.0, 66.6, 54.7, 49.8.

ν_{max} (neat): 3094, 2859, 1590, 1479, 1428, 1400, 1337, 1235, 1157, 1072, 951 cm^{-1} .

HRMS (Method A): calcd. for $\text{C}_{15}\text{H}_{18}\text{ClN}_4\text{O}_4\text{S}$ $[\text{M}+\text{H}]^+$ 385.0737; found 385.0733.

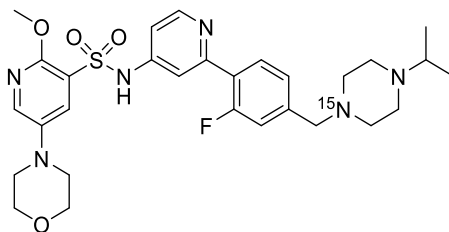


***N*-(2-(2-Fluoro-4-formylphenyl)pyridin-4-yl)-2-methoxy-5-morpholinopyridine-3-sulfonamide (187)**

To a microwave vial was added *N*-(2-chloropyridin-4-yl)-2-methoxy-5-morpholinopyridine-3-sulfonamide (226 mg, 0.59 mmol), (2-fluoro-4-formylphenyl)boronic acid (197 mg, 1.18 mmol), XPhos Pd G2 (92 mg, 0.12 mmol) and sodium carbonate (187 mg, 1.76 mmol). The vial was sealed and solids were suspended in 1,4-dioxane (4.5 mL) and water (0.5 mL). The atmosphere in the vial was purged with 3 nitrogen/vacuum cycles and the vial was heated in the microwave at 90 °C for 1 h 15 min. The reaction mixture was partitioned between EtOAc (60 mL) and water (50 mL). The layers were separated and the aqueous phase was extracted with EtOAc (3 x 50 mL). The combined organic extracts were dried by passing through a hydrophobic frit and concentrated under reduced pressure. The residue was dissolved in a minimum amount of DCM and purified by automated column chromatography on silica gel eluting with 0-100% EtOAc/cyclohexane over 25 CV. The product containing fractions were combined and concentrated under reduced pressure to afford the title compound as a beige solid (199 mg, 72% yield).

LCMS (Method B): t_R = 0.61 Min, $[\text{M}+\text{H}]^+$ = 473.09, 100% purity; ^1H NMR (400 MHz, $\text{DMSO}-d_6$) δ 10.04 (d, J = 1.4 Hz, 1H), 8.45 (d, J = 5.7 Hz, 1H), 8.12 – 8.03 (m, 2H), 7.88 – 7.78 (m, 3H), 7.59 – 7.54 (m, 1H), 7.10 (dd, J = 5.7, 2.1 Hz, 1H), 3.85 (s, 3H), 3.79 – 3.68 (m, 4H), 3.12 – 3.01 (m, 4H). 1H not observed (exchangeable); ^{13}C NMR (101 MHz, $\text{DMSO}-d_6$) δ 191.8, 161.0, 158.5, 152.8, 151.4, 150.2, 142.1, 138.9, 138.09 (d, J = 6.7 Hz), 131.8, 131.69 (d, J = 2.8 Hz), 127.5, 125.51 (d, J = 3.3 Hz), 121.0, 116.60 (d, J = 23.8 Hz), 113.03 (d, J = 9.7 Hz), 112.1, 65.8, 53.9, 48.8; ^{19}F

NMR (376 MHz, DMSO-*d*₆) δ -115.43 – -115.56 (m), ν_{max} (neat): 3089, 2843, 1692, 1596, 1580, 1482, 1456, 1397, 1342, 1234, 1158, 1107, 1067 cm⁻¹.

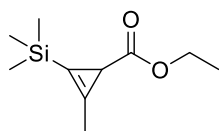


N-(2-(2-fluoro-4-((4-isopropylpiperazin-1-yl-1-¹⁵N)methyl)phenyl)pyridin-4-yl)-2-methoxy-5-morpholinopyridine-3-sulfonamide (167)

To a stirred solution of crude 1-isopropylpiperazine-4-¹⁵N, dihydrochloride (122 mg, 0.61 mmol) in DCM (5 mL) was added triethylamine (169 μ L, 1.21 mmol) and the reaction was stirred at room temperature for 5 min. To the previous reaction mixture was added a solution of *N*-(2-(2-fluoro-4-formylphenyl)pyridin-4-yl)-2-methoxy-5-morpholinopyridine-3-sulfonamide (143 mg, 0.30 mmol) in DCM (3 mL) followed by acetic acid (9 μ L, 0.15 mmol). The reaction mixture was stirred at room temperature for 30 min after which sodium triacetoxyborohydride (96 mg, 0.45 mmol) was added in one portion. The reaction mixture was stirred overnight at room temperature. The reaction was partitioned between DCM (30 mL) and a saturated aqueous sodium bicarbonate solution (30 mL). The layers were separated and the aqueous phase was further extracted with DCM (3 x 30 mL). The combined organic extracts were dried by passing through a hydrophobic frit and concentrated under reduced pressure. The residue was dissolved in a MeOH/DMSO solution (1:1, 2 mL) and purified by Mass Directed Automated Preparative HPLC (Method D, 2 x 1 mL injection). The product-containing fractions were freeze-dried to afford the title compound as a white solid (60 mg, 34%).

LCMS (Method B): t_R =0.68 Min, $[M+H]^+$ = 586.25, 100% purity, ¹H NMR (400 MHz, Chloroform-*d*) δ 8.46 (d, J = 5.6 Hz, 1H), 7.92 (d, J = 3.0 Hz, 1H), 7.87 – 7.81 (m, 2H), 7.49 – 7.42 (m, 1H), 7.17 (dd, J = 8.0, 1.6 Hz, 1H), 7.11 (dd, J = 12.4, 1.6 Hz, 1H), 6.99 (dd, J = 5.6, 2.2 Hz, 1H), 4.04 (s, 3H), 3.93 – 3.80 (m, 4H), 3.51 (s, 2H), 3.16 – 3.04 (m, 4H), 2.68 (sept, J = 6.5 Hz, 1H), 2.60 – 2.42 (m, 8H), 1.06 (d, J = 6.5

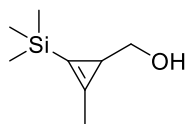
Hz, 6H). ¹H not observed (exchangeable); ¹³C NMR (101 MHz, Chloroform-*d*) δ 160.5 (d, *J* = 249.8 Hz), 154.5, 153.4, 150.5, 145.1, 142.6, 142.5, 139.7, 130.7 (d, *J* = 2.8 Hz), 128.8, 125.4, 125.3 (d, *J* = 2.7 Hz), 120.8, 116.6 (d, *J* = 23.4 Hz), 114.01 (d, *J* = 9.9 Hz), 112.1, 66.7, 62.3 (d, *J* = 3.5 Hz), 54.7, 54.6, 53.5 (d, *J* = 3.5 Hz), 49.8, 48.8, 18.8, HRMS (Method B): calcd. for C₂₉H₃₈FN₅¹⁵NO₄S [M+H]⁺ 586.2659; found 586.2637.



Ethyl 2-methyl-3-(trimethylsilyl)cycloprop-2-ene-1-carboxylate (195)^[68]

A suspension of dirhodium tetraacetate (0.42 g, 0.95 mmol) in trimethyl(prop-1-yn-1-yl)silane (28.2 mL, 190.43 mmol) was stirred under nitrogen for 5 minutes. To the previous reaction mixture was added ethyl 2-diazoacetate (9.22 mL, 76.27 mmol) using a syringe pump at a rate of 1.5 mL/h at room temperature. Once the addition was complete, the reaction mixture was stirred for an additional 18 h. The crude reaction mixture was loaded on top of a silica column and purified by column chromatography on silica gel eluting with 0-20% Et₂O/petroleum ether 40-60 °C. The product-containing fractions were identified by TLC (8:2 petroleum ether/Et₂O, KMnO₄ staining). The product-containing fractions were combined and concentrated carefully under reduced pressure (room temperature, 200 mbar) to afford the title compound as a pale yellow oil (10.2 g, 68% yield).

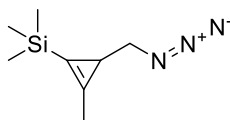
¹H NMR (500 MHz, Chloroform-*d*) δ 4.07 – 3.95 (m, 2H), 2.17 (s, 3H), 1.96 (s, 1H), 1.22 (t, *J* = 7.1 Hz, 3H), 0.17 (s, 9H); ¹³C NMR (126 MHz, CDCl₃) δ 177.2, 122.7, 104.3, 59.9, 21.4, 14.6, 12.0, -1.5; ν_{max}(DCM): 2964, 1441, 1364, 1840, 1718, 1325, 1175, 1043, 832 cm⁻¹, HRMS: calcd. for C₁₀H₁₉O₂Si [M+H]⁺ 199.1154; found 199.1159.



(2-Methyl-3-(trimethylsilyl)cycloprop-2-en-1-yl)methanol (196)^[68]

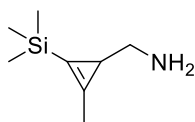
To an oven dried round-bottom flask was added ethyl 2-methyl-3-(trimethylsilyl)cycloprop-2-ene-1-carboxylate (6.03 g, 30.40 mmol) which was dissolved in dry Et₂O (40 mL). The resulting solution was cooled to 0 °C. DIBAL-H 1 M in DCM (69.9 mL, 69.90 mmol) was then added to the flask over 25 min and the reaction mixture was stirred at 0 °C under N₂ atmosphere for 3 h. The reaction was quenched by the addition of MeOH (30 mL) and a saturated aqueous Rochelle's salt solution (100 mL). The biphasic mixture was stirred for 10 min at room temperature after which a thick transparent gel had formed. More Et₂O (150 mL) was added. The layers were separated and the aqueous was further extracted with Et₂O (4 x 100 mL). The combined organic layers were dried by passing through a hydrophobic frit and concentrated under reduced pressure (room temperature, 200 mbar). The crude was taken in a minimum amount of DCM and purified by column chromatography on silica gel eluting with 0-50% Et₂O/petroleum ether. The product-containing fractions were identified by TLC (1:1 petroleum ether/Et₂O, KMnO₄ staining) and concentrated under reduced pressure (room temperature, 250 mbar). Remaining solvent was removed by flushing compressed air to afford the title compound as a colourless oil (4.06 g, 85% yield).

¹H NMR (500 MHz, Chloroform-*d*) δ 3.50-3.39 (m, 2H), 2.19 (s, 3H), 1.55 (t, *J* = 4.7 Hz, 1H), 0.14 (s, 9H); ¹³C NMR (126 MHz, CDCl₃) δ 135.7, 111.4, 69.4, 22.3, 13.5, -1.0; ν_{max}(DCM): 3330, 2953, 2915, 1801, 1430, 1248, 1187, 998, 832 cm⁻¹



(3-(Azidomethyl)-2-methylcycloprop-1-en-1-yl)trimethylsilane (197)^[68]

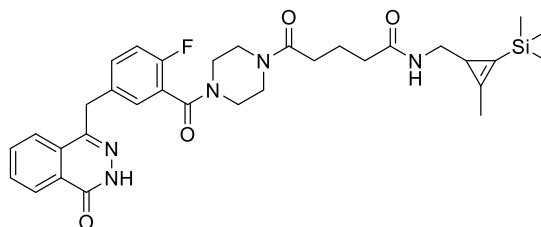
To a stirred solution of (2-methyl-3-(trimethylsilyl)cycloprop-2-en-1-yl)methanol (1.39 g, 8.89 mmol) in THF (20 mL) cooled to 0°C was added DBU (1.86 mL, 12.45 mmol) followed by DPPA (2.68 mL, 12.45 mmol) under N₂. The reaction was allowed to warm to room temperature overnight and turned into a milky suspension after a few minutes. Most of the THF was removed by flushing compressed air and the remaining suspension was passed through celite and eluted with a 1:1 solution of petrol ether 40-60/Et₂O (200 mL). The solvents were removed under reduced pressure (room temperature, 200 mbar). Remaining solvents were removed by flushing compressed air without completely evaporating to dryness. The material was immediately taken forward into the following step without further purification.



(2-Methyl-3-(trimethylsilyl)cycloprop-2-en-1-yl)methanamine (192)^[68]

The crude cyclopropene azide was dissolved in THF (10 mL) and water (2 mL) and triphenylphosphine (3.03 g, 11.56 mmol) was added. The reaction was stirred at room temperature overnight. A 1 M aqueous HCl solution (15 mL) was added to the reaction mixture and most of the THF was removed by flushing compressed air. The aqueous was then extracted with Et₂O (2 x 25 mL). The pH of the aqueous layer was adjusted to pH 8 by the addition of a saturated aqueous sodium bicarbonate solution (approx. 30 mL). The aqueous was then extracted with DCM (3 x 40 mL). The DCM organic layer was dried by passing through a hydrophobic frit and concentrated under reduced pressure (200 mbar, room temperature) without completely evaporating to dryness. The remaining DCM was removed by briefly flushing compressed air to afford crude cyclopropene amine as a yellow oil (698 mg, 51% yield over 2 steps). The cyclopropene amine is not stable to long term storage and was used straight away in the following step without further purification.

^1H NMR (500 MHz, Chloroform-*d*) δ 3.03 (bs, 2H), 2.70 – 2.60 (m, 1H), 2.57 – 2.48 (m, 1H), 2.19 (s, 3H), 1.45 (t, J = 4.6 Hz, 1H), 0.13 (s, 9H); ^{13}C NMR (126 MHz, Chloroform-*d*) δ 136.7, 112.4, 48.5, 22.6, 13.5, -0.9.

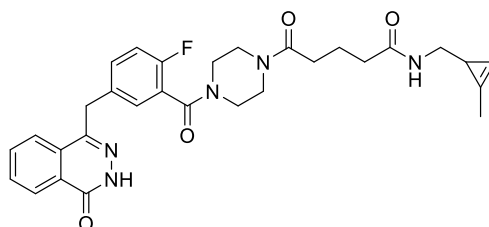


5-(4-(2-Fluoro-5-((4-oxo-3,4-dihydrophthalazin-1-yl)methyl)benzoyl)piperazin-1-yl)-N-((2-methyl-3-(trimethylsilyl)cycloprop-2-en-1-yl)methyl)-5-oxopentanamide (190)

To a stirred solution of 4-(4-fluoro-3-(piperazine-1-carbonyl)benzyl)phthalazin-1(2*H*)-one (510 mg, 1.39 mmol) in DCM (12 mL) was added glutaric anhydride (175 mg, 1.53 mmol) followed by triethylamine (213 μL , 1.53 mmol). The reaction was stirred at room temperature for 2 h. To the previous reaction mixture was added *N,N'*-disuccinimidyl carbonate (464 mg, 1.81 mmol) and the reaction was stirred at room temperature for 30 min. To the previous reaction mixture was added a solution of (2-methyl-3-(trimethylsilyl)cycloprop-2-en-1-yl)methanamine (688 mg, 4.43 mmol) in DCM (5 mL). The reaction was stirred at room temperature for 2 h. The reaction was partitioned between DCM (60 mL) and water (60 mL). The layers were separated and the aqueous was further extracted with DCM (3 x 60 mL). The combined organics extracts were dried by passing through a hydrophobic frit. The residue was dissolved in a minimum amount of DCM and purified by automated column chromatography on silica gel eluting with 0-25% MeOH/EtOAc over 20 CV. The product-containing fractions were combined and concentrated under reduced pressure to afford the title compound as a pale yellow solid (703 mg, 82% yield).

LCMS (Method B): t_{R} = 1.09 Min, $[\text{M}+\text{H}]^+ = 618.26$, purity 100%; ^1H NMR (700 MHz, Chloroform-*d*) (1:1 mixture of rotamers) δ 10.73 (bs, 0.5H), 10.64 (bs, 0.5H), 8.42 (dd, J = 7.3, 2.0 Hz, 1H), 7.76 – 7.66 (m, 3H), 7.33 – 7.28 (m, 2H), 7.01 – 6.97

(m, 1H), 5.50 (bs, 1H), 4.26 (s, 2H), 3.83 – 3.54 (m, 4H), 3.54 – 3.20 (m, 4H), 3.20 – 3.13 (m, 1H), 3.06 – 2.95 (m, 1H), 2.46 – 2.34 (m, 2H), 2.26 – 2.20 (m, 2H), 2.15 – 2.11 (m, 3H), 1.96 – 1.86 (m, 2H), 1.41 – 1.37 (m, 1H), 0.11 (s, 9H); ^{13}C NMR (176 MHz, Chloroform-*d*) (1:1 mixture of rotamers) 172.1, 171.5, 165.2 (d, $J = 23.1$ Hz), 160.9, 157.0 (d, $J = 247.5$ Hz), 145.4, (135.9, 135.8), 134.5, 133.6 (d, $J = 8.1$ Hz), 131.7 (d, $J = 8.0$ Hz), 131.5, 129.6, 129.2 (d, $J = 18.3$ Hz), 128.3, 127.1, 123.7 (d, $J = 18.0$ Hz), 116.2 (d, $J = 21.9$ Hz), 111.8, (47.2, 46.8, 45.8, 45.7, 45.2), (46.4, 46.3), (42.2, 42.0, 41.7, 41.2), (37.7, 37.6), (35.5, 35.2), (32.7, 32.3), (21.3, 21.2), (19.3, 19.2), 13.2, -1.1; ^{19}F NMR (376 MHz, Chloroform-*d*) δ -117.57 – -117.83 (m); ν_{max} (neat): 3177, 2907, 1797, 1633, 1552, 1494, 1432, 1354, 1245, 1117, 1011, 838 cm^{-1} ; HRMS: calcd. for $\text{C}_{33}\text{H}_{41}\text{FN}_5\text{O}_4\text{Si}$ $[\text{M}+\text{H}]^+$ 618.2912; found 618.2908.

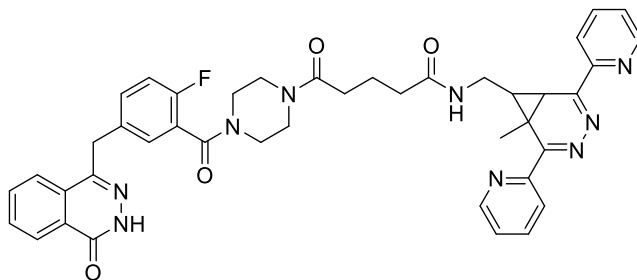


5-(4-(2-Fluoro-5-((4-oxo-3,4-dihydrophthalazin-1-yl)methyl)benzoyl)piperazin-1-yl)-N-((2-methylcycloprop-2-en-1-yl)methyl)-5-oxopentanamide (189)

To a stirred solution of 5-(4-(2-fluoro-5-((4-oxo-3,4-dihydrophthalazin-1-yl)methyl)benzoyl)piperazin-1-yl)-N-((2-methyl-3-(trimethylsilyl)cycloprop-2-en-1-yl)methyl)-5-oxopentanamide (251 mg, 0.41 mmol) in THF (7 mL) was added TBAF 1.0 M in THF (0.45 mL, 0.45 mmol) and the reaction was stirred at room temperature for 1 h. More TBAF 1.0 M in THF (0.45 mL, 1.1 equiv.) was added and the reaction was stirred at room temperature for an additional 2 h. Volatiles were removed under reduced pressure. The crude was dissolved in a minimum amount of DCM and purified by automated column chromatography on silica gel eluting with 0-20% MeOH/DCM over 20 CV. The product-containing fractions were combined and concentrated under reduced pressure. The compound was dissolved in MeCN/water (1:1, 6 mL) and freeze-dried overnight to afford the title compound as a white solid (188 mg, 85% yield).

LCMS (Method B): t_R = 0.82 Min, $[M+H]^+ = 546.20$, purity 100%.

1H NMR (400 MHz, Chloroform- d) (1:1 mixture of rotamers) δ 10.50 (bs, 0.5H), 10.37 (bs, 0.5H), 8.52 – 8.39 (m, 1H), 7.85 – 7.64 (m, 3H), 7.35 – 7.29 (m, 2H), 7.13 – 6.92 (m, 1H), 6.57 (s, 1H), 5.58 (bs, 1H), 4.28 (s, 2H), 3.88 – 3.65 (m, 3H), 3.63 – 3.46 (m, 3H), 3.37 – 3.19 (m, 3H), 3.18 – 3.08 (m, 1H), 2.52 – 2.42 (m, 1H), 2.42 – 2.36 (m, 1H), 2.29 – 2.21 (m, 2H), 2.13 – 2.08 (m, 3H), 2.03 – 1.88 (m, 2H), 1.59 – 1.51 (m, 1H); ^{13}C NMR (101 MHz, Chloroform- d) (1:1 mixture of rotamers) δ 172.3, 171.6, 165.2 (d, $J = 18.2$ Hz), 160.4, 157.3 (d, $J = 248.9$ Hz), 155.9, 145.6, (134.4, 134.3), 133.8, 133.6, 131.9 (d, $J = 8.4$ Hz), 131.8, 130.9, 129.7, 129.5 (d, $J = 15.8$ Hz), 128.5, 127.4, 125.1 (d, $J = 4.0$ Hz), 123.8 (d, $J = 17.1$ Hz), 116.4 (d, $J = 22.6$ Hz), 103.0, (47.4, 46.9, 46.5, 46.0), 45.4, (42.4, 42.1, 41.9, 41.4), (37.8, 37.7), (35.6, 35.4), (32.7, 32.4), (21.5, 21.4) (18.1, 18.0), 11.7; ^{19}F NMR (376 MHz, Chloroform- d) -117.55 – -117.82 (m); ν_{max} (neat): 3194, 2914, 1632, 1551, 1494, 1465, 1432, 1354, 1224, 1118, 1011, 838 cm^{-1} ; HRMS (Method B): calcd. for $C_{30}H_{33}FN_5O_4$ $[M+H]^+ 546.2517$; found 546.2523.



5-(4-(2-Fluoro-5-((4-oxo-3,4-dihydrophthalazin-1-yl)methyl)benzoyl)piperazin-1-yl)-N-((1-methyl-2,5-di(pyridin-2-yl)-3,4-diazabicyclo[4.1.0]hepta-2,4-dien-7-yl)methyl)-5-oxopentanamide (208)

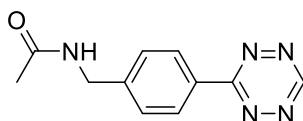
To a stirred solution of 5-(4-(2-fluoro-5-((4-oxo-3,4-dihydrophthalazin-1-yl)methyl)benzoyl)piperazin-1-yl)-N-((2-methylcycloprop-2-en-1-yl)methyl)-5-oxopentanamide (50 mg, 0.092 mmol) in MeOH (5 mL) was added 3,6-di(pyridin-2-yl)-1,2,4,5-tetrazine (33 mg, 0.14 mmol). The reaction was stirred at room temperature for 15 min during which the characteristic red colour of the tetrazine progressively disappeared. Solvent was removed under reduced pressure. The residue was dissolved in MeOH/DMSO (1:1, 2 mL) and purified by Mass Directed Automated Preparative

HPLC (Method C, 2 x 1 mL injections). The product-containing fractions were freeze-dried to afford the title compound as a pale yellow solid (31 mg, 45% yield).

LCMS (HPH method, WF110359-1): $t_R = 0.83$ Min, $[M+H]^+ = 754.31$, purity 78%.

1H and ^{13}C NMR spectra were recorded and showed multiple sets of signals, attributable to a mixture of rotamers and diastereo-isomers, as the major components and some minor signals which may be regio-isomers or other related impurities. The major signals are consistent with the regio-chemistry depicted in the key part of the molecule where the reaction has occurred.

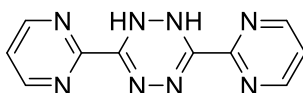
ν_{max} (neat): 3283, 3064, 2930, 1638, 1555, 1494, 1466, 1434, 1354, 1225, 1151, 1012 cm^{-1} ; HRMS (Method B): calcd. for $C_{42}H_{41}FN_9O_4$ $[M+H]^+ 754.3266$; found 754.3268.



***N*-(4-(1,2,4,5-Tetrazin-3-yl)benzyl)acetamide (209)**

To a stirred solution of (4-(1,2,4,5-tetrazin-3-yl)phenyl)methanamine, hydrochloride (25 mg, 0.11 mmol) in DCM (3 mL) was added DIPEA (39 μ L, 0.22 mmol) followed by acetic anhydride (13 μ L, 0.13 mmol). The reaction was stirred at room temperature for 30 min. Solvents were removed under reduced pressure. The residue was dissolved in a minimum amount of DCM and purified by automated column chromatography on silica gel eluting with 0-10% MeOH/DCM over 20 CV. The product-containing fractions were combined and concentrated under reduced pressure to afford the title compound as a pink solid (20 mg, 78% yield).

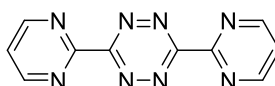
LCMS (Method A): $t_R = 0.64$ Min, $[M+H]^+ = 230.09$; 1H NMR (400 MHz, Chloroform-*d*) δ 10.21 (s, 1H), 8.58 (d, $J = 8.4$ Hz, 2H), 7.51 (d, $J = 8.4$ Hz, 2H), 5.95 (bs, 1H), 4.56 (d, $J = 6.0$ Hz, 2H), 2.08 (s, 3H); ^{13}C NMR (101 MHz, Chloroform-*d*) δ 170.2, 166.4, 158.0, 144.1, 131.0, 128.8, 128.7, 43.5, 23.4; ν_{max} (neat): 3298, 1039, 2929, 1644, 1536, 1437, 1348, 1271, 1185, 1141, 903 cm^{-1} ; HRMS (Method A): calcd. for $C_{11}H_{12}N_5O$ $[M+H]^+ 230.1042$; found 230.1042.



3,6-Di(pyrimidin-2-yl)-1,2-dihydro-1,2,4,5-tetrazine (214)

To a stirred solution of pyrimidine-2-carbonitrile (1.01 g, 9.61 mmol) in THF (13 mL) was added HCl 37% (1.58 mL, 19.22 mmol). Then, hydrazine hydrate (2.70 mL, 55.70 mmol) was added dropwise and the flask was equipped with a condenser. The resulting mixture was stirred at reflux overnight. The reaction mixture was partitioned between DCM (80 mL) and water (80 mL). The layers were separated and the aqueous phase was further extracted with DCM (3 x 80 mL). The combined organic extracts were dried by passing through a hydrophobic frit and concentrated under reduced pressure to afford crude title compound as an orange solid (1.26 g, 55% yield). The product was deemed pure enough to be used in the following step without further purification.

LCMS (Method B): t_R = 0.52 Min, $[M+H]^+$ = 241.02; 1H NMR (400 MHz, DMSO- d_6) δ 9.08 (bs, 2H), 8.93 (d, J = 4.9 Hz, 4H), 7.63 (t, J = 4.9 Hz, 2H); ^{13}C NMR (101 MHz, DMSO) δ 157.7, 155.8, 145.1, 122.2; ν_{max} (neat): 3377, 3340, 3059, 2977, 1637, 1570, 1554, 1430, 1378, 1276, 1116, 980 cm^{-1} ; HRMS (Method B): calcd. for $C_{10}H_9N_8$ $[M+H]^+$ 241.0950; found 241.0949.

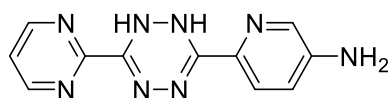


3,6-Di(pyrimidin-2-yl)-1,2,4,5-tetrazine (210)

Crude 3,6-di(pyrimidin-2-yl)-1,2-dihydro-1,2,4,5-tetrazine (470 mg, 1.96 mmol) was dissolved in acetic acid (12 mL). To the previous solution was added sodium nitrite (202 mg, 2.93 mmol) upon which the orange solution turned red/pink and gas evolved. The reaction was stirred at room temperature for 20 min. The reaction mixture was diluted with DCM (40 mL), transferred to a separatory funnel and more DCM (150 mL). A saturated aqueous sodium bicarbonate solution (350 mL) was added until pH was neutral. The layers were separated and the aqueous was further extracted with DCM (5 x 90 mL). The combined organic layers were dried by passing through a

hydrophobic frit and concentrated under reduced pressure. The residue was triturated with acetone (10 mL) and the solid was isolated by vacuum filtration. The solid was washed with more acetone (3 x 10 mL) and dried under vacuum to afford the title compound as a purple solid (141 mg, 30% yield).

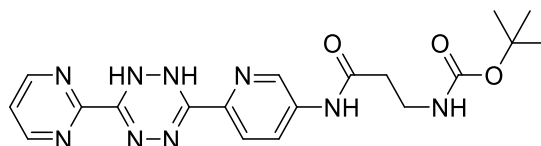
^1H NMR (400 MHz, Chloroform-*d*) δ 9.18 (d, J = 4.9 Hz, 4H), 7.62 (t, J = 4.9 Hz, 2H); ^{13}C NMR (101 MHz, Chloroform-*d*) δ 163.9, 159.6, 158.7, 122.8; $\nu_{\text{max}}(\text{neat})$: 3072, 1567, 1557, 1447, 1372, 1316, 1245, 1163, 991, 911, 828 cm^{-1} .



6-(6-(Pyrimidin-2-yl)-1,2-dihydro-1,2,4,5-tetrazin-3-yl)pyridin-3-amine (216)^[58]

5-Aminopicolinonitrile (1.50 g, 12.59 mmol) and pyrimidine-2-carbonitrile (1.32 g, 12.59 mmol) were mixed with hydrazine hydrate (2.44 mL, 50.40 mmol) and heated to 90 °C overnight behind a blast shield. The reaction mixture turned to a dark red solution after a few minutes and then to a thick orange suspension. The mixture was allowed to cool to room temperature. The orange precipitate was isolated by filtration and washed with cold water (200 mL). The crude solid was dissolved in DCM/MeOH (3:1, 250 mL). Florisil was added and solvents were removed under reduced pressure to adsorb the compound. Purification was carried out by automated column chromatography on silica gel eluting with 0-15% MeOH/DCM over 20 CV. The product-containing fractions were combined and concentrated under reduced pressure to afford the title compound as an orange solid (862 mg, 27% yield).

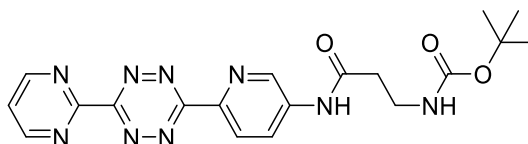
LCMS (Method B): t_R = 0.57 Min, $[\text{M}+\text{H}]^+ = 255.12$; ^1H NMR (400 MHz, DMSO-*d*₆) δ 8.92 (d, J = 4.9 Hz, 2H), 8.82 (bs, 1H), 8.65 (bs, 1H), 7.94 (d, J = 2.7 Hz, 1H), 7.66 (d, J = 8.6 Hz, 1H), 7.60 (t, J = 4.9 Hz, 1H), 7.01 (dd, J = 8.6, 2.7 Hz, 1H), 5.88 (bs, 2H); ^{13}C NMR (101 MHz, DMSO-*d*₆) δ 157.6, 156.1, 146.7, 146.1, 146.0, 134.1, 134.0, 122.0, 121.9, 120.3; $\nu_{\text{max}}(\text{neat})$: 3446, 3321, 3085, 1626, 1583, 1561, 1469, 1439, 1378, 1321, 1272, 1147, 1085 cm^{-1} .



***tert*-Butyl (3-oxo-3-((6-(6-(pyrimidin-2-yl)-1,2-dihydro-1,2,4,5-tetrazin-3-yl)pyridin-3-yl)amino)propyl)carbamate (217)**

To a stirred solution of Boc- β -Ala-OH, (447 mg, 2.36 mmol) in DMF (10 mL) was added DMAP (72 mg, 0.59 mmol) and EDC hydrochloride (565 mg, 2.95 mmol). The reaction was stirred at room temperature for 5 min after which 6-(6-(pyrimidin-2-yl)-1,2-dihydro-1,2,4,5-tetrazin-3-yl)pyridin-3-amine (300 mg, 1.18 mmol) was added in one portion. The reaction was stirred at room temperature for 2 h. The reaction mixture was partitioned between EtOAc (150 mL) and a saturated aqueous sodium bicarbonate solution (100 mL). The layers were separated and the aqueous was further extracted with EtOAc (3 x 80 mL). The combined organic extracts were washed with a 5% aqueous LiCl solution (3 x 100 mL), dried by passing through a hydrophobic frit and concentrated under reduced pressure. The residue was dissolved in DCM, florisil was added and solvents were removed under reduced pressure to adsorb the compound. Purification was carried out by automated column chromatography on silica gel eluting with 0-15% MeOH/DCM over 20 CV. The product-containing fractions were combined and concentrated under reduced pressure to afford the title compound as an orange solid (249 mg, 50% yield).

^1H NMR (400 MHz, DMSO- d_6) δ 10.38 (bs, 1H), 9.03 (bs, 1H), 8.92 (d, J = 4.9 Hz, 2H), 8.85 (bs, 1H), 8.82 (d, J = 2.4 Hz, 1H), 8.16 (dd, J = 8.6, 2.4 Hz, 1H), 7.93 (d, J = 8.6 Hz, 1H), 7.61 (t, J = 4.9 Hz, 1H), 6.88 (bs, 1H), 3.29 – 3.20 (m, 2H), 2.54 (t, J = 7.1 Hz, 2H), 1.37 (s, 9H); ^{13}C NMR (101 MHz, DMSO- d_6) δ 170.2, 157.7, 156.0, 155.5, 145.63, 145.55, 141.3, 138.9, 137.2, 126.7, 122.1, 121.4, 77.6, 36.8, 36.3, 28.2 ν_{max} (neat): 3317, 3059, 2972, 1710, 1689, 1563, 1541, 1480, 1433, 1365, 1234, 1166, 1066 cm^{-1} ; HRMS (Method A): calcd. for $\text{C}_{19}\text{H}_{24}\text{N}_9\text{O}_3$ $[\text{M}+\text{H}]^+$ 426.2002; found 426.2003.



***tert*-Butyl (3-oxo-3-((6-(6-(pyrimidin-2-yl)-1,2,4,5-tetrazin-3-yl)pyridin-3-yl)amino)propyl)carbamate (211)**

To a stirred solution of *tert*-butyl (3-oxo-3-((6-(6-(pyrimidin-2-yl)-1,2-dihydro-1,2,4,5-tetrazin-3-yl)pyridin-3-yl)amino)propyl)carbamate (152 mg, 0.36 mmol) in acetic acid (7 mL) was added sodium nitrite (30 mg, 0.43 mmol) upon which the orange solution turned red and gas evolved. The reaction was stirred at room temperature for 30 min. The reaction was partitioned between DCM (100 mL) and a saturated aqueous sodium bicarbonate solution (250 mL) until pH was neutral. The layers were separated and the aqueous was further extracted with DCM (3 x 80 mL). The combined organic extracts were dried by passing through a hydrophobic frit and concentrated under reduced pressure. The crude was dissolved in a minimum amount of DCM and purified by automated column chromatography on silica gel eluting with 0-15% MeOH/DCM over 20 CV. The product-containing fractions were combined and concentrated under reduced pressure to afford the title compound as a red solid (88 mg, 58% yield).

LCMS (Method B): $t_R = 0.79$ Min, $[M+H]^+ = 424.15$, purity 96%; 1H NMR (400 MHz, DMSO- d_6) δ 10.59 (bs, 1H), 9.19 (d, $J = 4.9$ Hz, 2H), 9.06 (d, $J = 2.5$ Hz, 1H), 8.65 (d, $J = 8.6$ Hz, 1H), 8.42 (dd, $J = 8.6, 2.5$ Hz, 1H), 7.83 (t, $J = 4.9$ Hz, 1H), 6.91 (bs, 1H), 3.34 – 3.23 (m, 2H), 2.60 (t, $J = 7.0$ Hz, 2H), 1.38 (s, 9H); ^{13}C NMR (101 MHz, DMSO- d_6) δ 170.7, 162.8, 162.7, 159.1, 158.5, 155.6, 143.6, 141.3, 138.5, 126.1, 125.2, 122.9, 77.7, 36.9, 36.3, 28.2; $\nu_{max}(\text{neat})$: 3307, 2977, 1714, 1697, 1568, 1525, 1431, 1388, 1251, 1165, 1151, 1059 cm^{-1} ; HRMS (Method B): calcd. for $C_{19}H_{22}N_9O_3$ $[M+H]^+ 424.1846$; found 424.1849

8.3. 2nd order rate constant (k_2) determination for reaction between Olaparib-cyclopropene 2 and various tetrazines

Reaction mixtures consisting of Olaparib-cyclopropene 2 (**189**) and the different 1,2,4,5-tetrazines in 1:1 MeCN/PBS (total volume = 100 μ L) were prepared in separate wells of a 96-well plate at 25 °C so that a final concentration of 1 mM tetrazine and 10, 13 and 17 mM of **189** was achieved. Immediately after the 1,2,4,5-tetrazines solution being added to the well to initiate the IEDDA cycloaddition, the progress of the reaction was monitored by recording the decay of the tetrazines absorbance with a SpectraMax M2 multimode plate reader and SoftMax Pro 6.5 software for 2 minutes (2 seconds interval) at a wavelength of 520 nm. The pseudo-first order rate constants (K_{obs}) were then determined by linear fit of $\ln ([A]/[A_0])$ against reaction time using the pseudo-first order rate equation: $A = A_0 \cdot \exp(-k \cdot [\mathbf{189}] \cdot t)$ where A = absorbance at time t , A_0 = initial absorbance, $k \cdot [\mathbf{189}]$ = pseudo-first order rate constant (K_{obs}), t = time. This procedure was repeated three times for each concentration of Olaparib-cyclopropene 2 and the average of the observed rates K_{obs} was plotted against the concentration of **189** to obtain the second-order rate constants (k_2). All data processing was performed using GraphPad PRISM 8 software.

8.4. Cellular Imaging of PI3K δ TCO Chemical Probes

8.4.1. Imaging of PI3K δ TCO chemical probes in Hut78 cells

▪ **Reagent information table**

Reagent name	# number	Lot	Supplier
Dulbecco's phosphate buffered saline (PBS)	14190-094	1906040	Gibco
Paraformaldehyde 16% solution (PFA)	28908	SL2492801	Thermo scientific
Triton X-100	X100-1L	106K0177V	Sigma
Tween 20	P1379-500ML	SZBC1240V	Sigma
RPMI	21875	1901507	Gibco
PBS	14190-144	1892388	Life Technologies

Hut78 cells at passage 13 in media (200 mL IMDM + 20% FCS) were transferred in a 500 mL FALCON bottle and centrifuged at 1500 rpm for 7 min. Media was removed and pellet were resuspended in 10 mL of media. Cells were diluted to a final concentration of 5×10^6 cells/mL and for each condition 2 mL of cell suspension were used. Cells were distributed to 6 well plate and 4 μ L of compound solution) were added. The cells were incubated for 90 min at 37°C, 5% CO₂ on a shaker.

For competition experiments with covalent PI3K δ inhibitor **149**, cells were incubated for 1 h at 37°C, 5% CO₂ on a shaker with covalent PI3K δ inhibitor. After 1 h, cells were incubated with the TCO chemical probes. The cells were then incubated for 90 min at 37°C, 5% CO₂ on a shaker.

▪ **FACS readout**

After the incubation time, the cells were transferred to FACS tubes (each sample was distributed to 3 FACS tubes, 500 μ L per tube). The tubes were centrifuged for 5 min, 1200 rpm and the supernatant was removed completely. Cells were fixed with 500 μ L/tube 4% PFA solution for 10 min at room temperature in the dark. Cells were washed twice with 500 μ L PBS to remove all PFA and were then permeabilized with

500 μ L 0.5% Triton X-100 solution for 5 min at room temperature. All centrifugation steps after permeabilization were performed for 3 min at 1800 rpm. Cells were washed twice with 500 μ L/tube PBST before 500 μ L/ tube 100 nM Cy5-tetrazine were added for 5 min at room temperature in the dark. Cells were washed 3 times with 500 μ L/ tube PBST and once with 500 μ L/ tube PBS. Then, cells were resuspended in 200 μ L PBS for FACS acquisition.

The cells were then subjected to flow cytometric analysis using a FACS Calibur instrument (BD Biosciences, San Jose, CA). A total of 50,000 events was collected for each sample, and the forward- and side-scatter properties were used to exclude doublets, dead cells, and debris. Cells were excited with a red laser (635 nm) and Cy5 fluorescence was detected using a 660/20 band pass filter (FL4-H channel). A gate for Cy5-positive cells was defined in a FL1-H/FL4-H scatter plot (FL1-H detecting cell autofluorescence), and the percentage of Cy5-positive cells among all cells was calculated based on the number of events recorded within that gate. The data were analyzed using GraphPad Prism. The error bars represent standard deviations from at least two independent replicates.

Washing step with cell media after incubation with compounds: After the incubation time, the cells from the conditions that required a washing step were transferred to 15 mL FALCON tubes and centrifuged for 5 min, 1200 rpm. The supernatant was removed completely. The pellets were resuspended in 5 mL of media. The FALCON tubes were centrifuged for 5 min, 1200 rpm and the supernatant was removed completely. 2 mL of 4% PFA solution were added to each FALCON tube. 500 μ L from each FALCON tubes were immediately transferred into FACS tubes and analysed as previously described.

▪ **Microscopy readout**

After incubation with probes, 50 μ L of cells were taken and transferred to Eppendorf tube. Cells were then centrifuge for 5 min at 400g (Eppendorf centrifuge, 5417R), medium was removed and cell pellet was resuspended in 250 μ L of 4% PFA solution.

Cytofunnels were placed in the Cytospin. After 7 min of fixation, 200 μ L of cell suspension was added to each cytofunnel and samples were centrifuged for 5 min at 1500 rpm. Cytoslides were removed from the funnel and washed once with PBS. Afterwards slides were placed in the chamber with PBS for further washing. Slides were washed with PBS by exchanging the solvent in the chamber. Cells were then permeabilized with 0.5% Triton X-100 solution for 5 min at room temperature. Cells were then washed twice with PBST. Slides were then placed under a fume-hood protected from light and 200 μ L per slide of 100 nM Cy5-tetrazine were added for 5 min at room temperature in the dark (drop on the top of cells). Afterwards, slides were placed again in the chamber and washed three times with PBST. Slides were placed again under the fume-hood and incubated with 200 μ L per slide of Hoechst solution for 10 min at room temperature in the dark. Slides were placed again in the chamber and were washed three times with PBS. Slides were let to dry briefly with air and 30 μ L of Moviol solution was added on the top of cells. Cover slip was placed and all bubbles were removed by pressing the cover slip against the slide. Finally, nail polish was used to glue the borders of the cover slip. For acquisition a Zeiss NLO 780 microscope was used (Zen software).

Settings for imaging:

- Hoechst: ex: 405nm, em: 410-468nm
- Cy5: ex: 633, em: 638-690nm

The objective used was 63x oil. Image analysis was done using Fiji/ImageJ open source, NIH, USA.

8.4.2. Imaging of PI3K δ TCO chemical probes in HeLa cells

▪ Reagent information table

Reagent name	# number	lot	supplier
Dulbecco's phosphate buffered saline (PBS)	14190-094	2078356	Gibco
0.05% Trypsin-EDTA	25300-054	2063501	Gibco
Chambered coverglass system (8 chamber)	155411	11465012209	Lab-Tek
Paraformaldehyde 16% solution (PFA)	15710	171207-06	Electron Microsc. Sci.
Hoechst	H3569	1417663	Life Tech.
Triton X-100	X100-1L	106K0177V	Sigma
Tween 20	P1379-500ML	SLBR9241V	Sigma
37°C incubator Hera Cell 240			Thermo Scientific

▪ Plating of cells

HeLa cells (passage 12) were washed once with 10 mL PBS. Cells were detached from the plate by addition of 3 mL Trypsin and incubation for ~ 5 min at 37°C, 5% CO₂. Trypsin was neutralized with 10 mL of media (MEM + 10% FCS + 1% NEAA, sodium pyruvate at a final concentration of 1 mM) and cells were collected into a 50 mL Falcon tube. The cell concentration was adjusted to 0.2x10⁶ cells/mL and 200 μ L of diluted cells were plated per well in all wells of Lab-Tek dishes and were left for 23 h at 37°C, 5% CO₂ to adhere.

▪ Treatment with compound

Media was removed from the wells by aspiration with a Pasteur pipette. 200 μ L of fresh media were added into wells of the two Labtek dishes. Next, 50 μ L of compound stock solution (or DMSO solution) were added (250 μ L final volume) and cells were incubated with chemical probes for 1 h at 37°C, 5% CO₂. After 1 h incubation, media was removed and cell were washed once with PBS (200 μ L per well).

▪ **Fixation and permeabilization**

Cells were fixed with 200 µL/well 4% PFA solution for 10 min at room temperature in the dark. Cells were washed twice with 200 µL PBS to remove all PFA. Next, cells were permeabilized with 200 µl 0.5% Triton X-100 solution for 5 min at room temperature. Cells were washed twice with 200 µL/well PBST, then 200 µL/ well 100 nM Cy5-tetrazine were added for 7 min at room temperature in the dark. Cells were washed five times with 200 µL/well PBST and then incubated with 200 µL/well Hoechst (1:2000) and WGA-Alexa488 (1:500) solution for 10 min at room temperature in the dark. Cells were washed three times with 200 µL/well PBST, two times with PBS and kept in PBS for acquisition.

▪ **Acquisition**

Images were acquired with a Zeiss NLO 780 microscope equipped with Zen software.

- Hoechst: ex: 405 nm, em: 410-468 nm, 0.2% laser power.
- Cy5: ex: 633 nm, em: 638-690 nm, 0.4-4.5% laser power.
- WGA: ex. 488, em. 506-603nm, 0.8% laser power.

The objective used was 63x oil. Image analysis was done using Fiji / ImageJ open source, NIH, USA.

8.5. NanoSIMS Imaging

Cell Culture

HeLa cells are a human derived cervix adenocarcinoma epithelial cell line (ATTC CCL-2, USA). The cells were cultured in 75 cm² cell culture flasks (Corning, USA). The medium solution used was ATCC-formulated Dulbecco's Modified Eagle's Medium (DMEM), Catalogue No. 30-2002. To make the growth medium complete, the following components were added to the base medium: fetal bovine serum to a final concentration of 10%. The cells were grown for 2 passages and at passage 3 the cells were seeded at 1x10⁵ cell per well on 6 well-plates containing a silicon chip (Ted Pella, 16008) and in a T175cm² per condition, the cells were left to grow for 48 hours,

the media was then changed, and the compounds were added so the concentration was 0.5, 1, 5 and 20 μM .

The cells were counted using a cell Counter (and approximately 1×10^7 cell per condition were obtained from each flask or concentration. $3 \times 2 \mu\text{L}$ of cells were at a density of $1 \times 10^6/\text{mL}$ were taken for each silicon chip from each concentration. The rest was centrifuged again and resuspended in fixative, and EM prep was performed. After 2-hour incubations the cells on silicon chips were washed 3 times with PBS and freeze-dried using the Advantage VirTis wizard 2.0, they were then shipped to the National Physical Laboratory (NPL) and run on the CAMECA NanoSIMS.

The cells grown on $T175\text{cm}^2$ flasks were also treated with the compounds at the 4 different concentrations and after 2 hours washed with PBS, trypsinized, and centrifuged to form a pellet this pellet was then fixed with 4% Formaldehyde/1% Glutaraldehyde (minimum 24 hours).

EM preparation protocol was performed as follows:

After fixation a 2% Aqueous Osmium Tetroxide was added to the cell pellet for 1 hour. Samples were dehydrated in graded series of Ethanol's 30%, 70% 90% and finally 100% followed by 2 changes of Acetone. Samples were infiltrated with Agar 100 epoxy resin and embedded into rubber moulds and polymerised overnight at 60 $^{\circ}\text{C}$. Sections for NanoSIMS were cut on a Leica Ultramicrotome at approximately 500 nm. Sections were then placed onto silicon chips.

Imaging

NanoSIMS measurement was performed using a CAMECA NanoSIMS 50L (Grenneville France). A Cesium primary ion beam was used and negative ions were detected. The impact energy of the primary ion beam was 16 keV/ion. The detectors were moved to the appropriate radii to detect ^{12}C (Detector 1), ^{16}O (Detector 2), $^{12}\text{C}^{14}\text{N}$ (Detector 3), $^{12}\text{C}^{15}\text{N}$ (Detector 4), ^{29}Si (Detector 5), ^{31}P (Detector 6) and ^{32}S (Detector 7). Pulse height distributions were measured on detectors 3 and 4 and voltage gains and thresholds adjusted to ensure proper calibration for isotope measurements. Counts

for ^{12}C ^{14}N were then measured on each detector by changing the magnetic field to ensure the count rates were the same on both detectors as a final check. Imaging was performed by rastering the ion beam across the sample surface with fields of view typically in the range of 25-40 mm. The raster size in pixels was 256 x 256. A primary ion beam aperture diameter of 150 mm was used (D1-4), which would enable a spot size of ~ 100-150 nm. Dwell time per pixel was 4 ms. Mass resolution was ~7000 measured at ^{12}C ^{14}N using a 30 mm width entrance slit (Es-3) and a 350 mm width aperture slit (As-1). Mass spectra were checked at each detector prior to each image acquisition and the deflection voltage at each detector was set to ensure only the desired mass was deflected through the exit slit to the detector. All images scaled from 38 to 50 for the ratio images.

9. References

- [1] Prescher, J. A., Bertozzi, C. R., *Nat. Chem. Biol.*, **2005**, *1*, 13-21.
- [2] Alcolea, M. P., Jones, P. H., *Nat. Rev. Cancer*, **2013**, *13*, 161-171.
- [3] Tsien, R. Y., *Annu. Rev. Biochem.*, **1998**, *67*, 509-544.
- [4] Lippincott-Schwartz, J., Patterson, G. H., *Science*, **2003**, *300*, 87-91.
- [5] Zhang, J., Campbell, R. E., Ting, A. Y., Tsien, R. Y., *Nat. Rev. Mol. Cell. Biol.*, **2002**, *3*, 906-918.
- [6] Swenson, E. S., Price, J. G., Brazelton, T., Krause, D. S., *Stem cells (Dayton, Ohio)*, **2007**, *25*, 2593-2600.
- [7] Remington, S. J., *Prot. Sci.*, **2011**, *20*, 1509-1519.
- [8] Alberts, B., *Mol. Biol. Cell*, **2002**,
- [9] Sletten, E. M., Bertozzi, C. R., *Angew. Chem. Int. Ed.*, **2009**, *48*, 6974-6998.
- [10] Baskin, J. M., Prescher, J. A., Laughlin, S. T., Agard, N. J., Chang, P. V., Miller, I. A., Lo, A., Codelli, J. A., Bertozzi, C. R., *Proc. Natl. Acad. Sci. U.S.A.*, **2007**, *104*, 16793-16797.
- [11] Lang, K., Chin, J. W., *ACS Chem. Biol.*, **2014**, *9*, 16-20.
- [12] Lim, R. K. V., Lin, Q., *Chem. Commun.*, **2010**, *46*, 1589-1600.
- [13] Murrey, H. E., Judkins, J. C., am Ende, C. W., Ballard, T. E., Fang, Y., Riccardi, K., Di, L., Guilmette, E. R., Schwartz, J. W., Fox, J. M., Johnson, D. S., *J. Am. Chem. Soc.*, **2015**, *137*, 11461-11475.
- [14] Oliveira, B. L., Guo, Z., Bernardes, G. J. L., *Chem. Soc. Rev.*, **2017**, *46*, 4895-4950.
- [15] Griffin, R. J., *Prog. Med. Chem.*, **1994**, *31*, 121-232.
- [16] Hendricks, S. B., Pauling, L., *J. Am. Chem. Soc.*, **1925**, *47*, 2904-2920.
- [17] Agard, N. J., Baskin, J. M., Prescher, J. A., Lo, A., Bertozzi, C. R., *ACS Chem. Biol.*, **2006**, *1*, 644-648.
- [18] Saxon, E., Bertozzi, C. R., *Science*, **2000**, *287*, 2007-2010.
- [19] Staudinger, H., Meyer, J., *Helv. Chim. Acta*, **1919**, *2*, 635-646.
- [20] Lin, F. L., Hoyt, H. M., van Halbeek, H., Bergman, R. G., Bertozzi, C. R., *J. Am. Chem. Soc.*, **2005**, *127*, 2686-2695.

- [21] Saxon, E., Luchansky, S. J., Hang, H. C., Yu, C., Lee, S. C., Bertozzi, C. R., *J. Am. Chem. Soc.*, **2002**, *124*, 14893-14902.
- [22] Prescher, J. A., Dube, D. H., Bertozzi, C. R., *Nature*, **2004**, *430*, 873-877.
- [23] Boyce, M., Bertozzi, C. R., *Nat. methods*, **2011**, *8*, 638-642.
- [24] Saxon, E., Armstrong, J. I., Bertozzi, C. R., *Org. Lett.*, **2000**, *2*, 2141-2143.
- [25] Soellner, M. B., Nilsson, B. L., Raines, R. T., *J. Am. Chem. Soc.*, **2006**, *128*, 8820-8828.
- [26] Debets, M. F., van der Doelen, C. W. J., Rutjes, F. P. J. T., van Delft, F. L., *ChemBioChem*, **2010**, *11*, 1168-1184.
- [27] McKay, Craig S., Finn, M. G., *Chem. Biol.*, **2014**, *21*, 1075-1101.
- [28] Kolb, H. C., Finn, M. G., Sharpless, K. B., *Angew. Chem., Int. Ed.*, **2001**, *40*, 2004-2021.
- [29] Hong, V., Steinmetz, N. F., Manchester, M., Finn, M. G., *Bioconjugate Chem.*, **2010**, *21*, 1912-1916.
- [30] Wright, M. H., Sieber, S. A., *Nat. Prod. Rep.*, **2016**, *33*, 681-708.
- [31] Huisgen, R., *Angew. Chem. Int. Ed.*, **1963**, *2*, 565-598.
- [32] Huisgen, R., *Angew. Chem. Int. Ed.*, **1963**, *2*, 633-645.
- [33] Rostovtsev, V. V., Green, L. G., Fokin, V. V., Sharpless, K. B., *Angew. Chem. Int. Ed.*, **2002**, *41*, 2596-2599.
- [34] Presolski, S. I., Hong, V. P., Finn, M. G., *Curr. Prot. Chem. Biol.*, **2011**, *3*, 153-162.
- [35] Wolbers, F., ter Braak, P., Le Gac, S., Luttge, R., Andersson, H., Vermes, I., van den Berg, A., *Electrophoresis*, **2006**, *27*, 5073-5080.
- [36] Li, L., Zhang, Z., *Molecules*, **2016**, *21*,
- [37] Agard, N. J., Prescher, J. A., Bertozzi, C. R., *J. Am. Chem. Soc.*, **2004**, *126*, 15046-15047.
- [38] Wittig, G., Krebs, A., *Chem. Ber.*, **1961**, *94*, 3260-3275.
- [39] Jewett, J. C., Bertozzi, C. R., *Chem. Soc. Rev.*, **2010**, *39*, 1272-1279.
- [40] Sletten, E. M., Bertozzi, C. R., *Acc. Chem. Res.*, **2011**, *44*, 666-676.
- [41] Fukui, K., Yonezawa, T., Shingu, H., *J. Chem. Phys.*, **1952**, *20*, 722-725.

- [42] Codelli, J. A., Baskin, J. M., Agard, N. J., Bertozzi, C. R., *J. Am. Chem. Soc.*, **2008**, *130*, 11486-11493.
- [43] Sletten, E. M., Bertozzi, C. R., *Org. Lett.*, **2008**, *10*, 3097-3099.
- [44] Ning, X., Guo, J., Wolfert, M. A., Boons, G.-J., *Angew. Chem. Int. Ed.* **2008**, *47*, 2253-2255.
- [45] Sletten, E. M., Nakamura, H., Jewett, J. C., Bertozzi, C. R., *J. Am. Chem. Soc.*, **2010**, *132*, 11799-11805.
- [46] Laughlin, S. T., Baskin, J. M., Amacher, S. L., Bertozzi, C. R., *Science*, **2008**, *320*, 664-667.
- [47] Debets, M. F., van Berkel, S. S., Dommerholt, J., Dirks, A. J., Rutjes, F. P. J. T., van Delft, F. L., *Acc. Chem. Res.*, **2011**, *44*, 805-815.
- [48] Blackman, M. L., Royzen, M., Fox, J. M., *J. Am. Chem. Soc.*, **2008**, *130*, 13518-13519.
- [49] Diels, O., Alder, K., *Justus Liebigs Ann. Chem.*, **1928**, *460*, 98-122.
- [50] Saracoglu, N., *Tetrahedron*, **2007**, *63*, 4199-4236.
- [51] Carboni, R. A., Lindsey, R. V., Jr., *J. Am. Chem. Soc.*, **1959**, *81*, 4342-4346.
- [52] Blackman, M. L., Royzen, M., Fox, J. M., *J. Am. Chem. Soc.*, **2008**, *130*, 13518-13519.
- [53] Taylor, M. T., Blackman, M. L., Dmitrenko, O., Fox, J. M., *J. Am. Chem. Soc.*, **2011**, *133*, 9646-9649.
- [54] Steigel, A., Sauer, J., Kleier, D. A., Binsch, G., *J. Am. Chem. Soc.*, **1972**, *94*, 2770-2779.
- [55] Rossin, R., van, d. B. S. M., Ten, H. W., Carvelli, M., Versteegen, R. M., Lub, J., Robillard, M. S., *Bioconjugate Chem.*, **2013**, *24*, 1210-1217.
- [56] Bach, R. D., *J. Am. Chem. Soc.*, **2009**, *131*, 5233-5243.
- [57] Darko, A., Wallace, S., Dmitrenko, O., Machovina, M. M., Mehl, R. A., Chin, J. W., Fox, J. M., *Chem. Sci.*, **2014**, *5*, 3770-3776.
- [58] Uttamapinant, C., Howe, J. D., Lang, K., Beranek, V., Davis, L., Mahesh, M., Barry, N. P., Chin, J. W., *J. Am. Chem. Soc.*, **2015**, *137*, 4602-4605.
- [59] Kozma, E., Varga, B. R., Kele, P., Nikic, I., Aramburu, I. V., Kang, J. H., Lemke, E. A., Fackler, O. T., *ChemBioChem*, **2016**, *17*, 1518-1524.

- [60] Lambert, W. D., Scinto, S. L., Dmitrenko, O., Boyd, S. J., Magboo, R., Mehl, R. A., Chin, J. W., Fox, J. M., Wallace, S., *Org. Biomol. Chem.*, **2017**, *15*, 6640-6644.
- [61] Luscombe, C., GSK: 2018, Unpublished results.
- [62] <http://www.daylight.com/dayhtml/doc/clogp/index.html#PCMsc1.1.2>, accessed on 30th January 2019.
- [63] Siegl, S. J., Vázquez, A., Dzijak, R., Dračinský, M., Galeta, J., Rampmaier, R., Klepetářová, B., Vrabel, M., *Chem. Eur. J.*, **2018**, *24*, 2426-2432.
- [64] Šekut, J., Devaraj, N. K., *Curr. Opin. Chem. Biol.*, **2013**, *17*, 761-767.
- [65] Wieczorek, A., Buckup, T., Wombacher, R., *Org. Biomol. Chem.*, **2014**, *12*, 4177-4185.
- [66] Devaraj, N. K., Upadhyay, R., Haun, J. B., Hilderbrand, S. A., Weissleder, R., *Angew. Chem. Int. Ed.*, **2009**, *121*, 7147-7150.
- [67] Andrews, U. H., Baldwin, J. E., Grayston, M. W., *J. Org. Chem.*, **1982**, *47*, 287-292.
- [68] Thalhammer, F., Wallfaher, U., Sauer, J., *Tetrahedron Lett.*, **1990**, *31*, 6851-6854.
- [69] Kamber, D. N., Nazarova, L. A., Liang, Y., Lopez, S. A., Patterson, D. M., Shih, H.-W., Houk, K. N., Prescher, J. A., *J. Am. Chem. Soc.*, **2013**, *135*, 13680-13683.
- [70] Patterson, D. M., Nazarova, L. A., Xie, B., Kamber, D. N., Prescher, J. A., *J. Am. Chem. Soc.*, **2012**, *134*, 18638-18643.
- [71] Ravasco, J. M. J. M., Monteiro, C. M., Trindade, A. F., *Org. Chem. Front.*, **2017**, *4*, 1167-1198.
- [72] Yang, J., Liang, Y., Seckute, J., Houk, K. N., Devaraj, N. K., *Chem. Eur. J.* **2014**, *20*, 3365-3375.
- [73] Yang, J., Seckute, J., Cole, C. M., Devaraj, N. K., *Angew. Chem., Int. Ed.*, **2012**, *51*, 7476-7479.
- [74] Fattorusso, E., Magno, S., Mayol, L., Santacroce, C., Sica, D., *Tetrahedron*, **1975**, *31*, 1715-1716.
- [75] Itoh, T., Sica, D., Djerassi, C., *J. Org. Chem.*, **1983**, *48*, 890-892.
- [76] Lin, H.-C., Tsai, R.-T., Wu, H.-P., Lee, H.-Y., Lee, G.-A., *Tetrahedron*, **2016**, *72*, 184-191.

- [77] Sheshenev, A. E., Baird, M. S., Croft, A. K., Starikova, Z. A., Shashkov, A. S., Zhuze, A. L., Bolesov, I. G., *Tetrahedron Lett.*, **2006**, 47, 2839-2843.
- [78] Carter, F. L., Frampton, V. L., *Chem. Rev.*, **1964**, 64, 497-525.
- [79] Karver, M. R., Weissleder, R., Hilderbrand, S. A., *Bioconjugate Chem.*, **2011**, 22, 2263-2270.
- [80] Kumar, P., Jiang, T., Li, S., Zainul, O., Laughlin, S. T., *Org. Biomol. Chem.*, **2018**, 16, 4081-4085.
- [81] Kalia, J., Raines, R. T., *Curr. Org. Chem.*, **2010**, 14, 138-147.
- [82] Devaraj, N. K., *ACS Cent. Sci.*, **2018**, 4, 952-959.
- [83] Row, R. D., Prescher, J. A., *Acc. Chem. Res.*, **2018**, 51, 1073-1081.
- [84] Bunnage, M. E., Chekler, E. L. P., Jones, L. H., *Nat. Chem. Biol.*, **2013**, 9, 195-199.
- [85] Rix, U., Superti-Furga, G., *Nat. Chem. Biol.*, **2009**, 5, 616-624.
- [86] Kang, K., Park, J., Kim, E., *Proteome Sci.*, **2017**, 15, 45/41-45/13.
- [87] Arrowsmith, C. H., Audia, J. E., Austin, C., Baell, J., Bennett, J., Blagg, J., Bountra, C., Brennan, P. E., Brown, P. J., Bunnage, M. E., Buser-Doepner, C., Campbell, R. M., Carter, A. J., Cohen, P., Copeland, R. A., Cravatt, B., Dahlin, J. L., Dhanak, D., Edwards, A. M., Frye, S. V., Gray, N., Grimshaw, C. E., Hepworth, D., Howe, T., Huber, K. V. M., Jin, J., Knapp, S., Kotz, J. D., Kruger, R. G., Lowe, D., Mader, M. M., Marsden, B., Mueller-Fahrnow, A., Muller, S., O'Hagan, R. C., Overington, J. P., Owen, D. R., Rosenberg, S. H., Roth, B., Ross, R., Schapira, M., Schreiber, S. L., Shoichet, B., Sundstrom, M., Superti-Furga, G., Taunton, J., Toledo-Sherman, L., Walpole, C., Walters, M. A., Willson, T. M., Workman, P., Young, R. N., Zuercher, W. J., *Nat. Chem. Biol.*, **2015**, 11, 536-541.
- [88] Rutkowska, A., Thomson, D. W., Vappiani, J., Werner, T., Mueller, K. M., Dittus, L., Krause, J., Muelbaier, M., Bergamini, G., Bantscheff, M., *ACS Chem. Biol.*, **2016**, 11, 2541-2550.
- [89] Arrowsmith, J., Miller, P., *Nat. Rev. Drug Discov.*, **2013**, 12, 569-569.
- [90] Fong, P. C., Boss, D. S., Yap, T. A., Tutt, A., Wu, P., Mergui-Roelvink, M., Mortimer, P., Swaisland, H., Lau, A., O'Connor, M. J., Ashworth, A., Carmichael, J., Kaye, S. B., Schellens, J. H. M., de Bono, J. S., *N. Engl. J. Med.*, **2009**, 361, 123-134.

- [91] Cantley, L. C., *Science*, **2002**, 296, 1655-1657.
- [92] Jean, S., Kiger, A. A., *J. Cell Sci.*, **2014**, 127, 923-928.
- [93] Vanhaesebroeck, B., Whitehead, M. A., Pineiro, R., *J. Mol. Med.*, **2016**, 94, 5-11.
- [94] Martin, T. F. J., *Annu. Rev. Cell Dev. Biol.*, **1998**, 14, 231-264.
- [95] Walker, E. H., Perisic, O., Ried, C., Stephens, L., Williams, R. L., *Nature*, **1999**, 402, 313-320.
- [96] Wymann, M. P., Marone, R., *Curr. Opin. Cell Biol.*, **2005**, 17, 141-149.
- [97] Carracedo, A., Pandolfi, P. P., *Oncogene*, **2008**, 27, 5527-5541.
- [98] Vanhaesebroeck, B., Stephens, L., Hawkins, P., *Nat. Rev. Mol. Cell Biol.*, **2012**, 13, 195-203.
- [99] Mader, C., *Yale J. Biol. Med.*, **2007**, 80, 91-91.
- [100] Amzel, L. M., Huang, C.-H., Mandelker, D., Lengauer, C., Gabelli, S. B., Vogelstein, B., *Nat. Rev. Cancer*, **2008**, 8, 665-669.
- [101] Berndt, A., Miller, S., Williams, O., Le, D. D., Houseman, B. T., Pacold, J. I., Gorrec, F., Hon, W.-C., Liu, Y., Rommel, C., Gaillard, P., Rueckle, T., Schwarz, M. K., Shokat, K. M., Shaw, J. P., Williams, R. L., *Nat. Chem. Biol.*, **2010**, 6, 117-124.
- [102] Jimenez, C., Hernandez, C., Pimentel, B., Carrera, A. C., *J. Biol. Chem.*, **2002**, 277, 41556-41562.
- [103] Jia, S., Liu, Z., Zhang, S., Liu, P., Zhang, L., Lee, S. H., Zhang, J., Signoretti, S., Loda, M., Roberts, T. M., Zhao, J. J., *Nature*, **2008**, 454, 776-779.
- [104] Jackson, S. P., Schoenwaelder, S. M., Goncalves, I., Nesbitt, W. S., Yap, C. L., Wright, C. E., Kenche, V., Anderson, K. E., Dopheide, S. M., Yuan, Y., Sturgeon, S. A., Prabakaran, H., Thompson, P. E., Smith, G. D., Shepherd, P. R., Daniele, N., Kulkarni, S., Abbott, B., Saylik, D., Jones, C., Lu, L., Giuliano, S., Hugan, S. C., Angus, J. A., Robertson, A. D., Salem, H. H., *Nat. Med.*, **2005**, 11, 507-514.
- [105] Crabbe, T., Welham, M. J., Ward, S. G., *Trends Biochem. Sci.*, **2007**, 32, 450-456.
- [106] Rommel, C., Camps, M., Ji, H., *Nat. Rev. Immunol.*, **2007**, 7, 191-201.
- [107] Engelman, J. A., Luo, J., Cantley, L. C., *Nat. Rev. Genet.*, **2006**, 7, 606-619.
- [108] Khan, A., Southworth, T., Worsley, S., Sriskantharajah, S., Amour, A., Hessel, E. M., Singh, D., *Clin. Exp. Pharmacol. Physiol.*, **2017**, 44, 932-940.

- [109] Allen, R. A., Brookings, D. C., Powell, M. J., Delgado, J., Shuttleworth, L. K., Merriman, M., Fahy, I. J., Tewari, R., Silva, J. P., Healy, L. J., Davies, G. C. G., Twomey, B., Cutler, R. M., Kotian, A., Crosby, A., McCluskey, G., Watt, G. F., Payne, A., *J. Pharmacol. Exp. Ther.*, **2017**, *361*, 429-440.
- [110] Vanhaesebroeck, B., Guillermet-Guibert, J., Graupera, M., Bilanges, B., *Nat. Rev. Mol. Cell Biol*, **2010**, *11*, 329-341.
- [111] Bi, L., Okabe, I., Bernard, D. J., Wynshaw-Boris, A., Nussbaum, R. L., *J. Biol. Chem.*, **1999**, *274*, 10963-10968.
- [112] Samuels, Y., Wang, Z., Bardelli, A., Silliman, N., Ptak, J., Szabo, S., Yan, H., Gazdar, A., Powell, S. M., Riggins, G. J., Willson, J. K. V., Markowitz, S., Kinzler, K. W., Vogelstein, B., Velculescu, V. E., *Science*, **2004**, *304*, 554.
- [113] Koyasu, S., *Nat. Immunol.*, **2003**, *4*, 313-319.
- [114] Foster, J. G., Blunt, M. D., Carter, E., Ward, S. G., *Pharmacol. Rev.*, **2012**, *64*, 1027-1054.
- [115] Ghigo, A., Damilano, F., Braccini, L., Hirsch, E., *BioEssays*, **2010**, *32*, 185-196.
- [116] Sriskantharajah, S., Hamblin, N., Worsley, S., Calver, A. R., Hessel, E. M., Amour, A., *Ann. N. Y. Acad. Sci*, **2013**, *1280*, 35-39.
- [117] Thomas, M., Owen, C., *Curr. Opin. Pharmacol.*, **2008**, *8*, 267-274.
- [118] Sriskantharajah, S., Hamblin, N., Worsley, S., Calver, A. R., Hessel, E. M., Amour, A., *Ann. N.Y Acad. Sci.*, **2013**, *1280*, 35-39.
- [119] Barnes, P. J., Wedzicha, J. A., Burney, P. G. J., Silverman, E. K., Celli, B. R., Vestbo, J., Wouters, E. F. M., *Nat. Rev. Dis. Primers*, **2015**, *1*, 15076.
- [120] Gonda, I., *J. Aerosol Med.*, **2006**, *19*, 47-53.
- [121] Lotvall, J., *Respir. Med.*, **1997**, 29-31.
- [122] Patton, J. S., Byron, P. R., *Nat. Rev. Drug Discov.*, **2007**, *6*, 67-74.
- [123] Patton, J. S., Fishburn, C. S., Weers, J. G., *Proc. Am. Thorac. Soc.*, **2004**, *1*, 338-344.
- [124] Chrystyn, H., *Br. J. Clin. Pharmacol.*, **2001**, *51*, 289-299.
- [125] Down, K., Amour, A., Baldwin, I. R., Cooper, A. W. J., Deakin, A. M., Felton, L. M., Guntrip, S. B., Hardy, C., Harrison, Z. A., Jones, K. L., Jones, P., Keeling, S. E., Le, J., Livia, S., Lucas, F., Lunniss, C. J., Parr, N. J., Robinson, E., Rowland, P.,

- Smith, S., Thomas, D. A., Vitulli, G., Washio, Y., Hamblin, J. N., *J. Med. Chem.*, **2015**, 58, 7381-7399.
- [126] Sutherlin, D. P., Baker, S., Bisconte, A., Blaney, P. M., Brown, A., Chan, B. K., Chantry, D., Castanedo, G., DePledge, P., Goldsmith, P., Goldstein, D. M., Hancox, T., Kaur, J., Knowles, D., Kondru, R., Lesnick, J., Lucas, M. C., Lewis, C., Murray, J., Nadin, A. J., Nonomiya, J., Pang, J., Pegg, N., Price, S., Reif, K., Safina, B. S., Salphati, L., Staben, S., Seward, E. M., Shuttleworth, S., Sohal, S., Sweeney, Z. K., Ultsch, M., Waszkowycz, B., Wei, B., *Bioorg. Med. Chem. Lett.*, **2012**, 22, 4296-4302.
- [127] Duong-Ly, K. C., Peterson, J. R., *Curr. Prot. Pharmacol.*, **2013**, Chapter 2, Unit2.9, 1-14.
- [128] Garces, A. E., Stocks, M. J., *J. Med. Chem.*, **2018**, Ahead of Print.
- [129] Begg, M., Edwards, C. D., Hamblin, J. N., Pefani, E., Wilson, R., Gilbert, J., Vitulli, G., Mallett, D., Morrell, J., Hingle, M. I., Uddin, S., Ehtesham, F., Marotti, M., Harrell, A., Newman, C. F., Fernando, D., Clark, J., Cahn, A., Hessel, E. M., *J. Pharmacol. Exp. Ther.*, **2019**, 369, 443-453.
- [130] Smith, D. A., Beaumont, K., Maurer, T. S., Di, L., *J. Med. Chem.*, **2015**, 58, 5691-5698.
- [131] Anderson, G. P., Linden, A., Rabe, K. F., *Eur. Respir. J.*, **1994**, 7, 569-578.
- [132] Kazmi, F., Hensley, T., Pope, C., Funk, R. S., Loewen, G. J., Buckley, D. B., Parkinson, A., *Drug Metab. Dispos.*, **2013**, 41, 897-905.
- [133] Chakraborty, K., Leung, K., Krishnan, Y., *eLife*, **2017**, 6, 1-21.
- [134] Daniel, W. A., *Nova Acta Leopold.*, **2003**, 87, 101-111.
- [135] Trapp, S., Rosania, G. R., Horobin, R. W., Kornhuber, J., *Eur. Biophys. J.*, **2008**, 37, 1317-1328.
- [136] Morrell, J., GSK, Unpublished results.
- [137] Taylor, T. E., Zigel, Y., Egan, C., Hughes, F., Costello, R. W., Reilly, R. B., *Sci. Rep.*, **2018**, 8, 1-14.
- [138] Helmer, E., Watling, M., Jones, E., Tytgat, D., Jones, M., Allen, R., Payne, A., Koch, A., Healy, E., *Eur. J. of Clin. Pharmacol.*, **2017**, 73, 581-591.
- [139] Rao, V. K., Webster, S., Dalm, V. A. S. H., Sediva, A., van Hagen, P. M., Holland, S., Rosenzweig, S. D., Christ, A. D., Sloth, B., Cabanski, M., Joshi, A. D.,

- de Buck, S., Doucet, J., Guerini, D., Kalis, C., Pylvaenaeinen, I., Soldermann, N., Kashyap, A., Uzel, G., Lenardo, M. J., Patel, D. D., Lucas, C. L., Burkhardt, C., *Blood*, **2017**, *130*, 2307-2316.
- [140] Barton, N., Convery, M., Cooper, A. W. J., Down, K., Hamblin, J. N., Inglis, G., Peace, S., Rowedder, J., Rowland, P., Taylor, J. A., Wellaway, N., *J. Med. Chem.*, **2018**, *61*, 11061-11073.
- [141] GSK, Unpublished results.
- [142] Thomson, D., Rutkowska, A., Cellzome (a GSK company), Unpublished results.
- [143] Hamm, G., Nilsson, A., Fihn, B.-M., Strittmatter, N., Andrén, P., Goodwin, R. J. A., Fridén, M., *Drug Deliv.*, **2018**, *25*, 838-845.
- [144] Frye, S. V., *Nat. Chem. Biol.*, **2010**, *6*, 159-161.
- [145] Livia, S., GSK, Unpublished results.
- [146] Edney, D., Hulcoop, D. G., Leahy, J. H., Vernon, L. E., Wipperman, M. D., Bream, R. N., Webb, M. R., *Org. Process Res. Dev.*, **2018**, *22*, 368-376.
- [147] Goo, Koley, D., Hermann, H., Thiel, W., *Chem. Commun.*, **2004**, 2141-2143.
- [148] Grushin, V. V., Alper, H., *Chem. Rev.*, **1994**, *94*, 1047-1062.
- [149] Kinzel, T., Zhang, Y., Buchwald, S. L., *J. Am. Chem. Soc.*, **2010**, *132*, 14073-14075.
- [150] Biscoe, M. R., Fors, B. P., Buchwald, S. L., *J. Am. Chem. Soc.*, **2008**, *130*, 6686-6687.
- [151] Bruno, N. C., Tudge, M. T., Buchwald, S. L., *Chem. Sci.*, **2013**, *4*, 916-920.
- [152] Abdel-Magid, A. F., Carson, K. G., Harris, B. D., Maryanoff, C. A., Shah, R. D., *J. Org. Chem.*, **1996**, *61*, 3849-3862.
- [153] Imada, Y., Yuasa, M., Nakamura, I., Murahashi, S.-I., *J. Org. Chem.*, **1994**, *59*, 2282-2284.
- [154] Wissmann, H., *Phosphorus Sulfur Silicon Relat. Elem.*, **1987**, *30*, 645-648.
- [155] Dunetz, J. R., Magano, J., Weisenburger, G. A., *Org. Process. Res. Dev.*, **2016**, *20*, 140-177.
- [156] Gorelsky, S. I., Lapointe, D., Fagnou, K., *J. Am. Chem. Soc.*, **2008**, *130*, 10848-10849.
- [157] Lafrance, M., Fagnou, K., *J. Am. Chem. Soc.*, **2006**, *128*, 16496-16497.

- [158] Kotha, S., Lahiri, K., Kashinath, D., *Tetrahedron*, **2002**, 58, 9633-9695.
- [159] Ishiyama, T., Murata, M., Miyaura, N., *J. Org. Chem.*, **1995**, 60, 7508-7510.
- [160] Mkhalid, I. A. I., Barnard, J. H., Marder, T. B., Murphy, J. M., Hartwig, J. F., *Chem. Rev.*, **2010**, 110, 890-931.
- [161] Hartwig, J. F., *Acc. Chem. Res.*, **2012**, 45, 864-873.
- [162] Cho, J.-Y., Iverson, C. N., Smith, M. R., *J. Am. Chem. Soc.*, **2000**, 122, 12868-12869.
- [163] Ishiyama, T., Takagi, J., Ishida, K., Miyaura, N., Anastasi, N. R., Hartwig, J. F., *J. Am. Chem. Soc.*, **2002**, 124, 390-391.
- [164] Larsen, M. A., Hartwig, J. F., *J. Am. Chem. Soc.*, **2014**, 136, 4287-4299.
- [165] Ishiyama, T., Nobuta, Y., Hartwig, J. F., Miyaura, N., *Chem. Commun.*, **2003**, 2924-2925.
- [166] Vanchura, I. I. B. A., Preshlock, S. M., Roosen, P. C., Kallepalli, V. A., Staples, R. J., Maleczka, J. R. E., Singleton, D. A., Smith, I. I. I. M. R., *Chem. Commun.*, **2010**, 46, 7724-7726.
- [167] Bryan, M. C., Dunn, P. J., Entwistle, D., Gallou, F., Koenig, S. G., Hayler, J. D., Hickey, M. R., Hughes, S., Kopach, M. E., Moine, G., Richardson, P., Roschangar, F., Steven, A., Weiberth, F. J., *Green Chem.*, **2018**, 20, 5082-5103.
- [168] Bream, R., GSK, Unpublished results.
- [169] Das, S., Addis, D., Junge, K., Beller, M., *Chem. Eur. J.*, **2011**, 17, 12186-12192.
- [170] Young, R. J., Green, D. V. S., Luscombe, C. N., Hill, A. P., *Drug Discov. Today*, **2011**, 16, 822-830.
- [171] Bhattachar, S. N., Wesley, J. A., Seadeek, C., *J. Pharm. Biomed. Anal.*, **2006**, 41, 152-157.
- [172] Almeling, S., Ilko, D., Holzgrabe, U., *J. Pharm. Biomed. Anal.*, **2012**, 69, 50-63.
- [173] Kansy, M., Senner, F., Gubernator, K., *J. Med. Chem.*, **1998**, 41, 1007-1010.
- [174] Cheng, Y.-C., Prusoff, W. H., *Biochem. Pharmacol.*, **1973**, 22, 3099-3108.
- [175] Bantscheff, M., Eberhard, D., Abraham, Y., Bastuck, S., Boesche, M., Hobson, S., Mathieson, T., Perrin, J., Raida, M., Rau, C., Reader, V., Sweetman, G., Bauer, A., Bouwmeester, T., Hopf, C., Kruse, U., Neubauer, G., Ramsden, N., Rick, J., Kuster, B., Drewes, G., *Nat. Biotechnol.*, **2007**, 25, 1035-1044.

- [176] Golkowski, M., Vidadala, R. S. R., Lombard, C. K., Suh, H. W., Maly, D. J., Ong, S.-E., *J. Proteome Res.*, **2017**, *16*, 1216-1227.
- [177] Medard, G., Pachl, F., Ruprecht, B., Klaeger, S., Heinzlmeir, S., Helm, D., Qiao, H., Ku, X., Wilhelm, M., Kuehne, T., Wu, Z., Dittmann, A., Hopf, C., Kramer, K., Kuster, B., *J. Proteome Res.*, **2015**, *14*, 1574-1586.
- [178] Lea, J., Chitty, C., GSK, Unpublished results.
- [179] Campbell, J. D. M., Foerster, A., Lasmanowicz, V., Niemoeller, M., Scheffold, A., Fahrendorff, M., Rauser, G., Assenmacher, M., Richter, A., *Clin. Exp. Immunol.*, **2011**, *163*, 1-10.
- [180] Soond, D. R., Bjorgo, E., Moltu, K., Dale, V. Q., Patton, D. T., Torgersen, K. M., Galleway, F., Twomey, B., Clark, J., Gaston, J. S. H., Tasken, K., Bunyard, P., Okkenhaug, K., *Blood*, **2010**, *115*, 2203-2213.
- [181] Routledge, P. A., *Br. J. Clin. Pharmacol.*, **1986**, *22*, 499-506.
- [182] Tillement, J. P., Albengres, E., Urien, S., *Eur. J. Drug Metab. Pharmacokinet.*, **1979**, *4*, 123-127.
- [183] Obach, R. S., Lombardo, F., Waters, N. J., *Drug Metab. Dispos.*, **2008**, *36*, 1385-1405.
- [184] Valko, K., Nunhuck, S., Bevan, C., Abraham, M. H., Reynolds, D. P., *J. Pharm. Sci.*, **2003**, *92*, 2236-2248.
- [185] Elcock, T., Mallett, D., Edwards, C., GSK, Unpublished results.
- [186] Wan, H., Rehngren, M., *J. Chromatogr. A*, **2006**, *1102*, 125-134.
- [187] Waters, N. J., Jones, R., Williams, G., Sohal, B., *J. Pharm. Sci.*, **2008**, *97*, 4586-4595.
- [188] Serban, G. M., Manescu, I. B., Manu, D. R., Dobreanu, M., *Acta Med. Marisiensis*, **2018**, *64*, 83-90.
- [189] Kimura, M., Tsuruta, S., Yoshida, T., *Clin. Exp. Immunol.*, **1999**, *118*, 192-196.
- [190] Bunn, P. A., Jr., Foss, F. M., *J. Cell. Biochem.*, **1996**, 12-23.
- [191] Lavis, L. D., Raines, R. T., *ACS Chem. Biol.*, **2008**, *3*, 142-155.
- [192] <https://www.thermofisher.com/uk/en/home/references/molecular-probes-the-handbook/introduction-to-fluorescence-techniques.html>, accessed on 15th January 2019.

- [193] Monici, M., *Biotechnol. Annu. Rev.*, **2005**, *11*, 227-256.
- [194] Wall, K. P., Dillon, R., Knowles, M. K., *Biochem. Mol. Biol. Educ.*, **2015**, *43*, 52-59.
- [195] Rurack, K., Spieles, M., *Anal. Chem.*, **2011**, *83*, 1232-1242.
- [196] Devaraj, N. K., Hilderbrand, S., Upadhyay, R., Mazitschek, R., Weissleder, R., *Angew. Chem., Int. Ed.*, **2010**, *49*, 2869-2872.
- [197] Carlson, J. C. T., Meimetis, L. G., Hilderbrand, S. A., Weissleder, R., *Angew. Chem. Int. Ed.*, **2013**, *52*, 6917-6920.
- [198] Vazquez, A., Dzajak, R., Dracinsky, M., Rampmaier, R., Siegl, S. J., Vrabel, M., *Angew. Chem. Int. Ed.*, **2017**, *56*, 1334-1337.
- [199] Rutkowska, A., Krause, J., Cellzome (a GSK company), Unpublished results.
- [200] https://spirochrome.com/documents/datasheet_SiR-tetrazine.pdf, accessed on 13th January 2019.
- [201] <https://www.jenabioscience.com/click-chemistry/click-reagents-by-chemistry/tetrazine-reagents/fluorescent-dyes/clk-015-tetrazine-cy5>, accessed on 18th April 2018.
- [202] Schnyder, A., Indolese, A. F., Studer, M., Blaser, H.-U., *Angew. Chem. Int. Ed.*, **2002**, *41*, 3668-3671.
- [203] Dalton, S. E., Dittus, L., Thomas, D. A., Convery, M. A., Nunes, J., Bush, J. T., Evans, J. P., Werner, T., Bantscheff, M., Murphy, J. A., Campos, S., *J. Am. Chem. Soc.*, **2018**, *140*, 932-939.
- [204] <https://www.news-medical.net/life-sciences/The-Endoplasmic-Reticulum-and-Golgi-Body-Whats-the-Difference.aspx>, accessed on 2nd April 2020.
- [205] Kellokumpu, S., *Front. Cell Dev. Biol.*, **2019**, *7*, 93.
- [206] Kaufmann, A. M., Krise, J. P., *J. Pharm. Sci.*, **2007**, *96*, 729-746.
- [207] Goldman, S. D. B., Funk, R. S., Rajewski, R. A., Krise, J. P., *Bioanalysis*, **2009**, *1*, 1445-1459.
- [208] <https://www.thermofisher.com/order/catalog/product/W11261>, accessed on 6th December 2018.
- [209] Morgan, G. W., Kail, M., Hollinshead, M., Vaux, D. J., *Anal. Biochem.*, **2013**, *441*, 21-31.

- [210] Haranczyk, N. A., Pochee, E. A., *Kosmos*, **2016**, 65, 1-10.
- [211] <http://tools.thermofisher.com/content/sfs/manuals/mp07525.pdf>, accessed on 4th March 2020.
- [212] <https://www.thermofisher.com/order/catalog/product/L7528#/L7528>, accessed on 4th March 2020.
- [213] Griffiths, R. J., Burley, G. A., Talbot, E. P. A., *Org. Lett.*, **2017**, 19, 870-873.
- [214] Cobice, D. F., Goodwin, R. J. A., Andren, P. E., Nilsson, A., MacKay, C. L., Andrew, R., *Br. J. Pharmacol.*, **2015**, 172, 3266-3283.
- [215] Boxer, S. G., Kraft, M. L., Weber, P. K., *Annu. Rev. Biophys.*, **2009**, 38, 53-74.
- [216] Bodzon-Kulakowska, A., Suder, P., *Mass Spect. Rev.*, **2016**, 35, 147-169.
- [217] Nunez, J., Renslow, R., Cliff, J. B., 3rd, Anderton, C. R., *Biointerphases*, **2017**, 13, 03B301.
- [218] Aguei-Gonzalez, P., Jaehne, S., Phan, N. T. N., *J. Anal. At. Spectrom.*, **2019**, 34, 1355-1368.
- [219] Gyngard, F., Steinhäuser, M. L., *J. Anal. At. Spectrom.*, **2019**, 34, 1534-1545.
- [220] Steinhäuser, M. L., Lechene, C. P., *Semin. Cell Dev. Biol.*, **2013**, 24, 661-667.
- [221] Chandra, S., *Appl. Surf. Sci.*, **2003**, 203-204, 679-683.
- [222] Cheng, C., Sun, J., Xing, L., Xu, J., Wang, X., Hu, Y., *J. Org. Chem.*, **2009**, 74, 5671-5674.
- [223] Yang, J., Liang, Y., Seckute, J., Houk, K. N., Devaraj, N. K., *Chem. Eur. J.*, **2014**, 20, 3365-3375.
- [224] Yang, J., Liang, Y., Šečutè, J., Houk, K. N., Devaraj, N. K., *Chem. Eur. J.*, **2014**, 20, 3365-3375.
- [225] Paulissen, R., Reimlinger, H., Hayez, E., Hubert, A. J., Teyssie, P., *Tetrahedron Lett.*, **1973**, 2233-2236.
- [226] Doyle, M. P., *Chem. Rev.*, **1986**, 86, 919-940.
- [227] Doyle, M. P., *Acc. Chem. Res.*, **1986**, 19, 348-356.
- [228] Doyle, M. P., Griffin, J. H., Bagheri, V., Dorow, R. L., *Organometallics*, **1984**, 3, 53-61.
- [229] Hosmane, R. S., Liebman, J. F., *Struct. Chem.*, **2002**, 13, 501-503.
- [230] Dallinger, D., Kappe, C. O., *Aldrichimica Acta*, **2016**, 49, 57-66.

- [231] Snyder, J. P., Padwa, A., Stengel, T., Arduengo, A. J., Jockisch, A., Kim, H.-J., *J. Am. Chem. Soc.*, **2001**, *123*, 11318-11319.
- [232] Cotton, F. A., Dikarev, E. V., Feng, X., *Inorg. Chim. Acta*, **1995**, *237*, 19-26.
- [233] Sargent, A. L., Rollog, M. E., Eagle, C. T., *Theor. Chem. Acc.*, **1997**, *97*, 283-288.
- [234] Nakamura, E., Yoshikai, N., Yamanaka, M., *J. Am. Chem. Soc.*, **2002**, *124*, 7181-7192.
- [235] Yates, P., *J. Am. Chem. Soc.*, **1952**, *74*, 5376-5381.
- [236] Felthouse, T. R., *Prog. Inorg. Chem.*, **1982**, *29*, 73-166.
- [237] Pirrung, M. C., Morehead, A. T., Jr., *J. Am. Chem. Soc.*, **1996**, *118*, 8162-8163.
- [238] Hoye, T. R., Dinsmore, C. J., *J. Am. Chem. Soc.*, **1991**, *113*, 4343-4345.
- [239] Bonge, H. T., Hansen, T., *J. Org. Chem.*, **2010**, *75*, 2309-2320.
- [240] Nowlan, D. T., Gregg, T. M., Davies, H. M. L., Singleton, D. A., *J. Am. Chem. Soc.*, **2003**, *125*, 15902-15911.
- [241] Jennings, P. W., Johnson, L. L., *Chem. Rev.*, **1994**, *94*, 2241-2290.
- [242] Davies, H. M. L., Hodges, L. M., Matasi, J. J., Hansen, T., Stafford, D. G., *Tetrahedron Lett.*, **1998**, *39*, 4417-4420.
- [243] Loibner, H., Zbiral, E., *Helv. Chim. Acta*, **1977**, *60*, 417-425.
- [244] Lal, B., Pramanik, B. N., Manhas, M. S., Bose, A. K., *Tetrahedron Lett.*, **1977**, 1977-1980.
- [245] Thompson, A. S., Humphrey, G. R., DeMarco, A. M., Mathre, D. J., Grabowski, E. J. J., *J. Org. Chem.*, **1993**, *58*, 5886-5888.
- [246] Gololobov, Y. G., Kasukhin, L. F., *Tetrahedron*, **1992**, *48*, 1353-1406.
- [247] Bickelhaupt, F. M., Houk, K. N., *Angew. Chem., Int. Ed.*, **2017**, *56*, 10070-10086.
- [248] Liu, F., Liang, Y., Houk, K. N., *J. Am. Chem. Soc.*, **2014**, *136*, 11483-11493.
- [249] Liu, F., Paton, R. S., Kim, S., Liang, Y., Houk, K. N., *J. Am. Chem. Soc.*, **2013**, *135*, 15642-15649.
- [250] Fan, X., Ge, Y., Lin, F., Yang, Y., Zhang, G., Ngai, W. S. C., Lin, Z., Zheng, S., Wang, J., Zhao, J., Li, J., Chen, P. R., *Angew. Chem., Int. Ed.*, **2016**, *55*, 14046-14050.
- [251] Pinner, A., *Chem. Ber.*, **1897**, *30*, 1871-1890.

[252] Audebert, P., Miomandre, F., Clavier, G., Vernieres, M.-C., Badre, S., Meallet-Renault, R., *Chem. Eur. J.*, **2005**, *11*, 5667-5673.

[253] Yang, J., Karver, M. R., Li, W., Sahu, S., Devaraj, N. K., *Angew. Chem. Int. Ed.*, **2012**, *51*, 5222-5225.

[254] Chen, W., Wang, D., Dai, C., Hamelberg, D., Wang, B., *Chem. Commun.*, **2012**, *48*, 1736-1738.